Radiation mechanisms of astrophysical objects: classics today

Proceedings of the conference
in honor of the 100th birthday of Academician V.V. Sobolev
held at St. Petersburg on September 21–25, 2015

Edited by
V. P. Grinin, H. Harutyunian, V. B. Il'in,
A. F. Kholtygin, A. Nikoghossian

EDIT
PRINT
publishing house

Editors:
Vladimir P. Grinin
Hayk Harutyunian
Vladimir B. Il'in
Alexander F. Kholtygin
Artur Nikoghossian

Radiation mechanisms of astrophysical objects: classics today —
Proceedings of the conference in honor of the 100th birthday of Academician Victor V. Sobolev held at St. Petersburg on September 21–25, 2015.

Studies of radiation mechanisms and processes of spectra formation in astronomical objects are among the fundamental tasks of modern astrophysics. A powerful tool for the solution of these problems is provided by the theory of radiative transfer, which has been substantially contributed to and developed by Victor Victorovich Sobolev. The conference highlighted recent advances in the field of the interests of V.V. Sobolev. The proceedings provide the permanent record of what was presented at the meeting and include various papers on radiative transfer theory, interstellar matter, stellar atmospheres and circumstellar matter, planetary atmospheres, and high-energy astrophysics and cosmology.

ISBN
Printed in the Republic of Armenia

EDIT PRINT
12 Toumanyan str., Yerevan
Tel.: (374 10) 520 848
www.editprint.am
info@editprint.am

Contents

Preface

We are very pleased to introduce the proceedings of the international conference "Radiation mechanisms of astrophysical objects: classics today" held at the St. Petersburg State University and Main (Pulkovo) Astronomical Observatory from September 21 to 25, 2015. The meeting was related to the 100th anniversary of Academician Victor Victorovich Sobolev celebrated on September 2, 2015 and highlighted recent advantages in the research fields to which V.V. Sobolev contributed prominently.

The conference was highly successful. It included the plenary sessions featuring review talks by internationally recognized experts as well as a memorial session. Original scientific results were presented in the sections: i) radiative transfer theory; ii) interstellar matter; iii) stellar atmospheres, circumstellar matter, and planetary atmospheres; iv) high-energy astrophysics and cosmology. There were all together about 130 contributions, with many papers being focused on the development of Sobolev's ideas in modern astrophysics. The program, book of abstracts, some presentations, a large photogallery and other materials including these proceedings are available at the conference web site *http://www.astro.spbu.ru/Sobolev100*.

The proceedings provide the permanent record of what was presented at the meeting. The plan of the book follows the conference program: four parts of the book correspond to the above mentioned sections. Each part begins with review papers, then the oral presentations follow in the alphabetic order of their first author, and finally a few poster papers are placed. In an appendix written by V.V. Ivanov in Russian, one can find a brief biography of V.V. Sobolev, a clear resume on his main scientific achievements and a brilliant description of his features as a pedagogue, an organizer, and just a person. It should be added that extended versions of 10 conference papers on radiative transfer theory have been published in the special issue of Journal of Quantitative Spectroscopy and Radiative Transfer (2016, vol. 183) entitled "Victor V. Sobolev and his scientific legacy."

We would like to thank participants for their contributions to the conference and these proceedings. The meeting could not also have happened without the Local Organizing Committee, who made a tough work to assemble and run the conference, and the Scientific Organizing Committee, who guided the direction of the conference and assisted with its program. We are glad to acknowledge the financial support from the St. Petersburg State University and the Russian Foundation for Basic Research. We are also deeply indebted to the Byurakan Astrophysical Observatory that sponsored the publication of the proceedings. Last but not least, we would like to thank Yulia Milanova, Roman Baluev, and Alexander Pocheketa for their very valuable assistance in preparation of this book.

The Editors

List of the Conference Participants

Martin Abrahamyan, Yerevan State University, Armenia
Yulia Aikasheva, Herzen State Pedagogical University, Russia
Vitaly Akimkin, Institute of Astronomy of the RAS (INASAN), Russia
Alexey Alakoz, Astro Space Center of Lebedev Physical Institute (ASC LPI), Russia
Ilya Alekseev, Crimean Astrophysical Observatory (CrAO), Russia
Sofya Alexeeva, Institute of Astronomy of the RAS (INASAN), Russia
Elena Babina, Crimean Astrophysical Observatory (CrAO), Russia
Sergei Balashev, Ioffe Institute, Russia
Dmitry Barsukov, Ioffe Institute, Russia
Oksana Belova, Sternberg Astronomical Institute (SAI MSU), Russia
Svetlana Berdyugina, Kiepenheuer Institute for Solar Physics (KIS), Germany
Alexander Berezhnoi, St. Petersburg branch of Astronomical-Geodesic Society, Russia
Nina Beskrovnaya, Main (Pulkovo) Astronomical Observatory, Russia
Ilfan Bikmaev, Kazan (Volga region) Federal University (KFU), Russia
Anastasia Bisyarina, Ural Federal University (UrFU), Russia
Sergey Blinnikov, Institute for Theoretical and Experimental Physics (ITEP), Russia
Valeria Borovik, Main (Pulkovo) Astronomical Observatory, Russia
Konstantin Bychkov, Sternberg Astronomical Institute (SAI MSU), Russia
Andrey Bykov, Ioffe Institute, Russia
Alex Carciofi, University of São Paulo, Brazil
Sandip Chakrabarty, S.N. Bose National Centre for Basic Sciences, India
Pascal Chardonnet, University of Savoy Mont Blanc, France
Anatol Cherepashchuk, Sternberg Astronomical Institute (SAI MSU), Russia
Gennadiy Chernov, N. Pushkov Institute of Terrestrial Magnetism, Ionosphere and Radio Wave Propagation of the RAS (IZMIRAN), Russia
Eugene Churazov, Space Research Institute, Russia and Max-Planck-Institute for Astrophysics (MPA), Germany
Rustam Dagkesamanskii, Pushchino Radio Astronomy Observatory (PRAO), Russia
Andrey Dementyev, St. Petersburg State University (SPbSU), Russia
Tatiana Demidova, Main (Pulkovo) Astronomical Observatory, Russia
Zhanna Dlugach, Main Astronomical Observatory (MAO NASU), Ukraine
Denis Dmitriev, St. Petersburg State University (SPbSU), Russia
Helmut Domke, Berlin, Germany
Viacheslav Dushin, St Petersburg State University (SPbSU), Russia
Tamara Ermolaeva, Main (Pulkovo) Astronomical Observatory, Russia
Andres Escala, University of Chile, Chile
Sergei Fabrika, Special Astrophysical Observatory (SAO RAS), Russia
Marat Gil'fanov, Space Research Institute, Russia
Yuri Gnedin, Main (Pulkovo) Astronomical Observatory, Russia
Ol'ga Golubchina, St. Petersburg branch of SAO RAS, Russia
Mikhail Gornostaev, Sternberg Astronomical Institute (SAI MSU), Russia
Vitaliy Grigoryev, St. Petersburg State University (SPbSU), Russia
Vladimir Grinin, Main (Pulkovo) Astronomical Obseravatory, Russia

Hayk Harutyunian, Byurakan Astrophysical Observatory (BAO), Armenia
Swetlana Hubrig, Leibniz Institute for Astrophysics Potsdam (AIP), Germany
Subhon Ibadov, Institute of Astrophysics, Tajik Academy of Sciences (IA TAS), Tajikistan
Nazar Ikhsanov, St. Petersburg State University (SPbSU), Russia
Vladimir Il'in, St. Petersburg State University (SPbSU) and Main (Pulkovo) Astronomical Observatory, Russia
Nariman Ismailov, Shamakhi Astrophysical Observatory (ShAO ANAS), Azerbaijan
Alexander Ivanchik, Ioffe Institute, Russia
Pavel Ivanov, Astro Space Centre of Lebedev Physical Institute (ASC LPI), Russia
Natalia Kalinina, Ural Federal University (UrFU), Russia
Alexander Kaminker, Ioffe Institute, Russia
Maria Katsova, Sternberg Astronomical Institute (SAI MSU), Russia
Natalia Katysheva, Sternberg Astronomical Institute (SAI MSU), Russia
Andrey Kazantsev, Pushchino Radio Astronomy Observatory ASC LPI (PRAO), Russia
Edward Khachikian, Byurakan Astrophysical Observatory (BAO), Armenia
Alexander Kholtygin, St. Petersburg State University (SPbSU), Russia
Vitaliy Kim, Main (Pulkovo) Astronomical Obseravatory, Russia
Nikolai Kiselev, Main Astronomical Observatory (MAO NASU), Ukraine
Alexander Kolesov, St. Petersburg State University (SPbSU), Russia
Serguei Komissarov, University of Leeds, United Kingdom
Flera Kopylova, Special Astrophysical Observatory (SAO RAS), Russia
Maria Kostina, St. Petersburg State University (SPbSU), Russia
Yuri Kovalev, Astro Space Center, Lebedev Physical Institute (ASC LPI), Russia
Olesya Kozlova, Crimean Astrophysical Observatory (CrAO), Russia
Jacek Krelowski, Nicolaus Copernicus University, Poland
Sergey Levshakov, Ioffe Institute, Russia
Moisey Livshits, N. Pushkov Institute of Terrestrial Magnetism, Ionosphere and Radio Wave Propagation of the RAS (IZMIRAN), Russia
Alexander Lutovinov, Space Research Institute, Russia
Leonid Lyubimkov, Crimean Astrophysical Observatory (CrAO), Russia
Olga Maryeva, Special Astrophysical Observatory (SAO RAS), Russia
Liudmila Mashonkina, Institute of Astronomy of the RAS (INASAN), Russia
Aleksei Medvedev, St. Petersburg State University (SPbSU), Russia
Khidir Mikayilov, Shamakhi Astrophysical Observatory (ShAO ANAS), Azerbaijan
Yulia Milanova, St. Petersburg State University (SPbSU), Russia
Michael Mishchenko, NASA Goddard Institute for Space Studies, United States
Anna Mokrushina, Main (Pulkovo) Astronomical Observatory, Russia
Egor Morchenko, Sternberg Astronomical Institute (SAI MSU), Russia
Maria Murga, Institue of Astronomy of the RAS (INASAN), Russia
Alexander Mushtukov, Tuorla Observatory, Finland and Main (Pulkovo) Astronomical Observatory, Russia
Dmitrij Nagirner, St. Petersburg State University (SPbSU), Russia
Valery Nagnibeda, St. Petersburg State University (SPbSU), Russia
Aleksandr Nesterenok, Ioffe Institute, Russia
Arthur Nikoghossian, Byurakan Astrophysical Observatory (BAO), Armenia
Evgeniya Nikolaeva, Kazan (Volga region) Federal University (KFU), Russia

Bulat Nizamov, Sternberg Astronomical Institute (SAI MSU), Russia
Lidia Oskinova, University of Potsdam, Germany
Yaroslav Pavlyuchenkov, Institute of Astronomy of the RAS (INASAN), Russia
Oganes Pikichyan, Byurakan Astrophysical Observatory (BAO), Armenia
Mikhail Pogodin, Main (Pulkovo) Astronomical Observatory, Russia
Konstantin Postnov, Sternberg Astronomical Institute (SAI MSU), Russia
Alexander Potekhin, Ioffe Institute, Russia
Ilya Potravnov, Main (Pulkovo) Astronomical Observatory, Russia
Juri Poutanen, University of Turku, Finland
Marina Prokopieva, St. Petersburg State University (SPbSU), Russia
Dmitriy Rodionov, Herzen State Pedagogical University, Russia
Nikolai Rogovtsov, Belarusian National Technical University (BNTU), Belarus
Bayram Rustamov, Shamakhi Astrophysical Observatory (ShAO ANAS), Azerbaijan
Nail Sakhibullin, Kazan (Volga region) Federal University (KFU), Russia
Svetlana Salii, Ural Federal University (UrFU), Russia
Igor' Savanov, Institute of Astronomy of the RAS (INASAN), Russia
Elena Seifina, Sternberg Astronomical Institute (SAI MSU), Russia
Alexander Semyannikov, Volgograd State University (VolSU), Russia
Alexey Semyonov, Main (Pulkovo) Astronomical Observatory, Russia
Asoke Kumar Sen, Assam University, India
Nadezhda Shakhvorostova, Lebedev Physical Institute (LPI RAS), Russia
Margarita Sharina, Special Astrophysical Observatory (SAO RAS), Russia
Yuri Shchekinov, Southern Federal University (SFU), Russia
Vladislav Shimansky, Kazan (Volga region) Federal University (KFU), Russia
Sergei Shulman, St. Petersburg State University (SPbSU), Russia
Gustav Shved, St. Petersburg State University (SPbSU), Russia
Nikolai Silant'ev, Main (Pulkovo) Astronomical Observatory, Russia
Tatiana Sitnova, Institute of Astronomy of the RAS (INASAN) and Sternberg Astronomical Institute (SAI MSU), Russia
Ksenia Smirnova, Ural Federal University (UrFU), Russia
Andrej Sobolev, Ural Federal University (UrFU), Russia
Dmitry Sokoloff, Moscow State University and IZMIRAN, Russia
Natalia Sotnikova, St. Petersburg State University (SPbSU), Russia
Svetlana Starikova, Smithsonian Astrophysical Observatory (SAO), United States
Natalia Sudnik, St. Petersburg State University (SPbSU), Russia
Rashid Syunyaev, Space Research Institute, Russia
Larisa Tambovtseva, Main (Pulkovo) Astronomical Observatory, Russia
Anatoliy Tarasov, Crimean Astrophysical Observatory (CrAO), Russia
Daria Teplykh, Pushchino Radio Astronomy Observatory ASC LPI (PRAO), Russia
Lev Titarchuk, University of Ferrara, Italy
Olga Tsiopa, Main (Pulkovo) Astronomical Observatory, Russia
Dmitri Varshalovich, Ioffe Institute, Russia
Evgenii Vasiliev, Southern Federal University (SFU), Russia
Oleg Verkhodanov, Special Astrophysical Observatory (SAO RAS), Russia
Vitaly Vertogradov, Herzen State Pedagogical University, Russia
Tõnu Viik, Tartu Observatory, Estonia

Alexey Vikhlinin, Smithsonian Astrophysical Observatory (SAO), United States
Alexander Vinokurov, Special Astrophysical Observatory (SAO RAS), Russia
Yaroslav Voronov, Herzen State Pedagogical University, Russia
Nikolai Voshchinnikov, St. Petersburg State University (SPbSU), Russia
Dmitri Wiebe, Institute of Astronomy of the RAS (INASAN), Russia
Dmitry Yakovlev, Ioffe Institute, Russia
Svetlana Yakovleva, Herzen State Pedagogical University, Russia
Valeria Yakovleva, St. Petersburg State University (SPbSU), Russia
Valentine Yankovsky, St. Petersburg State University (SPbSU), Russia
Saleem Zaroubi, University of Groningen, The Netherlands

Section I
Radiative Transfer Theory

V.V. Sobolev and Analytical Radiative Transfer Theory

D.I. Nagirner[1]

E-mail: *dinagirner@gmail.com*

The review of Sobolev's publications on the analytical radiative transfer theory is presented. A short review is also given of the results published by his disciples.

1 Introduction

The basic equations of the Radiative Transfer Theory (RTT) were formulated at the turn of the 20th century. Initially transfer theory developed as a purely analytical instrument since the calculation of radiation fields was problematic with the computational facilities of that time. Between 1940 and 1980 the exact and sufficiently accurate approximate solutions to the basic equations of the theory were found, and for various limiting cases the asymptotic theory was developed. The peculiarities and difficulties of the description and computation of multiple scattering were thus revealed. By comparing numerical results with the analytical solutions it became possible to evaluate the benefits and drawbacks of various numerical methods and give estimates of their accuracy.

V.V. Sobolev made a definitive contribution to the creation of the analytical RTT. In the 1940s he developed a method of calculating populations of atomic levels in expanding non-planar dilute gaseous media, the method which is still in use. This method is known now as *the Sobolev theory*. He also developed an effective approximate method to solve problems of anisotroping multiple light scattering. As early as in 1941, he formulated the approximation of Complete Frequency Redistribution (CFR) in problems of radiative transfer in spectral lines. In the 1950s he developed the method of exact solution of the basic integral equations describing multiple light scattering, both monochromatic and with CFR. He was also the first to investigate multiple scattering of polarized radiation and non-stationary radiation fields. He applied his theoretical findings to the interpretation of observations of many types of astrophysical objects. Dozens of former Sobolev's students form a team of theorists known as the Sobolev astrophysical school. In what follows we present a brief review of the main results found by V.V. Sobolev and his disciples.

We begin with the description of contributions to the analytical RTT by V.A. Ambartsumian (who was Sobolev's Ph.D. adviser).

[1] Sobolev Astronomical Institute, St. Petersburg State University, Russia

V. Grinin et al. (eds) Radiation mechanisms of astrophysical objects. Yerevan: Edit Print, 2017, pp. 3–28.

2 Contribution of V.A. Ambartsumian

V.A. Ambartsumian founded the chair of astrophysics (1934) in the St. Petersburg (Leningrad) University. He published the first Russian manual on theoretical astrophysics [1].

He studied the radiation regime in an infinite plane medium with sources at the infinite depth, thus modeling deep layers of a semi-infinite medium with anisotropic monochromatic scattering [2].

Ambartsumian revealed the important role of radiation pressure by spectral line photons in the dynamics of planetary nebulae and stellar envelopes, particularly, the pressure exerted by the photons of the hydrogen L_α-line [3]. He suggested a new method to describe the influence of absorption lines on the temperature regime in stellar atmospheres [4].

Ambartsumian introduced innovative approaches to RTT problems known as the invariance principles and the method of adding of layers [5]. Using these new methods he expressed the reflection and transmission coefficients of a plane layer which are functions of two angular variables in terms of auxiliary functions of one variable [6]. For these functions he found nonlinear integral equations and studied the asymptotic behavior of their solutions for the case of a layer of large optical thickness [7, 8].

He expressed the mean number and the mean square of the number of scattering events in terms of the radiation intensity [9].

He studied also the problem of light scattering in semi-infinite medium with reflecting surface [10].

The main Ambartsumian's publications on RTT are reprinted in the book [11]. The proceedings of the conference dedicated to the 40th anniversary of the Invariance Principle are published in [12].

V.A. Ambartsumian studied many other astrophysical problems: the lifetimes of stars, star clusters, stellar associations, the Milky Way brightness fluctuations, formation of galaxies, variable stars, etc.

V.V. Sobolev continued studies of his teacher in RTT. He discovered new branches and created new methods of RTT, formulated and solved a lot of new problems.

3 Early Sobolev's publications

V.V. Sobolev proposed a method of approximate solution to the problem of anisotropic scattering of monochromatic radiation. According to this method the first scattering is taken into account exactly, with the real phase function, whereas higher order scatterings are treated approximately, with the two-term phase function [13]. V.V. Sobolev applied the developed theory to terrestrial and planetary atmospheres [14, 15]. Later, this approximate method was applied to problems with spherical geometry: scattering in a homogeneous sphere with a point source at its center [16] (a model of dust nebula) and in a spherical shell

illuminated by a parallel radiation flux [17] (model of a planetary atmosphere, coauthor I.N. Minin).

V.V. Sobolev showed that the idea of accelerated expansion of planetary nebulae adopted at that time is incorrect because it was based on the assumption that line radiation does not change its frequency when scattered. In fact, the scattered photon reduce its frequency because a part of its momentum and energy passes to the scattering atom. Therefore the full momentum of stellar radiation is not transmitted to the nebula matter and does not accelerate it: radiation simply leaves the nebula in the wings of the line [18]. In [19] V.V. Sobolev simplified the calculation of the radiation regime in infinite plane medium.

The problems of radiative transfer in expanding media were studied in Sobolev's doctoral thesis and in his famous book [20]. The equations determining the populations of atomic levels were derived and solved using the method of local scattering. The method is known as *the Sobolev approximation* and is widely used till now. The essence of the method is the following. If a medium expands with a velocity gradient, the radiation in a line ceases to interact with atoms when it propagates in places where gas velocity is substantially different from the velocity at the site of its emission. As a result, the line radiation is not reabsorbed and propagates freely. The scattering becomes local. Due to this effect, in media moving with large gradient of gas velocity atomic excitation and degree of ionization change drastically [21].

Later, for the special case of the two-level atom and a constant velocity gradient in plane media, the integral equation was formulated, with the kernel depending on the absolute value of the difference of the arguments. The approximate solution of the equation was found using "on the spot" approximation [22].

In two papers [23] and [24] (with V.V. Ivanov) the intensities of hydrogen lines and the Balmer decrement in the spectra of hot stars were calculated. Lines are formed in their envelopes. By applying the approximation of local scattering, the equations governing the populations of atomic levels were reduced to algebraic ones.

4 Monochromatic scattering

4.1 Polarized radiation and non-stationary radiation fields

In [25] V.V. Sobolev formulated transfer equations for linearly polarized radiation for the case of Rayleigh scattering. He found the behavior of two intensities and the corresponding source functions in deep layers of semi-infinite medium. He also found the degree of polarization of the radiation emerging from purely electronic semi-infinite medium with the sources at infinite depth, thus modeling a hot atmosphere of an early type star. The largest degree of polarization, 11.7%, is reached at the limb of the stellar disk. This is known as the *Sobolev–Chandrasekhar polarization limit*.

Later V.V. Sobolev published several papers on Rayleigh scattering (with V.M. Loskutov). They calculated fields of polarized radiation in plane slabs for several distributions of primary sources [26]. The results were used for the interpretation of observed polarization of X-ray sources [27] and quasars [28].

For studying non-stationary radiation fields in stationary media V.V. Sobolev introduced two characteristic times [29]: t_1, the mean time a photon spends while absorbed by an atom and t_2, the mean time between two consecutive scatterings of a photon. He derived the equations describing non-stationary radiation fields in one-dimensional approximation and solved them for the case $t_2 = 0$, both for final and infinite optical thickness of the medium. The solutions thus found were used to interpret peculiarities of radiation fields in the ejecta of novae (see [30]).

Later on V.V. Sobolev continued studying the non-stationary scattering with his coauthor A.K. Kolesov [31, 32]. They presented the formulas and numerical data for the solutions to the problem of a point source in an infinite and semi-infinite one-dimensional media for alternative cases $t_2 \ll t_1$ and $t_1 \ll t_2$. The results were applied to interpret the flares of UV Ceti stars.

4.2 Reflecting boundaries and inhomogeneous media

V.V. Sobolev derived the equations for radiation fields in a plane media with a reflecting lower surface. Two particular cases were considered in more detail: orthotropic and mirror reflection. In the former case the all quantities with the reflecting surface were expressed by simple relations in terms that without it [33]. The results for the case of a mirror boundary were published in the book [30] and applied to the scattering in a cloudy slab of large optical thickness above the surface of the sea.

The problem of scattering in plane media if the probability of photon survival λ depends on the depth τ was considered [34, 35]. The calculations of the albedo and brightness coefficients were made for the cases:

1) λ is piecewise constant;
2) λ is an exponent of optical depth $\lambda = \lambda_0\, e^{-m\tau}$ or the sum of such exponents;
3) λ is a superposition (integral) of exponents.

Later the degree of polarization of the radiation emergent from the semi-infinite medium was calculated for the case 2) [36] (coauthor V.M. Loskutov).

4.3 New methods of calculation of radiation fields

V.V. Sobolev formulated the concept of photon escape probability from a medium: the product $2\pi p\,(\tau, \eta)\,\mathrm{d}\eta$ denotes the probability for a photon absorbed at a depth τ in isotropically scattering semi-infinite atmosphere to escape from this medium at an angle $\arccos\eta$ within a solid angle of $2\pi\,\mathrm{d}\eta$ after an arbitrary number of scatterings. It is easy to obtain the equations and relations for the escape probability from simple considerations. If this function is found, it is possible

with the known power of primary sources to calculate the intensity of emergent radiation by direct integration [30]. Apart from this, the majority of the functions and equations of RTT got the probability interpretation. The concept of the escape probability was applied to many problems of RTT for deducing the equations and solving them.

Another method which was applied by V.V. Sobolev is transformation from equations with integrals on optical depth τ to linear equations with integrals on angular variables which is equivalent to application of the Laplace transform. Such equations were derived for brightness coefficients, functions of one variable in terms of which these coefficients were expressed and other functions. It was such type equations that were used for the calculations of polarization fields with the Rayleigh scattering and were mentioned above.

4.4 Asymptotic theory of monochromatic scattering

The complete asymptotics of the source function and of the intensity in deep layers of a semi-infinite medium for the reflection problem were obtained by V.V. Sobolev (see [37]) using the relations between characteristics of anisotropic scattering in infinite and semi-infinite media which were found with the summation of layers method. Using these results and with the same method V.V. Sobolev deduced asymptotics for the brightness coefficients and other functions when the optical thickness of a slab τ_0 was large [38].

Another domain for which the asymptotic formulas were found is a nearly pure scattering when the survival probability is very close to unity: $1 - \lambda \ll 1$. Expansions of various functions on the power of $\sqrt{1-\lambda}$ (the first or second) were obtained. The results are given in the book [39].

5 Scattering in lines and the resolvent method

5.1 Frequency redistribution

V.V. Sobolev directed essential efforts to the study of scattering in spectral lines.

The laws describing the transformation of photon frequency in single scattering were deduced but they were too complicate and did not allow to solve the problem of line formation. Several authors (T. Holstein, L.M. Biberman, V.V. Sobolev, and others) proposed the approximation of complete redistribution in frequency (CFR), which implied that the photon frequencies before and after scattering do not correlate. In other words, the absorption and emission coefficients depend on frequency equally. The following additional approximations were accepted: atoms of the same kind have only two discrete levels (the two-level approximation) and continuum constant within the line; both radiative and collisional transitions are possible between these levels; the induced radiation was not taken into account because it leads to nonlinear equations, which do not permit analytical investigation.

To begin V.V. Sobolev derived some frequency redistribution laws and accepted as the approximation the CFR. Then he considered scattering in a one-dimensional medium and obtained differential equations for the intensity and integral equation for the source function. He solved them for homogeneous distribution of the sources and found the emissivity, the density and flux of energy, the light pressure and the emission profiles of emergent radiation. The results were close for various redistribution laws and strongly differed from the monochromatic scattering.

Then various equations were obtained for the probability $p(\tau, x_1, x_2)$ of photon escape from the medium of optical thickness τ_0 in line from the depth τ (x_1 and x_2 are dimensionless frequencies of the emitted and escaping photons). Also the equations were derived for the two introduced functions $\varphi(x, \tau_0)$ and $\psi(x, \tau_0)$. After that V.V. Sobolev found the equation for the brightness coefficients. The equations were solved for CFR and the profiles of the forming absorption lines were calculated. Better agreement with the observable ones than for monochromatic scattering were achieved. All these results are in his book [30].

The integro-differential and integral equations, describing the process of multiple photon scattering in spectral line in a plane layer on the assumption of CFR, were derived by V.V. Sobolev in [40]. The approximate solution of the integral equation based on the principle of local scattering was found. It is usually known as on the spot approximation. Later V.V. Sobolev developed the exact theory of multiple scattering known as resolvent method. At first it was done for isotropic monochromatic scattering [41, 42] and then for scattering in line with CFR [43, 44].

5.2 Resolvent method

This method is applicable to equations of the following form:

$$S(\tau) = S_0(\tau) + \frac{\lambda}{2} \int_{\tau_*}^{\tau_0} K(|\tau - \tau'|) S(\tau')\, d\tau'. \tag{1}$$

This equation is the basic integral equation of RTT. Here $S_0(\tau)$ is a given, and $S(\tau)$ is the sought-for source function, λ is photon survival probability per scattering. The limits of integration τ_* and τ_0 are the "depths" of the lower and upper boundaries of a plane medium. If $-\tau_* = \tau_0 = \infty$, the medium is infinite; if $\tau_* > -\infty$ and $\tau_0 = \infty$, the medium is semi-infinite; if $\tau_0 < \infty$, it is a finite plane slab. In the last two cases it can be assumed that $\tau_* = 0$. The kernel function $K(\tau)$ for both monochromatic and CFR scattering can be represented as a superposition (integral) of exponentials.

The resolvent is defined as a function that allows one to find the solution of Eq. (1) for arbitrary given $S_0(\tau)$

$$S(\tau) = S_0(\tau) + \int_{\tau_*}^{\tau_0} \Gamma(\tau, \tau') S_0(\tau')\, \mathrm{d}\tau'. \tag{2}$$

The notations of resolvents are as follows: for an infinite medium it is $\Gamma_\infty(\tau,\tau_1)$, for a semi-infinite medium $\Gamma(\tau,\tau_1)=\Gamma(\tau,\tau_1,\infty)$, and for a finite slab $\Gamma(\tau,\tau_1,\tau_0)$.

For an infinite medium the following obvious relation holds: $\Gamma_\infty(\tau,\tau_1) = \Gamma_\infty(|\tau-\tau_1|,0) \equiv \Phi_\infty(|\tau-\tau_1|)$. V.V. Sobolev has shown that the resolvent of the equation (1) can be expressed in terms of a function of one variable, namely, the particular value of the resolvent with one of its arguments set equal to 0. This function is called the *resolvent function*: $\Phi(\tau,\tau_0)\equiv\Gamma(\tau,0,\tau_0)$. If $\tau_*=0$, the explicit expression of Γ in terms of Φ is rather complicated

$$\Gamma(\tau,\tau_1,\tau_0)=\Phi(|\tau-\tau_1|,\tau_0)+\int_0^{\min(\tau,\tau_1)}\big[\Phi(\tau-t,\tau_0)\Phi(\tau_1-t,\tau_0) - \Phi(\tau_0-\tau+t,\tau_0)\Phi(\tau_0-\tau_1+t,\tau_0)\big]\,dt. \tag{3}$$

For semi-infinite medium one has to set $\tau_0=\infty$ and $\Phi(\infty,\infty)=0$.

For the kernel functions representable as a superposition of exponentials V.V. Sobolev derived linear and nonlinear equations for the Laplace transforms of the resolvents and the resolvent functions as well as equations for resolvent functions themselves of type (1) (with $S_0(\tau) = (\lambda/2)\,K(\tau)$) and of Volterra type. Some of these equations are generalizations of Ambartsumian's equations. For a finite slab alternative equations were derived, with the derivatives with respect to τ_0.

For isotropic monochromatic scattering V.V. Sobolev found the asymptotic form of $\Phi(\tau,\tau_0)$ for $\tau \gg 1$[45]. It is expressed in terms of the resolvent function of semi-infinite medium. For the latter the exact explicit expression is known.

V.V. Sobolev encouraged his pupils for further development of the theory of line formation with CFR.

5.3 Inhomogeneous, infinite and spherical media

The scattering theory in inhomogeneous media was extended to the scattering in a spectral line with CFR [46] taking into account continuous absorption. In [47] V.V. Sobolev and E.G. Yanovitsky applied the resolvent method to the case of scattering with variable $\lambda(\tau)$. In [48] the results for the variable λ were summarized.

In [49] it was shown that three problems of monochromatic isotropic scattering in three media, namely: in a semi-infinite medium with an ideally reflecting mirror boundary; in a stationary spherical shell geometrically thin but optically thick with the central source and also in an infinite medium with a point source, are reduced to scattering in infinite medium.

In [50] the case of a smoothly reflecting boundary was reduced to two integral equations and with two resolvent functions. In [51] along with the fact that the smooth reflection from the boundary is not ideal, the changing direction of radiation when crossing it was taken into account because the refraction

indexes differ on its two sides. For the problem of diffuse reflection the equations were obtained for the azimuthal harmonics of the reflection coefficient by assuming that such harmonics calculated without reflection from the boundary are known. Also, the equations were deduced for characteristics of emergent radiation in the Milne problem and of the regime of the radiation field in deep layers. These problems are to model the light scattering at sea.

Several papers were devoted to monochromatic scattering in a homogeneous sphere and in a spherical envelope. In [52] the problem of scattering in the sphere with spherically symmetric sources was reduced to the problem of a plane slab of double optical thickness. In [53] the asymptotic formulas were obtained for the intensity of emergent radiation $I(\eta, \tau_0)$ when there is a point source in the center of the sphere or in the center of a thin spherical envelope and when the optical thicknesses of the sphere and the envelope τ_0 are large. V.V. Sobolev and A.K. Kolesov found more exact asymptotics of $I(\eta, \tau_0)$ for illuminating a sphere both by a radiation flux [54] and by a point source in the center [55]. The summary of these researches was presented in [56].

5.4 The resolvent method for anisotropic scattering

The equations governing anisotropic scattering with an arbitrary phase function contain integrals over three variables τ, η and ϕ. It is possible to expand characteristics of scattering in the Fourier series (or finite sum) on azimuth ϕ, to separate azimuth harmonics and to deduce separate equations with double integrals for each of the harmonics.

The intensity of the emergent radiation in the problem of reflection and transmission may be expressed in terms of functions $\varphi_i^m(\eta, \tau_0)$ and $\psi_i^m(\eta, \tau_0)$. If the number of terms in the expansion of the phase function in the Legendre polynomials equals $n+1$, to get the harmonic with number m ($i = m, m+1, \ldots, n$) one has to find $2(n - m + 1)$ such functions. For semi-infinite medium the functions $\psi_i^m(\eta, \infty) = 0$. For semi-infinite medium V.V. Sobolev expressed all the functions $\varphi_i^m(\eta)$ for each of the harmonics in terms of one function $H^m(\eta)$. The functions $\varphi_i^m(\eta, \tau_0)$ and $\psi_i^m(\eta, \tau_0)$ were expressed in terms of two functions, $X^m(\eta, \tau_0)$ and $Y^m(\eta, \tau_0)$. The polynomials depending on η and λ entered these expressions as factors. They are given by recurrent relations. The resolvent for each of the harmonics is expressed in terms of one resolvent function $\Phi_m(\tau, \tau_0)$. These results are summarized in Sobolev's book [39].

6 Other Sobolev's works on RTT

6.1 Number of scatterings; strongly peaked phase function

In four of V.V. Sobolev's papers [57] the numbers of scatterings were expressed through the functions introduced in other works. In the fourth paper for the case of scattering in the spectral line with CFR in finite slab were obtained sufficiently

narrow upper and lower estimations of the number of scatterings for large optical thickness.

In the case of strongly elongated forward phase function V.V. Sobolev expanded the intensity according the Taylor formula of the second order in the powers of the difference between the polar angles of the scattered and the incident radiation, and replaced the integral over angles with the differential operator. With the help of the obtained equation he found the light regime in deep layers [58].

6.2 Scattering in planetary atmospheres

Twenty years after publishing [14] V.V. Sobolev resumed the study of scattering characteristics in the Venus atmosphere. In the first paper [59] he calculated the reflection coefficient for a two-term phase function with the terms proportional to $\sqrt{1-\lambda}$. In the second paper two models of the atmosphere were adopted: the homogeneous one consisting of molecules and large-grained particles; and the two-layer one in which a molecular slab is placed above a cloudy slab. The dependencies of the degree of polarization on the phase and wavelength were found.

In two papers [60, 61] (coauthors I.N. Minin) the radiation of planetary atmosphere was described for isotropic scattering. The atmosphere was assumed to be plane (with the dependence $\lambda(\tau)$), but the incident angles of solar radiation on the plane were chosen to be the same as those of a parallel flux on spherical atmosphere. The effect of orthotropic reflection from the surface was taken into account.

In [62] the formulas for the profile r_ν and equivalent width W of a line in a certain place of the planetary disk and from the whole disk were derived as functions of phase. In [63] a two-layer atmosphere was constructed of a semi-infinite medium and an optically thin slab above it with different optical properties (i.e. their phase functions and photon survival probabilities differed). The same formulas were obtained.

6.3 Emission of supernovae and electron scattering

In three papers [64, 65, 66] V.V. Sobolev (in the third coauthor A.K. Kolesov) calculated the continuous spectra, light curves, optical thickness of envelopes and spectrophotometric temperatures of supernovae on the early stages of expansion of the ejecta. It was adopted that the radiation of envelope was under strong effect of electron scattering.

The effect of electron scattering on the spectra of stationary hot stars was studied in [67, 68], which continued the study in [35]. The emergent flux and specrophotometric temperature were calculated using as a tool linear integral equations with the integrals on angular variable.

6.4 Global absorption and emission

V.V. Sobolev devoted several papers specially to determination of relation between two parts of radiation energy that enters into a scattering and absorbing medium. One part of this energy undergoes true absorption and transfers to other types of energy. The other part abandons the medium. In the most general form the problem was considered in [69]. The law of redistribution in frequency and direction as the fraction of reemitted photons could be different in different points of the medium of arbitrary form (in [70] scattering was supposed to be isotropic). The amount of energy absorbed from the flux illuminating the medium was shown to be connected with the amount of irradiated energy if the distribution of internal sources was uniform. Analogous relations were obtained for Rayleigh scattering of polarized radiation [71].

The usefulness of the obtained relation was demonstrated for isotropic monochromatic scattering as well as for scattering in a line with CFR in a semi-infinite medium, in a plane slab and in a homogeneous sphere [72]. V.V. Sobolev deduced the integral relations for the intensities of internal and emerging from a plane slab radiation in [73].

7 Contributions of Sobolev's disciples

Here we present a list of the main achievements made by Sobolev's students and disciples. More detailed reviews of their works and the works of other authors are presented in the symposiums proceedings [12, 74, 75, 76].

7.1 I.N. Minin

The papers published with V.V. Sobolev as a coauthor are [17, 60, 61].

I.N. Minin deduced the equation and proposed the method to calculate the radiation transfer in a medium with refraction [77, 78] and obtained the exact expression for the resolvent function for monochromatic isotropic scattering in semi-infinite medium [79].

I.N. Minin used the Laplace transforms on time for solving the non-stationary radiation transfer in a medium with monochromatic scattering and studied it in detail [80, 81]. He showed that in three particular cases when $t_2 = 0$, $t_1 = 0$ and $t_1 = t_2$ the solutions for $\lambda < 1$ can be expressed through the solutions for $\lambda = 1$. The exact and asymptotic formulas for characteristics of the radiation emerging from a finite one-dimensional medium were obtained in three mentioned cases [82].

In [83] many characteristics of radiation field in a semi-infinite medium with arbitrary values of t_1 and t_2 were expressed in terms of one function. The equation determining this function was derived. Time-dependent problems were also solved for non-stationary one-dimensional ($\tau(t) = \tau(0)e^{-\alpha t}$) [84] and inhomogeneous [85] media.

Anisotropic scattering in semi-infinite medium [86] and in the layer of finite optical thickness [87] was investigated. If the number of terms in the expansion of phase function in the Legendre polynomials is equal to $n+1$, then for azimuthal harmonic number m I.N. Minin introduced $(n+1-m)^2$ resolvent functions and derived equations for them. His results are in his reviews [88, 89] and book [90].

7.2 V.V. Ivanov

The derivation of various asymptotics that characterize scattering in a spectral line with CFR directly from the equations [91, 92].

The wide use of the concept of thermalization length $\tau_{\rm t}$ (depending on λ). Its value separates two regions. In the first one (depths $\tau < \tau_{\rm t}$) the scattering in line can be considered as conservative while in the second one ($\tau > \tau_{\rm t}$) photons are thermalized, i.e. the source function becomes proportional to the Planck function [93]. Asymptotic formulas for the resolvent functions $\Phi_\infty(\tau)$ and $\Phi(\tau)$ for $\tau \gg 1$ depend not τ and λ separately but in the essential parts only on $\tau/\tau_{\rm t}$.

Time-variations of the degree of excitation for two-level atoms and of the line profile formed in an infinite homogeneous medium with CFR and $t_1 = 0$ if initially the atoms are completely excited [94]. The leading terms of the asymptotics at large time intervals coincide with those obtained for a more exact law of redistribution.

The detailed description of the asymptotic theory of conservative scattering [95, 96] was made for the Milne problem with isotropic monochromatic scattering as well as for CFR scattering with the absorption coefficient decreasing in the line wings as a power of frequency. The asymptotics of X and Y-functions were expressed in terms of the Bessel functions. For the Doppler profile it was performed earlier [97]. It was the very first result of what is now known as the large-scale description.

The concept of the "mean length of a photon path" $\overline{T}$, i.e. path from the place of photon emission to the place where it is finally absorbed (i.e. thermalized) was introduced and the formulas determining $\overline{T}$ were derived [98].

The formulation of a high accuracy approximate solution [99] to the basic CFR integral equation of RTT, both for half-space and for plane layer of finite thickness.

The description of multiple scattering of spectral line photons as a stochastic process of the Lévy random walks was given. It was used to obtain various asymptotics of CFR RRT (with Sh.A. Sabashvili) [100].

The solution was found to the problem of diffuse reflection and transmission of radiation if $t_1 = 0$, $t_2 = 1$ and the boundary of anisotropically scattering layer of finite optical thickness τ_0 is illuminated by an instant light flash [101] (with S.D. Gutshabash). The asymptotic behavior of the brightness wave escaping the layer was found assuming the thickness of the layer $\tau_0 \gg 1$.

The process of frequency relaxation to CFR due to multiple scatterings with non-CFR redistribution functions was studied [102] (with A.B. Schneeweis).

Generalizations of the invariance principles for a semi-infinite medium with scalar anisotropic scattering [103] and for scattering of polarized radiation were formulated [104] (with H. Domke). The asymptotic forms of the basic functions were found explicitly.

New concepts for treating analytically the so called blanketing effect were introduced: the "partial intensity" , i.e. the contribution to the intensity by photons classified both by the value of the absorption coefficient and by the frequency, and the so-called "gray in the average" atmosphere, in which the opacity probability distribution function (OPDF) is the same along the whole spectrum. The equations describing the radiation transfer in such an atmosphere were given [105] (with A.G. Kheinlo).

Molecular and Rayleigh scattering of polarized radiation was studied in detail using the concept of matrix transfer equation (with V.M. Loskutov, S.I. Grachev, and T. Viik). In particular, the so called $\sqrt{\varepsilon}$ law of the scalar theory was generalized to incorporate polarization [106, 107, 108].

V.V. Ivanov with coauthors investigated scattering polarization of radiation in resonance lines under the assumption that angular and CFR frequency redistributions are not correlated [109].

The albedo shifting method when the kernel of the integral equation is changed to another one in order to accelerate the convergence of iterations was developed (with coauthors) [110, 111, 112].

Ivanov's results are published also in books [113, 114] and in review [115].

7.3 A.K. Kolesov

Articles with V.V. Sobolev [31, 32, 54, 55, 66].

In three papers [116, 117, 118] calculations were made for the Henyey–Greenstein phase function.

In the series of papers [119, 120, 121, 122] the radiation fields in two-layer and multilayer media with anisotropic scattering in the layers were studied. In the most general case the layers differed in the values of λ, phase functions and refraction indexes.

The expansions in the elementary solutions of the radiation transfer equation (the Case method) were applied for radiation fields in non-plane media with anisotropic scattering. In [123] the problem of scattering in a homogeneous sphere was reduced to the plane one. The same procedure was made for a point source in an infinite medium [124]. In [125] the expression for the Green function of the point source and in [126] the asymptotics of this function were obtained, and in [127] the intensity of radiation far from the point source in the infinite medium was expanded in the reversed powers of τ. The case of small true absorption was considered separately. In [128] and [129] the Case modes were found and the relations of their orthogonality were formulated for spherical and cylindrical symmetries.

Review [130].

7.4 E.G. Yanovitskij

With V.V. Sobolev [47].

Detailed investigation of anisotropic scattering in inhomogeneous [131] and multilayer media [132, 133, 134] (the first and the third papers with Zh.M. Dlugach).

Some formulas for the pure scattering were shown to coincide for an arbitrary scattering phase function [135].

For a semi-infinite medium [136] and a plane layer [137] the equations were formulated, which have the form of the transfer equation in the so-called pseudo problems of anisotropic scattering. These equations determine the intensity of radiation, which would correspond to the source functions equal to the resolvent functions $\Phi^m(\tau)$ and $\Phi^m(\tau, \tau_0)$ that were introduced by V.V. Sobolev.

A new form of the radiation transfer equation (called Q-form) was deduced, where the intensity was represented as the derivative on the optical depth of some linear integral operator of the same intensity [138].

The results of Yanovitskij and his coauthors can be found in his book [139].

7.5 D.I. Nagirner

Using the methods of the theory of complex variables the exact explicit solutions and their asymptotic forms were obtained for stationary [140, 141] and non-stationary ($t_2 = 0$) [142] multiple scattering with CFR in infinite and semi-infinite media. Large-scale and uniform asymptotics of the resolvent and other functions describing scattering in a plane layer [143] and sphere [144] of large optical thickness and radius were found, in particular, the mean number of scatterings and dispersion.

The exact and asymptotic formulas describing the process of damping of the atomic excitation in a homogeneous infinite medium, the excitation being created instantly at the initial moment [145]. The scattering in a line with CFR and the Lorentz absorption profile with an arbitrary ratio of t_1 and t_2 parameters was assumed.

The method was proposed to calculate the eigenvalues and eigenfunctions of the basic integral equation (continuous $\lambda(u) = 1/V(u)$ for a semi-infinite medium and discrete $\lambda_n(\tau_0) = 1/V(u_n(\tau_0))$ for a layer of finite thickness). The asymptotics (on n and $\tau_0 \gg 1$) of the eigenvalues were found for an optically thick layer [146].

The resolvent function, its asymptotic behavior and the asymptotics of the spectrum of the basic integral equation for a cylinder were obtained [147].

The method to calculate the scattering in a plane layer of finite optical thickness was proposed [148].

Reviews [149, 150, 151, 152, 153] and books [154, 155].

7.6 V.M. Loskutov

With V.V. Sobolev [26, 27, 28, 36] and V.V. Ivanov [108, 109].

With a given value of the characteristic number k the value of λ is found by the expansion in a chain fraction for the Henyey–Greenstein phase function [156].

The full phase matrix for the Rayleigh scattering is represented by the product $\mathbf{A}(\eta,\phi)\mathbf{A}^{\mathrm{T}}(\eta',\phi')$, where $\mathbf{A}(\eta,\phi)$ is a matrix of the size 3×6. This representation separates the angular variables of the incident (η',ϕ') and scattered (η,ϕ) radiation. For the six-term vector of the source functions the system of integral equations was obtained. Within the same approximation, in which redistribution depends on frequency and on angles independently as in [109], the matrix equation for the basic matrix was derived. The polarization degree of reflected radiation was calculated [157].

For the Lorentz absorption profile the polarization characteristics of radiation in a line emergent from a semi-infinite medium were calculated. It was noted that the polarization degree as a function of the absorption profile value (rather than the frequency) depends only slightly on the type of this profile (Lorentz, Doppler or rectangular) [158] (with V.V. Ivanov).

Review [159].

7.7 V.P. Grinin

The non-stationary radiation fields in a semi-infinite medium with anisotropic scattering and illuminated by a parallel external flux or a point source were studied [160]. The full radiation and the dependence of the radiation density on the distance from the source were found. The solutions were expressed through the function introduced by I.N. Minin [83].

The methods to calculate the radiation fields in expanding media were proposed [161].

The concept of non-local (large-scale) radiative interaction was introduced and the equations describing the interaction were deduced [162] (coauthor S.I. Grachev) and [163].

The radiation pressure in moving media with axial symmetry was studied [164].

Reviews [165, 166].

7.8 H. Domke

With V.V. Ivanov [104].

The radiative transfer theory in spectral lines was expanded to the presence of a weak magnetic field in [167].

The problem of conservative Rayleigh scattering of polarized radiation in a semi-infinite medium was reduced to searching for several source functions depending only on the optical depth and determined by the integral equations. For the Milne and the reflection problems the number of these functions is equal to two [168]. The results were transferred to a finite layer.

The general scattering matrix was expanded to the generalized spherical functions. The corresponding radiation fields were separated into the azimuthal harmonics [169].

The singular solutions to the equation of the polarized radiation transfer were determinated and the solutions to the multiple scattering problems were expanded in elementary modes [170, 171].

The methods to calculate the transfer of polarized radiation were proposed: the doubling method [172], the application of the invariance principles [173] and of the transfer equation in the Q-form [138] expanded to polarized radiation [174] (coauthor E.G. Yanovitskij).

The transformation of the equation for H-function in order to accelerate the convergence of iterations [175], which was followed by the albedo shifting method.

Book [176].

7.9 S.I. Grachev

With V.V. Ivanov [109] and with V.P. Grinin [162].

The characteristic lengths of radiation transfer in a one-dimensional infinite medium expanding with a constant velocity gradient (the thermalization length, the thickness of the boundary layer, the diffusion length) were determinated. The asymptotic behavior of the solutions were obtained by the factoring method for the rectangular, the Doppler and the power absorption profiles [177].

The asymptotics for the resolvent functions and the source functions for particular source distributions (uniform, exponential, point source) with scattering in an infinite medium isotropically expanding with a constant (small) velocity gradient were deduced. The scattering is considered to be conservative with the Doppler or power absorption profiles [178].

The asymptotic self-similar representations of the kernel and resolvent functions, which characterize the radiation fields in a three-dimensional infinite and semi-infinite media expanding with the velocity gradient were obtained [179].

The explicit expression of the resolvent function was deduced for the problem of the non-stationary line radiation field in a semi-infinite medium for scattering with CFR and $t_2 = 0$ [180] in terms of the eigenfunctions of the basic integral equation (1) found in [146].

The polarization in a spectral line was investigated. In [181] it was shown that the asymptotic expansion for the matrix of the source functions in the problem of the line scattering with CFR and the Doppler profile could be obtained directly from the matrix equation defining it. Some particular cases of the true absorption and the depolarization values were considered. In [182] the problem of calculating the line radiation fields in the medium with uniform distribution of sources was reduced to two nonlinear equations for the matrices of the dimension 6×6. For scattering with CFR (even with the Hanle effect) the two equations were replaced by one. In [183] the asymptotic and numerical solutions to this equation were obtained. Finally, in [184] the Hanle matrix was factorized and the matrix generalization of the so-called $\sqrt{\varepsilon}$ law ($\varepsilon = 1 - \lambda$) was deduced.

Review [185].

8 Conclusion

Thus, V.V. Sobolev and his disciples have succeeded in building the analytical radiative transfer theory for monochromatic scattering as well as for scattering in spectral lines, including the scattering of polarized and non-stationary radiation. Their calculations demonstrated characteristic features of various types of scattering and are in qualitative agreement with the observational data for a variety of astrophysical objects.

Certainly several other groups have been studying the same problems. Their works are described in the reviews mentioned in the text. These groups exchanged the information and results as well as cited the works by each other. In this review we summarize only the main works by V.V. Sobolev and his school.

Acknowledgments. The author is thankful to V.V. Ivanov for the improvement of the manuscript. The work was partly supported by grant SPbSU 6.38.18.2014.

References

1. *V.A. Ambartsumian*, Theoretical Astrophysics. Leningrad: GONTI, 1939 (in Russian).
2. *V.A. Ambartsumian*, "Scattering and absorption of light in planetary atmospheres," Trudy Astron. Obs. Leningr. Univ., **12**, 64–85, 1941.
3. *V.A. Ambartsumian*, "On the radiative equilibrium of a planetary nebula," Izv. Glav. Astron. Obs. Pulk., **13**, No. 114, 1–27, 1933.
4. *V.A. Ambartsumian*, "On the effect of absorption lines on the radiation equilibrium of the outer layers of stars," Trudy Astron. Obs. Leningr. Univ., **6**, 7–18, 1936.
5. *V.A. Ambartsumian*, "New method for calculation of light scattering in turbid medium," Izv. Akad. Nauk SSSR, Ser. Geogr. Geofiz., **3**, 97, 1942.
6. *V.A. Ambartsumian*, "Light scattering by planetary atmospheres," Astron. Zh., **19**, No. 5, 30–41, 1942.
7. *V.A. Ambartsumian*, "Diffusion of radiation in scattering medium of large optical thickness," Dokl. Akad. Nauk SSSR, **38**, No. 8, 257–260, 1943.
8. *V.A. Ambartsumian*, "Diffusion of radiation in scattering medium of large optical thickness," Dokl. Akad. Nauk SSSR, **43**, No. 3, 106–109, 1944.
9. *V.A. Ambartsumian*, "On the number of scatterings of photons diffusing in a turbid medium," Dokl. Akad. Nauk Arm. SSR, **8**, 101–104, 1948.
10. *V.A. Ambartsumian*, "On the problem of multiple light scattering in plane-parallel layer with internal reflection from boundary surface," Trudy Astron. Obs. Leningr. Univ., **20**, 3–9, 1964.
11. *V.A. Ambartsumian*, Scientific works, vol. 1. Yerevan: Arm. SSR Acad. Sci., 1960 (in Russian).

12. *M.A. Mnatsakanian, H.V. Pikichian (eds.)*, Principle of Invariance and its Applications. Yerevan: Acad. Sci. Arm. SSR, 1989 (in Russian).

13. *V.V. Sobolev*, "On the approximate solution of a problem of scattering of light in a medium with arbitrary scattering diagram," Astron. Zh., **20**, No. 5–6, 14–22, 1943.

14. *V.V. Sobolev*, "On the optical properties of the atmosphere of Venus," Astron. Zh., **21**, No. 5, 241–244, 1944.

15. *V.V. Sobolev*, "On the scattering of light in the atmospheres of Earth and planets," Trudy Astron. Obs. Leningr. Univ., **13**, 17–52, 1949.

16. *V.V. Sobolev*, "On the brightness of a spherical nebula," Astron. Zh., **37**, No. 1, 3–8, 1960.

17. *V.V. Sobolev, I.N. Minin*, "Light scattering in a spherical atmosphere. I.," Iskustv. Sputniki Zemli, No. 14, 7–12, 1962; II. – Kosmich. Issled., **1**, No. 2, 227–234, 1963; III. – *ibid.*, **2**, No. 4, 610–618, 1964.

18. *V.V. Sobolev*, "Radiation pressure in expanding nebula," Astron. Zh., **21**, No. 4, 143–148, 1944.

19. *V.V. Sobolev*, "On the intensity of radiation in the inner layers of absorbing and scattering medium," Izv. Akad. Nauk SSSR, Ser. Geogr. Geophys., **8**, No. 5, 273–280, 1944.

20. *V.V. Sobolev*, Moving Envelopes of Stars. Cambridge: Harvard Univ. Press, 1960 (Original in Russian: Dvizhushchiesya Obolochki Zvezd. Leningrad: Izd. Leningr. Univ., 1947).

21. *V.V. Sobolev*, "On excitation and ionization in expanding stellar envelopes," Astron. Zh., **23**, No. 4, 193–202, 1946.

22. *V.V. Sobolev*, "The diffusion of L_α radiation in nebulae and stellar envelopes," Astron. Zh., **34**, No. 5, 694–705, 1957.

23. *V.V. Sobolev*, "On the intensity of emission lines in spectra of early-type stars," Astron. Zh., **24**, No. 1, 13–24, 1947.

24. *V.V. Sobolev, V.V. Ivanov*, "On the intensity of hydrogen emission lines in stellar spectra," Trudy Astron. Obs. Leningr. Univ., **19**, 3–17, 1962.

25. *V.V. Sobolev*, "On polarization of scattered light," Trudy Astron. Obs. Leningr. Univ., **13**, 3–16, 1949.

26. *V.M. Loskutov, V.V. Sobolev*, "Polarization of radiation multiply scattered by a plane layer," Astrofiz., **17**, No. 3, 535–546, 1981.

27. *V.M. Loskutov, V.V. Sobolev*, "On the polarization of X-ray sources," Astrofiz., **18**, No. 1, 81–91, 1982.

28. *V.M. Loskutov, V.V. Sobolev*, "On the polarization of quasar light," Astrofiz., **23**, No. 2, 307–321, 1985.

29. *V.V. Sobolev*, "On the theory of non-stationary radiation field," Astron. Zh., **29**, I. – No. 4, 406–417, 1952; II. – No. 5, 517–525, 1952.

30. *V.V. Sobolev*, Perenos Luchistoj Energii v Atmosferah Zvezd i Planet. Moscow: GITTL, 1956 (in Russian) (Translated as A Treatise on Radiative Transfer. Princeton: Van Nostrand, 1963).

31. *A.K. Kolesov, V.V. Sobolev*, "Non-stationary radiation transfer in stellar atmospheres," Astron. Zh., **67**, No. 2, 357–366, 1990.

32. *A.K. Kolesov, V.V. Sobolev*, "On non-stationary radiation transfer," Trudy Astron. Obs. Leningr. Univ., **43**, 5–27, 1991.

33. *V.V. Sobolev*, "On the brightness coefficients of a plane layer of turbid medium," Dokl. Akad. Nauk SSSR, **61**, No. 5, 803–806, 1948.

34. *V.V. Sobolev*, "The transfer of radiation in inhomogeneous medium," Dokl. Akad. Nauk SSSR, **111**, No. 5, 1000–1003, 1956.

35. *V.V. Sobolev*, "On the theory of scattering photospheres," Astrofiz., **11**, No. 3, 499–510, 1975.

36. *V.M. Loskutov, V.V. Sobolev*, "Polarization of radiation scattered by an inhomogeneous atmosphere," Astrofiz., **17**, No. 1, 97–108, 1981.

37. *V.V. Sobolev*, "Diffusion of radiation in a medium of high optical thickness where scattering is non-isotropic," Dokl. Akad. Nauk SSSR, **179**, No. 1, 41–44, 1968.

38. *V.V. Sobolev*, "Anisotropic light scattering in an atmosphere of large optical thickness," Astrofiz., **4**, No. 3, 325–336, 1968.

39. *V.V. Sobolev*, Rassejanije Sveta v Atmosferah Planet. Moscow: Nauka, 1972 (in Russian) (Translated as Light Scattering in Planetary Atmospheres. Oxford: Pergamon Press, 1975).

40. *V.V. Sobolev*, "Non-coherent light scattering in stellar atmospheres," Astron. Zh., **26**, No. 3, 129–137, 1949.

41. *V.V. Sobolev*, "Radiation diffusion in a semi-infinite medium," Dokl. Akad. Nauk SSSR, **116**, No. 1, 45–48, 1957.

42. *V.V. Sobolev*, "Radiation diffusion in a plane layer," Dokl. Akad. Nauk SSSR, **120**, No. 1, 69–72, 1958.

43. *V.V. Sobolev*, "On the theory of diffusion of radiation in stellar atmospheres," Astron. Zh., **36**, No. 4, 573–578, 1959.

44. *V.V. Sobolev*, "Radiation diffusion in gas," In Theory of Stellar Spectra. Moscow: Nauka, 1966, pp. 105–126 (in Russian).

45. *V.V. Sobolev*, "Diffusion of radiation in a plane layer of large optical thickness," Dokl. Akad. Nauk SSSR, **155**, No. 2, 316–319, 1964.

46. *V.V. Sobolev*, "On the theory of line formation in stellar spectra," Astron. Zh., **53**, No. 4, 681–685, 1976.

47. *V.V. Sobolev, E.G. Yanovitsky*, "Radiation diffusion in the spectral line of inhomogeneous atmosphere," In Problems of Physics and Evolution of the Universe. Ed. L.V. Mirzoyan. Yerevan: Publ. House Arm. Acad. Sci., 1978, p. 359–369 (Original in Russian: Voprosy fiziki i evolutsii kosmosa. Yerevan: Arm. SSR Acad. Sci., 1978, pp. 370–380).

48. *V.V. Sobolev*, "Radiative transfer in inhomogeneous medium," In Principle of Invariance and its Applications. Yerevan: Arm. SSR Acad. Sci., 1989, pp. 55–61 (in Russian).

49. *V.V. Sobolev*, "On some problems of the theory of the diffusion of radiation," Dokl. Akad. Nauk SSSR, **129**, No. 6, 1265–1268, 1959.

50. *V.V. Sobolev*, "Diffusion of the radiation in a medium whose boudary reflects the rays as a mirror," Dokl. Akad. Nauk SSSR, **136**, No. 3, 571–574, 1961.

51. *V.V. Sobolev*, "On a theory of light scattering in water basins," Dokl. Akad. Nauk SSSR, **234**, No. 3, 568–571, 1977.

52. *V.V. Sobolev*, "Light scattering in a homogeneous sphere," Astrofiz., **8**, No. 2, 197–212, 1972.

53. *V.V. Sobolev*, "On the scattering of light in a spherical envelope and in a sphere," Dokl. Akad. Nauk SSSR, **273**, No. 3, 573–576, 1983.

54. *A.K. Kolesov, V.V. Sobolev*, "Diffuse radiation reflection from a spherical nebula," Astrofiz., **32**, No. 2, 278–289, 1990.

55. *A.K. Kolesov, V.V. Sobolev*, "The radiation from a spherical nebula due to a central star," Astrofiz., **33**, No. 2, 235–242, 1990.

56. *V.V. Sobolev*, "Luminescence of spherical nebula with different energy sources," Dokl. Ross. Akad. Nauk, **323**, No. 5, 861–864, 1992.

57. *V.V. Sobolev*, "Number of scatterings of diffusing photons, I.," Astrofiz., **2**, No. 2, 135–146, 1966; II. – *ibid.*, **2**, No. 3, 239–250, 1966; III. – *ibid.*, **3**, No. 1, 5–16, 1967; IV. – *ibid.*, **3**, No. 2, 137–154, 1967.

58. *V.V. Sobolev*, "Diffusion of radiation when the scattering phase function is greatly drawn out in length," Dokl. Akad. Nauk SSSR, **177**, No. 4, 812–815, 1967.

59. *V.V. Sobolev*, "An investigation of the atmosphere of Venus," Astron. Zh., **41**, No. 1, 97–103, 1964; II. – *ibid.*, **45**, No. 1, 169–176, 1968.

60. *V.V. Sobolev, I.N. Minin*, "Light scattering in a spherical atmosphere," Planet. Space Sci., **11**, No. 6, 657–662, 1963.

61. *I.N. Minin, V.V. Sobolev*, "On the theory of light scattering in planet atmosphere," Astron. Zh., **40**, No. 3, 496–503, 1963.

62. *V.V. Sobolev*, "On the theory of planet spectra," Astron. Zh., **49**, No. 2, 397–405, 1972.

63. *V.V. Sobolev*, "The spectrum of a planet with two-layer atmosphere," Dokl. Akad. Nauk SSSR, **211**, No. 1, 63–66, 1973.

64. *V.V. Sobolev*, "Theoretical light curves of supernovae," Astrofiz., **15**, No. 3, 401–411, 1979.

65. *V.V. Sobolev*, "On the continuous spectra of supernova stars," Astron. Zh., **59**, No. 3, 413–423, 1982.

66. *A.K. Kolesov, V.V. Sobolev*, "Supernova continuous spectra at the first times after the explosion," Astrofiz., **37**, No. 3, 433–445, 1994.

67. *V.V. Sobolev*, "The effect of electron scattering on continuous spectrum of a star," Astrofiz., **14**, No. 3, 383–391, 1978.

68. *V.V. Sobolev*, "On colour temperatures of objects with electron scattering," Astrofiz., **16**, No. 4, 695–706, 1980.

69. *V.V. Sobolev*, "Correlation between the emissivity and absorptivity at the arbitrary scattering law," Dokl. Akad. Nauk SSSR, **212**, No. 5, 1096–1098, 1973.

70. *V.V. Sobolev*, "The relationship between emissivity and absorptivity of medium," Dokl. Akad. Nauk SSSR, **209**, No. 5, 1071–1073, 1973.

71. *V.V. Sobolev*, "The integral relations in the transfer theory of polarized radiation," Dokl. Akad. Nauk SSSR, **295**, No. 1, 60–63, 1987.

72. *V.V. Sobolev*, "Some applications of the relationship between emissivity and absorptivity of a medium," Astrofiz., **9**, No. 4, 515–524, 1973.

73. *V.V. Sobolev*, "Integral relations and asymptotic formulae of radiative transfer theory," Astrofiz., **20**, No. 1, 123–132, 1984.

74. *V.V. Sobolev, V.G. Gorbatski, V.V. Ivanov (eds.)*, The Theory of Stellar Spectra, Moscow: Nauka, 1966 (in Russian).

75. *V.V. Sobolev (ed.)*, Stars, Nebulae, Galaxies. Yerevan: Arm. SSR Acad. Sci., 1969 (in Russian).

76. Trudy Astron. Obs. St. Petersburg Univ., **44**, 1994.

77. *I.N. Minin*, "Equation for the radiation transfer considering refraction," Opt. Spectrosk., **5**, No. 3, 337–340, 1958.

78. *I.N. Minin*, "On the calculation of light scattering in planetary atmosphere with refraction," Izv. Akad. Nauk SSSR, Fiz. Atmos. Okeana, **8**, No. 9, 985–987, 1972.

79. *I.N. Minin*, "On the theory of radiation diffusion in semi-infinite medium," Dokl. Akad. nauk SSSR, **120**, No. 1, 63–65, 1958.

80. *I.N. Minin*, "Non-stationary problems of the radiation transfer theory," Vestn. Leningr. Univ., **13**, 137–141, 1959.

81. *I.N. Minin*, "On the theory of non-stationary diffusion of radiation," Vestn. Leningr. Univ., **19**, 124–132, 1962.

82. *I.N. Minin*, "Non-stationary glow of a one-dimensional medium of finite optical thickness. I.," Astron. Zh., **48**, No. 2, 333–340, 1971.

83. *I.N. Minin*, "Unstationary light emission by semi-infinite medium," Dokl. Akad. Nauk SSSR, **154**, No. 5, 1059–1062, 1971.

84. *I.N. Minin*, "Light scattering in a one-dimensional non-stationary medium," Astrofiz., **1**, No. 2, 173–181, 1965.

85. *I.N. Minin*, "On the non-stationary diffusion of radiation in non-uniform medium," Astrofiz., **3**, No. 3, 345–350, 1967.

86. *I.N. Minin*, "Diffusion of radiation in semi-infinite medium with non-isotropic scattering. I.," Vestn. Leningr. Univ., **1**, 133–143, 1961; II. – *ibid.*, **13**, 106–118, 1963.

87. *I.N. Minin*, "The diffusion of radiation in a plane layer with non-isotropic scattering. I.," Astron. Zh., **43**, No. 6, 1244–1260, 1966; II. – *ibid.*, **45**, No. 2, 264–278, 1968.

88. *I.N. Minin*, "Non-stationary radiation field," In The Theory of Stellar Spectra. Moscow: Nauka, 1966, pp. 159–183 (in Russian).

89. *I.N. Minin*, "The theory of non-stationary radiation field," In Teor. i Prikladn. Probl. Rass. Sveta. Minsk: Nauka i Tekhnika, 1971, pp. 59–73 (in Russian).

90. *I.N. Minin*, The Radiative Transfer Theory in Planetary Atmospheres. Moscow: Nauka, 1988 (in Russian).

91. *V.V. Ivanov*, "Diffusion of radiation with frequency redistribution in semi-infinite medium," Trudy Astron. Obs. Leningr. Univ., **19**, 52–66, 1962.

92. *V.V. Ivanov*, "The diffusion of resonance radiation in stellar atmospheres and nebulae. I. Semi-infinite medium," Astron. Zh., **39**, No. 6, 1020–1032, 1962; "II. A layer of finite thickness" – *ibid.*, **40**, No. 2, 257–267, 1963.

93. *V.V. Ivanov*, "Determination of populations of excited levels in optically thick gas layer," In Theory of Stellar Spectra. Moscow: Nauka, 1966, pp. 127–158 (in Russian).

94. *V.V. Ivanov*, "Time variation of the profile of a Doppler broadened resonance line," Bull. Astron. Inst. Netherl., **19**, 192–196, 1967.

95. *V.V. Ivanov*, "On the Milne problem in the theory of line formation," Astrofiz., **4**, No. 1, 5–13, 1968.

96. *V.V. Ivanov*, "Transfer of resonance radiation in purely scattering media. I. Semi-infinite media," J. Quant. Spectrosc. Rad. Transf., **10**, 665–680, 1970; "II. Optically thick layer" – *ibid.*, 681–694.

97. *V.V. Ivanov*, "On the problem of light scattering in the atmosphere of finite optical thickness," Astron. Zh., **41**, No. 6, 1097–1107, 1964.

98. *V.V. Ivanov*, "Mean length of photon path in a scattering medium," Astrofiz., **6**, No. 4, 643–662, 1970.

99. *V.V. Ivanov*, "An approximate solution of the radiative transfer equation in line frequencies," Astron. Zh., **49**, No. 1, 115–120, 1972.

100. *V.V. Ivanov, Sh.A. Sabashvili*, "Transfer of resonance radiation and photon random walks," Astrophys. Space Sci., **17**, No. 1, 3–12, 1972.

101. *V.V. Ivanov, S.D. Gutshabash*, "Propagation of brightness wave in an optically thick atmosphere," Izv. Akad. Nauk SSSR, Fiz. Atmos. Okean., **10**, No. 8, 851–863, 1974.

102. *V.V. Ivanov, A.B. Shneivais*, "Frequency relaxation in multiple scattering of line radiation," Astrofiz., **12**, No. 2, 246–254, 1976.

103. *V.V. Ivanov*, "Invariance principles and internal radiation fields in semi-infinite atmospheres," Astron. Zh., **52**, No. 2, 217–226, 1975.

104. *H. Domke, V.V. Ivanov*, "Asymptotics of Green's function of the transfer equation for polarized light," Astron. Zh., **52**, No. 5, 1034–1037, 1975.

105. *V.V. Ivanov, A.G. Kheinlo*, "Radiative equilibrium of strongly non-gray atmospheres. I. General analysis," Astron. Zh., **52**, No. 6, 1252–1261, 1975.

106. *V.V. Ivanov*, "Generalized Rayleigh scattering. I. Basic theory," Astron. Astrophys., **303**, No. 2, 609-620, 1995; "III. Theory of I-matrices" – *ibid.*, **307**, No. 1, 319-331, 1996.

107. *V.V. Ivanov, A.M. Kasaurov, V.M. Loskutov*, "Generalized Rayleigh scattering. IV. Emergent radiation," Astron. Astrophys., **307**, No. 1, 332–346, 1996.

108. *V.V. Ivanov, A.M. Kasaurov, V.M. Loskutov, T. Viik*, "Generalized Rayleigh scattering. II. Matrix source functions," Astron. Astrophys., **303**, No. 2, 621–634, 1995.

109. *V.V. Ivanov, S.I. Grachev, V.M. Loskutov*, "Polarized line formation by resonance scattering. I. Basic formalism," Astron. Astrophys., **318**, No. 1, 315–326, 1996; "II. Conservative case" – *ibid.*, **321**, No. 3, 968–984, 1997.

110. *V.V. Ivanov*, "Albedo shifting: a new method in radiative transfer theory," Astron. Zh., **75**, No. 1, 102–112, 1998.

111. *V.V. Ivanov, A.M. Kasaurov*, "Albedo shifting technique in problems of anisotropic light scattering in plane atmospheres," Astrofiz., **41**, No. 4, 623–646, 1998.

112. *V.V. Ivanov, A.M. Kasaurov*, "Albedo shifting: source function in plane atmospheres," Astrofiz., **42**, No. 4, 485–500, 1999.

113. *V.V. Ivanov*, Perenos Izluchenija i Spectry Nebesnyh Tel. Moscow: Nauka, 1969 (in Russian).

114. *V.V. Ivanov*, Transfer of Radiation in Spectral Lines. Boulder: Nat. Bur. Stand. Special Publ., No. 385, 1973.

115. *V.V. Ivanov*, "Physics of radiative transfer," In Astronomia: Tradicii, Nastoyashchee, Budushchee, eds. V.V.Orlov et al., St. Petersburg, pp. 213–262, 2007 (in Russian).

116. *A.K. Kolesov*, "H-functions for some scattering phase functions with different values of asymmetry factor," Trudy Astron. Obs. Leningr. Univ., **28**, 39–51, 1971.

117. *A.K. Kolesov*, "Reflection and transmission of light by anisotropically scattering semi-infinite atmosphere," Trudy Astron. Obs. Leningr. Univ., **29**, 3–14, 1973.

118. *A.K. Kolesov*, "Azimuth-dependent diffuse reflection of light from semi-infinite planetary atmosphere," Trudy Astron. Obs. Leningr. Univ., **30**, 3–25, 1974.

119. *A.K. Kolesov*, "The reflection of radiation from a semi-infinite two-layer atmosphere," Trudy Astron. Obs. Leningr. Univ., **32**, 39–51, 1975.

120. *A.K. Kolesov*, "Brightness coefficients for two-layer atmosphere at anisotropic scattering. I.," Astrofiz., **12**, No. 1, 83–94, 1976; II. — *ibid.*, No. 3, 485–494.

121. *A.K. Kolesov*, "Radiation scattering in a medium consisting of two layers with different refraction indices. I.," Vestn. Leningr. Univ., **7**, 136–142, 1976; II. — *ibid.*, **1**, 127–134, 1977.

122. *A.K. Kolesov*, "Light scattering in a multilayer atmosphere," Trudy Astron. Obs. Leningr. Univ., **34**, 29–45, 1978.

123. *A.K. Kolesov*, "On radiative transfer in a homogeneous anisotropically scattering sphere," Vestn. Leningr. Univ., **1**, 97–104, 1982.

124. *A.K. Kolesov*, "Point source in an absorbing and anisotropically scattering infinite homogeneous medium," Sov. Phys. Dokl., **28**, 700–703, 1983.

125. *A.K. Kolesov*, "The Green's function for equation of radiative transfer in an infinite homogeneous medium with a radial distribution of the sources," Astrofiz., **20**, No. 1, 131–147, 1984.

126. *A.K. Kolesov*, "On asymptotic formulae on the theory of radiation transfer in sphere and a spherical envelopes," Astrofiz., **22**, No. 1, 177–187, 1985.

127. *A.K. Kolesov*, "The radiation field in infinite medium far from a point source," Vestn. Leningr. Univ., **22**, 62–67, 1990.

128. *A.K. Kolesov*, "Radiation field in media with spherical symmetry," Astrofiz., **22**, No. 3, 571–582, 1985.

129. *A.K. Kolesov*, "Radiative transfer in media with cylindrical symmetry," Dokl. Akad. Nauk SSSR, **287**, No. 1, 115–118, 1986.

130. *A.K. Kolesov*, "Light scattering in spherically symmetric media," Trudy Astron. Obs. St. Petersburg Univ., **44**, 114–130, 1994.

131. *E.G. Yanovitskij*, "Anisotropic light scattering in an inhomogeneous atmosphere. I. The case of pure scattering," Astron. Zh., **48**, No. 2, 323–332, 1971; "II. The radiation field in deep layers of semi-infinite atmosphere" – *ibid.*, **55**, No. 4, 713–721, 1978; "III. The case of nearly conservative scattering" – *ibid.*, **55**, No. 5, 1084–1092, 1978; "IV. Asymptotic separation of angular variables in optically thick layer" – *ibid.*, **57**, No. 6, 1277–1286, 1980; "V. Invariance principles and integrals of the radiative transfer equation" – *ibid.*, **58**, No. 1, 119–129, 1981.

132. *Zh.M. Dlugach, E.G. Yanovitskij*, "Light scattering in multilayer atmosphere. I. The problem of diffuse reflection," Astrofiz., **23**, No. 2, 337–348, 1985.

133. *E.G. Yanovitskij*, "Light scattering in multilayer atmosphere. II. The Milne problem," Astrofiz., **24**, No. 3, 535–548, 1986.

134. *E.G. Yanovitskij, Zh.M. Dlugach*, "The radiation field in multilayer plane atmosphere with arbitrary internal sources," Kinem. Fiz. Neb. Tel, **8**, No. 5, 12–30, 1992.

135. *E.G. Yanovitskij*, "Inhomogeneous semi-infinite atmosphere: the case of pure scattering," Dokl. Akad. Nauk SSSR, **189**, No. 1, 74–77, 1969.

136. *E.G. Yanovitskij*, "The field of radiation in a semi-infinite atmosphere with anisotropic scattering," Astron. Zh., **53**, No. 5, 1063–1074, 1976.

137. *E.G. Yanovitskij*, "The field of radiation in a plane atmosphere with anisotropic scattering. Separation of angular variables," Astrofiz., **16**, No. 2, 363–374, 1980.

138. *E.G. Yanovitskij*, "A new form of the equation of radiation transfer in anisotropically scattering atmosphere," Kinem. Fiz. Neb. Tel, **2**, No. 6, 3–13, 1986.

139. *E.G. Yanovitskij*, Light Scattering in Inhomogeneous Atmospheres. New York: Springer Verlag, 1997 (Original in Russian: Rassejanije Sveta v Neodnorodnyh Atmosferah. Kiev: Naukova Dumka, 1985).

140. *D.I. Nagirner*, "On the solution of integral equations of the theory of light scattering," Astron. Zh., **41**, No. 4, 669–675, 1964.

141. *D.I. Nagirner*, "Multiple light scattering in a semi-infinite medium," Trudy Astron. Obs. Leningr. Univ., **25**, 79–87, 1968.

142. *D.I. Nagirner*, "Non-stationary radiation fields in infinite media," Astrofiz., **5**, No. 1, 31–53, 1969.

143. *D.I. Nagirner*, "Transfer of resonance radiation in an optically thick layer," Astrofiz., **5**, No. 4, 507–524, 1969.

144. *D.I. Nagirner*, "Scattering of resonance radiation in a sphere," Astrofiz., **8**, No. 3, 353–368, 1972.

145. *D.I. Nagirner*, "Non-stationary luminescence of an infinite homogeneous medium," Vestn. Leningr. Univ., **7**, 138–143, 1977.

146. *D.I. Nagirner*, "The calculation of the spectrum of the integral equation of radiative transfer. I. Semiinfinite medium," Astrofiz., **15**, No. 2, 229–240, 1979; "II. Plane layer of finite optical thickness" – *ibid.*, No. 3, 485–495.

147. *D.I. Nagirner*, "Radiative transfer in a cylinder, I. The resolvent of the basic integral equation," Astrofiz., **37**, No. 1, 111–127, 1994; "II. Special problems" – *ibid.*, **37**, No. 4, 655–670, 1994; "III. Spectrum of the basic integral equation" – *ibid.*, **38**, No. 1, 75–88, 1995.

148. *D.I. Nagirner*, "Integral equation methods in radiative transfer theory," Trudy Astron. Obs. St. Petersburg Univ., **44**, 39–68, 1994.

149. *D.I. Nagirner*, "Theory of non-stationary transfer of radiation," Astrofiz., **10**, No. 3, 445–469, 1974.

150. *D.I. Nagirner*, "Theory of radiation transfer in spectral lines," Astrophys. Space Phys. Rev., **3**, 255–300, 1984.

151. *D.I. Nagirner*, "Polarization of radiation in spectral lines," In Photometric and polarimetric investigations of celestial bodies. Kiev: Naukova Dumka, 1985, pp. 118–128 (in Russian).

152. *D.I. Nagirner*, "Spectral line formation with partial frequency redistribution," Astrofiz., **26**, No. 1, 157–195, 1987.

153. *D.I. Nagirner*, "Transfer of spectral line radiation," Trudy Astron. Obs. St. Petersburg Univ., **44**, 172–202, 1994.

154. *D.I. Nagirner*, Lectures on Radiative Transfer Theory, St. Petersburg: St. Petersburg Univ., 2002 (in Russian).

155. *D.I. Nagirner*, "Analytical Methods in Radiative Transfer Theory," Astrophys. Space Phys. Rev., **13**, 1–439, 2006.

156. *V.M. Loskutov*, "Radiative field in deep layers of turbid medium with strongly anisotropic scattering," Vestn. Leningr. Univ., **13**, 143–149, 1969.

157. *V.M. Loskutov*, "Polarization in resonance lines: diffuse reflection," Astron. Zh., **81**, No. 1, 24–32, 2004.

158. *V.M. Loskutov, V.V. Ivanov*, "Polarized line formation by resonance scattering: Lorentz profile," Astrofiz., **50**, No. 2, 199–217, 2007.

159. *V.M. Loskutov*, "Transfer of polarized radiation: Rayleigh scattering," Trudy Astron. Obs. St. Petersburg Univ., **44**, 154–171, 1994.

160. *V.P. Grinin*, "On the theory of non-stationary radiation transfer for anisotropic scattering," Astrofiz., **7**, No. 2, 203–209, 1971.

161. *V.P. Grinin*, "Resonance radiation transfer in moving media. Approximate methods," Astrofiz., **10**, No. 2, 239–255, 1974.

162. *S.I. Grachev, V.P. Grinin*, "Analysis of line profiles in the QSO PHL 5200 spectrum," Astrofiz., **11**, No. 1, 33–47, 1975.

163. *V.P. Grinin*, "The transfer of resonance radiation in the moving media with largescale radiative coupling," Astrofiz., **14**, No. 2, 201–214, 1978.

164. *V.P. Grinin*, "The radiation pressure in spectral lines in envelopes with axial-symmetrical supersonic motions. I. The kinematics with the local radiative coupling," Astrofiz., **14**, No. 4, 537–551, 1978; "II. Gas and dust systems with local radiative coupling" – *ibid.*, **16**, No. 1, 123–137, 1980; "III. Gas and dust systems with largescale radiative coupling" – *ibid.*, **17**, No. 1, 109–123, 1981.

165. *V.P. Grinin*, "Formation of the emission spectra in the moving media," Astrofiz., **20**, No. 2, 365–417, 1984.

166. *V.P. Grinin*, "Non-stationary radiative transfer theory," Trudy Astron. Obs. St. Petersburg Univ., **44**, 236–249, 1994.

167. *H. Domke*, "Line formation in the presence of a magnetic field. I. Scattering matrix," Astrofiz., **5**, No. 4, 525–537, 1969; "II. Source functions" – *ibid.*, **7**, No. 1, 39–56, 1971; "III. Formation of a Zeeman triplet with non-splitted upper level. Estimation of the influence of the magnetic field" – *ibid.*, **7**, No. 4, 587–604, 1971.

168. *H. Domke*, "Radiative transfer with Rayleigh scattering. I. Semiinfinite atmosphere," Astron. Zh., **48**, No. 2, 341–355; "II. Finite atmosphere" – *ibid.*, No. 4, 777–789, 1971.

169. *H. Domke*, "Depth regime of polarized light in a semi-infinite atmosphere," Astrofiz., **10**, No. 2, 205–217, 1974.

170. *H. Domke*, "Transfer of polarized light in an isotropic medium. Singular eigensolutions of the transfer equation," J. Quant. Spectrosc. Rad. Transf., **15**, 669–679, 1975.

171. *H. Domke*, "Biorthogonality and radiative transfer in finite slab atmospheres," J. Quant. Spectrosc. Rad. Transf., **30**, 119–129, 1983.

172. *H. Domke, E.G. Yanovitskij*, "A simple computational method for internal polarized radiation. Fields of finite slab atmospheres," J. Quant. Spectrosc. Rad. Transf., **26**, 389–396, 1981.

173. *H. Domke, E.G. Yanovitskij*, "Principles of invariance applied to the computation of internal polarized radiation in multi-layered atmospheres," J. Quant. Spectrosc. Rad. Transf., **36**, 175–186, 1986.

174. *H. Domke, E.G. Yanovitskij*, "On a new form of the transfer equation with applications to multiple scattering of polarized light," J. Quant. Spectrosc. Rad. Transf., **43**, No. 1, 61–73, 1990.

175. *H. Domke*, "An equivalence theorem for Chandrasekhar H-function and its application for accelerating convergence," J. Quant. Spectrosc. Rad. Transf., **39**, No. 4, 283–286, 1988.

176. *J.W. Hovenier, C. van der Mee, H. Domke*, Transfer of Polarized Light in Planetary Atmospheres: Basic Concept and Practical Methods. Dordrecht: Kluwer Academic Publ., 2004.

177. *S.I. Grachev*, "Characteristic lengths in radiative transfer problems for moving medium," Astrofiz., **13**, No. 1, 185–197, 1977.

178. *S.I. Grachev*, "Transfer of resonance radiation in infinite isotropically expanding medium," Astrofiz., **14**, No. 1, 112–121, 1978.

179. *S.I. Grachev*, "Asymptotic scaling in the problems of resonance radiation transfer in linearly expanding media. I. Kernels of integral equations, photon escape probabilities," Astrofiz., **23**, No. 2, 323–336, 1985; "II. Solutions for infinite and semi-infinite media" – *ibid.*, No. 3, 551–568, 1985.

180. *S.I. Grachev*, "On non-stationary radiative transfer in a spectral line in stellar atmosphere," Astrofiz., **37**, No. 3, 447–453, 1994.

181. *S.I. Grachev*, "Asymptotic theory of polarized line formation by resonance scattering within the Doppler core," Astrofiz., **43**, No. 1, 95–114, 2000.

182. *S.I. Grachev*, "Polarized radiation transfer: nonlinear integral equations for I-matrices and for the case of resonance scattering in a weak magnetic field," Astrofiz., **44**, No. 3, 455–467, 2001.

183. *S.I. Grachev*, "The formation of polarized lines: allowance for the Hanle effect," Astron. Zh., **75**, No. 12, 1092–1098, 2001.

184. *S.I. Grachev*, "The formation of polarized lines: factorization of the Hanle phase matrix and $\sqrt{\epsilon}$ law in the most general form," Vestn. St. Petersburg Univ., **4**, 632–639, 2014.

185. *S.I. Grachev*, "Radiative transfer in moving astrophysical media," Trudy Astron. Obs. St. Petersburg Univ., **44**, 203–235, 1994.

Inhomogeneous Semi-Infinite Atmospheres – On Transforming Conservative Multiple Scattering to Non-Conservative Multiple Pseudo-Scattering

H. Domke[1]

E-mail: *helmut.domke@web.de*

The F- and K-integrals are used to transform the zeroth azimuthal Fourier component of the radiative transfer equation for conservative multiple scattering of polarized light in vertically inhomogeneous plane atmospheres into an equivalent transfer equation with a modified phase matrix corresponding to non-conservative pseudo-scattering. As an example, the transformation to non-conservative multiple pseudo-scattering is applied to express the surface Green's function matrix for conservative scattering in terms of the surface Green's function matrix for non-conservative pseudo-scattering.

1 Introduction

The exclusive property of the transfer equation for conservative multiple scattering, which permits to determine the first and second angular moments of the intensity of the radiation field, the so called F- and K-integrals, a priori, up to two constant parameters, has been pointed out by Chandrasekhar [1] as well as by Sobolev [2] and partly employed by them on treating radiative transfer problems in vertically homogeneous conservative plane media. Here, it is shown, that even for vertically inhomogeneous conservative media, the F- and K-integrals allow us to transform the conservative radiative transfer equation into an equivalent transfer equation of the same form corresponding to non-conservative pseudo-scattering.

2 The transfer equation

Let us consider the transfer of polarized radiation in a vertically inhomogeneous and source-free plane atmosphere with local conservative scattering properties assumed to be macroscopically isotropic and mirror symmetric. It is well known (c.f. [3]) that, after azimuthal Fourier decomposition, the only conservative

[1] Milinowskistrasse 1, D-14169 Berlin, Germany

V. Grinin et al. (eds) Radiation mechanisms of astrophysical objects. Yerevan: Edit Print, 2017, pp. 29–32.

transfer equation emerges for the two-component vector of the azimuthally averaged Stokes parameters I and Q

$$u\frac{\partial}{\partial\tau}\mathbf{I}(\tau,u) = -\mathbf{I}(\tau,u) + \frac{1}{2}\int_{-1}^{+1} dv\mathbf{W}_{IQ}(\tau;u,v)\,\mathbf{I}(\tau,v), \tag{1}$$

where $\tilde{\mathbf{I}}(\tau,u) = (I(\tau,u), \quad Q(\tau,u))$. Here, the tilde denotes transposition of the vector, τ is the optical depth in the atmosphere, and u is the cosine of the polar angle with respect to the inner normal at the top $\tau = 0$ of the atmosphere. The matrix $\mathbf{W}_{IQ}(\tau;u,v)$ is the azimuthally averaged I,Q-component of the complete phase matrix. Local macroscopic mirror symmetry and reciprocity imply [3]

$$\mathbf{W}_{IQ}(\tau;u,v) = \mathbf{W}_{IQ}(\tau;-u,-v) = \tilde{\mathbf{W}}_{IQ}(\tau;v,u), \tag{2}$$

respectively. For conservative scattering, there hold the integral relations

$$\frac{1}{2}\int_{-1}^{+1} dv\,\mathbf{W}_{IQ}(\tau;u,v)\,\mathbf{i}_0 = \mathbf{i}_0, \quad \frac{1}{2}\int_{-1}^{+1} dv\,\mathbf{W}_{IQ}(\tau;u,v)v\,\mathbf{i}_0 = \frac{u}{3}\beta_1(\tau)\,\mathbf{i}_0, \tag{3}$$

where $\tilde{\mathbf{i}}_0 = (1, \quad 0)$. By means of Eq. (1) in conjunction with Eqs. (2), and (3), we find that the flux of radiative energy will be constant, i.e.,

$$F(\tau) = \frac{1}{2}\int_{-1}^{+1} du\,u\,\tilde{\mathbf{i}}_0\,\mathbf{I}(\tau,u) = F = const, \tag{4}$$

and the K-integral is found to be

$$K(\tau) = \frac{1}{2}\int_{-1}^{+1} du\,u^2\,\tilde{\mathbf{i}}_0\mathbf{I}(\tau,u) = K(0) - \left(1 - \frac{\bar{\beta}_1(\tau)}{3}\right)\tau F. \tag{5}$$

Here, $\bar{\beta}_1(\tau)$ is defined as $\bar{\beta}_1(\tau) = \frac{1}{\tau}\int_0^\tau dt\bar{\beta}_1(t)$. Finally, two eigensolutions to the transfer equation (1) can be found

$$\mathbf{i}_0(\tau,u) = \mathbf{i}_0, \quad \mathbf{i}_1(\tau,u) = \left[\left(1 - \frac{\bar{\beta}_1(\tau)}{3}\right)\tau - u\right]\mathbf{i}_0. \tag{6}$$

3 The equivalent transfer equation

On defining a modified phase matrix

$$\mathbf{W}_c(\tau;u,v) = \mathbf{W}_{IQ}(\tau;u,v) - \left[c_1(\tau)\,u^2\,\mathbf{i}_0\,\tilde{\mathbf{i}}_0\,v^2 + c_2(\tau)\,u\,\mathbf{i}_0\,\tilde{\mathbf{i}}_0\,v\right], \tag{7}$$

and replacing the phase matrix in Eq. (1) by means of Eq. (7), and using also Eqs. (4) and (5), we rewrite the conservative transfer equation (1) in the form

$$\begin{aligned} u\frac{\partial}{\partial\tau}\mathbf{I}(\tau,u) &= -\mathbf{I}(\tau,u) + \frac{1}{2}\int_{-1}^{+1} dv\,\mathbf{W}_c(\tau;u,v)\,\mathbf{I}(\tau,v) \\ &+ c_1(\tau)\,u^2\,\mathbf{i}_0\left[K(0) - \left(1 - \frac{\bar{\beta}_1(\tau)}{3}\right)\tau F\right] + c_2(\tau)\,u\,\mathbf{i}_0 F. \end{aligned} \tag{8}$$

Obviously, the new transfer equation (8) describes non-conservative multiple pseudo-scattering, with some primary (pseudo-) source terms on the r.h.s. linearly dependent on two constants F and $K(0)$, which can be determined a posteriori. We note that a particular solution to the transfer equation (8) can be found in terms of the eigensolutions (6) of the original conservative transfer equation (1)

$$\mathbf{I}_p(\tau, u) = 3\,[\mathbf{i}_0 K(0) - \mathbf{i}_1(\tau, u)F]\,. \tag{9}$$

4 Semi-infinite medium surface Green's function matrix

The semi-infinite medium surface Green's function matrix $\mathbf{G}(\tau, u; 0, \mu_0)$, with $-1 \leq u \leq +1$, $0 \leq \mu_0 \leq 1$, and $0 < \tau < \infty$, is defined as the finite solution to the transfer equation

$$u\frac{\partial}{\partial\tau}\mathbf{G}(\tau, u; 0, \mu_0) = -\mathbf{G}(\tau, u; 0, \mu_0) + \frac{1}{2}\int_{-1}^{+1} dv\,\mathbf{W}(\tau; u, v)\,\mathbf{G}(\tau, v; 0, \mu_0), \tag{10}$$

subject to the half-range boundary condition

$$\mathbf{G}(+0, \mu; 0, \mu_0) = \frac{1}{\mu}\delta(\mu - \mu_0)\,\mathbf{E}, \quad \mu, \mu_0 \in [0, 1], \tag{11}$$

at the top, where $\mathbf{E} = \mathbf{diag}(1, 1)$. In terms of the surface Green's function, the matrix of diffuse reflection is given by

$$\mathbf{R}(\mu, \mu_0) = \frac{1}{2}\mathbf{G}(+0, -\mu; 0, \mu_0), \quad \mu, \mu_0 \in [0, 1], \tag{12}$$

where μ_o denotes the direction of incidence. Reciprocity implies $\mathbf{R}(\mu, \mu_0) = \tilde{\mathbf{R}}(\mu_0, \mu)$ (c.f. [3]). There is no net flux of radiative energy for finite radiation fields in a semi-infinite conservatively scattering atmosphere without internal primary sources. Thus, the F-integral of the corresponding surface Green's function matrix $\mathbf{G}_{IQ}(\tau, u; 0, \mu_0)$ becomes zero,

$$\tilde{\mathbf{F}}_{IQ}(\tau; 0, \mu_0) = \tilde{\mathbf{F}}_{IQ}(\tau; 0, \mu_0) = \frac{1}{2}\int_{-1}^{+1} du\,u\,\tilde{\mathbf{i}}_0\,\mathbf{G}_{IQ}(\tau, u; 0, \mu_0) = \mathbf{0}. \tag{13}$$

Instead of seeking the surface Green's function matrix $\mathbf{G}_{IQ}(\tau, u; 0, \mu_0)$ as the solution to the conservative transfer equation (10) with $\mathbf{W}(\tau; u, v) = \mathbf{W}_{IQ}(\tau; u, v)$, we apply the equivalent transfer equation (8) corresponding to non-conservative pseudo-scattering, where $\mathbf{I}(\tau, u)$ is replaced by the function matrix $\mathbf{G}_{IQ}(\tau, u; 0, \mu_0)$, while $F = 0$, and $K(0)$ is replaced by the transposed vector

$$\tilde{\mathbf{K}}_{IQ}(+0; 0, \mu_0) = \frac{1}{2}\int_{-1}^{+1} du\,u^2\,\tilde{\mathbf{i}}_0\,\mathbf{G}_{IQ}(+0, u; 0, \mu_0). \tag{14}$$

On taking into account the particular solution (9), we use the surface Green's function matrix $\mathbf{G}_c(\tau, u; 0, \mu_0)$ for non-conservative pseudo-scattering to get, after some algebra, the surface Green's function matrix for conservative scattering as

$$\mathbf{G}_{IQ}(\tau, u; 0, \mu_0) = \mathbf{G}_c(\tau, u; 0, \mu_0) + \frac{3}{D}\left[\mathbf{i}_0 - \int_0^1 d\eta\, \mathbf{G}_c(\tau, u; 0, \eta)\eta\, \mathbf{i}_0\right]\tilde{\mathbf{K}}_c(+0; 0, \mu_0) \tag{15}$$

with

$$\tilde{\mathbf{K}}_c(+0; 0, \mu_0) = \frac{1}{2}\left[\mu_0\, \tilde{\mathbf{i}}_0 + 2\int_0^1 d\mu\, \mu^2\, \tilde{\mathbf{i}}_0\, \mathbf{R}_c(\mu, \mu_0)\right], \tag{16}$$

and $D = 3\int_0^1 d\eta\, \tilde{\mathbf{K}}_c(+0; 0, \eta)\, \eta\, \mathbf{i}_0$, while $\tilde{\mathbf{K}}_c(+0; 0, \mu_0) = D\, \tilde{\mathbf{K}}_{IQ}(+0; 0, \mu_0)$. It is easy to verify that $\mathbf{G}_{IQ}(\tau, u; 0, \mu_0)$ as given by Eq. (15) satisfies the correct transfer equation (8) as well as the boundary condition (11). When specified with $\tau = +0$ and $u = -\mu$, Eq. (15) provides a simple formula for retrieving the reflection matrix $\mathbf{R}_{IQ}(\mu, \mu_0)$ for conservative scattering by means of the reflection matrix $\mathbf{R}_c(\mu, \mu_0)$ for non-conservative pseudo-scattering

$$\mathbf{R}_{IQ}(\mu, \mu_0) = \mathbf{R}_c(\mu, \mu_0) + \frac{3\,(1 - D)}{D^2\gamma}\, \mathbf{K}_c(+0; 0, \mu)\, \tilde{\mathbf{K}}_c(+0; 0, \mu_0), \tag{17}$$

where the constant $\gamma = 3\int_0^1 d\eta\, \eta^2\, \tilde{\mathbf{i}}_0\, \mathbf{K}_{IQ}(+0; 0, \eta) = \frac{3}{D}\int_0^1 d\eta\, \eta^2\, \tilde{\mathbf{i}}_0\, \mathbf{K}_c(+0; 0, \eta)$ is the so called extrapolation length well known in radiative transfer theory.

For practical methods to calculate reflection matrices for inhomogeneous semi-infinite atmospheres, which are applicable also to compute $\mathbf{R}_c(\mu, \mu_0)$ for non-conservative pseudo-scattering, we refer to the textbook of Yanovitsky [4] and references therein. Finally, we note that for homogeneous atmospheres the transformation to equivalent pseudo-scattering with reduced effective albedo of single scattering can be performed also for non-conservative scattering. This has been described in an earlier paper [5].

References

1. *S. Chandrasekhar*, Radiative Transfer. New York: Oxford University Press, 1950.
2. *V. V. Sobolev*, Light Scattering in the Atmospheres of Planets. Moscow: Nauka, 1972 (in Russian). Translated as Light Scattering in Planetary Atmospheres. Oxford: Pergamon Press, 1975.
3. *J. W. Hovenier, C. van der Mee, H. Domke*, Transfer of Polarized Light in Planetary Atmospheres: Basic Concepts and Practical Methods. Amsterdam: Elsevier, 2005.
4. *E. G. Yanovitsky*, Light Scattering in Inhomogeneous Atmospheres. New York: Springer Verlag, 1997.
5. *H. Domke*, Eigenvalue shifting – a new analytical-computational method in radiative transfer theory. In Photopolarimetry in Remote Sensing. Eds. G. Videen et al. Dordrecht: Kluwer Academic Publ., 2004, pp. 107–124.

Bilinear Expansions for Redistribution Functions

H.A. Harutyunian[1], G. Alecian[2], K.G. Khachatryan[1], A.V. Vardanyan[1]

E-mail: *hhayk@bao.sci.am*

We suggest here a method for construction of a bilinear expansion for an angle-averaged redistribution function. An eigenvalues and eigenvectors determination problem is formulated and the required matrices are found analytically, and numerical procedures for their computations are elaborated. A simple method for the accuracy evaluation of the numerical calculations is suggested. It is shown that a group of redistribution functions describing the light scattering process within the spectral line frequencies can be constructed if the eigenvalue problem is solved for the considered function. It becomes possible if various combinations of eigenvalues and eigenvectors with the basic functions are used.

1 The redistribution function $r_{II}(x', x)$

Let us first redefine the redistribution function $r(x', x)$ which has a rather simple physical meaning: the quantity $r(x', x)dx$ represents the probability that a photon with the dimensionless frequency x' will be absorbed by an atom and re-emitted then in the frequency interval $(x; x + dx)$. The introduced dimensionless frequencies show the distance of photon's frequency $\nu(\nu')$ from the line center frequency ν_0 in Doppler half widths $\left(x = \frac{\nu-\nu_0}{\Delta\nu_D}\right)$. This redistribution function differs from one defined by Hummer [1] by the constant factor $\left(\pi^{\frac{1}{4}} U(0, \sigma)\right)^{-1}$, where the function

$$U(x, \sigma) = \frac{\sigma}{\pi} \int_{-\infty}^{\infty} \frac{\exp(-t^2)}{(x - t)^2 + \sigma^2} dt \tag{1}$$

is the well known Voigt function and $\sigma = \frac{\Delta\nu_T}{\Delta\nu_D}$, where $\Delta\nu_T$ is the total half-width of the line caused by all the broadening mechanisms taken into account.

The redistribution function describing the photon scattering within the line frequencies of the model two-level atom the upper level of which is broadened due to radiation damping has been independently derived by Henyey [2], Unno [3] and Sobolev [4] assuming that in the atom's reference frame the scattering is coherent.

[1] V. Ambartsumian Byurakan Astrophysical Observatory, Armenia
[2] LUTH, Observatoire de Paris, CNRS, Université Paris Diderot, France

V. Grinin et al. (eds) Radiation mechanisms of astrophysical objects. Yerevan: Edit Print, 2017, pp. 33–42.

Then, using also Hummer's [1] designation, one can represent it in the following form:

$$r_{II}(x',x)=\frac{1}{\pi U(0,\sigma)}\int_{\frac{|\overline{x}-\underline{x}|}{2}}^{\infty}\exp(-t^2)\left[\arctan\frac{\underline{x}+t}{\sigma}-\arctan\frac{\overline{x}-t}{\sigma}\right]dt. \qquad (2)$$

In the expression (2) we used the following denotations: $\overline{x}=\sup(x',x)$ and $\underline{x}=\inf(x',x)$.

It is noteworthy that there has been known bilinear expansion for two out of four redistribution functions described in Hummer's paper [1], namely, $r_I(x',x)$ and $r_{III}(x',x)$ before their classification by him. This fact was rather important for solving the light scattering problems applying the Principle of Invariance (PI). However, up to nowadays no any "natural" bilinear expansion has been revealed for the function $r_{II}(x',x)$. Therefore, one might try to create such a bilinear expansion using some artificial procedures.

In order to construct numerically such an expansion, let us first introduce here another representation of $r_{II}(x',x)$ derived by Nikoghossian [5] (see also Heinzel's paper [6])

$$r_{II}(x',x)=\frac{\sigma}{\pi U(0,\sigma)}\int_{-\infty}^{\infty}\frac{r_I(x'+t,x+t)}{t^2+\sigma^2}dt. \qquad (3)$$

From Eq. (3) one finds easily that the function $r_{II}(x',x)$ transforms into the $r_I(x',x)$ when $\sigma=0$.

On the other hand, the function $r_I(x',x)$ allows the following bilinear expansion first derived by Unno [7]:

$$r_I(x',x)=\int_{|\overline{x}|}^{\infty}\exp(-t^2)dt=\sum_{k=0}^{\infty}\frac{\alpha_{2k}(x')\,\alpha_{2k}(x)}{2k+1}, \qquad (4)$$

where

$$\alpha_k(x)=(2^k\pi^{\frac{1}{2}}k!)^{-\frac{1}{2}}\,H_k(x)\exp(-x^2) \qquad (5)$$

and $H_k(x)$ are the Hermit polynomials.

The obvious connection between functions $r_{II}(x',x)$ and $r_I(x',x)$ expressed by relation (3) allows suggesting the functions (5) as basic ones for constructing the eigenfunctions of $r_{II}(x',x)$. Taking into account this connection, one can search for the bilinear expansion of $r_{II}(x',x)$ in the following form:

$$r_{II}(x',x)=\sum_{k=0}^{\infty}\frac{\omega_{2k}(x',\sigma)\,\omega_{2k}(x,\sigma)}{\zeta_k(\sigma)}, \qquad (6)$$

where

$$\omega_{2k}(x,\sigma)=\sum_{m=0}^{\infty}\gamma_{km}(\sigma)\,\alpha_{2k}(x). \qquad (7)$$

The vector $\zeta_k(\sigma)$ and matrix $[\gamma_{km}(\sigma)]$ are, respectively, the eigenvalues and eigenfunctions of the following problem (see, for example, [8, 9]):

$$\sum_{m=0}^{\infty} [\gamma_{km}(a_{mn} - \zeta_k(\sigma) b_{mn})] = 0, \tag{8}$$

where

$$a_{mn} = \int_{-\infty}^{\infty} \alpha_{2m}(x)\, \alpha_{2n}(x) dx, \tag{9}$$

and

$$b_{mn} = \int_{-\infty}^{\infty} \alpha_{2m}(x) dx \int_{-\infty}^{\infty} r_{II}(x', x)\, \alpha_{2n}(x') dx'. \tag{10}$$

It is evident that calculating the matrices $[a_{mn}]$ and $[b_{mn}]$ and solving the eigenvalue problem (8) one can numerically construct the bilinear expansion (6).

2 Calculation of the relevant matrices

Using the integral forms for the Hermit polynomials, one can easily find the following presentation for the introduced above basic functions [10]:

$$\alpha_k(x) = (2^k \pi^{\frac{1}{2}} k!)^{-\frac{1}{2}} \frac{2}{\sqrt{\pi}} \operatorname{Re}(-2i)^k \int_0^{\infty} t^k \exp(-t^2 + 2ixt) dt. \tag{11}$$

Then, using the following expression for the δ function:

$$\frac{1}{2\pi} \int_{-\infty}^{\infty} \exp(ixt) dt = \delta(t), \tag{12}$$

one finds directly

$$a_{mn} = (-1)^{m+n} \frac{(2m + 2n - 1)!!}{2^{m+n+\frac{1}{2}} \sqrt{(2m)!(2n)!}}. \tag{13}$$

For calculations of the matrix $[b_{mn}]$, one can suggest two different ways. One is the direct calculation of the threefold iterated integral (10) which is fraught with huge numerical difficulties arising due to the complicated behavior of the basic functions. Therefore, some simplifying analytical calculations before starting the numerical procedures would sufficiently facilitate the numerical procedures. One can find from Eq. (10) substituting Eq. (4) for the redistribution function $r_I(x', x)$ in the relation (3)

$$b_{mn} = \frac{\sigma}{\pi U(0, \sigma)} \sum_{k=0}^{\infty} \frac{1}{2k+1} \int_{-\infty}^{\infty} \frac{g_{km}(t)\, g_{kn}(t)}{t^2 + \sigma^2} dt, \tag{14}$$

where

$$g_{km}(t) = \int_{-\infty}^{\infty} \alpha_{2k}(x + t)\, \alpha_{2m}(x) dx = N_{km}\, \alpha_{km}\left(\frac{t}{\sqrt{2}}\right), \tag{15}$$

and

$$N_{km} = \frac{\pi^{\frac{1}{4}}}{2^{k+m+\frac{1}{2}}} \sqrt{\frac{(2k+2m)!}{(2k)!(2m)!}}. \tag{16}$$

Thus, one finds finally

$$b_{mn} = \frac{1}{U(0,\sigma)} \sum_{k=0}^{\infty} \frac{N_{km} N_{kn}}{2k+1} c_{k+m,k+n}, \tag{17}$$

where

$$c_{mn} = \frac{\sigma}{\pi} \int_{-\infty}^{\infty} \frac{\alpha_{2m}\left(\frac{t}{\sqrt{2}}\right) \alpha_{2n}\left(\frac{t}{\sqrt{2}}\right)}{t^2+\sigma^2} dt. \tag{18}$$

As a matter of fact, the threefold iterated integral is given now by an infinite series where only a single integration appears. However, the integrand is again a vastly oscillating function making the direct numerical computation extremely inefficient especially for greater values of indexes. Also it is not difficult to realize that for the smaller damping parameters the computing error gets larger. But at the same time in the limiting case when $\sigma = 0$, the integral (18) can be taken analytically to find

$$c_{mn}|_{\sigma=0} = \alpha_{2m}(0)\, \alpha_{2n}(0). \tag{19}$$

In order to calculate the integral (18) for the values $\sigma > 0$, let us use the formulae (5) and the Hermit polynomials definition (see, for example, [10])

$$H_{2k}(x) = (2k)! \sum_{l=0}^{k} \frac{(-1)^l}{(l)!(2k-2l)!} (2x)^{2k-2l}, \tag{20}$$

to obtain

$$\alpha_{2n}\left(\frac{t}{\sqrt{2}}\right) = \exp\left(-\frac{t^2}{2}\right) \frac{\sqrt{(2n)!}}{\pi^{\frac{1}{4}}} \sum_{k=0}^{n} \frac{(-1)^k t^{2n-2k}}{2^k k!(2n-2k)!}. \tag{21}$$

Then, taking into account that

$$t^{2k} = \frac{(2m)!}{2^{2m}} \sum_{j=0}^{m} \frac{H_{2j}(t)}{(2j)!\,(m-j)!}, \tag{22}$$

one can finally find

$$c_{mn} = \frac{\sqrt{(2m)!(2n)!}}{\pi^{\frac{1}{4}} 2^{2m+2n}} \sum_{k=0}^{m} \frac{(-2)^k}{k!\,(2m-2k)!} \sum_{l=0}^{n} \frac{(-2)^l}{l!\,(2n-2l)!}$$

$$\times\, (2m+2n-2k-2l)! \sum_{q=0}^{m+n-k-l} \frac{2^q \alpha_{2q}(0,\sigma)}{(m+n-k-l-q)!\sqrt{(2q)!}}, \tag{23}$$

where the following notation is introduced:

$$\alpha_{2q}(0,\sigma) = \frac{(-1)^q}{\pi^{\frac{1}{4}}\sqrt{(2q)!}} \sum_{p=0}^{\infty} \frac{2^p \sigma^{2p}}{(2p)!} \left[(2q+2p-1)!! - \frac{\sigma}{\sqrt{\pi}} \frac{2}{2p+1} (2q+2p)!! \right]. \quad (24)$$

The expression (23) obtained for description of elements of the required matrix, though explicit, is again rather complicated for direct numerical calculations. Therefore, any numerical procedure based on the ordinary accuracy of the used computer calculations cannot provide the required accuracy of the final results. These difficulties can be overcome only using methods of calculations based on the usage of a higher number of significant digits. For example, about one hundred twenty or more significant digits are needed to provide 15 correct digits for all the elements of the 100×100 matrix.

Nevertheless, it is possible to obtain a much simpler expression if one of the indexes of the matrix $[c_{mn}]$ is equal to zero (the first row or the first column). Then one out of the three sums disappears immediately and one obtains after some transformations

$$c_{0,n} = \frac{(-1)^n \sqrt{(2n)!}}{\pi^{\frac{1}{4}} 2^{2n}} \sum_{q=0}^{n} \frac{(-2)^q \, \alpha_{2q}(0,\sigma)}{(n-q)!\sqrt{(2q)!}} = c_{n,0}. \quad (25)$$

On the other hand, taking into account the relation of recurrence for the Hermit polynomials

$$H_{n+1}(x) = 2xH_n(x) - 2nH_{n-1}(x), \quad (26)$$

one can derive the following recurrence relation for the required elements of the matrix $[c_{mn}]$:

$$c_{mn} = \sqrt{\frac{2n+1}{2m}} d_{m-1,n+1} + \sqrt{\frac{n}{m}} d_{m-1,n-1} - \sqrt{\frac{2m-1}{2m}} c_{m-1,n}, \quad (27)$$

where

$$d_{mn} = c_{m+\frac{1}{2},n+\frac{1}{2}}. \quad (28)$$

Further, in terms of the physical meaning of the redistribution function one might conclude that its integral over one of the arguments should give the profile of the absorption coefficient

$$\int_{-\infty}^{\infty} r_{II}(x',x)dx' = \alpha(x,\sigma) = \frac{U(x,\sigma)}{U(0,\sigma)}, \quad (29)$$

and bearing in mind (5)–(7), one finds

$$\sum_{k=0}^{\infty} \frac{\gamma_{k,0}}{\zeta_k} \omega_{2k}(x,\sigma) = \frac{U(x,\sigma)}{U(0,\sigma)}. \quad (30)$$

Here the following normalization relation is used:

$$\int_{-\infty}^{\infty} \alpha_m(x)\, \alpha_n(x) dx = \delta_{mn}, \tag{31}$$

where δ_{mn} is the Kronecker symbol. Integrating Eq. (34) over all frequencies, one obtains finally

$$\int_{-\infty}^{\infty} dx \int_{-\infty}^{\infty} r_{II}(x', x) dx' = \sum_{k=0}^{\infty} \frac{{\gamma_{k0}}^2}{\zeta_k} = \sqrt{\pi}, \tag{32}$$

which can be used for the normalization purposes.

Now let us briefly consider the physical situation when both energetic levels are broadened. Heinzel [6] has shown that the redistribution function derived by Hummer [1] for description of this process is not correct and obtained a new expression allowing the following notation:

$$r_V(x', x) = \frac{{\sigma_i}^2}{\pi^2} \int_{-\infty}^{\infty} \frac{dt}{t^2 + {\sigma_i}^2} \int_{-\infty}^{\infty} \frac{r_{II}(x' + t, x + u)}{u^2 + {\sigma_i}^2} du. \tag{33}$$

Then, using Eq. (6), one will find a bilinear expansion for this function as well. Putting Eq. (6) into Eq. (33), one obtains

$$r_V(x', x) = \sum_{k=0}^{\infty} \frac{\omega_{2k}(x', \sigma_i, \sigma_j)\, \omega_{2k}(x, \sigma_i, \sigma_j)}{\zeta_k(\sigma_j)}, \tag{34}$$

where the functions

$$\omega_{2k}(x, \sigma_i, \sigma_j) = \sum_{m=0}^{\infty} \gamma_{km}(\sigma_j)\, \alpha_{2m}(x, \sigma_i) \tag{35}$$

depend on damping parameters of both energetic levels. The functions $\alpha_{2k}(x, \sigma)$ are defined by the relation

$$\alpha_k(x, \sigma) = (2^k \pi^{\frac{1}{2}} k!)^{-\frac{1}{2}} \frac{2}{\sqrt{\pi}} \operatorname{Re}(-2i)^k \int_0^{\infty} t^k \exp(-t^2 - 2\sigma t + 2ixt) dt. \tag{36}$$

Thus, constructing a bilinear expansion for the function $r_{II}(x', x)$ as described above, one arrives at a conclusion that this method provides a tool for constructing similar expansions for all the applicable redistribution functions. It can be done immediately, if one obtains the eigenfunctions $\gamma_{km}(\sigma)$ and eigenvalues $\zeta_k(\sigma)$ and also uses an appropriate numerical procedure for computing the functions $\alpha_k(x, \sigma)$. Then the corresponding redistribution functions could be constructed by the same procedure using the various values of the parameters σ_i and σ_j. It is easy to see that $r_V(x', x) = r_{III}(x', x)$, if $\sigma_j = 0$, $r_V(x', x) = r_{II}(x', x)$ for $\sigma_i = 0$ and, at last, $r_V(x', x) = r_I(x', x)$, if both damping parameters are equal to zero – $\sigma_j = \sigma_i = 0$.

3 The auxiliary functions $\alpha_k(x,\sigma)$

Obviously, besides the eigenvalue problem (8) one should overcome the second key computational difficulties for the eventual construction of the redistribution functions. That is the problem of the numerical evaluation of the corresponding auxiliary functions. The functions $\alpha_{2m}(x,\sigma)$ defined by Eq. (36) have been introduced and studied by Hummer [1], and a rather effective method for their calculation was suggested by him in the same paper. In order to simplify the initial expression (36), the exponent $\exp(-2\sigma t)$ is replaced by its power series. Then one should compute several terms of that series to provide the required accuracy of auxiliary functions. Following the Hummer's procedure in general, Harutyunian [11] has separated from each other the even and odd functions appearing in the derived series to obtain the following relation:

$$\alpha_k(x,\sigma) = (2^k \pi^{\frac{1}{2}} k!)^{-\frac{1}{2}} \sum_{m=0}^{\infty} \frac{(i\sigma)^m}{(2m)!} \left[M_{k+2m}(x) + \frac{\sigma}{2m+1} N_{k+2m+1}(x) \right], \qquad (37)$$

where

$$M_k(x) = \frac{2}{\sqrt{\pi}} \operatorname{Re}(-2i)^k \int_0^{\infty} t^k \exp(-t^2 + 2ixt) dt \qquad (38)$$

and

$$N_k(x) = \frac{2}{\sqrt{\pi}} \operatorname{Im}(-2i)^k \int_0^{\infty} t^k \exp(-t^2 + 2ixt) dt \qquad (39)$$

are the Hermit functions of the first and second kinds [10].

From Eqs. (38) and (39) one can easily find the following recurrent formulas well known from the mathematical textbooks (see, for example, [10]):

$$M_{k+1}(x) = 2xM_k(x) - 2kM_{k-1}(x) \qquad (40)$$

for the first kind functions and similarly

$$N_{k+1}(x) = 2xN_k(x) - 2kN_{k-1}(x) \qquad (41)$$

for the second kind functions. The first functions to be used for recurrent relations are defined as follows:

$$M_0(x) = \exp(-x^2), \quad M_1(x) = 2xM_0(x), \qquad (42)$$

$$N_0(x) = \frac{2}{\sqrt{\pi}}, \quad N_1(x) = 2xN_0(x) - \frac{2}{\sqrt{\pi}}. \qquad (43)$$

Here

$$F(x) = \int_0^{\infty} \exp(-t^2) \sin 2xt \, dt = \exp(-x^2) \int_0^x \exp(t^2) dt \qquad (44)$$

is the Dawson function connected with the error function of an imaginary argument and represents the solution of the following Cauchy problem:

$$F'(x) = 1 - 2xF(x) \tag{45}$$

with the initial condition $F(0) = 0$.

Numerical procedures for calculation of the Dawson function are considered in Hummer's paper [12]. Some earlier references could be found in the mentioned above review by Hummer [1]. Among the relatively recent studies one might refer to the papers [13–14]. The most efficient procedure for calculation of the Dawson function can be carried out using the power series [10]

$$F(x) = \sum_{n=0}^{\infty} \frac{(-1)^n\, 2^n}{(2n+1)!!} x^{2n+1}, \tag{46}$$

which converges for all values of the argument. However, one should take care for the accuracy issues when applying the relation (46) for numerical computations. Obviously, for the smaller values of the argument ($x \leq 1$) the series (46) converges rather rapidly and no big difficulties can arise. However, for the larger values of the argument, the need in much higher digit numbers for calculations grows up very rapidly. For instance, for $x = 12$ one can easily provide around 35 correct digits of the Dawson function if uses 120 significant digits for calculations. Nonetheless, the usage of the same number of significant digits provides only 12 correct digits in the final result if the argument reaches to the value $x = 15$. Many correct significant digits are very important not only for computing the Dawson function itself. The point is that the recurrent formula themselves are a perilous source of the error accumulation and therefore one needs to calculate the Dawson function with a bigger number of correct significant digits. Actually, the problem is absolutely the same that we encountered considering the matrix $[c_{mn}]$ in the previous paragraph.

Of course, on the other hand, one can find an asymptotic series for the larger arguments of the Dawson function which can be rather useful for the practical applications [10]

$$F(x) \approx \sum_{n=0}^{\infty} \frac{(2n)!}{2^{2n+1}\, n!\, x^{2n+1}}. \tag{47}$$

This asymptotic relation, as opposed to the series (46), is a diverging one. Nevertheless, a few first terms of this series will provide an applicable accuracy for various asymptotic estimates. Indeed, starting with the relations (42)–(43) and using the relation (47), one obtains for $x \to \infty$ the following asymptotic form:

$$N_k(x) \approx \frac{(-1)^k}{\sqrt{\pi} x^{k+1}} \sum_{n=0}^{\infty} \frac{(2n+k)!}{2^{2n}\, n!\, x^{2n}}, \tag{48}$$

which can be used in the series (37). It is easy to see that due to the exponentially decreasing behavior of the first kind Hermit functions for larger values of the argument they are falling much faster than the second kind functions. Therefore, one finds the asymptotic relation

$$\alpha_k(x,\sigma)=\frac{\sigma}{x^{k+2}\sqrt{\pi}}(2^k\pi^{\frac{1}{2}}k!)^{-\frac{1}{2}}\sum_{n=0}^{\infty}\frac{(2n+k+1)!}{x^{2n}}\sum_{m=0}^{n}\frac{(-1)^m\sigma^{2m}}{2^{2(n-m)}(2m+1)!(n-m)!},\tag{49}$$

which turns into the known asymptotic expression for the Voigt function [15]

$$U(x,\sigma)=\frac{\sigma}{x^2\sqrt{\pi}}\sum_{n=0}^{\infty}\frac{(2n+1)!}{x^{2n}}\sum_{m=0}^{n}\frac{(-1)^m\sigma^{2m}}{2^{2(n-m)}(2m+1)!(n-m)!}.\tag{50}$$

These asymptotic forms coupled with the exact formulas derived above provide one with all the necessary tools for building the bilinear expansions of redistribution functions and their usage for the practical purposes.

Preliminary calculations show that these numerical procedures easily can be performed on modern PC. Elaborated specially for these purposes software package HAHMATH allows one to perform computations with the needed number of significant digits when high accuracy calculations are required. However, extraordinary accuracies are needed only when the matrix $[c_{mn}]$ or Dawson function and its derivatives are calculated. Once calculated the matrix $[c_{mn}]$ can be used for building the matrix $[b_{mn}]$ and to continue all other computations with the ordinary accuracy of computers. There is no need for using the extremely long numbers when solving the corresponding eigenvalue problem. Calculated once the eigenvalues and eigenfunctions for the given damping factor might be used for further calculations.

Acknowledgments. Two of the authors (H.H. and G.A.) thank the Armenian SCS and French CNRS for the financial support given during the joint project implementation.

References

1. *D. Hummer*, Mon. Not. Roy. Astron. Soc., **125**, 21, 1962.
2. *L.G. Henyey*, Proc. Nat. Acad. Sci., **26**, 50, 1941.
3. *W. Unno*, Publ. Astron. Soc. Japan, **4**, 100, 1952.
4. *V.V. Sobolev*, Vestn. Leningr. Univ., No. 5, 85, 1955.
5. *A.G. Nikoghossian*, Dokl. Acad. Nauk Arm. SSR, **68**, 176, 1979.
6. *P. Heinzel*, J. Quant. Spectrosc. Rad. Transf., **25**, 483, 1981.
7. *W. Unno*, Astrophys. J., **129**, 388, 1959.

8. *N.B. Yengibarian*, Astrophys., **7**, 573, 1971.

9. *N.B. Yengibarian, A.G. Nikoghossian*, J. Quant. Spectrosc. Rad. Transf., **13**, 787, 1973.

10. *M. Abramowitz, I.A. Steagan (eds.)*, Handbook of Mathematical Functions with Formulas, Graphs, and Mathematical Tables. New York: Dover, 1972.

11. *H.A. Harutyunian*, Soobshch. Byurakan Obs., **52**, 137, 1980.

12. *D. Hummer*, Math. Comput., **18**, 317, 1964.

13. *L.A. Milone, A.A.E. Milone*, Astrophys. Space Sci., **147**, 189, 1988.

14. *G.B. Rybicki*, Computers in Phys., **3**, 85, 1989.

15. *G.N. Plass, D.I. Fivel*, Astrophys. J., **117**, 225, 1953.

About the Development of the Asymptotic Theory of Non-Stationary Radiative Transfer

A.K. Kolesov[1]

E-mail: *natakr4@gmail.com*

A brief review of the development of the asymptotic non-stationary radiative transfer theory is presented. In particular, the accuracy of the diffusion approximation is studied. It is shown that the replacement of the non-stationary transfer equation by the heat conductive equation should give satisfactory results when the single scattering albedo λ is close to the unity. But this approximation can lead to significant errors when $\lambda < 1$.

Studying time-dependent processes in various non-stationary objects is an important problem of modern astrophysics. The illumination of the dust nebula under the influence of radiation of a new star can be considered as an example of such process.

Sobolev initiated the systematic development of the theory of non-stationary radiation fields in the article [1] published in 1952. Fundamentals of this theory were presented in his book [2].

Non-stationary radiation fields are characterized by the finite speed of light c and a definite duration of the light scattering process.

Let t_1 be the mean time of the stay of a photon in the absorbed state. It is usually assumed that the probability of emission of a photon being in the absorbed state in the time interval from t to $t + dt$ depends on t by the exponential law, i.e., it is proportional to $e^{-\frac{t}{t_1}}\frac{dt}{t_1}$.

The probability of the photon absorption while travelling after his radiation during an interval of time from t to $t + dt$ depends on t also exponentially, e.g., it is proportional to $e^{-\frac{t}{t_2}}\frac{dt}{t_2}$, where $t_2 = \frac{1}{\alpha c}$ is the mean time of stay of a photon on the path between two consecutive scatterings. Here α is the volume absorption coefficient of the medium.

The values of t_1 and t_2 are usually very different from each other. Therefore, Sobolev has proposed to allocate the consideration of two limiting cases, i.e., the case A, when $t_1 \gg t_2$, and the case B, when $t_2 \gg t_1$.

The simplest model of non-stationary radiative transfer is a model based on the consideration of the one-dimensional homogeneous infinite medium with an energy source depending on time. Let us assume that the medium is illuminated by a momentary point source of luminosity L flashing at some initial moment of time. We note that an actual flash duration and a dependence of the luminosity $L(t)$

[1] St. Petersburg State University, Russia

V. Grinin et al. (eds) Radiation mechanisms of astrophysical objects. Yerevan: Edit Print, 2017, pp. 43–49.

on the time t can be taken into account by integrating over time the expressions for light field characteristics found in the case of a point source multiplied by the value of the luminosity $L(t)$.

Let $I_1(r,t)$ and $I_2(r,t)$ be intensities of the radiation spreading on distance r from the source at time t in the direction of increasing and decreasing values of the coordinate r, respectively. Instead of the geometric distances r, the physical time t and values t_1 and t_2, we use the corresponding dimensionless quantities

$$\tau = \alpha r, \quad u = \frac{t}{t_1 + t_2}, \quad \beta_1 = \frac{t_1}{t_1 + t_2}, \quad \beta_2 = \frac{t_2}{t_1 + t_2}. \tag{1}$$

Then the radiative transfer equation takes the following form:

$$\frac{\partial I_1(\tau,u)}{\partial \tau} + \beta_2 \frac{\partial I_1(\tau,u)}{\partial u} = -I_1(\tau,u) + B(\tau,u), \tag{2}$$

$$-\frac{\partial I_2(\tau,u)}{\partial \tau} + \beta_2 \frac{\partial I_2(\tau,u)}{\partial u} = -I_2(\tau,u) + B(\tau,u). \tag{3}$$

Here $B(\tau,u)$ is the source function defined by the equation of radiative equilibrium

$$B(\tau,u) = \frac{\lambda}{2} \int_0^u \left[I_1\left(\tau,u'\right) + I_2(\tau,u') \right] e^{-\frac{u-u'}{\beta_1}} \frac{du'}{\beta_1}, \tag{4}$$

where λ is the single scattering albedo. These equations are supplemented with the initial condition which takes into account the momentary point source of energy. The mean radiation intensity $J(\tau,u)$ and the radiation flux $H(\tau,u)$ are defined by the expressions

$$J(\tau,u) = \frac{1}{2}\left[I_1(\tau,u) + I_2(\tau,u) \right], \tag{5}$$

$$H(\tau,u) = I_1(\tau,u) - I_2(\tau,u). \tag{6}$$

Minin [3] obtained the exact solution of this problem by means of the Laplace transform.

Simple asymptotic expressions for characteristics of the non-stationary radiation field are obtained in the case when points of the medium are located at large optical distances from energy sources ($\tau \gg 1$) and scattering of light is close to conservative ($1 - \lambda \ll 1$). In this case Minin [4] proposed to use a simple technique for inverting the Laplace transform. As it is known from the theory of the Laplace transform, the value of the original at large values of the argument ($u \gg 1$) is determined using the expansion of the image in powers of the small parameter s. This expansion corresponds to the expansion of solutions of the stationary radiative transfer equation in powers of the small values of $1 - \lambda$. As a result of the Laplace transform in time, the non-stationary equation is converted

into the stationary one but the value of λ is replaced by the value $\frac{\lambda}{(1+\beta_1 s)(1+\beta_2 s)}$. Therefore, taking into account the fact that $\beta_1 + \beta_2 = 1$, we obtain $1 - \lambda = s$ with accuracy to members of the higher degrees of the parameter s. Hence, when receiving the asymptotic image, it is necessary to replace the small values of $1 - \lambda$ by s in the equation solution for the stationary case, and then to apply the inverse Laplace transform.

In the case of one-dimensional infinite medium illuminated by a momentary point source, we obtain for $J(\tau, u, \lambda)$ and $H(\tau, u, \lambda)$ the following expressions (for $\lambda = 1$, $\tau \gg 1$, $u > \tau$):

$$J_D(\tau, u, 1) = \frac{L}{4\sqrt{\pi u}}\, e^{-\frac{\tau^2}{4u}}, \tag{7}$$

$$H_D(\tau, u, 1) = \frac{L}{4\sqrt{\pi u}}\, \frac{\tau}{u}\, e^{-\frac{\tau^2}{4u}}. \tag{8}$$

The same expressions for these quantities are obtained in the diffusion approximation in the case of $\lambda = 1$. This approximation is based on using the heat conductivity equation

$$\frac{\partial^2 J(\tau, u, \lambda)}{\partial \tau^2} = \frac{\partial J(\tau, u, \lambda)}{\partial u} + (1 - \lambda)\, J(\tau, u, \lambda) \tag{9}$$

instead of the non-stationary radiation transfer equation. The solution of the equation (9) leads to the following expressions for the functions $J(\tau, u, \lambda)$ and $H(\tau, u, \lambda)$:

$$J_D(\tau, u, \lambda) = e^{-(1-\lambda)u} J_D(\tau, u, 1), \tag{10}$$

$$H_D(\tau, u, \lambda) = e^{-(1-\lambda)u} H_D(\tau, u, 1), \tag{11}$$

where $J_D(\tau, u, 1)$ and $H_D(\tau, u, 1)$ are given by the expressions (7) and (8).

The diffusion approximation was proposed by Compton [5] in 1923. However, in 1926 Milne [6] showed that the usage of this approximation for the calculation of non-stationary fields of radiation can lead to physically unreasonable results.

Kolesov and Sobolev [7] studied the accuracy of the diffusion approximation in the cases A and B.

Exact expressions for $J(\tau, u, \lambda)$ and $H(\tau, u, \lambda)$ in the case A have the form

$$J_A(\tau, u, \lambda) = \frac{L}{2\pi} \int_0^\infty e^{-\left(1 - \frac{\lambda}{1+x^2}\right)u}\, \frac{\cos x\tau}{1 + x^2}\, dx, \tag{12}$$

$$H_A(\tau, u, \lambda) = \frac{L}{\pi} \int_0^\infty e^{-\left(1 - \frac{\lambda}{1+x^2}\right)u}\, \frac{x \sin x\tau}{1 + x^2}\, dx. \tag{13}$$

When $\lambda u \gg 1$, we have the following asymptotic expressions:

$$J_A^{as}(\tau,u,\lambda) \approx \frac{L}{4\sqrt{\pi\lambda u}}\, e^{-(1-\lambda)u-\frac{\tau^2}{4\lambda u}}, \tag{14}$$

$$H_A^{as}(\tau,u,\lambda) \approx \frac{L}{4\sqrt{\pi\lambda u}}\, \frac{\tau}{\lambda u} e^{-(1-\lambda)u-\frac{\tau^2}{4\lambda u}}. \tag{15}$$

In the absence of true absorption, when $\lambda = 1$, these expressions coincide with the expressions (7) and (8) of the diffusion approximation.

In the case B for $\tau \geq 0$ and $u > \tau$, the exact expressions for these quantities are given by the expressions

$$J_B(\tau,u,\lambda) = \frac{\lambda L}{8}\left[I_0\left(\frac{\lambda}{2}\sqrt{u^2-\tau^2}\right) + \frac{u}{\sqrt{u^2-\tau^2}} I_1\left(\frac{\lambda}{2}\sqrt{u^2-\tau^2}\right)\right] e^{-\left(1-\frac{\lambda}{2}\right)u}, \tag{16}$$

$$H_B(\tau,u,\lambda) = \frac{\lambda L}{4}\frac{\tau}{\sqrt{u^2-\tau^2}} I_1\left(\frac{\lambda}{2}\sqrt{u^2-\tau^2}\right) e^{-\left(1-\frac{\lambda}{2}\right)u}, \tag{17}$$

where $I_0(z)$ and $I_1(z)$ are the modified Bessel functions. The asymptotic expressions for $u \gg \tau$ have the form

$$J_B^{as}(\tau,u,\lambda) \approx \frac{L}{4}\sqrt{\frac{\lambda}{\pi u}} e^{-(1-\lambda)u-\frac{\lambda\tau^2}{4u}}, \tag{18}$$

$$H_B^{as}(\tau,u,\lambda) \approx \frac{L\tau}{4u}\sqrt{\frac{\lambda}{\pi u}} e^{-(1-\lambda)u-\frac{\lambda\tau^2}{4u}}. \tag{19}$$

When $\lambda = 1$, these expressions also coincide with the expressions (7) and (8) of the diffusion approximation.

First of all, let us consider the case A. When $\lambda = 1$, the exact and approximate values of $J(\tau,u,\lambda)$ and $H(\tau,u,\lambda)$ are pretty close to each other, and the asymptotic expressions for these quantities coincide with the expressions for $J_D(\tau,u,1)$ and $H_D(\tau,u,1)$ in the diffusion approximation. The ratios J_A^{as}/J_D and H_A^{as}/H_D are shown in Table 1.

A different situation occurs when $\lambda < 1$. A comparison of the exact values $J_A(\tau,u,\lambda)$ and $H_A(\tau,u,\lambda)$ with the approximate values of these quantities shows that they can significantly differ from each other. The asymptotic expressions differs from the corresponding expressions in the diffusion approximation. Their ratio is equal to

$$\frac{J_A^{as}(\tau,u,\lambda)}{J_D(\tau,u,\lambda)} = \frac{H_A^{as}(\tau,u,\lambda)}{H_D(\tau,u,\lambda)} \approx \frac{1}{\sqrt{\lambda}}\, e^{-\frac{\tau^2}{4u}\left(\frac{1}{\lambda}-1\right)}. \tag{20}$$

Since λ is included in the exponent, these ratios may differ significantly from the unity.

Let us consider now the case B. We note that due to the finite speed of light $J(\tau,u,\lambda) = 0$ and $H(\tau,u,\lambda) = 0$ if $u < \tau$ but in the diffusion approximation

Table 1: Ratios of J_A^{as}/J_D and H_A^{as}/H_D for $\lambda = 1$

	$\tau = 1$		$\tau = 10$	
u	J_A^{as}/J_D	H_A^{as}/H_D	J_A^{as}/J_D	H_A^{as}/H_D
I	0.801	0.98	5.30×10^7	8.57×10^6
2	0.916	1.57	7.78×10^2	2.24×10^2
3	0.977	1.76	2.92×10^1	1.15×10^1
4	0.995	1.77	6.92	3.33
5	1.018	1.69	3.27	1.82
6	1.022	1.59	2.12	1.32
7	1.024	1.50	1.63	1.104
8	1.023	1.43	1.38	0.997
9	1.022	1.36	1.23	0.942
10	1.021	1.32	1.14	0.914
15	1.015	1.19	0.993	0.906
20	1.012	1.13	0.971	0.939
30	1.008	1.083	0.977	0.983
40	1.006	1.060	0.985	1.001
50	1.005	1.047	0.990	1.009
60	1.004	1.039	0.993	1.012
80	1.003	1.029	0.996	1.014
100	1.002	1.023	0.998	1.014

$J_D(\tau, u, \lambda) \neq 0$ and $H_D(\tau, u, \lambda) \neq 0$ under this condition as the finite speed of light is not taken into account in this approximation. A comparison of the exact and asymptotic expressions gives approximately the same results, as in the case of A, i.e. $J_B^{as}(\tau, u, 1) = J_D(\tau, u, 1)$ and $H_B^{as}(\tau, u, 1) = H_D(\tau, u, 1)$, but when $\lambda < 1$, $J_B^{as}(\tau, u, \lambda)$ and $H_B^{as}(\tau, u, \lambda)$ are significantly different from $J_D(\tau, u, \lambda)$ and $H_D(\tau, u, \lambda)$, as

$$\frac{J_B^{as}(\tau, u, \lambda)}{J_D(\tau, u, \lambda)} = \frac{H_B^{as}(\tau, u, \lambda)}{H_D(\tau, u, \lambda)} \approx \sqrt{\lambda}\, e^{\frac{\tau^2}{4u}(1-\lambda)}, \tag{21}$$

i.e., these ratios depend strongly on λ (see Tables 2 and 3).

From the above it follows that the replacement of the non-stationary radiation transfer equation by the heat conductive equation should give satisfactory results when $\lambda \approx 1$ and can lead to significant errors when $\lambda < 1$.

This conclusion is also valid in the cases of non-stationary radiative transfer in infinite three-dimensional media illuminated by planar or point sources. Let us give the expressions of the mean intensity and radiation flux in these cases (if one uses the Eddington approximation).

Let us consider an infinite medium illuminated by a momentary isotropic planar source which can be represented in the form of multiple isotropic point sources of luminosity L uniformly distributed on the plane $\tau = 0$ with a surface

Table 2: Values of $J_A(\tau,u)$, $J_D(\tau,u)$, $J_B(\tau,u)$ for $\lambda = 0.5$

	$\tau = 1$			$\tau = 10$		
u	$J_A(\tau,u)$	$J_D(\tau,u)$	$J_B(\tau,u)$	$J_A(\tau,u)$	$J_D(\tau,u)$	$J_B(\tau,u)$
I	5.50×10^{-2}	6.66×10^{-2}	3.32×10^{-2}	2.84×10^{-5}	1.19×10^{-12}	0
2	3.24×10^{-2}	3.24×10^{-2}	1.82×10^{-2}	3.82×10^{-5}	1.37×10^{-7}	0
3	1.88×10^{-2}	1.67×10^{-2}	1.01×10^{-2}	4.11×10^{-5}	4.37×10^{-6}	0
4	1.09×10^{-2}	8.96×10^{-3}	5.63×10^{-3}	3.91×10^{-5}	1.84×10^{-5}	0
5	6.30×10^{-3}	4.92×10^{-3}	3.18×10^{-3}	3.43×10^{-5}	3.49×10^{-5}	0
6	3.64×10^{-3}	2.75×10^{-3}	1.82×10^{-3}	2.84×10^{-5}	4.44×10^{-5}	0
7	2.11×10^{-3}	1.55×10^{-3}	1.04×10^{-3}	2.25×10^{-5}	4.53×10^{-5}	0
8	1.22×10^{-3}	8.85×10^{-4}	5.94×10^{-4}	1.73×10^{-5}	4.01×10^{-5}	0
9	7.08×10^{-4}	5.08×10^{-4}	3.43×10^{-4}	1.29×10^{-5}	3.25×10^{-5}	0
10	4.11×10^{-4}	2.93×10^{-4}	1.99×10^{-4}	9.37×10^{-6}	2.47×10^{-5}	7.78×10^{-5}
15	2.82×10^{-5}	1.98×10^{-5}	1.36×10^{-5}	1.51×10^{-6}	3.80×10^{-6}	6.95×10^{-6}
20	2.02×10^{-6}	1.41×10^{-6}	9.81×10^{-7}	1.90×10^{-7}	4.10×10^{-7}	5.79×10^{-7}
30	1.11×10^{-8}	7.81×10^{-9}	5.46×10^{-9}	2.09×10^{-9}	3.42×10^{-9}	3.78×10^{-9}
40	6.50×10^{-11}	4.57×10^{-11}	3.20×10^{-11}	1.81×10^{-11}	2.46×10^{-11}	2.41×10^{-11}
50	3.92×10^{-13}	2.76×10^{-13}	1.93×10^{-13}	1.40×10^{-13}	1.68×10^{-13}	1.54×10^{-13}
60	2.41×10^{-15}	1.70×10^{-15}	1.19×10^{-15}	1.02×10^{-15}	1.12×10^{-15}	9.82×10^{-16}
80	9.47×10^{-20}	6.68×10^{-20}	4.70×10^{-20}	4.99×10^{-20}	4.90×10^{-20}	4.06×10^{-20}
100	3.85×10^{-24}	2.71×10^{-24}	1.91×10^{-24}	2.32×10^{-24}	2.12×10^{-24}	1.70×10^{-24}

density of l and flashing at the initial moment of time ($u = 0$). Then, using the diffusion approximation, we have

$$J_D(\tau,u) = \frac{lL}{8\pi\sqrt{\pi}}\ \frac{\sqrt{3-x_1}}{\sqrt{u}}\ \exp\left(-\frac{(3-x_1)\,\tau^2}{4u}\right), \tag{22}$$

$$H_D(\tau,u) = \frac{lL}{4\sqrt{\pi}}\ \frac{\sqrt{3-x_1}}{u\sqrt{u}}\ |\tau|\ \exp\left(-\frac{(3-x_1)\,\tau^2}{4u}\right), \tag{23}$$

when $\tau \gg 1$, $1-\lambda \ll 1$, $u > \sqrt{3-x_1}\beta_2\tau$.

In the case of an infinite medium illuminated by a momentary point source of luminosity L we have

$$J_D(\tau,u) = \frac{L\alpha^2}{32\pi^2\sqrt{\pi}}\ \frac{(3-x_1)^{\frac{3}{2}}}{u\sqrt{u}} \exp\left(-\frac{(3-x_1)\,\tau^2}{4u}\right), \tag{24}$$

$$H_D(\tau,u) = \frac{L\alpha^2}{16\pi\sqrt{\pi}}\ \frac{(3-x_1)^{\frac{3}{2}}}{u^2\sqrt{u}}\ \tau\ \exp\left(-\frac{(3-x_1)\,\tau^2}{4u}\right), \tag{25}$$

when $\tau \gg 1$, $1-\lambda \ll 1$, $u > \sqrt{3-x_1}\beta_2\tau$.

Table 3: Values of $H_A(\tau,u)$, $H_D(\tau,u)$, $H_B(\tau,u)$ for $\lambda = 0.5$

	$\tau = 1$			$\tau = 10$		
u	$H_A(\tau,u)$	$H_D(\tau,u)$	$H_B(\tau,u)$	$H_A(\tau,u)$	$H_D(\tau,u)$	$H_B(\tau,u)$
I	8.69×10^{-2}	6.66×10^{-2}	7.38×10^{-3}	4.96×10^{-5}	1.19×10^{-11}	0
2	4.12×10^{-2}	1.62×10^{-2}	3.57×10^{-3}	6.18×10^{-5}	6.84×10^{-7}	0
3	1.96×10^{-2}	5.57×10^{-3}	1.75×10^{-3}	6.26×10^{-5}	1.46×10^{-5}	0
4	9.38×10^{-3}	2.24×10^{-3}	8.73×10^{-4}	5.64×10^{-5}	4.61×10^{-5}	0
5	4.52×10^{-3}	9.85×10^{-4}	4.41×10^{-4}	4.71×10^{-5}	6.98×10^{-5}	0
6	2.20×10^{-3}	4.58×10^{-4}	2.26×10^{-4}	3.73×10^{-5}	7.41×10^{-5}	0
7	1.08×10^{-3}	2.22×10^{-4}	1.17×10^{-4}	2.83×10^{-5}	6.47×10^{-5}	0
8	5.37×10^{-4}	1.11×10^{-4}	6.12×10^{-5}	2.08×10^{-5}	5.02×10^{-5}	0
9	2.69×10^{-4}	5.64×10^{-5}	3.24×10^{-5}	1.49×10^{-5}	3.61×10^{-5}	0
10	1.37×10^{-4}	2.93×10^{-5}	1.73×10^{-5}	1.04×10^{-5}	2.47×10^{-5}	8.64×10^{-5}
15	5.37×10^{-6}	1.32×10^{-6}	8.39×10^{-7}	1.41×10^{-6}	2.54×10^{-6}	4.78×10^{-6}
20	2.60×10^{-7}	7.07×10^{-8}	4.63×10^{-8}	1.52×10^{-7}	2.05×10^{-7}	2.91×10^{-7}
30	8.66×10^{-10}	2.60×10^{-10}	1.75×10^{-10}	1.27×10^{-9}	1.14×10^{-9}	1.25×10^{-9}
40	3.63×10^{-12}	1.14×10^{-12}	7.79×10^{-13}	8.74×10^{-12}	6.15×10^{-12}	5.60×10^{-12}
50	1.71×10^{-14}	5.51×10^{-15}	3.79×10^{-15}	5.57×10^{-14}	3.36×10^{-14}	3.04×10^{-14}
60	8.62×10^{-17}	2.83×10^{-17}	1.95×10^{-17}	3.43×10^{-16}	1.87×10^{-16}	1.62×10^{-19}
80	2.50×10^{-21}	8.35×10^{-22}	5.80×10^{-22}	1.27×10^{-20}	6.13×10^{-21}	5.04×10^{-21}
100	8.02×10^{-26}	2.71×10^{-26}	1.89×10^{-26}	4.71×10^{-25}	2.12×10^{-25}	1.63×10^{-25}

References

1. *V.V. Sobolev*, Astron. Zh., **29**, 406, 1952; *ibid.*, 517, 1952.
2. *V.V. Sobolev*, Transport of Radiant Energy in the Atmospheres of the Stars and Planets. Moscow: Gostekhizdat, 1956 (in Russian). Translated as A Treatise on Radiative Transfer, Princeton: Van Nostrand, 1963.
3. *I.N. Minin*, Vestn. Leningr. Univ., **19**, 124, 1962.
4. *I.N. Minin*, Theory of Radiative Transfer in Planetary Atmospheres, Moscow: Nauka, 1988 (in Russian).
5. *K.T. Compton*, Phil. Mag., **45**, 750, 1923.
6. *E.A. Milne*, J. London Math. Soc., **1**, 40, 1926.
7. *A.K. Kolesov, V.V. Sobolev*, Trudy Astron. Obs. Leningr. Univ., **43**, 5, 1991.

Some New Directions of Development of the Radiative Transfer Theory

A.G. Nikoghossian[1]

E-mail: *nikoghoss@yahoo.com*

It is shown that the problems of radiation transfer in homogeneous plane-parallel atmospheres admit a variational formulation, the equation of transfer then being the Euler–Lagrange equation and the known quadratic and bilinear relations being the conservation law due to form-invariance of the suitable Lagrangian. A group of transfer problems is revealed which are reducible to the source-free problem. We present a group-theoretical description of radiation transfer in inhomogeneous and multi-component atmospheres with plane-parallel geometry. The concept of composition groups is introduced for the media with different optical and physical properties. The group representations are derived for two possible cases of illumination of a composite finite atmosphere from outside. An algorithm for determining the global optical characteristics (reflectance and transmittance) of inhomogeneous and multi-component atmospheres is given. The group theory approach is also applied to determine the field of radiation inside the inhomogeneous atmosphere. The concept of a group of optical depth translations is introduced. The developed theory is illustrated with the problem of radiation diffusion with partial frequency distribution for the case where the inhomogeneity of the medium is due to the depth-variation of the scattering coefficient. It is shown that once reflectance and transmittance of a medium is determined, the internal field of radiation in the source-free atmosphere is found without solving any new equations.

1 Introduction

The research on the theory of radiative transfer carried out in recent two decades in Byurakan observatory develops Ambartsumian's ideas concerning the laws of addition of layers [1, 2] and the principle of invariance [2, 3, 4]. Being of importance for analytical theory itself, new results allow elaborating efficient computational schemes for various astrophysical applications involving radiation transfer in inhomogeneous absorbing and scattering atmospheres. In this context there is a need to define their place and importance in the modern transfer theory.

The report considers results obtained in two directions, the first of which concerns the variational formulation of radiation transfer problems in a plane-parallel homogeneous atmosphere.

[1] Byurakan Astrophysical Observatory, Armenia

V. Grinin et al. (eds) Radiation mechanisms of astrophysical objects. Yerevan: Edit Print, 2017, pp. 51–63.

2 Lagrangian formalism

Before turning to immediate description of the variational or Lagrangian approach to radiative transfer problems we will briefly dwell on premises of this research. The fact is that although Ambartsumian's principle of invariance has been known for a long time, but its physical meaning remained obscure. In particular, it was unclear what are the limits of applicability and efficiency of the principle. The second point concerns Rybicki's work [5], where some quadratic integrals of the transfer equation were derived referred by him to as Q- and R-integrals. He supposed that these integrals are possibly related with the principle of invariance. In some problems they lead to non-linear relations linking to each other some characteristics of the radiation field in the atmosphere. Further generalization of Rybicki's results for monochromatic and isotropic scattering in a plane-parallel medium was given in [6, 7], where new sorts of relations were obtained referred to as bilinear and two-point bilinear relations, which couple the radiation fields at different depths of a given atmosphere as well as the radiation fields in different atmospheres.

In frameworks of variational formalism we developed the equations of transfer are proved to be none the other than the Euler-Lagrange equations and the non-linear Q-relations are the conservation laws due to form-invariance of the suitable Lagrangian. In fact, a single functional comprises all the information on features of the problem and allows a systematic connection between symmetries and conservation laws. Being the first integrals of the Euler–Lagrange equation, this laws may facilitate the solution of the problem under consideration and contribute to its interpretation.

To demonstrate the approach, we write the transfer equations in terms of the function Y having the following probabilistic meaning: it characterizes the probability of the photon exit from atmosphere in the direction μ, if originally it was moving at depth τ with the directional cosine η.

We have

$$\pm\frac{dY(\tau,\pm\eta,\mu)}{d\tau} = -Y(\tau,\pm\eta,\mu) + \frac{\lambda}{2}\int_{-1}^{1} Y(\tau,\pm\eta',\mu)d\eta', \tag{1}$$

where λ is the scattering coefficient. The Lagrangian density L corresponding to Eq. (1) was obtained in [8]

$$L(\Phi,\Phi',\tau,\eta,\mu) = \Phi^2 + (\eta\Phi')^2 - 2\Phi U, \tag{2}$$

where we introduced notations

$$\Phi(\tau,\eta,\mu) = Y(\tau,\eta,\mu) + Y(\tau,-\eta,\mu), \qquad U(\tau,\mu) = \frac{\lambda}{2}\int_0^1 \Phi(\tau,\eta',\mu)d\eta'. \tag{3}$$

In accordance with the results of [8], the Euler–Lagrange equation has a form

$$\frac{\partial L}{\partial\Phi} - \frac{d}{d\tau}\frac{\partial L}{\partial\Phi'} + \lambda\int_0^1 \frac{\partial L}{\partial U}d\eta' = 0. \tag{4}$$

One will make sure that insertion of the Lagrangian (2) into Eq. (4) yields the transfer equation (1). It is important that both the transfer equation (1) and the Lagrangian density (2) do not depend explicitly on τ, or stated differently, they are form-invariant under infinitesimal transformation of the optical depth.

This implies that the transformation (or translation) of the optical depth is the symmetry transformation for the system (1). The derivation of conservation laws from direct study of the variational integral is based on Noether's theorem (see, for instance, [9]), which was generalized in [10] to encompass the integro-differential equations. For the problem under consideration, it suggests a conservation law as follows:

$$\int_0^1 \left[L - \frac{\partial L}{\partial \Phi} \Phi' \right] d\eta = const, \tag{5}$$

which, in view of Eq. (2), takes a form

$$\int_0^1 Y(\tau, \zeta, \mu)\, Y(\tau, -\zeta, \mu) d\zeta = \frac{\lambda}{4} \left(\int_{-1}^1 Y(\tau, \zeta, \mu) d\zeta \right)^2 + const. \tag{6}$$

This relation is, in essence, a prototype of the Q-integral obtained by Rybicki [5]. The above considerations imply that by its content the integral (6) is an analog of the momentum conservation law in mechanics and is due to the axes translation transformation. It holds everywhere where λ does not vary with depth.

The variational formalism allows one not only to elucidate the physical meaning of invariance principle but enables to derive along with many known results a great number of new relations of great importance for the theory and applications. It allows one also to find out some statistical characteristics of the diffusion process in the atmosphere [7, 11]. Some of the known non-linear relations possess a fairly obvious physical or/and probabilistic meaning and can be written immediately on the base of simple arguments.

This approach reveals a group of common radiation transfer problems of astrophysical interest which admit quadratic and bilinear integrals. All of them can be reduced to the source-free problem. This group of problems referred to as RSF-problems includes Milne's problem, the problem of diffuse reflection (and transmission in the case of the atmosphere of finite optical thickness) as well as problems with exponential and polynomial laws for the distribution of internal energy sources. The group problems are characterized at least by three features. First of all, the invariance principle implies bilinear relations connecting the solutions of the listed problems. It was shown in [12] that the group of the RSF-problems admits a class of integrals involving quadratic and bilinear moments of the intensity of arbitrarily high orders. Secondly, if the problem can be formulated for finite atmosphere then the principle allows connecting its solution with that of the proper problem for a semi-infinite atmosphere. Finally, knowledge of the

Ambartsumian φ-function reduces their solutions to the Volterra-type equations for the source function with the kernel-function

$$L(\tau) = \frac{\lambda}{2} \int_0^1 \varphi(\zeta) e^{-\frac{\tau}{\zeta}} \frac{d\varphi}{\zeta}. \tag{7}$$

While the variational approach is widely used in various branches of theoretical physics, it was not the case in the field of the radiative transfer theory, with the only exception being the paper of Anderson [8] who established the conservation law suitable for the case of non-isotropic scattering. We used the results of the rigorous mathematical theory in applying the Lagrangian formalism to the one-dimensional transfer problem [13].

3 Group-theoretical description of radiative transfer in inhomogeneous atmospheres

The next topic of the report concerns application of the group theory to solve the radiative transfer problems in inhomogeneous atmospheres under general assumptions on the frequency-angle distribution of the radiation field, the elementary event of scattering and properties of the medium. As we shall see, the theory we put forward can be regarded as a further extension of the layers adding method proposed first by Ambartsumian [1, 2] for one-dimensional homogeneous media and generalized by Nikoghossian [14, 15] over the case of inhomogeneous media. We remind that the method establishes summation laws for global optical properties of absorbing and scattering media (reflectance and transmittance), which express these properties of the combined medium through similar properties of its components. Of special interest is the particular limiting case of this method when optical thickness of one of the added components tends to zero. This allows one to find the global optical characteristics of a medium simultaneously for a family of the media of different thicknesses. This branch of the theory was developed by Bellman and his co-authors (see, e.g., [16, 17]) and is known as "invariant imbedding".

3.1 Composition groups

We start with considering the amalgamation procedure of the plane-parallel absorbing and scattering inhomogeneous media. It is assumed that the added components do not contain primary energy sources and are allowed to differ one from the other not only by optical thicknesses, but also by the nature of inhomogeneity. By inhomogeneity we mean that each of the physical parameters specifying the elementary event of scattering or physical state of the medium may vary with depth. Of them we note the profile of the absorption coefficient, the quantum scattering (or destruction) coefficient, Voigt's parameter, the phase function, the frequency redistribution function, the Stokes parameters in the case of polarized radiation, the correlation length for turbulent media, and

so on. However, in illustrating the approach, we restrict ourselves by treating the 1D transfer problem for the case of partial redistribution over frequencies by assuming that the only variable parameter is the scattering coefficient.

Now we introduce the concept of composition or transformation of scattering and absorbing inhomogeneous media, which refers to the addition of a new medium to the initial one. The transformations induced in this way form a group if under the group product (binary operation) one takes the resultant of two successive transformations. It is remarkable that this definition does not specify the nature of inhomogeneity of added media. It is easily seen that all the required conditions for forming a group are satisfied. In particular, the role of the unit element is played by the identity transformation, which leaves the initial medium unchanged, and the inverse element is the transformation which reverses the effect of the already performed transformation. The associativity of the group product is obvious. We refer to this group of transformations as the GN(2,C) group, which, evidently, is not commutative. As a result of the described compositions, one can construct different atmospheres composed of inhomogeneous components.

Of special interest is one of subgroups of the introduced group which describes the case when the added media are homogeneous. The components of such a composite atmosphere may differ from each other not only by optical thicknesses but also by any characteristics of the radiation diffusion in them. Such groups, referred nominally to as GNH(2,C), are two-, three- and multi-parameter dependent on the number of parameters changing in passing from one component to another. The groups of these types are infinite and non-commutative. They can serve as archetypes for a number of real radiating media of astrophysical importance. Finally, of independent interest is the narrower subgroup of the introduced two groups which involves compositions of homogeneous media with identical physical properties but, in general, of different optical thicknesses. These compositions obviously yield homogeneous medium. This one-parameter group, we call it GH(2,C), is infinite and commutative, i.e., Abelian [18]. It becomes continuous when the only parameter, optical thickness, varies continuously.

3.2 The group representations

In order to find the representations of introduced groups, consider a composite atmosphere consisted of two layers, which generally differ in both the optical thickness and functional behavior of parameters specifying the elementary event of scattering (Fig. 1). This means that both components are inhomogeneous and possess the property of polarity [14]. The scattering in the media is supposed occurring with redistribution over directions and frequencies so that the optical characteristics of media may be presented in the operator-matrix form with the matrix elements possessing probabilistic meaning (throughout the paper we use the probability language). They describe the angle and/or frequency dependent probabilities of a single event of reflection and transmission. Having in mind

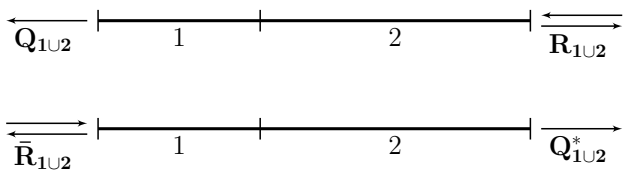

Figure 1: Reflection and transmission by inhomogeneous atmosphere.

the polarity property of inhomogeneous media, we introduce the notations $\mathbf{R}_i$, $\mathbf{Q}_i$ and $\bar{\mathbf{R}}_i$, $\bar{\mathbf{Q}}_i$ $(i = 1, 2)$ for the reflection and transmission coefficients of the components of a composite medium illuminated correspondingly from the right and left. In accordance with the principle of reversibility of optical phenomena, $\bar{\mathbf{Q}}_i = \mathbf{Q}_i^*$, where the transposed matrix is supplied by asterisk. Everywhere below we follow the designation $\mathbf{Q}_i^*$. An important role in this research belongs to the inverse of the transmittance matrix $\mathbf{P} = \mathbf{Q}^{-1}$ and the other three combined matrices $\mathbf{S} = \mathbf{RP}$, $\bar{\mathbf{S}} = \mathbf{P}\bar{\mathbf{R}}$, $\mathbf{M} = \mathbf{Q}^* - \mathbf{S}\bar{\mathbf{R}}$. These four matrices provide a complete description of the optical properties of an inhomogeneous absorbing and scattering medium independent of that what of its boundaries is illuminated from outside.

Let us treat now the transfer of radiation through composite medium when a photon falls on its right boundary (top drawing in Fig. 1). Taking account of possibility of multiple reflections between components of the medium, one can derive the following two relations (see [19]):

$$\mathbf{P}_{1\cup 2} = \mathbf{P}_2\mathbf{P}_1 - \bar{\mathbf{S}}_2\mathbf{S}_1, \tag{8}$$

$$\mathbf{S}_{1\cup 2} = \mathbf{S}_2\mathbf{P}_1 + \mathbf{M}_2\mathbf{S}_1, \tag{9}$$

where the quantities pertaining to composite medium are indexing with $1 \cup 2$.

Taking together, relations (8) and (9) can be presented in the more convenient compact form

$$\begin{pmatrix} \mathbf{P}_{1\cup 2} \\ \mathbf{S}_{1\cup 2} \end{pmatrix} = \begin{pmatrix} \mathbf{P}_2 & -\bar{\mathbf{S}}_2 \\ \mathbf{S}_2 & \mathbf{M}_2 \end{pmatrix} \begin{pmatrix} \mathbf{P}_1 \\ \mathbf{S}_1 \end{pmatrix}, \tag{10}$$

where we used the concepts of supervector and supermatrix [18, 20, 21]. The supermatrix entering in Eq. (10) is denoted by $\tilde{\mathbf{A}}$ (hereafter the supermatrices are supplied by tilde)

$$\tilde{\mathbf{A}} = \begin{pmatrix} \mathbf{P} & -\bar{\mathbf{S}} \\ \mathbf{S} & \mathbf{M} \end{pmatrix}. \tag{11}$$

The set of matrices $\tilde{\mathbf{A}}$ is the first of representations of the group of compositions GN(2,C) which also is a group (we denote it by g) and provides a one-to-one mapping of GN(2,C) to supervector space, i.e., the group product of two transformations $g_1 \bigotimes g_2$, corresponds to $\tilde{\mathbf{A}}_{1\cup 2} = \tilde{\mathbf{A}}_1\tilde{\mathbf{A}}_2$, or for representations $\Im(g_1 \bigotimes g_2) = \Im(g_1)\Im(g_2)$ (isomorphism). On the hand, the supermatrix $\tilde{\mathbf{A}}$ can be regarded as an operator mapping one supervector space to another one.

It is natural to refer nominally to this supermatrix as "composer". It plays an important role in the developed theory.

It is easy to see that the transformation realizing by $\tilde{\mathbf{A}}$ provides determination of optical properties of the composed medium partially, namely, only those for the right-hand side illumination. For complete description of optical properties of the composite medium, we need the matrices $\bar{\mathbf{S}}$ and $\mathbf{M}$ which obey the following transformations [19]:

$$\bar{\mathbf{S}}_{1\cup 2} = \mathbf{P}_2\bar{\mathbf{S}}_1 + \bar{\mathbf{S}}_2\mathbf{M}_1, \qquad \mathbf{M}_{1\cup 2} = \mathbf{M}_2\mathbf{M}_1 - \mathbf{S}_2\bar{\mathbf{S}}_1. \tag{12}$$

Note that these relations could be derived directly.

In the matrix-operator form they read

$$\begin{pmatrix} \mathbf{M}_{1\cup 2} \\ \mathbf{S}_{1\cup 2} \end{pmatrix} = \begin{pmatrix} \mathbf{M}_2 & -\mathbf{S}_2 \\ \bar{\mathbf{S}}_2 & \mathbf{P}_2 \end{pmatrix} \begin{pmatrix} \mathbf{M}_1 \\ \bar{\mathbf{S}}_1 \end{pmatrix}. \tag{13}$$

Thus, we are led to an alternative group of representations given by the supermatrix

$$\tilde{\mathbf{B}} = \begin{pmatrix} \mathbf{M} & -\mathbf{S} \\ \bar{\mathbf{S}} & \mathbf{P} \end{pmatrix}, \tag{14}$$

which we denote by $\bar{\Im}(g)$. It is evident that this group also is isomorphic to the group of compositions GN(2,C) and together with $\Im(g)$ gives a complete description of optical properties of the composite atmosphere illuminated from the right. In both cases the identity transformation is given by the supermatrix

$$\tilde{\mathbf{E}} = \begin{pmatrix} \mathbf{I} & \mathbf{0} \\ \mathbf{0} & \mathbf{I} \end{pmatrix}, \tag{15}$$

where $\mathbf{I}$ is the unit matrix. The supermatrices $\tilde{\mathbf{A}}$, $\tilde{\mathbf{B}}$ are non-degenerate, and two-sided inverse matrices exist with superdeterminant [21, 22, 23] equaled to one (see [19]).

By introducing the four-dimensional supervector $\tilde{\mathbf{Y}}$ with the components $(\mathbf{P}, \mathbf{S}, \mathbf{M}, \bar{\mathbf{S}})$, the group representations $\Im(g)$, $\bar{\Im}(g)$ can be joined and presented as a reducible representation

$$\tilde{\mathbf{Y}}_{1\cup 2} = \tilde{\mathbf{\Psi}}_2\tilde{\mathbf{Y}}_1, \tag{16}$$

where

$$\tilde{\mathbf{\Psi}} = \begin{pmatrix} \mathbf{P} & -\bar{\mathbf{S}} & \mathbf{0} & \mathbf{0} \\ \mathbf{S} & \mathbf{M} & \mathbf{0} & \mathbf{0} \\ \mathbf{0} & \mathbf{0} & \mathbf{M} & -\mathbf{S} \\ \mathbf{0} & \mathbf{0} & \bar{\mathbf{S}} & \mathbf{P} \end{pmatrix}. \tag{17}$$

We conclude that, given the optical properties of the component layers, the common matrix multiplications allow one to determine these properties for the compound atmosphere. If the atmosphere is homogeneous one can restrict oneself by transformation Eq. (10). Arguments analogous to those above in deriving Eq. (17) allow one to derive adding laws for the case when the composite atmosphere is illuminated from the side of the left boundary (bottom drawing in Fig. 1) [19].

3.3 The 1D source-free problem for partial redistribution over frequencies

Consider a subgroup of the composition group GNH(2,C) subjected to the only condition that the optical thickness of the medium obtained as a result of compositions must not exceed some presetting value of τ_0. When the optical thickness varies continuously, this infinite group is obviously continuous. Then this group together with its representation $\Im(g)$ are one-dimensional Lie groups [21, 22, 23]. With help of compositions of this groups one can construct a multi-component atmosphere with components which generally can differ one from the other by their physical characteristics.

As an example, let us treat the matrix problem of radiation diffusion in a one-dimensional inhomogeneous atmosphere illuminated from the boundary $\tau = \tau_0$ when the scattering obeys the angle averaged law of partial redistribution over frequencies. Suppose that the atmosphere consists of components of equal and sufficiently small thickness characterized by some constant values of the scattering coefficient λ, so that in the limit of the components thicknesses tending to zero it might be regarded as a continuous function of the optical depth.

The infinitesimal operator of this group of compositions at τ_0 can be represented in the form

$$\tilde{\mathbf{\Xi}}(\tau_0) = \lim_{\Delta\tau_0 \to 0} \frac{\widetilde{\mathbf{A}}(\tau_0 + \Delta\tau_0) - \widetilde{\mathbf{A}}(\tau_0)}{\Delta\tau_0} = \begin{pmatrix} \mathbf{m}(\tau_0) & -\mathbf{n}(\tau_0) \\ \mathbf{n}(\tau_0) & -\mathbf{m}(\tau_0) \end{pmatrix}, \tag{18}$$

where

$$\mathbf{m}(\tau_0) = \alpha - \mathbf{n}(\tau_0), \qquad \mathbf{n}(\tau_0) = \frac{\lambda(\tau_0)}{2}\mathbf{\Gamma}. \tag{19}$$

Here α and $\mathbf{\Gamma}$ are the discrete analogs correspondingly of the profile of the absorption coefficient and the law of the frequency redistribution [24]. For the sake of simplicity, they are supposed to be independent of depth. Evidently, $\mathbf{\Gamma}$ is a symmetric matrix and α is a diagonal matrix with the elements $\alpha_i = \alpha(x_i)$.

Transformation (8) implies [25]

$$\frac{d\mathbf{P}}{d\tau_0} = \mathbf{m}(\tau_0)\,\mathbf{P}(\tau_0) - \mathbf{n}(\tau_0)\,\mathbf{S}(\tau_0), \tag{20}$$

$$\frac{d\mathbf{S}}{d\tau_0} = \mathbf{n}(\tau_0)\,\mathbf{P}(\tau_0) - \mathbf{m}(\tau_0)\,\mathbf{S}(\tau_0), \tag{21}$$

with the initial conditions $\mathbf{P}(0) = \mathbf{I}$, $\mathbf{S}(0) = \mathbf{0}$, where $\mathbf{0}$ is the null matrix.

Inversion of the matrix $\mathbf{P}(\tau_0)$ found from the set of equations (20) and (21) allows one to determine the requisite values of the medium reflectance and transmittance. Analogously, by using the infinitesimal operator of the supermatrix $\tilde{\mathbf{B}}$ and Eq. (14), we are led to a new set of the matrix differential equations

$$\frac{d\mathbf{M}}{d\tau_0} = -\mathbf{m}(\tau_0)\,\mathbf{M}(\tau_0) - \mathbf{n}(\tau_0)\,\bar{\mathbf{S}}(\tau_0), \tag{22}$$

$$\frac{d\bar{\mathbf{S}}}{d\tau_0} = \mathbf{n}(\tau_0)\,\mathbf{M}(\tau_0) + \mathbf{m}(\tau_0)\,\bar{\mathbf{S}}(\tau_0), \tag{23}$$

with the initial conditions $\mathbf{M}(0) = \mathbf{I}$, $\bar{\mathbf{S}}(0) = \mathbf{0}$.

In the case of homogeneous atmosphere one can restrict oneself to solving the set of equations (20)–(21). Its solution can be presented in the form of the matrix exponential [25]. Note that from the sets of equations (20)–(23) one can derive separate matrix differential equations of the second order for unknown matrix-functions as it is the case in the scalar case [25].

Equations obtained with the group approach exhibit intimate connection between the group approach and the method of invariant imbedding [16, 17]. As a matter of fact, the invariant imbedding technique is equivalent to action of infinitesimal operators of the proper group representations introduced in the paper. For homogeneous atmosphere, the obtained equations admit invariants or conservation laws, the continual analogs of which were obtained in the mentioned papers [7, 8, 25, 26].

The efficiency of the developed theory becomes especially discernible when solving radiative transfer problems for atmospheres with a complex multi-layer structure. In applying any of the introduced composers, one needs to predetermine the global optical properties of each of the layers added to the boundary $\tau = \tau_0$, namely, the matrices $\mathbf{P}$, $\mathbf{S} = \mathbf{RP}$, $\bar{\mathbf{S}} = \mathbf{P}\bar{\mathbf{R}}$ and $\mathbf{M} = \mathbf{Q}^* - \mathbf{S}\bar{\mathbf{R}} = \mathbf{Q}^* - \mathbf{R}\bar{\mathbf{S}}$, i.e., the triad of matrices $\mathbf{R}$, $\bar{\mathbf{R}}$, $\mathbf{Q}$. The problem is simpler when the components are homogeneous. Particularly, in the scalar problems these quantities are determined analytically. In the general case of inhomogeneous components, we can turn to solutions of the systems of equations (20)–(23) with subsequent inversion of the matrix $\mathbf{P}$. This route is preferable in finding the field of radiation inside the medium to be discussed below. However, there exists an alternative way of determining the required optical properties by solving basic differential equations obtained in [12, 27], which are easily realizable initial-value problems.

Thus, the algorithm of solution of the transfer problem in the most general case of multi-component atmosphere is as follows. One starts with finding the reflectance and transmittance of the layers to be added by using one of the routes described above. Further, the compositions transformations are continued until the optical thickness of the composite atmosphere specified by the problem formulation is attained. Inversion of the matrix $\mathbf{P}(\tau_0)$ allows one to find $\mathbf{Q}(\tau_0)$ what, in its turn, determines other properties of the composite atmosphere. We shall see below that the obtained quantities are sufficient to find the field of radiation inside the medium.

In the special case when the supplemented layers are homogeneous and possess similar properties, we deal with the cyclic group and the composition process reduces to the action of powers of corresponding operators ($\tilde{\mathbf{A}}^n$, for instance). This naturally reduces the volume of computations to a great extent.

3.4 Radiation field inside the medium

The goal we pursue in this section is to extend the group theory approach over the field of radiation inside inhomogeneous media. Consider a plane-parallel inhomogeneous atmosphere of optical thickness τ_0, the boundary $\tau = \tau_0$ of which is illuminated from outside (Fig. 2). Light scattering is generally assumed occurring with the angle and frequency redistribution. The internal field of radiation we assign by the matrices $\mathbf{U}(\tau, \tau_0)$ and $\mathbf{V}(\tau, \tau_0)$, which specify the probabilities that the quantum with the angle-frequency characteristics (η, x) falling on the boundary $\tau = \tau_0$, will be found, as a result of diffusion in the medium, at the depth τ moving correspondingly to the boundaries $\tau = 0$, and $\tau = \tau_0$, generally with some other characteristics (η', x').

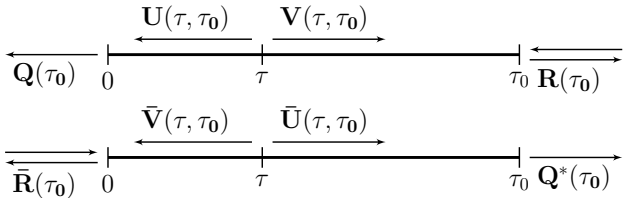

Figure 2: Description of the radiation field inside the inhomogeneous atmosphere.

Let us treat now the procedure of transition from one optical depth to another one by supplementing a new layer. The infinite set of such transitions obviously composes a group if the group product is defined as the result of two subsequent transitions. One can easily check that all the group postulates are satisfied. In accordance with the physics of the problem, the resulting value of the optical depth should not exceed the optical thickness of the medium $\tau \leq \tau_0$. This group is a subgroup of the group GN(2,C) and is equivalent to the similar subgroup considered in the preceding sections for composition of different media.

Taking into account the probability meaning of matrices $\mathbf{U}(\tau, \tau_0)$ and $\mathbf{V}(\tau, \tau_0)$, one can write

$$\mathbf{Q}(\tau_0) = \mathbf{Q}(\tau)\,\mathbf{U}(\tau, \tau_0), \quad \mathbf{V}(\tau, \tau_0) = \mathbf{R}(\tau)\,\mathbf{U}(\tau, \tau_0), \tag{24}$$

hence

$$\mathbf{U}(\tau, \tau_0) = \mathbf{P}(\tau)\,\mathbf{Q}(\tau_0), \quad \mathbf{V}(\tau, \tau_0) = \mathbf{S}(\tau)\,\mathbf{Q}(\tau_0). \tag{25}$$

The fact of separation of arguments in $\mathbf{U}(\tau, \tau_0)$ and $\mathbf{V}(\tau, \tau_0)$ is one of advantages of the applied approach. Equations (24) imply that the subgroup of representation $\Im(g)$ relevant to the media compositions group may be now regarded as representation of the depth-translation group.

Indeed, on the base of Eq. (10), one may write

$$\begin{pmatrix} \mathbf{U}(\tau + \delta\tau, \tau_0) \\ \mathbf{V}(\tau + \delta\tau, \tau_0) \end{pmatrix} = \begin{pmatrix} \mathbf{P}_\tau(\delta\tau) & -\bar{\mathbf{S}}_\tau(\delta\tau) \\ \mathbf{S}_\tau(\delta\tau) & \mathbf{M}_\tau(\delta\tau) \end{pmatrix} \begin{pmatrix} \mathbf{U}(\tau, \tau_0) \\ \mathbf{V}(\tau, \tau_0) \end{pmatrix}, \tag{26}$$

where $\delta\tau$ is an increment to the optical depth τ. The subscript τ indicates that the internal physical properties of supplemented layer are relevant to (or vary in) the interval $(\tau, \tau + \delta\tau)$.

Thus, the supermatrix $\tilde{\mathbf{A}}$ plays an important role not only in adding the media of different optical thicknesses but also in translating optical depths inside inhomogeneous atmosphere. Stating differently, it serves at the same time as "composer" of inhomogeneous atmospheres and as "translator" in transitions between optical depths inside the atmosphere. It is noteworthy that in the latter case only the global optical properties of the incremented layer provide the transformations. The internal physical characteristics do not take an immediate part in these transformations, so that the nature of inhomogeneity in different media or layers are allowed to be different.

To illustrate the obtained results, let us return to the matrix case of the transfer problem treated in Section 3.3, where we confined ourselves to the global optical characteristics of the medium. Our immediate objective now is to find the field of radiation inside the medium, where, again, the only parameter varying with depth is the scattering coefficient λ. In light of that said in Sect. 3.3, we conclude that the depth-translation group together with its representation are the Lie groups of the one-dimension.

Given the supermatrix (18), the transformation (26) leads to the customary differential equations of radiation transfer for the operator-functions $\mathbf{U}$ and $\mathbf{V}$

$$\frac{d\mathbf{U}}{d\tau_0} = \mathbf{m}(\tau)\,\mathbf{U}(\tau,\tau_0) - \mathbf{n}(\tau)\,\mathbf{V}(\tau,\tau_0), \tag{27}$$

$$\frac{d\mathbf{V}}{d\tau_0} = \mathbf{n}(\tau)\,\mathbf{U}(\tau,\tau_0) - \mathbf{m}(\tau)\,\mathbf{V}(\tau,\tau_0). \tag{28}$$

In place of the usual boundary conditions, one can now adopt the conditions at $\tau = \tau_0$, $\mathbf{U}(0,\tau_0) = \mathbf{Q}(\tau_0)$, $\mathbf{V}(0,\tau_0) = \mathbf{0}$, then reducing the problem to that with initial conditions. Derivation of the transfer equations (27)–(28) on the base of physical reasoning is straightforward, what is usually doing in the classical astrophysical literature. As it was shown, the operator-functions $\mathbf{P}(\tau)$ and $\mathbf{S}(\tau)$ satisfy the same set of equations (20)–(21) with the initial conditions $\mathbf{P}(0) = \mathbf{I}$, $\mathbf{S}(0) = \mathbf{0}$. By comparing the initial conditions of these two sets of equations, we are led to relations (24) written above on the base of probabilistic reasoning [26].

Bearing in mind the computations described in Section 3.4 for the composite inhomogeneous atmosphere as well as the equivalence of the medium-composition and the depth-translation subgroups of GNH(2,C), we arrive at an important conclusion that the internal field of radiation now can be found without solving any new equations. Indeed, it is sufficient to this end to multiply the obtained value of $\mathbf{Q}(\tau_0)$ by $\mathbf{P}$ and $\mathbf{S}$ found above in intermediate calculations in constructing the atmosphere under study.

The far reaching analogy between media composition and depths translation groups makes it possible to transfer different results obtained for global optical

properties of an atmosphere to quantities determining the internal field of radiation. For instance, if the atmosphere is homogeneous, one can derive conservation laws in terms of **U** and **V**, as it was done above for the matrices **P** and **S**. We do not deal with it here but refer the interested reader after continual analogs of these laws to [7, 26].

4 Conclusions

We discussed two directions of further development of the radiation transfer theory which, in our opinion, are promising from both the analytical and computational points of view. They generalize Ambartsumian's ideas concerning the principle of invariance and the layers adding laws. The variational approach allows one to reveal the physical nature and the scope of applicability of invariance principle. It is important that the solutions of some standard problems of astrophysical interest mathematically are reducible to the Volterra type integral equations.

The second direction concerns the group theory which is applied to solve the problems of radiative transfer in inhomogeneous absorbing and scattering atmospheres. The media composition groups and their representations introduced in the paper generalize the layers adding approach, which now covers inhomogeneous, particularly multi-component, atmospheres with allowance of the angle and frequency distribution of the radiation field. The group representations being expressed in terms of some combined discrete quantities allow one to find the most general summation laws for reflectance and transmittance of the plane-parallel media.

Employment of infinitesimal operators of the introduced groups makes it possible to establish the close connection of the introduced groups with the classical transfer equations and the equations ensuing from invariant imbedding. In fact, the first of them are connected with the depth translation groups, while the second – with composition groups for the media of different optical thicknesses.

An important result in considering the internal field of radiation is the separation of variables of the optical depth and thickness in the expression of quantities describing the optical properties. This implies that the introduced group of the optical depths translations is a subgroup of the group of the media compositions. In its turn, this means that after finding the reflectance and transmittance of an atmosphere, there is no need to solve any new equations to determine the internal field of radiation in the source-free atmosphere.

The theory we put forward is of sufficiently great generality since it does not depend on the nature of inhomogeneity of the media as well as on the angle and frequency distribution of the radiation field.

References

1. *V.A. Ambartsumian*, Izv. Acad. Nauk Arm. SSR, No. 1-2, 31, 1944.
2. *V.A. Ambartsumian*, Scientific Papers, vol. 1. Yerevan: Izd. Acad. Nauk Arm. SSR, 1960 (in Russian).

3. *V.A. Ambartsumian*, Dokl. Acad. Nauk SSSR, **38**, 257, 1943.
4. *V.A. Ambartsumian*, Ann. Rev. Astron. Astrophys., **18**, 1, 1980.
5. *G.B. Rybicky*, Astrophys. J., **213**, 165, 1977.
6. *V.V. Ivanov*, Astron. Zh., **23**, 612, 1978.
7. *A.G. Nikoghossian*, Astrophys. J., **483**, 849, 1977.
8. *D. Anderson*, Inst. Math. Applic., **12**, 551, 1973.
9. *I.M. Gelfand, S.V. Fomin*, Calculus of Variations. Englewood Cliffs: Prentice-Hall, 1965.
10. *M. Tavel*, Transp. Theory Stat. Phys., **1**, 271, 1971.
11. *A.G. Nikoghossian*, Astrophys., **43**, 337, 2000.
12. *A.G. Nikoghossian*, Light Scattering Reviews, **8**, 377, 2013.
13. *R.A. Krikorian, A.G. Nikoghossian*, J. Quant. Spectrosc. Rad. Transf., **56**, 465, 1996.
14. *A.G. Nikoghossian*, Astron. Astrophys., **422**, 1059, 2004.
15. *A.G. Nikoghossian*, Astrophys., **47**, 248, 2004.
16. *R. Bellman, G.M. Wing*, An Introduction to Invariant Imbedding. New York: Wiley, 1973.
17. *J. Casti, R. Kalaba*, Imbedding Methods in Applied Mathematics. Reading: Addison-Wesley, 1973.
18. *E. Wigner*, Group Theory. New York: Academic Press, 1959.
19. *A.G. Nikoghossian*, Astrophys., **57**, 272, 2014.
20. *R. Bellman*, Introduction to Matrix Analysis. New York: Mcgraw-Hill, 1960.
21. *F.A. Berezin*, The Method of Second Quantization. Boston: Academic Press, 1965.
22. *J.-Q. Chen, J. Ping, F. Wang*, Group Representation Theory for Physicists. Singapore: World Scientific, 2002.
23. *V. Heine*, Group Theory in Quantum Mechanics. Oxford: Pergamon Press, 1960.
24. *D. Mihalas*, Stellar Atmospheres. San Francisco: Freeman and Co., 1970.
25. *A.G. Nikoghossian*, Astrophys., **54**, 553, 2011.
26. *A.G. Nikoghossian*, J. Quant. Spectrosc. Rad. Transf., **61**, 345, 1999.
27. *A.G. Nikoghossian*, Astrophys., **55**, 261, 2012.

On the Linear Properties of the Nonlinear Problem of Radiative Transfer

H.V. Pikichyan[1]

E-mail: *hovpik@gmail.com*

We address the nonlinear problem of reflection/transmission of radiation from an anisotropic scattering/absorbing one-dimensional medium of finite geometrical thickness, when both of its boundaries are illuminated by intense monochromatic radiative beams. The new conceptual element of so-called "linear images" is noteworthy, which admits a probabilistic interpretation. The solution of nonlinear problem of reflection/transmission of radiation is reduced to a linear combination of linear images. They describe the reflectivity and transmittance of the medium for a single photon or their beam of unit intensity, incident on one of the boundaries of the layer, when the medium in real regime is still under the bilateral illumination by external exciting radiation of arbitrary intensity. To determine the linear images, we exploit three well known methods: (i) adding of layers, (ii) its limiting form described by differential equations of invariant imbedding, and (iii) a transition to the so-called functional equations of Ambartsumyan's "complete invariance".

1 Introduction

In linear problem of transfer of radiation energy, the resulting characteristics of the radiation field are formed in the process of multiple interactions of radiation with matter, when the physical properties of the medium are assumed to be unchanged. The very complexity of nonlinear problem, in contrast, is the functional dependence of the scattering/absorbing properties of each elementary volume $\Delta \to 0$ on the intensity of radiation incident on it from all sides. The characteristics of the diffusing in medium radiation field and the physical state of the medium itself are forming each other reciprocally, in a self-consistent manner.

It is well known that in the linear case, the solution of the problem of reflection-transmission (PRT) of radiation, i.e. seeking the intensities $u_L^{\pm}(x, y)$ of emerging radiation from the right "+" and left "−" boundaries of the anisotropic medium (of finite geometrical thickness L), which is illuminated from both boundaries simultaneously by intense radiation beams with intensities x and y, respectively, is reduced to a simple linear combination of the solutions of the two separate problems of its unilateral illumination (from left x, and from right y, separately):

$$u_L^{+}(x, y) = q^{+}\, x + r^{+}\, y, \tag{1}$$

[1] Byurakan Astrophysical Observatory, Armenia

V. Grinin et al. (eds) Radiation mechanisms of astrophysical objects. Yerevan: Edit Print, 2017, pp. 65–72.

$$u_L^-(x,y) = r^-\, x + q^-\, y, \tag{2}$$

where r^- and q^+ are the coefficients of reflection and transmission of an anisotropic medium of geometric thickness L, for a "single quantum", or their "beam of unit intensity", incident from its left boundary, while r^+ and q^- are their counterparts related to the right boundary. These coefficients can be readily interpreted as the probability densities of reflection and transmission of a single photon incident on one of the two boundaries of medium. In nonlinear case [1]–[5], the relations analogous to Eqs. (1)–(2) do not hold. The relationship of these two problems is now implemented (instead of Eqs. (1)–(2)) by Cauchy problems [1]–[5]. Moreover, it is obvious that in the nonlinear case, it makes no sense at all to operate with such concepts as "single photon", or their "beam of unit intensity", and the use of probabilistic interpretation of transference phenomena, which though are very efficient tools in the linear problems. This obstacle, in nonlinear problems of bilateral illumination of medium, still prevents to explore only the solution of equations for particular PRT of unilateral illumination of medium (such as seeking the variables $r^\pm$ and $q^\pm$ [6, 7] of the linear case). Therefore, the exact methods of determining the field of radiation emerging from the medium, such as: (i) adding of layers, (ii) its limiting form, described by differential equations of invariant imbedding, and (iii) the so-called functional equations of Ambartsumyan's "complete invariance" (ACI) [4, 5], are compelled here to apply directly to the functions $u_L^\pm(x,y)$ of bilateral illumination of medium, which significantly complicates their determination.

A major goal of this report is to simplify further the methods of nonlinear PRT by revealing and exploring some new functions of so-called "linear images" of the solution of PRT. It is noteworthy that the solution in quest of nonlinear PRT is expressed in terms of newly introduced functions explicitly, just as in the linear case, through a simple linear combination of the solutions of more particular PRT of unilateral illumination of medium. We show that the introduction of these linear images allows to handle effectively a random walk of a single quantum or their unit beam. Moreover, this ensures an application of Sobolev's probabilistic interpretation [8] of linear transfer problems, in nonlinear case too, as simple as in the linear case. For a determination of linear images, as a consequence of the systematic application of the principle of invariance [1] and [4]–[6], we explore in unified way the analogues of described above all three methods of solutions of PRT.

2 The linear images of nonlinear PRT

The idea of introduction of linear images is closely related to one observation of Ambartsumian [9, 2] that inevitably a translucence of medium occurs at high intensities of external radiation exiting it, which is due to the transition of essential fraction of atoms from the ground state to an excited. As a result, the proportion of absorbing neutral atoms in the medium decreases and a stationary regime was

established in the excited medium with a new, changed, optical thickness. The original problem becomes linear with respect to new values of the optical thickness, unknown in advance. This is just a physical meaning of the approach entitled "method of self-consistent optical depths", and further used very effectively by [10]. Following Ambartsumian, let us trace the path of a single quantum, randomly walking in an anisotropic scattering/absorbing medium, when certain steady state conditions are established in it. This constant level of an excitation of medium is maintained (stationary regime) during the whole process of random walk of a quantum. It means that an arbitrary chosen quantum just "lives" in a linear medium during this entire time. If x number of photons are incident on medium from the left, and y – from the right, then their total output, as in linear case, can be given by the relations analogous to Eqs. (1)–(2), with the only difference that the functions, $R_L^{\pm}(x,y)$ and $T_L^{\pm}(x,y)$, of the described above linear images of solution of original PRT, are dependent on the total number of photons (x,y), because of nonlinearity of the problem:

$$u_L^+(x,y) = T_L^+(x,y)\,x + R_L^+(x,y)\,y, \tag{3}$$

$$u_L^-(x,y) = T_L^-(x,y)\,y + R_L^-(x,y)\,x. \tag{4}$$

The functions $R_L^{\pm}(x,y)$ and $T_L^{\pm}(x,y)$ are the above-mentioned linear images of the solution of original PRT. They are, respectively, the probability densities of reflection and transmission of a single photon or their unit beam incident on the medium through from one of its two boundaries. Although these functions describe the behavior of a single quantum or their unit beam, but because of nonlinearity of the problem nevertheless depend upon the intensities (x,y) of entering medium radiation, due to which the acting level of an excitation of medium has been set. In asymptotic limit of weak fields $x + y \leq \delta^{\pm}$, these functions apparently become constants, which are the solutions of a linear problem, where $\delta^{\pm}$ is the asymptotic threshold of incident single quantum from the left and right, respectively.

3 Relations of the adding of layers for the linear images

As a first method for determining the linear images, let us employ a general method of adding of layers in the nonlinear problems of transfer [1, 2, 5]. Suppose the anisotropic one-dimensional medium of geometrical thickness of B is adjoined from the right to a similar medium of thickness A. Thereby the composite slab of finite thickness $A + B$ is illuminated from the left and right boundaries by radiation of intensities x and y, respectively. Required to determine the intensity of the radiation $u_{A+B}^{\pm}(x,y)$ emerging from this composite slab, when the solutions of similar problems for its both sub-layers, $u_A^{\pm}(x,y)$, $u_B^{\pm}(x,y)$, are previously known. From Eqs. (3)–(4), it is seen that the problem is reduced to determination

of the linear images $R^{\pm}_{A+B}(x,y)$ and $T^{\pm}_{A+B}(x,y)$ by means of known linear images $R^{\pm}_{A}(x,y)$, $T^{\pm}_{A}(x,y)$ and $R^{\pm}_{B}(x,y)$, $T^{\pm}_{B}(x,y)$. From the formulas of the nonlinear addition of layers [5], by virtue of Eqs. (3)–(4), we obtain

$$T^{+}_{A+B}(x,y) = T^{+}_{B}(p,y)\ p_{+}, \tag{5}$$

$$R^{+}_{A+B}(x,y) = R^{+}_{B}(p,y) + T^{+}_{B}(p,y)\ p_{-}, \tag{6}$$

$$R^{-}_{A+B}(x,y) = R^{-}_{A}(x,s) + T^{-}_{A}(x,s)\ s_{+}, \tag{7}$$

$$T^{-}_{A+B}(x,y) = T^{-}_{A}(x,s)\ s_{-}, \tag{8}$$

where the four auxiliary functions can be obtained exploring the explicit relations

$$p_{+} = \frac{T^{+}_{A}(x,s)}{1 - R^{+}_{A}(x,s)\ R^{-}_{B}(p,y)}, \quad s_{+} = \frac{R^{-}_{B}(p,y)\ T^{+}_{A}(x,s)}{1 - R^{-}_{B}(p,y)\ R^{+}_{A}(x,s)}, \tag{9}$$

$$p_{-} = \frac{R^{+}_{A}(x,s)\ T^{-}_{B}(p,y)}{1 - R^{+}_{A}(x,s)\ R^{-}_{B}(p,y)}, \quad s_{-} = \frac{T^{-}_{B}(p,y)}{1 - R^{-}_{B}(p,y)\ R^{+}_{A}(x,s)}. \tag{10}$$

The unknowns, p and s, can be found from the system

$$\begin{cases} p = T^{+}_{A}(x,s)\ x + R^{+}_{A}(x,s)\ s, \\ s = T^{-}_{B}(p,y)\ y + R^{-}_{B}(p,y)\ p, \end{cases} \tag{11}$$

or writing them in the form of separate equations

$$p = g^{+}(x,y;p,s) + K^{+}(x,y;p,s)\ p, \quad s = g^{-}(x,y;p,s) + K^{-}(x,y;p,s)\ s. \tag{12}$$

Here the proper kernels and free terms are defined by

$$\begin{aligned} K^{+}(x,y;p,s) &\equiv R^{+}_{A}(x,s)\ R^{-}_{B}(p,y), \\ K^{-}(x,y;p,s) &\equiv R^{-}_{B}(p,y)\ R^{+}_{A}(x,s), \\ K^{+}(x,y;p,s) &= K^{-}(x,y;p,s), \end{aligned} \tag{13}$$

$$g^{+}(x,y;p,s) \equiv T^{+}_{A}(x,s)\ x + R^{+}_{A}(x,s)\ T^{-}_{B}(p,y)\ y, \tag{14}$$

$$g^{-}(x,y;p,s) \equiv T^{-}_{B}(p,y)\ y + R^{-}_{B}(p,y)\ T^{+}_{A}(x,s)\ x. \tag{15}$$

When one of the equations (12) is already solved, the solution of the other can be obtained directly by using corresponding explicit relation (11). Whereas the attention is drawn to the fact that in the equations (12):

1. The discussed explicit structures have until now met only in linear problems, with the ensuing advantages.
2. Furthermore, an increase of the intensity of external radiation that excites the medium, in the form of direct dependence appears only in free terms g^{+}, g^{-} of these equations. This, as well known, does not affect a convergence of the iterative solutions of considered equations, because it is due only to the properties of kernels.
3. The kernels of equations K^{+}, K^{-} are just the probability densities.

Aforesaid ensures a convergence, for example, of a simple iterative scheme

$$p^{(n+1)} = g^{+}_{(n)} + K^{+}_{(n)}\, p^{(n)} \quad \text{at} \quad s^{(0)} = y, \tag{16}$$

where

$$g^{+}_{(n)} \equiv g^{+}\left(x,\, y;\, p^{(n)},\, s^{(n)}\right), \quad K^{+}_{(n)} \equiv K^{+}\left(x,\, y;\, p^{(n)},\, s^{(n)}\right). \tag{17}$$

In the framework of the method of adding of layers, to determine the linear images of nonlinear PRT, the following sequential scheme can be distinguished: to begin with, we determine p and s from Eqs. (11)–(17), next it will be $p_{\pm}$ and $s_{\pm}$ from Eqs. (9)–(10), afterward $R^{\pm}_{L}(x,y)$, $T^{\pm}_{L}(x,y)$ from Eqs. (5)–(8), and finally $u^{\pm}_{L}(x,y)$ from Eqs. (3)–(4).

4 A complete set of equations of invariant imbedding for the linear images

As a second method for determining the linear images, we derive a complete set of equations of invariant imbedding. More consistent way is to fulfill a limiting transition in the general relations of addition of layers, which were built above, i.e. successively letting one layer be elementary $\Delta \to 0$, while the other is left fixed: $A \equiv \Delta$, $B \equiv L$ and $A \equiv L$, $B \equiv \Delta$. For radiation characteristics of diffuse reflection-transmission of elementary volume can be obtained the explicit forms

$$\begin{aligned} T^{\pm}_{\Delta}(x,y) &= 1 - æ^{\pm}(x,y)\,\Delta + O\left(\Delta^2\right), \\ R^{\pm}_{\Delta}(x,y) &= \chi^{\pm}(x,y)\,\Delta + O\left(\Delta^2\right). \end{aligned} \tag{18}$$

The physical meaning of the functions $æ^{\pm}(x,y)$ and $\chi^{\pm}(x,y)$ is as follows: they represent the probability densities that the quantum moving in a certain direction will first be absorbed by elementary layer of the medium, and then: a) $æ^{\pm}(x,y)$ will not be re-emitted in the same direction; b) $\chi^{\pm}(x,y)$ will be re-emitted in backwards. Hence a complete set of the equations of invariant imbedding can be written as follows:

$$\left[\frac{\partial}{\partial L} - \hat{E}_{+}\right] T^{+} = -T^{+}\, æ^{+}\left(x,u^{-}\right) + T^{+}\,\chi^{+}\left(x,u^{-}\right)\, R^{-}, \tag{19}$$

$$\left[\frac{\partial}{\partial L} - \hat{E}_{+}\right] R^{+} = T^{+}\,\chi^{+}\left(x,u^{-}\right)\, T^{-}, \tag{20}$$

$$\begin{aligned} \left[\frac{\partial}{\partial L} - \hat{E}_{+}\right] R^{-} = {} & \chi^{-}\left(x,u^{-}\right) - R^{-}\, æ^{+}\left(x,u^{-}\right) - \\ & - æ^{-}\left(x,u^{-}\right)\, R^{-} + R^{-}\,\chi^{+}\left(x,u^{-}\right)\, R^{-}, \end{aligned} \tag{21}$$

$$\left[\frac{\partial}{\partial L} - \hat{E}_{+}\right] T^{-} = -æ^{-}\left(x,u^{-}\right)\, T^{-} + R^{-}\,\chi^{+}\left(x,u^{-}\right)\, T^{-}, \tag{22}$$

$$\left[\frac{\partial}{\partial L} - \hat{E}_{-}\right] T^{+} = -æ^{+}(u^{+},y)\, T^{+} + R^{+}\,\chi^{-}(u^{+},y)\, T^{+}, \tag{23}$$

$$\begin{aligned} \left[\frac{\partial}{\partial L} - \hat{E}_{-}\right] R^{+} = {} & \chi^{+}(u^{+},y) - æ^{+}(u^{+},y)\, R^{+} - \\ & - R^{+}\, æ^{-}(u^{+},y) + R^{+}\,\chi^{-}(u^{+},y)\, R^{+}, \end{aligned} \tag{24}$$

$$\left[\frac{\partial}{\partial L} - \hat{E}_-\right] R^- = T^- \chi^-(u^+, y)\, T^+, \tag{25}$$

$$\left[\frac{\partial}{\partial L} - \hat{E}_-\right] T^- = -T^- æ^-(u^+, y) + T^- \chi^-(u^+, y)\, R^+. \tag{26}$$

The first quartet of equations is a consequence of variations of the left boundary of medium, and the second quartet is that of the right boundary. The corresponding operators of radiation "response" of medium can be written [5]

$$\hat{E}_+ = \alpha^+\left(x, u_L^-\right) \frac{\partial}{\partial x}, \quad \hat{E}_- = \alpha^-(u^+, y) \frac{\partial}{\partial y}, \tag{27}$$

where $\alpha^\pm$ are the well-known integral of collisions of the problem. Without going into details, we note that the initial conditions in the corresponding Cauchy problem, in terms of the parameter of layer thickness, are $R^\pm|_{L=0} = 0$, $T^\pm|_{L=0} = 1$, and in terms of the energy variables (x, y) – more particular solutions of PRT of single quantum, when the medium is excited by radiation incident only on one boundary (for details, see Example in Sect. 6).

5 Ambartsumian's functional equations for linear images

A third method of solution of PRT corresponds to the case when simultaneously vary both boundaries of the layer (when the elementary layer of infinitesimal thickness is added to one boundary, and it is subtracted from the other boundary). At this, a geometry of the problem is not changed, i.e. the layer thickness remained constant, so the derivatives of the spatial variables naturally should be excluded. By pairwise exclusion of derivatives over thickness from Eqs. (19)–(26), we obtain four functional equations of ACI for the linear images:

$$\begin{aligned}\hat{A}T^+ = {} & T^+ æ^+\left(x, u^-\right) - æ^+(u^+, y)\, T^+ \\ & + R^+ \chi^-(u^+, y)\, T^+ - T^+ \chi^+\left(x, u^-\right) R^-,\end{aligned} \tag{28}$$

$$\begin{aligned}\hat{A}R^+ = {} & \chi^+(u^+, y) - æ^+(u^+, y)\, R^+ - R^+ æ^-(u^+, y) \\ & + R^+ \chi^-(u^+, y)\, R^+ - T^+ \chi^+\left(x, u^-\right) T^-,\end{aligned} \tag{29}$$

$$\begin{aligned}\hat{A}R^- = {} & -\chi^-\left(x, u^-\right) + R^- æ^+\left(x, u^-\right) + æ^-\left(x, u^-\right) R^- - \\ & - R^- \chi^+\left(x, u^-\right) R^- + T^- \chi^-(u^+, y)\, T^+,\end{aligned} \tag{30}$$

$$\begin{aligned}\hat{A}T^- = {} & æ^-\left(x, u^-\right) T^- - T^- æ^-(u^+, y) \\ & + T^- \chi^-(u^+, y)\, R^+ - R^- \chi^+\left(x, u^-\right) T^-.\end{aligned} \tag{31}$$

The corresponding operator of radiation "response" of medium, when simultaneously vary both boundaries, i.e. the ACI operator, is given by $\hat{A} = \hat{E}_+ - \hat{E}_-$:

$$\hat{A} \equiv \alpha^+\left(x, u_L^-\right) \frac{\partial}{\partial x} - \alpha^-\left(u_L^+, y\right) \frac{\partial}{\partial y}. \tag{32}$$

It is noteworthy that the equations of linear images (20)–(31) favorably differed from the corresponding equations of previously known [5], $u_L^{\pm}(x,y)$, in the followings: (i) they retain a constructive explicit structure distinctive only for the equations of linear case, (ii) the characteristics of the elementary act of scattering (dependent on level of excitation of medium) are clearly separated from the structural forms, which are caused by the multiple scattering. The characteristics of the elementary act – $æ^{\pm}(x,y)$ and $\chi^{\pm}(x,y)$ at the transition to the linear case are converted into constant, when explicit structural forms, those just caused by the multiple scattering, are naturally retained. A transition to the functional equations of ACI (i.e. turn from the second method to the third, for determining the linear images) provides additional simplification. The layer thickness here are figured as fixed parameter for the whole calculation, whereas in the same problem with a given value of the layer thickness, the use of invariant imbedding necessarily implies an additional calculation of the entire family of PRT, starting from the value of zero thickness and continuing until reaching its final value, intended beforehand.

6 Particular example

Let us investigate next the simple instructive model of isotropic medium, with the conservative and isotropic scattering. Here we have the simplifications $R^{\pm} \equiv R$, $T^{\pm} \equiv T$, $R + T = 1$. The ACI equations, for determining the linear image T of function $u \equiv u(x,y)$, can be put in the simple symmetrical form

$$\left[k\,(x+v)\,\frac{\partial}{\partial x} + k\,(y+u)\,\frac{\partial}{\partial y}\right] T = -T\,M(x,y), \tag{33}$$

where

$$\begin{aligned} M(x,y) =& M(y,x) \equiv \frac{k\,(x+v) - k\,(y+u)}{x-y}, \\ k\,(\xi) \equiv& n\,\frac{h\nu}{2}\,\frac{A_{21}\,B_{12}}{A_{21} + \frac{\xi}{2}\,(B_{12}+B_{21})}, \end{aligned} \tag{34}$$

$$u = (x-y)\,T + y, \qquad v = -\,(x-y)\,T + x. \tag{35}$$

The initial conditions for Eq. (33) will be $T\,(x,0) = \sigma\,(x)$ or $T\,(0,y) = \sigma\,(y)$, where the unknown function $\sigma\,(z)$ describes the passage of a single quantum through medium, when it is excited by radiation of intensity z incident only on one boundary, and determined from its equation of invariant imbedding

$$\left[\frac{\partial}{\partial L} + x\,\sigma\,\frac{k\,(2\,x - x\,\sigma)}{2}\,\frac{\partial}{\partial x}\right]\sigma = -\sigma^2\,\frac{k\,(2\,x - x\,\sigma)}{2}, \tag{36}$$

$$\sigma|_{L=0} = 1, \quad \text{or} \quad \sigma|_{x=0} = q, \tag{37}$$

where q is the transmittance of layer of geometrical thickness L, in linear problem of isotropic medium at conservative isotropic scattering. It is explicitly given by

$$q = \frac{1}{1 + \frac{1}{2}\,k_0\,L}. \tag{38}$$

Thus, in this particular example, the following sequence of solutions of the problem we have in short: first solved a linear problem by means of (38), then this solution is used to define a linear image of a particular nonlinear PRT of unilateral illumination of medium by considering the auxiliary Cauchy problem (36)–(37) (by means of the equation of invariant imbedding), and afterward then the quasi-linear system of ACI (33)–(35) was considered. Hence, the desired solution of the nonlinear PRT, in term of its linear image of transmission of a single quantum, is given in an explicit form by (35).

7 Conclusion

In conclusion I want to express my deep appreciation to organizers of the conference in honor of bright memory and the 100th anniversary of academician V.V. Sobolev. For my great fascination by the theory of radiative transfer, I fully obliged to the two outstanding achievements of the field: the first is the "principle of invariance" of my teacher V.A. Ambartsumian, and the second is the "probabilistic interpretation" of V.V. Sobolev. Their incorporation provides the researchers by a powerful tools and methods of effective analysis of transfer problems, and a clear vision of their future opportunities. I am sure that the representatives of many more generations of astrophysicists, like me, would be fascinated by this area of knowledge.

Acknowledgments. The very helpful and positive feedback from G. Ter-Kazarian in preparation of this report is much appreciated.

References

1. *V.A. Ambartsumian*, Dokl. Akad. Nauk Arm. SSR, **38**, 225, 1964.
2. *V.A. Ambartsumian*, in: The Theory of Stellar Spectra. Eds. V.V. Sobolev et al. Moscow: Nauka, 1966, p. 91.
3. *R. Bellman, R. Kalaba, M. Wing*, Proc. Nat. Acad. Sci., **46**, 1646, 1960.
4. *H.V. Pikichian*, in Proc. Conf. Evolution of Cosmic Objects Through Their Physical Activity (dedic. V. Ambartsumian's 100th anniversary). Eds. H. Harutyunian, A. Mickaelian, Y. Terzian. Yerevan: Publ. House NAS RA, 2010, p. 302.
5. *H.V. Pikichian*, Astrophys., **53**, 251, 2010.
6. *V.A. Ambartsumian*, Izv. Akad. Nauk Arm. SSR, Nat. Sci., No. 1–2, 31, 1944.
7. *V.A. Ambartsumian*, Dokl. Akad. Nauk Arm. SSR, **7**, 199, 1947.
8. *V.V. Sobolev*, Transport of Radiant Energy in the Atmospheres of the Stars and Planets. Moscow: Gostekhizdat, 1956 (in Russian). Translated as A Treatise on Radiative Transfer. Princeton: Van Nostrand, 1963.
9. *V.A. Ambartsumian*, Dokl. Akad. Nauk Arm. SSR, **39**, 159, 1964.
10. *N.B. Yengibarian*, Astrophys., **1**, 158, 1965.

On Some Applications of General Invariance Relations Reduction Method to Solution of Radiation Transfer Problems

N.N. Rogovtsov[1], F.N. Borovik[2]

E-mail: *rogovtsov@bntu.by, bfn@hmti.ac.by*

Foundations of the general invariance relations reduction method are presented outline. A number of solutions of problems of the radiation transfer theory, obtained by the help of this method, is described briefly.

1 Background of the general invariance relations reduction method (GIRRM)

Properties of symmetry and invariance are widely used practically in all fields of people activity [1]. Very often these properties and principles make sense of statements on invariance of some objects, systems, equations, constructions, solutions and so on with respect to sets of actions and operations that form group. However not all properties and principles of invariance can be formulated in the framework of group-theoretical approach [1, 2]. It is necessary to point out a number of the fundamental works in which the concept of the immutability (invariance) solutions of one-dimensional (in the space variables) problems of optics and radiation transfer theory (RTT) under the simplest of the above-mentioned actions and operations are used. These publications include works written by Stokes [3], Ambartsumian (see Refs. in [4]), Chandrasekhar [5], Bellman and Kalaba [6], and Sobolev (see Refs. in [7]). The first principles of invariance in the RTT were formulated by Ambartsumian [4] and Chandrasekhar [5]. Then in 1956 Bellman and Kalaba formulated in a sufficiently abstract way the classical principle of invariant imbedding (PII). More wide interpretation, generalization and application of classical principles of invariance of the RTT were given in a number of works (see Refs. in [2, 8]). The general invariance relations reduction method (GIRRM) was proposed by Rogovtsov [1, 2, 9, 10].

The most important basic GIRRM statements and constructions are the general invariance principle (GIP) and the general invariance relations (GIRs). More narrow formulation of the GIP (in framework of the RTT) was given by Rogovtsov [2, 10]. Most universal formulation of this principle was given in the monograph [1]. By the GIRs we understand consequences of invariance (partial

[1] Belarus National Technical University, Minsk, Belarus
[2] A.V. Luikov Heat and Mass Transfer Institute, Minsk, Belarus

V. Grinin et al. (eds) Radiation mechanisms of astrophysical objects. Yerevan: Edit Print, 2017, pp. 73–83.

invariance) of solutions of problems of the RTT and other mathematical physics problems in respect to above-mentioned actions and operations. The GIRs connect solutions of different or the same type RTT or MP problems. It should be noted that the GIRRM are an heuristic, general and effective method

2 A short list of the results obtained by using the GIRRM

2.1 About rigorous derivation of asymptotic formulas for the plane albedo and spherical albedo for the case of nearly conservative scattering

Using rigorous integral relations and some a priori assumptions Sobolev [7] obtained the following three-term asymptotic formulas:

$$A_{pl}(\mu_1;\omega_0) \sim 1 - 4\sqrt{\frac{1-\omega_0}{3-x_1}}u(\mu_1;1) + b_{Sob}(\mu_1)(1-\omega_0), \quad \omega_0 \to 1, \tag{1}$$

$$A_{sp}(\omega_0) \sim 1 - 4\sqrt{\frac{1-\omega_0}{3-x_1}} + D(3-x_1)^{-1}(1-\omega_0), \quad \omega_0 \to 1. \tag{2}$$

Here $A_{pl}(\mu_1;\omega_0) = 2\int_0^1 \rho^0_{[0,+\infty)}(\mu,\mu_1;\omega_0)\,\mu\,d\mu$ is the plane albedo and $\rho^0_{[0,+\infty)}(\mu,\mu_1;\omega_0)$ is the azimuthally averaged reflection function for a semi-infinite plane-parallel medium (ω_0 is a single scattering albedo), $A_{sp}(\omega_0) = 2\int_0^1 \mu_1 A_{pl}(\mu_1;\omega_0)d\mu_1$ is the spherical albedo, $u(\mu;\omega_0)$ is the function that defines the angular dependence of Milne's problem solution [7, 8], $b_{Sob}(\mu_1) = 15(5-x_2)^{-1}\big(\mu_1^2 - 2\int_0^1 \rho^0_{[0,+\infty)}(\mu,\mu_1;1)\mu^3 d\mu\big) + D(3-x_1)^{-1}u(\mu_1;1)$, where $D = 24\int_0^1 u(\mu;1)\mu^2 d\mu$, $\{x_s\}_{s\in N_0}$ is a sequence of expansion coefficients of the phase function $p(\mu)$ in Fourier series in the system of Legendre polynomials $\{P_s(\mu)\}_{s\in N_0}$ ($p(\mu) = \sum_{s=0}^{+\infty} x_s P_s(\mu); N_0 = \{0,1,2,\dots\}$). Without any a priori assumptions, using the GIRRM, we were strictly obtained Eq. (2) and such asymptotic formula:

$$A_{pl}(\mu_1;\omega_0) \sim 1 - 4\sqrt{\frac{1-\omega_0}{3-x_1}}u(\mu_1;1) + b_{R,B}(\mu_1;\omega_0)(1-w_0), \quad \omega_0 \to 1. \tag{3}$$

The value of $b_{R,B}(\mu_1;\omega_0)$ in Eq. (3) is equal to

$$\begin{aligned} b_{R,B}(\mu_1;\omega_0) = {} & D(3-x_1)^{-1}u(\mu_1;1) \\ & - 15(5-x_2)^{-1}\left[\mu_1^2 - 2\int_0^1 \mu^3 \rho^0_{[0,+\infty)}(\mu,\mu_1;1)d\mu\right] \\ & - 2\int_{-1}^{1} d\mu \int_{+0}^{+\infty} \left[\tilde{G}^*_{\infty;0}(\tau,\mu;0,\mu_1;\omega_0) - J(\tau,\mu,\mu_1;\omega_0)\right] d\tau, \\ J(\tau,\mu,\mu_1;\omega_0) = {} & 2\int_0^1 \mu' \tilde{G}^*_{\infty;0}(\tau,\mu,0,-\mu';\omega_0)\rho^0_{[0,+\infty)}(\mu',\mu_1;1)d\mu'. \end{aligned} \tag{4}$$

Table 1: Numerical values of the coefficients $b_{Sob}(\mu_1)$ and $b_{R,B;0}(\mu_1)$

μ_1	$g = 0.65$	$g = 0.75$	$g = 0.85$	$g = 0.97$	$g = 0.991$
0.0381347	1.613	2.339	3.901	18.37	60.14
0.238853	3.212	4.652	7.974	41.00	137.3
0.333212	4.080	5.863	9.993	51.15	171.1
0.434867	5.114	7.289	12.34	62.78	209.8
0.539374	6.285	8.894	14.97	75.66	252.6
0.642166	7.545	10.61	17.77	89.32	298.0
0.738751	8.829	12.60	20.60	103.1	343.7
0.824908	10.05	14.02	23.30	116.1	387.0
0.896871	11.14	15.49	26.68	127.6	425.0
0.951494	12.00	16.65	27.54	136.7	455.0
1.0	12.78	17.72	29.26	144.9	482.4

In the formula (4) the function $\tilde{G}^{*}_{\infty;0}(\tau, \mu; \tau', \mu'; \omega_0)$ has the meaning of not the main part of the contribution to the integrated over azimuth "volume" Green function [2, 11] of the dimensionless scalar radiative transfer equation (SRTE) for the case of an infinite plane-parallel medium. This part is generated by the subset of the spectrum of the reduced characteristic equation of the SRTT (it corresponds to zero azimuthal harmonic of phase function). The above-mentioned subset does not contain only the minimum in modulus eigenvalues. The asymptotic formulas (1) and (3) differ in shape (their third members have different forms). Nonetheless theoretical analysis and the series of numerical experiments showed that there are no differences (within the limits of calculation errors for sufficiently small values of q ($q = 1 - \omega_0$) between the coefficients $b_{Sob}(\mu_1)$ and $b_{R,B}(\mu_1; \omega_0)$.

Remark 1. *The coefficient $b_{R,B}(\mu_1; \omega_0)$ can be represented in form of the following series:*

$$b_{R,B}(\mu_1; \omega_0) = \sum_{l=0}^{+\infty} b_{R,B;l}(\mu_1)(1 - \omega_0)^l. \tag{5}$$

This series is convergent point-wise and uniformly on [-1,1] for sufficiently small values of q.

Remark 2. *Using the GIRRM the effective analytical and numerical algorithms for finding all the quantities in the asymptotic formulas* (2) *and* (3) *for any phase functions are developed.*

In Table 1 a number of numerical values of the coefficients $b_{Sob}(\mu_1)$ and $b_{R,B;0}(\mu_1)$ are given for the case of Henyey-Greenstein's phase function $\chi(\mu; g)$ [7, 8]. From the above-said and Table 1, it follows that the assumptions [7], which V.V. Sobolev used in the derivation of the formulas (1) and (2), are correct for situations considered.

2.2 The correct methods of derivation of multi-term asymptotics for the case of plane-parallel media

The GIRRM allows to derive asymptotic formulas for azimuthally averaged reflection and transmission coefficients [7] for the case of plane-parallel optically thick media without using a priori assumptions about their structures. It should be noted that it is necessary to take into account the implicit contribution of the entire spectrum of the characteristic equation (CE) of the SRTE in the above-mentioned coefficients in the process of rigorous derivation of these asymptotics. In particular, all of the elements (they belong to the spectrum of the CE), which do not coincide with minimal in modulus elements of the same spectrum, contribute some terms of the order of $(1-\omega_0)$ (if $\omega_0 \to 1$) to asymptotics of these coefficients. Using some constructions of the GIRRM, the principle of reciprocity [11] and the analytical representations (see [12, 13]) for the "volume" Green function of the SRTE for a infinite plane-parallel medium, we have proved the faithfulness of Sobolev's a priori assumptions and asymptotic formulas [7] for the above-mentioned coefficients for the cases of semi-infinite media and layers of a large optical thickness τ_0. In [14] multi-term formulas for the reflection and transmission coefficients when $\tau_0 \to \infty$ were first obtained in implicit form. These asymptotics were found by using Case's method. Then the methods of finding of multi-terms asymptotics of various radiative characteristics were proposed in [15, 16, 17]. The most effective algorithm for deriving of such asymptotics was described in [15]. This algorithm was based on the constructive ideas of the GIRRM. To illustrate capabilities of this algorithm we write down only some relations from [15]. Consider a macroscopically homogeneous and local isotropic plane-parallel turbid layer of an optical thickness τ_0. Then using standard constructions of the GIRRM [1, 2] the following GIRs:

$$\rho^0(|\mu|,\xi;\omega_0,\tau_0) = g_1^0(|\mu|,\xi;\omega_0,\tau_0) + \int_0^1 K(|\mu|,\mu'';\omega_0,\tau_0)\rho^0(\mu'',\xi;\omega_0,\tau_0)d\mu'', \quad (6)$$

$$\sigma^0(|\mu|,\xi;\omega_0,\tau_0) = g_2^0(|\mu|,\xi;\omega_0,\tau_0) + \int_0^1 K(|\mu|,\mu'';\omega_0,\tau_0)\sigma^0(\mu'',\xi;\omega_0,\tau_0)d\mu'', \quad (7)$$

$$(|\mu|,\xi \in [0,1],\ \omega_0 \in [0,1],\ \tau_0 \in (0,+\infty))$$

were obtained in [15]. In GIRs (6) and (7) the functions $\rho^0(|\mu|,\xi;\omega_0,\tau_0)$ and $\sigma^0(|\mu|,\xi;\omega_0,\tau_0)$ are the azimuthally averaged reflection and transmission coefficients [7, 8] of a layer correspondingly. The function $K(|\mu|,\mu'';\omega_0,\tau_0)$ is defined by the relation.

$$K(|\mu|,\mu'';\omega_0,\tau_0) = \mu'' \int_0^1 \mu' \tilde{G}_{[0,+\infty)}(0,-|\mu|;\tau_0,\mu';\omega_0)\tilde{G}_{[0,+\infty)}(0,-\mu';\tau_0,\mu'';\omega_0)d\mu'. \quad (8)$$

Here function $\tilde{G}_{[0,+\infty)}(\tau,\mu;\tau',\mu';\omega_0)$ is the "volume" Green function of the dimensionless SRTE for the case of a semi-infinite plane-parallel medium which

comprises the "sources" $\delta(\tau-\tau')\delta(\mu-\mu')$ $(\tau'>0)$. In turn the functions $g_1^0(|\mu|,\xi;\omega_0,\tau_0)$, $g_2^0(|\mu|,\xi;\omega_0,\tau_0)$ can be expressed in terms of values of this "volume" Green function (see [15]).

For example, using the principle of reciprocity [11], the representations for the Green function $\tilde{G}_{[0,+\infty)}(\tau,\mu;\tau',\mu';\omega_0)$ [12, 13], K-integral of the SRTE [7] and GIRs (6), (7) the following asymptotics:

$$\begin{aligned}
\sigma^0(|\mu|,\xi;1,\tau_0) &= Q(|\mu|,\xi;\tau_0)+(2u(|\mu|;1)+h_2(|\mu|;\tau_0))\gamma_1(\tau_0,x_1)\\
&\quad\times\left\{\int_0^1\mu'^2\rho^0_{[0,+\infty)}(\mu',\xi;1)d\mu'+h_1(\xi;\tau_0)+\gamma_2(\tau_0,\xi,x_1)\right\}\\
&\quad+O(\tau_0^{-1}\exp(-2k_2\tau_0)),\quad \tau_0\to+\infty,\\
\gamma_1(\tau_0,x_1) &= \left[(1-\frac{x_1}{3})\tau_0+4\int_0^1\mu'^2u(\mu';1)d\mu'+h(\tau_0)\right]^{-1},\\
\gamma_2(\tau_0,\xi,x_1) &= 2^{-1}\xi\Big(1-\exp\Big(-\frac{\tau_0}{\xi}\Big)\Big)-2^{-1}\Big(1-\frac{x_1}{3}\Big)\tau_0\exp\Big(-\frac{\tau_0}{\xi}\Big),
\end{aligned}\tag{9}$$

$$\begin{aligned}
\int_0^1\mu\sigma^0(\mu,\xi;1,\tau_0)d\mu &= \gamma_1(\tau_0,x_1)\left\{\int_0^1\mu'^2\rho^0_{[0,+\infty)}(\mu',\xi;1)d\mu'\right.\\
&\quad\left.+h_1(\xi;\tau_0)+\gamma_2(\tau_0,\xi,x_1)\right\}\\
&\quad+O(\tau_0^{-2}\exp(-2k_2\tau_0)),\quad \tau_0\to+\infty,
\end{aligned}\tag{10}$$

were obtained in [15]. The functions $Q(|\mu|,\xi;\tau_0)$, $h(\tau_0)$, $h_1(\xi;\tau_0)$, $h_2(|\mu|;\tau_0)$ are expressed explicitly in terms of the functions $u(|\mu|;1)$, $\rho^0_{[0,+\infty)}(|\mu|,\xi;1)$, $\tilde{G}^*_{\infty;0}(\tau,\mu;\tau',\mu';\omega_0)$. In addition there are asymptotics $h(|\mu|;\tau_0)=O(\exp(-k_2\tau_0))$, $h_1(\xi;\tau_0)=O(\exp(-k_2\tau_0))$, $h_2(|\mu|;\tau_0)=O(\exp(-k_2\tau_0))$, $\tau_0\to+\infty$. In Eqs. (9), (10) under symbol k_2 it should be understood the second non-negative root of the reduced characteristic equation of the SRTE (if it exists). If a root does not exist under the symbol k_2 it is necessary to understand the positive number $(1-\varepsilon)$, where ε is a small enough positive number. Eq. (9) is a generalization of asymptotics for $\sigma^0(|\mu|,\xi;1,\tau_0)$ obtained by Sobolev [7].

2.3 Constructive theory of scalar characteristic equations of the radiative transfer theory

The constructive theory of scalar characteristic equations of the RTT was suggested in [12, 13, 18]. The construction of solutions of these equations in analytic form can be reduced to finding solutions of infinite tridiagonal systems of linear algebraic equations. Effective analytical and numerical algorithms for finding discrete spectra, eigenfunctions and normalizing constants for reduced scalar characteristic equations of the SRTE was described in above-mentioned works. New two-term recursion formulas and analytic representations for solutions of infinite tridiagonal systems of linear algebraic equations were suggested in [13]. In addition, Rogovtsov obtained a general analytic expression for the "volume"

Green function of a two-dimensional (with respect to the angular variables) integro-differential equation of the radiative transfer for the case in which the phase function satisfies the Hölder condition on [-1, 1].

2.4 Effective algorithms for finding the reflection function, plane and spherical albedo for any phase function

Properties of invariance are used in the RTT in developing the effective algorithms for finding the reflection function, plane and spherical albedo. Point out two algorithms, in which these properties are used in an explicit form. The first algorithm is based on the use of Ambartsumian's non-linear integral equations for the reflection function and its azimuthal harmonics. The second algorithm was developed through the use of Fredholm special integral equations. The nonlinear integral above-mentioned equations were obtained by Ambartsumian by using the principle of invariance which he formulated in 1943 (see Refs. in [4]). Special Fredholm equations were found through the use of rigorous mathematical considerations or some properties of invariance in a number of papers (see, for example, [2, 12, 19, 20, 21] and references therein). The first algorithm was used, in particular, in [22]. The second algorithm is actually used in [2, 12]. It should be noted that the correct application of both algorithms requires the use of additional information about solutions of other problems of the RTT. For example, the quantities describing the deep regime of the radiation intensity in a semi-infinite medium and the Sobolev–van de Hulst relation [7, 8, 22] was used in the first algorithm [22] as an additional information in the construction of a sustainable iterative algorithm for solving nonlinear scalar Ambartsumian's integral equations. Previously it is necessary to find "volume" Green function of the SRTE for the case of an infinite plane-parallel turbid medium if special Fredholm integral equations are taken as the initial equations when finding of the reflection function. Before developing effective analytical and numerical algorithms for finding the above-mentioned Green function for cases of arbitrary phase functions it was practically impossible to use this kind of equations. Such algorithms were constructed and effectively used in [2, 12, 13]. These algorithms can be applied for the cases of sharply anisotropic phase functions. To illustrate the effectiveness of the algorithms developed in [2, 12, 13] we give below Table 2 for the quantities $A_{pl}(\mu_1;\omega_0)$, $A_{sp}(\omega_0)$ for the case of the phase function $\chi(\mu;g)$.

2.5 Exact expressions, asymptotic formulas, inequalities and asymptotic inequalities for the average characteristics of radiative fields in turbid media of different configurations

Different GIRs can be used for finding the integral invariants of the stationary and non-stationary SRTE. Moreover a number of average characteristics of radiative fields in turbid media of different configurations can be found using the GIRs. In the most simple form such results were obtained by Rogovtsov (see [1, 2, 13] and

Table 2: Values for plane and spherical albedo $A_{pl}(\mu_1;\omega_0)$, $A_{sp}(\omega_0)$ $(g = 0.993)$

μ_1	$\omega_0 = 0.99$	0.993	0.997	0.999	0.9999	0.99999
0.844195×10^{-2}	0.6995	0.7326	0.7996	0.8668	0.9504	0.9834
0.381347×10^{-1}	0.5356	0.5833	0.6836	0.7879	0.9206	0.9734
0.880185×10^{-1}	0.4097	0.4643	0.5860	0.7191	0.8939	0.9643
0.155914	0.3135	0.3670	0.5027	0.6575	0.8691	0.9558
0.238853	0.2407	0.2948	0.4314	0.6016	0.8453	0.9476
0.434867	0.1456	0.1906	0.3202	0.5057	0.8010	0.9318
0.642166	0.09391	0.1294	0.2442	0.4312	0.7622	0.9174
0.738751	0.07811	0.1097	0.2170	0.4020	0.7456	0.9111
0.896871	0.05896	0.08970	0.1803	0.3598	0.7200	0.9011
1.0	0.04964	0.07264	0.1605	0.3353	0.7040	0.8948
$A_{sp}(\omega_0)$	0.1079	0.1431	0.2542	0.4351	0.7612	0.9167

Refs. in therein) for the cases turbid media having forms of layer, sphere, infinite circular cylinder and regular polyhedral. In these works the average duration of the luminescence and radiative fluxes were required quantities. In turn the asymptotic inequalities for the mean intensity of the radiation, the average number of scattering of a photon, the average density of radiation, radiative fluxes and spherical albedo were found by Rogovtsov, Karpuk and Samson (corresponding Refs. are given in [2, 13]). These authors considered the process of radiative transfer in turbid media that have the forms of layer, sphere, finite and infinite circular cylinders, spheroids, spherical shell and non-concavity body bounded by a smooth boundary. In some of the above-mentioned publications the presence of underlying surfaces was allowed.

2.6 On the asymptotic expressions for the Green functions of the SRTE when turbid medium contains mono-directional point or line sources

2.6.1. Let turbid "medium" $\tilde{V}$ be a macroscopically homogeneous or two-layer non-conservative semi-infinite "medium" $\tilde{V}_{[0,\infty)}$, which is irradiated by an infinitely narrow mono-directional beam of radiation or contains near its border $\tilde{S}_{[0,\infty)}$ a point mono-directional source (see Figs. 1a, 1b).

Then the intensity of the radiation (or Green functions) at an optical depth τ_0 (when $\tau_0 \to +\infty$) at any observation point P can be represented in a simple analytical form (see [23]). In addition, the principle terms of asymptotic formulas are expressed in terms of elementary functions and solutions of special BVPs for the case of a plane-parallel anisotropic absorbing semi-infinite turbid "medium".

Remark 3. *Under the above-mentioned assumptions the forms of relative intensities for deep regime behaviors tend asymptotically to each other when a semi-infinite turbid medium is irradiated by an infinitely wide mono-directional beam of radiation or infinitely narrow mono-directional beams of radiation.*

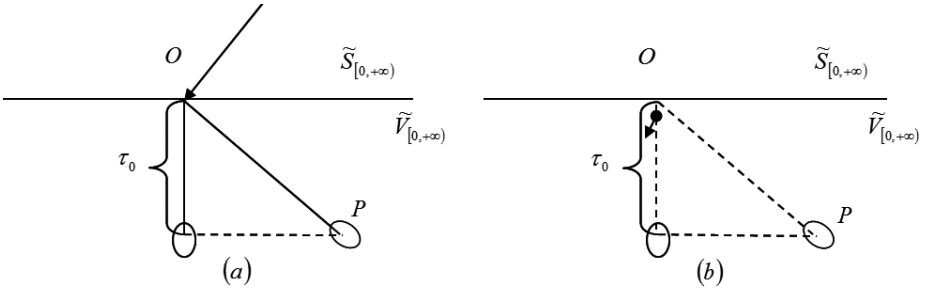

Figure 1: Geometries of problems for the cases of external and internal sources of radiation.

Remark 4. *Let the observation point P be at a large optical depth τ_0 and the shortest optical distance from point P to a perpendicular to $\tilde{S}_{[0,\infty)}$ (it passes through the point of incidence of external radiation) is equal τ_1. Then for the case of a macroscopically homogeneous turbid medium the principle term of the asymptotics of "volume" Green function of the dimensionless SRTE will be in form [24]*

$$\tilde{G}_{[0,+\infty)}\left(\vec{\tau},\vec{\Omega};\vec{0},\vec{\Omega}_1;\omega_0\right) \sim \frac{k_1 \exp(-k_1\tau_0)}{2\pi^2\tau_0}\, i(\mu;\omega_0)\, u(\mu_1;\omega_0), \qquad (11)$$
$$\omega_0 \in (0,1), \quad \tau_0 \to +\infty, \quad (\tau_1/\sqrt{\tau_0}) \to 0$$

Here functions $i(\mu;\omega_0)$ and $u(\mu_1;\omega_0)$ are the classic functions of the SRTT [7, 8]; k is the smallest positive element of the discrete spectrum of characteristic equation of the SRTT [7, 8, 13].

2.6.2. Let $\tilde{V}_{[0,\tau_0]}$ be a macroscopically uniform non-conservative scattering "layer" of an optical thickness τ_0 which is irradiated by a mono-directional infinitely narrow beam of radiation (see Fig. 2). Then with the help of the GIRRM the principle term of asymptotics of the "surface" Green function [11] of the dimensionless the SRTE for any position of observation point P, which is on the second boundary $\tilde{S}_2$ of the layer $\tilde{V}_{[0,\tau_0]}$, can be found. Here τ_0 tends to $+\infty$.

Remark 5. *Let the shortest optical distance from an observation point P to the perpendicular to $\tilde{S}_1$ which passes through the point of incidence of external*

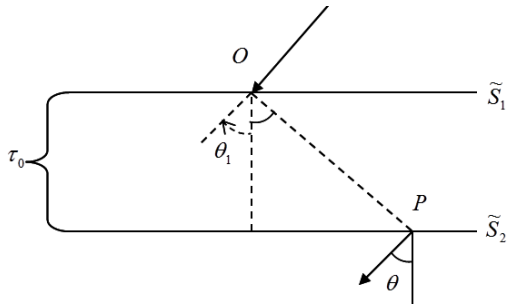

Figure 2: Geometry of problem for the case of the layer irradiated by the external beam of radiation.

radiation be equal to τ_1. *Then the principle term of the asymptotics of the "surface" Green function* $\tilde{G}_{\tilde{S}}(\tau, \vec{\Omega}; \vec{0}, \vec{\Omega}_1; \omega_0; \tilde{V}_{[0,\tau_0]})$ *of the SRTE can be presented in the form [24]*

$$\begin{aligned} &\tilde{G}_{\tilde{S}}(\vec{\tau}, \vec{\Omega}; \vec{0}, \vec{\Omega}_1; \omega_0; \tilde{V}_{[0,\tau_0]}) \sim \mu_1 \frac{M k_1 \exp(-k_1\tau_0)}{2\pi^2\tau_0} u(\mu; \omega_0)\, u(\mu_1; \omega_0), \\ &\tau_0 \to +\infty, \quad \frac{\tau_1}{\sqrt{\tau_0}} \to 0, \quad \omega_0 \in (0,1), \\ &M = 2\int_{-1}^{1} \mu\, i^2(\mu; \omega_0) d\mu, \quad \mu = \cos\theta, \quad \mu_1 = \cos\theta_1. \end{aligned} \tag{12}$$

2.6.3. Let $\tilde{V}$ be a non-conservative scattering "medium" having the shape of a sphere, the center of which is the point mono-directional "source" $\delta(\vec{\tau})\delta(\vec{\Omega} - \vec{\Omega}_1)$. In addition, the optical radius of $\tilde{V}$ is equal to τ_0. Then the asymptotic formula (see Refs. in [1, 2])

$$\tilde{G}(\vec{\tau}, \vec{\Omega}; \vec{0}, \vec{\Omega}_1; \omega_0; \tilde{V}) \sim \frac{k_1 \exp(-k_1\tau_0)}{2\pi^2\tau_0} u((\vec{n}\cdot\vec{\Omega}))\, i((\vec{n}\cdot\vec{\Omega}_1)), \tag{13}$$

$$\tau_0 \to +\infty, \quad ((\vec{n}\cdot\vec{\Omega}) \geq \varepsilon > 0)$$

holds. Here $\vec{n}$ is the unit dimensionless external normal to the boundary $\tilde{S}$ of the "medium" $\tilde{V}$ in a observation point (it is specified by an optical radius-vector $\vec{\tau}$) which lies at this boundary.

2.6.4. Let $\tilde{V}$ be a non-conservative scattering "medium" which has the shape of an infinite circular cylinder and contains (on the axis of symmetry) a linear mono-directional "source" $\delta(\vec{x})\delta(\vec{y})\delta(\vec{\Omega} - \vec{\Omega}_1)$ (see Fig. 3). Then the asymptotic formula (see Refs. in [1, 2])

$$\int_{-\infty}^{+\infty} \tilde{G}(\vec{\tau}_p, \vec{\Omega}; \tilde{z}\vec{e}_3, \vec{\Omega}_1; \omega_0; \tilde{V}) d\tilde{z} \sim \frac{1}{\pi}\sqrt{\frac{k_1}{2\pi\tau_0}} \exp(-k_1\tau_0)\, u((\vec{n}\cdot\vec{\Omega})\, i(\vec{n}\cdot\vec{\Omega}_1)), \tag{14}$$

$$\tau_0 \to +\infty \quad ((\vec{n}\cdot\vec{\Omega}) \geq \varepsilon > 0), \quad \omega_0 \in (0,1)$$

holds. Here $\vec{e}_3$ is the unit dimensionless vector which defines the direction of $\tilde{Z}$-axis of a dimensionless Cartesian right rectangular coordinate system $O\tilde{X}\tilde{Y}\tilde{Z}$ (the axis $\tilde{Z}$ coincides with symmetry axis of this cylinder), $\vec{\tau}_p$ specifies an observation point P, which is on the boundary of the cylinder.

2.6.5. Let V be a non-conservative scattering medium, which has a disk shape (see Fig. 4). We will assume that the local optical characteristics of V can depend only on the depth z in a Cartesian right rectangular coordinate system $OXYZ$. Assume that a plane OXY is parallel to the plane parts of the boundary of the disk V and the point O is situated on the axis of symmetry of the disk (this point should be situated inside the disk). Let the disk V contain a point isotropic "source" $\delta(\vec{r})$, which is located at the point O.

Using the GIRRM an asymptotic formula for the "volume" Green function was obtained when the observation point P is situated on the lateral boundary

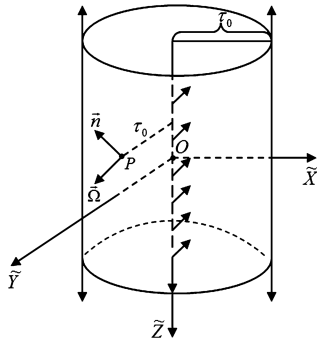

Figure 3: Geometry of the problem for the case of the infinite circular cylinder

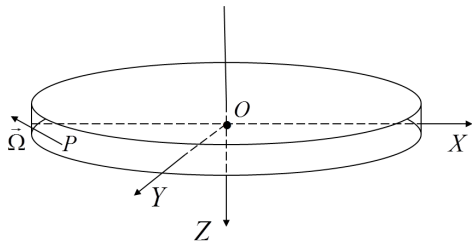

Figure 4: Geometry of the problem for the case of the disk

of the disc and the radius R of the disk tends to $+\infty$. This asymptotics has the following form (see Refs. in [1, 2]):

$$\tilde{G}(\vec{r}_p, \vec{\Omega}; \vec{0}; V) \sim \frac{c_1}{\sqrt{R}} \exp(-k^* R)\, B(z; \vec{\Omega}), \quad R \sup_{z\in[a,b]}\{\alpha(z)\} \to +\infty. \tag{15}$$

Here k^* is the smallest positive root of the non-classical characteristic equation of the SRTT, the constant c_1 is expressed through the first eigenvalue and the corresponding eigenfunction of this equation, $\alpha(z)$ is an attenuation coefficient, the function $B(z; \vec{\Omega})$ is expressed through solutions of one-dimensional and two-dimensional (in space variable) BVPs (the initial BVP is three-dimensional).

Acknowledgments. The authors are graceful to Yauheni Khnykin for help with design work.

References

1. *N.N. Rogovtsov*, Properties and Principles of Invariance. Application to Solving of Problems of Mathematical Physics, Part 1. Minsk: BGPA, 1999.

2. *N.N. Rogovtsov*, General Invariance Relations Reduction Method and Its Applications to Solutions of Radiative Transfer Problems for Turbid Media of Various Configurations, in Light Scattering Reviews, vol. 5. Ed. A.A. Kokhanovsky. Chichester: Springer-Praxis, 2010, pp. 243-327.

3. *G.G. Stokes*, Proc. Roy. Soc. Lond., **11**, 545, 1862.

4. *V.A. Ambartsumian*, Nauchnye trudy, Vol.1. Yerevan: Publ. Co. Acad. Sci. Arm. SSR, 1960.

5. *S. Chandrasekhar*, Radiative Transfer. London: Oxford University Press, 1950.

6. *R. Bellman, R. Kalaba*, Proc. Nat. Acad. Sci., **42**, 629, 1956.

7. *V.V. Sobolev*, Light Scattering in Planetary Atmospheres. New York: Pergamon Press, 1975.

8. *E.G. Yanovitskij*, Light Scattering in an Inhomogeneous Atmosphere. New York: Springer-Verlag, 1997.

9. *N.N. Rogovtsov*, J. Appl. Spectrosc., **34**, 241, 1981; *ibid*, **35**, 1354, 1981.

10. *N.N. Rogovtsov*, Dokl. Akad. Nauk BSSR, **25**, 420, 1981.

11. *K.M. Case, P.F. Zweifel*, Linear Transport Theory. Massachusetts: Addison-Wesley Publ. Co., 1967.

12. *N.N. Rogovtsov, F.N. Borovik*, The Characteristic Equations of Radiative Transfer Theory, in Light Scattering Reviews, vol. 4 Ed. A.A. Kokhanovsky. Chichester: Springer-Praxis, 2009, pp. 347–429.

13. *N.N. Rogovtsov*, Diff. Equat., **51**, 268, 2015; *ibid*, **51**, 661, 2015.

14. *N.V. Konovalov*, Preprint No. 65, Moscow: Inst. Appl. Math., 1974.

15. *N.N. Rogovtsov*, Teoreticheskaya i Prikladnaya Mekhanika (Minsk), **22**, 72, 2007.

16. *N.N. Rogovtsov, A.M. Samson*, Astrophys., **23**, 468, 1985.

17. *N.N. Rogovtsov*, Dokl. Akad. Nauk BSSR, **41**, 52, 1997.

18. *N.N. Rogovtsov*, in Boundary-Value Problems, Special Functions and Fraction Calculus. Ed. A.A. Kilbas. Minsk: BGU, 1996, pp. 305–312.

19. *N.N. Rogovtsov*, Izv. Atmos. Ocean. Phys., **16**, 160, 1980.

20. *N.N. Rogovtsov, A.M. Samson*, J. Appl. Spectrosc., **25**, 1164, 1976.

21. *H. Domke*, J. Quant. Spectrosc. Rad. Transf., **16**, 973, 1976.

22. *M.I. Mishchenko, J.M. Dlugach, E.G. Yanovitskij, N.T. Zakharova*, J. Quant. Spectrosc. Rad. Transf., **63**, 409, 1999.

23. *N.N. Rogovtsov*, Izv. Akad. Nauk SSSR, Fiz. Atmos. Okean., **26**, 1082, 1990.

24. *N.N. Rogovtsov*, Astrophys., **29**, 781, 1988.

On the Complex Radiative Transfer in an Optically Finite Homogeneous Atmosphere

T. Viik[1]

E-mail: *tonu.viik@to.ee*

In this paper we consider the classical problem in radiative transfer – the planetary problem – in an isotropically scattering homogeneous optically finite medium where the albedo of single scattering may be defined anywhere in the complex plane.

To solve this problem we use the method of approximating the kernel in the integral equation for the Sobolev resolvent function. This approach allows to define easily determinable auxiliary functions which help us to express almost all the relevant functions of transfer for this problem.

1 Statement of the problem

Usually the albedo of single scattering λ or c is assumed real in radiative transfer. But when we consider the Laplace transformed time-dependent transport equation λ may turn complex. We met another such problem when we tried to determine the photon path-length distribution function in an optically semi-infinite atmosphere. It appeared that the non-linear integral equation for the complex H-function is valid even in the complex plane [1]. This interesting fact directed the author to a deeper treatment of the problem and to try to find for such a case the radiation field in general.

In order to solve this problem we used the kernel approximation method first proposed by Krook [2] and later developed by Rybicki [3] and Vainikko et al. [4]. Rybicki approximated the kernel in the integral equation – the exponential integral – for the Sobolev resolvent function Φ by a Gauss-Legendre sum while Krook and Vainikko et al. used the method of kernel approximation for the integral equation of the source function.

The substitution of the kernel by a Gauss-Legendre sum allows us to solve the obtained approximate equation for the Sobolev resolvent function Φ [5] exactly while the solution is a weighted sum of exponents. This approach allowed us to define simple auxiliary functions for determining the radiation field.

Here we have chosen to consider the planetary problem in a homogeneous isotropically scattering optically finite atmosphere where the albedo of single scattering is complex

$$\lambda = \lambda_1 + i\lambda_2. \tag{1}$$

[1] Tartu Observatory, Estonia

V. Grinin et al. (eds) Radiation mechanisms of astrophysical objects. Yerevan: Edit Print, 2017, pp. 85–90.

We assume that in this case the source function B for a large range of radiative transfer problems in given type of atmospheres can still be described by the well-known Fredholm integral equation

$$B(\tau,\kappa,T)=\frac{1}{2}\lambda\int_0^T E_1(t-\tau)B(t,\kappa,T)dt+\frac{1}{4}\lambda F\exp\left(-\tau/\kappa\right), \tag{2}$$

where τ is the optical depth, T is the optical thickness of the atmosphere, πF is the flux of the incident radiation normal to the plane of stratification, κ is the direction cosine of the angle of incidence referred to the outward normal of the atmosphere and the exponential integral is expressed in the form

$$E_n(x)=\int_0^1 \exp(-|x|/s)s^{n-2}ds. \tag{3}$$

Since the Sobolev resolvent function is the regular part of the Green function for Eq. (2) we may immediately write that the solution of Eq. (2) for the planetary case is

$$B(\tau,\kappa,T)=\frac{1}{4}\lambda F\left[\exp\left(-\tau/\kappa\right)+\int_0^\tau \Phi(t,T)\exp\left(-t/\kappa\right)dt\right], \tag{4}$$

where the Sobolev resolvent function satisfies the following Fredholm integral equation [6]

$$\Phi(\tau;T)=\frac{1}{2}\lambda\int_0^T E_1(t-\tau)\,\Phi(t;T)dt+\frac{1}{2}\lambda E_1(\tau). \tag{5}$$

Now the task is all set for the solution of Eq. (5) by approximating the kernel of this equation.

2 Solution of the equation for the approximate resolvent function

Eq. (5) is one of the most important equations in the radiative transfer since all the relevant functions of transfer can be expressed through the resolvent function.

We try to solve Eq. (5) by approximating the kernel of it by a sum of exponents

$$E_1(\tau)=\sum_{n=1}^{N} w_n\exp(-\tau/u_n)u_n^{-1}, \tag{6}$$

where w_n are the weights and u_n are the points of a Gauss quadrature rule of the order of N in the interval (0,1). After substitution of this approximation into

Eq. (5) the resulting equation can be solved exactly and the solution is

$$\Phi(\tau, T) = a_1 + b_1\tau + \sum_{i=2}^{N} \left\{ a_i \exp(-s_i\tau) + b_i \exp[s_i(T-\tau)] \right\}. \tag{7}$$

If $\lambda_1 \neq 1$ then $a_1 = b_1 = 0$ outside of the summation sign and the summation begins at $i = 1$. This rule applies throughout the paper. The unknown coefficients s_i are the zeros of the equation

$$1 - \lambda \sum_{n=1}^{N} \frac{w_n}{1 - s^2 u_i^2} = 0. \tag{8}$$

The approximate characteristic equation – Eq. (8) – can simply be solved when λ is real and positive since we know beforehand in which intervals to search for the zeros. This is not the case when λ is complex or negative but if we write Eq. (8) in the polynomial form

$$\sum_{i=1}^{N} c_i s_i^{2i} = 0, \tag{9}$$

we may apply the code DZROOTS from Numerical Recipes [7].

The coefficients a_i and b_i are to be found from linear algebraic systems of equations

$$\begin{aligned} \alpha_1 + \sum_{i=2}^{N} \alpha_i \left[\frac{1}{1 - s_i u_j} + \frac{\exp(-s_i T)}{1 + s_i u_j} \right] &= u_j^{-1}, \\ \beta_1 (T + 2u_j) + \sum_{i=2}^{N} \beta_i \left[\frac{1}{1 - s_i u_j} - \frac{\exp(-s_i T)}{1 + s_i u_j} \right] &= u_j^{-1}, \quad j = 1, 2, \ldots, N, \end{aligned} \tag{10}$$

while

$$\begin{aligned} &a_i = (\alpha_i + \beta_i)/2, \quad b_i = (\alpha_i - \beta_i)/2, \quad i = 2, \ldots, N; \\ &a_1 = (\alpha_1 - \beta_1 T)/2, \quad b_1 = \beta_1. \end{aligned} \tag{11}$$

This system may be solved, e.g., using algorithms ZGECO and ZGESL from LINPACK.

Thus, the solution of the approximate equation for the Sobolev resolvent function is completed.

3 The complex radiation field

Next we define the auxiliary functions x and y as the generalizations of the well-known Ambartsumian–Chandrasekhar functions X and Y

$$x(\tau,\kappa,T) = 1 + \int_{\tau}^{T} \Phi(t;T)\exp\left[-(t-\tau)/\kappa\right]dt,$$

$$y(\tau,\kappa,T) = \exp\left(-\tau/\kappa\right) + \int_{0}^{\tau} \Phi(t;T)\exp\left[-(\tau-t)/\kappa\right]dt. \tag{12}$$

By the use of these functions we may express the solution of Eq. (2) [8] as

$$B(\tau,\kappa,T) = \frac{1}{4}\lambda F\{X(\kappa,T)y(\tau,\kappa,T) - Y(\kappa,T)[x(T-\tau)-1]\}. \tag{13}$$

Evidently, the Ambartsumian–Chandrasekhar functions X and Y are the special cases of x and y

$$\begin{aligned} X(\kappa,T) &= x(0,\kappa,T), \\ Y(\kappa,T) &= y(T,\kappa,T). \end{aligned} \tag{14}$$

As the next step we use the well-known definitions for the intensities and find that for the upward moving radiation, i.e. for the intensities towards the smaller optical depths we have

$$\begin{aligned} I(\tau,-\mu,\kappa,T) = \frac{\lambda F}{4}\frac{\kappa}{\mu+\kappa}\{&X(\kappa,T)[x(\tau,\mu,T) + y(\tau,\kappa,T) - 1] \\ &- Y(\kappa,T)[x(T-\tau,\kappa,T) + x(T-\tau,\mu,T) - 1]\} \end{aligned} \tag{15}$$

and for the intensities towards the larger optical depths

$$\begin{aligned} I(\tau,\mu,\kappa,T) = \frac{\lambda F}{4}\frac{\kappa}{\mu-\kappa}\{&X(\kappa,T)[y(\tau,\mu,T) - y(\tau,\kappa,T)] \\ &- Y(\kappa,T)[x(T-\tau,\mu,T) - x(T-\tau,\kappa,T)]\}. \end{aligned} \tag{16}$$

The seeming discontinuity in Eq. (16) may be eliminated by the L'Hopital rule.

4 Results

We have performed calculations for different set of atmospheric parameters and we are convinced that at least for the region $-8 \le \lambda_1 \le 8$ and $-8 \le \lambda_2 \le 8$ our method works well. We checked the results by solving the Ambartsumian–Chandrasekhar differential equations [9] for X and Y functions and coincidence of the results even for the modest $N = 7$ was very good.

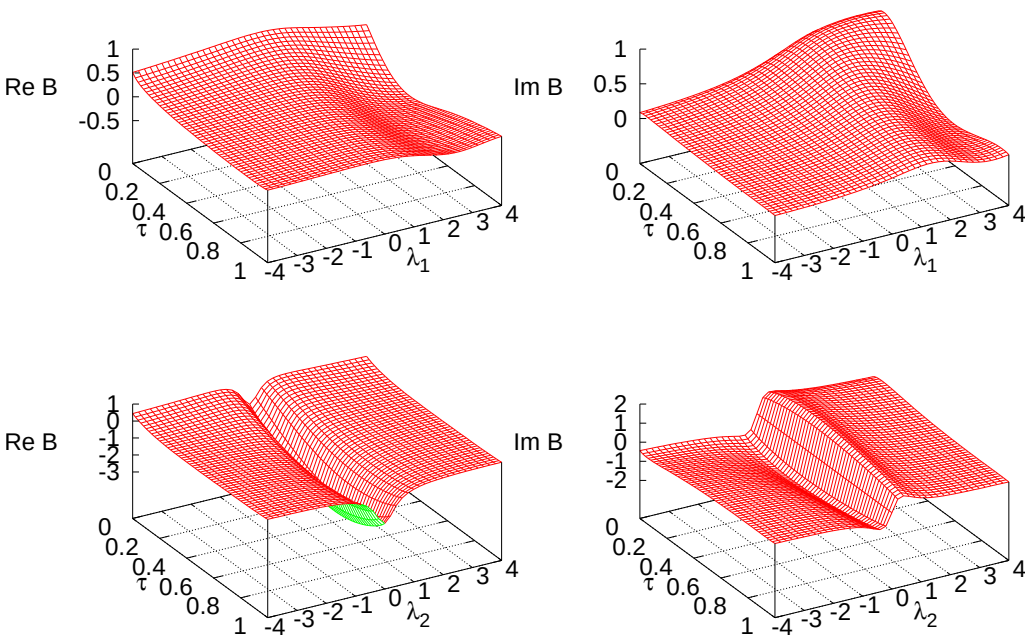

Figure 1: The real and imaginary parts of the source function ($\kappa = 1.0$, $T = 1.0$). Upper panel: $\lambda_2 = 2$, lower panel: $\lambda_1 = 2$.

In Fig. 1 we have presented some results for the source function. One may notice that for the fixed λ_2 the surfaces – both for the real and imaginary parts – of B are quite smooth while these for the fixed λ_1 have jumps at $\lambda_2 = 0$. We met a similar behavior when computing the complex H function [1].

Acknowledgments. The author thanks Prof. C.E. Siewert and Dr. H. Domke for fruitful discussions on the subject of this paper.

This work has been supported by the Estonian Ministry of Education and Research within Project No. SF0060030s08.

References

1. *T. Viik*, Astrophys. Space Sci., **209**, 255, 1993.
2. *M. Krook*, Astrophys. J., **122**, 488, 1955.
3. *G.B. Rybicki*, J. Quant. Spectrosc. Rad. Transf., **11**, 827, 1971.
4. *G. Vainikko, L. Karpenko, A. Shilman*, Proc. Eston. Acad. Sci., **25**, 118, 1976.
5. *T. Viik, R. Rõõm, A. Heinlo*, Publ. Tartu Astrophys. Obs., **76**, 3, 1985 (in Russian).
6. *V.V. Sobolev*, Light Scattering in Planetary Atmospheres. Oxford: Pergamon Press Ltd, 1975.
7. *W.H. Press, B.P. Flannery, S.A. Teukolsky, W.T. Vetterling*, Numerical Recipes, 3rd edition. Cambridge: Cambridge University Press, 2007.

8. *V. V. Sobolev*, Astron. Zh., **36**, 573, 1959.

9. *S. Chandrasekhar*, Radiative Transfer. New York: Dover, 1960.

* The color figure is available online in the Proceedings at *http://www.astro.spbu.ru/sobolev100/* .

Polarization of Resonance Lines in the Case of Polarized Primary Sources of Radiation

A.V. Dementyev[1]

E-mail: *a.dementiev@spbu.ru*

Transfer of polarized radiation in a spectral line in a non-magnetic semi-infinite plane-parallel atmosphere is considered. Complete frequency redistribution is assumed. It is supposed that primary sources of the radiation distributed in the atmosphere are partially polarized. The dependence on the optical depth of these sources is described by the product of a polynomial in the exponent. The problem is to find the radiation emergent from the atmosphere. The general theory of $\widehat{\mathbf{I}}$-matrices is applied to this problem. It turns out that the solution of the problem with any of the primary sources of this type is reduced to the solution of the so-called standard problem, and the subsequent simple numerical integration.

We consider multiple resonance scattering of radiation in a spectral line that takes place in a semi-infinite plane-parallel atmosphere without a magnetic field. Due to the symmetry, the radiation field can be described by two Stokes parameters I and Q. Therefore, the scattering is completely described by the two-component Stokes vector $\mathbf{i}(\tau, x, \mu) = (I, Q)^T$; its arguments are the usual optical depth averaged over line τ, the dimensionless frequency measured from the center of the line x, and the cosine of the zenith angle μ. Also, complete frequency redistribution is assumed. There are polarized primary sources of radiation embedded in the atmosphere; we suggest they are given by the vector function

$$\mathbf{s}_k(\tau) = \tau^k \, e^{-\tau/z_0} \, \mathbf{s}_0, \quad k = 0, 1, 2, \ldots, \tag{1}$$

where $z_0 \in (0, \infty)$ is a parameter, and $\mathbf{s}_0$ is a known constant vector.

In the works [1, 2] the theory of $\widehat{\mathbf{I}}$-matrices was developed. This theory makes possible to generalize a number of well-known results of the standard scalar theory of line formation to the problems when polarization of the radiation is taken into account. The scalar version of the problem considered here was studied in [3]. All the details regarding the theory of $\widehat{\mathbf{I}}$-matrices, for example, the relation of the matrix transfer equation to the vector one, as well as designations used here can be found in [1, 2].

By definition, the Stokes matrix $\widehat{\mathcal{I}}(\tau, z)$ is a solution of the matrix transfer equation

$$z \, \frac{\partial \widehat{\mathcal{I}}(\tau, z)}{\partial \tau} = \widehat{\mathcal{I}}(\tau, z) - \widehat{\mathbf{S}}(\tau). \tag{2}$$

[1] Saint Petersburg State University, Russia

V. Grinin et al. (eds) Radiation mechanisms of astrophysical objects. Yerevan: Edit Print, 2017, pp. 91–92.

Here $z \equiv \mu/\phi(x)$, $\phi(x)$ is the line absorption profile, and the matrix source function $\widehat{\mathbf{S}}(\tau)$ is given by

$$\widehat{\mathbf{S}}(\tau) = \widehat{\mathbf{S}}_*(\tau) + \int_{-\infty}^{+\infty} dz'\, \widehat{\mathbf{G}}(z')\, \widehat{\mathcal{I}}(\tau, z'), \tag{3}$$

$$\widehat{\mathbf{S}}_*(\tau) = \mathrm{diag}(s_I^*(\tau),\, s_Q^*(\tau)), \tag{4}$$

where $s_I^*(\tau)$ and $s_Q^*(\tau)$ are the components of the vector source function of the *scattered* radiation, $\widehat{\mathbf{G}}$ is directly related to the phase matrix of resonance scattering.

The problem with $\widehat{\mathbf{S}}_* \equiv \mathrm{diag}(\sqrt{1-\lambda}, \sqrt{1-0.7W\lambda})$ is called standard (λ is the albedo of single scattering, W is the depolarization parameter). It was analyzed in detail and solved numerically in the works [1, 2] and, also, in [4] where absorption in the continuum was taken into account. In particular, it was shown that the Stokes matrix at $\tau = 0$ for the standard problem can be found from the solution of the matrix generalization of the integral Ambartsumian–Chandrasekhar equation. We denote the solution of this equation by $\widehat{\mathbf{I}}(z)$ (it is the $\widehat{\mathbf{I}}$-matrix).

For the source function matrix $\widehat{\mathbf{S}}(\tau)$ of the problem under consideration it is not difficult to write an integral equation similar to the equation for the analogous scalar source function, when the polarization of the radiation is not taken into account. Application of Sobolev's resolvent method in the case of the atmosphere with an exponential distribution of primary sources (i.e., when $k = 0$ in Eq. (1)) provides the following Stokes matrix for the emergent diffuse radiation:

$$\widehat{\mathcal{I}}(0, z) = \widehat{\mathbf{I}}(z) \left[\frac{z_0^2\, \widehat{\mathbf{I}}^T(z_0)}{z_0 + z} \int_{-\infty}^{\infty} \frac{\widehat{\mathbf{F}}(z')\, dz'}{z_0 + z'} - z_0 \int_0^{\infty} \frac{z'\, \widehat{\mathbf{I}}^T(z')\, \widehat{\mathbf{F}}(z')\, dz'}{(z_0 - z')(z' + z)} \right], \tag{5}$$

where $\widehat{\mathbf{F}}$ is expressed through elements of the matrix $\widehat{\mathbf{G}}$.

In general case, if $k > 0$, it is not difficult to show that the Stokes matrix satisfies the recurrence formula

$$\widehat{\mathcal{I}}_k(0, z) = z_0^2\, \frac{\partial}{\partial z_0}\, \widehat{\mathcal{I}}_{k-1}(0, z). \tag{6}$$

Thus, in the case of primary sources (1), the Stokes matrix of the emergent radiation for any of such sources is expressed in terms of the solution of standard problem $\widehat{\mathcal{I}}(z)$ via the equations (5) and (6).

References

1. *V. V. Ivanov, S.I. Grachev, V.M. Loskutov*, Astron. Astrophys., **318,** 315, 1997.
2. *V. V. Ivanov, S.I. Grachev, V.M. Loskutov*, Astron. Astrophys., **321,** 968, 1997.
3. *V. V. Ivanov, D.I. Nagirner*, Astrophys., **1,** 86, 1965.
4. *A. V. Dementyev*, Astrophys., **52,** 545, 2009.

Radiative Transfer and Spectra in Stochastic Atmospheres

N.A. Silant'ev[1], G.A. Alekseeva[1], V.V. Novikov[1]

E-mail: *nsilant@bk.ru*

Various cosmic objects – stars, active galactic nuclei, accretion discs, etc., suffer the stochastic variations of temperature, large and small scales gas motions, magnetic fields, number densities of atoms and molecules. These stochastic variations give rise to changes of absorption factors, Doppler widths of lines and so on. The existence of numerous reasons for fluctuations lead to a Gaussian distribution of fluctuations. The observed spectra represent quantities averaged over the time and space. The common model explanations do not include the effect of fluctuations. In many cases, the consideration of fluctuations improves the agreement between theoretical explanations and observed values.

1 The radiative transfer equation in stochastic atmosphere

In a stochastic atmosphere the absorption factor has a fluctuating component: $\alpha = \langle\alpha\rangle + \alpha' \equiv \alpha^{(0)} + \alpha'$, $\langle\alpha'\rangle = 0$. The change of radiation intensity along the path s is determined by the equation

$$dI(\mathbf{n}, s) = -[\alpha^{(0)}(s) + \alpha'(s)]\, I(\mathbf{n}, s) ds. \tag{1}$$

The solution of this equation is

$$I(\mathbf{n}, s) = I(\mathbf{n}, 0) \exp\left[-\int_0^s ds'(\alpha^{(0)}(s') + \alpha'(s'))\right] \equiv I(\mathbf{n}, 0) \exp\left(-(\tau^{(0)} + \tau')\right). \tag{2}$$

The average of this expression, adopting for Gaussian probability distribution for fluctuations, gives

$$\langle I(\mathbf{n}, s)\rangle = I(\mathbf{n}, 0) \exp\left[-\left(\tau^{(0)} - \frac{1}{2}\langle\tau'^2\rangle\right)\right] \equiv I(\mathbf{n}, 0) \exp\left(-\tau_{eff}(s)\right). \tag{3}$$

It is seen from this expression that the averaged intensity $\langle I(\mathbf{n}, s)\rangle$ in stochastic medium decreases with the distance weaker than when accounting for the mean absorption factor $\alpha^{(0)}$.

[1] Central Astronomical Observatory at Pulkovo of Russian Academy of Sciences, Russia

V. Grinin et al. (eds) Radiation mechanisms of astrophysical objects. Yerevan: Edit Print, 2017, pp. 93–95.

The radiative transfer equation for $\langle I(\mathbf{n},s)\rangle$ has the form

$$\frac{d\langle I\rangle}{ds} = -\left[\alpha^{(0)}(s) - \langle\alpha'(s)\tau'(s)\rangle\right]\langle I\rangle + \left[\alpha^{(0)}_{sc}(s) - \langle\alpha'_{sc}(s)\tau'_{sc}(s)\rangle\right] \times \int d\mathbf{n}'\,\kappa(\mathbf{n}\cdot\mathbf{n}')\langle I(\mathbf{n}',s)\rangle + \langle S\rangle. \tag{4}$$

Here $\kappa(\mathbf{n}\cdot\mathbf{n}')$ is the phase function, $\langle S(\mathbf{n},s)\rangle$ is the averaged source function. Note that $\alpha(s) = \alpha_{sc}(s) + \alpha_{abs}(s)$. The detailed derivation of radiative transfer equations for all Stokes parameters in turbulent magnetized atmosphere is presented in [1].

2 Influence of Doppler width fluctuations on the center of absorption lines

The centers of absorption lines have a Gaussian form, i.e. the broadening is determined by Doppler's mechanism. Fluctuations of the thermal $u_{th} = u^{(0)}_{th} + u'_{th}$ and turbulent $u_{turb} = u^{(0)}_{turb} + u'_{turb}$ velocities give rise to fluctuations of the Doppler width

$$\Delta\lambda_D = \Delta^{(0)}_D + \Delta\lambda'_D, \quad \langle\Delta\lambda'_D\rangle = 0. \tag{5}$$

The level of fluctuations η is determined by the ratio $\eta = |\Delta\lambda'_D|/\Delta\lambda^{(0)}_D$. The averaged value of absorption factor up to $\eta \le 0.3$ has the form

$$\langle\alpha_\lambda(x)\rangle = \left\langle \frac{\alpha_0}{\Delta\lambda_D}\exp\left[-\left(\frac{\lambda-\lambda_0}{\Delta\lambda_D}\right)^2\right]\right\rangle \simeq \alpha^{(0)}(x)\exp\left(3x^2\eta^2\right)\left[(1+\eta^2)\,\cosh\left(2\eta x^2\right) - \eta\,\sinh\left(2\eta x^2\right)\right], \tag{6}$$

where $x = (\lambda-\lambda_0)/\Delta\lambda^{(0)}_D$ and $\alpha^{(0)}(x) = (\alpha_0/\Delta\lambda^{(0)}_D)\exp(-x^2)$. It is seen from this expression that in the center of the line ($x = 0$)

$$\langle\alpha_\lambda(0)\rangle \simeq \alpha^{(0)}(0)\,(1+\eta^2). \tag{7}$$

Thus, the stochastic effect gives rise to additional increase of line's depth. Note that non-LTE models and also synthetic spectra often lead to an increase in the depth of the absorption line. Nevertheless, sometimes this increase is insufficient to explain the observed depth of the line. In these cases the consideration of stochastic effect may help.

3 The influence of fluctuations on spectra in the continuum

The convective and turbulent motions and the magnetic field evolution lead to temperature fluctuations in stellar atmospheres, active galactic nuclei and

other cosmic objects. First, we demonstrate the nature of statistical effects by considering two realizations with temperatures $T_0 + T'$ and $T_0 - T'$. The mean value of Planck function (in Wien's limit) is equal to

$$\begin{aligned}\langle B_\lambda(T)\rangle &= \frac{1}{2}\,\frac{2hc^2}{\lambda^5}\left\{\exp\left[-\left(\frac{h\nu}{k(T_0+T')}\right)\right] + \exp\left[-\left(\frac{h\nu}{k(T_0-T')}\right)\right]\right\} \\ &\simeq B_\lambda(T_0)\cosh\left(\frac{h\nu}{kT_0}\,\frac{T'}{T_0}\right) \geq B_\lambda(T_0).\end{aligned} \tag{8}$$

Here we accepted $T' \ll T_0$. This simple example demonstrates that the averaged value $\langle B_\lambda(T_0)\rangle$ is larger than $B_\lambda(T_0)$. Analogously one can see that the averaged value of absorption factor $\langle \alpha_\lambda(T)\rangle$ may be either larger than $\alpha_\lambda(T_0)$ or smaller than this value, depending on specific form of function $\alpha_\lambda(T)$. The averaged radiation flux $\langle H_\lambda\rangle$ with allowance for temperature fluctuations is determined as

$$\langle H_\lambda\rangle = 2\pi \int_0^\infty d\langle\tau_\lambda\rangle \int_0^1 d\mu\, \exp\left[-\frac{\langle\tau_\lambda\rangle}{\mu}\right] \frac{\langle\alpha_\lambda(T)B_\lambda(T)\rangle}{\langle\alpha_\lambda(T)\rangle}, \tag{9}$$

where $d\langle\tau_\lambda\rangle = \langle\alpha_\lambda(T)\rangle ds$ determines the averaged optical length. It is interesting that in the Wien limit $\langle H_\lambda\rangle$ can be derived directly from observed spectrum, from the first and second derivatives over λ of the observed spectrum. The fluctuation effects are considered in the papers [2–4].

References

1. *N.A. Silant'ev*, Astron. Astrophys., **433**, 1117, 2005.
2. *N.A. Silant'ev, G.A. Alekseeva, V.V. Novikov*, Astrophys., **54**, 642, 2011.
3. *N.A. Silant'ev, G.A. Alekseeva, V.V. Novikov*, Astrophys. Space Sci., **342**, 433, 2012.
4. *N.A. Silant'ev, G.A. Alekseeva*, Astron. Astrophys., **479**, 207, 2008.

Section II
Interstellar Matter

V.V. Sobolev and Physics of Gaseous Nebulae

A.F. Kholtygin[1], Yu.V. Milanova[1]

E-mail: *afkholtygin@gmail.com*

First works by V.V. Sobolev were devoted to gaseous nebulae. He proposed a method for determining the nebula temperature based on the analysis of the energy balance of the electron gas. He also investigated the transfer of L_α and L_c radiation and the role of light pressure in their dynamics. The works by V.V. Sobolev were at the bases of constructing the ionization models of gaseous nebulae. The Sobolev method is widely used in solving the problems of radiation transfer in the nebulae. In our report we review the impact of the ideas and methods proposed by V.V. Sobolev on both the classic and contemporary researches in physics of gaseous nebulae.

1 Introduction

There were about 200 papers published in 1800 – 1941 (according to ADS) before V.V. Sobolev started to study gaseous nebulae. First planetary nebulae, the Dumbbell Nebula M 27, was discovered by Ch. Messier in 1764 (see, e.g., [10]). W. Herschel proposed in 1791 that PNe derive their energy from a nearby star.

The first step towards an understanding of the nature of PNe was made by W. Huggins in 1864 with his spectroscopic observation of NGC 6543 [5]. He saw a single bright line in the spectra. Subsequent observations, with better resolution, showed that this bright line was actually the famous N_1+N_2 doublet.

Studying H_β, Menzel (1926) suggested that all the stellar outputs beyond the Lyman limit (912 Å) should be utilized to ionize the hydrogen atom [11]. In 1927 Zanstra supposed that H-lines are the result of the recombination of ionized hydrogen [20]. In 1928 Bowen identified the 8 strongest nebular lines as being due to metastable states of NII, OII and OIII [3].

In 1929 Perrine interpreted the broad (or even split) emission lines in PNe spectra as a result of an expansion of PNe [13] (not rotation as had been supposed before). In 1933 Ambartsumian found that the mean electron temperature of PNe is about of 10000 K [2].

For determination of the parameters of central stars (CS) of PNe, the methods by Zanstra [21] and Stoy [18] were proposed. In 1938 Whipple established that PNe ages are in the interval 10^3–10^5 years [19]. The physics of PNe was considered in the series of 18 papers written by Menzel and Aller in 1937–1945 (see [1]).

Here we review the papers by V.V. Sobolev which influenced on our understanding of the physics of planetary nebulae.

[1] Saint Petersburg State University, Russia

V. Grinin et al. (eds) Radiation mechanisms of astrophysical objects. Yerevan: Edit Print, 2017, pp. 99–104.

2 Sobolev's works on physics of gaseous nebulae

V.V. Sobolev started to study the PNe when he was still a graduate student by V.A. Ambartsumian.

Here we list the early papers by Sobolev which were not included in ADS:

1) *V.V. Sobolev,* "Determination of electron temperatures of planetary nebulae and improvement of the method of nebulium to determine the temperature of their central stars," Trudy Astron. Obs. Leningr. Univ., **12**, 3–16, 1941;
2) *V.V. Sobolev,* "Light pressure in the expanding nebula," Astron. Zh., **21**, 143–148, 1944;
3) *V.A. Ambartsumian, E.R. Mustel, A.B. Severnyi, V.V. Sobolev,* Teoreticheskaya Astrophysika. Moscow: GITTL, 1952;
4) *V.V. Sobolev,* "Physics of planetary nebulae," Voprosy Kosmogonii, **VI**, 112–155, 1958.

Results of the paper [1] were included in the PhD thesis of V.V. Sobolev.

A short review of other papers by V.V. Sobolev devoted to physics of PNe is as follows. The diffusion of L_α radiation in nebulae and stellar envelopes was studied in [15]. The problem of the brightness of a spherical nebula was considered in [16]. The scattering of radiation of the central star in a spherical nebula was investigated by Kolesov and Sobolev in [7, 8].

Many problems devoted to physics of the nebulae were generalized in the famous Sobolev's Course in Theoretical Astrophysics [17].

3 Energy balance in gaseous nebulae

In his paper [14] V.V. Sobolev used the law of energy conservation in the following form:

$$n_1 \alpha \varepsilon = n_e n^+ \sum_{i=1}^{\infty} \varepsilon_i + \mathsf{E} + n_1 n_e \left(\gamma h\nu_0 + \sum_{i=2}^{\infty} D_i h\nu_{1i} \right). \qquad (1)$$

In the left part of the equation the energy gained by electrons due to photoionization of the hydrogen atom is given, in the right part the energy losses are enumerated. Here n_1 is the population of the first atom level, α is the rate of ionization of the neutral hydrogen atom due to the radiation of the central star of the PN, and ε is the mean energy obtained by photoelectron after photoionization.

The value n_e is the electron number density, n^+ is the number density of ionized hydrogen atoms, ε_i is the part of energy lost by electrons at recombination to level i, E is the energy spent to emission in OIII lines N_1 ($\lambda\,5007$ Å) and N_2 ($\lambda\,5007$ Å, see Fig. 1, left panel), $h\nu_0$ is the energy of the hydrogen atom ionization from the ground level, γ is the rate of the H atom ionization by electron collisions, and D_i is the rate of energy lost by electrons due to collision excitation from

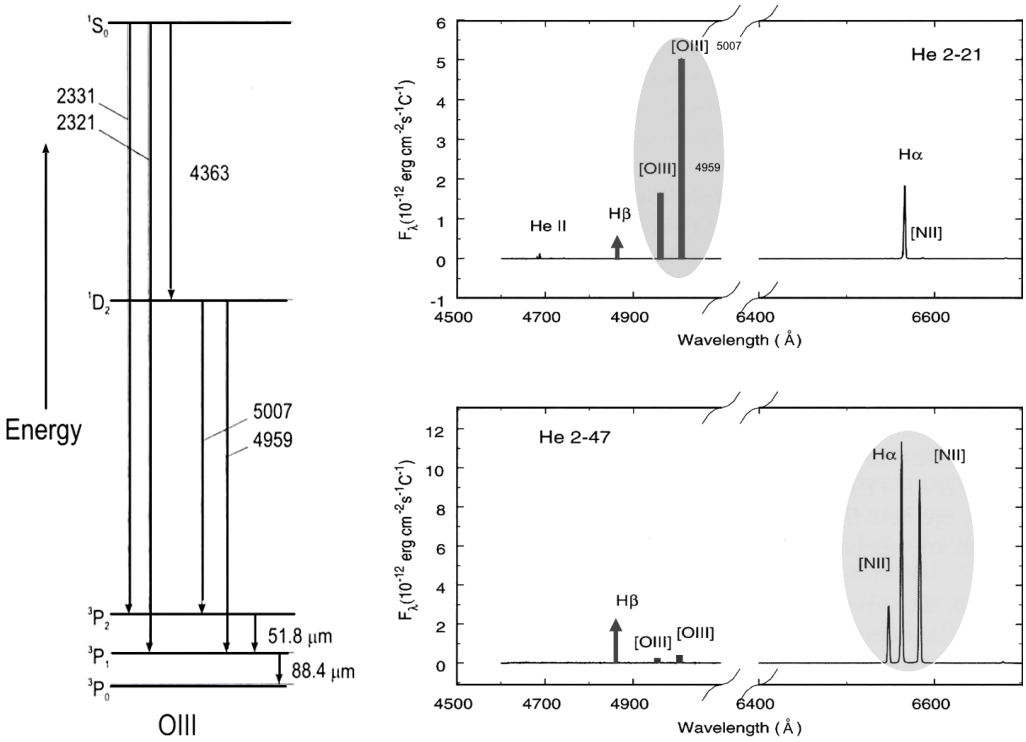

Figure 1: Left panel: ground and metastable OIII levels and corresponding forbidden lines. Right panel: spectra of the high and low excitation nebulae (based on Fig. 12.3 in [9]).

the ground level to level i (in units of $h\nu_1$ being the energy of excitation of the level i).

The left part of Eq. (1) was calculated by Sobolev, supposing that the emission of the central star (CS) of the PNe can be presented as the black-body emission with the temperature emission and for $\propto \nu^{-3}$ dependence of the photoionization cross sections of the H atoms with the ground level $i = 1$.

The same approximation for a dependence of the photoionization cross sections of the H atoms for an arbitrary level i was used to calculate the first term in the right part of Eq. (1).

In the time when Sobolev wrote his paper the values of effective cross sections for excitation of the upper levels of ion O^{2+} were unknown, so he estimated the value of E via the line intensity ratio $I(N_2)/I(H_\beta)$ supposing that the ratio $I(N_1)/I(N_2) = 3$. Then

$$\mathsf{E} = \int EdV = 4\frac{I(N_2)}{I(H_\beta)} A_{42} h\nu_{42} \int n_4 dV, \tag{2}$$

where A_{42} is the transition probability for line H_β, $h\nu_{42}$ is the energy of the transition $4 \to 2$ and n_4 is the population of the level $n = 4$ of hydrogen. It means that $\mathsf{E} \propto I(N_2)/I(H_\beta)$.

Table 1: Calculations by Sobolev in a comparison with the data of other authors

Name	Nebular parameters					Contribution		
	$\frac{I(\mathrm{N_2})}{I(\mathrm{H}_\beta)}$	$\frac{T_*^{VVS}}{10^3\mathrm{K}}$	$\frac{T_*}{10^3\mathrm{K}}$	$\frac{T_\mathrm{e}^{VVS}}{10^3\mathrm{K}}$	$\frac{T_\mathrm{e}}{10^3\mathrm{K}}$	Recom-bination	N_1+N_2	Excita-tion HI
IC 4593	1.7	25	28[a]	13	6.0[c]	0.25	0.60	0.15
NGC 6543	1.6	41	47[a]	16	7.9[c]	0.20	0.30	0.50
NGC 6572	2.4	48	66[a]	18	8.9[c]	0.15	0.40	0.45
NGC 6826	2.0	29	33[a]	13	8.3[c]	0.20	0.60	0.20
NGC 7009	3.1	45	98[b]	15	6.5[c]	0.15	0.55	0.30
NGC 7662	3.7	76	118[b]	19	12.3[c]	0.10	0.30	0.60

Notes: [a]Kaler, Jacobi (1991), [b]Capriotti, Kovach (1968), [c]Milanova, Kholtygin (2009).

The last term in Eq. (1) is determined by the value of n_1 which is the mean population of the ground level of hydrogen. For PNe, the ratio $n_1/n(\mathrm{H}) \ll 1$, where $n(\mathrm{H})$ is the full hydrogen number density. It means that the last term in Eq. (1) is proportional to n_1/n^+.

The final equation connecting the black-body temperature of the CS T_* and the mean electron temperature of the nebula T_e is as follows (Eq. 19 in [14]):

$$AT_* = BT_\mathrm{e} + C\,\frac{I(\mathrm{N_2})}{I(\mathrm{H}_\beta)} + D\,\frac{n_1}{n^+}. \tag{3}$$

Here the ionization ratio n^+/n_1 can be determined using the equation of the ionization balance

$$\frac{n_\mathrm{e}n^+}{n_1} = W\sqrt{\frac{T_\mathrm{e}}{T_*}}\,\frac{(2\pi mkT_*)^{3/2}}{h^3}e^{-\frac{h\nu_0}{kT_*}}, \tag{4}$$

where W is the dilution factor, m is the mass of electron, k is the Boltzmann constant, h is the Planck constant, and $h\nu_0$ is the ionization potential for the ground level of H.

The coefficients A, B, C, D were calculated by Sobolev for $T_*/10^3\,\mathrm{K} \in [20, 80]$ and $T_\mathrm{e}/10^3\,\mathrm{K} \in [1, 50]$ (see Tables 1, 2 in [14]). He used these calculations to estimate the parameters T_e and $T*$ for selected PNe.

In Table 1 we list the values T_*^{VVS} and T_e^{VVS} obtained by Sobolev in [14] (columns 3 and 5) in a comparison with the data obtained in papers [4, 6, 12] (columns 4 and 6). In the columns 7–9 of Table 1 the contributions of different sources of cooling in the total cooling rate in Eq. (1) calculated by Sobolev are presented.

It is worth to note that the temperature of the central stars of the PNe obtained in the cited papers essentially exceeds the values given by Sobolev. Conversely, Sobolev's electronic temperatures for these PNe (in column 5) are significantly higher than the modern data by Milanova and Kholtygin [12] (column 6).

Table 2: Corrected cooling process contributions

Name	Contribution			$q(N_1+N_2)$
	Recombination	All collisions	Excitation HI	
IC 4593	0.13	0.87	–	0.66
NGC 6543	0.08	0.92	0.0002	0.32
NGC 6574	0.06	0.94	0.0003	0.31
NGC 6826	0.13	0.87	0.002	0.65
NGC 7009	0.03	0.97	–	0.24
NGC 7662	0.04	0.95	0.01	0.23

The main reason for this discrepancy in our opinion is underestimation of the energy loss due to excitation of the metastable levels of not only OIII but numerous ions of the other elements. If we look at Fig. 1 (right panel) we see that the fluxes of N_1+N_2 lines in the spectra of some nebulae are small in a comparison of the fluxes of other forbidden lines. It means that one has to add the new terms in the value E in Eq. (1).

The corrected energy balance equation (3) can be rewritten as

$$AT_* = BT_\mathrm{e} + E' + D\frac{n_1}{n^+}, \tag{5}$$

where E' is the corrected value of the energy losses due to excitation of *all* collisional transitions.

To estimate the value of E' we use the following procedure. Firstly, we take more exact than obtained by Sobolev values of T_* and T_e, which are given in the columns 4 and 6 of Table 1. Secondly, we calculate the coefficients A, B, D and the ratio n_1/n^+, using the data of Tables 1–4 in the paper [14] for these updated values of T_* and T_e.

Substituting those coefficients into Eq. (5), one can evaluate the full energy loss value E' and the ratio

$$q(\mathrm{N}_1 + \mathrm{N}_2) = C\left(\frac{I(\mathrm{N}_2)}{I(\mathrm{H}_\beta)}\right)\Big/E',$$

the fraction of the energy excitation of N_1+N_2 lines in all collision energy losses E'.

In the columns 2–4 of Table 2 we give the corrected values of the relative contributions of the cooling processes for the same nebulae which are considered in Table 1. In the last column we present the ratio $q(N_1+N_2)$. Comparing Tables 1 and 2, we can conclude that the part of the energy losses which is spent to the excitation of hydrogen is negligible due to the lower electron temperatures than accepted in [14]. In the same time the recombination losses appear to be significantly less important than they were estimated by Sobolev. This result is in an agreement with Sobolev's main assumption that the collision processes give the most contribution to the energy loss by electron in the PNe.

4 Conclusions

Sobolev's works on physics of gaseous nebulae were among the first Foundation Stones of physics of planetary nebulae. Our review of Sobolev's work dedicated to physics of the nebulae showed that the main ideas proposed by Sobolev appear to be correct, but due to the poor knowledge of the atomic parameters in the time when Sobolev wrote his paper, the important corrections to the parameters of the PNe obtained by him have to be done.

References

1. *L.H. Aller, D.H. Menzel*, Astrophys. J., **102**, 239, 1945.
2. *V. Ambartsumian*, Tsirk. Pulkovo Obs., No. 6, 10, 1933.
3. *I.S. Bowen*, Astrophys. J., **67**, 1, 1928.
4. *E.R. Capriotti, W.S. Kovach*, Astrophys. J., **151**, 991, 1968.
5. *W. Huggins, W.A. Miller,* Phil. Trans. Roy. Soc., **154**, 437, 1864.
6. *J.B. Kaler, G.H. Jacoby*, Astrophys. J., **372**, 215, 1991.
7. *A.K. Kolesov, V.V. Sobolev*, Astrophys., **33**, 235, 1991.
8. *A.K. Kolesov, V.V. Sobolev*, Astrophys., **35**, 304, 1993.
9. *S. Kwok*, The Origin and Evolution of Planetary Nebulae. Cambridge: Cambridge University Press, 2000.
10. *S. Kwok*, Proc. IAU Symp., **283**, 1, 2012.
11. *D.H. Menzel*, Publ. Astron. Soc. Pacif., **38**, 295, 1926.
12. *Yu.V. Milanova, A.F. Kholtygin*, Astron. Lett., **35**, 518, 2009.
13. *C.D. Perrine*, Astron. Nachr., **237**, 89, 1929.
14. *V.V. Sobolev*, Trudy Astron. Obs. Leningr. Univ., **12**, 3, 1941.
15. *V.V.Sobolev*, Sov. Astron., **1**, 678, 1958 (original paper in Astron. Zh., **34**, 694, 1957).
16. *V.V. Sobolev*, Sov. Astron., **4**, 1, 1960.
17. *V.V. Sobolev*, Course in Theoretical Astrophysics. Moscow: Nauka, 1967 (1st edition), 1975 (2nd edition), 1985 (3rd edition).
18. *R.H. Stoy*, Mon. Not. Roy. Astron. Soc., **93**, 588, 1933.
19. *F.L. Whipple*, Harvard Coll. Obs. Bull., No. 908, 17, 1938.
20. *H. Zanstra*, Astrophys. J., **65**, 50, 1927.
21. *H. Zanstra*, Z. Astrophys., **2**, 1, 1931.

Diffuse Interstellar Bands Approaching Centenary

J. Krełowski[1]

E-mail: *jacek@umk.pl*

The paper presents in short the history of the investigations of diffuse interstellar bands (DIBs) – the longest standing unsolved problem of the whole spectroscopy. The importance of "peculiar" objects is emphasized as well as a search for the relations of DIBs to other (identified) interstellar spectral features. Some suggestions, concerning possible carriers of diffuse bands are presented as well.

1 Statement of the problem

The problem of DIBs is located in a broader subject matter of the physics and chemistry of the interstellar medium (ISM), which consists of atomic gas, molecules, and dust grains. The origin of these bands is as puzzling as since their first detection, more than 90 years ago.

DIBs appeared in the literature more than 90 years ago [1] as described in a nice, recent paper by McCall and Griffin [2]. However, the term "diffuse interstellar bands" was introduced later by P.W. Merrill (1938) who was the first to investigate these puzzling features systematically. At that time only six DIBs were known but their interstellar origin considered as certain. Fig. 1 demonstrates why the features are interstellar – they are stationary as well as NaI interstellar lines in the sharp contrast to stellar lines – and why they are known as "diffuse" – they are much shallower but broader than the NaI lines.

The application of solid state detectors to DIB observations led to discoveries of new features. Currently, the list of known DIBs contains 414 entries [3]; a majority of them – very shallow. Such a rich spectrum cannot share a common carrier; moreover the DIB profiles differ seriously from as narrow ones as about 1 Å (e.g. 6196) to more than 40 Å (e.g. 4430). They bear the name "diffuse" because their profiles are always broader than those of many of the well known atomic/molecular lines, even though the latter are much stronger (Fig. 1).

Nearly all conceivable forms of matter – from hydrogen anion to dust grains – have already been proposed as DIB carriers, so far with no generally accepted success. The abundance of elements in the Universe constrains the chemical composition of the DIB carriers. They ought to be built out of the most abundant elements: H, O, C, N, a small contribution of other elements also cannot be

[1] Center for Astronomy, Nicolaus Copernicus University, Toruń, Poland

V. Grinin et al. (eds) Radiation mechanisms of astrophysical objects. Yerevan: Edit Print, 2017, pp. 105–114.

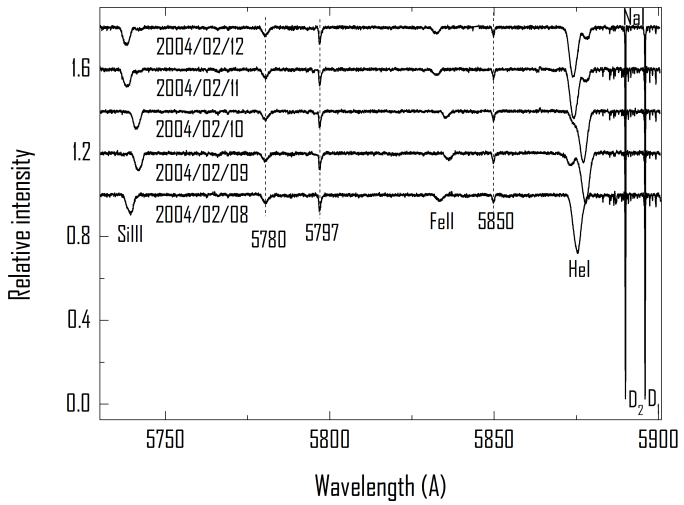

Figure 1: Interstellar NaI lines (right) and three diffuse bands in the spectra of HD 23180 – the spectroscopic binary with a 4.5 day period. Stellar lines (identified) perform the Doppler "dance". Note that strong interstellar NaI lines are narrower than the indicated DIBs.

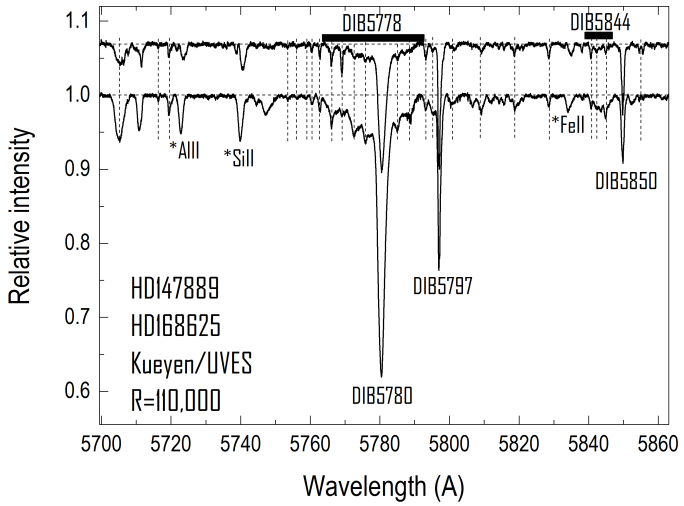

Figure 2: The spectral range in which M.L. Heger found the first two DIBs allows now to trace about 30 features, marked with vertical lines – a vast majority very shallow.

excluded. Among this group of elements carbon is in an exceptional position, since it can form a great number of stable compounds with a linear, planar and spherical structure. Bare carbon chains of 5 to 15 C atoms have been proposed as carriers of diffuse interstellar bands by Douglas [4]. Fulara et al. [5] and Freivogel et al. [6] later extended this hypothesis to the whole class of linear, unsaturated hydrocarbons. The interstellar medium (star forming regions) contains a lot of molecules based on carbon chain skeletons. Their vibrational and electronic transitions cause features in the spectral range full of diffuse bands. Apart

from (hydro)carbon chains and polycyclic aromatic hydrocarbons (PAHs), also fullerenes (recently identified in circumstellar shells by [7]) fall in this category having features in visible and near infrared spectral ranges. Unfortunately, the existing spectra of the above mentioned molecules obtained in gas phase experiments (see for reviews [8, 9]) do not match the astrophysical ones. On the other hand, the spectra which have been acquired using the matrix isolation spectroscopy (MIS) cannot be directly compared to the astrophysical spectra. The features in MIS spectra are broadened and wavelength-shifted with respect to the gas phase (the magnitude of the shift remains unknown); the rotational structure is missing. However, the MIS spectra are necessary to determine relative strength ratios of molecular features as the CRDS technique (Cavity Ring Down Spectroscopy) – the method of acquiring gas-phase spectra of molecules – allows only to scan a single feature in a single experiment.

The fine structure (reminiscent of the rotational contours of bands of polyatomic molecules) has been detected in some DIBs [10, 11] giving a strong support to the idea of molecular origin of DIBs.

It is evident that the only way to identify the DIB carriers is to compare observed spectra with those of suspect molecules acquired in gas phase experiments. It is extremely important to keep in mind that what we observe are stellar spectra with interstellar features superimposed. No star is just a lamp, producing continuous spectrum. Stellar spectra contain many atomic lines originating in their atmospheres of the intensities depending on their temperatures, profiles depending on the luminosity class and widths – on rotational speed. This is why not every star allows to separate properly every interstellar feature from its spectrum. The additional problem is the likely present in a majority of targets Doppler splitting of interstellar features. DIB profiles modified in this fashion must not be compared to laboratory ones. This condition shrinks seriously the number of possible targets in which the DIB profiles can be used for such comparison.

The author is collecting high resolution echelle spectra of OB stars since 1993 using different instruments at both hemispheres. The latter is of basic importance for a reliable comparison between laboratory and astrophysical spectra. Very likely the recent attempts to identify neutral PAHs in translucent clouds [12, 13] failed because there are (most likely) a lot of different species in the space and thus abundances of individual PAHs are very small pushing their features below the detection level. Still much higher S/N ratio is necessary to discover ultraviolet PAH features. The very high S/N ratio spectrum of HD 169454 seems to contain the strongest feature of benzo[ghi]perylene (Fig. 3) – one of the investigated PAHs. The evident, neighbour C_3 band, is observed for the first time in this object [14]. High resolution echelle spectra allow to observe several spectral features of simple molecular species: CH, CH^+, CN, OH, OH^+, NH, C_2 and C_3; recently also SH [15]. It is interesting whether their abundance ratios are similar in all objects or not. The existing data suggest that CH and OH are closely related while NH and CH^+ behave in a different fashion [16, 17]. Let's emphasize that the above list allows

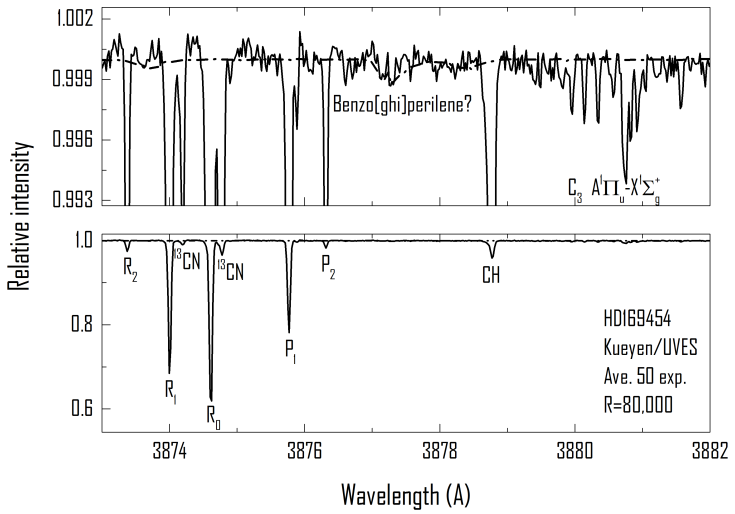

Figure 3: The extremely shallow feature in between of strong CN and CH bands, suggesting the presence of benzo[ghi]perylene in the spectrum of heavily reddened star. The dash-dot line is the laboratory spectrum, courtesy of F. Huisken.

to constrain chemistry of all most important elements: hydrogen, carbon, oxygen and nitrogen. The suggestion that profile widths of (some?) DIBs are related to rotational temperatures of simple carbon centrosymmetric species [18] needs a broader survey.

A comparison of band strength measurements, DIB profile details and their mutual relations require very high resolution, S/N ratio and a broad wavelength range. The necessary observations are very time-consuming and require well-designed procedures of data acquiring and reducing.

2 Families of diffuse bands?

The term "families" was used for the first time in the literature in relation to DIBs by Krełowski and Walker [19]. High resolution and high SNR spectra demonstrated that the strength ratio of the major DIBs: 5780 and 5797 changes from object to object. A similar result, confirming the variable DIB strength ratio was published soon after by Josafatsson and Snow [20] confirming that they are not of common origin but belong to different "families" considered as sets of features of common origin. Since 1975 the set of known DIBs was reasonably large [21] which also could suggest diverse origin of the whole DIB spectrum.

The two first objects, in which the variable ratio of major DIBs was observed as early as 1983, are HD 147165 (σ Sco) and HD 149757 (ζ Oph). The result was, however, published a couple of years later [22] for it looked incredible at that time. The terms σ and ζ type clouds, popular now, are rooted in that "ancient" project. The objects were later observed several times and the σ and ζ type clouds were connected not only to the 5780/5797 ratio but also to the shapes

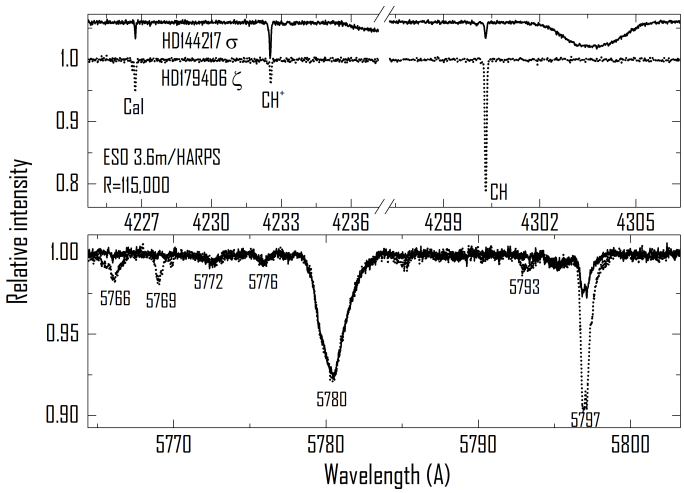

Figure 4: Major DIBs (lower panel) and the bands of simple interstellar radicals, observed in the spectra of HD 144217 and HD 179406 – the typical of σ and ζ type clouds. Note the identical intensity and profile of the 5780 DIB.

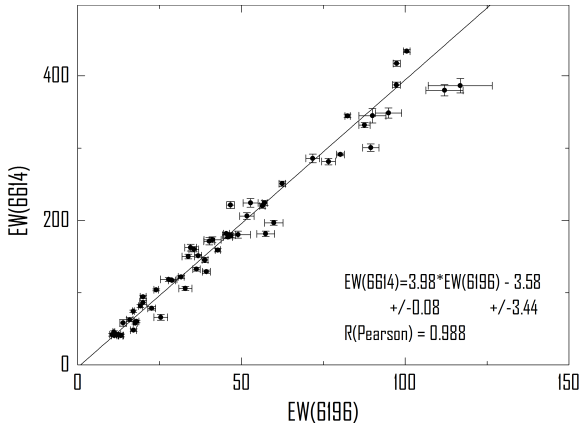

Figure 5: The nearly perfect correlation of the strengths of 6196 and 6614 DIBs.

of extinction curves (see [23]) and to the relative abundances of simple interstellar radicals [24]. Both DIBs and bands carried by simple molecules are depicted in Fig. 4, presenting the two σ and ζ type clouds of similar $E(B-V)$.

Naturally the very first idea was that one "family" members should share the carrier and thus – should be of constant strength ratio. The first DIB survey [25] found a pair that correlates almost perfectly: 6196 and 6614. The former is quite narrow while the latter is quite broad which does not support the idea of common origin. Their equivalent width ratio is nearly 4. This tight correlation was confirmed later by other teams, e.g [26] – it is thus established beyond a reasonable doubt. However, Galazutdinov et al. [11] demonstrated that while the strengths of the two DIBs are well correlated, their FWHMs (full-width half-maxima) are not. Figure 5 presents the above mentioned tight correlation based on spectra from three major world spectrographs: HARPS fed with the

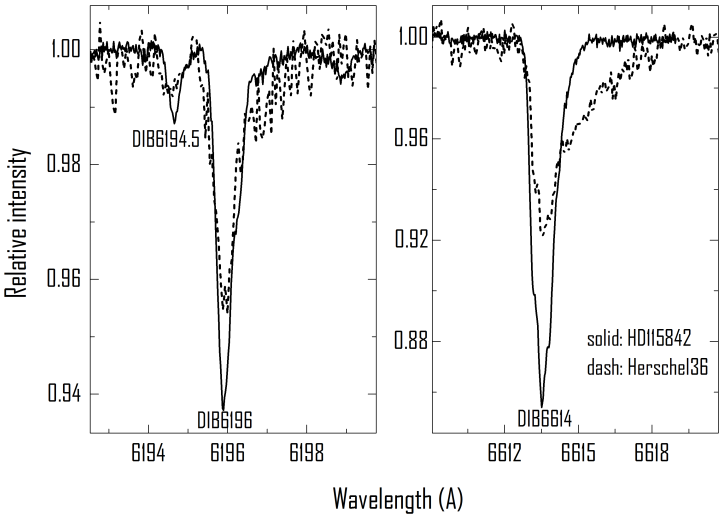

Figure 6: The lack of correlation between FWHM's of 6196 and 6614 DIBs. Note that also some differences of the strength ratio may be physically grounded.

3.6m ESO LaSilla telescope, UVES – attached to the Kueyen mirror of the VLT at Paranal and BOES – fed with the national Korean telescope at Bohyunsan. The very high correlation coefficient is shown. It is, however, a necessary but not a sufficient condition. Analyzing a spectrum of the Herschel 36, it is possible to find more spectacular evidence that FWHMs of the two DIBs do not behave in unison (Fig. 6). Moreover, the scatter, seen in Fig. 5, is very likely caused by different physical conditions inside individual clouds – not by just the measurements' errors.

3 Rest wavelengths

Rest wavelengths of DIBs are necessary to identify these puzzling features. However, having no identification we must not have the laboratory wavelengths of any spectral line or band. It is natural that the observed wavelengths of interstellar features are Doppler shifted because of the relative motions of interstellar clouds, the Sun and the Earth. One can shift the wavelength scale of any spectrum to that of some interstellar identified line; this may allow to determine the laboratory wavelengths of unidentified features providing they share the place of origin with the chosen identified line. This may be complicated because not all identified interstellar lines or bands share the same radial velocity.

Seemingly the only proper way to determine rest wavelengths of DIBs is to find an object (or a couple of objects) where radial velocities of all identified lines or bands are identical and their profiles – free of the Doppler splitting. Such objects are very scarce. They should be reasonably bright to allow acquiring high S/N spectra and reasonably heavily reddened to make the tracing of weak DIBs possible. The additional difficulty follows the fact that DIB profiles are not

just Gaussians and thus their central wavelengths may not coincide in different publications. This is broadly discussed in the paper by Bondar [27] where the rest wavelengths of 336 DIBs are determined using high quality spectra of 10 stars. However, even this method may not always lead to proper results. The example is the Orion Trapezium [28] where the observed DIBs are apparently red-shifted.

There is no explanation of this effect. Anyway it creates possible doubts on how far the wavelengths of DIBs, shifted to the rest wavelength frames of interstellar lines, are equal to the laboratory ones.

4 Profiles of diffuse bands

As mentioned above, the intrinsic profiles of diffuse bands are not just Gaussians; the profiles are not only quite broad but also asymmetric with possible substructures inside. Since the first such analysis [29] it was established that practically all narrow diffuse bands demonstrate some substructure patters, suggesting their molecular origin. It was demonstrated clearly in the paper by Galazutdinov et al. [11]. The profiles of very well correlated 6196 and 6614 DIBs apparently change from object to object where no Doppler splitting is observed in identified lines. The influence of the Doppler splitting on the observed DIB profiles was demonstrated, e.g., by Westerlund and Krełowski [30]. This mechanical broadening makes difficult a comparison of observed and laboratory DIB profiles.

It seems reasonable that changes of DIB profiles are results of different rotational temperatures of their carriers if the latter are molecules as well. It is much easier to find differences in rotational temperatures of centrosymmetric molecules as such temperatures may cover a very broad range [31].

Herschel 36 is a very specific object – the only such one in the sky. Oka et al. [32] found the CH and CH^+ molecules in its spectrum to be rotationally excited. The exceptionally high rotational temperatures of the simple, polar radicals are apparently related to severely broadened profiles of some DIBs (Fig. 7). However, not all profiles are broadened; for example that of the 5850 DIB is free of any visible broadening.

Another unique object in the sky is HD 34078 (AE Aur). Adamkovics et al. [31] found the exceptionally high rotational temperature of the C_3 molecule in this object. The object seems extremely interesting as the spectral features in its spectrum, carried by simple interstellar radicals, decline with time. Despite of this the profiles of diffuse bands seem to be broadened and their gravity centers – blue-shifted [33]. Also in this case one can expect that the rotational temperatures of the DIB carriers may be responsible for the observed changes of profiles.

The star taken for comparison is HD 27778. Apparently, the 5797 profile resembles that, observed by Oka et al. [32] in 9 Sgr. It is interesting that the DIB is broadened in HD 34078 as well but it looks also blue-shifted. The rotational components of CH^+ and CH are not observed in HD 34078 and so the rotational temperature of these species is apparently lower than in Herschel 36.

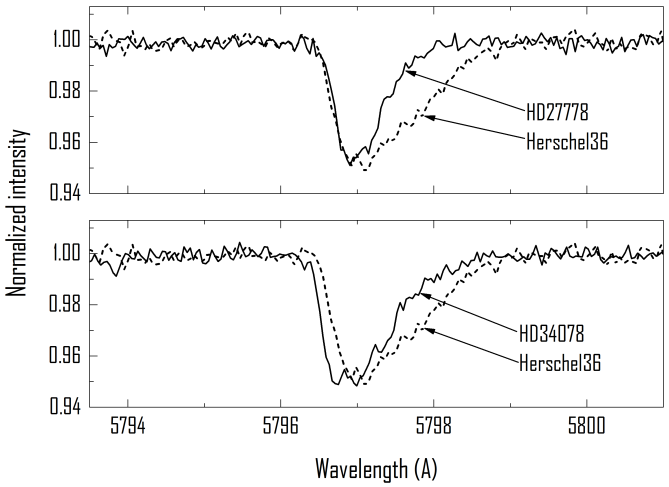

Figure 7: 5797 DIB profiles broadened in the spectra of Herschel 36 and HD 34078. The comparison of HD 27778 with Herschel 36 closely resembles Fig. 3 of [32]. Apparently the DIB is broadened in HD 34078 but not as much as in Herschel 36. The spectra of HD 34078 and HD 27778 are from MIKE (R = 67 000) while that of Herschel 36 from Feros (R = 48 000). All spectra are shifted to the rest wavelength velocity frame using the KI 7699 Å line.

"Peculiar" cases, like AE Aur or Herschel 36, are extremely interesting because they do reflect some specific situations which can take place only in individual clouds (likely homogeneous environments). Unfortunately such cases are extremely rare; it is of basic importance to hunt for more such "peculiar" objects – perhaps they will allow to understand the physics and chemistry leading to the formation of the DIB spectrum.

5 Identification propositions

The first proposition of a DIB identification, but signed with a question mark, is the CH_2CN^- molecule proposed as the carrier of the 8037 Å DIB by Cordiner and Sarre [34]. This feature is located in the wavelength range severely contaminated with telluric lines and fringes. Thus it is very difficult to check whether the identification is reliable because the profile of it is clearly seen only in a few objects and no more its features are proposed.

Recently we found a very weak DIB which coincides with the electronic, gas-phase band of HC_4H^+; this finding [35] supports DIB molecular origin. The identification was disputed by Maier et al. [36]; this fact clearly demonstrates the necessity of close cooperation between experimentalists and observers. The lack of the latter leads to obvious confusions. The wavelength of the above mentioned feature may be a bit floating due to different rotational temperature of the carrier. Unfortunately, the band is so weak that a proper statistics of observations is hardly available.

Another overlap between a lifetime broadened absorption spectrum, recorded through a hydrocarbon plasma and a stronger DIB at 5450 Å was reported by [37]; an identification of the carrier was not possible yet. If l-C_3H_2 can produce the 5450 Å DIB, as proposed by Maier et al. [38] then the carrier is unacceptably abundant; moreover the second l-C_3H_2 feature, near 4883 Å is clearly of another origin [39].

The recently published by Campbell et al. [40] gas phase spectra of the C_{60}^+ reactivated the dormant idea of this species to be the carrier of two near infrared DIBs: 9577 and 9632. According to the authors the cation of C_{60}^+ exhibits four relatively strong spectral lines centered at 9365.9, 9428.5, 9577.5 and 9632.7 Å with relative intensity 0.2, 0.3, 1.0 and 0.8, respectively, and the wavelength precision not worse than 0.1Å. However, the authors did not collect big enough sample of spectra allowing a comparison with the laboratory data. The strength ratio of both strong, observed features may seriously differ from the laboratory predictions; moreover the ratio is apparently variable if observed in a pretty big sample of targets. Also the rest wavelengths of both DIBs do not match the laboratory ones inside the possible errors.

Acknowledgments. The author is very indebted to Dr. G.A. Galazutdinov for very helpful discussions. The paper was financially supported by the grant 2015/17/B/ST9/03397 of the Polish National Science Center.

References

1. *M.L. Heger*, Lick Obs. Bull., **10**, 141, 1922.
2. *B.J. McCall, E. Griffin*, Proc. Roy. Soc. A, **469**, 20120604, 2013.
3. *L.M. Hobbs, D.G. York, J.A. Thorburn et al.*, Astrophys. J., **705**, 32, 2009.
4. *A.E. Douglas*, Nature, **269**, 130, 1977.
5. *J. Fulara, D. Lessen, P. Freivogel, J.P. Maier*, Nature, **366**, 439, 1993.
6. *P. Freivogel, J. Fulara, J.P. Maier*, Astrophys. J., **431**, 151, 1994.
7. *J. Cami, J. Bernard-Salas, E. Peeters, S.E. Malek*, Science, **329**, 1180, 2010.
8. *E.B. Jochnovitz, J.P. Maier*, Ann. Rev. Phys. Chem., **59**, 519, 2008.
9. *H. Linnartz*, in Cavity Ring-down Spectroscopy Techniques and Applications. Eds. G. Berden, R. Engeln. Wiley-Blackwell, 2009, p. 145.
10. *T.H. Kerr, R.E. Hibbins, S.J. Fossey et al.*, Astrophys. J., **495**, 941, 1998.
11. *G.A. Galazutdinov, C. Moutou, F. Musaev, J. Krełowski*, Astron. Astrophys., **384**, 215, 2002.
12. *F. Salama, G. Galazutdinov, L. Biennier et al.*, Astrophys. J., **728**, 154, 2011.
13. *R. Gredel, Y. Carpentier, G. Rouill et al.*, Astron. Astrophys., **530**, 26, 2011.
14. *M.R. Schmidt, J. Krełowski, G.A. Galazutdinov et al.*, Mon. Not. Roy. Astron. Soc., **441**, 1134, 2014.

15. *D. Zhao, G. Galazutdinov, H. Linnartz, J. Krełowski*, Astron. Astrophys., **579**, 1, 2015.

16. *T. Weselak, G. Galazutdinov, Y. Beletsky, J. Krełowski*, Mon. Not. Roy. Astron. Soc., **402**, 1991, 2010.

17. *T. Weselak, G. Galazutdinov, Y. Beletsky, J. Krełowski*, Astron. Astrophys., **499**, 783, 2009.

18. *M. Kazmierczak, P. Gnaciński, M.R. Schmidt et al.*, Astron. Astrophys., **498**, 785, 2009.

19. *J. Krełowski, G.A.H. Walker*, Astrophys. J., **312**, 860, 1987.

20. *K. Josafatsson, T.P. Snow*, Astrophys. J., **319**, 436, 1987.

21. *G.H. Herbig*, Astrophys. J., **196**, 129, 1975.

22. *J. Krełowski, B.E. Westerlund*, Astron. Astrophys., **190**, 339, 1988.

23. *E.L. Fitzpatrick, D. Massa*, Astrophys. J., **663**, 320, 2007.

24. *J. Krełowski, T.P. Snow, C.G. Seab, J. Papaj*, Mon. Not. Roy. Astron. Soc., **258**, 693, 1992.

25. *C. Moutou, J. Krełowski, L. d'Hendecourt, J. Jamroszczak*, Astron. Astrophys., **351**, 680, 1999.

26. *B.J. McCall, M.M. Drosback, J.A. Thorburn et al.*, Astrophys. J., **708**, 1628, 2010.

27. *A.V. Bondar*, Mon. Not. Roy. Astron. Soc., **423**, 725, 2012.

28. *J. Krełowski, G.A. Galazutdinov, G. Mulas et al.*, Mon. Not. Roy. Astron. Soc., **451**, 3210, 2015.

29. *B. Westerlund, J. Krełowski*, Astron. Astroph., **218**, 216, 1988.

30. *B. Westerlund, J. Krełowski*, Astron. Astroph., **189**, 221, 1988.

31. *M. Adamkovics, G.A. Blake, B.J. McCall*, Astrophys. J., **595**, 235, 2003.

32. *T. Oka, D.E. Welty, S. Johnson et al.*, Astrophys. J., **773**, 42, 2013.

33. *G.A. Galazutdinov, G. Manico, J. Krełowski*, Mon. Not. Roy. Astron. Soc., **366**, 1075, 2006.

34. *M.A. Cordiner, P.J. Sarre*, Astron. Astrophys., **472**, 537, 2007.

35. *J. Krełowski, Y. Beletsky, G. Galazutdinov et al.*, Astrophys. J. Lett., **714**, L64, 2010.

36. *J.P. Maier, S. Chakrabarty, F.J. Mazzotti et al.*, Astrophys. J. Lett., **729**, L20, 2011.

37. *H. Linnartz, N. Wehres, H. van Winckel et al.*, Astron. Astrophys., **511**, 3, 2010.

38. *J.P. Maier, G.A.H. Walker, D.A. Bohlender et al.*, Astrophys. J., **726**, 41, 2011.

39. *J. Krełowski, G. Galazutdinov, R. Kołos*, Astrophys. J., **735**, 124, 2011.

40. *E.K. Campbell, M. Holz, D. Gerlich, J.P. Maier*, Nature, **523**, 322, 2015.

41. *M. Kazmierczak, M.R. Schmidt, G.A. Galazutdinov et al.*, Mon. Not. Roy. Astron. Soc., **408**, 1590, 2010.

Interstellar Extinction and Polarization and Star Formation in Dark Clouds

A.K. Sen[1], V.B. Il'in[2,3], M.S. Prokopjeva[2], N.V. Voshchinnikov[2], R. Gupta[4]

E-mail: *asoke.kumar.sen@aus.ac.in*

Polarimetry of stars background to dark clouds provides an important tool to map the magnetic field in the cloud. These polarimetric measurements have significance as the magnetic field plays a key role in star formation dynamics. However, simultaneous interpretation of extinction and polarization for such clouds poses problems for theoreticians. Some of these problems are discussed in the present work and possible explanations are provided.

1 Introduction

It is well known that light from celestial sources, when passes through the interstellar medium, gets polarized due to the aligned dichroic interstellar dust grains. At times, the light passes through denser parts of the interstellar medium which usually contain *interstellar clouds*. Some of these clouds are undergoing gravitational collapse and may form stars. The amount of the polarization caused by such intervening clouds provides valuable information and acts as a good diagnostic to understand various processes associated with star formation.

The dichroic grains present in such clouds generally get aligned by various mechanisms, where the magnetic field is an important component [1]. The same magnetic field also plays a key role in the dynamics of star formation and helps in deciding the shape of the clouds [2]. Some of these clouds have rotations, which together with the magnetic field sometimes impede the gravitational collapse [3]. The grains, on the other hand, absorb radiation at shorter wavelengths and *reradiate in the infrared,* helping the energy balance mechanism. The thermally re-radiated emission also shows polarization [4, 5].

In our galaxy we have many small compact dark clouds (known as Bok globules), undergoing gravitational collapse, that may form low mass stars [6, 7]. They mainly contain molecular gas and dust, having the gas temperature ∼10–30 K and density $\sim 10^4$ cm^{-3}, the total mass about 10–100 $M_\odot$ and the size

[1] Dept. of Physics, Assam University, India
[2] St. Petersburg University, Russia
[3] Pulkovo Observatory, Russia
[4] IUCAA, India

V. Grinin et al. (eds) Radiation mechanisms of astrophysical objects. Yerevan: Edit Print, 2017, pp. 115–120.

about 1–2 pc. The role of gravity is to be understood in a situation, where we have thermal outward pressure, turbulence, rotation and the magnetic field (also electrostatic charging [8] and so on). Towards the cloud core the total extinction can be as large as $A_V > 25$ mag, whereas in the outer periphery, where most of the optical polarimetric observations are carried out, $A_V < 5$ mag (see, e.g., [9]).

With this background, over the last few decades many dense interstellar clouds were astronomically observed by various groups in polarimetry, to understand the star formation processes in them. In spite of that, we still have a number of unresolved critical issues associated with such observation and analysis, namely: *Are background star polarimetry and re-emission polarimetry really capable of estimating magnetic field? Why the extinction data most often do not seem to be related to the polarization data? How interstellar polarization measurement is related to background star polarimetry?*

In this paper, we go through some of these issues and draw conclusions.

2 Interstellar extinction and polarization

The interstellar extinction and polarization over a wide wavelength range have been studied by many authors, which helped to characterize the grains' composition, shape and size, and also the number density distribution and the magnetic field. For instance, Gupta et al. [10] considered mixtures of silicate and graphite oblate spheroidal grains of the aspect ratio $a/b = 1.33$ within the wavelength range 0.1–3.4 μm to simulate the interstellar extinction. On the other hand, Das et al. [11], considering homogenous carbonaceous and silicates spheroids containing C, O, Mg, and Fe and the imperfect Davis–Greenstein (DG) alignment mechanism, explained the interstellar extinction as well as polarization curves. Voshchinnikov and Henning [12] also made such studies with a special emphasis on the dust composition and found that the dust phase abundance of Si, Fe, Mg played an important role to decide some of the observed phenomena. Many other aspects of interpretation of the interstellar polarization and extinction observations have been recently reviewed in [13].

3 Background star extinction and polarization for dark clouds

For the stars background to diffuse clouds, we know that the dichroic grains absorb optical radiation from background stars, resulting in the optical polarization. The same set of dust reradiates thermally resulting in the sub-mm and IR polarization. In past, Vrba et al. [14], Joshi et al. [15], Goodman et al. [16], Myers and Goodman [17], Kane et al. [18], Sen et al. [19], Whittet [20], Andersson and Potter [21] and other authors made such optical polarimetric studies. The works on polarization by the thermal re-emission were reported, e.g., by Ward-Thompson et al. [22] and Henning et al. [23] among others.

The background star polarimetric results are generally analyzed in the same way as interstellar polarization values. But since sometimes we encounter many problems while interpreting results of background star polarimetry, it appears that, understanding the processes in the background star polarimetry is not as simple as understanding the interstellar polarization.

Some of the observations of the background star polarization need attention:

1. Optical and NIR polarimetry does not show an increase in the polarization degree as one goes closer to the center of a dark cloud (signifying an increase in the optical depth) (e.g., [15, 9]).
2. The extinction and corresponding polarization for a set of background stars should be related for dark clouds, but most of the recent studies show they are not. So, Goodman et al. [24] questioned the validity of this technique to study the magnetic fields within the clouds.
3. For a set of eight clouds, Sen et al. [25] found that the perfect DG mechanism could not explain the observed polarization. Many other investigators also noted that the DG mechanism predicted much higher values of polarization than the actually observed ones. The question naturally arises, is polarization in the optical caused by grains which are aligned by DG mechanism or other processes? If we understand the process, then we can map the magnetic field more confidently.
4. Again far-IR observation gives polarization values which are consistent with the thermal re-emission from grains [27, 26].
5. Not only that, these far-IR polarization values are also consistent with the absorption polarization in the optical region. The polarization in this region comes from the low density region ($A_V \sim 1$–5 mag) of the cloud (near the periphery), while in the sub-mm domain (850 μm) does from near the core ($A_V \sim 10$–100 mag). The optical polarization direction is parallel to the magnetic field. The sub-mm polarization is due to the preferential emission from aligned elongated grains and should be *perpendicular* to the magnetic field. A comparison of the optical (from the Indian telescope) and sub-mm (from the SCUBA data archive) polarization vectors confirmed these findings [27]. Recent Planck data give a deeper insight on the relation between the sub-mm and visual polarization [5].
6. As found by Sen et al. [25] from a study of eight clouds, turbulence within the cloud was influencing (rather disturbing) the grain alignment and this could be modeled through a mathematical relation (see Fig. 1).
7. As an exception to point (2) above, Sen et al. [28] found that at least for some clouds, there was a positive correlation between polarization and extinction.

Basing on points (1) to (3), one could say that the intervening cloud has no role in the polarization that we observe for the stars background to the cloud. But in that case, we can not explain the points (4) to (6) listed above, which suggests that the polarization observed for background stars must have something intrinsic to the cloud.

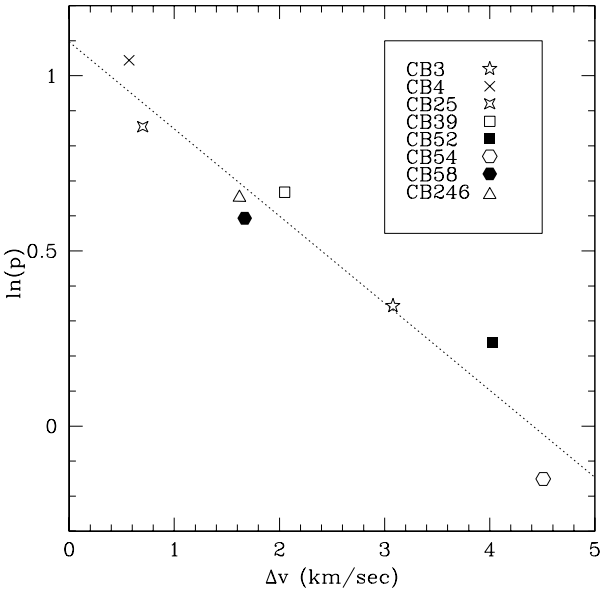

Figure 1: The log of the average observed polarization $\ln(p)$ against the turbulence velocity Δv (in km/s) for different clouds according to [25]. The line of the best fit $\ln(p) = 1.08 - 0.24\,\Delta v$ is shown.

There *exist* various possibilities which can explain the present situation. There are now doubts that the DG-like mechanisms play a role as large as thought earlier, and many researchers believe that the most important aligning force could be radiative torques [29]. However, it does not exclude the role of other mechanisms which can align grains.

It is very possible that some particular mechanism works in some parts of the cloud as compared to others. Also a particular alignment mechanism may be more effective for grains with a particular size and composition. Voshchinnikov [13], while working on the interstellar polarization, discussed such possibilities. And for dark clouds, it may be even more complicated. Within such a cloud, along the line of sight different values of the parameters of the magnetic field (or other aligning forces) are possible.

As listed in [30], a set of conditions should be fulfilled to get polarization out of aligned grains. If these conditions are not satisfied, we can get extinction, but not polarization.

Any misadjustment in these conditions should result in a poor correlation between polarization and extinction. The grain shape, size, magnetic properties (composition), alignment procedure are important parameters and some of these physical properties should vary within the clouds. And recent studies of extinction law, scattered light and sub-mm emissivity have already inferred changes in dust properties with an increase of depth inside a cloud (see [31] and references therein). So, the polarization observed for stars background to dark clouds may appear to be quite different from the polarization observed for the diffuse interstellar medium.

4 Conclusions

We can conclude as follows:

1. It is clear that the polarization values observed for stars behind dark clouds are influenced by the physical processes within these clouds.
2. However, the physical processes responsible for producing the polarization *in* the clouds are not well understood.
3. The processes producing the interstellar polarization and the polarization of background star radiation in dark clouds are definitely not the same.
4. The processes responsible for the polarization in dark clouds should be *more* clearly understood, as we find the situation is not as simple as in the interstellar medium. Only after this, we can use in the full manner the background star polarimetry to investigate star formation processes in dark clouds.

Acknowledgments. The authors acknowledge a partial support of the work by the grants of RFBR 16-02-00194, DST-RFBR 16-52-45005 and SPbGU 6.38.18.2014.

References

1. *R.M. Crutcher*, Ann. Rev. Astron. Astrophys., **50**, 29, 2012.
2. *H.-B. Li, A. Goodman, T.K. Sridharan et al.*, In: Protostars & Planets, VI. Tucson: Univ. Arizona Press, 2014, p. 101.
3. *P. Hennebelle, C. Charbonnel (eds.)*, Angular Momentum Transport during the Formation and Early Evolution of Stars. EAS Publ. Ser., **62**, 2013.
4. *B.T. Draine, A. Fraisse*, Astrophys. J., **696**, 1, 2009.
5. *Planck Collaboration*, Astron. Astrophys., **576**, A106, 2016.
6. *B.J. Bok, E.F. Reilly*, Astrophys. J., **105**, 255, 1947.
7. *B.J. Bok*, Astron. J., **61**, 309, 1956.
8. *C.B. Dwivedi, A.K. Sen, S. Bujarbarua*, Astron. Astrophys., **345**, 1049, 1999.
9. *V.B. Il'in, Y.S. Efimov, T.N. Khudyakova, M.S. Prokopjeva*, 2016, this conference.
10. *R. Gupta, T. Mukai, D.B. Vaidya et al.*, Astron. Astrophys., **441**, 555, 2005.
11. *H.K. Das, N.V. Voshchinnikov, V.B. Il'in*, Mon. Not. Roy. Astron. Soc., **404**, 265, 2010.
12. *N.V. Voshchinnikov, Th. Henning*, Astron. Astrophys., **517**, A45, 2010.
13. *N.V. Voshchinnikov*, J. Quant. Spectrosc. Rad. Transf., **113**, 2334, 2012.
14. *F.J. Vrba, G.V. Coyne, S. Tapia*, Astrophys. J., **243**, 489, 1981.

15. *U.C. Joshi, P.V. Kulkarni, H.C. Bhatt et al.*, Mon. Not. Roy. Astron. Soc., **215**, 275, 1985.

16. *A.A. Goodman, R.M. Crutcher, C. Heiles et al.*, Astrophys. J. Lett., **338**, L61, 1989.

17. *P.C. Myers, A.A. Goodman*, Astrophys. J., **373**, 509, 1991.

18. *B.D. Kane, D.P. Clemens, R.W. Leach, R. Barvainis et al.*, Astrophys. J., **445**, 269, 1995.

19. *A.K. Sen, R. Gupta, A.N. Ramaprakash, S.N. Tandon*, Astron. Astrophys., **141**, 175, 2000.

20. *D.C.B. Whittet, P.A. Gerakines, J.H. Hough, S.S. Shenoy*, Astrophys. J., **547**, 872, 2001.

21. *B.-G. Andersson, S.B. Potter*, Astrophys. J., **665**, 369, 2007.

22. *D. Ward-Thompson, J. Kirk, R. Crutcher et al.*, Astrophys. J. Lett., **537**, L135, 2000.

23. *Th. Henning, S. Wolf, R. Launhardt, R. Waters*, Astrophys. J., **561**, 871, 2001.

24. *A.A. Goodman, T.J. Jones, E.A. Lada, P.C.Myers*, Astrophys. J., **448**, 748, 1995.

25. *A.K. Sen, T. Mukai, R. Gupta, H.S. Das*, Mon. Not. Roy. Astron. Soc., **361**, 177, 2005.

26. *B.T. Draine*, IAU Gen. Assembly, Meet. #29, id.2253136, 2015.

27. *D. Ward-Thompson, A.K. Sen, J.M. Kirk, D. Nutter*, Mon. Not. Roy. Astron. Soc., **398**, 394, 2009.

28. *A.K. Sen, V.F. Polcaro, I. Dey, R. Gupta*, Astron. Astrophys., **522**, 45, 2010.

29. *B-G. Andersson, A. Lazarian, J.E. Vaillancourt*, Ann. Rev. Astron. Astrophys., **53**, 501, 2015.

30. *N.V. Voshchinnikov, T. Henning, M.S. Prokopjeva, H.K. Das*, Astron. Astrophys., **541**, A52, 2012.

31. *J.B. Foster, K.S. Mandel, J.E. Pineda et al.*, Mon. Not. Roy. Astron. Soc., **428**, 1606, 2013.

Estimates of Brightness Temperatures for Maser Sources of the Galaxy Observed by Space Interferometer "RadioAstron"

N.N. Shakhvorostova[1], A.V. Alakoz[1], A.M. Sobolev[2]
on behalf of the RadioAstron maser survey team

E-mail: *nadya@asc.rssi.ru*

The ultra-high angular and high spectral resolutions of RadioAstron provide tight limits on the sizes of the most compact maser spots and the estimates of their brightness temperatures. We present the results of the maser survey obtained by RadioAstron during the first four years of operation. Very compact features with angular sizes not exceeding about 20–60 micro-arcseconds have been detected in star-forming regions. Corresponding linear sizes are about 5–10 millions of kilometers. Brightness temperatures for a number of maser sources are estimated. Estimates of the brightness temperatures provide the values from $\sim 10^{14}$ to $\sim 10^{16}$ K.

1 Observations of masers with RadioAstron

Maser sources represent one of the main targets of the RadioAstron (RA) science program along with active galactic nuclei and pulsars. The RadioAstron project allows us to observe maser emission in one quantum transition of water at 22.235 GHz and two transitions of hydroxyl at 1.665 and 1.667 GHz. Water and hydroxyl masers are found in star-forming regions of our and nearby galaxies, around mass-loosing evolved stars, and in accretion discs around super-massive black holes in external galaxies.

Masers have small angular sizes (a few milli-arcsec and smaller), very high flux densities (up to hundreds of thousand Jy), and small line widths (normally about 0.5 km/s and smaller). Due to that masers proved to be precise instruments for studies of kinematics and physical parameters of the objects in our and other galaxies.

The space radio interferometer RadioAstron provides a record of high angular resolution, in some cases reaching a few tens of micro-arcseconds. This provides tight limits on the sizes of the most compact maser spots and estimates of their brightness temperatures, which are necessary input for the studies of the pumping mechanisms.

[1] Astro-Space Center of LPI RAS, Russia
[2] Ural Federal University, Russia

V. Grinin et al. (eds) Radiation mechanisms of astrophysical objects. Yerevan: Edit Print, 2017, pp. 121–126.

Typical values of the minimal flux density detectable with RA for the water masers at 22 GHz and hydroxyl masers at 1.665/1.667 GHz are 15 Jy and 3.5 Jy, respectively. These values were calculated for a typical line width of 0.1 km/s and coherent accumulation time of 100 s and 600 s for 22 GHz and 1.665/1.667 GHz, respectively. So, the sensitivity in Jy for hydroxyl masers is better than for water masers. Anyhow, when we use the large ground-based antenna, for example 100-m GBT, and the source has wide line, RA proved ability to detect 3–4 Jy water maser source.

2 Statistics of maser observations for the first 4 years of operation

2.1 Maser observation program

The goal of the scientific program for the study of cosmic masers using space interferometer RadioAstron was observations of maser emission in quantum transitions of water at frequency 22 GHz and hydroxyl at frequencies 1.665 and 1.667 GHz. During the period from November 2011 to May 2012 interferometric mode of RA operation was tested. For that purpose a number of bright quasars and the brightest and most compact sources of maser emission were selected [1]. Basic conditions for choosing these sources were the existence of details that remain compact (i.e. unresolved) on the longest baseline projections and the highest brightness temperatures measured during VLBI and VSOP surveys. The first positive detections of maser sources by space interferometer were achieved for W51 (water) and W75N (hydroxyl) in two sessions in May and July 2012. Baseline projections were 1.0–1.5 and 0.1–0.8 Earth diameters (ED), respectively. Later, more sophisticated data analysis led to even more positive results in these test sessions: compact water maser features were detected in W3 IRS5 and W3(OH) in two sessions in February 2012. Baseline projections were 3.7–3.9 ED.

After the first successful tests the early science program started. The main purpose of these observations was to obtain first astrophysical results and measurements of the main parameters of the operating interferometer. List of observed sources has been significantly expanded, objects of other types were included in addition to the star-forming regions. Stellar masers in S Per, VY CMa, NML Cyg, U Her and extragalactic masers in Circinus and N113 were observed. It was proved that RadioAstron can observe cosmic masers with very high spectral resolution. This was not obvious at the beginning, indicates presence of the ultra-fine structure in the maser images, and that interstellar scattering does not prevent observations of masers in the galactic plane [1]. Positive detections for stellar and extragalactic masers were not obtained during the early science program.

The early science program was followed by the key and general research programs which were conducted (and the general program continues at the moment) on the basis of the open call for proposals received from research teams around the world. Details of the preparation and the conditions of the

Table 1: Maser sources detected on the space–ground baselines

Source	Observed line(s)	Projected baseline length, ED
W3 IRS5	22 GHz (H_2O)	2.5–2.8; 3.5; 3.9; 5.4; 6.0
W51_E8	22 GHz (H_2O)	0.4–2.3; 1.3; 1.4–1.8
Cepheus A	22 GHz (H_2O)	0.9–1.7; 1.1; 3.1–3.5
W49N	22 GHz (H_2O)	2.2–3.0; 9.4
Orion KL	22 GHz (H_2O)	1.9; 3.4
W75N	1.665 & 1.667 GHz (OH)	0.1–0.3; 0.1–0.8
Onsala 1	1.665 GHz (OH)	0.2–0.7; 1.0–1.9
W3(OH)	22 GHz (H_2O)	3.9
NGC4258	22 GHz (H_2O)	1.3

call for proposals are published at the RadioAstron project website [2]. The main objectives of this phase of the maser program are studying the kinematics and dynamics of the compact sources of maser emission in star-forming regions, as well as the study of extragalactic masers, such as NGC3079 and NGC4258. As a result, along with star-forming regions the signal from extragalactic maser NGC4258 was detected. This maser is associated with the accretion disk around super-massive black hole at the center of this galaxy. The projected baseline in this observing session was up to 2 ED, which corresponds to an angular resolution of 110 μas.

2.2 General statistics of maser source detections

This section provides statistics from the beginning of RA maser observations (November 2011) up to the present time (July 2015). During four years of operation a large amount of data was accumulated, and this allows us to sum up the first results of this work. 135 maser observation sessions were conducted, and 31 sources were observed. The majority of masers observed in RA program are related to star-forming regions – 19 sources in total. Eight masers sources in the envelopes of late-type stars of the Galaxy were observed, and 4 extragalactic masers in star-forming regions and circum-nuclear disks of external galaxies were observed.

Due to technical reasons the scientific data have been corrupted or lost in 10 sessions out of total 135. 103 observations of the remaining 125 sessions at the moment (August 2015) are processed, positive detections are obtained in 21 sessions. Thus, the current detection rate of fringes at space-ground baselines is about 20.4 %. Some scientific data is still under consideration at ASC LPI data processing center [3]. The final detection rate is likely to be higher.

All successful fringe detections for galactic masers at space-ground baselines were obtained for the sources associated with star-forming regions, – 20 positive detections. One detection was obtained for extragalactic maser. No fringes for the stellar masers were obtained at space-ground baselines yet. Probably, the spots of the brightest masers in the stellar envelopes are fully resolved at the space-ground baselines.

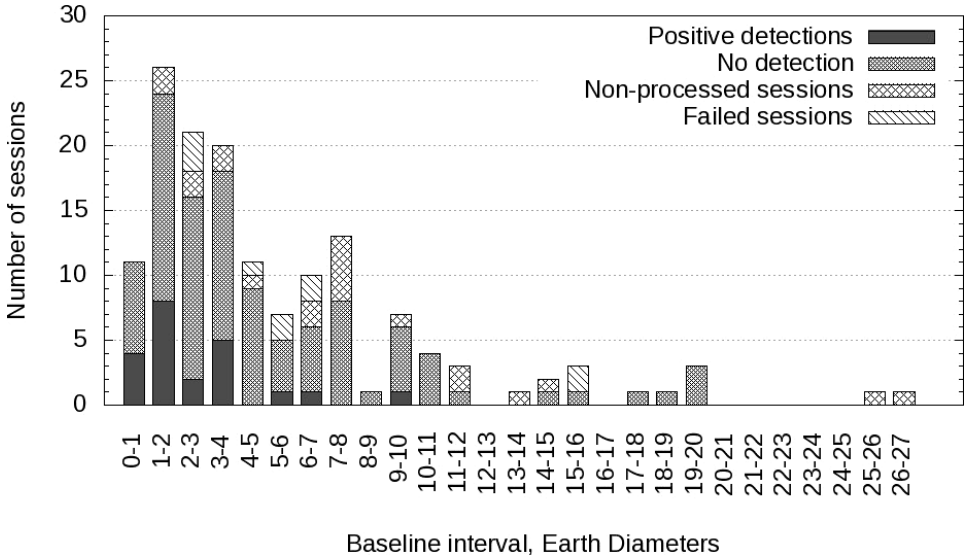

Figure 1: Statistics of maser observation results over projected baseline length of the space interferometer RadioAstron.

Table 1 provides information on the observational sessions which provided positive fringe detection with the space interferometer. The columns show source names, observed lines and projected lengths of the space-ground baselines at which the interferometric detection was obtained. Each baseline (or baseline interval) corresponds to one observational session with positive detection of the fringes.

It is instructive to show the distribution of the number of detections depending on the length of the baseline projection. Figure 1 presents statistics of observational sessions for the whole set of database lengths. It is seen that most of the positive detections fall in range from 1 to 4 ED.

3 Estimates of the minimal brightness temperatures for the maser sources of the Galaxy

Brightness temperature is one of the observational parameters of the maser emission which provides a basic and strong constraint on the theoretical models of maser pumping. Usually the brightness temperature is estimated from the source imaging using adequate range of baseline projections. This way requires involvement of many telescopes and a rather long duration of observations in order to obtain good sampling of the uv-plane. But at present the majority of RadioAstron maser data consists of the short observations with duration of about 1 hour with a few baseline sets, about 3 to 6. These are detection experiments which do not allow producing map of the source. Nevertheless, using some assumptions it is possible to estimate brightness temperature and size of the source even for such short sessions.

Table 2: Brightness temperature estimates for some H_2O masers observed by RadioAstron

Source	Baseline, ED	Resolution, μas	Minimal T_b, K	T_b, K
W3 IRS5	3.5	62	9.0×10^{14}	1.5×10^{15}
W3 IRS5	5.4	40	1.5×10^{15}	8×10^{15}
W3 OH	3.8	58	2.1×10^{14}	7×10^{14}
Cepheus A	3.4	64	1.2×10^{14}	3×10^{14}
Orion	3.3	66	1.2×10^{15}	6×10^{15}
W49N	9.6	23	4.5×10^{14}	2.6×10^{15}

For example, we can assume that the shape of the brightness distribution is a circular Gaussian. This proved to be a good approximation in many observed cases. Under this assumption we can estimate brightness temperature of the source using the formula proposed in [5]

$$T_{\rm b} = \frac{\pi}{2k} \frac{B^2 V_0}{\ln\left(V_0/V_q\right)}. \tag{1}$$

Here B is a baseline, V_q is an amplitude of visibility function at a single spatial frequency $q = B/l$, and V_0 is a space-zero visibility. It was shown [5] that $T_{\rm b}$ has its lowest value when $V_0/V_q = e$. This provides the minimal brightness temperature estimate $T_{\rm b,min}$ when the values of baseline and correlated flux are obtained from observations

$$T_{\rm b,min} \approx 3.09 \left(\frac{B}{\rm km}\right)^2 \left(\frac{V_q}{\rm mJy}\right) [K]. \tag{2}$$

Principles of the maser data processing have basic similarities to continuum data processing. However, maser observations greatly depend on the proper selection of the frequency band and need a large number of frequency channels for correlation. This imposes additional requirements on the correlator software. We carried out post-correlation data processing using the VLBI processing software package PIMA [4]. Source fluxes were calibrated using system temperature measurements provided by the telescopes participating in observations with RA.

4 Results and conclusions

Here we discuss some estimates of $T_{\rm b}$ and $T_{\rm b,min}$ obtained from the measured source flux S under the assumption that the brightness distribution is a circular Gaussian. Some results for compact features detected in star-forming regions W3 IRS5, Orion KL, W3 and Cepheus A are presented in Table 2. Each line corresponds to one observational session. In the second column the baselines in units of ED's are given. In the third column resolution in micro-arcseconds is given. The last two columns show estimates of the brightness temperatures $T_{\rm b}$ and $T_{\rm b,min}$ in Kelvin. The highest temperature is obtained for W3 IRS5 source (8×10^{15} K). Angular resolution is very high, so we observe very compact features of about 20 to 60 micro-arcseconds. Such angular sizes correspond to linear sizes of about 5–10 million km or several solar diameters.

The main conclusions of the work are the following:

1. Space-VLBI observations of the water and hydroxyl masers show that the bright details of the masers in galactic star-forming regions often remain unresolved at baseline projections which considerably exceed Earth diameter. Record resolution for the maser observations at present are obtained for W49N water maser – 23 micro-arcsec at projected baseline 9.6 ED.
2. Very compact water maser features with the angular sizes of about 20–60 micro-arcseconds are registered in galactic star-forming regions. These correspond to linear sizes of about 5–10 million km (several solar diameters).
3. Estimates of the brightness temperatures for the ultracompact interstellar water maser features range from $\sim 10^{14}$ to $\sim 10^{16}$ K.

Acknowledgments. The RadioAstron project is led by the Astro Space Center of the Lebedev Physical Institute of RAS and the Lavochkin Association of Russian Federal Space Agency, and is a collaboration with partner institutions in Russia and other countries. This research is partly based on observations with the 100 m telescope of the MPIfR at Effelsberg; radio telescopes of IAA RAS (Federal State Budget Scientific Organization Institute of Applied Astronomy of Russian Academy of Sciences); Medicina & Noto telescopes operated by INAF – Istituto di Radioastronomia; Hartebeesthoek, Torun, WSRT, Yebes, and Robledo radio observatories. The National Radio Astronomy Observatory is a facility of the National Science Foundation operated under cooperative agreement by Associated Universities, Inc. Results of optical positioning measurements of the Spektr-R spacecraft by the global MASTER Robotic Net [6], ISON collaboration, and Kourovka observatory were used for spacecraft orbit determination in addition to mission facilities.

References

1. *N.S. Kardashev, A.V. Alakoz, Y.Y. Kovalev et al.*, Solar Syst. Res., **49**, 573, 2015.
2. *RadioAstron – Space VLBI Mission*, *http://www.asc.rssi.ru/radioastron*
3. *N.S. Kardashev, V.V. Khartov, V.V. Abramov et al.*, Astron. Rep., **57**, 153, 2013
4. *L. Petrov*, PIMA – VLBI processing software, 2015, *http://astrogeo.org/pima*
5. *A. Lobanov*, Astron. Astrophys., **574**, A84, 2015.
6. *V. Lipunov, V. Kornilov, E. Gorbovskoy et al.*, Adv. Astron., **2010**, 349171, 2010.

Metal Ions in the Circumgalactic Medium

E.O. Vasiliev[1,2], M.V. Ryabova[1], Yu.A. Shchekinov[3]

E-mail: *eugstar@mail.ru*

Recent observations show high column densities of metal ions in extended haloes of galaxies within $z \sim 0$–0.5. For instance, to explain column densities of OVI ion observed around star-forming galaxies one should assume solar metallicity in the extended haloes, and in this case the haloes become the main reservoir of missing baryons and metals. Using time-dependent radiation field of a nearby starburst galaxy we study how ionic species depend on the galactic mass and star formation rate. We derive conditions for the high ionic states of metals to appear in extended galactic haloes.

1 Introduction and model description

High column densities of OVI and CIV ions in halos of star-forming galaxies lead to a conclusion on more massive galactic halos than thought before [1, 2]. In principle, this conclusion for galactic haloes to bear such a large gas mass might solve the problem of missing baryons and metals, though requiring enormously high oxygen production and mass ejection rates. Taking into account galactic ionizing radiation, the maximum OVI fraction can reach ∼0.4–0.9 that facilitates constrains on both gaseous mass and metallicity for massive star-forming galaxies [3]. Here we are interested in metal column densities in circumgalactic medium of less massive galaxies with special attention for CIV and OVI ions. We present only a brief description of our model, the details will be presented in our future paper.

Using the photoionization code CLOUDY [4] we calculate all ionization states of the elements H, He, C, N, O, Ne, Mg, Si and Fe. In our calculations the gas in the circumgalactic medium is in local thermal equilibrium that means the equality between cooling and heating rates in a gas parcel located at the radial distance r from the galactic center and exposed to both galactic (reached to such distance) and extragalactic radiation. In order to follow evolution of stellar mass, metallicity and galaxy spectrum, we use the spectrophotometric code PEGASE [5]. We assume a Schmidt-like power-law star formation rate (SFR) typical of star-forming galaxies: $\mathrm{SFR}(t) = \mathcal{M}_g^{p_1}/p_2$, where $\mathcal{M}$ is the normalized mass of gas in $M_\odot$. In our model we assume a closed-box regime. To extend the spectrum to higher energies (up to $\sim 10^4$ eV), we use the empirical relation between the X-ray luminosity and the star formation rate [6]. For the extragalactic background we accept the

[1] Southern Federal University, Russia
[2] Special Astrophysical Observatory, Russian Academy of Sciences (RAS), Russia
[3] Astro Space Center of Lebedev Physical Institute of RAS, Russia

V. Grinin et al. (eds) Radiation mechanisms of astrophysical objects. Yerevan: Edit Print, 2017, pp. 127–132.

Table 1: List of the main models

Total mass of gas $M_g^i, M_\odot$	p_2, Myr/$M_\odot$ (Name of model)
10^{10}	3×10^5 (A1), 3×10^4 (A2), 3×10^3 (A3)
5×10^{10}	3×10^5 (B1), 3×10^4 (B2), 3×10^3 (B3)
10^{11}	3×10^5 (C1), 3×10^4 (C2), 3×10^3 (C3)

spectrum described in [7]. We suppose the density profile has a shape similar to the Milky Way galaxy [8] normalized to mass of the dark matter halo. The parameters of the models are listed in Table 1. A fiducial value of gas metallicity in our models is assumed to be equal to 0.1 $Z_\odot$.

2 Results

We consider gas in outer haloes of star-forming galaxies with stellar mass $\sim10^9 - 10^{11}$ $M_\odot$. Figure 1 shows the dependence of specific star formation rate, sSFR = SFR/M_*, on the stellar mass, M_*. Note that the value of p_2 increases from left to right. It is clearly seen that almost all points for the COS-Dwarfs galaxies are locked between tracks for models A1–C2 as well as the data for the star-forming COS-Halos galaxies are close to the tracks of the models C2–C3. Therefore, we expect that spectral properties of the galaxies observed in the COS-Dwarfs and COS-Halos surveys are similar to those in the models considered here during the latest ∼3–4 Gyrs of their evolution.

Figure 2 shows the dependence of CIV column densities (left panels) in a halo around a galaxy in models B*. The N(CIV) values become lower with a decrease of both impact distance b and HI column density in the disk. This is explained by an increase of photons ionized CIV, so that under such conditions carbon is locked mainly in CV state. High column densities, $N(\mathrm{CIV}) \gtrsim 10^{14}$ cm^{-2}, are found at impact distances $b \lesssim 0.3\,r_v$, moderate values $\sim10^{13.5}$–10^{14} cm^{-2} can be detected at larger distances $b \sim (0.3\text{–}0.5)\,r_v$. Certainly, the increase of SFR from model B1 (upper panel) to B3 (lower panel) leads to reducing N(CIV), especially this is clear for moderate values of HI column density $\sim10^{20}$–$10^{20.4}$ cm^{-2}. However, the N(CIV) values calculated for galaxies in models B* and $N(\mathrm{HI}) \gtrsim 10^{20.4}$ cm^{-2} are close to the measured ones in the COS-Dwarfs survey [2]. Note that the stellar masses and SFR in models B* are also similar to those detected for the host galaxies in the survey (Fig. 1). One can see that N(CIV) significantly depends on the absorption of galactic radiation.

Figure 2 shows the OVI column densities (right panels) in a halo around a galaxy in models B*. Similar to N(CIV) the OVI column density reaches values as high as $\sim10^{13.8}$ cm^{-2} at $b \lesssim 0.5\,r_v$, but contrary to CIV it increases for smaller absorption of the galactic radiation: N(OVI) becomes $\sim10^{14.2-15}$ cm^{-2} for $N(\mathrm{HI}) \lesssim 10^{20.3}$ cm^{-2}. Higher SFR is also favor to higher N(OVI). Such behavior is due to a growth of galactic photons being able to ionize OV.

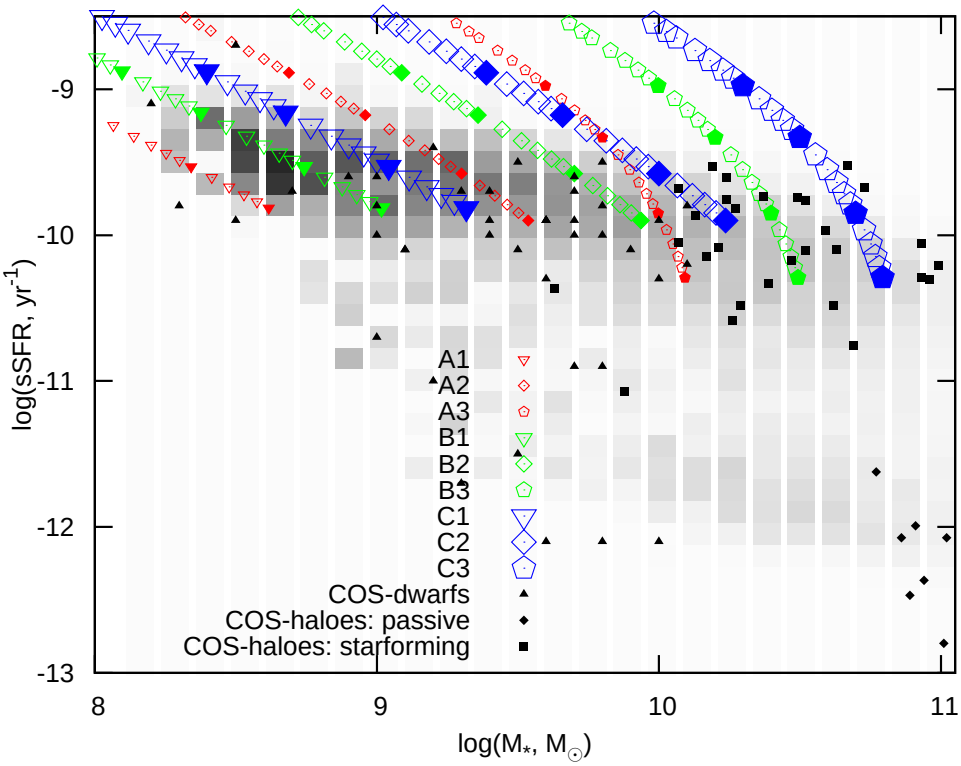

Figure 1: The dependence of specific star formation rate, sSFR = SFR/M_*, on the stellar mass, M_*, for the models A*, B* and C* showed by small, middle-size and large open symbols (Table 1). The value of p_2 increases from left to right. The filled symbols among open ones correspond to 1, 2, 5 and 10 billion years (from top-left to bottom-right points) passed from the beginning of the evolution of a galaxy. Data for the COS-Dwarfs galaxies from [2] are shown by small filled triangles and for the COS-Halos star-forming and passive galaxies from [1] are depicted by small filled squares and rhombuses, respectively. The gray-scale map is for SDSS+GALEX galaxies [9].

Note that both CIV and OVI column densities are as high as $\sim 10^{14-14.5}$ cm^{-2} and $\sim 10^{14.5-15}$ cm^{-2}, respectively, at small $b \lesssim 0.2$ for moderate values of N(HI) $\sim 10^{20.4}$ cm^{-2}. Whereas in other ranges of N(HI) and b either CIV or OVI has high column density, in other words, there takes place the bimodal distribution. It has been argued [2] that high CIV column densities can be found in halos of dwarf galaxies, whereas high OVI values are usual in a gas around massive star-forming galaxies [1], and have assumed the existence of bimodality over mass of a galaxy. Here we consider the same total and initial gaseous masses of a galaxy (in models B* the initial gaseous mass equals 5×10^5 $M_\odot$, see Table 1), but the SFR is taken different, so that during the evolution the stellar masses reach different values ranged by more than an order of magnitude (middle-size green symbols in Fig. 1). However, Figure 2 shows similar N(OVI) distributions for all three values of SFR and significant dependence of N(OVI) on HI column density.

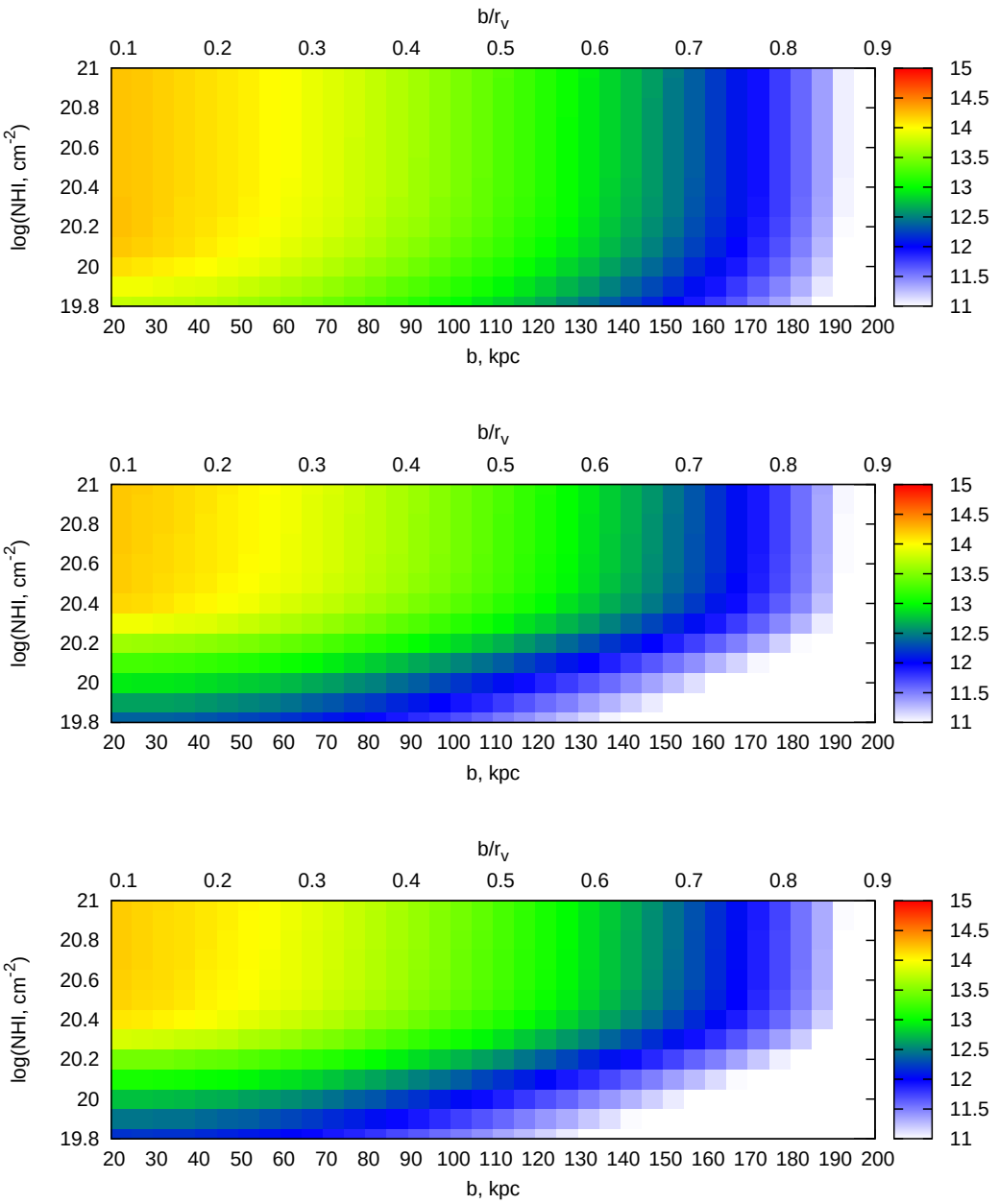

Figure 2: The dependence of CIV (*left* panels) and OVI (*right* panels) column densities (in logarithmic scale) in a halo around a galaxy in models B* on impact parameter b (which is given in kpc in the lower x-axis and in units of virial radius r_v of a galaxy in the upper x-axis) and the HI column density $\log N_{\rm HI}$ in the galactic disk. The upper row corresponds to model B1 ($M = 5 \times 10^{10}\ M_\odot$, $p_2 = 3 \times 10^5$ Myr$/M_\odot$), the middle is for model B2 ($M = 5 \times 10^{10}\ M_\odot$, $p_2 = 3 \times 10^4$ Myr$/M_\odot$), and the lower one is for B3 ($M = 5 \times 10^{10}\ M_\odot$, $p_2 = 3 \times 10^3$ Myr$/M_\odot$). The virial radius r_v of a galaxy with $M = 5 \times 10^{10}\ M_\odot$ at $z = 0$ equals $\sim$218 kpc.

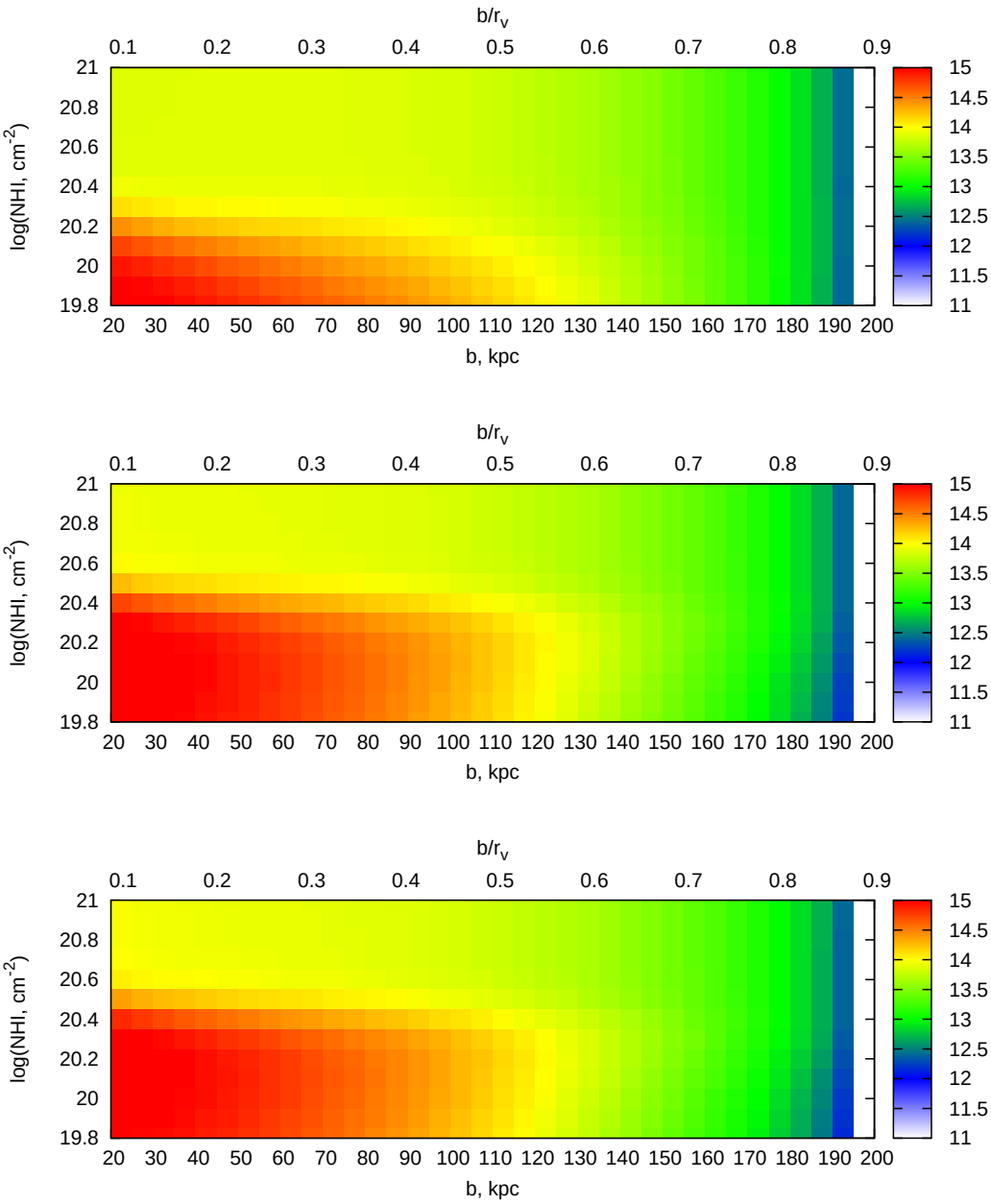
b/r_v
0.1 0.2 0.3 0.4 0.5 0.6 0.7 0.8 0.9
log(NHI, cm^-2)
21 20.8 20.6 20.4 20.2 20 19.8
15 14.5 14 13.5 13 12.5 12 11.5 11
20 30 40 50 60 70 80 90 100 110 120 130 140 150 160 170 180 190 200
b, kpc
b/r_v
0.1 0.2 0.3 0.4 0.5 0.6 0.7 0.8 0.9
log(NHI, cm^-2)
21 20.8 20.6 20.4 20.2 20 19.8
15 14.5 14 13.5 13 12.5 12 11.5 11
20 30 40 50 60 70 80 90 100 110 120 130 140 150 160 170 180 190 200
b, kpc
b/r_v
0.1 0.2 0.3 0.4 0.5 0.6 0.7 0.8 0.9
log(NHI, cm^-2)
21 20.8 20.6 20.4 20.2 20 19.8
15 14.5 14 13.5 13 12.5 12 11.5 11
20 30 40 50 60 70 80 90 100 110 120 130 140 150 160 170 180 190 200
b, kpc

Acknowledgments. E.V. is supported by the Russian Scientific Foundation (grant 14-50-00043). M.R. and Y.S. are supported by the RFBR (grants 15-02-08293, 15-52-45114).

References

1. *J. Tumlinson, C. Thom, J.K. Werk et al.*, Science, **334**, 948, 2011.
2. *R. Bordoloi, J. Tumlinson, J.K. Werk et al.*, Astrophys. J., **796**, 136, 2014.
3. *E.O. Vasiliev, M.V. Ryabova, Yu.A. Shchekinov*, Mon. Not. Roy. Astron. Soc., **446**, 3078, 2015.
4. *G.J. Ferland, K.T. Korista, D.A. Verner et al.*, Publ. Astron. Soc. Pacif., **110**, 761, 1998.
5. *M. Fioc, B. Rocca-Volmerange*, Astron. Astrophys., **326**, 950, 1997.
6. *M. Gilfanov, H.-J. Grimm, R. Sunyaev*, Mon. Not. Roy. Astron. Soc., **347**, L57, 2004.
7. *F. Haardt, P. Madau*, in Clusters of Galaxies and High Redshift Universe Observed in X-rays. Eds. D.M. Neumann, J.T.V. Tran. Rencon. Moriond, 2001.
8. *R. Feldmann, D. Hooper, N.Y. Gnedin*, Astrophys. J., **763**, 21, 2013.
9. *D. Schiminovich, T.K. Wyder, D.C. Martin et. al.*, Astrophys. J. Suppl., **173**, 315, 2007.

* The color figures are available online in the Proceedings at *http://www.astro.spbu.ru/sobolev100/*.

Energy Budget in Multiple Supernova Explosions

E.O. Vasiliev[1,2], B.B. Nath[3], Yu.A. Shchekinov[4]

E-mail: *eugstar@mail.ru*

Standard models of large scale galactic outflows in starburst galaxies assume a high efficiency of SNe in heating the gas in central regions of starburst galaxy in order to launch outflows. We study the heating efficiency of the interstellar gas by multiple supernovae (SNe) within 3D simulations. We argue that SNe remnants have to act coherently in space and in time in order to minimize radiative losses. We show that interacting expanding shells from different SNe restrict the heating efficiency of multiple SNe even when they explode with a high rate. As a result the heating efficiency can considerably differ from a commonly assumed value (0.1–0.3).

1 Introduction

Heating of the interstellar medium by multiple supernovae (SNe) explosions is at the heart of producing galaxy-scale outflows in starburst galaxies. Standard models of outflows assume a high efficiency of SNe in heating the gas to X-ray emitting temperatures and filling the central region of starburst with hot gas, in order to launch vigorous outflows. The collective effect of clustered SNe is believed to form a superbubble (e.g., [1]) whose shell of swept up mass moves faster than the typical speed of OB associations (few km s^{-1}) and which therefore contains most of the SNe arising from the association. The study of the evolution of these superbubbles has mostly assumed continuous energy release from the center.

This problem becomes acute in the context of supernovae driven galactic winds in which it is assumed that SNe can sufficiently heat up the ISM gas, at least in the central region of disc galaxies, in order to launch a wind. This process assumes that although SNe lose most energy in radiation in isolated cases, the efficiency of heating the ISM can be large in the central region filled with hot and low density gas and that the gas in this region is thermalized [2, 3]. Numerical simulations (e.g., [4, 5, 6]) also implement the initial conditions leading to galactic winds making similar assumptions. It is believed that in a multiphase medium and in the case of multiple SNe events, the efficiency of SNe heating – the fraction of the total explosion energy transferred into thermal energy – can be larger than $\sim$0.1. These

[1] Southern Federal University, Russia
[2] Special Astrophysical Observatory, Russian Academy of Sciences (RAS), Russia
[3] Raman Research Institute, India
[4] Astro Space Center of Lebedev Physical Institute of RAS, Russia

V. Grinin et al. (eds) Radiation mechanisms of astrophysical objects. Yerevan: Edit Print, 2017, pp. 133–136.

estimates came from the numerical and analytical studies of energy loss in *isolated* supernova remnants, which showed that the fractional energy retained in the hot interior gas of remnants was of order ∼0.1. Larson [7] had first pointed out the importance of cooling with regard to galactic outflows, and derived a critical supernova rate density required to compensate for cooling.

The question of heating efficiency of SNe crucially depends on the evolution of multiple SNe which has not yet been studied in detail. Nath and Shchekinov [8] have argued that the energy input from multiple SNe in the central regions of starbursts cannot heat the gas to $T \geq 10^6$ K unless the SNe events act coherently in space and time. Here we study two aspects of the problem of multiple SNe with gas-dynamic simulations, namely, we test the importance of coherency condition and consider the time scale and conditions under which percolation of hot gas becomes possible. This allows us to study the efficiency of heating by multiple SNe events, in particular the efficiency of heating gas to high temperature.

2 Numerical method and initial conditions

We use three-dimensional unsplit TVD code based on the MUSCL-Hancock scheme and the HLLC method (e.g., [9]) as an approximate Riemann solver. In the energy equation we take into account cooling processes adopted the tabulated non-equilibrium cooling curve [10]. This cooling rate is obtained for a gas cooled isobarically from 10^8 down to 10 K. The heating rate is adopted to be constant whose value is chosen so that the background gas does not cool.

We have carried out 3-D gasdynamic simulations (Cartesian geometry) of multiple SNe explosions using periodic boundary conditions. The computational domains have size 200^3 pc^3 which consists of 300^3 cells corresponding to a physical cell size of 0.75 pc. The background number density considered ranges between 0.1–10 cm^{-3}, the background temperature is 10^4 K. The metallicity is constant within the domain, and we consider the cases with $Z = 0.1$, 1 $Z_\odot$. We inject the energy of each SN in the form of thermal energy in a region of radius $r_i = 1.5$ pc. SNe are distributed uniformly and randomly over the computational domain.

3 Results

We have performed runs with SNe exploding continuously in the computational domain of 200^3 pc^3 with resolution of 1 pc and gaps of $\Delta t = 10^3$, 10^4, 2×10^4, 3×10^4, 4×10^4 and 10^5 yr. In other words, one supernova explodes after every Δt. The positions of SNe are distributed randomly in space. Figure 1 shows the results of heating efficiencies (left) and filling factors (right) for gas with different temperatures, for all time delays (from short to long delays, from top to bottom). We denote the efficiency of heating gas to $\geq 10^{6.5}$ K by $\eta[10^{6.5}]$ and define it as the ratio of thermal energy stored in gas with $T \geq 10^{6.5}$ K at any given time to the total explosion energy deposited up to that time. It is clear that the case of more frequent SNe ($\Delta t = 10^3$ yr) shows continuous decline in the

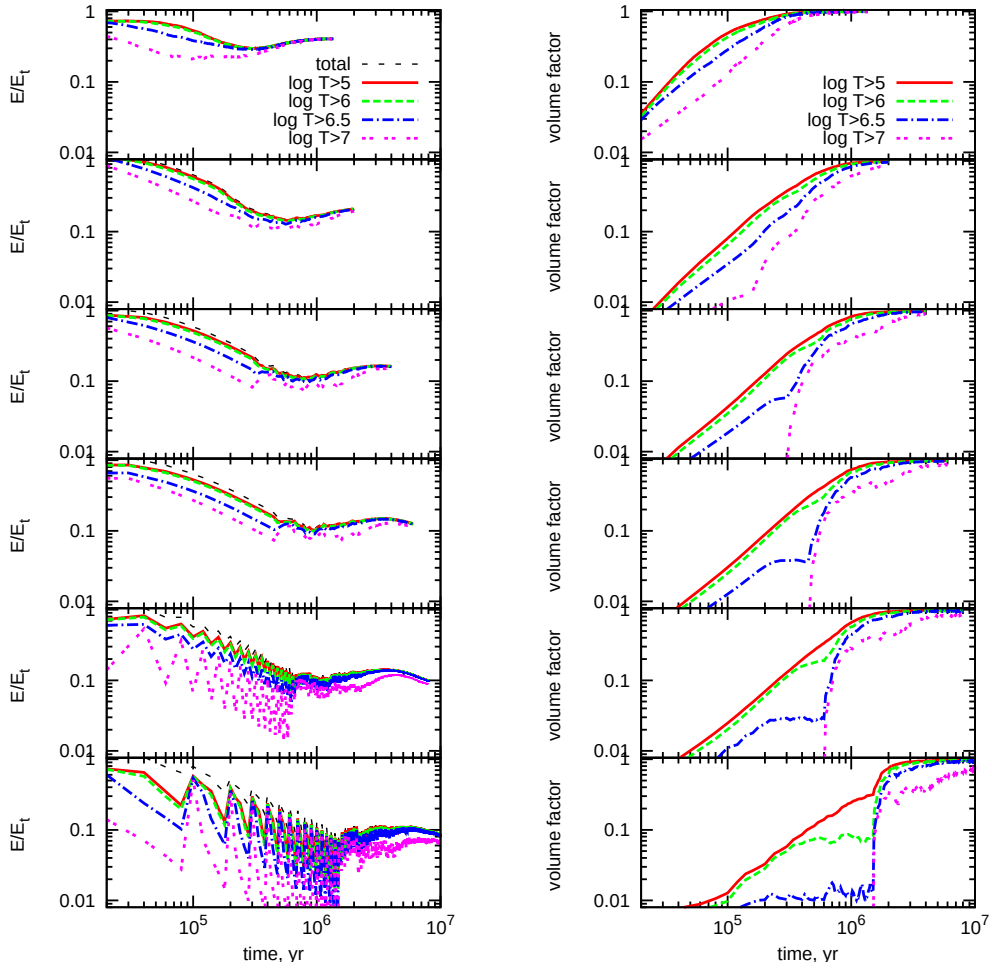

Figure 1: The evolution of the heating efficiency (left) and filling factors (right) for gas with different temperatures for a continuous series of SNe separated by time delay $\Delta = 10^3$, 10^4, 2×10^4, 3×10^4, 4×10^4, 10^5 yr (from top to bottom).

heating efficiency $\eta[10^{6.5}]$ and only after $t \simeq 10^5$ yr when the remnants practically fill the whole computational domain (60% of the volume), η increases to $\sim$0.4 because the subsequent SNe mostly expand into hot diffuse medium. Explosions with a longer delay of $\Delta t = 10^5$ yr (bottom most row) show on average similar trend on longer time scales, though as expected, with lower heating efficiency of order $\eta[10^{6.5}] \sim 0.1$. Similar to the previous model, the efficiency first declines and then increases after the remnants occupy roughly 30% of the computational zone at $t \simeq 10^6$ yr to $\eta[10^{6.5}] \sim 0.1$.

A common feature in the behavior of the heating efficiency in all models can be obviously noted: after a continuous decline down to $\eta(T) \lesssim 0.1$, it stabilizes and then grows slowly for all temperature fractions, particularly for the gas with $T \geq 3 \times 10^6$ K which carries a considerable amount of thermal energy. The most reasonable explanation is that the epoch of increasing η coincides with the state

when the filling factor of the corresponding temperature fraction reaches a critical value $f(T) \sim 0.3$ when different bubbles percolate.

The time required for the percolation of hot gas can be found by using the result that the threshold filling factor is $\sim$0.3 and can be estimated as [11]

$$t_{\rm perc} \approx 10\,{\rm Myr} \left(\frac{n}{E_{51}}\right)^{4/7} \left(\frac{\nu_{\rm SN}}{10^{-10}\,{\rm pc^{-3}\,yr^{-1}}}\right)^{-4/7}. \quad (1)$$

For a typical starburst SNe rate density of $\sim 10^{-9}$ pc^{-3} yr^{-1} and gas density of $n \sim 10$ cm^{-3} in starburst nuclei, the time scale for heating efficiency to become ≥ 0.1 is of order 10 Myr.

It is interesting to note that recent observations of 10 starburst galaxies show that there is a time lag of $\sim$10 Myr between the onset of star formation and the excitation of galactic winds [12]. Our simulations and the important result of percolation of hot gas when the overall filling factor crosses a threshold of $\sim$0.3, therefore, allow us to interpret this time lag as required for heating efficiency to become sufficiently large for an outflow to be launched.

Using our simulations for different gas densities (n = 0.3, 1, 3, 10 cm^{-3}) and keeping the SNe frequency a constant, we can infer the scaling of the heating efficiency with the SNe rate density and ambient density [11]. We find that roughly $\eta[10^{6.5}] \propto \nu_{\rm SN}^{0.2}\, n^{-0.6}$ for the heating efficiency of X-ray emitting gas.

Acknowledgments. E.V. is supported by the Russian Scientific Foundation (grant 14-50-00043). Yu.S. is grateful for partial support from the RFBR through the grants 15-02-08293 and 15-52-45114.

References

1. *M-M. Mac Low, R. McCray*, Astrophys. J., **324**, 776, 1988.
2. *R.A. Chevalier, A.W. Clegg*, Nature, **317**, 44, 1985.
3. *M. Sharma, B.B. Nath*, Astrophys. J., **763**, 17, 2013.
4. *A.A. Suchkov, D.S. Balsara, T.M. Heckman, C. Leitherer*, Astrophys. J., **430**, 511, 1994.
5. *D. Strickland, I.R. Stevens*, Mon. Not. Roy. Astron. Soc., **314**, 511, 2000.
6. *A. Fujita, C.S. Marttin, M.-M. Mac Low et al.*, Astrophys. J., **698**, 693, 2009.
7. *R. Larson*, Mon. Not. Roy. Astron. Soc., **169**, 229, 1974.
8. *B.B. Nath, Yu.A. Shchekinov*, Astrophys. J. Lett., **777**, L12, 2013.
9. *E. Toro*, Riemann Solvers and Numerical Methods for Fluid Dynamics. A Practical Introduction. Berlin: Springer-Verlag, 1999.
10. *E.O. Vasiliev*, Mon. Not. Roy. Astron. Soc., **431**, 638, 2013.
11. *E.O. Vasiliev, B.B. Nath, Yu.A. Shchekinov*, Mon. Not. Roy. Astron. Soc., **446**, 1703, 2015.
12. *R.G. Sharp, J. Bland-Hawthorn*, Astrophys. J., **711**, 818, 2010.

* The color figure is available online in the Proceedings at *http://www.astro.spbu.ru/sobolev100/*.

Dust in Outer Layers of B5 Globule

V.B. Il'in[1,2], Y.S. Efimov[3], T.N. Khudyakova[1], M.S. Prokopjeva[1]

E-mail: *ilin55@yandex.ru*

We present results of $UBVRI$ polarimetry of about 30 stars in a vicinity of the well-studied Bok globule Barnard 5 (B5). We find a correlation of the maximum polarization wavelength λ_{max} with extinction in the cloud when $A_V > 1.5$ mag. We conclude that multicolor polarimetry of background stars can be a useful tool to characterize dust in outer regions of dark clouds.

The properties of dust in dark clouds are still not well understood. Recent studies of extinction law, scattered light and submm emissivity have inferred changes in dust properties with an increase of depth inside a cloud (e.g., [1]). However, there are doubts that the wavelength dependence of polarization $P(\lambda)$ of background stars can be useful to characterize dust grains as different factors can affect this dependence in typical molecular clouds [2]. For globules, being smaller and more simple geometrically and physically, the situation can be different, but observations of $P(\lambda)$ variations with the depth have not been made since the work [3].

We performed $UBVRI$ polarimetric observations of about 30 stars around B5 at 2.6-m ZTS and 1.25-m AZT-11 telescopes with the standard equipment at the Crimea Observatory in 1990–93. These polarimetric data supplemented with those available in the literature allowed us to derive much more reliable estimates of λ_{max} than in [3] (see as examples the values of λ_{max} in micron in the table).

Stars	data from [3]	this work
J1	0.79 ± 0.06	0.77 ± 0.02
J6	0.80 ± 0.11	0.55 ± 0.06

Stars	data from [3]	this work
J2	0.85 ± 0.08	0.76 ± 0.02
J16	1.11 ± 0.29	0.93 ± 0.12

For 20 out of 36 stars considered, we accepted the spectral classes found from Vilnius system photometry in [4]. For other 8 stars, we took the classes given by HDEC and assumed that the stars belong to the MS. For the weakest rest 8 stars, we estimated spectral classes from 2MASS data in a usual way. That gave us estimates of A_V and distances to the stars as photometric data are available.

We used data from the COMPLETE survey that has given various detailed maps of several star-forming regions including that in Perseus with the globule B5 being located at its edge [5]. In the figure we show a map of B5 with the

[1] Sobolev Astronomical Institute of St.Petersburg University, Russia
[2] Pulkovo Observatory of the RAS, Russia
[3] Crimea Astrophysical Observatory, Crimea

V. Grinin et al. (eds) Radiation mechanisms of astrophysical objects. Yerevan: Edit Print, 2017, pp. 137–138.

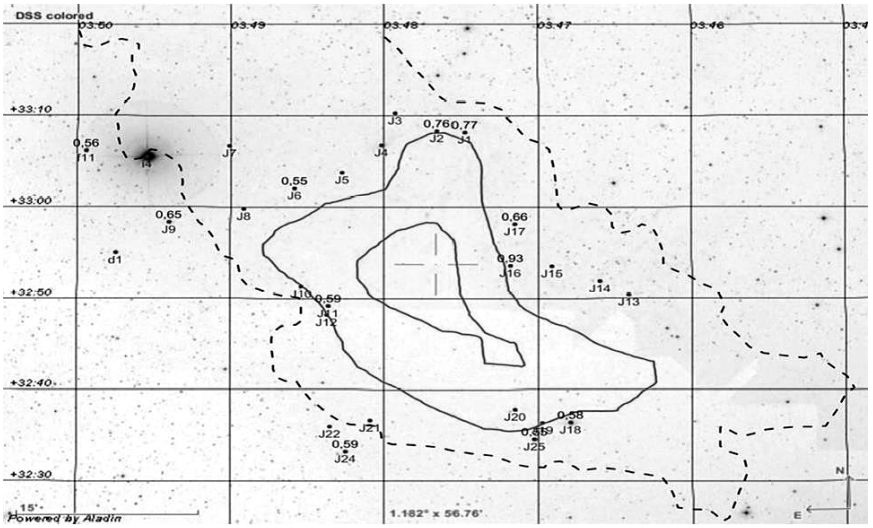

Figure 1: Map of B5 globule. Continuous lines present the extinction contours with $A_V = 3$ and 5 mag from [5]. Points with the number marks show our stars. Numbers above these marks give the obtained values of λ_{max} in micron.

extinction contours from this survey (and our stars with λ_{max} values derived). We find a good agreement of our estimates of A_V with those of [5].

For the field stars, we found locally increased $\lambda_{max} \approx 0.6 \pm 0.05\,\mu$m, which is typical of star-forming regions and is usually related to an effect of close stars.

Our data show that the stars J11, J18, J25 and F11 are foreground as the distance to them is less than that to B5 ($\sim$350 pc). For other stars, we see a certain increase of λ_{max} values when the cloud contribution to A_V grows.

Generally, we did not find clear effects of the halo on the maximum polarization wavelength, but detected a certain increase of λ_{max} when the contribution of the outer layers was significant ($A_V > 1.5$ mag).

Acknowledgments. The work was supported by grants RFBR 16-02-00194 and DST-RFBR 16-52-45002.

References

1. *J.B. Foster, K.S. Mandel, J.E. Pineda et al.*, Mon. Not. Roy. Astron. Soc., **428**, 1606, 2013.
2. *B.G. Andersson, A. Lazarian, J.E. Vaillancourt*, Ann. Rev. Astron. Astrophys., **53**, 501, 2015.
3. *H.C. Bhatt*, Mon. Not. Roy. Astron. Soc., **222**, 383, 1986.
4. *K. Cernis*, Balt. Astron., **2**, 214, 1993.
5. *N.A. Ridge, J. Di Francesco, H. Kirk et al.*, Astron. J., **131**, 2921, 2006.

Section III

Stellar Atmospheres and Circumstellar Matter, Planetary Atmospheres

The Sobolev Approximation in the Development and Astrophysical Applications

V.P. Grinin[1,2]

E-mail: *grinin@gao.spb.ru*

The Sobolev approximation is one of the most effective methods of the modeling of emission spectra of astrophysical objects of various types. It plays also an important role in the radiative hydrodynamics. In this short review, after an introduction to the Sobolev method, I discuss the main steps in its development and astrophysical applications.

1 Introduction to the Sobolev method

Emission spectra of many astrophysical objects are formed in the media with large-scale differential motions which velocities are much greater than the thermal velocity of atoms. In these conditions, the Doppler shift of the radiation frequency leads to strong changes in optical properties of the gas in the line frequencies. This circumstance strongly complicates the solution of the radiative transfer problem. However, as shown by V.V. Sobolev [58], in the media with the large velocity gradient, the solution of this problem can be significantly simplified.

The essence of this approximation is as follows: for large velocity gradients, due to the shift between resonance frequencies of the emitting and absorbing atoms, the radiative interaction at each point of the medium $\vec{r}$ is determined by its local vicinity. The characteristic size of this vicinity is equal to the distance from the given point to that, where the aforementioned shift in resonance frequencies is equal to the half-width of the line profile function $\Delta\nu_D$ determined by the thermal (or turbulent) velocity v_t,

$$s_0 = v_t/|dv_{\vec{s}}/ds|. \tag{1}$$

Here $dv_{\vec{s}}/ds$ is the velocity gradient in the comoving coordinate system at the point $\vec{r}$ in the direction $\vec{s} = \vec{r}\,' - \vec{r}$; $s = |\vec{s}| \ll |\vec{r}\,|$), and $dv_{\vec{s}}/ds \simeq [\vec{v}(\vec{r}\,') - \vec{v}(\vec{r})]/s$ (see Fig. 1).

For rough estimates, the velocity gradient in this expression can be replaced by the ratio v/R, where v is the characteristic velocity of large-scale motions and R is the characteristic size occupied by the emitting gas. As a result, we obtain the approximate relation: $s_0 \approx R(v_t/v)$. The parameter s_0, which was subsequently called the "Sobolev length", is the main parameter of the Sobolev method, characterizing the size of the local vicinity of the point.

[1] Pulkovo Astronomical Observatory, St. Petersburg, Russia
[2] Sobolev Astronomical Institute, St. Petersburg University, St. Petersburg, Russia

V. Grinin et al. (eds) Radiation mechanisms of astrophysical objects. Yerevan: Edit Print, 2017, pp. 141–150.

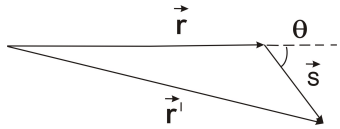

Figure 1

In general case, the equation for the source function has a form

$$S(\vec{r}) = \lambda \int_V K(\vec{r}, \vec{r}\,')\, S(\vec{r}\,')\, d\vec{r}\,' + g(\vec{r}). \tag{2}$$

Here $K(\vec{r}, \vec{r}\,')$ is the kernel function determining the density probability of a transfer of the radiative excitation from the point $\vec{r}$ to the point $\vec{r}\,'$, λ is the probability of a photon survival at a single scattering, V is the volume of the space filled in with atoms, and $g(\vec{r})$ represents the primary sources of excitation in the spectral line under consideration.

In the media with the large velocity gradient $s_0 \ll R$, Eq. (2) can be essentially simplified. In this case, one can approximately assume that the source function does not change in the vicinity of the point $\vec{r}$, and we can take it outside the integral by setting $S(\vec{r}\,') \approx S(\vec{r})$. A similar procedure can be done with the kernel function $K(\vec{r}, \vec{r}\,')$ if to replace its parameters that determine optical properties of the medium (atomic level populations, thermal or turbulent velocity) by the corresponding values at the point $\vec{r}$. Finally, one can neglect an influence of the boundaries and assume that the medium fills in an infinite volume of space. As a result, the integral equation with the very complicated kernel is transformed to the simple equation

$$S(\vec{r})\ [1 - \lambda + \lambda\beta(\vec{r})] = g(\vec{r}), \tag{3}$$

where β is the probability of a photon to escape the point of the medium $\vec{r}$ without scattering and absorption along the way

$$\beta(\vec{r}) = 1 - \int K(\vec{r}, \vec{r}\,')\, d\vec{r}\,'. \tag{4}$$

It should be noted that in the stationary medium the corresponding kernel function is always normalized to unit. This reflects the obvious fact that a photon emitted in an infinite medium will be absorbed somewhere in it. A principal difference of the radiative diffusion in a medium with a velocity gradient is that this normalization condition is violated, and the integral of the kernel function over infinite space is always less than unity. This means that because of enlightenment of the medium in the line frequencies due to the Doppler effect, there is a nonzero probability for a photon to escape from the point of the medium lying formally at the infinite distance from its boundary: $\beta(\infty) > 0$. This property of the radiation transfer in the line frequencies in moving media is the basis of the Sobolev approximation (SA).

It is important that the photon escape probability from an arbitrary point of the medium is expressed fairly simply in terms of the characteristics of the medium and the velocity field at the given point. For example, in a spherically-symmetric envelope expanding with the velocity $v(r)$ we have

$$\beta(r) = \int_0^1 \frac{1 - e^{-\tau(r,\mu)}}{\tau(r,\mu)}\, d\mu, \tag{5}$$

where $\tau(r,\mu)$ is the effective optical depth of the medium at the point r in the direction $\vec{s}$ forming an angle $\theta = \arccos\mu$ with the vector $\vec{r}$

$$\tau(r,\mu) = k(r)\, v_t |\psi(r,\mu)|^{-1}, \tag{6}$$

$k(r)$ is the integrated line opacity per unit volume (weighted with the line profile function), and

$$\psi(r,\mu) = \frac{dv_{\vec{s}}}{ds} = \frac{dv}{dr}\,\mu^2 + \frac{v}{r}\,(1-\mu^2). \tag{7}$$

In the particular case of an isotropically expanding medium (an example of which is the expanding Universe), $v(r) = Ar$, $\psi(r,\mu) = v/r$ and $\tau(r,\mu) = constant = k\, v_t/A$. As a result, $\beta(r) = (1-e^{-\tau(r)})/\tau(r)$. From this, we get $\beta = 1/\tau$ for $\tau \gg 1$.

Thus, if the primary sources of excitation $g(\vec{r})$ in the spectral line are known, then we can immediately calculate the source function from Eq. (3), and then calculate the intensity of the spectral line. This method has been originally developed by V.V. Sobolev for the case of a rectangular line profile function and the complete frequency redistribution in a comoving frame. Later, in 1957, he considered in [59] the general case of an arbitrary absorption coefficient. It turned out that the expression for the photon escape probability $\beta(r)$ does not depend on the type of the line profile function. This invariance is one of the most interesting properties of the process of radiative diffusion at line frequencies in moving media which has no analog in the case of stationary media. In the latter case, as we know, the escape probability depends sensitively on the type of the line profile function (see, e.g., the book of Ivanov [42]).

Due to its simplicity, the Sobolev approximation was widely used when modeling and interpreting the emission spectra of stars with circumstellar envelopes and other astrophysical objects. The role of this method in the solution of complex, multilevel problems was especially great. First steps in this direction were taken by Rublev [54, 55], Gorbatskii [20], Boyarchuk [4], Doazan [11], Luud and Il'mas [45], Gershberg and Shnol [18], Grinin and Katysheva [28], Castor and Lamers [7], Natta and Giovanardi [50], and many others (see a more detailed bibliography of the works on this subject in the review [24]).

In 1961 Sobolev's book "Moving Envelopes of Stars" was translated into English by S. Payne-Gaposchkin and published in the USA. Soon a series of fundamental discoveries in astronomy have been done, resulting in appearance of new astrophysical objects: quasars, neutron stars and maser sources. First

observations of ultraviolet spectra of stars from space led to the discovery of intense mass outflows (stellar winds) from hot supergiants. All this expanded considerably the field of the application of the SA and stimulated its further development in the papers by Castor [5, 6], Grachev [22], Rybicki and Hummer [57], Hummer and Rybicki [36, 37], Jeffery [39], Hutsemekers and Surdej [38], Petrenz and Puls [53], Dorodnitsyn [13], Grinin and Tambovtseva [30], and others (see below). In particular, the Sobolev approximation has been adapted for studying polarization in spectral lines [39], for the case of relativistic motions [38, 40] and conditions near black holes and neutron stars [12, 13, 14].

1.1 The SEI algorithm

The questions of the accuracy of the SA and the limits of its applicability naturally emerged. The development of numerical and asymptotic methods of the radiative transfer theory has made possible the solution of this problem. It turned out that the limits of applicability of the SA depend sensitively on the type of the line profile function and are determined by the asymptotic behavior of the kernel function in Eq. (2). These and related topics are discussed in more detail in the review papers by Grachev [23] and Grinin [24].

Using the numerical methods, Bastian et al. [2] and Hamann [31] investigated in detail the accuracy of the SA in models of spherically symmetric outflows. They have shown that the error in the calculations performed on the basis of the SA arises mainly when calculating the line profile, while accuracy of the source function calculations was quite good. Based on this result, Bertout [3] and Lamers et al. [44] suggested to use the exact expression for the intensity of the radiation emerging from the medium in the combination with the source function calculated in the Sobolev approximation. This algorithm is known as the Sobolev Exact Integration (SEI) method [44]. It yields a considerable gain in accuracy of the line profiles and is widely used when modeling the emission spectra.

2 The non-local approximation

In the seventies it was found that the presence of the large gradient velocity in the emitting region actually still does not guarantee the condition of locality of the radiative interaction at the line frequencies, and one additional condition must be fulfilled. Namely, the derivative of the velocity in the comoving coordinate system, $dv_{\vec{s}}/ds$ has to be a positive definite function of the angle θ between the vector $\vec{r}$ and the arbitrary direction $\vec{s}$. In the case of radially symmetric motions, this condition is fulfilled for the outflow with the acceleration ($dv/dr > 0$) and does not fulfilled in the case of decelerated outflows. The latter is also true in the case of accretion flows, including the quasi-Keplerian disks. In these cases, at each point $\vec{r}$ there are directions along which $dv_{\vec{s}}/ds = 0$, and the Sobolev length $s_0 = \infty$ (see Fig. 2).

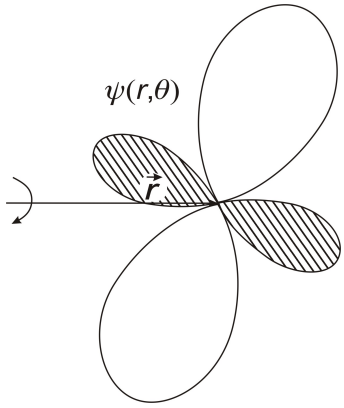

Figure 2: Azimuthal structure of the velocity gradient in the comoving frame in the plane of the quasi-Keplerian disk (from [29]). In the filled regions $\psi(r,\theta) < 0$.

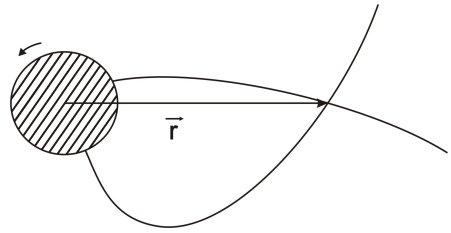

Figure 3: The common-point velocity surface in the rotating and collapsing envelope (from [24]).

These distinctions in the structure of the velocity field in the comoving frame are key for definition of a type of the radiative interaction in a moving medium. The equation for the source function in the case of the non-local radiative interaction was first obtained by Grachev and Grinin [21]. They showed that in shells expanding with deceleration, the source function is determined by the equation

$$S(\vec{r})\ [1-\lambda+\lambda\beta(\vec{r})] = \lambda \int_{\Omega_c} S(\vec{r}\,')\ \left[1-e^{-\tau(\vec{r}\,',\theta')}\right]\ \beta(\vec{r},\theta)\,\frac{d\Omega}{4\pi} + g(\vec{r}), \qquad (8)$$

which differs from Eq. (3) by the integral term. This additional term allows for the fact that besides the local vicinity of the point, a contribution to photoexcitations at the point $\vec{r}$ comes from the so-called surfaces of comoving points that are in resonance with the point $\vec{r}$ and satisfy the equation $(\vec{v}(\vec{r}\,') - \vec{v}(\vec{r}))\cdot\vec{s} = 0$. An example of such a surface is presented in Fig. 3. The existence of such surfaces provides for the non-local nature of the radiative interaction in media moving with large velocity gradients.

An equation similar to Eq. (8) was derived independently and investigated in detail by Rybicki and Hummer [56]. They introduced the term "the common points surface" which has now become generally accepted. We should also note a paper by Deguchi and Fukui [9] in which Eq. (8) was derived and used for calculations of the spectra of collapsing protostellar clouds as well as a version of a non-local radiative interaction between components of a resonance doublet in moving media, considered by Surdej [60].

Let us note that the integral term in this equation does not contain any new quantities in comparison with the local version of the Sobolev approximation. We see the same expressions for the escape probability β and for the effective optical depth τ as in Eq. (3). An analysis shows that the contribution of the integral term in Eq. (8) to the source function depends on two factors: on the behavior of the

primary sources of excitation $g(r)$ and on the solid angle Ω_c in which the surface of comoving points is seen from the point $\vec{r}$. For $\Omega_c \ll 4\,\pi$, the influence of the integral term on the source function can be neglected in most cases. The non-local version of the Sobolev approximation is applied to modeling the emitting regions around young stars (see, e.g., the works of Hartmann et al. [33], Muzerolle et al. [49]), black holes and neutron stars (the paper of Dorodnitsyn [14]), supernova shells (that of Fransson [16]) and other astrophysical objects. It is interesting to note that the non-local radiative interaction can take place near to the compact objects (black holes and neutron stars) in the *accelerating outflows* due to the gravitation red shift (the work of Dorodnitsyn [13]). In this case the P Cygni profile may have both red- and blue-shifted absorption troughs (in contrast with the classical theory).

3 The radiative force

Due to the large cross sections of the interaction with matter, radiation in spectral lines plays an important role in the dynamics of gas in high-luminosity astrophysical objects. In 1957 Sobolev [59] has obtained the formula for the radiative force in the plane-parallel layer expanding with a constant velocity gradient. Only diffuse radiation produced in the layer was taken into account. The next important step was made by Castor [5]. Developing the ideas laid down in the SA, he has obtained the expression for the radiative force exerted on the gas in a spherically symmetric expanding shell with absorption and scattering of continuous stellar radiation in the line frequencies. It has a simple form

$$f_{r,L} = \frac{k(r)\,F_c\,\Delta\nu_D}{c}\,\min(1, 1/\tau), \tag{9}$$

where F_c is the radiation flux at the stellar surface at the frequency of the spectral line under consideration, k is the integrated line opacity (normalized to a unit of mass), c is the speed of light, and τ is the optical depth defined by Eqs. (6)–(7). Castor, Abbott, and Klein (CAK) [8] subsequently calculated models of the expanding envelopes of hot supergiants and showed that the main contribution to the radiative force comes from a set of weak subordinate lines of ionized atoms such as CII, CIII, etc. It is needed to note that in the earlier attempts to solve this problem it was assumed that the main contribution to the radiative force provided the ultraviolet resonance lines (see the works of Lucy and Solomon [46], Lucy [47]). However, their effect was too small to explain the high mass loss rate from the hot supergiants.

The CAK theory has had a significant effect on the development of the theory of radiative driven stellar winds. Due to the efforts of Castor and his co-authors, this theory is now one of the most advanced fields of theoretical astrophysics. The results of this theory are applied not only to calculations of the radiative driven winds from hot stars but also to modeling of the envelopes and disk winds of quasars and active galactic nuclei.

3.1 The azimuthal component of the radiative force

Completing the topic of the radiative force in moving media, we note one non-trivial property of this mechanism. It consists in the fact that in envelopes with axially symmetric motions, along with the radial component $f_{r,L}$ of the radiative force there is also an azimuthal component $f_{\theta,L}$. Its appearance is related to the fact that in the general case of axially symmetric motions, the derivative of the velocity in the comoving frame in the plane of the motions includes the odd dependence on the angle θ between the vector $\vec{r}$ and the arbitrary direction $\vec{s}$ in the plane of motions

$$\frac{dv_{\vec{s}}}{ds} = \frac{dv}{dr}\,\cos^2\theta + \frac{v}{r}\,\sin^2\theta + \left(\frac{du}{dr} - \frac{u}{r}\right)\sin\theta\,\cos\theta. \tag{10}$$

For this reason, the Sobolev length $s_0(r,\theta)$ and, therefore, the optical properties of the medium at the line frequencies are asymmetric functions of the angle θ (Fig. 2). Radiation in the spectral line propagates in such a medium not along the radius vector $\vec{r}$ but at some angle to it. This angle depends on the ratio between the radial and tangential velocity components v and u. A result of this is an azimuthal component of the radiative force. Its sign depends on the physical conditions in the envelope, such as the gradient of the source function and the direction of the radial velocity (expansion or accretion). Depending on these parameters, the direction of the azimuthal radiative force can either coincide with the rotation of a gaseous envelope or act against the rotation. The efficiency of this mechanism, operating on the principle of "Segner's wheel", depends on the ratio between the radiation density at spectral lines frequencies and the kinetic energy of gas as well as on the ratio between the velocity components v and u. For example, in the accretion disks $v \ll u$, and the ratio $f_{\theta,L}/f_{r,L} \sim v/u \ll 1$. More detailed information on this radiative mechanism can be found in [25, 26, 27]. Here we only note that in 1995 Owocki, Cranmer, and Gayley [52] independently discovered a similar effect in a numerical solution of the radiative hydrodynamics equations in the envelopes of Be stars (see also [17]).

4 Molecular lines and cosmic masers

Despite the fact that the velocities of internal motions in interstellar molecular clouds do not exceed several kilometers per second, as a rule, they nevertheless can also be objects to which SA can be applied. Because of the low temperatures, the velocities of thermal motions of molecules in the clouds are also very small and often do not exceed several hundreds of meters per second. This fact has been used by many authors who have used the SA for the diagnostics of interstellar clouds based on molecular line intensities. In particular, Goldreich and Kylafis [19], and Deguchi and Watson [10] used the SA to study the polarization of molecular lines.

In cosmic masers the optical depth of the emitting region with an inverted population of molecular levels plays the role of the amplification factor, and in the case of powerful masers it can be much larger than unity. Under these conditions,

even a relatively small number of working molecules going out of resonance can cause considerable changes in the maser emission intensity (e.g., the paper of Watson and Wyld [63]). Maser lines are therefore the most sensitive indicators of internal motions of the medium, especially in the case of unsaturated regime. For the same reason, maser emission is also very sensitive to the type of radiative interaction in the medium. Really, only at the non-local radiative interaction, at each point of the medium there are directions in which the velocity gradient in the comoving coordinate system equals zero. In particular, in the quasi-Keplerian disk the equation $\psi(r, \mu) = 0$ has four solutions: $\mu_1, \ldots, \mu_4$ (Fig. 2). In terms of the SA, the optical depth in the line frequencies in these directions formally becomes infinite.

To determine the effective optical depth in this case, one must allow for the second order derivative of the velocity (see Fig. 4) from the work of Grinin and Grigor'ev [29]). Typical examples of such objects are the quasi-Keplerian disks (see, e.g., the paper by Babkovskaia et al. [1]) as well as protostellar clouds in the phase of gravitational contraction. It should be also noted that in addition to a velocity gradient, the maser lines can be also sensitive to the presence of magnetic field. These are the hydroxyl masers and some others. Calculations of such masers require joint allowance for the velocity and magnetic field gradients (see the work of Kegel and Varshalovich [41]).

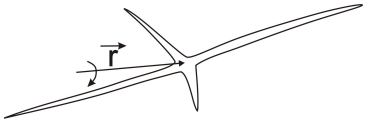

Figure 4: Azimuthal structure of the optical depth in the maser line in the plane of the quasi-Keplerian disk (from [29]).

Thus, despite the appearance of the effective numerical methods (see, e.g., [48, 35, 34] and references there), the Sobolev approximation is an important tool for modeling and diagnostics of emitting regions in the different kinds of astrophysical objects. It is applied in combination with the Monte Carlo method for modeling of the complex emitting regions near the young stars (see, e.g., the papers of Harries [32], Kurosawa et al. [43]). The unique object of application of the SA is the expanding Universe (e.g., the work of Dubrovich and Grachev [15]) which can be optically very thick for the L_α radiation at the large red shifts as shown by Varshalovich and Syunyaev [62]. It is also difficult to overestimate the role of the SA in the theory of the radiative driving stellar winds (see the paper of Owocki and Puls [51] and references therein).

References

1. *N. Babkovskaia, Ju. Poutanen, A.M.S. Richards, R. Szczerba*, Mon. Not. Roy. Astron. Soc., **370**, 1921, 2006.

2. *U. Bastian, C. Bertout, L. Stenholm, R. Wehrse*, Astron. Astrophys., **86**, 105, 1980.

3. *C. Bertout*, Astrophys. J., **285**, 269, 1984.
4. *A.A. Boyarchuk*, Izv. Krym. Astrofiz. Obs., **35**, 45, 1966.
5. *J. Castor*, Mon. Not. Roy. Astron. Soc., **149**, 111, 1970.
6. *J. Castor*, Mon. Not. Roy. Astron. Soc., **169**, 279, 1974.
7. *J. Castor, H.J.G.L.M. Lamers*, Astrophys. J. Suppl., **39**, 481, 1979.
8. *J. Castor, D.C. Abbott, R.I. Klein*, Astrophys. J., **195**, 157, 1975.
9. *S. Deguchi, Y. Fukui*, Publ. Astron. Soc. Japan, **29**, 683, 1977.
10. *S. Deguchi, W.D. Watson*, Astrophys. J., **285**, 126, 1984.
11. *V. Doazan*, Ann. Astrophys., **28**, 1, 1965.
12. *A.V. Dorodnitsyn, I.D. Novikov*, Astrophys. J., **621**, 932, 2005.
13. *A.V. Dorodnitsyn*, Mon. Not. Roy. Astron. Soc., **393**, 1433, 2009.
14. *A.V. Dorodnitsyn*, Mon. Not. Roy. Astron. Soc., **406**, 1060, 2010.
15. *V.K. Dubrovich, S.I. Grachev*, Astron. Lett., **31**, 359, 2005.
16. *C. Fransson*, Astron. Astrophys., **133**, 264, 1984.
17. *K.G. Gayley, S.P. Owocki*, Astrophys. J., **537**, 461, 2000.
18. *R.E. Gershberg, E.E. Shnol*, Izv. Krym. Astrofiz. Obs., **50**, 122, 1974.
19. *P. Goldreich, N.D. Kylafis*, Astrophys. J., **253**, 606, 1982.
20. *V.G. Gorbatskii*, Astron. Zh., **41**, 849, 1964.
21. *S.I. Grachev, V.P. Grinin*, Astrophys., **20**, 190, 1975.
22. *S.I. Grachev*, Astrophys., **13**, 95, 1977.
23. *S.I. Grachev*, Trudy Astron. Obs. St.Peterburg Univ., **44**, 203, 1994.
24. *V.P. Grinin*, Astrophys., **20**, 190, 1984.
25. *V.P. Grinin*, Astrophys., **14**, 537, 1978.
26. *V.P. Grinin*, Astrophys., **16**, 123, 1980.
27. *V.P. Grinin*, Astrophys., **17**, 109, 1981.
28. *V.P. Grinin, N.A. Katysheva*, Izv. Krym. Astrofiz. Obs. (Bull. Crimean Astrophys. Obs.), **62**, 59, 1980.
29. *V.P. Grinin, S.A. Grigor'ev*, Sov. Astron., **27**, 298, 1983.
30. *V.P. Grinin, L.V. Tambovtseva*, Astron. Rep., **55**, 704, 2011.
31. *W.-R. Hamann*, Astron. Astrophys., **93**, 353, 1981.
32. *T.J. Harries*, Mon. Not. Roy. Astron. Soc., **315**, 722, 2000.
33. *L. Hartmann, R., Hewett, N. Calvet*, Astrophys. J., **426**, 669, 1994.
34. *D.J. Hillier, D.L. Miller*, Astrophys. J., **496**, 407, 1998.

35. *D.J. Hillier*, Astron. Astrophys., **231**, 116, 1990.

36. *D.G. Hummer, G.B. Rybicki*, Astrophys. J., **293**, 258, 1985.

37. *D.G. Hummer, G.B. Rybicki*, Astrophys. J., **378**, 248, 1992.

38. *D. Hutsemekers, J. Surdej*, Astrophys. J., **361**, 367, 1990.

39. *D. Jeffery*, Astrophys. J. Suppl., **71**, 951, 1989.

40. *D. Jeffery*, Astrophys. J., **415**, 734, 1993.

41. *W.H. Kegel, D.A. Varshalovich*, Nature, **286**, 136, 1980.

42. *V.V. Ivanov*, Radiative Transfer and the Spectra of Celestial Bodies. Moscow: Nauka, 1969.

43. *R. Kurosawa, M.M. Romanova, T.J. Harries*, Mon. Not. Roy. Astron. Soc., **416**, 2623, 2011.

44. *H.J. Lamers, M. Cerruti-Sola, M. Perinotto*, Astrophys. J., **314**, 726, 1987.

45. *L. Luud, M. Il'mas*, Emission Lines in Stellar Spectra. Tartu, 1974.

46. *L.B. Lucy, P. Solomon*, Astrophys. J., **159**, 879, 1970.

47. *L.B. Lucy*, Astrophys. J., **163**, 95, 1971.

48. *D. Mihalas, P.B. Kunasz, D.G. Hummer*, Astrophys. J., **210**, 419, 1976.

49. *J. Muzerolle, P. D'Alessio, N. Calvet, L. Hartmann*, Astrophys. J., **617**, 406, 2004.

50. *A. Natta, C. Giovanardi*, Astrophys. J., **356**, 646, 1990.

51. *S.P. Owocki, J. Puls*, Astrophys. J., **510**, 355, 1999.

52. *S.P. Owocki, S.R. Cranmer, K.G. Gayley*, Astrophys. J. Lett., **472**, L115, 1996.

53. *P. Petrenz, J. Puls*, Astron. Astrophys., **358**, 956, 2000.

54. *S.V. Rublev*, Sov. Astron. **3**, 76, 1961.

55. *S.V. Rublev*, Sov. Astron. **7**, 492, 1964.

56. *G.B. Rybicki, D.G. Hummer*, Astrophys. J., **219**, 654, 1978.

57. *G.B. Rybicki, D.G. Hummer*, Astrophys. J., **274**, 380, 1983.

58. *V.V. Sobolev*, Moving Envelopes of Stars. Cambridge: Harvard Univ. Press, 1960 (Original in Russian: Dvizhushchiesya Obolochki Zvezd. Leningrad: Izd. Leningr. Univ., 1947).

59. *V.V. Sobolev*, Astron. Zh., **34**, 694, 1957.

60. *J. Surdej*, Astron. Astrophys., **60**, 303, 1978.

61. *J. Surdej, J.P. Swings*, Astron. Astrophys., **96**, 242, 1981.

62. *D.A. Varshalovich, R.A. Syunyaev*, Astrophys., **4**, 140, 1968.

63. *W.D. Watson, H.W. Wyld*, Astrophys. J., **350**, 207, 2000.

Polarized Scattering and Biosignatures in Exoplanetary Atmospheres

S.V. Berdyugina[1]

E-mail: *berdyugina@kis.uni-freiburg.de*

Polarized scattering in planetary atmospheres is computed in the context of exoplanets. The problem of polarized radiative transfer is solved for a general case of absorption and scattering, while Rayleigh scattering and Mie polarized scattering are considered as most relevant examples. We show that (1) relative contributions of single and multiple scattering depend on the stellar irradiation and opacities in the planetary atmosphere; (2) cloud (particle) physical parameters can be deduced from the wavelength-dependent measurements of the continuum polarization and from a differential analysis of molecular band absorption; (3) polarized scattering in molecular bands increases the reliability of their detections in exoplanets; (4) photosynthetic life can be detected on other planets in visible polarized spectra with high sensitivity. These examples demonstrate the power of spectropolarimetry for exoplanetary research for searching for life in the universe.

1 Polarized radiative transfer

Radiative processes in planetary atmospheres are a classical subject, simply for the reason that we live in one. Extensive theoretical studies were carried out during the second half of the twentieth century by such giants as Sobolev [1] and Chandrasekhar [2] as well as the renown radiative transfer school at the Saint Petersburg (Leningrad) State University [3]. Most recently, physics of planetary atmospheres has become one of the most acclaimed subjects because of applications for Earth climate studies and the detection of a large variety of extrasolar planets. This paper provides the theoretical basis for studying atmospheres of exoplanets using techniques of spectropolarimetry available to us. In particular, using molecular band and continuum spectropolarimetry, one can reveal the composition of the gaseous atmosphere, particle layers (clouds, hazes, etc.) and the planetary surface, including the land, water, and life. Modeling these cases is described in this paper.

We start from solving a self-consistent radiative transfer problem for polarized scattering in a planetary atmosphere illuminated by a host star. We solve this problem under the following assumptions:

1) the atmosphere is plane-parallel and static;
2) the planet is spherically symmetric;

[1] Kiepenheuer Institut für Sonnenphysik, Freiburg, Germany

V. Grinin et al. (eds) Radiation mechanisms of astrophysical objects. Yerevan: Edit Print, 2017, pp. 151–162.

3) stellar radiation can enter the planetary atmosphere from different angles and can be polarized;
4) an incoming photon is either absorbed or scattered according to opacities in the atmosphere;
5) an absorbed photon does not alter the atmosphere (model atmosphere includes thermodynamics effects of irradiation);
6) photons can be scattered multiple times until they escape the atmosphere.

These assumptions expand those in [4], namely that multiple scattering is allowed, stellar irradiation can be polarized and vary with an incident angle, and the planetary atmosphere can be inhomogeneous in both longitude and latitude.

Then, the radiative transfer equation for the Stokes vector $\mathbf{I} = (I, Q, U, V)^{\mathrm{T}}$ of scattered polarized radiation of a given frequency (omitted for clarity) towards ($\mu = \cos\theta$, φ) is

$$\mu \frac{d\,\mathbf{I}(\tau,\mu,\varphi)}{d\tau} = \mathbf{I}(\tau,\mu,\varphi) - \mathbf{S}(\tau,\mu,\varphi) \tag{1}$$

with the total source function

$$\mathbf{S}(\tau,\mu,\varphi) = \frac{\kappa(\tau)\,\mathbf{B}(\tau) + \sigma(\tau)\,\mathbf{S}_{\rm sc}(\tau,\mu,\varphi)}{\kappa(\tau)+\sigma(\tau)}, \tag{2}$$

where κ and σ are absorption and scattering opacities, $\mathbf{S}_{\rm sc}$ and $\mathbf{B}$ are the scattering source function and the unpolarized thermal emission, respectively, and τ is the optical depth in the atmosphere with $\tau = 0$ at the top. The formal solution of Eq. (1) is (e.g., [1])

$$\mathbf{I}(\tau,\mu,\varphi) = \mathbf{I}(\tau_*,\mu,\varphi)\,e^{-(\tau_*-\tau)/\mu} + \int_\tau^{\tau_*} \mathbf{S}(\tau',\mu,\varphi)\,e^{-(\tau'-\tau)/\mu}\,\frac{d\tau'}{\mu}, \tag{3}$$

where τ_* is either the optical depth at the bottom of the atmosphere for the Stokes vector $\mathbf{I}^+(\tau,\mu,\varphi)$ coming from the bottom to the top ($\theta < \pi/2$) or the optical depth at the top of the atmosphere ($\tau_* = 0$) for the Stokes vector $\mathbf{I}^-(\tau,\mu,\varphi)$ coming from the top to the bottom ($\theta > \pi/2$).

The scattering source function $\mathbf{S}_{\rm sc}$ is expressed via the scattering phase matrix $\hat{\mathbf{P}}(\mu,\mu';\varphi,\varphi')$, depending on the directions of the incident (μ', φ') and scattered (μ, φ) light

$$\mathbf{S}_{\rm sc}(\tau,\mu,\varphi) = \int \hat{\mathbf{P}}(\mu,\mu';\varphi,\varphi')\,\mathbf{I}(\tau,\mu',\varphi')\,\frac{d\Omega'}{4\pi}. \tag{4}$$

It has contributions from scattering of both incident stellar light and intrinsic thermal emission. Their relative contributions depend on the frequency. For instance, for Rayleigh scattering the intensity of the thermal emission of a relatively cold planet in the blue part of the spectrum may become negligible compared to that of the scattered stellar light. The phase matrix $\hat{\mathbf{P}}(\mu,\mu';\varphi,\varphi')$ is a 4×4 matrix with six independent parameters for scattering cases on particles with a symmetry [5]. In this paper we employ the Rayleigh and Mie scattering phase matrices but our formalism is valid for other phase functions too.

The Stokes vector of the light emerging from the planetary atmosphere $\mathbf{I}(0, \mu, \varphi)$ is obtained by integrating iteratively Eqs. (2) and (3) for a given vertical distribution of the temperature and opacity in a planetary atmosphere. Boundary conditions are defined by stellar irradiation at the top, planetary thermal radiation at the bottom, and (if present) reflection from the planetary surface. Stellar irradiation can be polarized, but the planetary thermal radiation is unpolarized. In particular, stellar limb darkening and linear polarization due to scattering in the stellar atmosphere [7, 8] can be taken into account, including the influence of dark spots on the stellar surface [9]. This effect is not very large but may be important for cooler stars with large spots and planets on very short-period orbits (when the stellar radiation incident angle noticeably varies depending on the stellar limb angle). Also, stellar magnetic fields causing polarization in stellar line profiles due to the Zeeman effect can be included for given atomic and molecular lines [6]. This effect is only important for high-resolution spectropolarimetry which is not yet possible for exoplanets. Depending on the structure of the phase matrix and the boundary conditions, the equations are solved for all or a fewer Stokes vector components. Normally it takes 3–7 iterations to achieve a required accuracy. The radiation flux is then obtained by integrating the Stokes vector over the illuminated planetary surface with a coordinate grid ($6^\circ \times 6^\circ$) on the planetary surface for a given orbital phase angle as described in [4].

Our model includes the following opacity sources:

(1) Rayleigh scattering on H I, H_2, He I, H_2O, CO, CH_4 and other relevant molecules, Thomson scattering on electrons, and Mie scattering on spherical particles with a given size distribution, with all scattering species contributing to the continuum polarization;

(2) absorption in the continuum due to free-free and bound-free transitions of H I, He I, H^-, H_2^+, H_2^-, He^-, metal ionization, and collision-induced absorption (CIA) by H_2–H_2;

(3) absorption and scattering in atomic and molecular lines for particular frequencies where they contribute.

Number densities of the relevant species are calculated with a chemical equilibrium code described in [6]. Here we employ model atmospheres from [10] and [11] for stellar and planetary atmospheres, respectively, according to their effective temperatures ($T_{\rm eff}$). This is appropriate for illustrating radiative transfer effects discussed in Sect. 2 and applicable for the case of highly irradiated hot Jupiters and substellar components. In particular, a model atmosphere of a hot Jupiter has to match the infrared thermal radiation of the planet originating in deeper layers, while upper layers contributing to the optical radiation are completely dominated by the incident stellar radiation. Planetary atmosphere models with specific chemical compositions and temperature–pressure (TP) structures can be also employed. For instance, the planetary atmosphere can be inhomogeneous with the vertical composition and TP-structure varying with latitude and longitude.

2 Results

2.1 Rayleigh scattering

In this section we assume that scattering in the planetary atmospheres occurs only on atoms, molecules or particles which are significantly smaller than the wavelength of scattered light, i.e., we employ the Rayleigh scattering phase matrix, including isotropic scattering intensity. In particular, we focus here on examples of resulting Stokes parameters and source functions depending on stellar irradiation and wavelength.

Figure 1 shows examples of depth dependent Stokes I source functions (top panels) and normalized emerging Stokes I and Q (bottom panels) for three distances between the star and the planet (left to right) at the wavelength of 400 nm. Here, the star is of $T_{\rm eff} = 5500\,{\rm K}$, and the planet is of $T_{\rm eff} = 1500\,{\rm K}$. Stokes Q is assumed to be positive when polarization is perpendicular to the scattering plane.

By studying the behavior of the source functions and Stokes parameters depending on various parameters, we conclude the following facts:

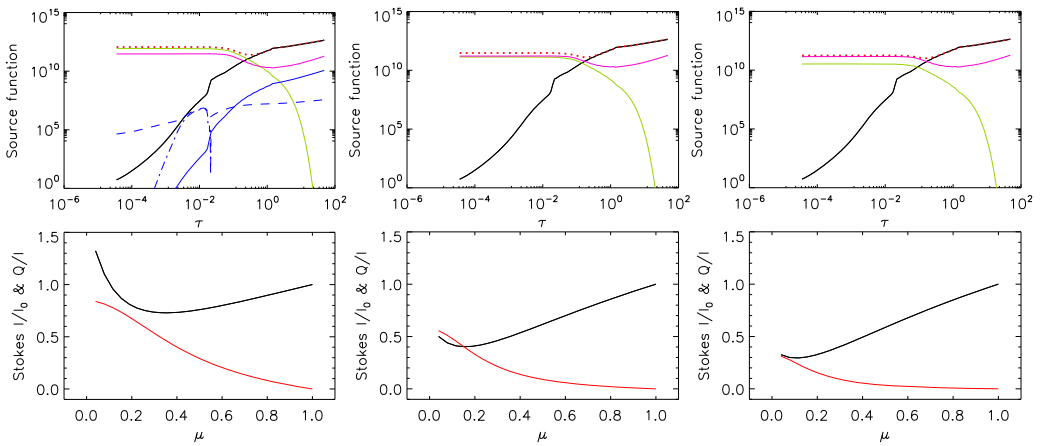

Figure 1: Stokes I source functions (top panels) and normalized emerging Stokes I and Q parameters (bottom panels) for three distances between the star and the planet: 0.02, 0.05, and 0.1 AU (left to right). The source functions are shown separately for thermal radiation of the planet (black), single scattered stellar radiation (green), multiple scattered stellar and planetary radiation (magenta), and the total one (red dotted line). The top left plot also shows relative scattering (dashed blue) and absorption (solid blue) opacities and separately particle scattering (dashed-dotted blue) as a cloud layer in the original model atmosphere (it is the same for all three panels). In the lower panels, the Stokes I/I_0 (black) is normalized to the intensity at the planet disk center ($\mu = 0$). The Stokes Q/I (red) is normalized to I at given μ. Both are at $\tau = 0$. Notice the increase of the single scattering contribution with respect to that of multiple scattering as the distance to the planet decreases (i.e., the stellar flux increases). Accordingly, the planet limb polarization and brightening increase too.

- The polarization at a given depth in the atmosphere arises due to its anisotropic irradiation, i.e., unequal illumination coming from the top and from the bottom (assuming here an azimuthal symmetry). Hence, anisotropy and polarization are small in deeper layers, where planet thermal radiation dominates, and they are larger in upper layers, where stellar irradiation dominates. The depth where this dominance alternates depends on the relative contribution of the scattering and absorption coefficients to the total opacity (which is wavelength dependent). It turns out that in cool gaseous atmospheres this occurs very deep in the atmosphere for the continuum radiation, but can be higher for radiation in cores of strong absorption atomic and molecular lines.
- This anisotropy (and, hence, polarization) is sensitive to the incident stellar flux (cf., number of photons arriving to the planet) at wavelengths where Rayleigh scattering is most efficient, i.e., in the blue part of the spectrum. Thus, hotter stars hosting closer-in planets are systems potentially producing larger polarization in the blue.
- Relative contribution of single-scattered photons with larger polarization with respect to multiple-scattered photons with lower resulting polarization increases with stellar irradiation at shorter wavelengths.
- Depending on stellar irradiation, the intensity distribution on the planetary disk, i.e., $I(0,\mu)/I(0,1)$ can decrease or increase with μ. In fact, the μ value where limb darkening turns into limb brightening approximates the optical depth τ where single and multiple scattering contributions become comparable.
- Planet limb polarization is very sensitive to the stellar irradiation because of the effects listed above. For a larger stellar flux, a larger polarization is seen for a wider range of angles.
- Considering the high sensitivity of planet polarization to stellar irradiation, variability of the stellar flux incident on the planet, e.g., caused by dark (magnetic) spots or flares, can result in a variable *amplitude* of planet polarization, while its orbital phase dependence is preserved, since the latter depends on orbital parameters only (see [4]).

The models presented in Fig. 1 are close to the case of the HD 189733b hot Jupiter which is at about 0.03 AU from its K-dwarf star with the effective temperature of about 5500 K. The relatively high polarization measured from this planet in the blue band (B-band) [12, 13] is well explained by the dominance of the single-scattered stellar photons in its upper atmosphere because of the high irradition and Rayleigh scattering cross-section in the blue. This was first proposed in [13] and further demonstrated with a simple model in [14]. Here, with the precise calculations of the polarized radiative transfer, we show that this hypothesis is valid. Moreover, multi-wavelength polarimetry allowed for estimating the planet albedo and determining its blue color. The relation between the

geometrical albedo and polarization is however not so simple as was assumed in [13]. An analysis of this relation for various planetary and stellar parameters using this theory will be carried out in a separate paper.

2.2 Mie scattering

In this section we consider scattering caused by spherical particles of various sizes which can be comparable or larger than the wavelength of scattered light, i.e., we employ the Mie scattering phase matrix. For smaller particles and/or longer wavelengths, it approximates Rayleigh scattering.

Following examples in earlier literature (e.g., [5] and references therein), we assume "gamma" distribution of particle sizes: $n(r) = \mathrm{C}r^{(1-3b)/b}e^{-r/ab}$, with a and b being the effective particle radius and the effective size variance, respectively. Also, we use the so-called size parameter $2\pi a/\lambda$ which can be recalculated to λ for a given a, and vice versa. Particles are characterized by the refractive index n_r with its real part being responsible for scattering. With this, we can reproduce numerical examples in [5] as well as results for Venus in [15]. Here, we investigate scattering on highly refractive materials ($n_r > 1.5$) which are expected to be present in hot Jupiter atmospheres. For instance, olivine, which is common in the Solar system, and its endmembers forsterite Mg_2SiO_4 and fayalite Fe_2SiO_4 have a range of the refractive index from 1.6 to 1.9.

In Fig. 2 we show examples of two Mie phase matrix elements: intensity P_{11} and percent polarization $-100\%P_{21}/P_{11}$ for single scattering on particles with n_r of 1.6 (upper panels) and 1.9 (lower panels), depending on the size parameter and the scattering angle. The latter is 0° for forward and 180° for backward scattering. These examples illustrate the following known facts (e.g., [16, 15, 5]):

- Forward scattering dominates the intensity for larger particles.
- For the smallest particle size parameters, polarization is strong (up to 100%) and positive near scattering angle 90° due to Rayleigh scattering. For the largest size parameters, polarization approaches that of the geometrical optics, i.e., it is small at small scattering angles because of largely unpolarized diffracted light, and it is negative for a wide range of angles because of two refractions within a sphere.
- Strong positive polarization maximum near 165°–170° is the primary rainbow. It can reach 100% polarization for certain size-angle combinations.
- Strong negative polarization near 140°–150° is a "glory"-like phenomenon caused by surface waves on the scattering particle. The "glory" itself, which is a sharp maximum in polarization in the backscattering direction, can be seen on particles with larger size parameters.
- Weak positive polarization near 20°–30° is due to "anomalous diffraction" caused by interference of the diffracted, reflected and transmitted light in the forward direction.

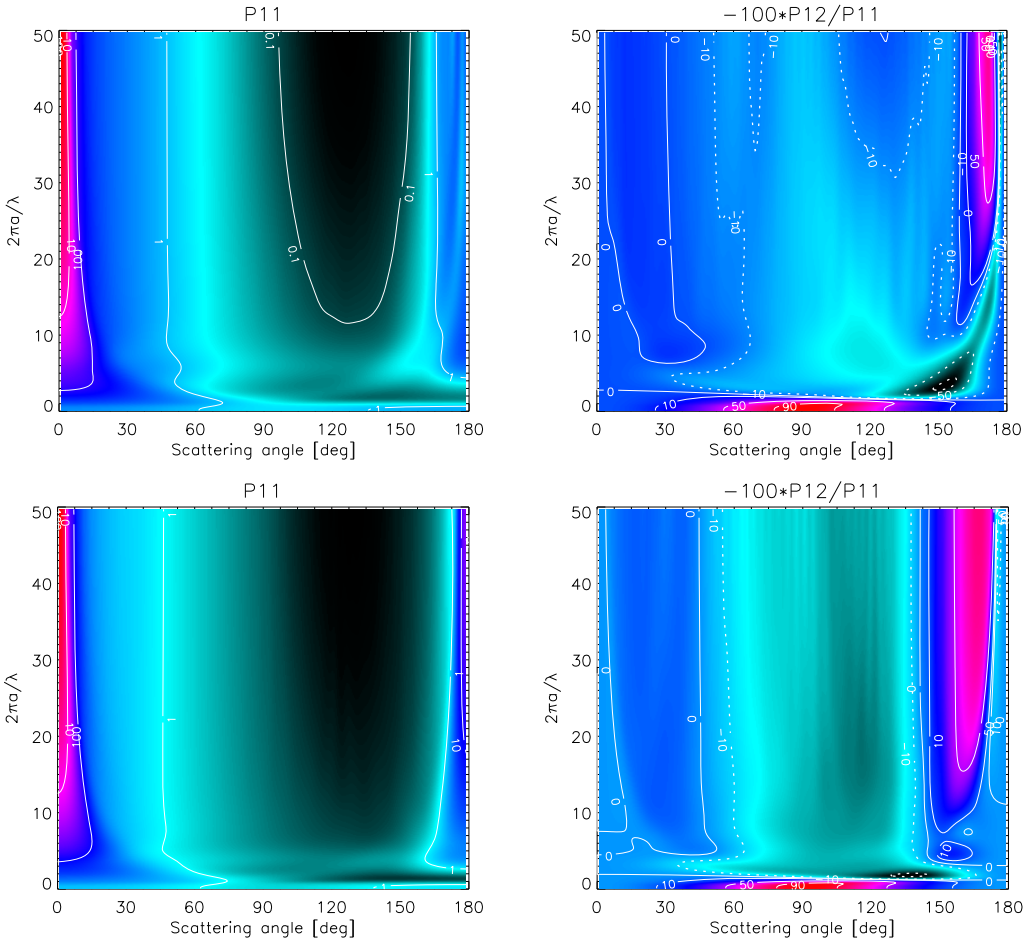

Figure 2: Mie scattering phase matrix elements P_{11} (intensity) and $-100\%P_{21}/P_{11}$ (percent polarization) for single scattering on particles with $n_r = 1.6$ (top panels) and $n_r = 1.9$ (bottom panels) and the effective particle size variance $b = 0.07$. Dotted lines are contours for negative polarization (parallel to the scattering plane).

Now we can model effects of particle scattering on limb intensity and polarization distribution in planetary atmospheres by solving the polarized radiative transfer problem as described in Sect. 1 with the corresponding phase functions. As in Sect. 2.1, we investigate radiative transfer effects depending on irradiation and atmosphere properties. We use the same model atmospheres as before but replace the original layer of scattering particles in the planetary atmosphere with layers of various properties at different heights, imitating a variety of clouds. This *ad hoc* approach allows us to study intensity and polarization depending on particle (cloud) properties. Three examples are shown in Fig. 3. One can see that clouds can significantly affect the brightness of the irradiated atmosphere at depths (angles) where scattering and absorption opacities are comparable. In the presented example of the highly irradiated

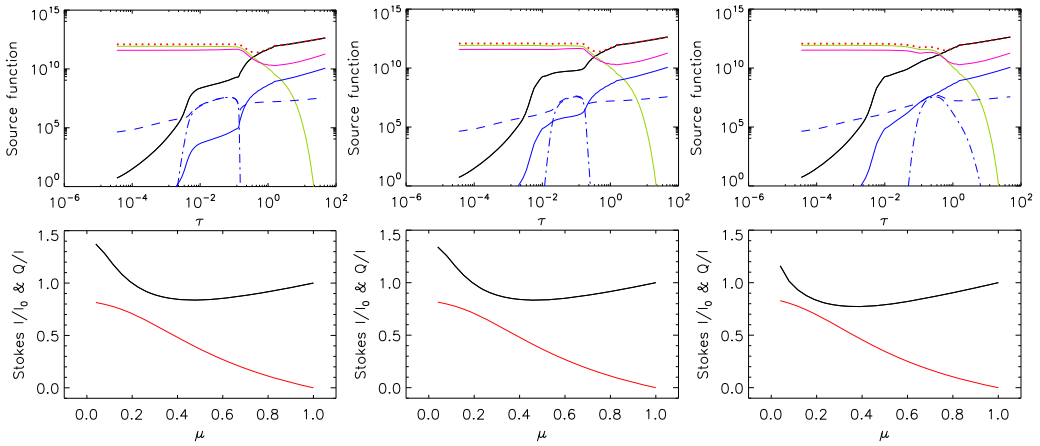

Figure 3: The same as Fig. 1 but for a planet at 0.02 AU from the star with an atmosphere containing *ad hoc* particle layers. The particles are assumed to have an effective size of 20 nm, and the layers are at the depths of 70, 80, and 90 km from the top of the atmosphere (plots are from left to right, respectively).

planetary atmosphere the polarization is still determined by the single-scattered stellar photons. In less irradiated atmospheres, the influence of particles is larger, but still according to the scattering and absorption profiles. More examples with a larger variety of clouds will be published elsewhere.

2.3 Molecular bands

Detecting molecular bands in planetary spectra is the key to their chemical composition and to their habitability assessment. By analyzing the molecular composition we can establish whether the atmosphere is in equilibrium or it is affected by such non-equilibrium processes like stellar activity or life.

Including molecular bands into polarized radiative transfer requires computation of both line absorption and scattering coefficients. We compute molecular line absorption, following [6], and molecular line scattering, following [17], where magnetic field effects on molecular absorption and scattering (the Zeeman, Paschen–Back and Hanle effects) are also included and can be employed for exoplanets. These line opacities augment the continuum opacities at molecular band wavelengths. In addition, depending on the molecular number density distribution, the maximum absorption and scattering for different molecules and bands can occur at different heights [6]. This is an important diagnostics of the atmosphere thermodynamics, e.g., TP profiles.

Despite the growing amount of information, the molecular composition of exoplanetary atmospheres is still largely unknown. Several reported detections of molecular bands were disputed by later measurements (e.g., see overview and references in [18]). Also, a few exoplanets were found to lack any spectral features in the near infrared, which was interpreted as the presence of high clouds

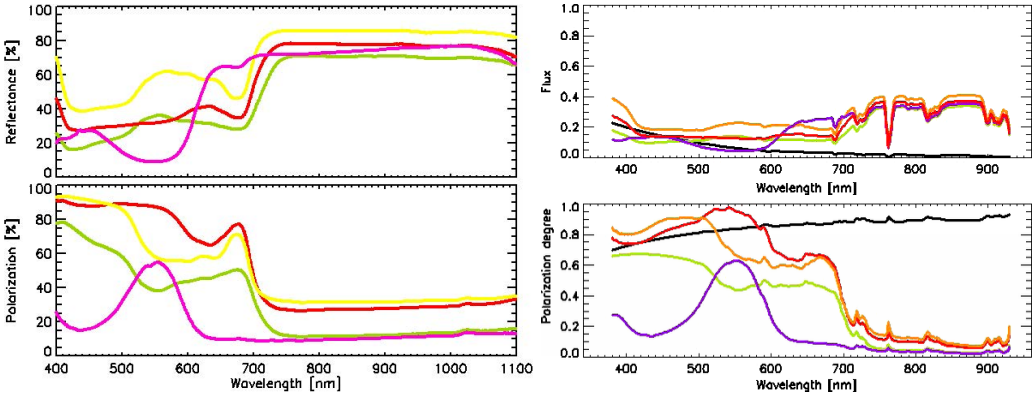

Figure 4: *Left:* reflectance and linearly polarized spectra of plant samples containing various assemblies of biopigments: chlorophyll (green), anthocyanins (red), carotenoids (yellow), phycobiliproteins (purple) [24]. Note that the higher polarization occurs at the wavelengths where these biopigments most efficiently absorb photons. The so-called "red edge" near 700 nm is clearly visible. Also, polarization and reflectance are elevated if the surface of the plant is glossy (wavelength independent), cf., in the red and yellow samples. *Right:* modeled reflectance spectra (top) and linear polarization degree spectra (bottom) for planets with the Earth-like atmosphere, 80% surface coverage by either of the four pigmented organisms shown on the left and 20% ocean surface coverage (visible hemisphere only). The high linear polarization degree clearly distinguishes the presence of the biopigments in contrast to the flux spectra. Black curve represents a planet with an ocean only [26]. The glint from its surface is highly polarized.

masking molecular absorption (e.g., [19]). To explain the presence or absence of molecular bands, synthetic flux absorption and emission thermal spectra in clear and cloudy planetary atmospheres were computed. Recently, it was proposed that cloud physical parameters can be constrained by a differential analysis of various molecular bands forming at different heights in the atmosphere with respect to the cloud height and extent [18]. For instance, water vapor bands at 1.09 μm and 1.9 μm show noticeably different sensitivity to particle size and cloud extent and position at intermediate depths in the atmosphere. This is a sensitive spectral diagnostics of clouds.

Polarized scattering in molecular bands was observed in the solar atmosphere and solar system planets (e.g., [17, 20]). To model this polarization we employ the radiative transfer theory described in Sect. 1 with the line scattering coefficient strongly dependent on wavelength (within line profiles), line polarizability and magnetic field (if included, via the Hanle effect) [17, 21]. The first order radiative transfer effect leads to an apparent correlation of line scattering with absorption. This effect increases the contrast of detection of weak signals in distant planets. For example, model spectra from [26] for the Earth atmosphere (Fig. 4, right panels) show polarization in molecular oxygen and water vapour bands in red wavelengths. However, because of the line-dependent polarizability and magnetic sensitivity, line polarization does not in general correlate with line absorption,

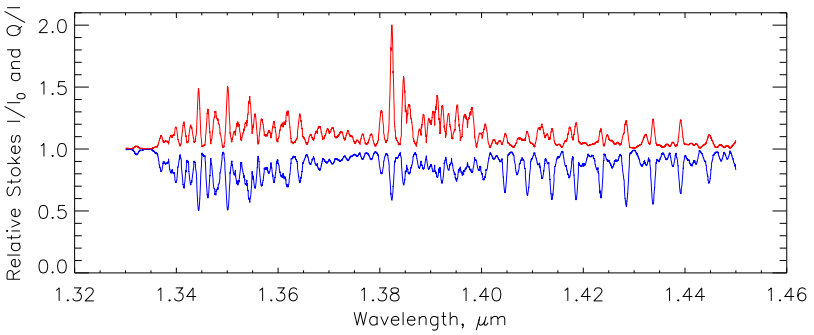

Figure 5: H_2O relative polarization (red) and absorption (blue) spectra plotted, respectively, up and down for clarity, taking into account line polarizability. Note that there is no exact correlation between polarization and absorption.

as is observed in the Second solar spectrum [21]. Neglecting these effects impedes the quantitative interpretation of polarization and the inferred planet parameters. An example taking the polarizability effect into account for about 3500 H_2O lines near 1.4 μm is shown in Fig. 5.

2.4 Biosignatures

A planetary surface visible through an optically thin atmosphere can be searched remotely for spectral and polarized imprints of organisms reflecting and absorbing stellar light. Due to the accessibility and amount of energy provided by the stellar radiation, it seems natural for life to evolve a photosynthetic ability to utilize it as an energy source also on other planets. Thus, flux spectral signatures of biological pigments arising from photosynthesis have been proposed as biosignatures on exoplanets [22, 23]. Moreover, it was recently shown that photosynthetic organisms absorbing visible stellar radiation with the help of various biopigments demonstrate a high degree of linear polarization associated with such absorption bands (see Fig. 4). This effect was also proposed as a sensitive biosignature for high-contrast remote sensing of life [24].

Capturing stellar energy by photosynthetic organisms relies on complex assemblies of biological pigments. While chlorophyll *a* is the primary pigment in cyanobacteria, algae and plants, there are up to 200 accessory and secondary (synthesized) biopigments, including various forms of chlorophyll (*b*, *c* and *d*), carotenoids, anthocyanins, phycobiliproteins, etc. [25]. Various spectral sensitivity of biopigments contribute to their ability to absorb almost all light in the visible range (Fig. 4).

Present and near future observations of Earth-like planets around distant stars cannot resolve the planet surface and image its structures directly. However, uneven distribution of land masses and their various surface properties as on Earth seen from space produce rotational modulation of the reflected light which can be detected and used to constrain the overall surface coverage of various components

which can be distinguished with flux and polarization measurements at different wavelengths. To calculate the biosignature effect, we add surface below the atmosphere which implies new lower boundary conditions in Eq. (3). We allow the planetary surface to contain patches due to the presence of photosynthetic organisms, minerals, sands and water and include also scattering and absorption in the planetary atmosphere and clouds. The Earth atmosphere, ocean and clouds are the same as in [26]. Examples are shown in Fig. 4.

The presence of clouds masking the surface dilutes the information on the surface structure and composition. A completely cloudy atmosphere will obviously disguise the presence of biopigments (and everything else) on the planet surface. A small cloud coverage of around 20% will only marginally reduce polarization effect (see [24]). Thus, clouds are the most disturbing factor in detecting surface biosignatures, but weather variability should assist in successful detection if a planet is monitored long enough to reveal long-lived features on the surface.

The effect of the water ocean is also interesting [24]. The optical thickness of the ocean is basically infinite, so its surface is dark in most colors except for the blue, where it reflects the blue light scattered in the atmosphere. However, there is a bright glint at the subsolar location, which moves around the globe as the planet rotates. This glint is due to specular reflection and is highly polarized and practically white. Hence, an ocean only, cloud-free planet with an Earth-like atmosphere will appear somewhat blue (due to Rayleigh scattering in the atmosphere) and highly polarized. It seems therefore that the presence of an ocean and optically thin atmosphere is most favourable for remote polarimetric detection of exoplanets and biopigments.

To conclude, we have presented a broad range of interesting examples where spectropolarimetry provides novel insights into physics of exoplanets and life. The theoretical components outlined in this paper have been developed since the 1950s, and they were successfully employed for probing atmospheres of the Earth, Sun, solar system planets, and other stars. It is imperative now to make a full use of these techniques for advancing our understanding of exoplanets and for searching for life in the universe.

Acknowledgments. This work was supported by the European Research Council Advanced Grant HotMol (ERC-2011-AdG 291659). The author was fortunate to have studied at the Saint Petersburg University under the guidance of Prof. V.V. Sobolev and the professors and docents of his Department. The joint work in the group of Prof. Jan Stenflo at ETH Zurich was also a great benefit for this research.

References

1. *V.V. Sobolev*, Transfer of Radiant Energy in the Atmospheres of the Stars and Planets. Moscow: Gostekhizdat, 1956 (in Russian).
2. *S. Chandrasekhar*, Radiative Transfer. New York: Dover, 1960.
3. *D.I. Nagirner*, J. Quant. Spectrosc. Rad. Transf., **183**, 4, 2016.

4. *D.M. Fluri, S.V. Berdyugina*, Astron. Astrophys., **512**, A59, 2010.

5. *J.E. Hansen, L.D. Travis*, Space Sci. Rev., **16**, 527, 1974.

6. *S.V. Berdyugina, S.K. Solanki, C. Frutiger*, Astron. Astrophys., **412**, 513, 2003.

7. *N.M. Kostogryz, S.V. Berdyugina*, Astron. Astrophys., **575**, A89, 2015.

8. *N.M. Kostogryz, I. Milic, S.V. Berdyugina, P.H. Hauschildt*, Astron. Astrophys., **586**, A87, 2016.

9. *N.M. Kostogryz, T.M. Yakobchuk, S.V.Berdyugina*, Astrophys. J., **806**, 97, 2015.

10. *F. Allard, P.H. Hauschildt, D.R. Alexander et al.*, Astrophys. J., **556**, 357, 2001.

11. *S. Witte, C. Helling, P.H. Hauschildt*, Astron. Astrophys., **506**, 1367, 2009.

12. *S.V. Berdyugina, A.V. Berdyugin, D.M. Fluri, V. Piirola*, Astrophys. J. Lett., **673**, L83, 2008.

13. *S.V. Berdyugina, A.V. Berdyugin, D.M. Fluri, V. Piirola*, Astrophys. J. Lett., **728**, L6, 2011.

14. *S.V. Berdyugina*, in Solar Polarization 6. Eds. J.R. Kuhn et al., Astron. Soc. Pacif. Conf. Ser., **437**, 219, 2011.

15. *J.E. Hansen, J.W. Hovenier*, J. Atmos. Sci., **31**, 1137, 1971.

16. *H.C. van de Hulst*, Light Scattering by Small Particles. New York: Wiley, 1957.

17. *S.V. Berdyugina, J.O.Stenflo, A.Gandorfer*, Astron. Astrophys., **388**, 1062, 2002.

18. *N. Afram, S.V. Berdyugina*, Astron. Astrophys., 2016, submitted.

19. *L. Kreidberg, J.L. Bean, J.-M. Désert et al.*, Nature, **505**, 69, 2014.

20. *F. Joos, H.M. Schmid*, Astron. Astrophys., **463**, 1201, 2007.

21. *J.O. Stenflo*, Solar Magnetic Fields. Dordrecht: Kluwer, 1994.

22. *N.Y. Kiang, J. Siefert, Govindjee, R.E. Blankenship*, Astrobiol., **7**, 222, 2007.

23. *N.Y. Kiang, A. Segura, G. Tinetti et al.*, Astrobiol., **7**, 252, 2007.

24. *S.V. Berdyugina, J.R. Kuhn, D.M. Harrington et al.*, Int. J. Astrobiol., **15**, 45, 2016.

25. *G.D. Scholes, G.R. Fleming, A. Olaya-Castro, R. van Grondelle*, Nature Chem., **3**, 763, 2011.

26. *D.M. Stam*, Astron. Astrophys., **482**, 989, 2008.

* The color figures are available online in the Proceedings at *http://www.astro.spbu.ru/sobolev100/*.

On the Localization of Emission Line Region in Mira Stars

O. Belova[1]

E-mail: *whitecanvas05122010@mail.ru*

New evidence is obtained that hydrogen emission lines as well as metallic ones originate below the molecular absorption layers in Mira stars.

The time scale t_c of gas cooling behind a shock front propagating through the stellar atmosphere when the gas temperature tends to its preshock value T_0 equal to 2800–3000 K corresponding to the molecular layers, is calculated as a function of temperature T at the final stage. This calculation shows that the gas does not have sufficient time to be cooled to its preshock state. So, T_0 should be greater than the temperature of the molecular layers.

This result agrees with the spectra of Mira-like stars available in the literature. The emission lines show a complex structure with asymmetric or multi-component profiles because of molecular line absorption.

1 Introduction

Mira-like stars belong to a class of long-period pulsating variables on the Asymptotic Giant Branch stage [1]. They pulsate with the largest visible amplitude greater than 2.5 mag and the longest period of about some hundred days. The Miras have complex spectra including molecular absorption bands (TiO and VO), absorption lines of metals (Ca, Fe, Ti, V), and strong emission lines of hydrogen and some metals (MgI, MgII, FeI, FeII and others). The emission lines are observed during approximately $70 - 80\%$ of time: they appear before the luminosity maximum and disappear after the luminosity minimum.

Gorbatskii [2] suggested a shock wave model (similar to that of Cepheids) to explain the emission lines in the spectra of Mira variables. In solving the problem of the shock wave in Mira's atmosphere, one usually considers the regions in which the radiation is mainly formed. These regions are rapidly cooled on the timescale of less than a day. Less attention was paid to further cooling of the gas to the preshock temperature, but estimating the time required for complete relaxation of the gas may be important.

It is shown below that the radiative cooling rate of the gas declines at low temperatures and the cooling time can exceed a half of the period.

[1] SAI MSU, Russia

V. Grinin et al. (eds) Radiation mechanisms of astrophysical objects. Yerevan: Edit Print, 2017, pp. 163–166.

2 Cooling timescale

Let us consider the process of gas cooling in the final stage when the gas temperature T (electron temperature is nearly equal to temperature of atoms and ions) tends to the preshock value T_{bg} (see [3] for more details).

At this stage the main processes are photorecombination, free-free transitions, electron-collisional excitation. The ionization state is determined by photoprocesses as the contribution of electron-collisional ionization to the electron density at the gas temperature of 5000 K is far less than the contribution of photoprocesses at the photosphere temperature of 3000 K. The energy gain due to photoionization and energy losses due to recombination cancel each other out. Thus, the cooling is determined by electron collisions and bremsstrahlung.

In general terms, the equation for the temperature in the final stage of cooling may be written as follows:

$$\frac{dT}{dt} = \Phi\left(\varphi_{ff}(T), Q_{ex}(T)\right) = \Phi(T), \tag{1}$$

where $\varphi_{ff}(T)$ is the contribution of bremsstrahlung, $Q_{ex}(T)$ is that of collisional excitation.

The right side of Eq. (1), designated by $\Phi(T)$, is a function of temperature T under the conditions of quasi-stationary ionization. Consequently, the cooling timescale can be calculated as the integral

$$t(T_{\rm beg}, T_{\rm fin}) = \int\limits_{T_{\rm fin}}^{T_{\rm beg}} \frac{dT}{\Phi(T)}, \tag{2}$$

where $T_{\rm beg}$ is the temperature from the interval 4000–5000 K at which the integration begins. The timescale t is determined by the final temperature $T_{\rm fin}$.

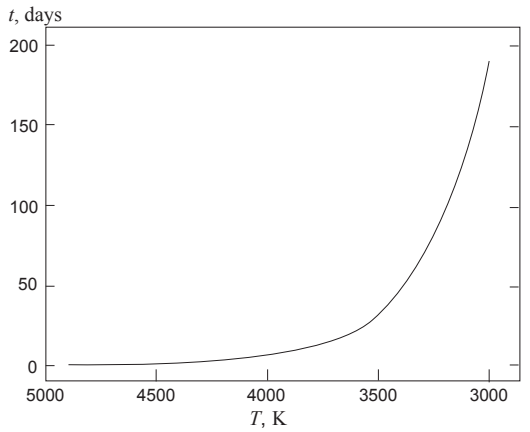

Figure 1: The cooling time as a function of the final temperature $T_{\rm fin}$.

Some results of our calculations are presented in Fig. 1. As can be seen, the gas is rapidly cooled to a temperature of order of 3700–3500 K, but the rate of cooling significantly decreases for $T_{\rm fin}$ below 3500 K. So, the time of cooling to the temperature equal to 3000 K is approximately 200 days, and that to the temperature of 2800 K is even much more.

It is clear from Table 1 that the cooling time exceeds a half of the period for the majority of Mira variables. Therefore, the gas does not have time to return to the undisturbed value of the temperature. This means that the shock wave passes through the regions under the layer of molecular gas. This fact should be manifested in the spectra of Miras.

Table 1: Typical periods of Mira variables

Star	Period, days	Star	Period, days
o Cet	332	S CrB	360
U Her	406	R Aql	284
S Car	150	RS Vir	354
T Her	165	R Leo	310
T Col	150	R Hya	389

3 Information on emission-line profiles

Let us compare the results of calculations with the observational data. Spectra of Mira variables suitable for analyzing the structure of emission lines were published in [4]–[7].

Gillet et al. [4] studied the Hα profile in the spectra of *o* Cet from the maximum ($\phi \sim -0.05$) to the minimum ($\phi \sim 0.60$). The Hα line has complex structure: there are blue- and red-shifted components. The blue-shifted component has 4 components during about a quarter of period (till $\phi \sim 0.23$): three absorption lines are observed against the emission profile. After the phase $\phi \sim 0.23$, the absorption lines are not separated, but the blue-shifted component has an asymmetric profile. The red-shifted component appears in the spectrum after the phase $\phi \sim 0.14$ and also has an asymmetric shape. These features of the Hα line are associated with the absorption band (γ system) of TiO.

Other papers include emission profiles of Balmer series (Hα–H12) and metal lines (MgI, MgII, FeI, FeII, SiI, MnI) for different Miras. All the profiles demonstrate an asymmetric shape. This is attributed to the effect of scattering by atoms and molecules and absorbing by molecules, mainly TiO.

Thus, emission lines are influenced by atomic and molecular absorption. In this case, the shock wave motion should occur in the layers located below the molecular one. Such a model of Mira's atmosphere is shown in Fig. 2.

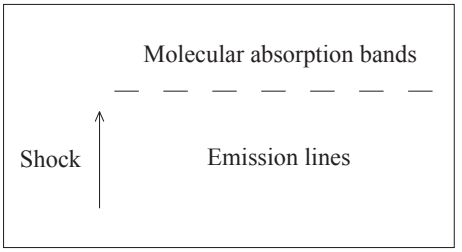

Figure 2: Model of Mira's atmosphere.

4 Conclusion

The problem of cooling of the gas behind the shock front in Mira variables was considered. The cooling time of the gas was calculated as a function of the final temperature and was compared to the typical periods of Mira stars. For most Miras, the cooling time is more than a half of the period, so the gas does not have time to cool down to the unperturbed temperature. In this case, the shock wave should propagate under the layers where molecular absorption bands are formed. This conclusion is confirmed by the available high-resolution optical spectra which show the influence of molecular bands on the emission line profiles.

Acknowledgments. This work was supported by the Russian Foundation for Basic Research (project 15-03-03302) and NSh 9670.2016.2.

References

1. *P.R. Wood*, Mem. Soc. Astron. Ital., **81**, 883, 2010.
2. *V.G. Gorbatskii*, Astron. Zh., **38**, 256, 1961.
3. *O.M. Belova, K.V. Bychkov, G.M. Rudnitskii*, Astron. Rep., **58**, 922, 2014.
4. *M.W. Fox, P.R. Wood, M.A. Dopita*, Astrophys. J., **286**, 337, 1984.
5. *He. Richter, P.R. Wood*, Astron. Astrophys., **369**, 1027, 2001.
6. *D. Gillet, E. Maurice, D. Baade*, Astron. Astrophys., **128**, 384, 1983.
7. *D. Gillet*, Astron. Astrophys., **192**, 206, 1988.

Ionization from Excited Levels as a Cause of Hydrogen Level Non-Stationary Occupation during Radiative Cooling behind a Shock Wave

O.M. Belova[1], K.V. Bychkov[1]

E-mail: *bychkov@sai.msu.ru*

It is shown that for physical conditions typical of late giant star atmospheres, the discrete level occupations are of necessity non-stationary in the case of radiative cooling of hydrogen behind a shock wave. They depend on the whole cooling process as well as on the current values of temperature and electronic density. This fact is due mainly to impact ionization from the excited discrete hydrogen levels.

1 Introduction

Hydrogen contributes significantly to the cooling rate of a shocked gas and defines emission spectrum during flares in stellar atmospheres of the stars whose spectral class is later than A. Both the cooling rate and emission spectra are determined by the relative occupations of discrete levels ν_k and the ionization state x. We assume that N_a and N_p are the atomic and ion hydrogen number densities, respectively, N_k is the number density of hydrogen on the level with the main quantum number k, and N is the total hydrogen number density. So,

$$N = N_a + N_p, \quad x = N_p/N, \quad \nu_k = N_k/N, \quad y_k = N_k/N_1. \tag{1}$$

The discrete level occupations of hydrogen and its ionization state are non-stationary as it follows from our calculations of radiative cooling of shocked gas [1]. This result calls for an explanation. Indeed, transitions between discrete levels are rather quick in stellar atmospheres, and one could expect that both functions of time $\nu_k(t)$ and $x(t)$ are nearly completely determined by the current values of electron temperature $T_e(t)$ and electron density $N_e(t)$, i.e. there is a "quasi-stationary" flow. The Lagrangian coordinate t is the time passed from the beginning of the process, i.e. since the moment when the gas element passed the shock front.

Let us consider a simple model of the two-level atom where the level occupations are controlled by electron impact and spontaneous radiative

[1] SAI MSU, Russia

V. Grinin et al. (eds) Radiation mechanisms of astrophysical objects. Yerevan: Edit Print, 2017, pp. 167–172.

transitions. The occupation y_2 of the excited level is described by the simple formula

$$y_2(t) = y_{2\infty} - (y_{2\infty} - y_{20})\, e^{-\lambda t}, \tag{2}$$

where $y_{20} = y_2(0)$ and $y_{2\infty}$ is the steady state value. The parameter λ is the inverse e-folding time which is expressed through the interaction rates as follows:

$$\lambda = A^*_{21} + Q_{21} + Q_{12}, \tag{3}$$

where Q_{ij} is the excitation ($i<j$) or deexcitation ($i>j$) rate, A^*_{21} is spontaneous emission probability. The value of $1/\lambda$ is rather large compared with the temperature evolution time scale. So, if the set of processes is restricted only by the transitions between the discrete levels, we could obtain "quasi-stationary" values of ν_k. However, electron impact ionization from the excited levels changes the time scale. It tends to establish the stationary ionization and occupation states simultaneously, and as a result the whole process is slowed down. The influence of ionization can be demonstrated by the analytical solution of a simple two-level system.

2 Analytical solution

Let us write the kinetic equations for a two-level atom taking into account transitions between discrete levels and ionization by electron impact. All the coefficients are suggested to be constant, and Q_{12} is used for impact excitation rate, R_{21} for deactivation rate (radiative and impact), and Q_{ic} for impact ionization from levels $i = 1, 2$. Recombination is not included, and hence both ν_1 and ν_2 tend to zero. The equations describing evolution of the level occupations are as follows:

$$\frac{d\nu_1}{dt} = -(Q_{12} + Q_{1c})\nu_1 + R_{21}\nu_2, \tag{4}$$

$$\frac{d\nu_2}{dt} = -(R_{21} + Q_{2c})\nu_2 + Q_{12}\nu_1. \tag{5}$$

The characteristic equation has two roots

$$\lambda_1 = \frac{s+d}{2}, \quad \lambda_2 = \frac{s-d}{2}, \tag{6}$$

where

$$s = Q_{12} + R_{21} + Q_{1c} + Q_{2c}, \tag{7}$$

$$p = Q_1\, R_{21} + Q_2\, (Q_{12} + Q_{1c}), \tag{8}$$

$$d = \sqrt{s^2 - 4p}\,. \tag{9}$$

With chosen initial conditions

$$\nu_{10} = 1, \quad \nu_{20} = 0, \tag{10}$$

the solution is

$$\nu_1 = \frac{Q_{12} + Q_{1c} - \lambda_2}{\lambda_1 - \lambda_2} e^{-\lambda_1 t} + \frac{\lambda_1 - Q_{12} - Q_{1c}}{\lambda_1 - \lambda_2} e^{-\lambda_2 t}, \tag{11}$$

$$\nu_2 = \frac{Q_{12}}{\lambda_1 - \lambda_2} \left(e^{-\lambda_2 t} - e^{-\lambda_1 t} \right). \tag{12}$$

The excitation coefficient Q_{12} and the ionization coefficient from the ground level Q_{1c} are often small compared to the deactivation rate

$$Q_{12} + Q_{1c} \ll R_{21}. \tag{13}$$

Then Eqs. (6) for λ_1 and λ_2 are simplified

$$\lambda_1 \approx s, \quad \lambda_2 \approx m/s, \tag{14}$$

where

$$m = Q_1 \left(Q_2 + R_{21} \right) + Q_{12} Q_2. \tag{15}$$

Note that the simplified value of λ_1 is near to λ from Eq. (2). They coincide if we substitute A^*_{21}+Q_{21} instead of R_{21} and omit Q_{1c} and Q_{2c} in the expression for s. The inequality $m \ll s$ follows from Eq. (13), and hence

$$\lambda_2 \ll \lambda_1. \tag{16}$$

So, ionization changes significantly the evolution of excited level occupation in comparison with Eq. (2). Now the whole process develops in two stages. Occupation changes quickly at the first stage on the "short" time scale which is defined by deactivation. The final value of occupation establishes on the "long" time scale $1/\lambda_2$ in which ionization from the excited level plays the important role.

Equation (12) contains all these features. The occupation ν_2 quickly grows on the time scale $1/\lambda_1$ due to diminishing the negative term $e^{-\lambda_1 t}$ in Eq. (12), reaches a maximum at the moment t_m such as

$$t_m = \frac{\ln(\lambda_1/\lambda_2)}{\lambda_1 - \lambda_2}, \tag{17}$$

and drops exponentially after the maximum on the "long" scale $1/\lambda_2$. All these features are drawn on Fig. 1.

3 Radiative cooling behind a shock front

Here we consider numerical results for a multilevel system to which the analytical approach is not applicable. Let the unperturbed equilibrium gas pass through the shock front at the velocity 50 km s^{-1}, with the temperature T_0 and number density N_0 being typical of Mira Ceti atmospheres: $T_0 = 3000$ K and $N_0 = 10^{12}$ cm^{-3}.

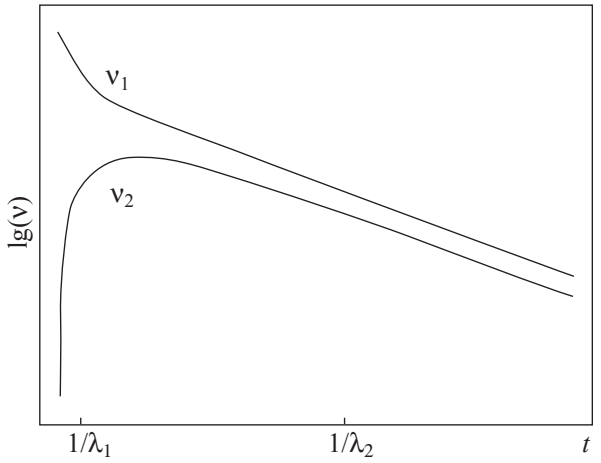

Figure 1: Analytical solution for a two-level system.

We have written the differential equations for the problem in [1]. Here we rewrite the equation describing the occupations of excited hydrogen levels as follows:

$$\begin{aligned}\frac{d\nu_k}{dt} = &-\left[q_{kc}N_e + \sum_{k>i}\left(A^*_{ki} + q_{ki}N_e\right) + \sum_{k<i} q_{ki}N_e\right]\nu_k \\ &+ \left(r_k + \gamma_k N_e\right)N_e x + \sum_{i>k}\left(A^*_{ik} + q_{ik}N_e\right)\nu_i + N_e\sum_{k<i} q_{ik}\nu_i,\end{aligned} \tag{18}$$

where q_{ki} are the coefficients of electron impact transitions between discrete levels k and i for excitation ($k<i$) and deactivation ($k>i$), r_k and γ_k are for radiative and triple recombination on the level k, respectively, x is the proton relative concentration, A^*_{ij} designs the spontaneous radiative transition probability taking into account the line scattering

$$A^*_{ij} = A_{ij}/\zeta_{ij}, \tag{19}$$

with ζ_{ij} being the scattering number before a quantum leaves the cooling gas. For ν_k and x, we have

$$\sum_{k=1}^{K}\nu_k + x = 1. \tag{20}$$

The upper limit K is the main quantum number of the highest level which is realized under the given conditions. We obtain $K = 25$ using Inglis–Teller equation.

Some results of calculations of non-stationary cooling of the shocked gas are drawn on Fig. 2 as functions of time $T_e(t)$ and $\nu_5(t)$. Note that T_e can rise when the gas cools behind the shock. Time t on the bottom axis is measured in seconds. A fragment of gas evolution during about 0.007 s is selected at about 3 seconds

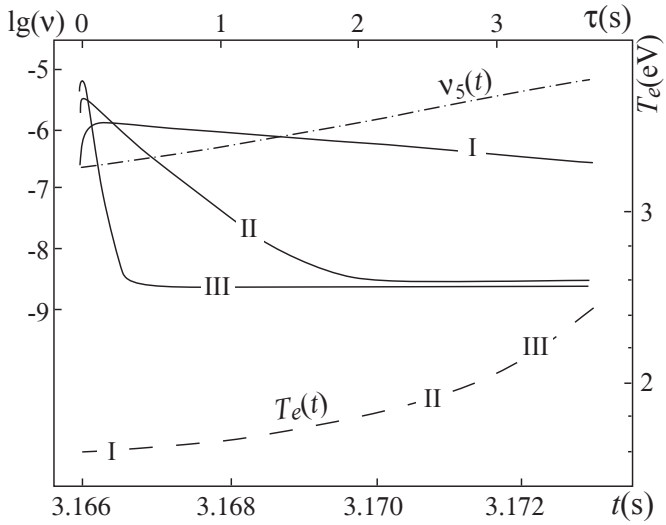

Figure 2: Electron temperature T_e (dashed) and non-stationary occupation ν_5 (dash-dot) evolution of the shocked gas behind a shock: the lower horizontal axis is the time (in sec) elapsed from the shock passed, the right vertical axis is T_e in eV, the left one is occupation in logarithmic scale, the upper horizontal axis is τ (in sec), solid lines I, II and III describe evolution $\nu_5^{(\mathrm{qs})}(\tau)$ as a solution of Eq. (18) for the temperature values I, II, and III.

after passing the shock. The lower dashed line describes the function $T_e(t)$, while $\nu_5(t)$ is drawn by the upper dash-dot line in the logarithmic scale. The right vertical axis is the electron temperature measured in electron-volts, and the left one is decimal logarithm of the occupation ν_5.

Three solid curves (I, II, and III) are the solutions of the system (17) for a given value of $T_e(t)$. These curves show "quasi-stationary" functions $\nu_5^{(\mathrm{qs})}(T_e(t), \tau)$ with the initial conditions $\nu_k(\tau = 0) = \nu_k(t)$, where $T_e(t)$ is a parameter and the independent variable τ is the time elapsed from the moment t. The values of τ are given on the upper horizontal axis. Three values of the parameter $T_e(t)$, chosen and noted by I, II, and III on the lower dashed curve, are as follows: $T_e^{(\mathrm{I})} = 1.6\,\mathrm{eV}$, $T_e^{(\mathrm{II})} = 1.9\,\mathrm{eV}$, $T_e^{(\mathrm{III})} = 2.2\,\mathrm{eV}$.

The functions $\nu_5^{(\mathrm{qs})}(T_e(t), \tau)$ make sure that $\nu_5(t)$ corresponds to a properly non-stationary process. All solid curves are similar to the analytical solution: a fast rise from the initial value followed by slow transition to a maximum and after that to a constant value $\nu_\infty(T_e(t))$.

Comparing the three solid curves with the lower dashed line, we see that the time for any $\nu_5^{(\mathrm{qs})}(T_e(t), \tau)$ to reach its steady state value $\nu_\infty(T_e(t))$ is longer than the time needed for T_e to grow up. This is the first evidence for non-stationary cooling process. And comparing the solid lines with the dash-dot one, we obtain the second evidence. The numerical difference between $\nu_5(t)$ and the corresponding steady state values are very large and can reach orders of magnitude (one for the curve I, and 3–4 orders for II and III).

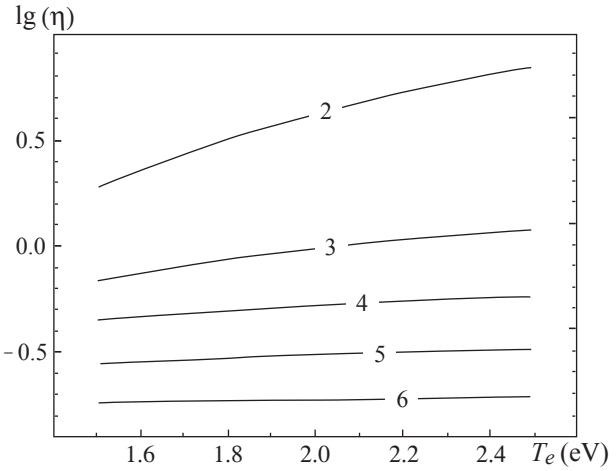

Figure 3: Ratio $q_{kc}/q_{k,k-1}$ vs T_e.

4 Ionization and deexcitation rates

We see that ionization from the excited states is an important factor which determines non-stationary character of shocked gas cooling. Its efficiency depends on the ratio

$$\eta_k = \frac{q_{kc}}{q_{k,k-1}}. \tag{21}$$

The greater η_k, the more effective the influence of ionization is. This relation is drawn on Fig. 3 for the first five excited levels of hydrogen atom as a function of the electron temperature T_e. The temperature range $1.5\,\text{eV} < T_e < 2.5\,\text{eV}$ is typical of a flow behind the front in a cold star atmosphere. The electron impact coefficients q_{kc} and $q_{k,k-1}$ were calculated from the Johnson formulas [2]. As follows from Fig. 3, ionization prevails in the case of the second level ($n = 2$), and the value of η_k remains sufficient up to $n = 6$.

So, electron impact ionization from the excited hydrogen levels ($n \leqslant 6$) is the cause of non-stationary cooling of the shocked gas.

Acknowledgments. This work was supported by the Russian Foundation for Basic Research (project 15-03-03302) and NSh 9670.2016.2.

References

1. *O.M. Belova, K.V. Bychkov, E.S. Morchenko, B.A. Nizamov*, Astron. Rep., **58**, 650, 2014.

2. *L.C. Johnson*, Astrophys. J., **174**, 227, 1972.

Variability of [OI] 6300 Å and [OI] 6363 Å Emission in HD 200775

A.P. Bisyarina[1], A.M. Sobolev[1], S.Yu. Gorda[1]

E-mail: *bisyarina_nastya@mail.ru*

Variability of the emission in [OI] 6300 Å and [OI] 6363 Å lines from Herbig Be binary star HD 200775 is reported for the first time. The system has the common disk observed in IR-emission and an accretion disk around the primary component which is probably formed due to accretion of the common disk material. The orbital period of the binary system is about 3.7 years. The [OI] line profiles from the newly-obtained spectral data and the archival ones, derived during the last 20 years or so, were examined. The major part of the data was obtained with the 1.2 m telescope at Kourovka Astron. Obs., Ural Federal Univ. Similarity of the line profiles obtained at the same orbital phases in different epochs and with different instruments was found. So, the variability of [OI] line emission is related to the binarity of the system.

1 Context

HD 200775 (V380 Cep, MWC 361) is a Herbig Be binary star with the orbital period of about 3.7 years. Mid-infrared interferometric observations of the binary orbit [1] and a number of spectroscopic works [1]–[7] were performed to estimate the orbital parameters. Periodic maximum activity phases related to the binarity were recognized in the spectra of the star [2]. This activity is characterized by an increase in the equivalent width of the Hα line formed in the material associated with the primary component.

The authors of [8, 9] observed diffuse IR-emission from the system and suggested that it was originated from the common circumbinary disk. In [8, 6] the presence of an accretion disk close to the primary (more massive) component of the system was pointed out. This disk is probably formed by the material accretion from the common disk onto the primary component. There is no evidence of any disk material near the secondary component.

Forbidden OI line emission in Herbig Ae/Be and T Tauri stars is often observed as a blue-shifted high-velocity component originated from an outflow and a low-velocity component (e.g., [10, 11]). The origin of the latter is unclear, it might be formed on the disk surface or in the slow disk wind. A review of [OI] line emission in 49 Herbig Ae/Be stars, including HD 200775, has been performed

[1] Kourovka Astronomical Observatory of the Ural Federal University, Russia

V. Grinin et al. (eds) Radiation mechanisms of astrophysical objects. Yerevan: Edit Print, 2017, pp. 173–176.

in [12]. However, variability of [OI] lines in spectra of this binary star is for the first time reported in this paper.

2 Observational data

Our data were obtained from May 2, 2012 to April 2, 2015 using a high-resolution spectrograph mounted at the 1.2 m telescope of the Kourovka Astronomical Observatory of the Ural Federal University. The operating wavelength range was 4000–7800 Å, an effective exposure was 1 hour (each image is a median average of three 20-min CCD images). One spectrum was obtained in 2013 with NES spectrograph of the Special Astrophysical Observatory of Russian Academy of Science (SAO RAS). We also used archival spectral data obtained from 1994 till 2011 with ELODIE and SOPHIE spectrometers of Observatoire de Haute-Provence, the ESPaDOnS spectrometer from Canadian-France Hawaii Telescope, as well as NES data from the SAO RAS archive.

3 Results

In the spectra of HD 200775 we see a broad low-velocity component of the [OI] line (Fig. 1). There is no evidence of the high-velocity one. Unfortunately, the wavelength region around the [OI] 6300 Å line includes a number of telluric lines and narrow atmospheric oxygen emission. But these lines only arise at well-defined wavelengths, while at the other wavelengths variations in stellar emission still can be seen. The most significant changes (except for atmospheric components) occur near the values of −65, 30 and 55 km/s.

We have also considered emission in the [OI] 6363 Å line (Fig. 1, right panel). This line is about twice less intensive than the [OI] 6300 Å one. So, the signal-to-noise ratio of many of our spectra did not allow us to examine the line. On the other hand, the spectral region near this line is free from telluric lines. Thus,

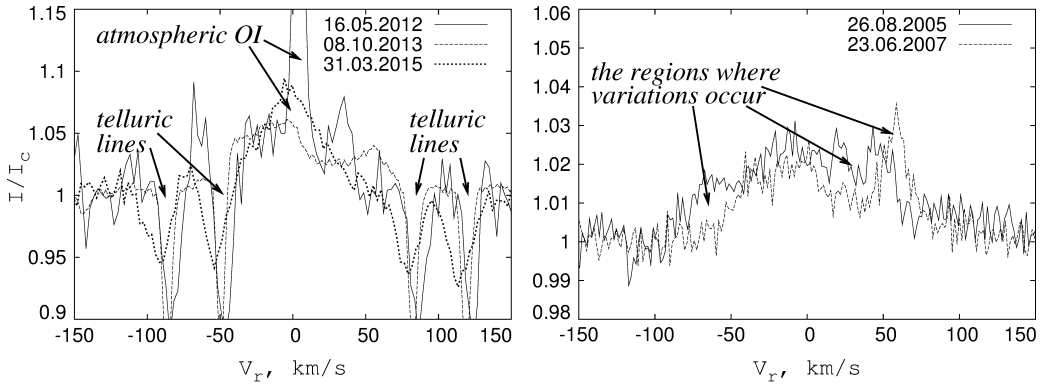

Figure 1: [OI] 6300 Å (left panel) and [OI] 6363 Å (right panel) lines profiles in HD 200775 at different epochs.

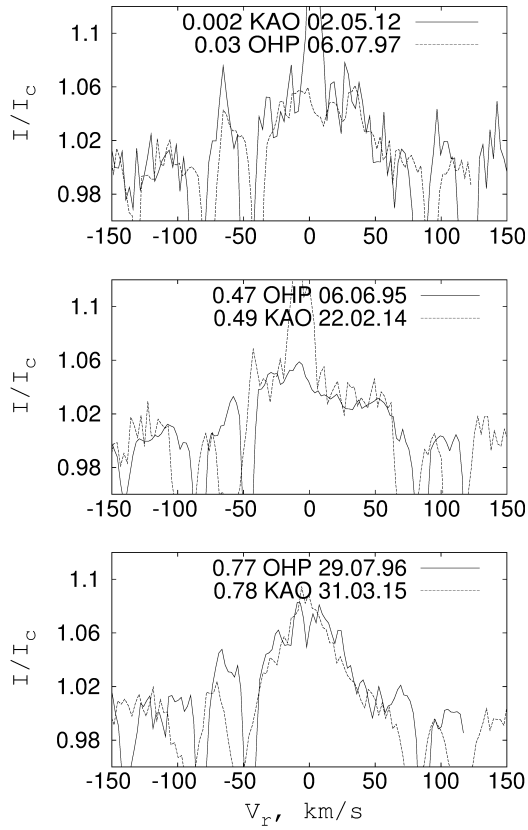

Figure 2: Comparison of [OI] 6300 Å line profiles. The line profiles are different on different panels but similar inside the panels for close orbital phases.

we can verify our results obtained for the [OI] 6300 Å line. We found that the variations in this line profile occur nearly at the same velocity values as for the [OI] 6300 Å line.

Estimating the orbital period, made on the basis of the data covering 20 years in our previous work [7], allowed us to use very accurate values of orbital phases. As a result, we noticed that the [OI] 6300 Å line profiles in the spectra, obtained with different instruments and at different observational epochs but at the same orbital phases, are similar (Fig. 2). This means that the variability of [OI] emission is related to the binarity of the system.

4 Summary

Variability of the [OI] emission in the spectra of HD 200775 is reported for the first time. Significant changes of the lines profiles appear in three components – near −65, 30 and 55 km/s for both [OI] 6300 Å and [OI] 6363 Å lines. They were examined on the basis of 20 years data including new and archival high-resolution

spectra. We found that the line profiles in spectra obtained in different epochs but at the same orbital phases are similar. Thus, we showed that the variations are related to the binarity of the system. The mechanism of the [OI] line variability in HD 200775 is still an open question.

Acknowledgments. The work was supported by the Russian Science Foundation, grant No. 15-12-10017.

References

1. *J.D. Monnier, J.-P. Berger, R. Millan-Gabe et al.*, Astrophys. J., **647**, 444, 2006.
2. *A.S. Miroshnichenko, C.L. Mulliss, K.S. Bjorkman et al.*, Publ. Astron. Soc. Pacif., **110**, 883, 1998.
3. *N.Z. Ismailov*, Astron. Rep., **47**, 206, 2003.
4. *M.A. Pogodin, A.S. Miroshnichenko, A.E. Tarasov et al.*, Astron. Astrophys., **417**, 715, 2004.
5. *E. Alecian, C. Catala, G.A. Wade et al.*, Mon. Not. Roy. Astron. Soc., **385**, 391, 2008.
6. *M. Benisty, K. Perraut, D. Mourard et al.*, Astron. Astrophys., **555**, A113, 2013.
7. *A.P. Bisyarina, A.M. Sobolev, S.Yu. Gorda*, Astron. Bull., **70**, 243, 2015.
8. *J.D. Monnier, P.G. Tuthill, M. Ireland et al.*, Astrophys. J., **700**, 491, 2009.
9. *Y.Z. Okamoto, H. Kataza, M. Honda et al.*, Astrophys. J., **706**, 665, 2009.
10. *J. Kwan, E. Tademaru*, Astrophys. J. Lett., **332**, L41, 1988.
11. *G.A. Hirth, R. Mundt, J. Solf*, Astron. Astrophys., **285**, 929, 1994.
12. *B. Acke, M.E. van den Ancker, C.P. Dullemond*, Astron. Astrophys., **436**, 209, 2005.

Non-Stationary Processes in Atmospheres of Early-Type Stars: Influence on Forbidden to Intercombination Ratio f/i

V.V. Dushin[1], A.F. Kholtygin[1]

E-mail: *v.dushin@spbu.ru*

We report the results of non-stationary level population modeling of highly ionized atoms in the atmospheres of early-type stars. We studied the influence of the fast heating and cooling processes on the ratio of forbidden to intercombination line intensities $R = f/i$ for He-like ions (CV, NVI, OVII, etc.) in X-ray spectra.

It is shown that the instantaneous ratio $R_{\rm m}$ for the non-stationary plasma varies by up to 4 orders of magnitude on short time scales (milliseconds) in comparison with the value for the stationary plasma. In the same time the value of $R_{\rm a}$ averaged on long time scales (hours and minutes) varies by up to 20%. Using the ratio R calculated in the case the stationary plasma for the non-stationary plasma can lead to an overestimation of the plasma electron density by up to 1–2 orders of magnitude.

1 Introduction

The density diagnostics of the X-ray emitted plasma of the early-type stars based on the forbidden-to-intercombination line ratio R showed that this ratio is much lower than that predicted for the homogeneous non-stationary plasma (e.g., [1]). This could be explained as follows:

- The stellar UV-radiation excites electrons in the upper level 1s2s ^{3}S$_1$ of the forbidden line f and populates the upper level 1s2p ^{3}P$_{1,2}$ of the intercombination line i, which weakens the line f and strengthens the line i.
- Bound electrons are excited from the upper level of the line f by free electrons, which decreases the line f. This happens if the X-ray radiation originates from the dense clouds in stellar atmospheres.

In this paper we outline an alternative hypothesis.

2 Processes in non-stationary plasma

We suppose that the level population in the stellar atmospheres can become non-stationary.

[1] St. Petersburg State University, Russia

V. Grinin et al. (eds) Radiation mechanisms of astrophysical objects. Yerevan: Edit Print, 2017, pp. 177–180.

Non-stationarity could be caused by collisions of the plasma flows in the region on the stellar magnetic equator or by nano-flares in the stellar atmosphere similarly to the solar ones.

The non-stationary level population can be described by the following equation:

$$\frac{dx_i}{dt} = n_e \sum_{j\neq i}^{N} x_j q_{ji} + \sum_{j=i+1}^{N} x_j A_{ji} - x_i \left(\sum_{j=1}^{i-1} A_{ij} + n_e \sum_{j\neq i}^{N} q_{ij} \right). \qquad (1)$$

Here x_i is the relative population of the i-th level, N is the number of levels considered, n_e is the electron density, q_{ji} is the excitation/deexcitation rate from the level j to the level i, A_{ij} is the corresponding Einstein A-value. In our models we used $N = 50$ levels, which was enough for a precise modeling.

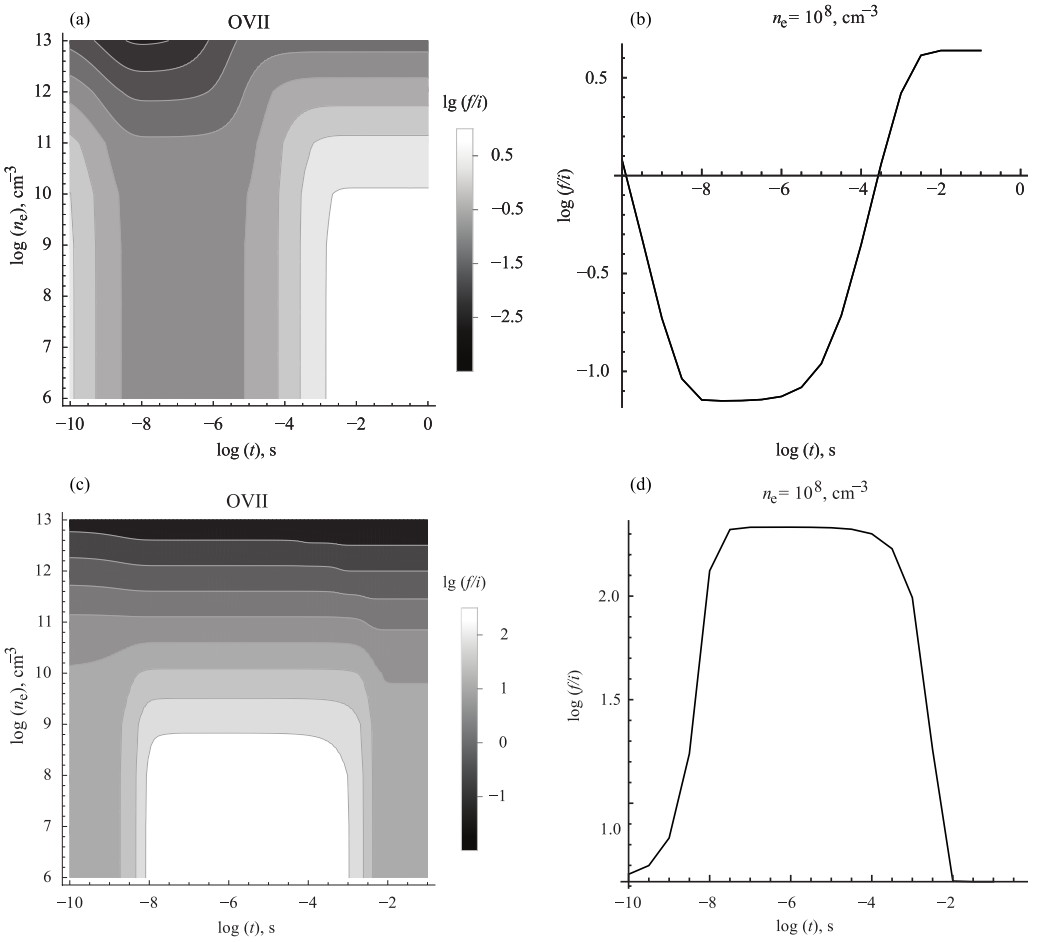

Figure 1: *Panel a*: Dependence of the ratio R_m on time and electron number density for OVII in the model for rapidly heated plasma. At $t = 0$, the plasma instantaneously heats from $T_\mathrm{e} = 10^6$ K to $T_\mathrm{e} = 10^7$ K, after the heating the temperature remains constant. *Panel b*: the same but for $n_\mathrm{e} = 10^8$ cm^{-3}. *Panels c, d*: the same as the upper row, but for rapid cooling from $T_\mathrm{e} = 10^7$ K to $T_\mathrm{e} = 10^6$ K.

Table 1: The parameters of the models: T_c is the plasma temperature in the "cool" state, t_c is the time of cooling, R_c is the stationary line ratio for T_c, the similar parameters for plasma heating are indexed with "h"

Model	T_c, K	t_c, s	T_h, K	t_h, s	R_c	R_h
A	5×10^5	3×10^{-2}	10^8	10^{-5}	9×10^{-3}	4×10^{-2}
B	5×10^5	10^{-5}	10^8	10^{-5}	3	2.75
C	5×10^5	3×10^{-2}	10^8	10^{-5}	9×10^{-4}	4×10^{-3}
D	5×10^5	10^{-3}	10^7	3×10^{-3}	7.5×10^{-1}	1.34
E	5×10^5	3×10^{-2}	10^8	10^{-5}	4.44	2.94
F	5×10^5	3×10^{-2}	10^8	10^{-5}	4.26	2.93
G	5×10^5	3×10^{-3}	10^7	2×10^{-3}	1.78	2.94
H	5×10^5	10^1	10^7	10^{-1}	5.61	8.25
I	5×10^5	10^{-3}	10^8	10^{-5}	2.98	2.75

Table 2: The results of the modeling, where n_e is the input model electron density, R_a is the averaged line ratio f/i, $\bar{n}_e$ is the electron density derived from R_a, when supposing the stationarity of the plasma

Model	Ion	n_e, cm^{-3}	R_a	$\bar{n}_e$, cm^{-3}	$\lg(n_e/\bar{n}_e)$
A	OVII	10^{13}	10^{-2}	8×10^{12}	0.1
B	OVII	10^{10}	–	–	–
C	OVII	10^{14}	2×10^{-3}	5×10^{13}	0.3
D	OVII	10^{11}	1.18	5×10^{10}	0.3
E	OVII	10^8	3.48	6×10^9	−1.8
F	OVII	10^9	3.35	6×10^9	−0.8
G	NVI	10^{10}	2.12	8×10^9	0.1
H	CV	10^9	6.24	8×10^8	0.1
I	OVII	10^{10}	2.93	–	–

3 Modeling and discussion

We used both a modified APEC [2] code and an additional code written in Mathematica to solve equation (1). We calculated the ratio R for various conditions of the plasma heating and cooling.

It can be seen that in the case of fast heating of low density plasma the ratio R decreases dramatically for a short time (see the "valley" in Fig. 1b). A similar behavior holds for the case of cooling: we can see the dramatic increase of the ratio R in the first second (the "plateau" in Fig. 1d). For stationary case, R holds in the interval 1–10.

Unfortunately, such fast processes could not be observed, since the exposure time of X-ray satellites is of the order of 10^4 s and above. That is why we studied the influence of non-stationary processes on the average f/i-ratio (R_a). The model

parameters are presented in Table 1, results of the modeling are summarized in Table 2. It can be seen that the models E and F show significant difference between $R_{\rm a}$ and $R_{\rm c}$ and $R_{\rm h}$. It means that using the ratios R for the stationary plasma leads to the overestimation of the $n_{\rm e}$ derived from observations.

The parameters of heating and cooling which are given in the captions to Fig. 1 are typical of solar nano-flares or similar events in stellar atmospheres.

4 Conclusion

We showed that non-stationary processes could affect on the instantaneous forbidden-to-intercombination ratio $R_{\rm m}$ which increases (for fast cooling) or decreases (for fast heating) by up to 1–3 orders of magnitude during the first second. These processes could also strongly change the averaged ratio $R_{\rm a}$ by decreasing it by up to 20%. In this case one can incorrectly estimate the plasma electron density (errors can be of up to 2 orders of magnitude), when supposing the stationary level population in the plasma.

Acknowledgments. Some of our results were previously published in [3]. The authors acknowledge St. Petersburg State University for research grant 6.38.18.2014.

References

1. *W.L. Waldron, J.P. Cassinelli*, Astrophys. J. Lett., **548**, L45, 2001.
2. *R.K. Smith, N.S. Brickhouse, D.A. Liedahl, J.C. Raymond*, Astrophys. J. Lett., **556**, L91, 2001.
3. *V.V. Dushin, A.F. Kholtygin*, Astron. Rep., **59**, 709, 2015.

Properties of Emission of Coronal Holes on the Sun according to Observations in Radio Range

O.A. Golubchina[1]

E-mail: *golubchina_olga@mail.ru*

This paper is a brief review devoted to the investigation of coronal holes (CHs) on the Sun. The special attention is paid to CHs research in the millimeter and centimeter wavelength ranges. Observations in the millimeter range and from satellites in ultraviolet and soft X-ray ranges, as well as observations of Solar eclipse on March 29, 2006 at centimeter waves with the radio telescope RATAN-600 have yielded new data for understanding of the physical nature of coronal holes on the Sun.

1 Statement of the problem

Coronal holes (CHs) are areas of low temperature and density at the surface of the Sun. These areas are unipolar, with an open configuration of the magnetic field. Polar coronal holes are always visible on the poles of the Sun during the periods of a minimum solar activity as the rotary directed dipole component of the magnetic field prevails at this phase. During the periods of an increased solar activity, CH can exist at any latitude of the Sun. A CH is formed by random convective motions of the open magnetic field lines in the photosphere and reconnection of lines of the open magnetic field with the closed coronal lines. Lines of the open magnetic field in CH expand super-radially. Carrying out a stream of the charged particles from CH and low rate of emergence of new magnetic flux [1] can explain low density of particles in CH on the Sun. For the first time, observations of a CH above the solar limb were performed by Waldmeier [2] in a green line (5303 Å) with coronograph of the Zurich observatory. CHs above the limb were observed as the least intensive and long-living formations. A progress in studying CHs started in 1973–1974 with spacecraft observations in the ultra-violet (EUV) and soft X-ray (3–60 Å) ranges. The CH areas are seen in EUV and soft X-ray ranges as very dark places on the Sun because of low density and temperature in CH. CHs are identified with the areas of increased brightness in the line HeI 10830 Å as they possess the lowest absorption in the line [3, 4]. Therefore, radiation in this line often serves as an indicator of a CH. CHs represent a huge interest not only as a phenomenon in the physics of the Sun, but also as the source of quasi-stationary high-speed streams of solar plasma – the solar wind which extends to

[1] St. Petersburg Branch of Special Astrophysical Observatory, Russia

V. Grinin et al. (eds) Radiation mechanisms of astrophysical objects. Yerevan: Edit Print, 2017, pp. 181–185.

the limits of the Solar System. The high-speed solar wind ($V = 700 - 800$ km/s) is the source of recurrent geomagnetic disturbances. By means of observations of solar eclipses in white light and from satellites in the ultra-violet (EUV) and X-ray ranges, a precise correlation between the high-speed solar wind and polar CHs, large low-latitude CHs was established [3, 5]. Magnitosphere protects the Earth from dangerous influence of the solar wind. It is obvious that the study of CHs is very important for human survival not only on the Earth, but also in space.

2 Observations of polar CHs at mm-wavelengths

Large coronal holes on the Sun emerge within approximately 7 years near a minimum of solar activity and are absent within 1–2 years near to a maximum [6]. Observations of polar CHs were first made in CRAO at the wavelengths of 8.2 and 13.5 mm with the radio telescope RT-22 (1974–1977) and in Australia (CSIRO) at 3.5 mm with the 4 m paraboloid (1977) [7]. Polar CHs are investigated at the solar latitude φ of up to 80°. Observations are impossible in the radio range if $\varphi > 80°$ as there is a steep temperature gradient near to the limb of the Sun. It was shown that the polar CHs are areas of the increased intensity of radio emission at mm-wavelengths. (If T is the excess of temperature over the temperature of the quiet Sun, $T = 1500$ K at $\lambda = 8.2$ mm, and $T = 2200$ K at $\lambda = 13.5$ mm.) Similar observations made in Japan on a radio telescope with the diameter $d = 45$ m have shown a considerably smaller temperature excess of $T = (240–560)$ K at $\lambda = 8.3$ mm. The temperature excess was not revealed in a polar area of the Sun at the wavelength of 3.1 mm [9]. More careful researches of polar CHs were performed in Finland (Metsähovi Radio Observatory) by means of a radio telescope of 14 m in diameter at 3.4, 3.5, and 8 mm with attraction of observations in the ultraviolet (EUV SOHO/EIT) and soft-X-ray (0.25–4) keV ranges and in white light. The polar areas at up to 70° of the solar latitude were studied with this radio telescope. Observations of polar CHs in Metsähovi Radio Observatory revealed that at the frequency of 87 GHz ($\lambda = 3.5$ mm) polar areas can demonstrate enhanced brightness as well as depressions. Sometimes a polar CH is visible as a radio depression with local brightening inside it [10, 11]. Comparisons of the obtained radio maps with the images of the Sun in the EUV and soft X-ray ranges allowed establishing the fact that the brightness increase in polar area at the mm-wavelengths correlates with polar plumes, diffuse EUV emission and bright points inside the CH. An increase of intensity of the radio emission in the mm-range coincides with the dark surfaces on images in the EUV and soft X-ray ranges (SOHO/EIT). However, from these observations it was impossible to determine, whether the increase of intensity of radiation from polar CH at the mm wavelengths is due to a thermal or non-thermal mechanism. Note that inside of the areas of an increased radio emission of polar CHs, there are medium and strong magnetic fields.

3 Emission of polar and low-latitude CHs in cm-range

CHs are areas of low radio emission at cm-wavelengths and are always identified with the most dark sites (except for floccules) on the surface of the Sun in EUV and soft X-ray emission. A depression of intensity of radio emission in CHs was revealed by 19 observations (1975–1987) on various radio telescopes in the range 1.38–21.4 cm. The average contrast of the CH radiation in relation to the level of the quiet Sun is 0.9. Radiation in the helium line HeI 10830 Å is weakly absorbed in CHs. Therefore, at cm-wavelengths CHs correlate with the bright areas on the Sun observed in this helium line. The intensity of magnetic fields in CHs is equal to 1–3 G. Observations of CH above the North Pole of the Sun on March 29, 2006 at cm-wavelengths (1.03, 1.38, 2.7, 6.2, 13, 30.7 cm) have been made on the northeast sector of the RATAN-600 by the method of "relay race" [12] during the maximum phase (0.998) of the solar eclipse. A center of the directional pattern (DP) was shifted at $h = +15$ arc min to investigate the radio emission above the North Pole of the Sun. The observation of the solar eclipse at RATAN-600 allowed us to determine physical characteristics of the CH above the North Pole of the Sun at the minimum of solar activity. The distribution of brightness temperature and electron density was reliably determined in the Northern polar CH on the Sun at the distances from 1 to 2 solar radii from the observations at $\lambda = 1.03$, 1.38, 2.7, 6.2, 6.3, 13, 30.7 cm and and their computer simulation [13]. As a first approximation, the electron density can be calculated at the wavelengths of 1.03 and 1.38 cm. It was established that the distribution of the electron density from the solar limb up to $2R_c$, where R_c is the radius of the optical disk of the Sun, is close to the distribution obtained in white light at the minimum of solar activity [13, 18]. As a consequence, a question arise, whether the physical characteristics of a large low-latitude CH and a polar CH are identical. Results of observations of the quiet Sun and low-latitude CHs on the background of the quiet Sun which were earlier obtained with RATAN-600 for a minimum of solar activity [8] have been utilized to answer this question. The coincidence of brightness temperatures of the quiet Sun with brightness temperatures found from the observations of the polar CH during the solar eclipse at $\lambda = 1.03$, 1.38, 2.7 cm testifies that a CH above the North Pole of the Sun is not visible at such short wavelengths. Low-latitude coronal holes on the background of the quiet Sun are not visible at short wavelengths either. Sharply dropping brightness temperature is revealed from the observational data for the solar eclipse at $\lambda = 6.2$, 13, and 30.7 cm over the range of distances (1.005–1.03) R_c, which testifies to a detection of a CH at these wavelengths. Investigation of low-latitude CHs also confirmed the detection of a CH if the wavelengths were greater than 4 cm. The simulated brightness temperatures of the low-latitude CHs were compared with the temperatures at the nearest points to the limb of the Sun which were obtained from the observations of the solar eclipse. It revealed their coincidence on close

wavelengths. The coincidence of the above-mentioned properties of cm-radio emission of the low-latitude CHs and CHs above the North Pole of the Sun testifies to the same nature of large CHs regardless of the place of their location on the Sun.

4 Radio emission of CHs in meter and decameter ranges

CH researches were conducted on interferometers, multi-element radio telescopes and radio heliographs in the meter and decameter ranges ($\lambda = 73-970$ cm) during 1974–1989. In the meter range a lowered intensity of radio emission of CHs was detected [14]. These CHs are well correlated with the dark areas on the EUV-images of the Sun. The temperature of CHs was found to be $T = 0.8 \times 10^6$ K, and the average temperature outside of CHs was $T = 1.0 \times 10^6$ K, i.e. the lower intensity of the radio emission of CHs has been detected [14, 15, 16] according to the observations of CHs in the meter range at 3.75 m (80 MHz) and 1.88 m (160 MHz) in 1972. The study of CHs showed both the increased and lowered intensities of radio mission in the decameter range. This is connected with the uncertainty of identification of the observed areas on the Sun because of the influence of strong radio refraction [17].

5 Results

Summarizing, it is possible to briefly formulate the basic characteristics of coronal holes in various wavelength ranges.

CHs in the radio range correlate with the most dark sites on the surface of the Sun observed in the ultra-violet and X-ray (3–60 Å) ranges and with areas of the increased brightness in the line HeI 10830 Å. Polar coronal holes at mm-wavelengths can show both a brightness increase and a depression. In the cm-range of wavelengths CHs are observed as areas of a reduced intensity, starting from the wavelengths of about 4–6 cm. CHs on the surface of the Sun are not visible at short wavelengths of the cm-range. At cm-wavelengths the distribution of electron density in the CHs above the pole of the Sun at the distances from the solar limb up to $2R_c$ is close to that obtained in white light during the epoch of a minimum of solar activity. The temperature characteristics of big CHs in the cm-range do not depend on their location on the Sun. CHs are the areas of a lower intensity in the meter- and dm-ranges. CHs show both increased and lowered intensities of radio emission at decameter wavelengths. This is connected with the uncertainty of identification of the observed area on the Sun because of strong radio refraction.

References

1. *V.I. Abramenko, L.A. Fisk, V.B. Yurchyshyn*, Astrophys. J. Lett., **641**, L65, 2006.
2. *M. Waldmeier*, Z. Astrophys., **38**, 219, 1956.
3. *S.R. Cranmer*, Living Rev. Solar Phys., **6**, 3, 2009.
4. *H. Zirin*, The Solar Atmosphere. Waltham: Blaisdell Publ. Co., 1966.
5. *Y.-M. Wang*, Astrophys. J., **660**, 882, 2007.
6. *K.L. Harvey, F. Recely*, Sol. Phys., **211**, 31, 2002.
7. *A.N. Babin, S.I. Gopasuk, V.A. Efanov et al.*, Izv. Krym. Astrofiz. Obs., **55**, 3, 1976.
8. *V.N. Borovik, M.S. Kurbanov, M.A. Livshits, B.I. Ryabov*, Sov. Astron., **34**, 522, 1990.
9. *T. Kosugi, M. Ishiguro, K. Shibasaki*, Publ. Astron. Soc. Japan, **38**, 1, 1986.
10. *S. Pohjolainen, F. Portier-Fozzani, D. Ragaigne*, Astron. Astrophys. Suppl., **143**, 227, 2000.
11. *A. Riehokainen, S. Urpo, E. Valtaoja et al.*, Astron. Astrophys., **366**, 676, 2001.
12. *O.A. Golubchina, G.S. Golubchin*, Astrofiz. Issled. (Izv. Spec. Astrofiz. Obs.), **14**, 125, 1981.
13. *O.A. Golubchina, A.N. Korzhavin*, Geomag. Aeron., **54**, 1039, 2014.
14. *G.A. Dulk, K.V. Sheridan, S.F. Smerd, G.L. Withbroe*, Sol. Phys., **52**, 349, 1977.
15. *Z. Wang, E.J. Schmahl, M.R. Kundu*, Sol. Phys., **111**, 419, 1987.
16. *K. Shibasaki, C.E. Alissandrakis, S. Pohjolainen*, Sol. Phys., **273**, 309, 2011.
17. *P. Lantos, C.E. Alissandrakis, T. Gergely, M.R. Kundu*, Sol. Phys., **112**, 325, 1987.
18. *V.V. Zheleznyakov*, Radioemission of the Sun and Planets. Moscow: Nauka, 1964 (in Russian).

Magnetic Fields in Massive Stars: New Insights

S. Hubrig[1], M. Schöller[2], A.F. Kholtygin[3], L.M. Oskinova[4], I. Ilyin[1]

E-mail: *shubrig@aip.de*

Substantial progress has been achieved over the last decade in studies of stellar magnetism due to the improvement of magnetic field measurement methods. We review recent results on the magnetic field characteristics of early B- and O-type stars obtained by various teams using different measurement techniques.

1 Massive O-type stars with different spectral designations and kinematic characteristics

During the last years, a number of magnetic studies focused on the detection of magnetic fields in massive early B- and O-type stars. The characterization of magnetic fields in massive stars is indispensable to understand the conditions controlling the presence of those fields and their implications for the stellar physical parameters and evolution. Accurate studies of the age, environment, and kinematic characteristics of magnetic stars are also promising to give us new insights into the origin of the magnetic fields. While a number of early B-type stars were detected as magnetic already several decades back, the first magnetic field detection in an O-type star was achieved only 13 years ago, even though the existence of magnetic O-type stars had been suspected for a long time. Indirect observational evidences for the presence of magnetic fields were the many unexplained phenomena observed in massive stars, which are thought to be related to magnetic fields, like cyclical wind variability, Hα emission variation, chemical peculiarity, narrow X-ray emission lines, and non-thermal radio/X-ray emission.

However, direct measurements of the magnetic field strength in massive stars, using spectropolarimetry to determine the Zeeman splitting of the spectral lines, are difficult since only a few spectral lines are available for these measurements. In addition, these spectral lines are usually strongly broadened by rapid rotation and macroturbulence and frequently appear in emission or display P Cyg profiles. In high-resolution spectropolarimetric observations, broad spectral lines frequently extend over adjacent orders, so that it is necessary to adopt order

[1] Leibniz-Institut für Astrophysik Potsdam (AIP), Germany
[2] European Southern Observatory, Germany
[3] Astronomical Institute, St. Petersburg State University, Russia
[4] Institut für Physik und Astronomie, Universität Potsdam, Germany

V. Grinin et al. (eds) Radiation mechanisms of astrophysical objects. Yerevan: Edit Print, 2017, pp. 187–196.

shapes to get the best continuum normalization. Furthermore, most of the existing high-resolution spectropolarimeters are operating at smaller telescopes and cannot deliver the necessary high signal-to-noise (SNR) observations for a majority of the massive stars. Especially, O-type stars and Wolf-Rayet (WR) stars are rather faint. Indeed, the Bright Star Catalog contains only about 50 O-type stars and only very few WR stars.

In view of the large line broadening in massive stars, to search for the presence of magnetic fields, the low-resolution VLT instrument FORS 2 – and prior to that FORS 1 – appears to be the most suitable instrument in the world, offering the appropriate spectral resolution and the required spectropolarimetric sensitivity, giving access to massive stars even in galaxies in our neighborhood. Only the Faint Object Camera and Spectrograph at the Subaru Telescope has an operating spectropolarimetric mode, and, pending the commissioning of the PEPSI spectrograph in polarimetric mode installed at the Large Binocular Telescope, no further high-resolution spectropolarimetric capabilities are available on any of the 8–10 m class telescopes.

The first spectropolarimetric observations of O-type stars at ESO started with FORS 1 already in 2005. During a survey of thirteen O-type stars, the discovery of the presence of a magnetic field was announced in the Of?p star HD 148937 [3]. The class of Of?p stars was introduced by Walborn [5] and includes only five stars in our Galaxy. Of?p stars display recurrent spectral variations in certain spectral lines, sharp emission or P Cygni profiles in He I and the Balmer lines, and strong C III emission lines around 4650 Å. In the last years, it was shown that all Of?p stars are magnetic with field strengths from a few hundred Gauss to a few kG. Among them, only two Of?p stars, HD 148937 and CPD–28 2561 are observable from Paranal and, noteworthy, the first magnetic field detections were achieved through FORS 1 and FORS 2 observations [4].

All FORS 1/2 observations of HD 148937 are presented in Fig. 1 together with the ESPaDOnS observations obtained at CFHT [2]. This figure demonstrates the excellent agreement between the FORS 2 and ESPaDOnS measurements, highlighting the outstanding potential of FORS 2 for the detection of magnetic fields and the investigation of the magnetic field geometry in massive stars. Notably, while an exposure time of 21.5 h at the CFHT was necessary to obtain seven binned measurements, the exposure time for the individual FORS 2 observations accounted only for two to four minutes and only 2.3 h were used for the observations at six different epochs, including telescope presets and the usual overheads for readout time and retarder waveplate rotation.

Also the FORS 2 measurements of the mean longitudinal magnetic field of the second Of?p star, CPD–28 2561, were consistent with a single-wave variation during the stellar rotation cycle, indicating a dominant dipolar contribution to the magnetic field topology with an estimated polar strength of the surface dipole B_d larger than 1.15 kG [6]. Interestingly, in the studies of these two Of?p stars, none of the reported detections reached a 4σ significance level. While 3σ detections with FORS 2 can not always be trusted

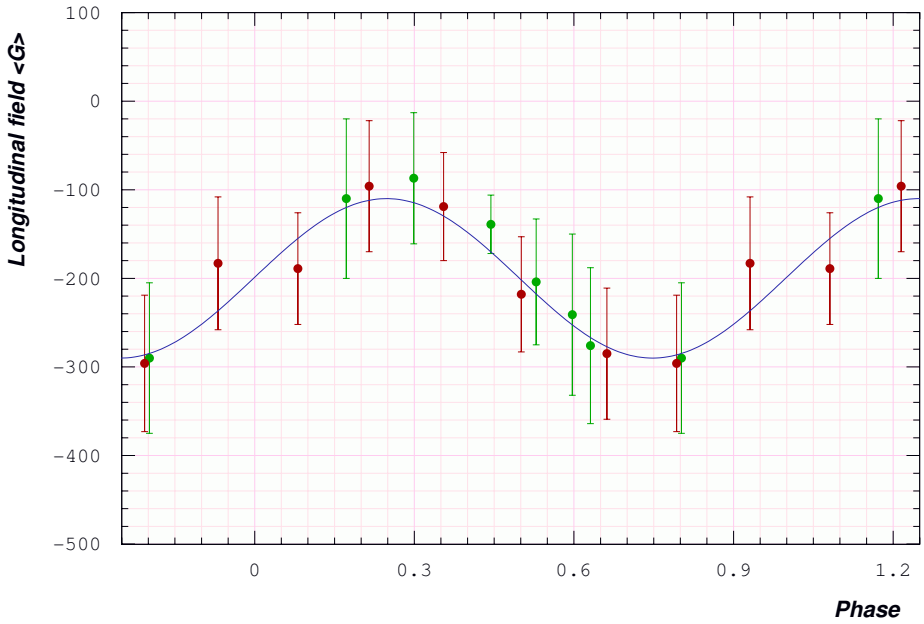

Figure 1: Longitudinal magnetic field variation of the Of?p star HD 148937 according to the 7.032 d period determined by Nazé et al. [1]. Red symbols correspond to ESPaDOnS observations [2], while green symbols are FORS 1 and FORS 2 measurements [3, 4]. Note that the measurement errors for both ESPaDOnS and FORS 1/2 observations are of similar order.

for single observations, they are genuine if the measurements show smooth variations over the rotation period, similar to those found for the Of?p stars HD 148937 and CPD–28 2561. The detection of rotational modulation of the longitudinal magnetic field is important to constrain the global field geometry necessary to support physical modeling of the spectroscopic and light variations.

To identify and to model the physical processes responsible for the generation of their magnetic fields, it is important to establish whether magnetic fields can also be detected in massive stars that are fast rotators and have runaway status. Recent detections of strong magnetic fields in very fast rotating early B-type stars indicate that the spindown timescale via magnetic braking can be much longer than the estimated age of these targets (e.g. [7]). Furthermore, current studies of their kinematic status identified a number of magnetic O and Of?p stars as candidate runaway stars (e.g. [8]). Increasing the known number of magnetic objects with extreme rotation, which are probably products of a past binary interaction, is important to understand the magnetic field origin in massive stars. The star ζ Ophiuchi (=HD 149757) of spectral type O9.5V is a well-known rapidly rotating runaway star, rotating almost at break-up velocity with $v \sin i = 400\,\mathrm{km\,s^{-1}}$ [9]. The analysis of the FORS 2 observations showed the presence of a weak magnetic field with a reversal of polarity [4] and

an amplitude of about 100 G. The resulting periodogram for the magnetic field measurements using all available lines showed a dominating peak corresponding to a period of about 1.3 d which is roughly double the period of 0.643 d determined by Pollmann [10], who studied the variation of the equivalent width of the He I 6678 line.

The presence of magnetic fields might change our whole picture about the evolution from O stars via WR stars to supernovae or gamma-ray bursts. Neglecting magnetic fields could be one of the reasons why models and observations of massive-star populations are still in conflict. Another potential importance of magnetic fields in massive stars concerns the dynamics of stellar winds. A few years ago, Hubrig et al. [11] carried out FORS 2 observations of a sample of Galactic WR stars including one WR star in the Large Magellanic Cloud. Magnetic fields in WR stars are especially hard to detect because of wind-broadening of their spectral lines. Moreover, all photospheric lines are absent and the magnetic field is measured on emission lines formed in the strong wind. Remarkably, spectropolarimetric monitoring of WR 6, one of the brightest WR stars, revealed a sinusoidal nature of $\langle B_z \rangle$ variations with a period of 3.77 d with an amplitude of only 70–90 G.

2 Pulsating massive stars

Recent high-precision uninterrupted high-cadence space photometry using a number of satellites (e.g., WIRE, MOST, CoRoT, Kepler, BRITE) led to a revolutionary change in the observational evaluation of variability of massive stars. Supported by results of photometric monitoring, it is expected that a large fraction of massive stars show photometric variability due to either β Cep- or SPB-like pulsations, or stochastic p-modes, or convectively-driven internal gravity waves.

High-resolution spectropolarimetric observations of pulsating stars frequently fail to show credible measurement results, if the whole sequence of subexposures at different retarder waveplate angles has a duration comparable to the timescale of the pulsation variability. As an example, even for the bright fourth magnitude β Cephei star ξ^1 CMa with a pulsation period of 5 h, a full HARPS sequence of subexposures requires about 30 min. In contrast, one FORS 2 observation of the same star lasts less than 10 min. Owing to the strong changes in the line profile positions and the shapes in the spectra of pulsating stars, a method using spectra averaged over all subexposures leads to erroneous wavelength shifts and thus to wrong values for the longitudinal magnetic field.

For the first time, FORS 1 magnetic field surveys of slowly pulsating B (SPB) stars and β Cephei stars were carried out from 2003 to 2008. As a number of pulsating stars showed the presence of a magnetic field, our observations implied that β Cephei and SPB stars can no longer be considered as classes of non-magnetic pulsators. Notably, although the presence of magnetic fields

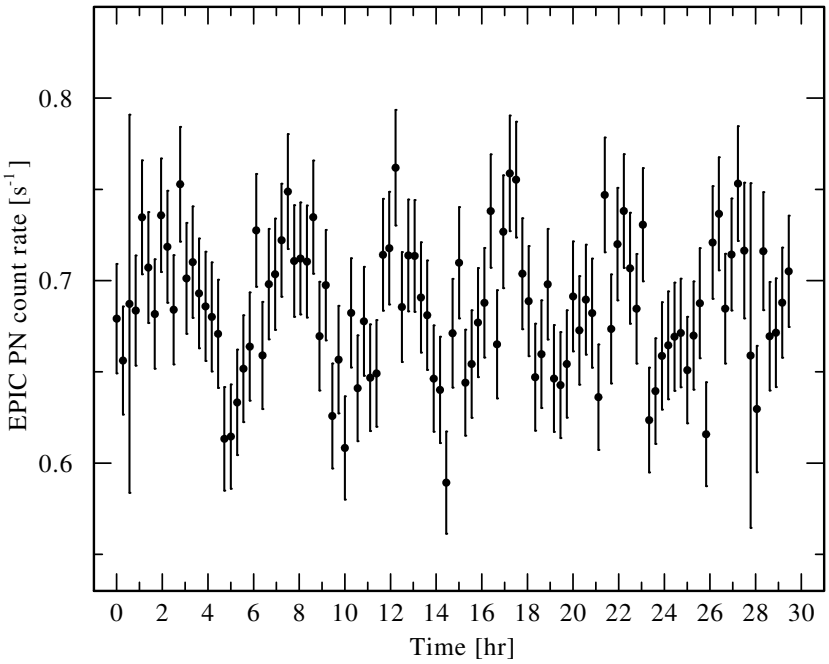

Figure 2: X-ray light curve of ξ^1 CMa in the 0.2 keV – 10.0 keV (1.24 Å – 62 Å) energy band, where the background was subtracted. The horizontal axis denotes the time after the beginning of the observation in hours. The data were binned to 1000 s. The vertical axis shows the count rate as measured by the EPIC PN camera. The error bars (1σ) correspond to the combination of the error in the source counts and the background counts.

in these stars is already known for more than ten years, the effect of these fields on the oscillation properties is not yet understood and remains to be studied. ξ^1 CMa, discovered as magnetic with FORS 1 observations long ago, is still the record holder with the strongest mean longitudinal magnetic field among the β Cephei stars of the order of 300–400 G [12]. Using FORS 2 measurements obtained in service mode in 2009/10, Hubrig et al. [13] detected a rotational modulation of its magnetic field with a period of about 2.19 d and estimated a magnetic dipole strength of about 5.3 kG.

Fully unexpected, observations of this particular star with the *XMM-Newton* telescope revealed for the first time X-ray pulsations with the same period as the stellar radial pulsation [14]. In Figs. 2 and 3, we present the observed X-ray light curve and the X-ray/optical light curves phased with the pulsation period. This first discovery of X-ray pulsations from a non-degenerate massive star stimulates theoretical considerations for the physical processes operating in magnetized stellar winds.

Observations of pulsating stars also allowed the first detection of a magnetic field in another β Cephei star, ϵ Lup [15], which is an SB2 system and recently received attention due to the presence of a magnetic field in both components.

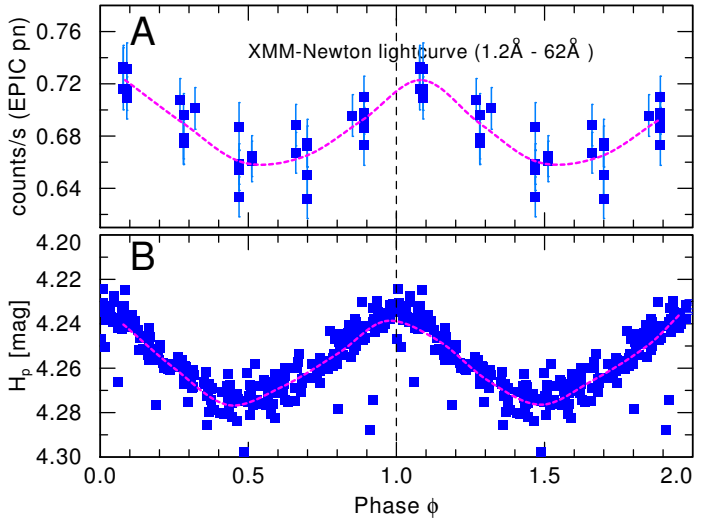

Figure 3: X-ray (upper panel) and optical (lower panel) light curves of ξ^1 CMa, phased with the stellar pulsation period. The X-ray light curve is produced from the data obtained with the *XMM-Newton* EPIC PN camera, using 1 h binning. The dashed red line interpolates the averages in phase bins of $\Delta\phi = 0.1$. The lower panel shows the *Hipparcos* Catalogue Epoch Photometry data. The abscissa is the magnitude H_p in the *Hipparcos* photometric system (330–900 nm with maximum at about 420 nm). The dashed red line interpolates the averages.

Since binary systems with magnetic components are rather rare, the detection of a magnetic field in this system using low resolution FORS spectropolarimetry indicates the potential of FORS 2 also for magnetic field searches in binary or multiple systems.

3 Improvements in the measurement techniques

During the last years, the measurement strategy for high-resolution and low-resolution spectropolarimetric observations was modified in many aspects. To measure the mean longitudinal magnetic fields in high-resolution polarimetric spectra obtained with ESPaDOnS, NARVAL, and HARPS, most teams are using the moment technique introduced by Mathys [16] and the Least-Squares Deconvolution (LSD) introduced by Donati et al. [17]. In the last years, Carroll et al. [18] developed the multi-line Singular Value Decomposition (SVD) method for Stokes Profile Reconstruction. The basic idea of SVD is similar to the Principal Component Analysis approach, where the similarity of the individual Stokes V profiles allows one to describe the most coherent and systematic features present in all spectral line profiles as a projection onto a small number of eigenprofiles (e.g. [19]). The excellent potential of the SVD method, especially in the analysis of extremely weak fields, e.g. in the Herbig Ae/Be star PDS 2, was recently demonstrated by Hubrig et al. ([20], right side of their Fig. 4).

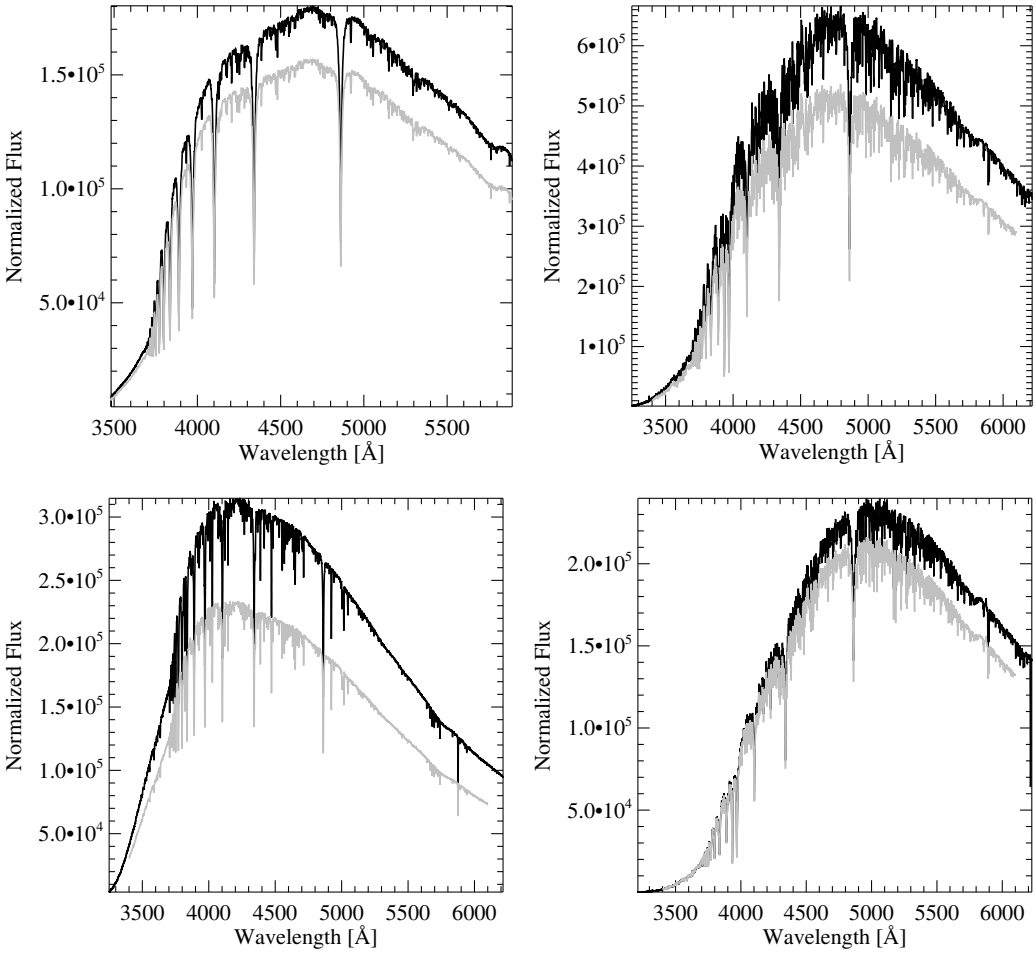

Figure 4: Fluxes extracted by Bagnulo et al. [22] (grey color) compared to those using our own pipeline (black color). The differences in the fluxes are presented (from left to right) for the HgMn star α And, the δ Scuti star HD 21190, the nitrogen rich early B-type star HD 52089, and the Herbig Ae star PDS 2. All these stars were announced in studies by Hubrig et al. as magnetic.

In the reduction process of low-resolution spectropolarimetric observations, Hubrig et al. [21] perform rectification of the V/I spectra and calculate null profiles, N, as pairwise differences from all available V profiles. From these, 3σ-outliers are identified and used to clip the V profiles. This removes spurious signals, which mostly come from cosmic rays, and also reduces the noise. A full description of the updated data reduction and analysis will be presented in a paper by Schöller et al. (*in preparation*).

The mean longitudinal magnetic field, $\langle B_{\rm z}\rangle$, is defined by the slope of the weighted linear regression line through the measured data points, where the weight of each data point is given by the squared signal-to-noise ratio of the Stokes V spectrum. The formal 1σ error of $\langle B_{\rm z}\rangle$ is obtained from the standard relations for

weighted linear regression. This error is inversely proportional to the rms signal-to-noise ratio of Stokes V. Finally, we apply the factor $\sqrt{\chi^2_{\rm min}/\nu}$ to the error determined from the linear regression, if larger than 1.

Since 2014, Hubrig et al. [21] also implement the Monte-Carlo bootstrapping technique, where they typically generate $M = 250\,000$ statistical variations of the original dataset, and analyze the resulting distribution $P(\langle B_{\rm z}\rangle)$ of the M regression results. Mean and standard deviation of this distribution are identified with the most likely mean longitudinal magnetic field and its 1σ error, respectively. The main advantage of this method is that it provides an independent error estimate.

A number of discrepancies in the published measurement accuracies has been reported by Bagnulo et al. [22] who used the ESO FORS 1 pipeline to reduce the full content of the FORS 1 archive. The same authors already published a few similar papers in the last years suggesting that very small instrument flexures, negligible in most of the instrument applications, may be responsible for some spurious magnetic field detections, and that FORS detections may be considered reliable only at a level greater than 5σ. However, no report on the presence of flexures from any astronomer observing with the FORSes was ever published in the past. The authors also discuss the impact of seeing, if the exposure time is comparable with the atmospheric coherence time, which they incorrectly assume to be in seconds and not in milliseconds. In the most recent work do the authors present for the first time the level of intensity fluxes for each image and report which spectral regions were used for the magnetic field measurements. However, no fluxes for left-hand and right-hand polarized spectra are available, thus the reproduction of their measurements is not possible. Notably, already small changes in the spectral regions selected for the measurements can have a significant impact on the measurement results [23].

Since the measurement accuracies predominantly depend on photon noise, an improper extraction of the spectra, for instance the use of smaller extraction windows, would explain why Bagnulo et al. [22] disregarded 3σ detections by other authors. Indeed, the inspection of the levels of intensity fluxes for each subexposure compiled in the catalog of Bagnulo et al. [22] shows that their levels are frequently lower, down to 70% in comparison to those obtained in our studies. In Fig. 4 we present the comparison of fluxes for a few stars for which detections were achieved and published by Hubrig et al. during the last years. It is obvious that the detection of weak magnetic fields is especially affected if the extracted fluxes are low. From the consideration of the SNR values presented by Bagnulo et al. [22], we also noted that emission lines are not taken into account during the measurements. The reason for this is not clear to us as there is no need to differentiate between absorption and emission lines: the used relation between the Stokes V signal and the slope of the spectral line wing holds for both type of lines, so that the signals of emission and absorption lines add up rather than cancel.

4 Summary

To increase the reliability of magnetic field detections, but also to carry out a quantitative atmospheric analysis and to probe spectral variability, it is certainly helpful to follow up FORS 2 detections with high-resolution HARPS observations. To our knowledge, the only collaboration that uses FORS 2 and HARPS to monitor magnetic fields is the BOB ("B-fields in OB stars") collaboration [24], which is focused on the search of magnetic fields in massive stars. Combining observations with different instruments allowed the BOB collaboration to report during the last couple of years the presence of magnetic fields in a number of massive stars. As an example, the first detection of a magnetic field in the single slowly rotating O9.7 V star HD 54879 was achieved with FORS 2 and follow-up HARPS observations could show that HD 54879 is, so far, the strongest magnetic single O-type star detected with a stable and normal optical spectrum [25].

References

1. *Y. Nazé, A. Ud-Doula, M. Spano et al.*, Astron. Astrophys., **520**, A59, 2010.
2. *G.A. Wade, G. Grunhut, G. Gräfener et al.*, Mon. Not. Roy. Astron. Soc., **419**, 2459, 2012.
3. *S. Hubrig, M. Schöller, R.S. Schnerr et al.*, Astron. Astrophys., **490**, 793, 2008.
4. *S. Hubrig, M Schöller, I. Ilyin et al.*, Astron. Astrophys., **551**, A33, 2013.
5. *N.R. Walborn*, Astron. J., **78**, 1067, 1973.
6. *S. Hubrig, M. Schöller, A.F. Kholtygin et al.*, Mon. Not. Roy. Astron. Soc., **447**, 1885, 2015.
7. *T. Rivinius, R.H.D. Townsend, O. Kochukhov et al.*, Mon. Not. Roy. Astron. Soc., **429**, 177, 2013.
8. *S. Hubrig, N.V. Kharchenko, M. Schöller*, Astron. Nachr., **332**, 65, 2011.
9. *E. Kambe, R. Hirata, H. Ando*, Astron. Astrophys., **273**, 435, 1993.
10. *E. Pollmann*, Inf. Bull. Var. Stars, No. 6034, 1, 2012.
11. *S. Hubrig, K. Scholz, W.-R. Hamann et al.*, Mon. Not. Roy. Astron. Soc., **458**, 3381, 2016.
12. *S. Hubrig, M. Briquet, M. Schöller et al.*, Mon. Not. Roy. Astron. Soc., **369**, L61, 2006.
13. *S. Hubrig, I. Ilyin, M. Schöller et al.*, Astrophys. J. Lett., **726**, L5, 2011.
14. *L.M. Oskinova, Y. Nazé, H. Todt et al.*, Nature Commun., **5**, 4024, 2014.
15. *S. Hubrig, M. Briquet, P. De Cat et al.*, Astron. Nachr., **330**, 317, 2009.
16. *G. Mathys*, Proc. IAU Coll., **138**, 232, 1993.

17. *J.F. Donati, M. Semel, B.D. Carter et al.*, Mon. Not. Roy. Astron. Soc., **291**, 658, 1997.

18. *T.A. Carroll, K.G. Strassmeier, J.B. Rice, A. Künstler*, Astron. Astrophys., **548**, A95, 2012.

19. *T.A. Carroll, M. Kopf, K.G. Strassmeier, I. Ilyin*, Proc. IAU Symp., **259**, 633, 2009.

20. *S. Hubrig, T.A. Carroll, M. Schöller, I. Ilyin*, Mon. Not. Roy. Astron. Soc., **449**, L118, 2015.

21. *S. Hubrig, M. Schöller, A.F. Kholtygin*, Mon. Not. Roy. Astron. Soc., **440**, 1779, 2014.

22. *S. Bagnulo, L. Fossati, J.D. Landstreet, C. Izzo*, Astron. Astrophys., **583**, A115, 2015.

23. *S. Hubrig, D.W. Kurtz, S. Bagnulo et al.*, Astron. Astrophys., **415**, 661, 2004.

24. *T. Morel, N. Castro, L. Fossati et al.*, The Messenger, **157**, 27, 2014.

25. *N. Castro, L. Fossati, S. Hubrig et al.*, Astron. Astrophys., **581**, A81, 2015.

* The color figures are available online in the Proceedings at *http://www.astro.spbu.ru/sobolev100/*.

Relative Intensities of Hydrogen Lines as a Tool to Study Astrophysical Plasma

N.A. Katysheva[1], V.P. Grinin[2,3]

E-mail: *natkat2006@mail.ru*

The hydrogen lines play an important role in diagnostics of astrophysical plasma. In recent years, the lines of higher hydrogen series became the objects of the research, thanks to the rapid development of the infrared spectroscopy. In this paper we investigate the relative intensities of the Paschen and Brackett lines as well as the ratio of $I(L_\alpha)/I(H_\alpha)$ over a large range of the optical depth of gas. The calculations are fulfilled on the basis of the Sobolev approximation for collisional excitations and ionizations of atoms for the electron temperature $T_e < 10000$ K. The behavior of the electron density N_e at the gas thermalization is investigated. It is shown that a very sharp jump in the degree of ionization is observed near the LTE conditions. The obtained results can be used both for the diagnostics of emitting regions and for determining the extinction for the objects with strong absorption.

1 Introduction

Emission hydrogen lines are present in spectra of different astrophysical objects – from cool stars to quasars and Seyfert galaxies. They indicate the deviation from the local thermodynamic equilibrium (LTE). Earlier, the visible spectral range was the basic one, and the Balmer emission lines were observed most frequently, making the theory of Balmer decrement (B.D.) one of the main methods of the diagnostics of emitting gas. The most detailed calculations of B.D. for a multi-level hydrogen atom were carried out on the basis of the escape probability method by V.V. Sobolev [1] for different cases of excitation and ionization of the gas. Boyarchuk [2], Hirata and Uesugi [3] calculated B.D. for radiative excitations and ionizations, Gershberg and Schnol [4], Grinin and Katysheva [5] computed B.D. just for collisional ones. Ilmas [6], Grinin and Katysheva [7] considered both the cases. The relative intensities of the Paschen, Brackett and Pfund series of hydrogen were calculated by Luud and Ilmas [8] to explain the spectra of γ Cas [8].

The Lyman and Balmer decrements for collisional excitations and ionizations were computed in [5] for a wide range of the electron temperatures ($T_e = 10000$–20000 K), electron number densities ($N_e = 10^7$–10^{13} cm^{-3}) and the escape probabilities ($\beta_{12} = 1$–10^{-8}), where β_{12} was the photon escape probability

[1] Sternberg State Astronomical Institute, Lomonosov Moscow State University, Russia
[2] Main Astronomical Observatory, Pulkovo, Russia
[3] Sobolev Astronomical Institute, St. Petersburg State University, Russia

V. Grinin et al. (eds) Radiation mechanisms of astrophysical objects. Yerevan: Edit Print, 2017, pp. 197–202.

in the Lyman α line. This quantity is connected with the optical depth τ_{12} of the Lyman α line (in the 1D model) by the following formula:

$$\beta_{12} = (1 - \exp(-\tau_{12}))/\tau_{12}. \quad (1)$$

In the paper [5] it was originally shown that for $T_e = 10000$ K the theoretical ratio of Lyα and Baα line intensities, $I(L_\alpha)/I(H_\alpha)$, could be of the order of unity or smaller, for large N_e and large optical thickness of emitting gas. On the basis of those calculations, the intensities of the Lyman, Balmer and Paschen lines of quasars and Seyfert galaxies were discussed in [9].

2 The ratio $I(L_\alpha)/I(H_\alpha)$

The progress in new astronomical equipment in recent years allowed an inclusion of the lines of Lyman and far infrared series of hydrogen in the analysis. The ratio $I(L_\alpha)/I(H_\alpha)$ is of considerable interest. The first data on $I(L_\alpha)/I(H_\alpha)$ in solar outbursts, quasars and Seyfert galaxies were obtained in the middle of the 1970s. In the case of the recombination mechanism (Menzel's case A), this ratio is more than 10. Zirin [10], and Canfield and Puetter [11] presented first results of observations of Lyman and Balmer lines. They found that the ratio $I(L_\alpha)/I(H_\alpha)$, on average, was of the order of 1. Then, Allen et al. [12] measured the $I(L_\alpha)/I(H_\alpha)$ ratio for some quasars, where it was in the range 0.8–3. McCarthy et al. [13] found that $I(L_\alpha)/I(H_\alpha)$ was equal to 4.7($\pm$1.8) and 3.5($\pm$1.3) for the radio galaxies with redshift of about 2.4: B3 0731+438 and MRC 0406-244, respectively. Explanations of the discrepancy between Menzel's case A and obtained $I(L_\alpha)/I(H_\alpha)$ were suggested in the papers [14]–[18]. It was shown that a small ratio $I(L_\alpha)/I(H_\alpha)$ could be derived for large optical depth and strong radiation.

In this paper, we continued our calculations and computed the populations of the hydrogen atomic levels and the line intensities on the base of the Sobolev approximation for the case of collisional excitations and ionizations, using our program described in [5]. We considered the model of a 15-level atom for the gas velocity $V = 300$ km/s. The model parameters were: $T_e = 8000$ and 9000 K and hydrogen density $N_H = 10^{11}$ and 10^{12} cm^{-3}.

In Fig. 1 the dependence of the $I(L_\alpha)/I(H_\alpha)$ ratio on the geometrical depth of the emitting gas, Z, is presented. The graph shows that an increase of Z (and, correspondingly, an increase of the optical depth) leads to a decrease of this ratio – firstly smooth and later sharp – from about 700 down to 1 or less. Such a behavior of the relative intensities is caused by approaching the physical state of gas to the LTE.

It is interesting to consider the electron density N_e as a function of the layer geometrical thickness Z. In Fig. 2 we show results of the calculations for two values of T_e (8000 and 9000 K) and two values of the hydrogen density N_H. We see that for low thickness Z, the degree of ionization is small and N_e is practically constant.

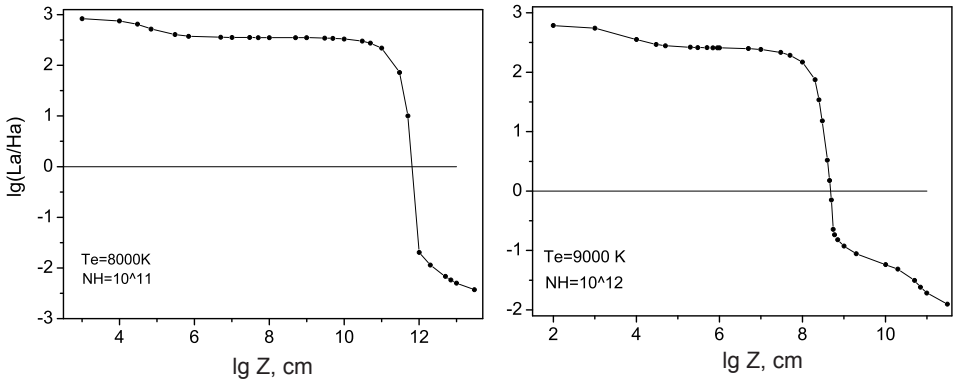

Figure 1: The ratio $I(L_\alpha)/I(H_\alpha)$ vs the geometrical depth Z (in cm) of the emitting gas for $T_e = 8000$ K, $N_H = 10^{11}$ cm^{-3} (left) and $T_e = 9000$ K, $N_H = 10^{12}$ cm^{-3} (right).

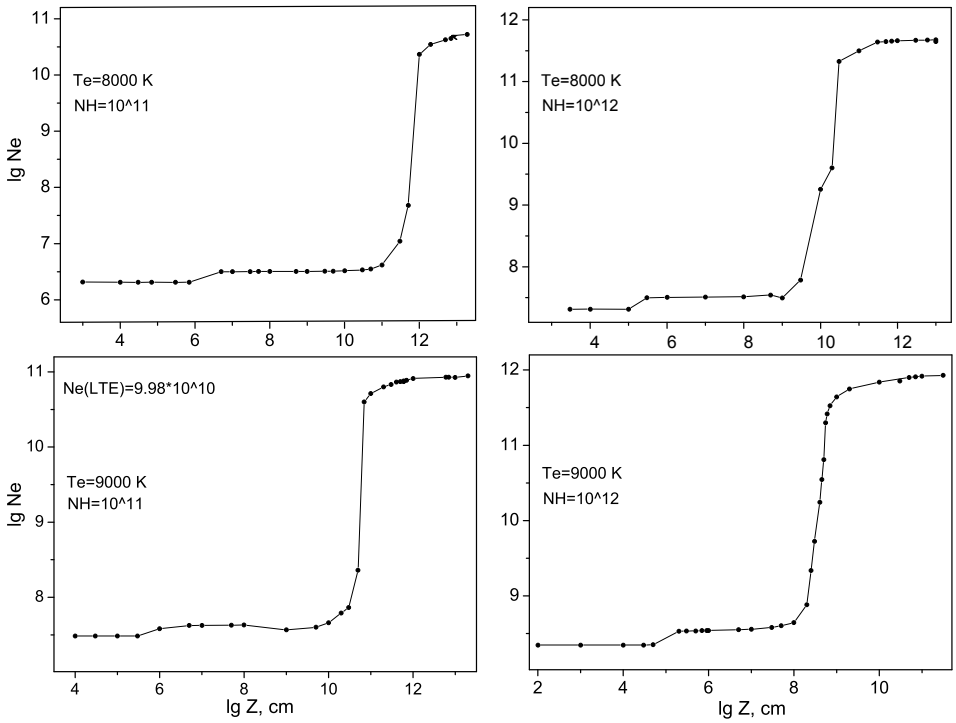

Figure 2: N_e vs the geometrical depth Z for $T_e = 8000$ and 9000 K, $N_H = 10^{11}$ cm^{-3} (left) and 10^{12} cm^{-3} (right).

At $Z \approx 10^5$ cm a small step is visible on the curves as N_e increases slightly due to the blocking of the radiation beyond the Lyman jump. Further growth of Z leads to an increase of the degree of ionization. A dramatic stepwise rise of the degree of ionization by about 10^4 times (!) occurs at a comparatively small interval of Z (depending on T_e and N_H). The comparison of Fig. 2 and Fig. 1 shows that a sharp increase of N_e and a strong decrease of $I(L_\alpha)/I(H_\alpha)$ occur in the same thickness range in which the gas conditions are close to the LTE.

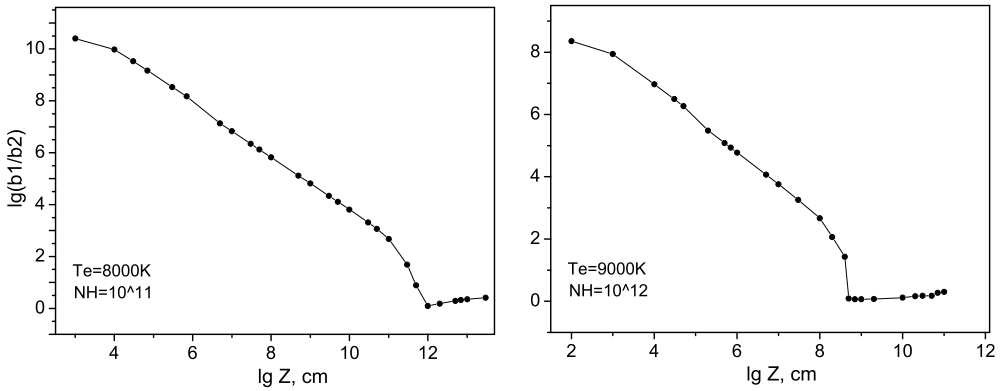

Figure 3: The ratio of Menzel parameters b_1/b_2 as a function of the geometrical depth Z for $T_e = 8000$ K, $N_H = 10^{11}$ cm^{-3} (left) and $T_e = 9000$ K, $N_H = 10^{12}$ cm^{-3} (right).

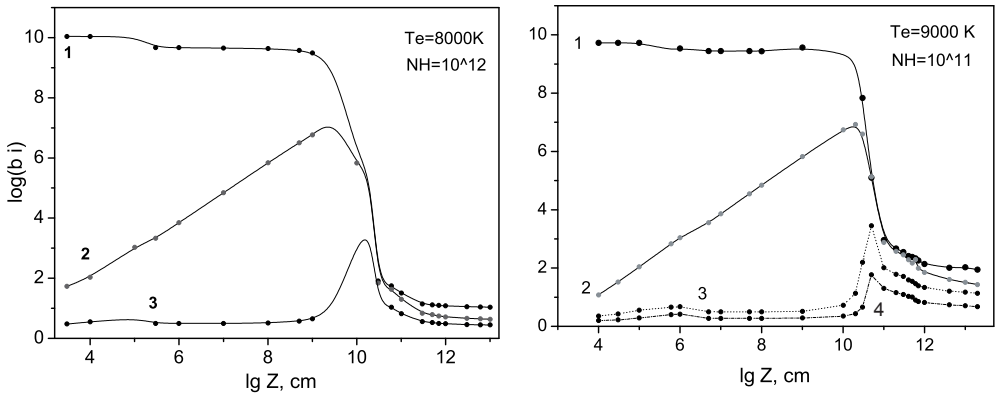

Figure 4: Dependence of b_i on the geometrical depth Z for $T_e = 8000$ K, $N_H = 10^{12}$ cm^{-3} (left) and 9000 K, $N_H = 10^{11}$ cm^{-3} (right). Indices 1, 2, 3 near the curves indicate the number of the atomic level.

What is the reason of such a sharp jump of N_e and, correspondingly, of the degree of ionization? Figs. 3 and 4 show, respectively, the ratio of Menzel parameters b_1/b_2 and the parameters b_1, b_2, b_3 (in a logarithmic scale) as a function of Z. In Fig. 3 we see a graduate decline of the ratio (b_1/b_2) from small Z to a certain geometrical depth, and then the value of b_1/b_2 becomes practically constant. The reason is the large optical depth of gas in the L_α and H_α lines at which the emitting gas becomes thermalized.

In Fig. 4 we see that the curve 1 decreases slowly with the increasing optical depth in the Lyman and then the Balmer lines, while curve 2 increases, and this corresponds to the decline in Fig. 3. If the optical depth of higher series is small, the values b_3 and b_4 change weakly. When the emitting gas becomes optically thick in the Paschen lines, the parameters b_3 and b_4 increase. Further thermalization of gas quickly reduces the Menzel parameters b_1 and b_2, and the role of collisional excitations from the excited levels and multi-cascade ionization increases essentially.

3 Infrared lines

Last years the far infrared spectroscopy developed very actively. For instance, high-resolution IR spectra of hot stars γ Cas, HD 45677, P Cyg with multiple lines of hydrogen (from Pfund to Humphrey series) were obtained. Lenorzer [19] presented ISO (Infrared Space Observatory) spectra and used them to diagnose the radiating gas, by considering fluxes in the lines Hu(14-6), Brα, Pfγ, and their ratios. They showed that on the diagram Hu(14-6)/Brα vs Hu(14-6)/Pfγ, there was a split of optically thin stellar winds and optically thick discs. For example, the fluxes of P Cyg and η Car are close to the optically thin case, whereas γ Cas to the optically thick one. Therefore, the lines of high series can give an additional information about the gas parameters.

Edwards et al. [20] carried out spectroscopic observations of 16 T Tauri stars, analyzed intensities of the Paschen and Brackett lines and compared them to the theoretical ones for Menzel's case B and those calculated by Kwan and Fischer [21]. The statistics of the observed intensity ratios $I(P_\alpha)/I(P_\beta)$ showed that they were less than 1, and P_β/Br_γ ratio was in the range from 3 to 6.

So, the diagnostics of IR-lines could give a significant contribution to study of stellar envelopes. Let us consider the ratio of the line intensities $Br7/P7 = Br_\gamma/P_\delta = 0.420\,\beta_{47}/\beta_{37}$ and $P7/H7 = P_\delta/H_\varepsilon = 0.303\,\beta_{37}/\beta_{27}$. Since these lines are formed by the transitions from the same upper (seventh) level, the intensity ratios of these lines depend only on the corresponding values of the gas optical depths.

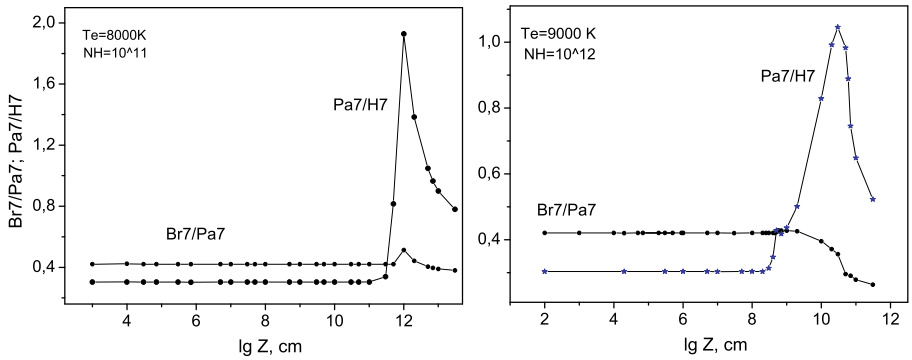

Figure 5: Ratios $I(Br_\gamma)/I(Pa_\delta)$ and $I(Pa_\delta)/I(H_\varepsilon)$ vs the geometrical thickness Z.

Fig. 5 presents the dependence of the ratios $I(Br_\gamma)/I(P_\delta)$ and $I(P_\delta)/I(H_\varepsilon)$ on Z. As it follows from the theoretical relations for the gas optically thin in the Paschen–Brackett series, these values are constant. With an increase of the optical depth $\tau_{L\alpha}$, the Menzel parameters b_i tend to equilibrium ones ($\sim$1).

If we known that the optical depth of P_α is less than 1, then it is possible to use the ratio of the lines mentioned above to estimate the interstellar or circumstellar extinction. Detailed calculations of $I(P_\alpha)/I(H_\alpha)$ have been carried out by Katysheva [9] for the case of collision ionizations and excitations for $T_e = 10000$–20000 K.

4 Conclusion

The results of the calculations presented above show that the role of the multi-cascade ionizations grows rapidly with the increase of the optical depth in the subordinate lines as a result of line-blocking in these lines. This is a natural reaction of the gas approaching the LTE. Such a gas state is observed in the dense emitting regions, for example, in the flares of UV Cet-type stars [22, 23, 24].

Acknowledgments. This work was partly supported by Russian President grant NSh-1675.2014.2 (N.K.) and the RFBR grant 15-02-09191 (V.G.).

References

1. *V.V. Sobolev*, Moving Envelopes of Stars. Cambridge: Harvard University Press, 1960.
2. *A.A. Boyarchuk*, Bull. Crim. Astrophys. Obs., **35**, 45, 1966.
3. *R. Hirata, A. Uesugi*, Contrib. Kwasan Obs. Kyoto, **156**, 1967.
4. *R.E. Gershberg, E.E. Shnol*, Izv. Krym. Astrofiz. Obs., **50**, 1122, 1974.
5. *V.P. Grinin, N.A. Katysheva*, Bull. Crim. Astrophys. Obs., **62**, 52, 1980.
6. *M. Ilmas*, Hydrogen Lines in Spectra of Cool Stars. Tartu, 1974.
7. *V.P. Grinin, N.A. Katysheva*, Bull. Crim. Astrophys. Obs., **62**, 47, 1980.
8. *L. Luud, M. Ilmas*, Hydrogen Lines in Spectra of Stars. Tartu, 1974.
9. *N.A. Katysheva*, Astrophys., **19**, 32, 1983.
10. *H. Zirin*, Astrophys. J. Lett., **222**, L105, 1978.
11. *R.C. Canfield, R.C. Puetter*, Astrophys. J. Lett., **236**, L7, 1980.
12. *D. Allen, J.R. Barton, P.R. Gillingham, R.F. Carswell*, Mon. Not. Roy. Astron. Soc., **200**, 271, 1982.
13. *P.J. McCarthy, R. Elson, P. Eisenhardt*, Astrophys. J. Lett., **387**, L20, 1992.
14. *S.A. Drake, R.K. Ulrich*, Astrophys. J. Suppl., **42**, 351, 1980.
15. *R.C. Canfield, R.C. Puetter*, Astrophys. J., **236**, 390, 1981.
16. *R.C. Canfield, R.C. Puetter, P.J. Ricchiazzi*, Astrophys. J., **249**, 383, 1981.
17. *J. Kwan, J.H. Krolik*, Astrophys. J. Lett., **233**, L91, 1979.
18. *J.H. Krolik, C.F. McKee*, Astrophys. J. Suppl., **37**, 459, 1978.
19. *A. Lenorzer, B. Vandenbussche, P. Morris et al.*, Astron. Astrophys., **384**, 473, 2002.
20. *S. Edwards, J. Kwan, W. Fischer et al.*, Astrophys. J., **778**, 148, 2013.
21. *J. Kwan, W. Fischer*, Mon. Not. Roy. Astron. Soc., **411**, 2383, 2011.
22. *V.P. Grinin, V.V. Sobolev*, Astrophys., **13**, 348, 1977.
23. *V.V. Sobolev, V.P. Grinin*, Astrophys., **38**, 15, 1995.
24. *W.E. Kunkel*, Astrophys. J., **161**, 503, 1970.

Polarimetric Properties of Icy Moons of the Outer Planets

N.N. Kiselev[1,4], V.K. Rosenbush[1], V.L. Afanasiev[2], S.V. Zaitsev[1], S.V. Kolesnikov[3,4], D.N. Shakhovskoy[4]

E-mail: *kiselevnn@yandex.ru*

The progress in the study of polarization phenomena exhibited by planetary moons is reviewed. Besides previously published data, we focus primarily on the new results of our recent polarimetric observations of the Galilean satellites of Jupiter, bright satellites of Saturn (Enceladus, Dione, Rhea, Iapetus), and the major moons of Uranus (Ariel, Umbriel, Titania, Oberon) at backscattering geometries, including phase angles approaching zero. In addition to a negative branch of polarization, which is typical of atmosphereless solar system bodies (ASSBs), some high-albedo objects, including E-type asteroids, reveal a backscattering polarization feature in the form of a spike-like negative polarization minimum. These optical phenomena serve as important tests of modern theoretical descriptions of light scattering by regolith surfaces. We found the polarimetric properties of different ASSBs near opposition are highly various. The possible reasons for such behavior are discussed.

1 Introduction

The surfaces of planetary satellites are covered with regolith particles which are likely to be aggregates. The properties of the regolith (the structure and packing density of the aggregates, the sizes of constituents, compositions, shapes, and orientation) can be inferred from measurements of the polarization characteristics, namely, the degree P and the plane of linear polarization θ. The degree of polarization P varies with the phase angle α (the angle between the Sun and the observer as viewed from the object), producing polarization phase curve.

Many atmosphereless solar system bodies (ASSBs) exhibit a brightening and negative values of the degree of linear polarization (NPB) near the opposition $\alpha \leq 20^\circ$. A class of high-albedo ASSBs (satellites of planets, E-type asteroids) reveals a unique combination of a nonlinear increase of brightness, so-called brightness opposition effect (BOE), and a sharp minimum of polarization (POE) centered at exactly the backscattering direction. There is also the so-called polarization longitude effect (PLE), i.e., a difference between the polarization

[1] Main Astronomical Observatory of the National Academy of Sciences of Ukraine
[2] Special Astrophysical Observatory of the Russian Academy of Sciences, Russia
[3] Observatory of Odessa National University, Ukraine
[4] Crimean Astrophysical Observatory, Crimea

V. Grinin et al. (eds) Radiation mechanisms of astrophysical objects. Yerevan: Edit Print, 2017, pp. 203–209.

curves for the leading and trailing hemispheres of satellites. Until the mid 1990s, the available polarimetric data, even for the bright Galilean moons of Jupiter, were rather limited and even mutually contradictory [1]. Polarization measurements of moons of the outer planets were scarce. Therefore, our goal was to fill in the missing data for the satellites of planets with different albedo which show the BOE. The objects of our program are the high-albedo Galilean moons of Jupiter (Io, Europa, Ganymede), Saturn's moons (Enceladus, Dione, Rhea, and Iapetus). We also include in our program the major moons of Uranus (Ariel, Umbriel, Titania, Oberon) as well as Jupiter's moon Callisto which are moderate-albedo objects, but demonstrate a sharp surge of brightness.

2 Observations

The polarimetric observations of the planetary satellites near opposition were carried out during different observing runs with different instruments in 1998–2015. The one-channel photopolarimeter of the 2.6 m Shain telescope and the UBVRI photopolarimeter of the 1.25 m telescope of the Crimean Astrophysical Observatory (CrAO) were used. A small part of observations was conducted at the 0.7 m telescope of the Chuguyev Observation Station of the Institute of Astronomy of Kharkiv National University (IAKhNU) and the 1 m telescope of the CrAO (Simeiz) using a one-channel photoelectric polarimeter of the IAKhNU. A description the polarimeters is given in [2]. The faint satellites of Uranus (Ariel, Umbriel, Titania, Oberon) were observed at the 6-m BTA telescope of the SAO with the multimode focal reducer SCORPIO-2 [3].

The degree of linear polarization P and the position angle of the polarization plane θ of the program objects were obtained with reduction programs specially designed for each polarimeter [2, 4]. From the observations of standard stars, we found the instrumental polarization fairly stable, always below 0.2% for all

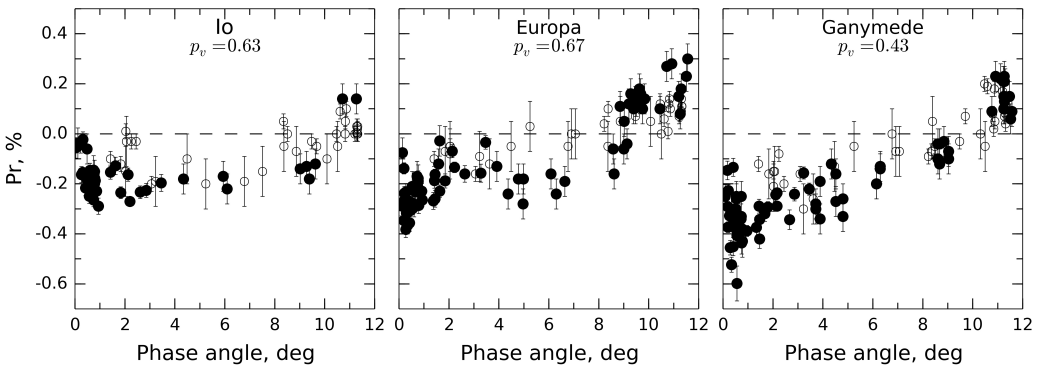

Figure 1: NPB for Io, Europa, and Ganymede with sharp minima of polarization centered at small phase angles. Dark symbols correspond to the present work, filters R and WR; open symbols to data from [5], filter V.

instruments. It was taken into account. A typical random error in the degree of linear polarization ranges from 0.02% to 0.1%, depending on the brightness of the satellite, the count accumulation time, and the observing conditions.

In planetary astrophysics, the polarization quantity of interest is $P_r = P\cos 2\theta_r$, where θ_r is the angle between the measured direction of the plane of linear polarization and the normal to the scattering plane. Thus, we present the results of our observations in the form of the phase–polarization curves (P_r versus α).

3 Results

3.1 The Galilean satellites: Io, Europa, Ganymede, and Gallisto

The polarization–phase curves for Io, Europa, and Ganymede are plotted in Fig.1.

We found that for all observations with $P \gg \sigma_P$, angle θ_r lies near 90°, and the values P_r are negative at all phase angles smaller than the inversion angle. As one can see in Fig. 1, the sharp asymmetric features with polarization minima about $-(0.3 \div 0.4)\%$ at phase angles $< 1°$ are observed. The shape of the negative polarization branches (NPB) of the satellites varies considerably from almost flat for Io up to strongly asymmetric curve for Ganymede.

Europa clearly demonstrates two minima at the NPB: $P_{min} \approx -0.4\%$ at $\alpha \approx 0.8°$ and $P_{min} \approx -0.2\%$ at $\alpha \approx 5.5°$. The same effect can be seen for Io and Ganymede, although less pronounced. The sharp secondary minimum of polarization centered at very small phase angle, called polarization opposition effect, was predicted by Mishchenko for high-albedo ASSBs [8].

A detailed study of the PLE for Callisto was carried out by Rosenbush [6]. The NPBs for the leading and trailing hemispheres of Callisto are the regular curves of polarization without any sharp asymmetric features like the POE (see Fig. 2).

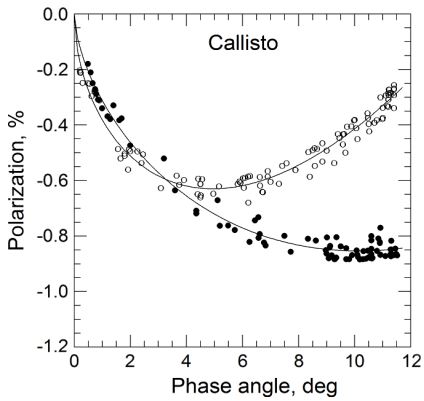

Figure 2: NPB for the leading (dark symbols) and trailing (open symbols) hemispheres of Callisto in the V filter after the correction for the orbital longitudinal variations [6]. Solid curves represent the best fit to the data by a trigonometric expression [7].

3.2 Saturn's moons: Enceladus, Dione, Rhea, and Iapetus

The NPBs for Enceladus, Dione, Rhea are plotted in Fig. 3. Enceladus is a unique object having the highest albedo ($p_v = 1.38$) of any object in the solar system. Moreover, Enceladus shows the ice fountains over the south polar region. Data for NPB of Enceladus are still rather limited because they are obtained for the first time. The asymmetric NPBs with polarization minima $P_{min} \approx -0.8\%$ at $\alpha_{min} \approx 1.8^\circ$ are observed for Rhea and Dione. The NPB for Rhea is more sharp asymmetric than that for Diona.

Iapetus is a unique moon of Saturn with the greatest albedo asymmetry of any object in the Solar System. Its leading hemisphere has albedo $p_v = 0.02$–0.05, whereas the trailing hemisphere has $p_v = 0.6$. As a result, the large variations of polarization degree with longitude of Iapetus are revealed. In Fig. 4 we present the observations obtained for the bright trailing hemisphere (open symbols) as well as for the leading hemisphere (dark symbols). As one can see (Fig. 4, left panel), a strongly asymmetric phase curve of polarization for the bright trailing hemisphere with minimum $P_{min} \approx -0.7\%$ at $\alpha_{min} \approx 1.5^\circ$ is revealed. The PLE for Iapetus is shown in Fig. 4 (right bottom panel). It is in a good agreement with the albedo distribution (Fig. 4, right upper panel) which is derived from a mosaic of Cassini images [9].

3.3 The major moons of Uranus: Ariel, Titania, Oberon, and Umbriel

Observations of the satellites were carried out at the 6 m BTA telescope [4] within the phase angle range of $0.06 - 2.37^\circ$. The NPB for Ariel, Titania, Oberon, and Umbriel in the V filter are presented in Fig. 5 (left panel). For Ariel, the maximum branch depth $P_{min} \approx -1.4\%$ is reached at the phase angle $\alpha_{min} \approx 1^\circ$; for Titania $P_{min} \approx -1.2\%$, $\alpha_{min} \approx 1.4^\circ$; for Oberon $P_{min} \approx -1.1\%$, $\alpha_{min} \approx 1.8^\circ$.

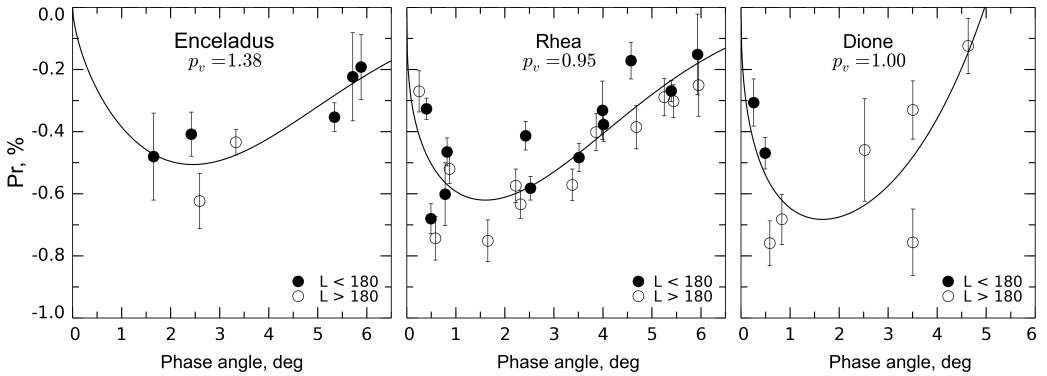

Figure 3: NPB for Enceladus, Rhea, and Dione. Dark and open circles show data for leading ($L < 180^\circ$) and trailing ($L > 180^\circ$) hemispheres, respectively. Solid curves represent the fit to the data by a trigonometric expression [7].

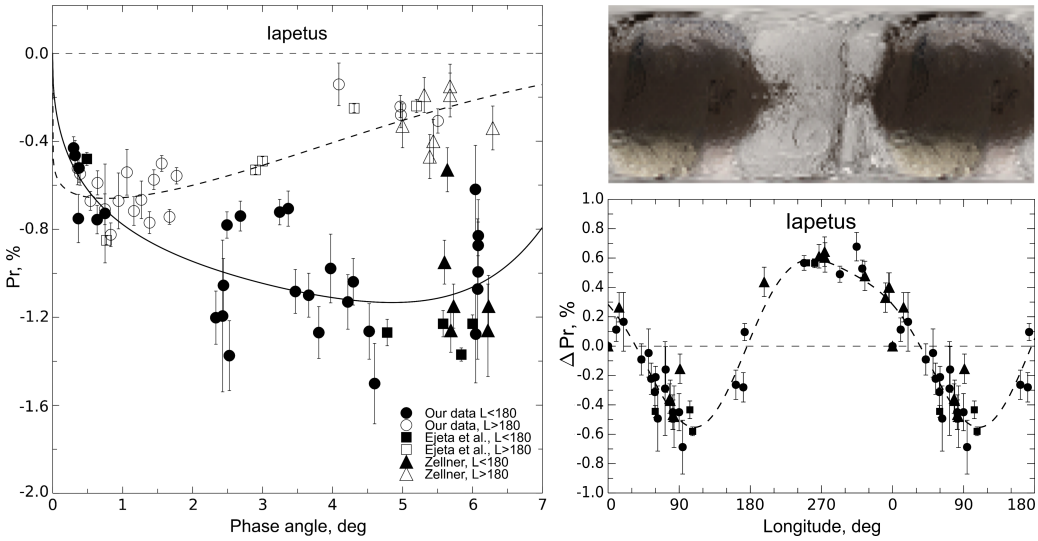

Figure 4: Phase-angle (left panel) and longitude (right bottom panel) dependencies of polarization for Iapetus. The albedo distribution map [9] is given in the right upper panel. Circles show our data, filters R and WR; squares data from [10, 11], filter R; triangles data by Zellner [12, 13], filter V.

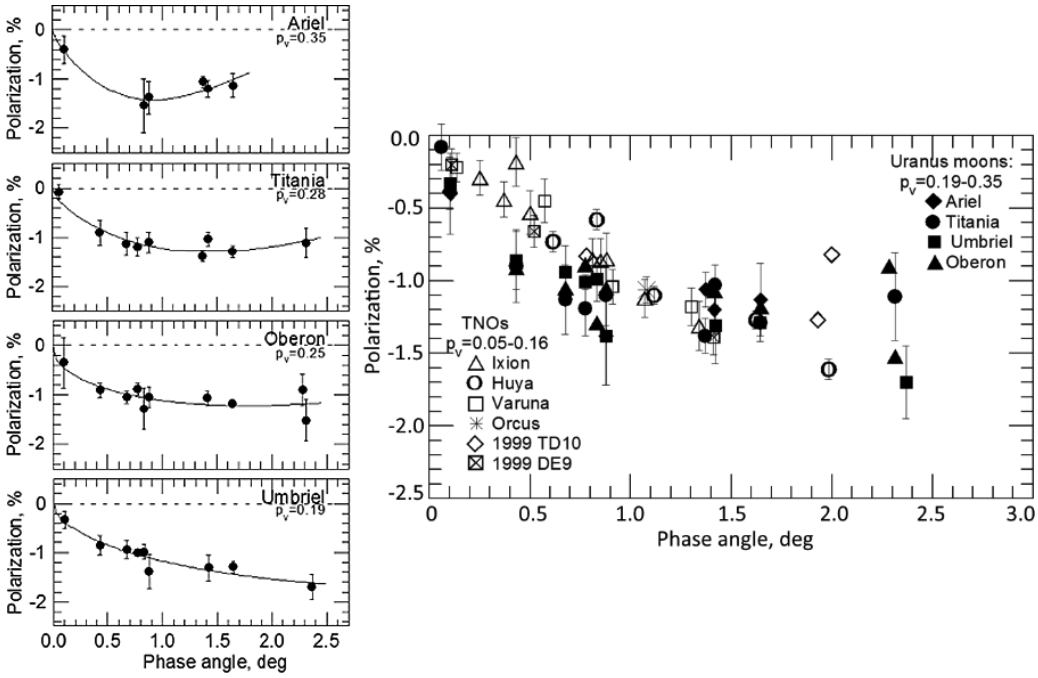

Figure 5: NPB for the Uranian satellites (left panel). Right panel shows a comparison of the phase-angle polarization dependencies of the Uranian moons (dark symbols) and TNOs (open symbols). Data for TNOs are taken from [14].

For Umbriel, the polarization minimum was not reached: for the last measurement point at $\alpha = 2.4°$, polarization amounts to -1.7%. The declining P_{min} and shifting α_{min} towards larger phase angles correlate with a decrease of the geometric albedo of the Uranian moons. There is no longitudinal dependence of polarization for the moons within the observational errors which indicates a similarity in the physical properties of the leading and trailing hemispheres [4].

We found (see Fig. 5, right panel) that for the Uranian moons the polarization phase dependencies are in a good agreement with the measured polarization of the group of small trans-Neptunian objects (Ixion, Huya, Varuna, Orcus, 1999 TD10, 1999 DE9) which are characterized by a large gradient of negative polarization, approximately 1% per degree in the $0.1-1°$ range of phase angles, according to [14].

4 Summary

The extensive polarimetric observations of moons of the outer planets, obtained during the past two decades, demonstrate that the behavior of the phase-angle dependence of polarization near the opposition is highly various. It is ranging from a bimodal curve consisting of a secondary minimum distinctly separated from the main minimum of the NPB (the Galilean satellites of Jupiter) to an asymmetric negative polarization branch (Saturn's and Uranian satellites). A quantitative analysis of these observational data in terms of specific physical parameters is hardly possible at this time because of the still limited data (limited range of phase angles and wavelengths). Nevertheless the data can be qualitatively interpreted in terms of the currently available light scattering mechanisms on the regolith surfaces. Shadow hiding, coherent backscattering, near-field effects, and anisotropic scattering by single particles are often considered as the dominant mechanisms that define the characteristics of the scattered radiation (intensity and polarization) at small phase angles. The shape of the NPB, as well as characteristics of BOE and POE, depend on the relative contributions of the mentioned mechanisms which, in turn, depend on the physical characteristics of the regolith layer and the scattering geometry. The packing density and the refractive index, as well as size and shape of the monomers constituting the aggregate particles, determine the effectiveness of each of the scattering mechanisms and, hence, the behavior of brightness and polarization near the opposition. This is what draws significant interest in the study of light scattering effects on surfaces of ASSBs, including planetary satellites, in terms of both observations and their modeling and development of light scattering theory.

References

1. *V. Rosenbush, N. Kiselev, V. Afanasiev*, in Polarimetry of Stars and Planetary Systems. Eds. L. Kolokolova, J. Hough, A.-Ch. Levasseur-Regourd. Cambridge: Cambridge Univ. Press, 2015, p. 340.
2. *M.I. Mishchenko, V.K. Rosenbush, N.N. Kiselev et al.*, Polarimetric Remote Sensing of Solar System Objects. Kyiv: Akademperiodika, 2010.

3. *V.L. Afanasiev, V.R. Amirkhanyan*, Astrophys. Bull., **67**, 438, 2012.
4. *V.L. Afanasiev, V.K. Rosenbush, N.N. Kiselev*, Astrophys. Bull., **69**, 121, 2014.
5. *A. Dollfus*, Icarus, **25**, 416, 1975.
6. *V.K. Rosenbush*, Icarus, **159**, 145, 2002.
7. *K. Lumme, K. Muinonen*, in Proc. IAU Symp. 160: Asteroids, Comets, Meteors. LPI Contrib. No. 810. Houston: Lunar Planet. Inst., 1993, p. 194.
8. *M.I. Mishchenko*, Astrophys. J., **411**, 351, 1993.
9. *S. Albers*, *http://laps.noaa.gov/albers/sos/saturn/iapetus/*
10. *C. Ejeta, H. Boehnhardt et al.*, Astron. Astrophys., **537**, A23, 2012.
11. *C. Ejeta, H. Boehnhardt et al.*, Astron. Astrophys., **549**, A61, 2013.
12. *B.H. Zellner*, Astrophys. J. Lett., **174**, L107, 1972.
13. *J. Veverka*, in Planetary satellites. Ed. J.A. Burns. Tucson: Univ. Arizona Press, 1977, p. 210.
14. *S. Bagnulo, I. Belskaya, K. Muinonen et al.*, Astron. Astrophys., **491**, L33, 2008.

Modeling of Spectral Variability of Romano's Star

O.V. Maryeva[1], V.F. Polcaro[2], C. Rossi[3], R.F. Viotti[2]

E-mail: *olga.maryeva@gmail.com*

The variable star GR 290 (M33/V532, Romano's Star) in the M 33 galaxy has been suggested to be a very massive star in the post-luminous blue variable (LBV) phase. In order to investigate links between this object, the LBV category and the Wolf-Rayet stars of the nitrogen sequence (WN), we have derived its basic stellar parameters and their temporal evolution. We confirm that the bolometric luminosity of the star has not been constant, it changes synchronously with stellar magnitude, being 50% larger during visual light maxima. Presently, GR 290 falls in the H-R diagram close to WN8h stars, being probably younger than them. In the light of current evolutionary models of very massive stars, we find that GR 290 has evolved from a 60 $M_\odot$ progenitor star and has an age of about 4 million years. From its physical characteristics, we argue that GR 290 has left the LBV stage and is presently moving from the LBV stage to a Wolf-Rayet stage of a late nitrogen spectral type.

1 Introduction

GR 290 was discovered as a variable star in 1978 by Giuliano Romano [1] and later classified by him as a Hubble–Sandage variable [2]. Peter Conti in 1984 merged Hubble-Sandage variables with S Dor variables in a united class – Luminous Blue Variables (LBVs), and GR 290 became a candidate LBV [3, 4]. Arguments for changing the class of GR 290 from candidate LBV to LBV were given in [5, 6, 7]. More detailed history of spectral and photometric investigations of GR 290 was described in [8].

However, in 2011 Polcaro et al. [9] suggested that, because of its very high luminosity and its extremely hot spectrum at the 2008 visual minimum (WN8h), GR 290 is probably not too far from the end of the LBV phase and may be evolving towards a late-WN-type star. In 2014 Humphreys et al. [10] also noticed that in recent years (2004–2010) GR 290 has shown large photometric variability of 1.5 mag in the blue, but no spectroscopic transition from a hot star spectrum (at the visual minimum) to the cool optically thick wind one at the visual maximum resembling an A to F-type supergiant that is typical of the LBV/S-Dor phenomenon. On the contrary, the spectrum of GR 290 varied from WN8h

[1] Special Astrophysical Observatory of the RAS, Russia
[2] INAF-IAPS, Italy
[3] Università La Sapienza, Italy

V. Grinin et al. (eds) Radiation mechanisms of astrophysical objects. Yerevan: Edit Print, 2017, pp. 211–214.

at minimum to WN11h at the recent visual maxima and to B, probably late type at its highest recorded maximum. In this regard, Humphreys et al. [10] speculate on whether GR 290 is a hot star in transition to the LBV stage (as suggested by Smith and Conti [11], for the WNh stars) or it may be in a post-LBV state.

Maryeva and Abolmasov [12] investigated the optical spectra of Romano's star in two different states: the brightness minimum of 2008 ($B = 18.5 \pm 0.05$ mag) and a moderate brightening in 2005 ($B = 17.1 \pm 0.03$ mag). Main result of the work [12] is that the bolometric luminosities (L_{bol}) of GR 290 were different in 2005 and 2008. L_{bol} of GR 290 in 2005 is 1.5 times higher, that is not typical of LBVs. This result confirms the suggestion of [9]. However, to refine the evolutionary status of the star, a more detailed investigation of intermediate states was also necessary, and in the present work we report on the results of such investigation.

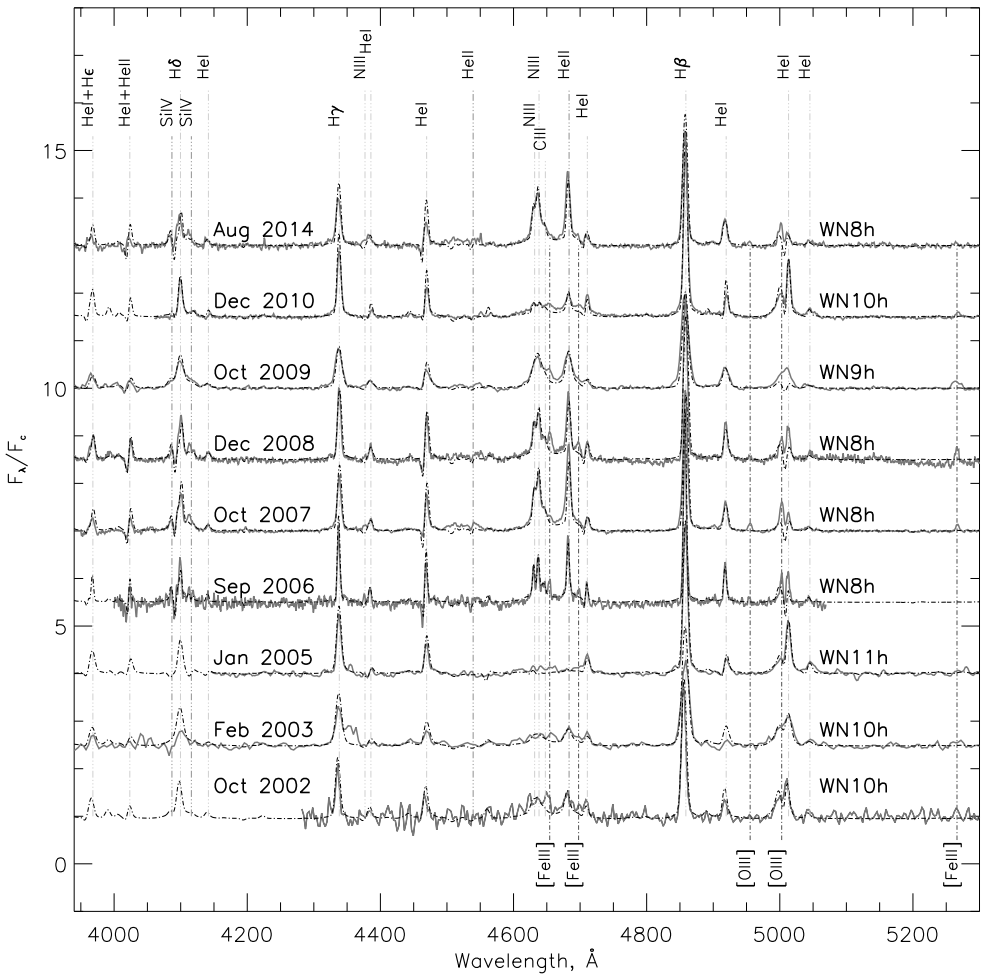

Figure 1: Normalized optical spectra of GR 290 compared with the best-fit CMFGEN models (dash-dotted line). The model spectra are convolved with a Gaussian instrumental profile.

Table 1: Derived properties of Romano's star. $R_{2/3}$ is the radius where the Rosseland optical depth is equal to 2/3, T_{eff} is the effective temperature at $R_{2/3}$, $\dot{M}_{cl}$ is the mass loss rate. For all models, we included clumping with the filling factor 0.15. For all dates, uncertainty of T_{eff} is 1 kK.

Date	V [mag]	Sp. type	T_{eff} [kK]	$R_{2/3}$ [$R_\odot$]	L_*, 10^5 [$L_\odot$]	$\dot{M}_{cl}$, 10^{-5} [$M_\odot \mathrm{yr}^{-1}$]	v_∞ [km/s]
Oct 2002	17.98	WN10h	28	39	8 ± 0.5	2.4 ± 0.3	250 ± 100
Feb 2003	17.70	WN10.5h	27.5	44	10.2 ± 0.7	2.6 ± 0.3	250 ± 50
Jan 2005	17.24	WN11h	23.5	61	$10.5^{+1.5}_{-3}$	4.0 ± 0.3	250 ± 50
Sep 2006	18.4	WN8h	31	28	6.7 ± 0.5	1.5 ± 0.3	250 ± 100
Oct 2007	18.6	WN8h	33.3	23.8	6.3 ± 0.5	1.9 ± 0.3	370 ± 50
Dec 2008	18.31	WN8h	31.5	28.5	7.2 ± 0.5	2.3 ± 0.3	370 ± 50
Oct 2009	18.36	WN9h	32	28.4	7.5 ± 0.5	2.0 ± 0.3	300 ± 100
Dec 2010	17.95	WN10h	26.7	42	8 ± 0.5	2.6 ± 0.3	250 ± 100
Aug 2014	18.74	WN8h	33	22.5	5.3 ± 0.5	1.7 ± 0.3	400 ± 100

2 Modeling

In order to see how the parameters of GR 290 changed with time, we modeled the most representative spectra with best quality obtained during October 2002 – December 2014, when the star displayed an ample range of variation in visual luminosity. This time interval covers two brightness maxima and three minima. For modeling we used CMFGEN atmospheric code [13] and constructed nine models (Fig. 1). We can see from Table 1 that the nature of the stellar wind significantly changes, being much denser and slower during the eruption in 2005, while during the minimum of brightness wind structure is fairly similar to the one of typical WN8h (non variable) stars.

The main result of this analysis is that the bolometric luminosity of GR 290 is variable, it is higher during the phases of greater optical brightness. The present model fitting of a large sample of spectra obtained during two successive luminosity cycles allows us to trace the recent path of the star in the Hertzsprung–Russell (H-R) diagram (Fig. 2).

3 Results

Combining the results of numerical modeling with data of photometric and spectral monitoring, we may conclude that we observed GR 290 in very rare evolutionary phase – post-LBV. The initial mass of GR 290 is near 60 $M_\odot$ and age is about 4 Myr. Probably, the changes of L_{bol} are due to the hydrogen mixing in the core generating a burst of nuclear energy: presently, such repeated nuclear events should be the extra-energy input to increase the bolometric luminosity of GR 290 during its last outbursts. They will end when the hydrogen percentage in the envelope will become too low to be mixed in the core.

More details are published in [14].

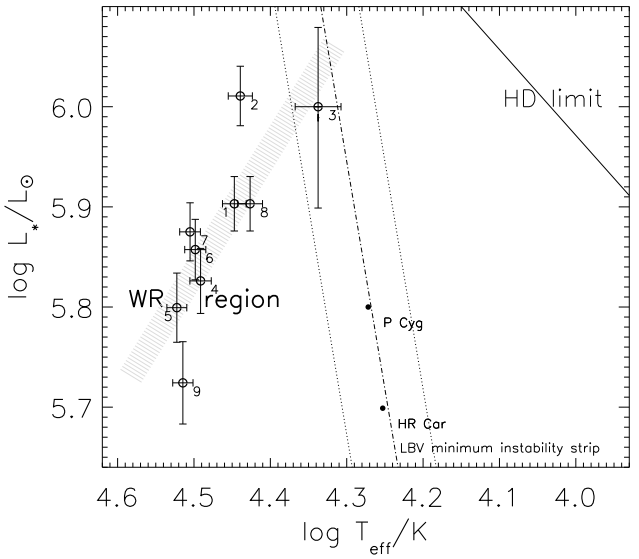

Figure 2: Position of GR 290 in the H-R diagram. HD limit line shows the Humphreys–Davidson limit [3]. 1 – Oct. 2002; 2 – Feb. 2003; 3 – Jan. 2005; 4 – Sep. 2006; 5 – Oct. 2007; 6 – Dec. 2008; 7 – Oct. 2009; 8 – Dec. 2010; 9 – Aug. 2014.

Acknowledgments. The authors would like to thank R. Gualandi, R. Haver and M. Calabresi for providing with new spectral and photometric data. O.M. thanks RFBR (project 14-02-00291) for a support.

References

1. *G. Romano*, Inf. Bull. Var. Stars, No. 1433, 1978.
2. *G. Romano*, Astron. Astrophys., **67**, 291, 1978.
3. *R.M. Humphreys, K. Davidson*, Publ. Astron. Soc. Pacif., **106**, 1025, 1994.
4. *T. Szeifert*, Liege Int. Astrophys. Coll., **33**, 459, 1996.
5. *R. Kurtev, O. Sholukhova et al.*, Rev. Mex. Astron. Astrofiz., **37**, 57, 2001.
6. *V.F. Polcaro, R. Gualandi, L. Norci et al.*, Astron. Astrophys., **411**, 193, 2003.
7. *S. Fabrika, O. Sholukhova, T. Becker et al.*, Astron. Astrophys., **437**, 217, 2005.
8. *O. Maryeva*, Balt. Astron., **23**, 248, 2014.
9. *V.F. Polcaro, C. Rossi, R.F. Viotti et al.*, Astron. J., **141**, 18, 2011.
10. *R.M. Humphreys, K. Weis, K. Davidson et al.*, Astrophys. J., **790**, 48, 2014.
11. *N. Smith, P.S. Conti*, Astrophys. J., **679**, 1467, 2008.
12. *O. Maryeva, P. Abolmasov*, Mon. Not. Roy. Astron. Soc., **419**, 1455, 2012.
13. *D.J. Hillier, D.L. Miller*, Astrophys. J., **496**, 407, 1998.
14. *V.F. Polcaro, O. Maryeva, R. Nesci et al.*, Astron. J., **151**, 149, 2016.

Magnetic Field Function for Early-Type Stars

A. Medvedev[1], A. Kholtygin[2]

E-mail: *a.s.medvedev@gmail.com*

We present a model describing the magnetic field function for early-type stars. The model relies on population synthesis to generate the ensemble of magnetic stars on the upper main sequence. It also includes the capabilities for statistical simulations and parameter estimation necessary for analysis of real data. Our model was able to reproduce the empirical magnetic field distributions for OBA stars. We estimated the model parameters, found constraints on dissipation of stellar magnetic fields and explored the hypothesis that magnetic properties of early-type stars (2–60 $M_\odot$) might be described by a single magnetic field function.

1 Introduction

Magnetic stars on the upper main sequence (upper MS) are particularly interesting for research. All of the theories proposed to explain the origin of the large-scale magnetic fields are closely related to our understanding of early stages of the pre-MS evolution and formation of intermediate-mass and massive stars [12]. Moreover, although these stars are the progenitors of isolated pulsars, their magnetic properties are not interrelated directly, but strongly suggest the evolution of the magnetic fields between the zero-age main sequence (ZAMS) and supernova explosion [7].

Potentially, a lot of information that might be vital for our understanding of stellar magnetism should be gained from the study of the distributions of the stellar magnetic fields. The great increase in the number of known magnetic stars [5, 13] that happened over the last decades, including the discovery of the magnetic O-type stars, provides us with the opportunity to study such distributions even for different groups of OBA stars [8]. It also opened the possibility to check some of the early hypotheses about properties of the stellar magnetic fields in the light of recently acquired data.

For these purposes, we model the magnetic field function for early-type stars. We create a tool that would be useful for analysis of the empirical magnetic field distributions. Our model is based on population synthesis to account for the diversities in stellar parameters that always will exist in real samples of magnetic stars. It is also able to simulate the magnetic field distribution for a sample of a given size and, what is important, to estimate the magnitude of its possible variations.

[1] Special Astrophysical Observatory, Nijnii Arkhyz, Russia
[2] St. Petersburg State University, Russia

V. Grinin et al. (eds) Radiation mechanisms of astrophysical objects. Yerevan: Edit Print, 2017, pp. 215–218.

2 The model

The population synthesis begins with the initial ensemble containing stars that are randomly generated assuming the standard initial mass function [9] and a constant birth-rate. The temporal evolution of the ensemble is computed with the SSE code [6] implemented within the AMUSE environment for astrophysical simulations [10]. The evolution time is set to be large enough for the ensemble to achieve stationarity for a number of MS stars.

The magnetic fields corresponding to ZAMS stars are generated, assuming the lognormal distribution for the initial net magnetic flux, which is defined by the mean logarithm of the net magnetic flux $\langle \log \Phi \rangle$ and its deviation Δ. The evolution of stellar magnetic fields on the MS is represented by the exponential decay of the magnetic flux [8]. The process is described by the dissipation parameter τ_d that coincides with the relative time-scale for the decay, expressed in terms of a stellar MS lifetime. The ensemble generation is accomplished when the root-mean-square (rms) magnetic fields $\mathcal{B}$ for all objects in the ensemble of magnetic stars are finally computed.

The ensemble is then used to obtain the magnetic field function and its appearance for the sample of a given size. This involves random sampling and raw statistical methods for estimating of the mean distribution and limits for its possible variations (Fig. 1).

3 Empirical magnetic field distributions

We obtained the magnetic field distributions for BA, OB and O-type stars using data from different sources [2, 4, 11], and applied our model for their analysis.

We find that the empirical magnetic field distributions for BA and OB stars are very similar. They both reveal the same regular shape, typical of the lognormal distribution. In particular, the distribution for BA stars can be fitted by the

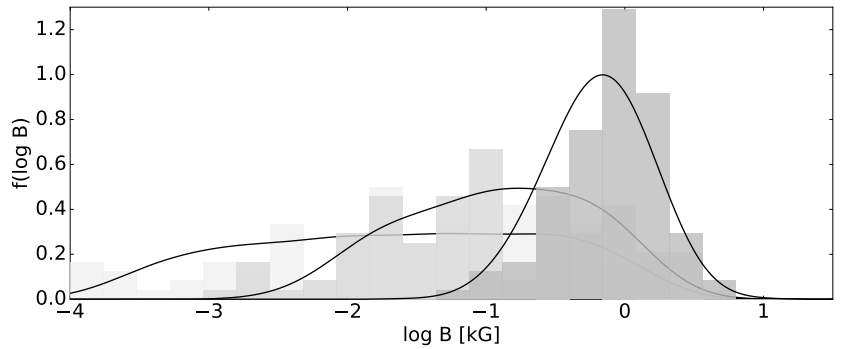

Figure 1: Magnetic field function for early-type stars calculated with our model. Black lines correspond to different values of the dissipation parameter τ_d: 0.15 (left curve), 0.3 (central curve) and ∞ (right curve). The gray histograms show the distribution for the same parameters, but for samples of $\sim$100 stars.

Table 1: Best-fit parameters obtained from the simultaneous approximation of the magnetic field distribution functions for BA, OB and O-type stars. The confidence intervals were obtained by using the C-statistics introduced by Cash [3]

Model	$\langle \log \Phi \rangle$, G cm^2	Δ	$\tau_{\rm d}$
I	$26.86^{+0.07}_{-0.21}$	$0.55^{+0.09}_{-0.13}$	∞
II	$27.23^{+0.11}_{-0.12}$	$0.38^{+0.1}_{-0.13}$	0.5

lognormal distribution with the mean $\langle \log \mathcal{B} \rangle \approx 0.5$ and the standard deviation $\sigma = 0.5$. It is inconsistent with the hypothesis of a "magnetic threshold" proposed by Aurière et al. [1] to explain the lack of stars with $B_d \lesssim 300$ G (or $\mathcal{B} \lesssim 60$ G), appeared in their sample. We found no peculiarities or other indications supporting this conjecture. A similar issue was also reported for OB stars in [5].

Also, we suppose that dissipation of the stellar magnetic fields is not very fast, otherwise we would expect very different appearances of the empirical distributions (Fig. 1). Our analysis shows that only for $\tau_{\rm d} \gtrsim 0.5$ it is possible to achieve the best agreement between the model and empirical distributions. This implies that the time-scales for magnetic field dissipation are at least comparable with the stellar MS lifetimes.

The sample of O-type stars consists of 11 stars only. Such a small size makes it difficult to draw reliable conclusions about the intrinsic magnetic field function. However, we assumed that the empirical distribution for O-type stars might also be drawn from the same magnetic field function as for BA and OB stars. Applying the procedure of simultaneous fitting, we were able to describe all of the empirical distributions with a single model (see Table 1). Therefore, it is not unlikely that magnetic properties of upper MS stars (with $M > 2$–$60\,{\rm M}_\odot$) are defined by a common magnetic field function.

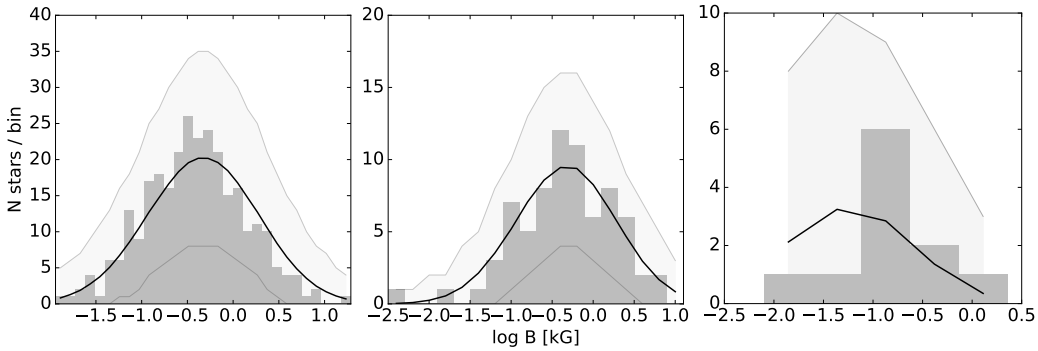

Figure 2: Simultaneous fitting of the magnetic field distributions for BA, OB and O-type stars (from left to right). The gray histograms represent the empirical data, while the black lines show the mean model distribution. The gray filled area corresponds to the 95% confidence limits for possible variations.

4 Conclusions

- We built a model describing distribution of magnetic fields for early-type stars and applied model for analysis of the empirical data.
- The empirical magnetic field distribution for BA and OB stars are very similar and both can be fitted by a lognormal distribution.
- It is possible to reproduce all of the empirical distributions with a single magnetic field function (Table 1).
- The estimated constraint on the dissipation parameter is $\tau_d \leq 0.5$, are in accordance with estimations by Kholtygin et al. [8].
- The empirical distributions for OBA stars provide with no evidence supporting the hypothesis of a "magnetic desert" [1].

Acknowledgments. The authors thank RFBR grant 16-02-00604a and RSF grant 14-50-00043 for the support.

References

1. *M. Aurière, G.A. Wade, J. Silvester et al.*, Astron. Astropys., **475**, 1053, 2007.
2. *V.D. Bychkov, L.V. Bychkova, J. Madej*, Mon. Not. Roy. Astron. Soc., **394**, 1338, 2009.
3. *W. Cash*, Astrophys. J., **228**, 939, 1979.
4. *L. Fossati, N. Castro, T. Morel et al.*, Astron. Astropys., **574**, A20, 2015.
5. *L. Fossati, N. Castro, M. Schöller et al.*, Astron. Astropys., **582**, A45, 2015.
6. *J.R. Hurley, O.R. Pols, C.A. Tout*, Mon. Not. Roy. Astron. Soc., **315**, 543, 2000.
7. *A.P. Igoshev, A.F. Kholtygin*, Astron. Nachr., **332**, 1012, 2011.
8. *A.F. Kholtygin, S.N. Fabrika, N.A. Drake et al.*, Astron. Lett., **36**, 370, 2010.
9. *P. Kroupa*, Science, **295**, 82, 2002.
10. *F.I. Pelupessy, A. van Elteren, N. de Vries et al.*, Astron. Astropys., **557**, A84, 2013.
11. *G.A. Wade*, Astron. Soc. Pacif. Conf. Ser., **494**, 30, 2015.
12. *R. Walder, D. Folini, G. Meynet*, Space Sci. Rev., **166**, 145, 2012.
13. *G.A. Wade, C. Neiner, E. Alecian et al.*, Mon. Not. Roy. Astron. Soc., **456**, 2, 2016.

Continuum and Line Emission of Flares on Red Dwarf Stars: Origin of the Blue Continuum Radiation

E.S. Morchenko[1]

E-mail: *morchenko@physics.msu.ru*

There are two types of models that explain the appearance of the quasi-blackbody radiation during the impulsive phase of stellar flares. Grinin and Sobolev [1] argue that this component of the optical continuum is formed in "the transition layer between the chromosphere and the photosphere." Katsova et al. [4] have "raised" the source of the white-light continuum up to the dense region in the perturbed chromosphere. In the present contribution (the main paper is published in "Astrophysics" [9]), we show that the statement in [4] is erroneous.

1 Introduction

Grinin and Sobolev [1] were the first who showed that the quasi-blackbody spectrum at the flare's maximum brightness is formed near the photosphere. Heating of the deep layers is due to the high energy proton or/and electron beams with the initial energy flux $F_0 \approx 10^{12}$ erg cm^{-2}s^{-1} and $F_0 \approx 3 \times 10^{11}$ erg cm^{-2}s^{-1}, respectively [2, 3].

Katsova et al. [4] calculated the first gas dynamic model of the impulsive stellar flares (the energy flux in the electron beam $F_0 = 10^{12}$ erg cm^{-2}s^{-1}). According to this model, the blue component of the optical continuum is formed in a chromospheric condensation. The condensation is located between a temperature jump and the front of the downward shock (the temperature wave of the second kind [5]). The physical parameters of this source of white-light continuum ($N_H \approx 2 \times 10^{15}$ cm^{-3}, $T \approx 9000$ K, and thickness $\Delta z \approx 10$km) lie in the range of the layer parameters in the model by Grinin and Sobolev [1] ($N_H \sim 10^{15}-10^{17}$ cm^{-3}, $T \sim 5000-20000$ K, and $\Delta z \gtrsim 10$ km). Here, N_H is equal to the sum of the proton and atom concentrations. However, the condensation is formed at height of about 1500 km above the quiescent photosphere of a red dwarf, i.e. in the upper chromosphere.

The downward shock [4] propagates through *a partially ionized gas* of the red dwarf chromosphere. The flow speed is subsonic for the electron component of the plasma but this speed is hypersonic for the ion-atom component [6]. Therefore, both ions and atoms are heated more intensively than electrons

[1] Sternberg Astronomical Institute, Moscow M.V. Lomonosov State University, Russia

V. Grinin et al. (eds) Radiation mechanisms of astrophysical objects. Yerevan: Edit Print, 2017, pp. 219–221.

at the shock front. Thus, the region between the temperature jump and the front of the downward shock is, in fact, *two-temperature* ($T_{ai} \gg T_e$) [7]. Here, T_{ai} is the ion-atom temperature, and T_e is the electron one.

2 Emission spectrum of a two-temperature layer

Morchenko et al. [7] calculated the emission spectrum of a homogeneous pure hydrogen layer with $6\,\mathrm{eV} \leq T_{ai} \leq 12\,\mathrm{eV}$ and $0.8\,\mathrm{eV} \leq T_e \leq 1.5\,\mathrm{eV}$. The layer density lies in the range $3 \times 10^{14}\,\mathrm{cm}^{-3} \leq N_H \leq 3 \times 10^{16}\,\mathrm{cm}^{-3}$.

Initially, we assume that the Lyman-α optical depth in the center of the layer, τ_{12}^D, is approximately equal to 10^7 (see Eq. (1) in [7]). However, at values of $N_H \sim 10^{16}\,\mathrm{cm}^{-3}$ the layer thickness, $\mathcal{L}$, is *small* ($\tau_{12}^D \propto N_1\mathcal{L}$ – see Eq. (53) in [7]). Here, N_1 is the concentration of the ground state atoms. Therefore, we consider the transition from the transparent gas to the gas whose emission is close to the Planck function under conditions when $\mathcal{L}$ is fixed (see the first paragraph of Sect. 7 in [7]).

The following elementary processes were taken into account: the electron impact ionization, excitation, and de-excitation, the triple recombination, the spontaneous radiative recombination, the spontaneous transitions between discrete energy levels. We consider the influence of the layer's radiation (bremsstrahlung and recombination) on the occupation of atomic levels. It is necessary as the flare luminosity is stronger in the optical range than that of the quiescent atmosphere of the whole star.

We take into account the scattering of line radiation in the framework of the Biberman–Holstein approximation [8]. Since $\tau_{12}^D \gg 1$, photons escape the flare plasma in the distant line wings [7]. The following asymptotic formula is valid for the resonance transition:

$$\theta_{12} \approx \left(\frac{\mathcal{B}_{21}\mathcal{E}_0}{\Delta\omega_{21}^D}\right)^{3/5} \frac{1}{(\tau_{12}^D)^{3/5}}. \tag{1}$$

Here, $\mathcal{B}_{21}$ is the Stark broadening parameter, $\mathcal{E}_0$ is the Holtsmark field strength, and $\Delta\omega_{21}^D$ is the Doppler width.

Our calculations [7] have shown that the Menzel factors do not differ from unity at values of $\tau_{12}^D \sim 10^7$ and higher. Moreover, the two-temperature 10 km layer with $N_H = 3 \times 10^{16}\,\mathrm{cm}^{-3}$, $T_{ai} = 10\,\mathrm{eV}$, $T_e = 1\,\mathrm{eV}$ generates the blue continuum radiation (the optical depth at wavelength $\lambda = 4170$ Å, τ_{4170}, is approximately equal to 6).

We also *proposed* that the non-stationary radiative cooling of the gas behind the downward stationary shock can produce an equilibrium region, which is responsible for the quasi-blackbody radiation during the impulsive phase of stellar flares (the last sentence in [7]).

3 Origin of the blue continuum radiation

The model [4] includes the one-temperature ($T_{ai} = T_e = T$) source of the white-light continuum. Let us investigate the applicability of the calculations [7] for a one-temperature layer with $\tau_{12}^D \gtrsim 10^7$. It is true that

$$\tau_{12}^D \propto \frac{1}{\sqrt{\pi}\Delta\omega_{21}^D} \propto {T_{ai}}^{-1/2}. \tag{2}$$

Therefore, the mean photon escape probability, θ_{12}, as well as the Menzel factors of the layer do not depend on the ion-atom temperature. Thus, at $T_e = T_{ai} = T$ numerical results [7] remain valid.

Then it is true that the 10 km layer with the parameters from the model by Katsova et al. [4] is *transparent* in the optical continuum (see the lower curve designated to "I" in Fig. 2 from [7]): $\tau_{4170} \ll 1$, Q.E.D.

In the paper [9] we briefly discuss the theoretical possibility of the origin of the blue continuum radiation behind the downward stationary shock with *radiative cooling*. Based on a simple estimate, it is shown that the Planck emission is formed only under conditions when the gas flows from the viscous jump on a small distance (approximately five hundred meters). Thus, our hypothesis [7] is not confirmed.

Finally, we hold that the quasi-blackbody spectrum during the impulsive phase of stellar flares is formed in the deep layers [1, 10].

References

1. *V.P. Grinin, V.V. Sobolev*, Astrophys., **13**, 348, 1977.
2. *V.P. Grinin, V.V. Sobolev*, Astrophys., **31**, 729, 1989.
3. *V.P. Grinin, V.M. Loskutov, V.V. Sobolev*, Astron. Rep., **37**, 182, 1993.
4. *M.M. Katsova, A.G. Kosovichev, M.A. Livshits*, Astrophys., **17**, 156, 1981.
5. *P.P. Volosevich, S.P. Kurdyumov, L.N. Busurina, V.P. Krus*, Comput. Math. Math. Phys., **3**, 204, 1963.
6. *S.B. Pikel'ner*, Izv. Krym. Astrofiz. Obs., **12**, 93, 1954.
7. *E. Morchenko, K. Bychkov, M. Livshits*, Astrophys. Space Sci., **357**, article id. 119, 2015.
8. *V.V. Ivanov*, Transfer of Radiation in Spectral Lines. Washington: Nat. Bur. Stand., 1973.
9. *E.S. Morchenko*, Astrophys., **59**, 475, 2016.
10. *S.W. Mochnacki, H. Zirin*, Astrophys. J. Lett., **239**, L27, 1980.

Optical Continuum of Powerful Solar and Stellar Flares

B.A. Nizamov[1], M.A. Livshits[2]

E-mail: *nizamov@physics.msu.ru, maliv@mail.ru*

The powerful optical continuum of solar and stellar flares is hard to explain within the concept of the gasdynamic response of the chromosphere to the impulsive heating. It requires too large amount of accelerated particles, in contradiction with the hard X-ray observations. The resolution of this trouble is to take into account the absorption of the short wavelength radiation of the hot flaring plasma by the optical emission source, i.e. the low temperature condensation. Our estimates show that this can help to explain the origin of the optical continuum of powerful impulsive flares on the Sun and red dwarfs and superflares on the young G stars.

1 Introduction

A large amount of the multi-wavelength observations of solar flares as well as the optical and X-ray observations of flares on red dwarfs have been analysed in the last years; non-stationary events with the total energy exceeding that of the most powerful phenomena on the Sun by 2–3 orders of magnitude were detected on some late-type low-mass stars by the *Kepler* spacecraft. This required a new analysis of the data on the stellar flares. Particularly, this refers to the possibility of the generation of the powerful continuous optical radiation of the superflares.

Theoretical investigation of the problem concerning the flares on red dwarfs was carried out in a series of papers by Grinin and Sobolev [8, 9, 10, 11].

It is clear that the heating by the accelerated particles, mainly electrons, should be accompanied by the gasdynamic motions. This dynamic response of the dense layers of the atmosphere was considered for the first time by Kostiuk and Pikelner [13] and later was considered in a numerous number of papers dedicated to the flares on the Sun and the stars [14, 7, 6, 2, 12, 3].

The optical emission in the gasdynamic model is known to originate in the dense low-temperature condensation between the front of the downward moving shockwave and the heating front. The plot of the density $n = n_{\mathrm{H\,I}} + n_{\mathrm{H\,II}}$ for several instants of a powerful solar flare is given in the left panel of Fig. 1. The density is seen to reach quite high values of the order 10^{15} cm^{-3} in a time of about 10 s.

[1] Sternberg State Astronomical Institute, Lomonosov Moscow State University, Russia
[2] Pushkov Institute of Terrestrial Magnetism, Ionosphere and Radiowaves Propagation (IZMIRAN), Russia

V. Grinin et al. (eds) Radiation mechanisms of astrophysical objects. Yerevan: Edit Print, 2017, pp. 223–228.

Although the aforementioned theoretical works were confirmed by the observations in various aspects, it still remains unclear: are such models able to account for the optical continuum arising in powerful flares on the Sun (and the stars)? In the present work an attempt is made to answer this question and find the conditions for the optical continuum in a flare to arise.

2 Method of solution

In the gasdynamic model the optical radiation arises in a peculiar low-temperature gas condensation. Can the radiation of the condensation give a contribution to the continuum? In order to answer this question, we made use of the calculation [2]. This *gasdynamic* calculation provides the gas density, the temperature, the ionization degree and some other parameters as functions of the column density ξ [cm^{-2}] (the gas is assumed to be pure hydrogen). In the right panel of Fig. 1 the thin solid line represents the electron density in the condensation (other lines will be explained later).

The lower boundary of the condensation (the right one in the figure) is a shock wave through which the undisturbed gas flows into the condensation and heats. This explains the high ionization at the lower boundary. The condensation is limited from above by the hot gas which also heats it due to the thermal conductivity. This explains the high ionization at the upper boundary. The ionization is low in the middle part of the condensation.

Given the density, the temperature and the electron number density, one can calculate the spectrum of the radiation emerging from the condensation. We performed such a calculation by the method described in [15], namely we solved the equations of radiative transfer and statistical equilibrium in the condensation

$$\mu \frac{dI_\nu}{d\tau_\nu} = I_\nu - S_\nu, \tag{1}$$

$$\sum_{j \neq i} n_i R_{ij} = \sum_{j \neq i} n_j R_{ji}. \tag{2}$$

It turned out that such a condensation gives no contribution to the continuum. However, it should be noted that the system of equations solved in [2] did not include either the equations of statistical equilibrium or the charge conservation law. Therefore, after solving the equations (1)–(2), it may turn out that the ion density is not equal to the electron density, i.e. the electroneutrality of the medium may be violated. And this is actually the case. In the right panel of Fig. 1 the thin solid line represents the electron density in the condensation which was taken from the gasdynamic calculation, and the dashed line represents the ion density which is obtained from the solution of the equations (1)–(2). In order to enforce the electroneutrality, one should add one more equation to the system, namely:

$$n_p = n_e, \tag{3}$$

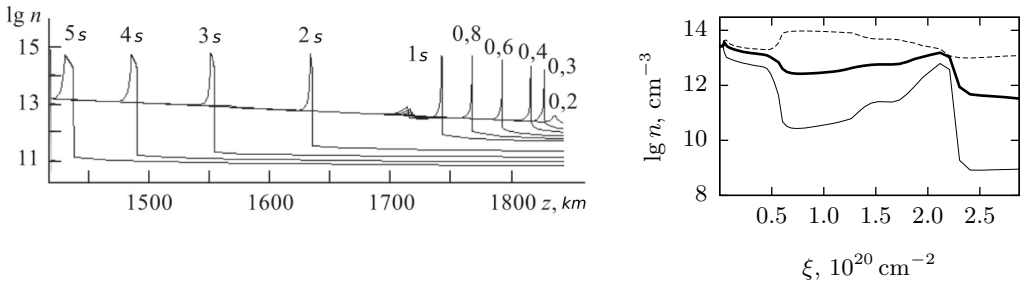

Figure 1: *Left.* The response of the solar atmosphere to the impulsive heating by the non-thermal electrons with the energy flux 10^{11}erg/cm^2/s and sufficiently hard spectrum which corresponds to a powerful solar flare [3]. *Right.* Thin solid line: electron number density in the gasdynamic model. Dashed line: corresponding number density of the ions. Thick solid line: electron and ion number density in case of electroneutrality concerned. The column density ξ is counted from the top of the condensation.

and the electron density should be calculated from the new system of equations instead of being taken from the gasdynamic model. The plot of the electron number density obtained in such a way is represented in the right panel of Fig. 1 by the thick solid line. It is clear from the comparison of this line with the thin solid one that the gasdynamic calculation tends to underestimate the electron density along with the optical depth of the gas in the continuum. Hence, the amount of the continuous radiation is also decreased.

Concerning the impossibility of explaining the optical continuum, we draw attention to one more factor which was not taken into account in [2], namely the irradiation of the condensation by the short-wavelength emission of the hot plasma filling the magnetic loop during the flare. This plasma has the temperature of the order 10^7 K and radiates in XEUV and SXR spectral regions. For a M2 class flare one can use the differential emission measure (DEM) provided by the CHIANTI package [5, 4]. Unfortunately, analogous data for the most powerful solar flares are absent for different reasons, therefore we assumed that for such flares the DEM(T) is an order of magnitude larger than that given in CHIANTI for a M2 class flare and calculated the spectrum of the gas with the density 10^9 cm^{-3} (Fig. 2). Note that this is the spectrum of the coronal gas only, therefore the flux in the He II 304 Å line can be underestimated.

First of all let us consider a simplified problem. Suppose there is a layer of hydrogen of a finite width with a given density and temperature (we call this temperature "initial"). The layer is irradiated by the photosphere. Moreover, in the layer there are artificial sources of heat which, along with the photospheric radiation and the radiation of the layer itself, maintain the given (initial) temperature. These artificial sources are introduced in order not to consider the evolution of the whole process in time, but instead to use the gasdynamic solution (or its analogue) for a certain instant. In other words, we replace the non-stationary problem with a stationary one. It is justified since beginning with approximately the time of 2 s, the evolution of the condensation is

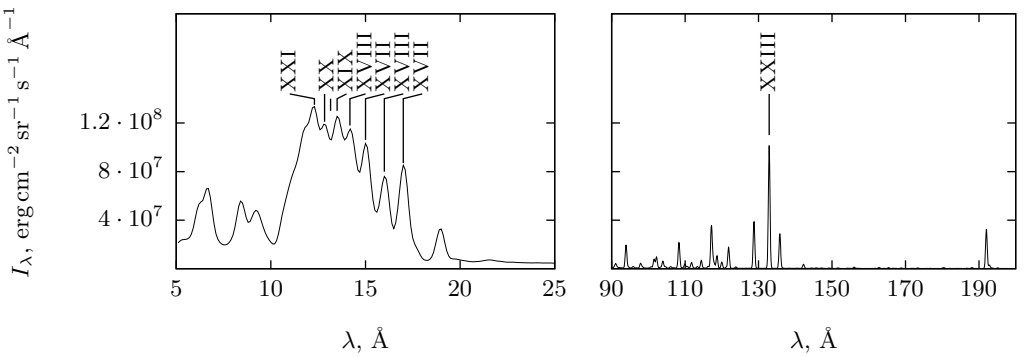

Figure 2: Two parts of the spectrum of the hot flaring plasma. The numbers indicate the ionization stage of the iron atom emitting the relevant line.

essentially quasi-stationary and its structure changes little with time (of course, up to a certain time). In fact, the parameters of the condensation depend on the time. In particular, the temperature is determined by the equation of energy. But taking into account the above consideration, we eliminate the dependence on the time, and in order to maintain the temperature at a given level, we introduce the artificial heat sources. Thus, we assume the validity of the condition of radiative equilibrium with the additional heat source in the layer. This condition takes the form

$$4\pi \int \eta_\nu d\nu = q + \int d\Omega \int I_\nu \chi_\nu d\nu, \tag{4}$$

where η_ν, χ_ν are the emissivity and opacity, and q is the power of the artificial sources. From this relation we find the power of the artificial sources

$$q = 4\pi \int \eta_\nu d\nu - \int d\Omega \int I_\nu \chi_\nu d\nu. \tag{5}$$

So, solving the equations (1)–(4) with the numerical values of q found from the equation (5), we obtain the populations of the atomic levels, the ionization degree and the temperature in the condensation, the latter being equal to the initial temperature. Now in order to take into account the X-ray source, we have to solve the equations (1)–(4) with *the same* sources q, but the upper boundary condition in the equation of radiative transfer should correspond to the X-ray emission falling on the condensation from above. As a result, we obtain the new populations, ionization degree and the new temperature which is higher than the initial one. We also calculate the spectrum of the radiation emerging from the condensation and can compare it with the spectrum of the quiet Sun to see if any additional continuum arises in the condensation and how large it is. Let us compare the specific intensity at the disc center of the radiation emerging from the condensation I_c and the radiation of the

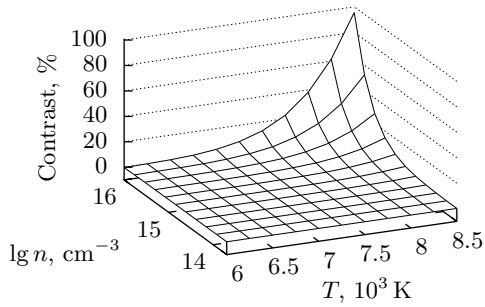

Figure 3: Contrasts in per cents for various values of the density and temperature of the condensation.

photosphere I_p at the wavelength 4500 Å. Let us term the quantity $(I_\mathrm{c} - I_\mathrm{p})/I_\mathrm{p}$ the contrast.

In our calculations we represent the condensation as a finite homogenous layer of the width 50 km as in the gasdynamic solution. The density and the initial temperature are varied in the ranges from 5×10^{13} to 10^{16} cm^{-3} and from 6000 to 8500 K, respectively. The plot of the contrasts is shown in Fig. 3.

It is seen that the high contrasts (>10%) are reached only at high densities ($\sim 10^{15}$ cm^{-3}) and temperatures (∼8500 K).

Taking into account the external radiation in the gasdynamic response of the chromosphere to the heating should change the physical conditions inside the condensation. Namely, at the beginning of the process, when the condensation is tenuous, the external radiation should prevent the strong cooling (and hence the decrease of the ionization degree) in the middle of the condensation. But by the end of the non-thermal particle heating (approximately in 10 s after the onset of the response) the condensation would propagate quite deep and its density would increase while the temperature throughout it would still be high due to the "preliminary" heating by the X-rays. This provides the generation of the optical continuum. In other words, the optical thickness of the condensation at the wavelength 4500 Å becomes $\gtrsim 0.03$.

3 Conclusions

The general idea of the relation between the origin of the optical continuum and the impact of the accelerated particles on the atmosphere which was put forward by Grinin and Sobolev is of current interest. The further development of the gasdynamic model with account of the absorption of the short-wavelength radiation is desired. Following this way may probably help to understand the emergence of the powerful optical continuum. Note that the radiation of the condensation is most likely related to the blue continuum whereas the lower-temperature red continuum can arise as a consequence of the irradiation of the upper photosphere by the soft X-rays from the large cloud of the hot plasma which forms during a flare (as it is stated in [1]).

Acknowledgments. We thank Farid Goryaev for his help with CHIANTI. This work was partially supported by Russian Foundation for Basic Research (grants No. 14-02-00922 and 15-02-06271) and by the grant from Russian Federation President supporting Leading Scientific Schools 1675.2014.2.

CHIANTI is a collaborative project involving the following Universities: Cambridge (UK), George Mason and Michigan (USA).

References

1. *J.C. Allred*, *A.F. Kowalski*, *M. Carlsson*, Astrophys. J., **809**, 104, 2015.
2. *A.Ya. Boiko*, *M.A. Livshits*, Astron. Rep., **39**, 338, 1995.
3. *A.Ya. Boiko*, *M.A. Livshits*, Astrophys. Space Sci., **274**, 299, 2000.
4. *G. Del Zanna*, *K.P. Dere*, *P.R. Young*, *E. Landi*, *H.E. Mason*, Astron. Astrophys., **582**, A56, 2015.
5. *K.P. Dere*, *J.W. Cook*, Astrophys. J., **229**, 772, 1979.
6. *A.G. Emslie*, Solar Phys., **121**, 105, 1989.
7. *G.H. Fisher*, *R.C. Canfield*, *A.N. McClymont*, Astrophys. J., **289**, 414, 1985.
8. *V.P. Grinin*, *V.V. Sobolev*, Astrophys., **13**, 348, 1977.
9. *V.P. Grinin*, *V.V. Sobolev*, Astrophys., **28**, 208, 1988.
10. *V.P. Grinin*, *V.V. Sobolev*, Astrophys., **31**, 729, 1989.
11. *V.P. Grinin*, *V.M. Loskutov*, *V.V. Sobolev*, Astron. Rep., **37**, 182, 1993.
12. *M.M. Katsova*, *A.Ya. Boiko*, *M.A. Livshits*, Astron. Astrophys., **321**, 549, 1997.
13. *N.D. Kostiuk*, *S.B. Pikelner*, Sov. Astron., **18**, 590, 1975.
14. *M.A. Livshits*, *O.G. Badalyan*, *A.G. Kosovichev*, *M.M. Katsova*, Solar Phys., **73**, 269, 1981.
15. *G.B. Rybicki D.G. Hummer*, Astron. Astrophys., **262**, 209, 1992.

Moving Inhomogeneous Envelopes of Stars

L.M. Oskinova[1], B. Kubátová[2,3], W.-R. Hamann[1]

E-mail: *lida@astro.physik.uni-potsdam.de*

Luminous hot massive stars drive strong stellar winds. New observations together with progress in model calculations reveal that these winds are highly inhomogeneous. Building on the foundations laid by V.V. Sobolev and his school, we are now developing new methods to analyze stellar spectra emerging from such winds. Among them are the new sophisticated 3D models of radiation transfer in inhomogeneous expanding media that elucidate the physics of stellar winds and improve empiric mass-loss rate diagnostics.

1 Empirical diagnostics of stellar winds using UV resonance lines

Strong ionizing radiation and stellar winds of massive stars with OB spectral types strongly influence the physical conditions in the interstellar medium and affect the formation of new generations of stars and planets.

Hot star winds are driven by their intense ultraviolet (UV) radiation [1]. Theory predicts that the winds remove the mass with a rate $\dot{M} \approx 10^{-7} - 10^{-5} M_\odot\,\mathrm{yr}^{-1}$ depending on the fundamental stellar parameters: $T_{\rm eff}$, $L_{\rm bol}$, and $\log g$ [2]. Hence, during the life time of a massive star (up to a few$\times 10^7$ yr), a significant fraction of its mass is removed by the wind. Thus, the mass-loss rate is a crucial factor of stellar evolution.

Empirical diagnostics of mass-loss rates largely rely on a spectroscopic analysis of resonance lines from abundant ions. When formed in a wind, these lines typically display P Cygni-type profiles. The resonance lines are produced by a photon scattering, hence the line strength and shape depend on the wind velocity and density. The latter obeys a continuity equation $\dot{M} = 4\pi v(r) r^2 \rho$. Therefore, by fitting a model line to the observed one, it is possible to estimate the wind velocity, density, and the mass-loss rate.

Line formation in a moving stellar envelope was studied by V.V. Sobolev [3]. It was shown that *if* the thermal motions in the atmosphere can be neglected compared to the macroscopic velocity, the radiative transfer problem can be significantly simplified [4]. This is now known as the *Sobolev approximation.*

Hot star winds are fast, with typical velocities of a few$\times 1000\,\mathrm{km\,s}^{-1}$, justifying the use of Sobolev approximation for modeling their resonance lines [5, 6].

[1] Institute for Physics and Astronomy, University of Potsdam, Germany
[2] Astronomický ústav AV ČR, Czech Republic
[3] Matematički institut SANU, Serbia

V. Grinin et al. (eds) Radiation mechanisms of astrophysical objects. Yerevan: Edit Print, 2017, pp. 229–234.

Such models were used to estimate mass-loss rate already from the first available UV spectra of O-type stars [7, 8].

However, with time it became clear that the high turbulence in stellar winds limits the applicability of the Sobolev approximation. The error in the modeling arises mainly from the treatment of the formal integral and, to a lesser extent, from the approximated source function [9]. This is accounted for in the "Sobolev with Exact Integration" method (SEI), which treats the source function in Sobolev approximation, while finding exact integration for the transfer equation [10]. As a result, the model provides significantly better fit to the observed lines [11], and allows for more precise mass-loss rate determinations [12].

From the observational side, the problem with mass-loss determinations is that the strong resonance lines of the CNO elements are saturated in spectra of Galactic O-type stars. Therefore, these lines are not sensitive to the precise values of mass-loss rates. On the other hand, the resonance doublet of P V $\lambda\lambda$1117, 1128 Å is never saturated because of a low phosphorus abundance ($\sim$1000 times less than the carbon one). Moreover, P V is a dominant ionization stage in O stars, hence its ionization fraction is nearly unity. This makes P V doublet very useful for the mass-loss rate measurements [13].

The Far Ultraviolet Spectroscopic Explorer (*FUSE*) measured spectra of P V for many O-type stars. The observed lines were weak, and the mass-loss rates derived from their modeling with the SEI method were found to be much smaller than expected [13]. It was concluded that either the true mass-loss rates are very small, or the traditional diagnostics of resonance lines are not suitable because of the strong stellar wind clumping.

2 Stellar wind clumping

There are clear evidences of stellar wind inhomogeneity. E.g., stochastic variability in the He II λ4686 Å emission line in the spectrum of an O supergiant was explained by a clump propagating in its stellar wind [14]. The line-profile variability of Hα observed in a large sample of O-type supergiants was attributed to the presence of shell fragments in structured winds [15]. Using spectral diagnostics, it was shown that the winds of B supergiants are clumped [16]. The spectral lines of OB stars are variable on various time scales likely because of the wind clumping and structuring [17]. In high-mass X-ray binaries, accretion from the clumped stellar wind onto a neutron star powers strongly variable X-ray emission [18].

Stellar wind clumping is included in the modern non-LTE stellar atmosphere models [20, 21], using the usual approximation of *microclumping*, i.e. an assumption that all clumps in stellar wind are optically thin. Hence, the radiative transfer is significantly simplified in such models.

Assume that the density inside the clumps is enhanced by a factor D compared to a smooth model with the same mass-loss rate $\dot{M}$, while the interclump medium is void (i.e. the clump volume filling factor is $f_{\rm V} = D^{-1}$). Then, in the stellar

atmosphere models, the rate equations have to be solved only for the clumps with the density $D\rho$ (instead of ρ as in the smooth wind case). In this case the mass-loss rates derived from fitting the lines that depend on the square of the density (such as, e.g., the recombination Hα line) will be by a factor $\sqrt{D}$ lower compared to the smooth wind models. On the other hand, mass-loss rates derived from the resonance lines (where both absorption and re-emission scales linearly grow with density) are not affected by microclumping.

3 Macroclumping

Albeit microclumping approximation is very convenient, it is too stringent for realistic stellar winds. Since optical depth in the UV resonance lines is high and the line photon mean free path is short, the wind clumps are likely to be optically thick at these wavelengths [19, 16]. To understand how such optically thick clumping ("macrocluming") affects the resonance line formation, it is useful to consider the Sobolev approximation. According to this approximation, only the matter close to the constant radial velocity surface contributes to the line optical depths. In a clumped wind, this surface will be porous (Fig. 1). Moreover,

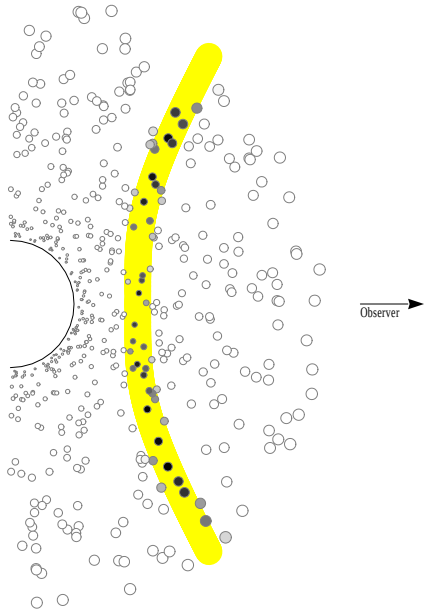

Figure 1: Sketch of a clumped stellar wind. In a smooth wind, rays of a given observer's frame frequency encounter line opacity only close to the "constant radial velocity surface" (thick shaded line). In a clumpy wind, assuming that the clumps move with the same velocity law as in the homogeneous wind, only those clumps interact with the ray that lie close to the corresponding constant radial velocity surface (dark-shaded circles). All other clumps are transparent (open circles) if the continuum opacity is small, so the wind is porous with respect to line absorption, even when the total volume is densely packed with clumps. Adopted from Oskinova et al. [19].

the opacity depends not only on geometrical matter distribution, but also on the Sobolev length $v_{\rm D}(dv/dr)^{-1}$, where $v_{\rm D}$ denotes the velocity dispersion within a clump. Correspondingly, the smaller the velocity dispersion within each clump, the narrower the constant radial velocity surface. Consequently, a smaller number of clumps can contribute to opacity, farther reducing it.

Adopting a statistical treatment of effective opacity $\kappa_{\rm eff}$, a correction factor for macroclumping that can be easily included in a sophisticated non-LTE codes was derived [19]. One can show that

$$\kappa_{\rm eff} = \kappa_{\rm f} \, \frac{1 - e^{-\tau_{\rm C}}}{\tau_{\rm C}} \equiv \kappa_{\rm f} \, C_{\rm macro}. \tag{1}$$

The factor $C_{\rm macro}$ describes how macroclumping changes the opacity in the microclumping limit $\kappa_{\rm f}$. Note that for optically thin clumps ($\tau_C \ll 1$), the microclumping approximation ($\kappa_{\rm eff} \approx \kappa_{\rm f}$) is recovered. For optically thick clumps ($\tau_C \gtrsim 1$), however, the effective opacity is reduced by a factor $C_{\rm macro}$ compared to the microclumping approximation.

4 Radiative transfer using realistic 3D Monte-Carlo wind models

The statistical treatment of macroclumping provides only a first approximation for radiative transfer in clumped winds. For in-depth studies, the full 3D models of clumped winds are developed [22, 23]. In these models the density and velocity of the wind can be arbitrarily defined in a 3D space and can be non-monotonic. The photons are followed along their paths using the Monte Carlo approach. Allowing for an arbitrary optical depth, clumps can be optically thick in the cores of resonance lines, while they remain optically thin at all other frequencies. The model lines are calculated and compared to the observed ones.

Detailed study showed that strengths and shape of the resonance lines depend on the spatial distribution of clumping, density contrast, and velocity field [22]. Overall, these 3D models confirmed that macroclumping reduces effective opacity in the resonance lines, and rigorously proved that in realistic winds the P Cygni profiles of resonance lines are different from those in smooth and stationary 3D winds.

The models were compared with the observed spectra of five O-type stars to measure their mass-loss rates and other wind parameters [23]. This was done using a combination of the non-LTE Potsdam Wolf-Rayet (PoWR) stellar atmospheres (Fig. 2) and the Monte Carlo routine for the transfer of radiation in resonance lines. It was shown that the strength of model P V lines is reduced in realistic 3D models compared to the smooth wind models. Therefore, the observed lines could be fitted with high mass-loss rates similar to those theoretically expected (Fig. 3).

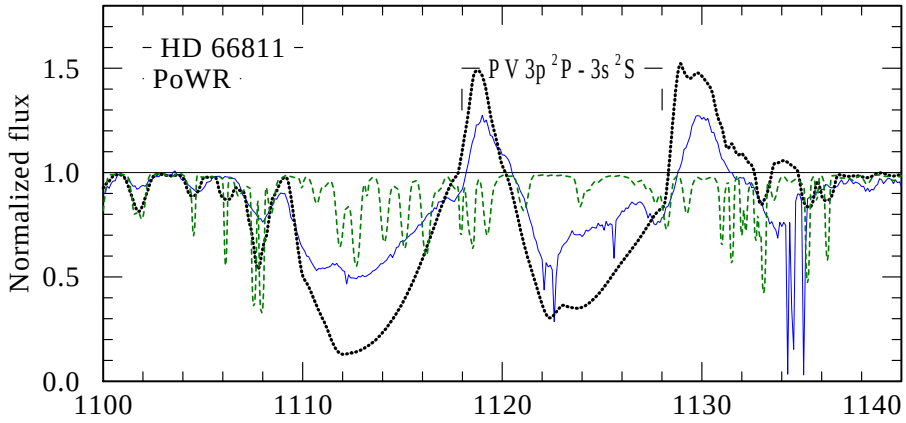

Figure 2: Comparison of observed and model spectra of P V in the O4I star HD 66811 (ζ Pup). Thin solid-blue lines is the observed spectrum. Dotted black line is the PoWR model spectrum adopting $\dot{M} = 2.5 \times 10^{-6}\, M_\odot\, \mathrm{yr}^{-1}$. The dashed-green lines are from the same model, but only accounting for the photospheric lines while wind contribution is suppressed.

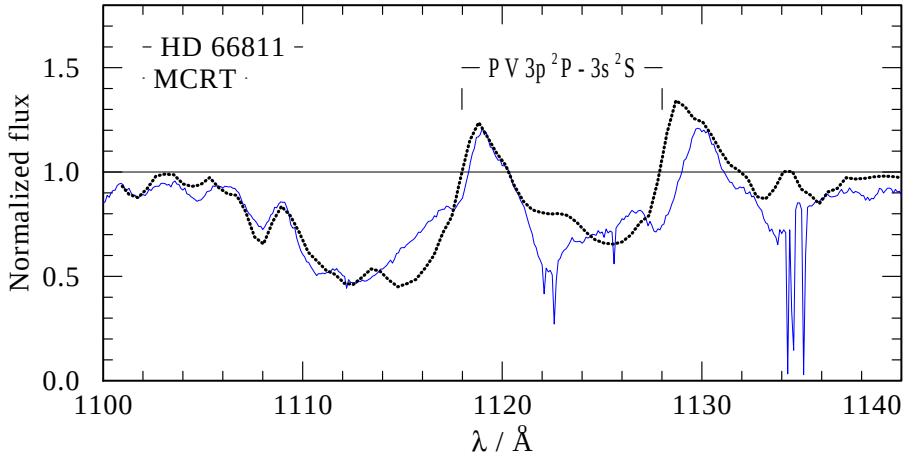

Figure 3: The same as in Fig. 2, but now the dotted black line is computed with the 3D Monte Carlo wind model, using the PoWR photospheric spectrum as input. The adopted mass-loss rate is $\dot{M} = 2.5 \times 10^{-6}\, M_\odot\, \mathrm{yr}^{-1}$. The line strength is significantly reduced compared to Fig. 2 despite the same adopted $\dot{M}$. See model details in Surlan et al. [23].

To summarize, the advances of macroclumping approach and 3D wind modeling improved empiric mass-loss rate diagnostics and showed that the mass-loss rates of OB supergiants are in good agreement with the theoretical predictions. Depending on the adopted clumping parameters, the observed spectra can be well reproduced with only a factor of 1–3 reduction compared to the predicted ones.

Thus, macroclumping is a new step in our quest for realistic descriptions of stellar wind, which would have been not possible without deep insights of V.V. Sobolev and his school into the physics of moving stellar envelopes.

References

1. *J.I. Castor, D.C. Abbott, R.I. Klein*, Astrophys. J., **195**, 157, 1975.
2. *A. Pauldrach, J. Puls, R.P. Kudritzki*, Astron. Astrophys., **164**, 86, 1986.
3. *V.V. Sobolev*, Moving Envelopes of Stars. Cambridge: Harvard Univ. Press, 1960 (Original in Russian: Dvizhushchiesya Obolochki Zvezd. Leningrad: Izd. Leningr. Univ., 1947).
4. *V.P. Grinin*, Astrophys., **44**, 402, 2001.
5. *J.I. Castor*, Mon. Not. Roy. Astron. Soc., **149**, 111, 1970.
6. *L.B. Lucy*, Astrophys. J., **163**, 95, 1971.
7. *J.I. Castor, H.J.G.L.M. Lamers*, Astrophys. J. Suppl., **39**, 481, 1979.
8. *P.S. Conti, C.D. Garmany*, Astrophys. J., **238**, 190, 1980.
9. *W.-R. Hamann*, Astron. Astrophys., **100**, 169, 1981.
10. *H.J.G.L.M. Lamers, M. Cerruti-Sola, M. Perinotto*, Astrophys. J., **314**, 726, 1987.
11. *M.A.T. Groenewegen, H.J.G.L.M. Lamers*, Astron. Astrophys. Suppl., **79**, 359, 1989.
12. *H.J.G.L.M. Lamers, S. Haser, A. de Koter, C. Leitherer*, Astrophys. J., **516**, 872, 1999.
13. *D. Massa, A.W. Fullerton, G. Sonneborn, J. B. Hutchings*, Astrophys. J., **586**, 996, 2003.
14. *T. Eversberg, S. Lépine, A.F.J. Moffat*, Astrophys. J., **494**, 799, 1998.
15. *N. Markova, J. Puls, S. Scuderi, H. Markov*, Astron. Astrophys., **440**, 1133, 2005.
16. *R.K. Prinja, D.L. Massa*, Astron. Astrophys., **521**, L55, 2010.
17. *S. Lépine, A.F.J. Moffat*, Astron. J., **136**, 548, 2008.
18. *L.M. Oskinova, A. Feldmeier, P. Kretschmar*, Mon. Not. Roy. Astron. Soc., **421**, 2820, 2012.
19. *L.M. Oskinova, W.-R. Hamann, A. Feldmeier*, Astron. Astrophys., **476**, 1331, 2007.
20. *W.-R. Hamann, L. Koesterke*, Astron. Astrophys., **335**, 1003, 1998.
21. *D.J. Hillier, D.L. Miller*, Astrophys. J., **519**, 354, 1999.
22. *B. Šurlan, W.-R. Hamann, J. Kubát, L.M. Oskinova, A. Feldmeier*, Astron. Astrophys., **541**, A37, 2012.
23. *B. Šurlan, W.-R. Hamann, A. Aret, J. Kubát, L.M. Oskinova, A.F. Torres*, Astron. Astrophys., **559**, A130, 2013.

* The color figures are available online in the Proceedings at *http://www.astro.spbu.ru/sobolev100/*.

Outflows and Accretion on the Late Phases of PMS Evolution. The Case of RZ Psc

I.S. Potravnov[1], V.P. Grinin[1,2], D.E. Mkrtichian[3], D.N. Shakhovskoy[4]

E-mail: *ilya.astro@gmail.com*

We consider the spectral variability of the post T Tauri star RZ Psc. The star does not show clear accretion traces, but at the same time it has distinct variable blue-shifted features in the Na I D resonance doublet and lines of other alkali metals which indicate the matter outflow from the stellar vicinity. We suppose that in case of RZ Psc we deal with the special type of interaction between the remnants of accreting gas and stellar magnetosphere in the "magnetic propeller" regime. It is expected that accretion in the propeller regime exists in some others young stars.

1 Introduction

Over three recent decades the magnetospheric accretion paradigm was developed and improved to explain the observed activity among young solar type stars. These so-called T Tauri stars actively accrete the matter from their protoplanetary disks and possess the notable spectroscopic evidences for complex gas motion in the near vicinity of the star. The profiles of the strong hydrogen emission lines and lines of some metals reveal the accretion infall as well as the less significant matter outflow due to the magnetospheric conical and X-wind. The overview of the basic concepts of the theory and its application to the observations can be found in the review by Bouvier et al. [1].

According to the recent investigations of several open clusters and young stellar associations, the phase of the actively accreting T Tauri star lasts only few million years (Myr) (see, e.g., the review by Williams and Chieza [2]). During this period the circumstellar disk evolves from an optically thick gaseous and dusty protoplanetary disk into an optically thin debris disk consisting of large particles, planetesimals, and planets. From the observational point of view, this evolution is reflected by a difference between the "Classical" (CTTS), "Weak line" (WTTS), and "Post" T Tauri stars. The last two subclasses in this sequence possess the mild characteristics of activity which decay with their age. Fedele et al. [3] show that on the timescale of 10 Myr accretion becomes vanishingly small (less than

[1] Pulkovo Astronomical observatory, Russia
[2] Sobolev Astronomical Institute of the St. Petersburg University, Russia
[3] National Astronomical Research Institute of Thailand
[4] Crimean Astrophysical Observatory, Crimea

V. Grinin et al. (eds) Radiation mechanisms of astrophysical objects. Yerevan: Edit Print, 2017, pp. 235–240.

$10^{-11} M_\odot$ yr^{-1}). Hence, the spectroscopic traces of the accretion/outflow process should also disappear on such a timescale.

The careful investigation of the stars near or even above this limit has the crucial importance for our understanding of the late stages of Pre-Main Sequence evolution. In the systems with the low accretion rate some special cases of interaction between stellar magnetosphere and remnants of the accreting gas can arise and can be studied in its "pure form". Such observational traces are not masked by the more prominent accretion features typical of early stages of the PMS evolution.

One of such unique objects is the star RZ Psc.

2 RZ Psc and its spectroscopic behavior

RZ Psc belongs to the family of young variable UX Ori type stars. The photometric and polarimetric activity of these stars is caused by the variable circumstellar (CS) extinction [4]. RZ Psc is one of the coolest (Sp = K0 IV) and eldest member of the family. According to the latest estimates, based on calculating the trajectory of the star in the gravitational potential of Galaxy, its age is about 25±5 million years [5, 6]. This value is considerably higher than the characteristic lifetime of the accretion disks and means that the star is surrounded by the significantly evolved accretion disk.

The spectrum of the RZ Psc strongly resembles the spectrum of a star that already passed the stage of the T Tauri stars, without any prominent emission features above the continuum level. There is the only important exception: the lines of the resonance sodium doublet Na I D show the blue-shifted absorption components which manifest the gas motion from the star toward the observer [7]. These absorption details were initially discovered in the spectra obtained in

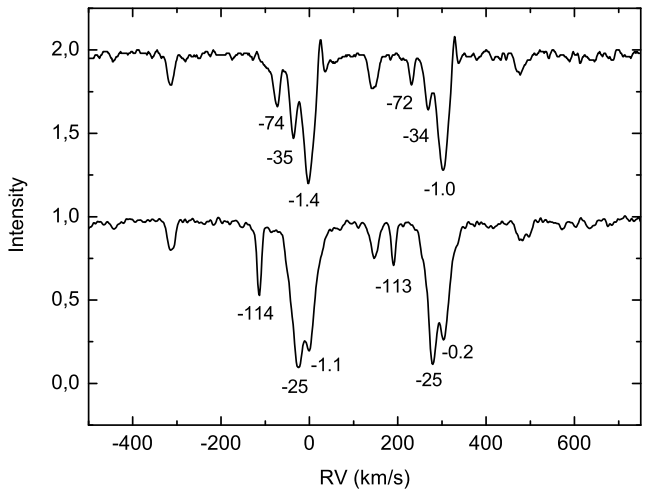

Figure 1: The Na I D lines in the spectra of RZ Psc observed with NOT.

the Peak Terskol Observatory during the seasons 2009–2012 with the moderate spectral resolution $R \sim 13500$ [7]. It should be stressed that despite blue-shifted absorptions are highly variable, no red-shifted details or signs of emission in Na D lines has been observed.

These details are very notable on the pair of the high-resolution FIES spectra ($R \sim 46000$), obtained in August and November 2013 by I. Ilyin with 2.56 m Nordic Optical Telescope (see [9] and Fig. 1).

The subsequent observations were carried out by one of the authors of our paper (D.E.M.) at the 2.4 m telescope of the Thai National Observatory with MRES echelle spectrograph in December 2014. The covered region was from 4400 to 8800 Å that allowed us to include lines of other alkali metals K I and Ca II into consideration. These lines are presented in Fig. 2.

One can see an appearance of the variable blue-shifted absorption components in Na I D lines which are accompanied by the similar structures in the K I 7699 Å line. The features in the K I line are less prominent due to the lower potassium abundance, but reach their maximum when the sodium lines also show the strongest additional absorption. The Ca II 8542 Å line belongs to the calcium IR triplet and demonstrates more complicated picture. The line core is filled in by the variable emission, while the additional low-velocity absorption appears on several dates. Nevertheless, RZ Psc still does not possess any clear accretion signs in its spectra.

The possible key to this mystery came from observations of the Hα line. It also has the pure absorption profile in RZ Psc spectrum. But a careful comparison of it with the synthetic profile and profile observed in the spectrum of the standard star σ Dra (K0 V) reveals the presence of the weak variable emission component in the central part of the Hα line. The spectral subtraction technique shows the narrow emission peak, that can be probably attributed to the chromospheric activity, and the broad (up to $\pm$ 200 km s^{-1}) emission base forms in the accreting matter (Fig. 3).

3 Discussion and conclusions

Measurement of the equivalent width (EW) of the Hα emission in RZ Psc spectra gives the mean value of about 0.5 Å. This value is significantly less than the standard value of 10 Å which separates the actively accreting CTTS from WTTS. According to this criteria, we can call RZ Psc as "the very Weak line T Tauri star". Measurement of Hα emission EW allows us to estimate the accretion rate in the system, using the empirical relationship between the observed emission line luminosity and total accretion luminosity from [8]. The obtained value $\dot{M} \sim 7 \times 10^{-12} M_{\odot}\,\mathrm{yr}^{-1}$ is an upper limit of the real accretion rate, because the Hα line in the RZ Psc spectrum possibly arises not only in the accreting matter but also in the stellar chromosphere. Nevertheless, this accretion rate is the lowest one known from the literature.

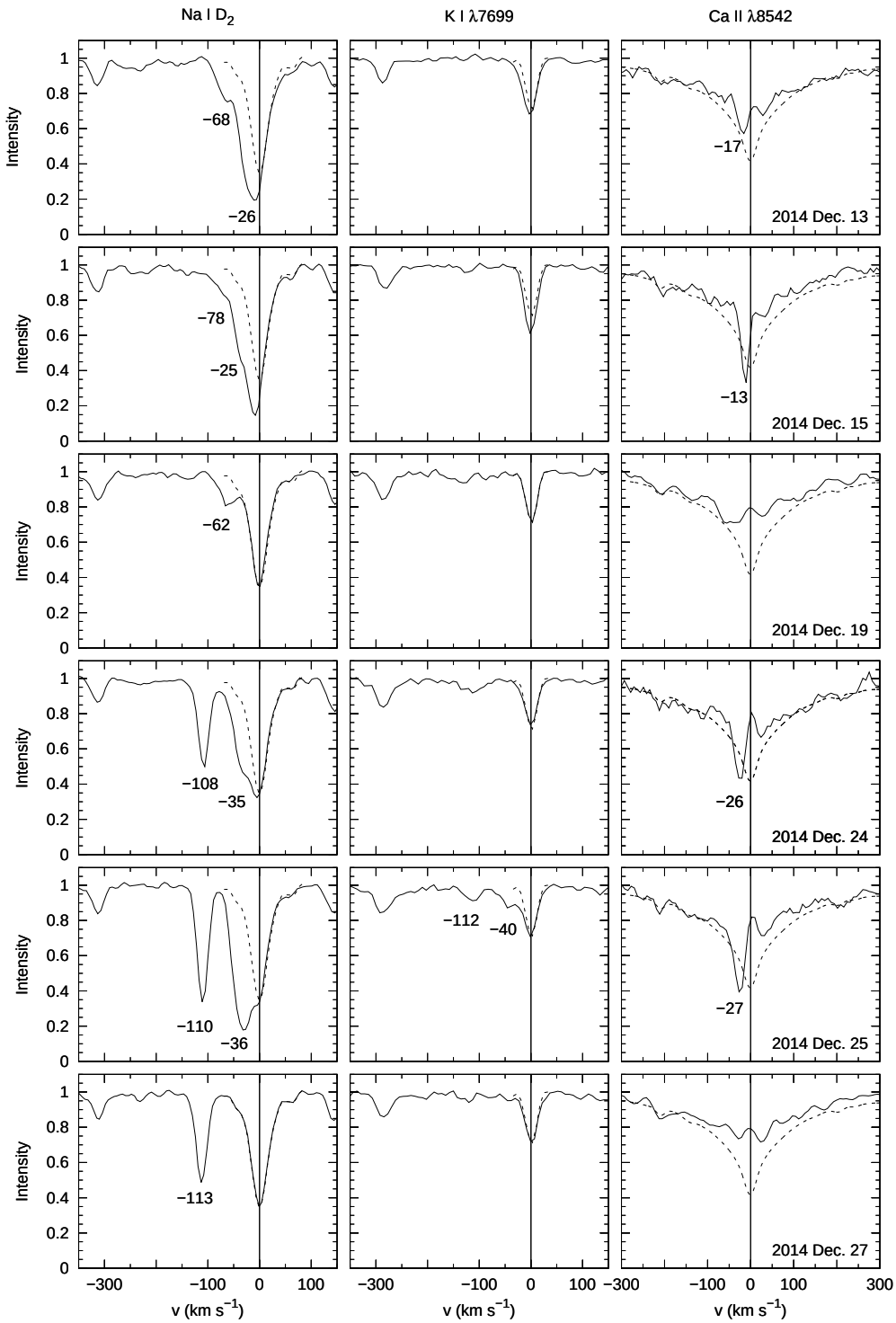

Figure 2: Alkali metal lines observed in the RZ Psc spectra with the MRES. The velocities in km s^{-1} of the variable absorption components are labeled. The reference photospheric profiles are plotted by dashed line.

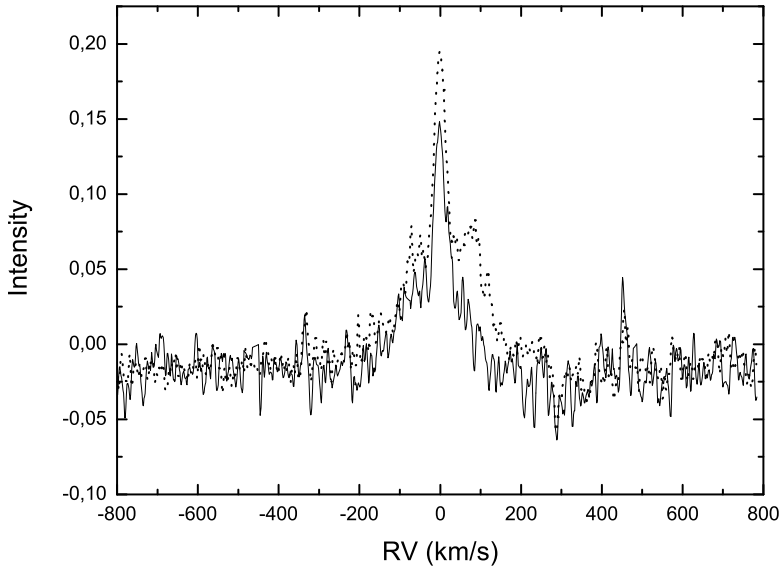

Figure 3: The emission components of the Hα line obtained after subtraction of the synthetic profile from the observed ones. Solid line corresponds to the observations obtained on Aug. 19, 2013, while the dotted line shows spectrum obtained on Nov. 21, 2013.

Hence, in the case of RZ Psc, we deal with the extremely low accretion rate and, at the same time, with nontrivial spectroscopic signs of the matter outflow. We supposed that the gaseous outflow from the RZ Psc vicinity was a result of the action of the so-called "propeller mechanism" arising at the interaction between the stellar magnetosphere and remnants of the gas in the circumstellar disk [9]. This mechanism is realized when the angular velocity of the star (and the magnetosphere) exceeds the angular velocity of the Keplerian disk at the truncation radius in the region where the magnetic field still controls the motion of the gas. The ratio between the corotation and truncation radii depends inversely on the mass accretion rate. When it is small, the truncation radius can significantly exceed the corotation radius. Under this conditions, most of the accreting matter is scattered into the surrounding space.

There are observational evidences (so-called AA Tau effect) that the situation, when the axis of magnetic dipole does not coincide with the rotational axis of the star, is not rare among young T Tauri stars (see, e.g., [10, 11]). Numerical simulations by Romanova et al. [12] showed that interaction between the accreting gas and inclined magnetic dipole produced the special case of a biconical outflow consisted of two expanding spiral structure. The multiple intersection of the line of sight by the spiral can produce the corresponding absorption lines shifted relatively to the star velocity.

Similar narrow absorption details are observed in the NaI D lines in the spectra of some other young stars such as MWC 480, NY Ori and BBW 76. However, these objects are at earlier evolutionary stages and show spectroscopic

signs of accretion. However, the magnetic propeller regime is not necessary phase of the evolution of T Tauri stars. The unstable behavior of the gaseous outflow significantly complicates the theoretical modeling. Sobolev's theory for the medium with large velocity gradients was developed and applied to the media where the gas density was determined from the continuity equation. In the case of RZ Psc, the situation is quite different: narrow absorption components in the lines of the sodium doublet in combination with the lack of the emission in these lines indicate that the absorbing gas fills in only the minor part of the whole solid angle 4π (see [9]). It is important to learn how to calculate the profiles and intensities of the spectral lines formed in such conditions.

A more detailed description and discussion of the spectral variability of RZ Psc will be forthcoming.

Acknowledgments. This research has been supported in part by the Russian Foundation for Basic Research (Projects 15-02-09191 and 15-02-05399).

References

1. *J. Bouvier, S.H.P. Alencar, T.J. Harries et al.*, in Protostars and Planets V. Eds. Bo Reipurth et al. Tucson: Univ. Arizona Press, 2007, p. 479.
2. *J.P. Williams, L.A. Cieza*, Ann. Rev. Astron. Astrophys., **49**, 67, 2011.
3. *D. Fedele, M.E. van den Ancker, Th. Henning et al.*, Astron. Astrophys., **510**, A72, 2010.
4. *V.P. Grinin, N.N. Kiselev, G.P. Chernova et al.*, Astrophys. Space Sci., **186**, 283, 1991.
5. *V.P. Grinin, I.S. Potravnov, F.A. Musaev*, Astron. Astrophys., **524**, A8, 2010.
6. *I.S. Potravnov, V.P. Grinin*, Astron. Lett., **39**, 776, 2013.
7. *I.S. Potravnov, V.P. Grinin, I.V. Ilyin*, Astrophys., **56**, 453, 2013.
8. *E. Rigliaco, A. Natta, L. Testi et al.*, Astron. Astrophys., **548**, A56, 2012.
9. *V.P. Grinin, I.S. Potravnov, I.V. Ilyin et al.*, Astron. Lett., **41**, 407, 2015.
10. *J. Bouvier, S.H.P. Alencar, T. Boutelier et al.*, Astron. Astrophys., **463**, 1017, 2007.
11. *O.Yu. Barsunova, V.P. Grinin, S.G. Sergeev*, Astrophys., **56**, 395, 2013.
12. *M.M. Romanova, G.V. Ustyugova, A.V. Koldoba et al.*, Mon. Not. Roy. Astron. Soc., **399**, 1802, 2009.

Activity and Cool Spots on the Surfaces of Stars with Planetary Systems and G-type Stars with Superflares from Kepler Observations

I.S. Savanov[1]

E-mail: *isavanov@inasan.ru*

Based on the photometric observations obtained with the Kepler telescope, we investigated the properties of the active regions (cold spots) on the surfaces of stars with planetary systems (exoplanets) and G type superflare stars. Three methods for determining the spottedness (S) of stellar surfaces were used. We studied the dependencies of the spottedness of the stars with exoplanets on the effective temperature and on the period of their axial rotation. In most cases the spottedness of stars with planetary systems does not exceed 5% of the area of their surface. The properties of active regions (cool spots) on the surfaces of 279 G-type stars in which more than 1500 superflares with energies of 10^{33}–10^{36} erg were analyzed. Three groups of stars with different surface spottednesses can be distinguished in a plot of superflare energy vs. cool-spot area. It is confirmed that the flare activity is not related directly to circumpolar active regions, since the majority of the points on the diagram lie to the right of the dependence for $B = 1000$ G and $i = 3°$.

1 Observational data and methods of analysis

Using the high-accuracy photometric observations obtained with the Kepler telescope, we studied the properties of the active areas (cool spots) on the surfaces of stars with planetary systems. The analysis was carried out using the data on 737 objects for which the rotation periods were estimated in [1] and reliable estimates of atmospheric parameters were available. Three methods of stellar surface spottedness estimation from the photometric observations were reviewed (the values $S1$, $S2$, and $S3$). On the example of two stars (KOI 877 and KOI 896) from the full sample of 737 stars, we compared the results of the $S1$–$S3$ estimation with the three mentioned methods. It was found that the results of the accurate calculations ($S1$) and estimations ($S2$) by the method of [2] correspond to each other, although the values of the latter are systematically higher.

It was shown that the method proposed in [3] and modified by us in [2] can be applied to a large enough sample of objects and, most importantly, it

[1] Institute of Astronomy, Russian Academy of Sciences, Russia

V. Grinin et al. (eds) Radiation mechanisms of astrophysical objects. Yerevan: Edit Print, 2017, pp. 241–244.

yields homogeneous data which can be used for statistical estimation and finding dependencies of general nature. This allowed us from the brightness variability data for 34 030 objects from [4] to find the S parameters for the analysis of the distribution of the S on the effective temperature for different objects.

For the late type stars with planetary systems, we used the data from Table 1 in [1] for 12 Quarters of observations (Q3–Q14). In the final sample we included the data on 737 objects for which in [1] the rotation periods were estimated and reliable estimates of the atmospheric parameters were available (the effective temperature and gravities) and which are not eclipsing binaries (i.e., their photometric variability is associated mainly with the cold spots). According to [1], the estimated rotation periods for the 737 stars under study are in the range of 0.9 to 62 days and the values of the photometric variability R_{var} are in the range of 0.18 to 64 mmag.

Based on our approach we used the specified technique for the analysis of activity of 279 stars in which Shibayama et al. [5] have reported 1547 superflares. For this purpose, we used the data of Table 2 from [5], which contained information both about the photometric variability of these stars and their flare activity.

2 The dependence of the spottedness on the effective temperature and rotation period

We examined the variation of the spottedness ($S2$) for the stars with planetary systems as a function of the effective temperature of these objects and the period of their axial rotation. The $S2$ value for these stars in most cases does not exceed 5% of the area of their surface. The three objects for which it exceeds 5 percent were examined in detail. We have not found any indications that the magnetic activity of a star with exoplanets has any special features that distinguish it from the activity of the stars from a wider sample from [4]. It was found that for the stars with effective temperatures smaller than 5750 K, the spottedness values decrease monotonously with the stellar rotation period decrease. The absence of stars with small S values (smaller than 0.002) was established for the stars with effective temperatures lower than 5750 K and rotation periods up to 10 days. The stars with effective temperatures higher than 5750 K have a very small spottedness for fast-rotating stars, which increases for the objects with the rotation periods of about 20–25 days.

In the case of G-type superflare stars we carried out additional analyses of diagrams plotting the energy of superflares against parameters of the stellar activity (the area of their magnetic spots) and also conducted more extensive studies of the activity of two stars with the highest numbers of superflares [5]. For this aim, we analyzed the properties of the active regions (cool spots) on the surfaces of 279 G stars displaying more than 1500 superflares with energies of 10^{33}–10^{36} erg.

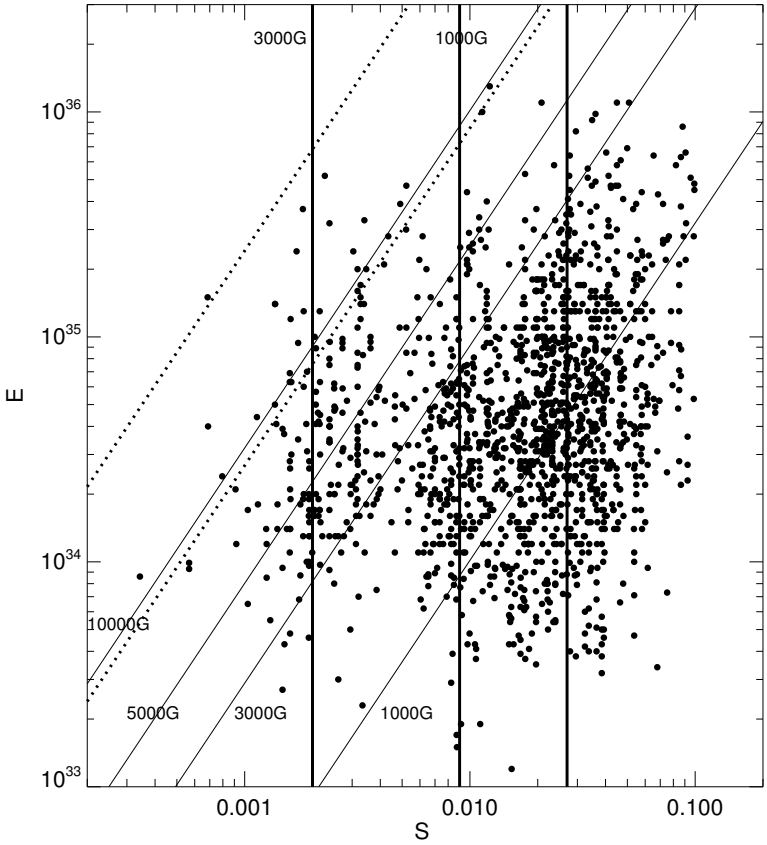

Figure 1: Comparison of the superflare energy E with the spotted area S.

We supplemented the conclusion of [5] that the maximum energy of superflares is independent of the stellar rotational periods P with the suggestion that the entire range of variations of the flare energies is independent of P. Analysis of the diagrams displaying comparisons of the superflare energy and the area occupied by cool spots (Fig. 1) suggests the possible existence of three groups of objects: stars whose spotted areas S exceed 1–1.1 % of the visible area of the star (the most numerous group), stars for which S more than 0.9 %, and stars for which S is less than 0.1 %. The majority of points on this diagram lie to the right of the dependence corresponding to $B = 3000$ G and $i = 90°$ (the first two groups of objects). Based on our new, more precise determinations of the parameter S we have confirmed the conclusion of [6] that the flare activity is not directly related to circumpolar active regions, since the vast majority of points in Fig. 1 lie to the right of the dependence for $B = 1000$ G and $i = 3°$ (the stars are essentially viewed pole-on). Our analysis of stars from a sample including objects with more than 20 superflares indicated that substantial variations in the flare energy can be achieved in the presence of only small variations in S for a single star (the range of flare energy can reach two orders of magnitude with essentially the same area occupied by magnetic spots). Only two objects in the sample displayed

substantial variations in their spottedness (by factors of five to six; KIC 10422252 and KIC 11764567). Variations in the flare energy by orders of magnitude were observed for any level of spottedness.

3 Results

Using the high-accuracy photometric observations obtained with the Kepler telescope, we studied the properties of the active areas (cool spots) on the surfaces of stars with planetary systems. The analysis was carried out using the data on 737 objects. We have not found any indications that the magnetic activity of a star with exoplanets has any special features that distinguish it from the activity of the stars from a wider sample.

We also analyzed the properties of active regions (cool spots) on the surfaces of 279 G-type stars in which more than 1500 superflares with energies of 10^{33}–10^{36} erg were detected. Diagrams of superflare energy against activity parameters of the stars (the area of their magnetic spots) were considered. The range of variation of the superflare energies (up to two orders of magnitude) is realized over the entire interval of rotation periods. It is proposed that the plot of superflare energy vs. rotational period is bimodal. Three groups of stars with different surface spottednesses can be distinguished in a plot of superflare energy vs. cool-spot area. The range of variation of the flare energy within a group is roughly the same for these three groups. Most of the points on this diagram lie to the right of the dependence corresponding to $B = 3000$ G and an inclination $i = 90°$ (the first two groups of objects). It is confirmed that the flare activity is not related directly to circumpolar active regions, since the majority of the points on the diagram lie to the right of the dependence for $B = 1000$G and $i = 3°$.

Additional detailed information can be found in our publications [7, 8, 9, 10].

References

1. *A. McQuillan, T. Mazeh, S. Aigrain*, Astrophys. J. Lett., **775**, L11, 2013.
2. *I.S. Savanov*, Astron. Rep., **58**, 478, 2014.
3. *S.S. Vogt*, Astrophys. J., **250**, 327, 1981.
4. *A. McQuillan, T. Mazeh, S. Aigrain*, Astrophys. J. Suppl., **211**, 24, 2014.
5. *T. Shibayama, H. Maehara, S. Notsu et al.*, Astrophys. J. Suppl., **209**, 5, 2013.
6. *Y. Notsu, T. Shibayama, H. Maehara et al.*, Astrophys. J., **771**, 127, 2013.
7. *I.S. Savanov*, Astrophys. Bull., **70**, 83, 2015.
8. *I.S. Savanov*, Astrophys. Bull., **70**, 292, 2015.
9. *I.S. Savanov, E.S. Dmitrienko*, Astron. Rep., **59**, 879, 2014.
10. *I.S. Savanov, E.S. Dmitrienko*, Astrophys. Bull., **71**, 59, 2016.

Non-LTE Models of the Emitting Regions in Young Hot Stars

L.V. Tambovtseva[1], V.P. Grinin[1,2]

E-mail: *lvtamb@mail.ru*

Various disk and outflow components of the circumstellar environment of young Herbig Ae/Be stars may contribute to the hydrogen line emission. These are a magnetosphere, disk wind (photoevaporative, magneto-centrifugal, conical or X-wind), gaseous accretion disk (both hot surface layers (inward of 10 AU) and innermost hot midplane of the accretion disk heated by the viscous dissipation (inward of 0.1 AU). Non-LTE modeling was performed to show the influence of the model parameters on the intensity and shape of the line profiles for each emitting region, to present the spatial distribution of the brightness for each component and to compare the contribution of each component to the total line emission. The modeling shows that the disk wind is the dominant contributor to the hydrogen lines compared to the magnetospheric accretion and gaseous accretion disk.

1 Introduction

The star formation theory developed for T Tauri stars (TTSs) successfully explains magnetospheric accretion [1, 2, 3], and magneto-centrifugal disk wind and jet formation [4, 5, 6]. To improve our knowledge of the physical processes in Herbig Ae/Be stars, it is useful to investigate them with theoretical models developed for TTSs, taking into account the special features of HAEBEs (the large luminosity, rapid rotation, weak magnetic fields).

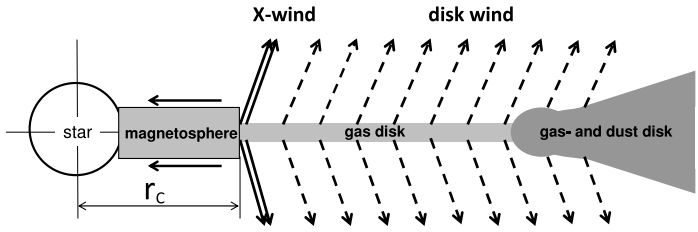

Figure 1: A sketch of line emitting regions in Herbig Ae star.

The promising method to probe the inner environment of young stars is to simultaneously reproduce both the hydrogen emission spectra and the observables of infrared long-baseline interferometry, that is, visibilities, wavelength-differential phases, and closure phases, e.g. [7, 8, 9, 10]. Let us consider

[1] Pulkovo Astronomical observatory, St. Petersburg, Russia
[2] Sobolev Astronomical Institute of St. Petersburg University, Russia

V. Grinin et al. (eds) Radiation mechanisms of astrophysical objects. Yerevan: Edit Print, 2017, pp. 245–252.

schematic picture of the environment of the young intermediate-mass Herbig Ae/Be stars (HAEBEs) (Fig. 1). It presents several gaseous regions emitting the hydrogen lines: (1) magnetospheric accretion region, (2) disk wind which can be presented in the different form (magneto-centrifugal wind, X-wind, conical wind and photoevaporative wind), (3) gaseous accretion disk, and (4) probably polar stellar wind. In this paper, we summarize results of our simultaneous non-LTE modeling of the Brγ emission lines in the spectra of several Herbig Ae/Be stars and interferometric variables obtained for these stars.

1.1 Computational scheme

For all emitting components we performed the non-LTE modeling solving the radiative transfer problem. Differences are in geometry of the regions, and, consequently, in the form of the mass continuity equation and velocity gradient. Solution of the radiative transfer problem has been made as follows. We calculated the excitation and ionization state with the help of numerical codes developed by [11, 12, 13] for the media with the large velocity gradient. The radiative terms in the equations of the statistical equilibrium which take into account transitions between the discrete levels are calculated in the Sobolev approximation [14]. The intensity of the disk wind radiation emergent at the frequencies within the spectral line has been calculated by exact integration over spatial co-ordinates in the approximation of the full redistribution over the frequencies in the co-moving coordinate system. We considered 15 atomic levels and continuum. The

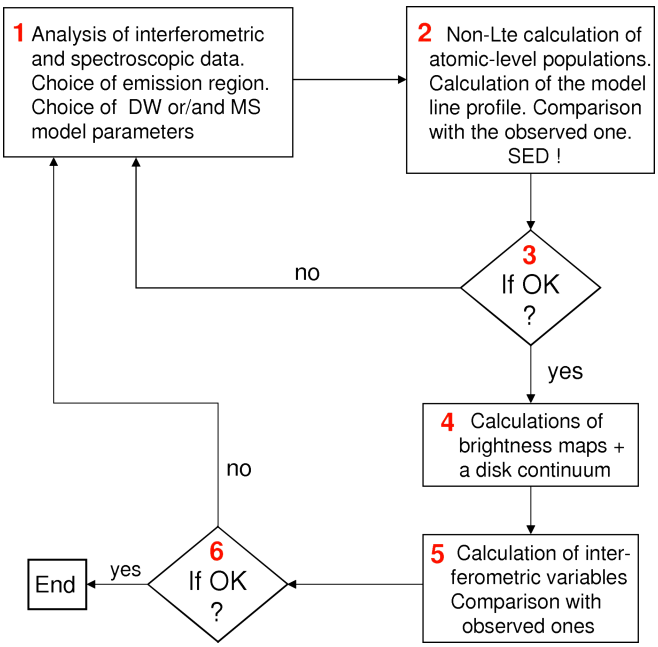

Figure 2: A principle algorithm of simultaneous calculations of emission in the line and interferometric variables.

algorithm of simultaneous calculations of the line emission and interferometric functions is shown in Fig. 2:

1) We choose the appropriate model parameters and compute the velocity and density distribution throughout the region.
2) We divide the integration region by the grid with cells over co-ordinates $[l, \theta, \varphi]$, assuming a wind/accretion temperature distribution. We solve the equation system of statistical equilibrium for the hydrogen atoms in each cell and find the populations of the atomic levels and ionization state in the media.
3) We compare the line profile with the observed one. In the case of a good agreement, we calculate brightness maps at the given frequencies.
4) We calculate the interferometric functions (visibilities, differential and closure phases) and compare them with the observed ones. In the case of the bad agreement we change the model of emitting region. Modeling process is described in details in [15, 16].

2 Models of emitting regions

2.1 Disk wind

Blandford and Payne [17] showed that if an open magnetic field passed through an infinitely thin, Keplerian disk, and is "frozen" into it, and if the field lines make with the disk surface an angle equal to or less than 60°, then gas from the disk surface will be flung out centrifugally along the field lines and can be accelerated to super-Alfvenic velocities. Father from the disk the toroidal component of the field collimates the outflow into two jets which are perpendicular to the disk plane.

There is a method of parametrization where the velocity and temperature distributions can be expressed in a parametric form (see, e.g. [3]). We applied it for HAEBEs. We divide the region of the disk wind by several streamlines, which are going out from point S (Fig. 3). We solve the mass continuity equation for each streamline using a sphere with the center in S. For simplicity, the disk wind consists of hydrogen atoms with a constant temperature (∼10 000 K) along

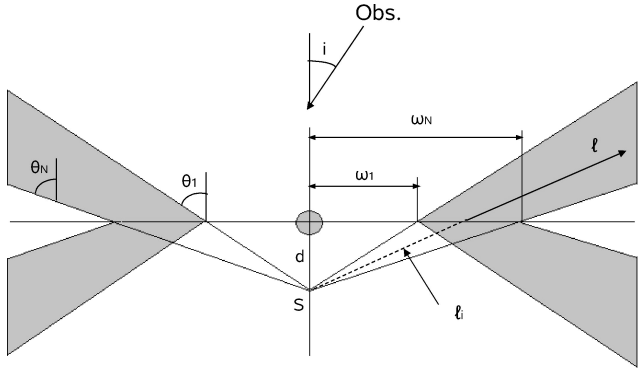

Figure 3: A sketch of the disk-wind region (not to scale).

Table 1: Disk wind model parameters

Model	θ_1	$\omega_1 - \omega_N$	γ	β	$\dot{M}_w$ in $M_\odot$ yr^{-1}
1	30°	$2R_* - 30R_*$	3	4	3×10^{-8}
2	30°	$2R_* - 20R_*$	3	5	3×10^{-8}
3	30°	$2R_* - 20R_*$	3	5	1×10^{-8}

the wind streamlines. As showed by Safier [18], the wind is rapidly heated by ambipolar diffusion to a temperature of ∼10 000 K. The wind electron temperature in the acceleration zone near the disk surface is not high enough to excite the Br line emission. Therefore, in our model, the low-temperature region below a certain height value does not contribute to the line emission. A full description of the disk wind model can be found in [15, 7].

Model parameters are as follows: ω_1 and ω_N are foot points of the disk wind launch region for the first and last trajectories of motion, or streamlines, respectively, θ_1 is the half opening angle between the 1st streamline and the vertical axis. The tangential velocity component $u(\omega)$ and poloidal velocity component $v(l)$ change along the streamlines, as given by

$$u(\omega) = u_K(\omega_i)\,(\omega/\omega_i)^{-1}, \tag{1}$$

$$v(l) = v_0 + (v_\infty - v_0)\,(1 - l_i/l)^\beta. \tag{2}$$

Here, $u_K\,(\omega_i) = (G\,M_*/\omega_i)^{1/2}$ at the starting point ω_i, v_0 and v_∞ are the initial and terminal velocities, respectively, G is the gravitation constant, M_* is the stellar mass, and β is a parameter. We assume v_0 to be the sound velocity in the disk wind, $v_\infty = f u_K(\omega_i)$, where $u_K(\omega_i)$ is the Keplerian velocity at distance ω_i from the star, and f is a scale factor. The two last parameters are the mass loss rate $\dot{M}_w$ and γ. The latter regulates the mass loading among the streamlines.

Examples of Hα and $H\beta$ line profiles (model 1 from Table 1) are presented in Fig. 4, where the profiles are shown for inclination angels from nearly pole-on

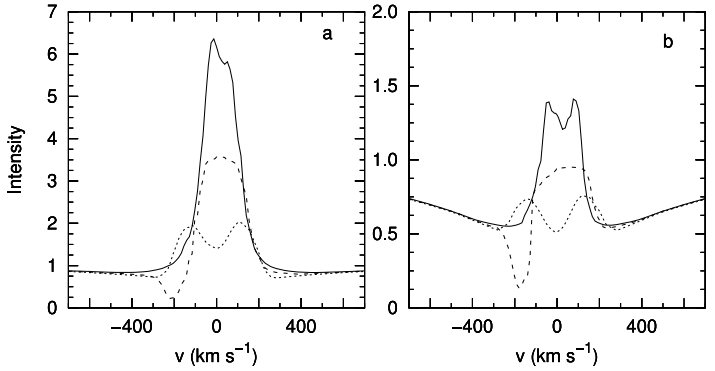

Figure 4: Hα (a) and Hβ (b) line profiles in the disk-wind model 1. Inclination angles are 30° (solid line), 47° (dashed line), and 85° (tiny dashed line); 0° corresponds to the face-on inclination.

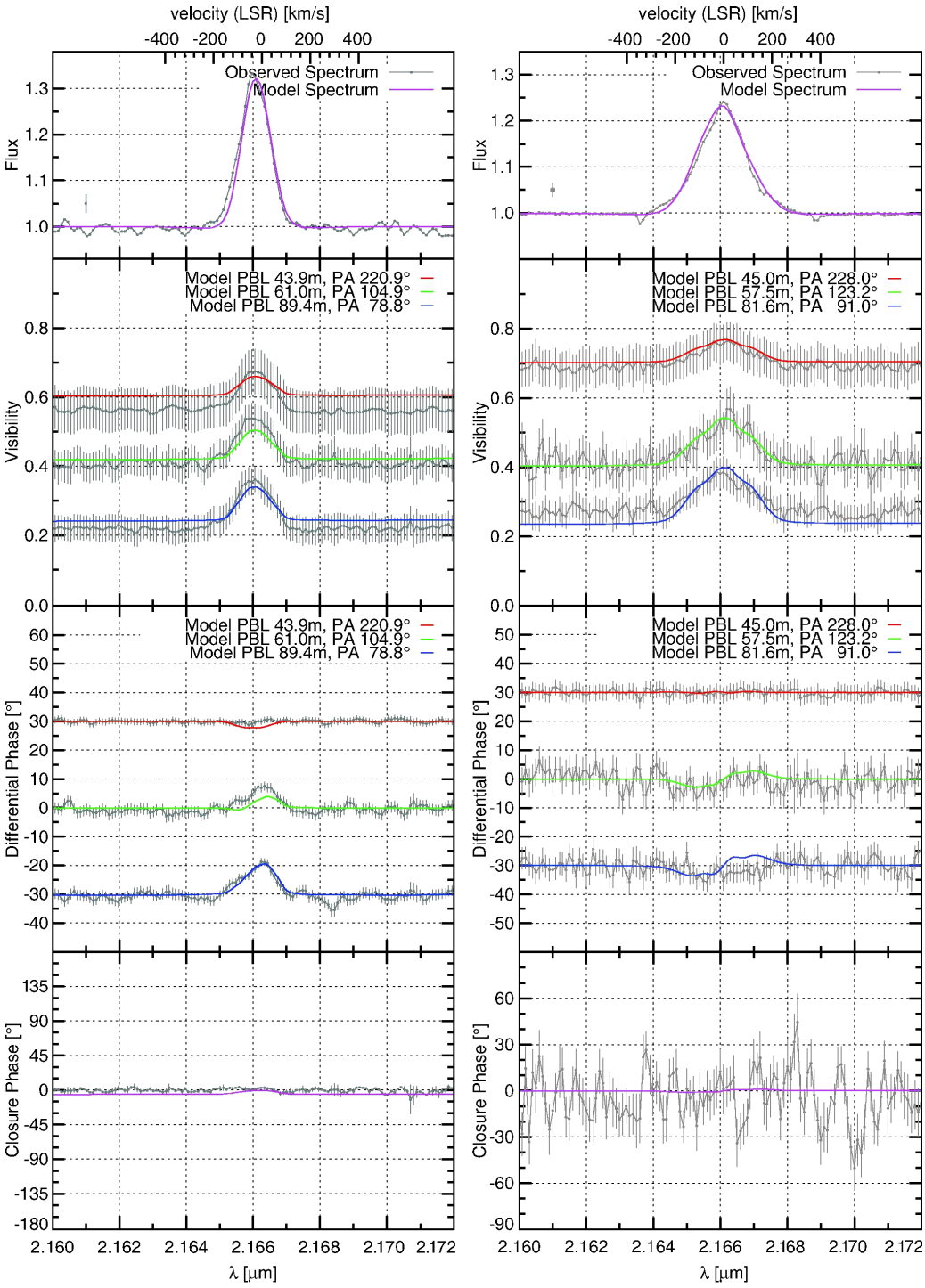

Figure 5: Brγ line profiles and interferometric variables observed and calculated in the framework of the disk wind models for the Herbig Be star HD 98922 (left) and the Herbig Ae star MWC 275 (right).

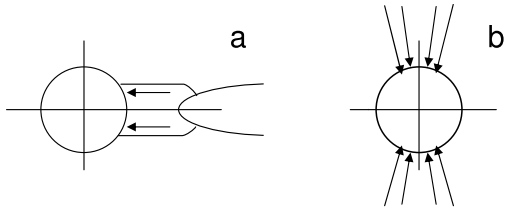

Figure 6: Sketch of the disk (a) and magnetospheric (b) accretion in HAEBEs.

to edge-on view. One can see modification of the line profile from a single one to P Cygni and double-peaked profiles. Modeling with simultaneous calculations of the Brγ line profiles and infrared interferometric variables was performed for several Herbig Ae/Be stars (MWC 297, MWC 275, and HD 98922 – [7, 8, 9]). Details and model parameters can be found in the papers cited. Examples of the observed and calculated line profiles and interferometric functions are presented in Fig. 5.

2.2 Magnetosphere and accretion disk

In our papers [13, 19, 16], we adapted the classical magnetospheric accretion model for TTSs to intermediate-mass Herbig Ae/Be stars. Taking into account that HAEBEs are luminous and rapidly rotating stars, we used a very compact disk-like magnetosphere with rotating gas in free-fall motion (Fig. 6a). This configuration can be used if the stellar magnetic field is weak enough to allow the accreting gas to approach the star surface at the low latitudes. Another configuration of the accreting zone (Fig. 6b) is expected if the magnetic field of the star is strong enough to transport the gas onto the pole regions [20]. In this case we can model the magnetospheric accretion zone by bi-polar thin cones because these regions contribute much more to the hydrogen line emission than outer parts of magnetosphere (not shown in Fig. 6b) due to the smaller gas temperatures in the outer regions. Our calculations of the infrared Brγ line emission (that probes the innermost stellar environment) together with interferometric functions showed that the contribution of the magnetospheric region to the hydrogen emission is no more than 40%. Our conclusion for hydrogen lines (including Balmer lines) is as follows: the emission from the magnetospheric accretion region is able to change the shape of the line profile, for example, to increase the wings of the profile and/or make it asymmetric. In calculations we used the ratio $\dot{M}_w/\dot{M}_{acc} =$ 0.1–0.3 $M_\odot$ yr^{-1}. Many examples of the Hα and Brγ lime profiles can be found in [19, 16].

We also considered the inner gaseous accretion disk as a possible source of the hydrogen emission. For formation of the hydrogen line, the temperature and density of the gas have to be high enough. We considered two components of the inner accretion disk: hot layers of the inner gaseous accretion disk (inward of 10 AU) and the innermost hot midplane of the accretion disk heated by viscous dissipation (inward of 0.1 AU) based on the study by Muzerolle et al. [21]

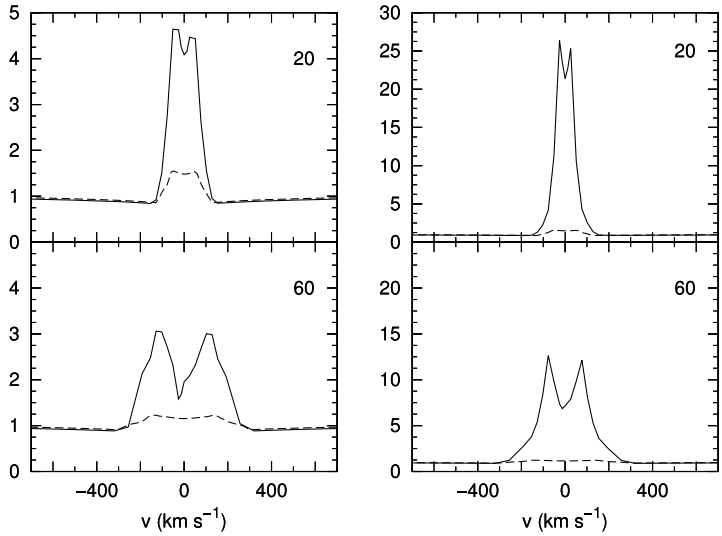

Figure 7: Brγ line profiles in the disk wind models (solid line) and the inner gaseous disk (dashed line) for inclination angles 20° and 60°. *Left*: the disk wind model 2; *right*: the disk wind model 3. Intensities are given in the units of the stellar continuum.

(see details in [16]). All of them contribute *less* Brγ and Hα emission than the *magneto-centrifugal disk*. Several examples of Brγ line profiles from the disk wind and inner gaseous disk are presented in Fig. 7. All they are normalized to the stellar continuum. At these frequencies the disk also emits in the continuum. The profiles for 20° and 60° inclination angles are presented. The same model of the inner disk heated by the viscous dissipation is compared with the disk wind models 2 and 3 from Table 1. Parameters of the disk model are: $R_{in} = 2R_*$, $R_{out} = 10R_*$, $\dot{M}_{acc} = 1 \times 10^{-7} M_\odot$ yr^{-1}. The gas temperature is equal to 6000 K near R_{in} and decreases with the distance r. The emission from the hot midplane of the inner gaseous accretion disk can also slightly change the line profile and increase the intensity of the line profile but is substantially less than that from the disk wind.

The hot layers of the inner gaseous accretion disk are not able to contribute strongly into the hydrogen line emission but together with the emission from the outer photoevaporating wind they are able to modify the shape of the line profile, for example, to fill in a small gap between two peaks with additional emission and transform the shape of the profile from double-peaked to single-peaked.

3 Conclusion

Unlike low-mass T Tauri stars, the disk wind of Herbig Ae/Be stars contributes substantially to the hydrogen emission spectra; nevertheless, the region of the magnetosphere is also a source of the emission and has to be taken into account.

Combination of the disk wind parameters and inclination angles permits us to obtain a large variety of profile shapes.

Calculation of the interferometric functions together with the emission lines modeling gives strong constraints to model parameters and provides us with an additional information about the star plus disk system.

Acknowledgments. This research has been supported in part by the Russian Foundation for Basic Research (Projects 15-02-05399 and 15-02-09191).

References

1. *L. Hartmann, R. Hewett, N. Calvet*, Astrophys. J., **426**, 669, 1994.
2. *J. Muzerolle, N. Calvet, L. Hartmann*, Astrophys. J., **550**, 944, 2001.
3. *R. Kurosawa, T.J. Harries, N.H. Symington*, Mon. Not. Roy. Astron. Soc., **370**, 580, 2006.
4. *A. Königl, R.E. Pudritz*, in Protostars and Planets IV. Eds. V. Mannings, A.P. Boss, S.S. Russell. Tucson: Univ. Arizona Press, 2000, p. 759.
5. *J. Ferreira*, Jets from Young Stars. Lect. Not. Phys., No. 723. Berlin: Springer-Verlag, 2007, p. 181.
6. *J. Ferreira, C. Dougados, S. Cabrit*, Astron. Astrophys., **453**, 785, 2006.
7. *G. Weigelt, V.P. Grinin, J.H. Groh et al.*, Astron. Astrophys., **527**, 103, 2011.
8. *R. Garcia Lopez, L.V. Tambovtseva, D. Schertl et al.*, Astron. Astrophys, **576**, A84, 2015.
9. *A. Caratti o Garatti, L.V. Tambovtseva, R. Garcia Lopez et al.*, Astron. Astrophys., **282**, 44, 2015.
10. *I. Mendigutía, W.J. de Wit, R. Oudmaijer et al.*, Mon. Not. Roy. Astron. Soc., **453**, 2126, 2015.
11. *V.P. Grinin, N.A. Katysheva*, Izv. Krym. Astrofiz. Obs. (Bull. Crim. Astrophys. Obs.), **62**, 59, 1980.
12. *V.P. Grinin, A.S. Mitskevich*, Astrophys., **32**, 216, 1990.
13. *L.V. Tambovtseva, V.P. Grinin, B. Rodgers, O.V. Kozlova*, Astron. Rep., **45**, 442, 2001.
14. *V.V. Sobolev*, Moving Envelopes of Stars. Cambridge: Harvard Univ. Press, 1960.
15. *V.P. Grinin, L.V. Tambovtseva*, Astron. Rep., **55**, 704, 2011.
16. *L.V. Tambovtseva, V.P. Grinin, G. Weigelt*, Astron. Astrophys., submitted, 2016.
17. *R.D. Blandford, D.G. Payne*, Mon. Not. Roy. Astron. Soc., **199**, 883, 1982.
18. *P. Safier*, Astrophys. J., **408**, 115, 1993.
19. *L.V. Tambovtseva, V.P. Grinin, G. Weigelt*, Astron. Astrophys., **562**, A104, 2014.
20. *F.H. Shu, J. Najita, E. Ostriker, F. Wilkin*, Astrophys. J., **429**, 781, 1994.
21. *J. Muzerolle, P. D'Alessio, N. Calvet, L. Hartmann*, Astrophys. J., **617**, 406, 2004.

Relative Content of Be Stars in the Young Open Clusters

A.E. Tarasov[1]

E-mail: *aetarasov@mail.ru*

Based on high and medium resolution spectra, we analyze the population of Be stars in young open clusters. We have found a clear dependence of the relative content of early-type (B0–B3) stars on the cluster age. The relative concentration of Be stars of spectral types B0–B3 gradually increases with the cluster age, reaching its maximum value of 0.46 in clusters with ages of 12–20 Myr. The almost complete absence of Be stars in older clusters can be easily explained by the fact that B stars leave the main sequence. The few emission objects in clusters with ages of 1–7 Myr are most likely Herbig Be stars. Such a distribution of Be stars in clusters unequivocally points to the evolutionary status of the Be phenomenon. We also briefly consider the causes of this pattern.

1 Introduction

The Be phenomenon, the presence of emission (usually HI) lines in the spectra of normal B-type dwarfs and giants, is widespread. The relative content of Be stars is currently estimated to be about 17% of total number of Galactic B stars [1]. It is not completely clear why the geometrically thin and extended disks are formed [2]. These can be both the weakly decretion disks of single stars or binaries after mass exchange and the accretion disks of massive binaries at the first mass exchange stage [3]. The Be phenomenon is commonly observed in stars with a rotation velocity higher than its average and is probably unrelated to the ordinary outflow of matter from the star's equator [2, 4] unless it rotates with a critical velocity [5].

One of the key problems for understanding the Be phenomenon is to answer the question of whether the disks around B stars appear immediately after they have reached the main sequence (MS) or this is a characteristic of objects at the end of their MS life. Young open clusters undoubtedly are a good test for verifying these assumptions.

One of the first investigation of Be stars in open clusters was made in [6] where it was concluded that stars with a high angular momentum become Be stars at the end of their evolution on MS. In [7] the authors also obtained a similar result that Be stars occupy the entire MS, but the fraction of Be stars is at a maximum in clusters with the turn-off point in the region of spectral types B1–B2, and their

[1] Crimean Astrophysical Observatory of RAS, Russia

V. Grinin et al. (eds) Radiation mechanisms of astrophysical objects. Yerevan: Edit Print, 2017, pp. 253–260.

population decreases with increasing age. No clear age dependence was revealed in subsequent papers [8, 1].

Later on, the authors of [9] showed that the Be phenomenon is nevertheless an evolutionary stage and is observed for B stars in the second half of their MS life. Using photometry and spectroscopy for Be stars in open clusters, they concluded that emission objects are present in clusters with ages of less than 10 Myr, but these are mostly Herbig Ae/Be stars or other pre-main-sequence objects. In contrast, classical Be stars appear in clusters with age of 10 Myr, and the maximum number of such objects is observed in clusters with age of 12–25 Myr.

A plot of the relative population of Be star against the cluster age was constructed in [10]. It showed no clear dependence, although a larger number of Be stars is contained in clusters with ages of 25–100 Myr and, according to [11], in clusters with ages of 10–40 Myr. The authors of [11] point out that the maximum fraction of B stars with emission in their spectra is observed in clusters with ages 0–10 and 20–30 Myr. When studying the population of Be stars, the authors of [12] investigated objects of spectral types B0–B3 and separately B4–B5. They found that the fraction of Be stars of spectral types B0–B3 increases in clusters of the Magellanic Clouds with ages of 10–25 Myr.

As we see, the available data are so far insufficient, they give a blurred and largely contradictory picture of the nature of the Be phenomenon. Since the number of well-studied clusters is small, most of the authors analyzed Be stars of all spectral types, when studying the Be phenomenon, while objects of later spectral types (later than B3) are known to usually exhibit a weak line emission. Given that many authors studied the emission based on narrow-band Hα photometry or low-resolution spectroscopy, there is a high probability that not all later-type Be stars have been identified. These methods do not allow a weak emission to be clearly revealed in Be stars. In addition, the MS lifetime of late B stars is longer by order of magnitude. Therefore, since most authors use

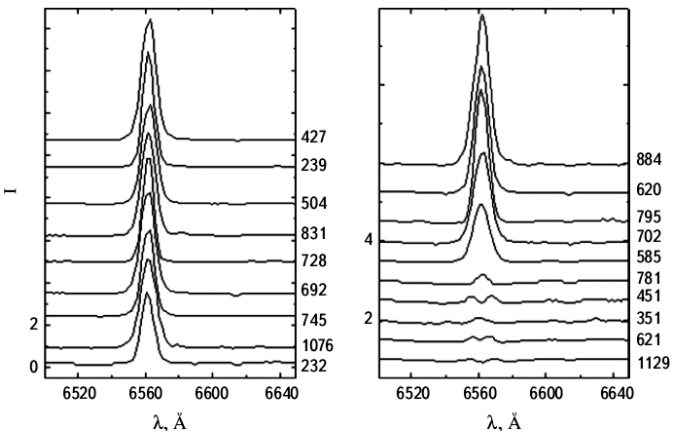

Figure 1: The Hα profiles of the selected Be stars in the open stellar cluster NGC 7419 [15]. Estimated age of the cluster is 14 Myr.

observational data for all B and Be, the age dependence of the fraction of Be stars is indistinct. For a proper analysis of the evolutionary status of Be stars, it is also important to determinate their position on the color-magnitude diagram and, accordingly, to determine the reddening coefficient. Considering Be stars in open clusters can partly help in this determinations. In some cases, however, significant reddening non-uniformity is observed within the cluster field, besides the additional reddening introduced by the envelopes of the Be stars themselves cannot be accurately taken into account either.

The spectroscopic data and, what is important, homogeneous studies of the age dependence of the population of B stars are very scarce, and the question about the nature of Be phenomenon currently remains unsolved [13, 14]. Therefore, the problem of studying Be stars in young open clusters based on high and medium resolution spectra remains topical.

2 Observations and age dependence of the Be stars fraction in clusters

During the last decade, based on high and medium resolution spectra taken with the 2.6 m telescope of the Crimean Astrophysical Observatory, we studied B and Be stars in nine open clusters with ages of 30–40 Myr: NGC 457, NGC 659, NGC 663, NGC 869, NGC 884, NGC 6871, NGC 6913, NGC 7419 and Berkley 86. To obtain a sample being complete and identical for B and Be stars and to analyze the age dependence, where possible, we restricted our study only to objects of early spectral types (B0–B3) when investigating the population of Be stars in young open clusters. Accordingly, the choice of clusters was also limited by the age less than 40 Myr, although there are Be stars in relatively older clusters, but these are generally stars of later spectral types (later than B3). We considered at least 60% of the Be stars in NGC 869, NGC 884, NGC 6913, NGC 7419 and took the spectra of all Be stars in NGC 457, NGC 659, NGC 5871 and Berkley 86. The example of Hα profiles of found and new Be stars in the open stellar cluster NGC 7419 is presented in Fig. 1. The results of our analysis of the relative content of early-type Be stars in the clusters studied are presented in [15, 16, 17, 18] and Table 1.

Table 1: The content of Be stars of spectral types B0–B3 in open clusters

Cluster name	Age, Myr	N(Be)	N(B+Be)	N(Be)/N(B+Be)
Berkley 86	6–8	1 (3)	15	0.07
NGC 457	11–20	4 (5)	15	0.27
NGC 659	12–20	4 (5)	16	0.25
NGC 663	18–25	16 (20)	50	0.32
NGC 869	12–14	20	47	0.43
NGC 884	12–14	18	39	0.46
NGC 7419	14	35 (37)	80	0.43
NGC 6871	6–12	2 (3)	14	0.14
NGC 6913	3–6	3	43	0.07

When constructing the age dependence of the fraction of Be stars, we took into account the data only for B0–B3 stars. However, since there is no spectral classification for some cluster member, we used the spectra in the wavelength range 4050–5200 Å for all observed objects to estimate their atmospheric parameters or to perform their spectral classification. The fraction of Be stars in the clusters was found as the ratio of the number of Be stars to the number of all B0–B3 objects (including the Be stars). When constructing the dependence, we also took into account the uncertainty in the relative number of Be stars and the estimated cluster ages. We calculated the upper limit for the estimated fraction of Be stars by taking into account the identified Be stars of spectral types B0–B3 and the Be candidates of the same spectral type.

The objects without any well-defined spectral type but with a probability that they are B0–B3 stars (as a rule, we used color-magnitude diagram for clusters) or objects, whose low-resolution spectroscopy showed some features indistinctly designed by the authors of the papers, were considered to be candidates. The third column (N(Be)) in Table 1 gives the number of Be stars and the possible maximum number of Be stars in the cluster (in parentheses), i.e. the sum of the identified Be stars and Be candidates.

Apart from the absence of spectral classification, the problem of cluster age determination also arose, because the estimations obtained by different methods often differ significantly. In addition, there are also large discrepancies in age determination when using the same method but with a different sample of program objects. We attempted to critically estimate the cluster ages. For all clusters, we constructed their color-magnitude diagrams with a set of isochrones (constructed from the data from [19]). We constructed the isochrones for each cluster by taking into account the already available reddening and distance modulus and then chose the most satisfactory reddening and distance modulus parameters. An example of this procedure is presented in Fig. 2. This allows us to estimate the age in a more homogeneous way. Our estimates of the ages, the number of B and Be stars, and the fraction of Be stars in each of clusters are given in Table 1.

In Fig. 3 the relative content of Be stars in the program clusters is plotted against the age. These data have a sufficient statistical significance, because we investigated almost all of the B0–B3 objects for their belonging to Be stars. As we see from the figure, the fraction of Be stars increases appreciably in clusters with ages of more than 10 Myr. This suggests that with a high probability the Be phenomenon is an evolutionary effect.

3 Discussion

Let us analyze in more details the data presented in Fig. 4 showing the gradual increase in the relative fraction of Be stars of spectral types B0–B3 with the cluster age.

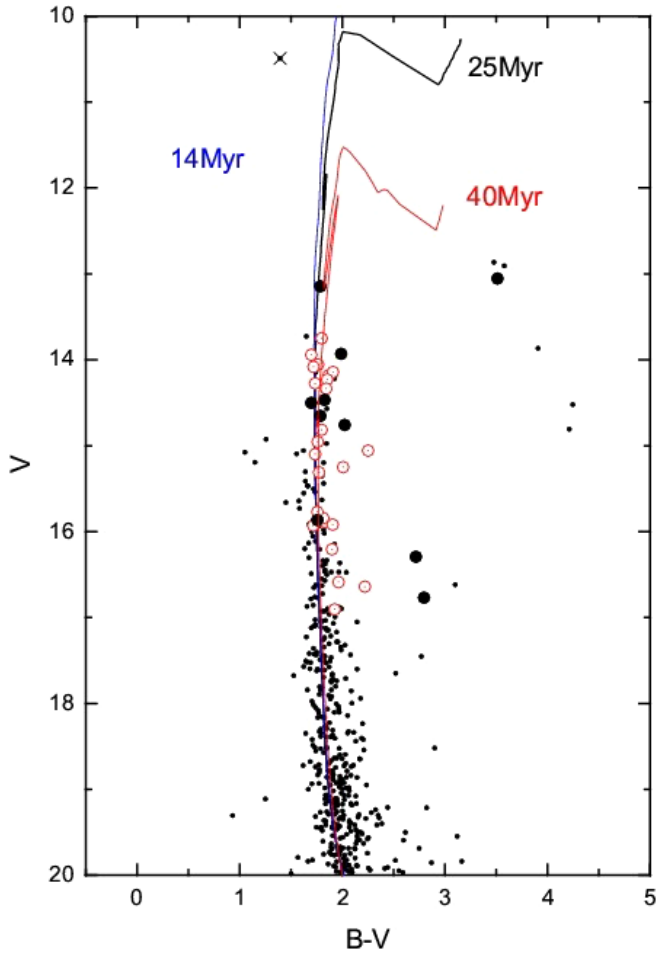

Figure 2: Example of the color-magnitude $((B-V)-V)$ diagram for the open stellar cluster NGC 7419 [16]. Open circles are for observed spectroscopically Be stars, large black circles for observed B stars. Three isochrones are presented for 14, 25 and 40 Myr.

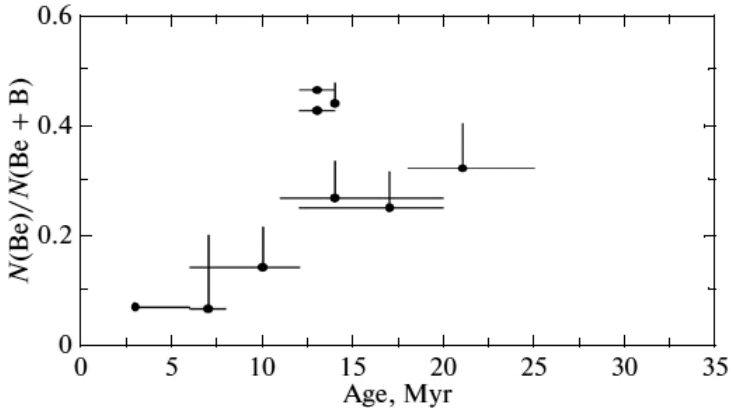

Figure 3: Relative number of Be stars versus cluster age (based on the data from Table 1).

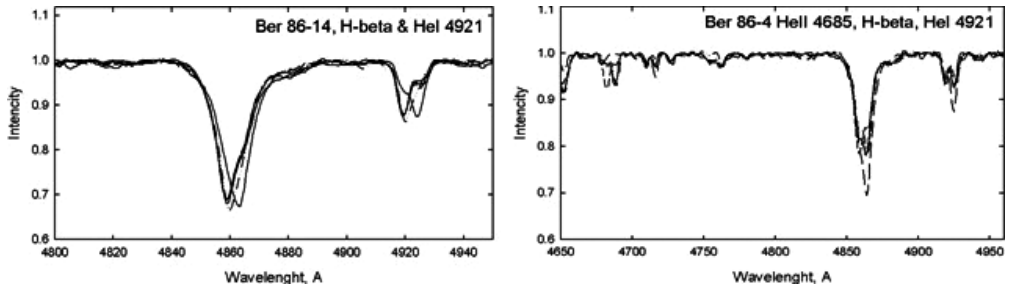

Figure 4: Two examples of spectral variability of the line double systems Ber 86 - 14 ($P_{orb} < 4$ days) and Ber 86-4 ($P_{orb} < 2$ days) in a very young open cluster Berkley 86 with age 6-8 Myr. Both systems have MS components.

According to [20], three evolutionary scenarios leading to the formation of disks around B stars are possible:

(A) Be stars were born as rapidly rotating B stars, and the HI line emission is observed throughout their MS life.

(B) The Be phenomenon arises in a single, sufficiently rapidly rotating B star during the change in its V/V_{crit} ratio (where V is the star's equatorial rotation velocity and V_{crit} is the critical equatorial rotating velocity) as the star moves from the zero-age main sequence (ZAMS) to the terminal age main sequence (TAMS) [13].

(C) Be stars are binary systems at the stage after active mass exchange.

Case A should probably be excluded from consideration. As we can see from Fig. 3, classical Be stars are observed very rarely in very young clusters, with ages of less than 8 Myr, and can be Herbig Be stars or pre-main-sequence objects with a high probability.

Case B, where V/V_{crit} ratio increases in the second half of the MS life of a rapidly rotating B star, was considered in detail in [13]. In particular, they showed that when the star is on MS, the equatorial rotation velocity of the star decreases significantly at the very end of its MS life. Thus, the V/V_{crit} ratio becomes the most important parameter. Assuming $V/V_{crit} \geq 0.7$ and solar metallicity for Be stars, any non-stationarities of the outer layers of Be stars, such as, for example, non-radial oscillations, can contribute to the outflow of matter from the stellar photosphere. According to these authors, a noticeable fraction of Be stars, 10-20% or, in a more optimistic case, up to 35%, are formed from single, rapidly rotating B stars during their MS life. For B0–B3 stars, this corresponds to an age of about 15–25 Myr. A comparison of these data based on the evolution theory and Fig. 3 obtained from observations suggest that this scenario is possible.

Case C, the formation of Be stars through mass and angular momentum exchange in close binary systems, was considered in detail by several authors (see [20, 21]). Spectroscopic studies of several young clusters in [14] point to

an appreciable fraction of massive binaries in young clusters (about 25% of the total number of B stars). Moreover, since the latter authors performed only 2–3 episodic observations at close dates, one might expect that they revealed only short-period ($P_{orb} < 20$ days) massive binaries and did not detect numerous systems with the periods of 30–1000 days, typical of Be stars and mass ratio differing noticeably from one. Thus, the data from [14] may be reliably considered to be a lower limit for the fraction of binaries with B-type components in young open clusters. Clearly, all of the detected binaries will enter the phase of rapid mass exchange as soon as the more massive component leaves MS. In this case, the previously more massive component will become inaccessible to optical observations, because it will become either a helium star, or a white dwarf, or, in the most massive systems, an X-ray binary [20].

Our spectroscopic observations confirm data of [14]. In Fig. 4 we present two examples of spectroscopic binaries in a very young open cluster Berkley 86 (age of 6–8 Myr). The cluster has only one (possibly 3) early type Be stars but we found at least three short orbital period double systems and all of them have MS components.

Obviously, the scenario C is most natural as was pointed out, for example, in [21], and qualitatively describes our dependence of the relative content of Be stars at the end of their MS life. In the case where the V/V_{crit} ratio for a single B star evolves, it is necessary to prove that this star is actually a single object rather than a binary system with $P_{orb} < 1000$ days and a secondary degenerate component. This problem is known to be difficult and allows one to investigate only the brightest objects, which usually do not include the B and Be stars in open clusters.

Modern statistical investigations of the field B stars showed that among OB stars, whose evolution leads to the phase of active mass exchange, the relative fraction of double systems decreased with decreasing of spectral type of the primary MS component. As it was shown, for example, by authors of [22], among of O7–O9 stars relative concentration of double systems reaches 80%, 65% for B0–B1.5 stars and 55% for MS stars of spectral types B2–B3. Nearly the same values were found during the studying of Scorpios OB2 association [23]. These authors found that the relative fraction of double and multiple systems among B0–B3 stars and B4–B9 stars is 80% and 50%, respectively. All these statistical data again support the scenario C as the most natural explanation of our statistical results presented in Table 1 and Fig. 3.

4 Conclusions

The data considered revealed the pattern of distribution of the relative content of early-type Be stars in clusters of different ages. The maximum number of Be stars is observed in clusters with ages of 12–25 Myr. The increase in the number of Be stars in clusters with a certain age confirms the hypothesis that Be stars emerge when they leave the main sequence. On the other hand, the Be

phenomenon can arise in binaries when the more massive component leaves the main sequence, which leads to mass exchange in the system and produces hydrogen emission lines in the spectrum. Both these effects operate simultaneously for single stars and binary systems.

References

1. *J. Zorec, D. Briot*, Astron. Astrophys., **318**, 443, 1997.
2. *J.E. Bjorkman, J.P. Cassinelly*, Astrophys. J., **409**, 429, 1993.
3. *A.E. Tarasov*, in Proc. IAU Coll. No. 175. The Be Phenomenon in Early Type Stars. Eds. M.A. Smith, H.M. Henrichs, J. Fabregat. Astron. Soc. Pacif. Conf. Ser., **214**, 644, 2000.
4. *Y. Flemat, J. Zorec, A.-M. Hubert, M. Floquet*, Astron. Astrophys., **440**, 305, 2005.
5. *R.H.D. Townsend, S.P. Owocki, I.D. Howarth*, Mon. Not. Roy. Astron. Soc., **350**, 189, 2004.
6. *R.E. Schild, W. Romanishin*, Astrophys. J., **204**, 493, 1976.
7. *J.C. Mermilliod*, Astron. Astrophys., **109**, 48, 1982.
8. *A. Slettebak*, Astrophys. J. Suppl., **59**, 759, 1985.
9. *J. Fabregat, J.M. Torrejon*, Astron. Astrophys., **375**, 451, 2000.
10. *M.V. McSwain, D.R. Gies*, Astrophys. J. Suppl., **161**, 118, 2005.
11. *B. Mathew, A. Subramaniam, B.Ch. Bhatt*, Mon. Not. Roy. Astron. Soc., **388**, 1879, 2008.
12. *J.P. Wisniewski, K.S. Bjorkman*, Astrophys. J., **652**, 458, 2006.
13. *S. Ekström, G. Meynet, A. Maeder, F. Barblan*, Astron. Astrophys., **478**, 467, 2008.
14. *W. Huang, D.R. Gies*, Astrophys. J., **648**, 580, 2006.
15. *C.L. Malchenko, A.E. Tarasov*, Astrophys., **51**, 250, 2008.
16. *C.L. Malchenko*, Odessa Astron. Publ., **21**, 60, 2008.
17. *C.L. Malchenko, A.E. Tarasov*, Astrophys., **52**, 235, 2009.
18. *C.L. Malchenko, A.E. Tarasov*, Astrophys., **54**, 52, 2011.
19. *T. Lejeune, D. Schaerer*, Astron. Astrophys., **366**, 538, 2001.
20. *O.R. Pols, I. Cote, L.M.F.M. Waters, J. Heise*, Astron. Astrophys., **241**, 419, 1991.
21. *W. Huang, D.R.. Gies, M.V. McSwain*, Astrophys. J., **722**, 605, 2010.
22. *R. Chini, V.H. Hoffmeister, A. Nasseri et al.*, Mon. Not. Roy. Astron. Soc., **424**, 1925, 2012.
23. *N.B.N. Kouwenhoven, A.G.A. Brown, H. Zinnecker et al.*, Astron. Astrophys., **430**, 137, 2005.

* The color figure is available online in the Proceedings at *http://www.astro.spbu.ru/sobolev100/* .

Model Approach for Inelastic Processes in Collisions of Heavy Particles with Hydrogen

S.A. Yakovleva[1], A.K. Belyaev[1]

E-mail: *cvetaja@gmail.com*

The quantum model approach within the framework of the Born–Oppenheimer formalism has been recently proposed to evaluate physically reliable data on rate coefficients for inelastic processes in collisions of atoms and positive ions of different chemical elements with hydrogen atoms and negative ions.

1 Introduction

Formation of spectral lines in stellar atmospheres is determined by many physical processes. Collisions of atoms and positive ions of different species with hydrogen atoms and anions are one of the main sources of uncertainties for non-LTE studies due to the high concentration of hydrogen [1].

The best way to get information on the rate coefficients for hydrogen collisions is to carry out full quantum studies. But these calculations are very time-consuming, and only a few collisional partners have already been studied at low collision energies. These are hydrogen collisions with hydrogen [2], helium [3], lithium [4, 5], sodium [6], and magnesium [7].

The data for hydrogen collisions are still rare, so the Drawin formula was widely used to estimate inelastic collision rate coefficients, although it has been shown [8] that the Drawin formula does not provide reliable data and can not be applied to charge transfer processes, which have been found to be the most important in astrophysical applications. A comparison of the rate coefficients obtained in full quantum studies and with the Drawin formula was performed in [8]. The rate coefficients obtained in quantum calculations are not larger than 10^{-8} cm^3/s, while the highest values for estimations by means of the Drawin formula are up to 10^{-2} cm^3/s, which is a huge value for an inelastic rate coefficient. Moreover, this formula gives zero rates for charge transfer processes, such as mutual neutralization and ion pair formation, which have been shown to have one of the largest values according to quantum calculations.

That is why it is important to develop and apply quantum model approaches that would provide reliable data, even approximate. Such quantum model approach for collisions of atoms and positive ions of different chemical elements with hydrogen atoms and negative ions was recently proposed in [9, 10].

[1] Dep. of Theoretical Physics and Astronomy, Herzen University, St. Petersburg, Russia

V. Grinin et al. (eds) Radiation mechanisms of astrophysical objects. Yerevan: Edit Print, 2017, pp. 261–264.

2 Quantum model approach

Low-energy atomic collisions are well described within the quantum Born-Oppenheimer approach. Within this framework the problem is solved in two steps. The first step includes electronic structure calculations. It can be based on accurate quantum-chemical data, if available. For many cases, accurate quantum-chemical data are not available, and approximate adiabatic potentials can be constructed via modeling of ionic-covalent interaction as described in [9]. Also it is possible to combine modeled potentials for higher-lying states with available *ab initio* potentials for low-lying states.

The second step includes non-adiabatic nuclear dynamics calculations. In the case, when adjacent states form several non-adiabatic regions, the probability current method described in [9] can be applied. The other option is to use multichannel formulas [10, 11], but they are only applicable for the case of ionic-covalent interaction (every pair of adjacent states form only one non-adiabatic region).

3 Results

The comparison of the results given by the quantum model approach and by full quantum study was performed in [7] for the case of magnesium-hydrogen collisions. Rate coefficients obtained in these studies are shown in Fig. 1.

The vertical axis represents results of the quantum model calculations, while the horizontal axis does results of the full quantum study. The symbols in Fig. 1 correspond to the rate coefficients of the partial processes, associated with

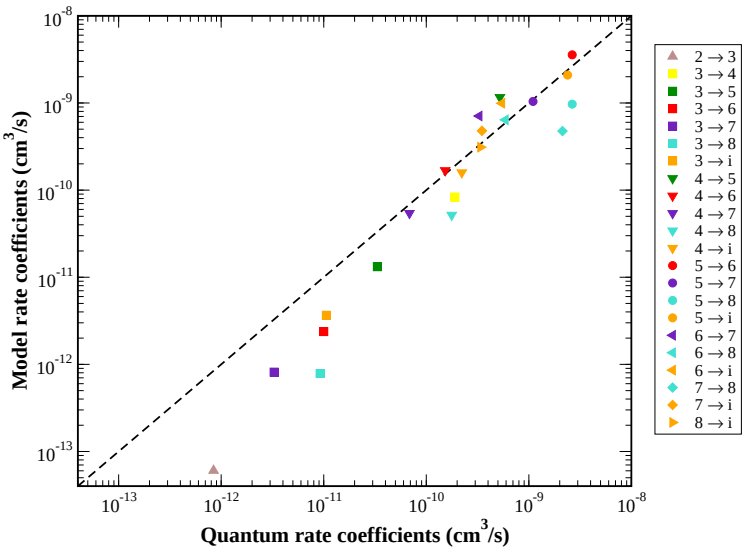

Figure 1: Comparison of the rate coefficients at $T = 6000$ K for the case of Mg-H collisions.

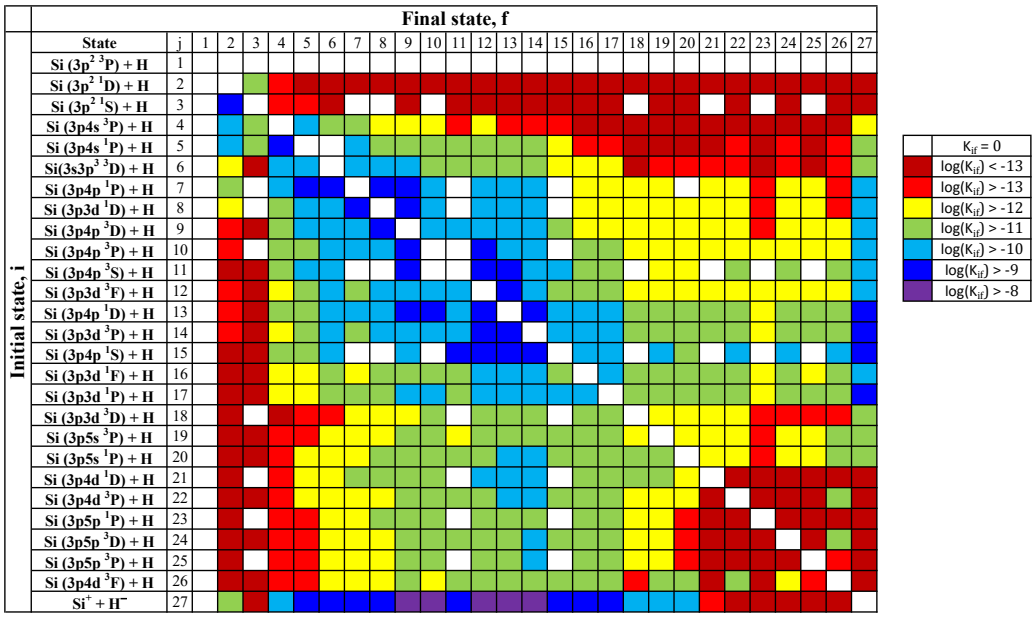

Figure 2: Rate coefficients (in cm^3/s) at $T = 6000\,\mathrm{K}$ for the case of Si-H collisions.

transitions between different molecular states numbered starting from the ground one (the index i corresponds to the ionic state). It is seen that the agreement for the rate coefficients with high and moderate values is quite good. While there are some deviations for the processes with small values of the rate coefficients, for which both the quantum model approach and the full quantum study give negligibly small values.

In [10], the quantum model approach was applied to silicon-hydrogen collisions. These calculations included 27 molecular states, and the heat map with the rate coefficients for different inelastic processes is represented in Fig. 2. The purple squares correspond to the highest rates, while white ones correspond to zero rates. It is seen that the highest values correspond to the charge transfer processes such as mutual neutralization and ion pair formation.

Acknowledgments. The partial support of the work from the Ministry for Education and Science (Russian Federation) and from the Dinasty foundation is gratefully acknowledged.

References

1. *M. Asplund*, Ann. Rev. Astron. Astrophys., **43**, 481, 2005.
2. *M. Stenrup, Å. Larson, N. Elander*, Phys. Rev. A, **79**, 012713, 2009.
3. *A.K. Belyaev*, Phys. Rev. A, **91**, 062709, 2015.
4. *H. Croft, A.S. Dickinson, F.X. Gadéa*, J. Phys. B, **32**, 81, 1999.

5. *A.K. Belyaev, P.S. Barklem*, Phys. Rev. A, **68**, 062703, 2003.

6. *A.K. Belyaev, P.S. Barklem, A.S. Dickinson, F.X. Gadéa*, Phys. Rev. A, **81**, 032706, 2010.

7. *M. Guitou, A. Spielfiedel, D.S. Rodionov et al.*, Chem. Phys., **462**, 94, 2015.

8. *P.S. Barklem, A.K. Belyaev, M. Guitou et al.*, Astron. Astrophys., **530**, A94, 2011.

9. *A.K. Belyaev*, Phys. Rev. A, **88**, 052704, 2013.

10. *A.K. Belyaev, S.A. Yakovleva, P.S. Barklem*, Astron. Astrophys., **572**, A103, 2014.

11. *A.K. Belyaev*, Phys. Rev. A, **48**, 4299, 1993.

* The color figures are available online in the Proceedings at *http://www.astro.spbu.ru/sobolev100/*.

Low-Energy Inelastic Magnesium-Hydrogen Collisions

D.S. Rodionov[1], A.K. Belyaev[1]

E-mail: *virtonoobne@bk.ru*

Available quantum calculations of cross sections for inelastic processes in Mg + H and $Mg^+ + H^-$ collisions, that is, the processes of astrophysical interest, are analyzed. It is shown that cross sections with large values are calculated with high accuracy. The calculations include all transitions between the nine lowest adiabatic $MgH(^2\Sigma^+)$ molecular states, with the uppermost of those diabatically extended to the ionic molecular state in the asymptotic region. Calculations also include transitions between five lowest adiabatic $MgH(^2\Pi)$ molecular states. The inelastic cross sections with large values are stable with respect to a number of channels treated. The non-adiabatic nuclear dynamical calculations have been performed by means of the reprojection method in the framework of the Born–Oppenheimer approach, which provides reliable physical results.

1 Aims

The measurement of abundances of chemical elements in stellar atmospheres, as interpreted from stellar spectra, is of fundamental importance in modern astrophysics. Inelastic processes in collisions of different atoms with hydrogen atoms are important for the non-local thermodynamic equilibrium modeling of stellar spectra which is the main tool for obtaining relative and absolute chemical abundances [1, 2].

Magnesium is of particular astrophysical interest since it is an α-element produced by supernovae of type II. The spectral lines of such α-element provide diagnostic tools to study distribution with time of chemical abundances in stellar populations [2, 3, 4]. Neutral Mg lines give many spectral features in different wavelength ranges and are easily observed in spectra of late-type stars, even in the most extreme metal-poor stars, e.g. the oldest stars in the Galaxy. Thus, the need for investigation of inelastic collisions of hydrogen atoms with magnesium atoms is well justified.

2 Methods and results

Non-adiabatic nuclear dynamical calculations have been performed by means of the reprojection method [5] in the framework of the standard Born–Oppenheimer approach, which provides reliable physical results. The method takes into account

[1] Herzen State Pedagogical University, St. Petersburg, Russia

V. Grinin et al. (eds) Radiation mechanisms of astrophysical objects. Yerevan: Edit Print, 2017, pp. 265–266.

non-vanishing asymptotic non-adiabatic matrix elements, provides the correct incoming and outgoing asymptotic total wave functions, and removes non-adiabatic transitions between atomic-state channels in the asymptotic region. The present analysis of the reprojection procedure within the reprojection method shows a reliable convergence with respect to a number of channels treated.

We have performed full quantum calculations [6, 7] of cross sections and rate coefficients for all excitation and de-excitation processes for all transitions between the eight lowest atomic states of Mg in inelastic collisions with H, as well as for mutual neutralization processes in $Mg^+ + H^-$ collisions and their inverse processes, the ion-pair formation ones, involving these Mg atomic states.

The first group of partial processes consists of the processes with large values of the cross sections, typically larger than $10\,Å^2$ for endothermic processes. The processes with the largest cross sections are $Mg(3s4s\,^1S) + H \to Mg^+ + H^-$, $Mg(3s4s\,^1S) + H \to Mg(3s3d\,^1D) + H$, $Mg(3s4p\,^3P) + H \to Mg(3s3d\,^3D) + H$. The present calculations show that these cross sections are rather stable with respect to variation of a number of channels treated.

The second group consists of inelastic processes with moderate values of cross sections, typically with the values between $0.1\,Å^2$ and a few $Å^2$. This is the largest group. The processes of these two groups are important for astrophysical applications [2].

The third group consists of the processes with low cross sections. The inelastic processes for transitions between, from and to low-lying states (including the ground one) are typically in this group due to large energy splittings, which result in small non-adiabatic transition probabilities.

Acknowledgments. The work was partly supported by Ministry for Education and Science (Russian Federation).

References

1. *P.S. Barklem*, J. Phys. Conf. Ser., **397**, 012049, 2012.
2. *Y. Osorio, P.S. Barklem, K. Lind et. al.*, Astron. Astrophys., **579**, A53, 2015.
3. *R. Cayrel, E. Depagne, M. Spite et. al.*, Astron. Astrophys., **416**, 1117, 2004.
4. *K. Fuhrmann*, Mon. Not. Roy. Astron. Soc., **384**, 173, 2008.
5. *A.K. Belyaev*, Phys. Rev. A, **82**, 060701(R), 2010.
6. *A.K. Belyaev, P.S. Barklem, A. Spielfiedel et. al.*, Phys. Rev. A, **85**, 032704, 2012.
7. *M. Guitou, A. Spielfiedel, D.S. Rodionov et. al.*, Chem. Phys., **462**, 94, 2015.

Orbital Parameters and Variability of the Emission Spectrum Massive Double System 105 Tau

A.E. Tarasov[1]

E-mail: *aetarasov@mail.ru*

Using high resolution spectroscopy, we detected the weak lines of the secondary component in the known massive binary system 105 Tau. Orbital parameters of the system are derived. Observations show that both components are MS stars with the more evolved primary star. The orbital variability of the weak emission component in the profile of Hα line is found. Accretion disk is formed around the less massive secondary component.

Some massive double systems with the Main Sequence (MS) components demonstrate, as a rule, the presence of a weak emission component in the core of the Hα line. One of such systems is the well known single-lined binary system 103 Tau (HR 1659, HD 32990, Sp B3V, V = 5.3^m). The system was discovered as a single-lined spectroscopic binary in 1924 [1]. Its period ($P_{orb} = 58.25^d$) and orbital elements were found in [2] and corrected in [3]. The star has a weak emission component in the core of the Hα line [4].

For understanding nature of emission in the Hα line and obtaining an improved orbital solution of the system, we carried out high resolution spectroscopy of 103 Tau in the region of lines HeI λ 6678 Å and Hα in the coude focus of 2.6 m telescope of CrAO with the spectral resolution 30000 in 2001–2004.

In Fig. 1a we present two typical spectra in the region of the HeI λ 6678 Å line. As it is seen from the figure, we found a faint secondary component in orbital elongations and its intensity allows us to construct the orbit of the secondary and obtain the complete spectroscopic orbital solution of the system. Using the code FOTEL [5], we obtained an improved orbital solution with $P_{orb} = 58.305(3)$, $e = 0.277(27)$, $K_{prim} = 44.8(2.8)\,\mathrm{km\,s^{-1}}$, $K_{sec} = 79.3(8.7)\,\mathrm{km\,s^{-1}}$, $\gamma = 14.6(1.0)$, $M_{prim}\sin^3 i = 6.6\,M_\odot$, $M_{sec}\sin^3 i = 3.7\,M_\odot$, $a\sin i = 50\,R_\odot$ and $b\sin i = 88\,R_\odot$. Variability of the radial velocities with the phase of the orbital period and the orbital solution obtained are presented in Fig. 1b.

The rotational velocities of both components of the system are synchronized in periastron. For the primary component, $v\sin i = 47 \pm 11\,\mathrm{km\,s^{-1}}$ [6] is identical to $K_{prim} = 45.7 \pm 2.1\,\mathrm{km\,s^{-1}}$. Our estimates of the rotational velocity of the secondary have lower quality because of low intensity of the line, but it is less than 80 $\mathrm{km\,s^{-1}}$ and is close to the orbital value $K_{sec} = 78.9 \pm 6.2\,\mathrm{km\,s^{-1}}$.

[1] Crimean Astrophysical Observatory of RAS, Russia

V. Grinin et al. (eds) Radiation mechanisms of astrophysical objects. Yerevan: Edit Print, 2017, pp. 267–268.

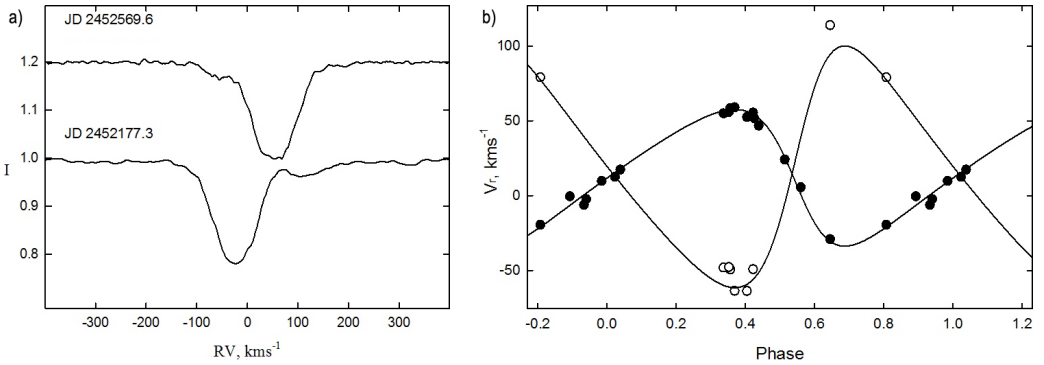

Figure 1: a) Spectral region around the HeI λ 6678 Å line. b) Radial velocity changes with the phase of the orbital period. Dots show the radial velocities of the primary component, open circles do the radial velocities of the secondary component.

Our analysis of the orbital variability of the faint emission component in the core of Hα line allows us to locate it in the Roche lobe of the secondary, which most probably is a late B star on MS. The primary, more massive component, is a MS or normal giant star that definitely has not reached its Roche lobe and cannot be an active mass loser. For the secondary, synchronization of the rotational and orbital velocities in periastron means that the accretion disc has appeared, which says about sporadic mass loss by the primary or recently started mass exchange.

References

1. *S.N. Adams, A.H. Joy, R.F. Sanford*, Publ. Astron. Soc. Pacific, **36**, 137, 1924.
2. *S.N. Hill*, Publ. Domin. Astrophys. Obs., **4**, 261, 1929.
3. *H.A. Abt, A.E. Gomez, S.G. Levy*, Astrophys. J. Supll., **74**, 551, 1990.
4. *J. Boulon, V. Doazan, N. Letourneur*, Astron. Astrophys., **40**, 203, 1975.
5. *P. Hadrava*, Prep. Astron. Inst. Czech. Acad. Sci., 1, 1991.
6. *W. Huang, D.R. Gies, M.V. McSwain*, Astrophys. J., **722**, 605, 2010.

Atomic Data for Inelastic Processes in Collisions of Beryllium and Hydrogen

Ya.V. Voronov[1], S.A. Yakovleva[1], A.K. Belyaev[1]

E-mail: *voronov_yaroslav@mail.ru*

The recently proposed model approach is applied to low-energy inelastic beryllium-hydrogen collisions for the purpose of obtaining quantum data for inelastic processes in beryllium-hydrogen collisions. The cross sections and the rate coefficients for the excitation, de-excitation, mutual neutralization and ion-pair formation processes are calculated.

1 Introduction

Atomic and molecular data on the inelastic processes in low-energy collisions of beryllium with hydrogen are important for astrophysical modeling of stellar atmospheres. Accurate quantum calculations are time-consuming and require accurate quantum-chemical input data. For this reason, it is important to develop and apply reliable model approaches, e.g. the approach described in [1, 2]. The approach is developed within the framework of the Born–Oppenheimer formalism and based on the asymptotic method [1] for construction of potential energy curves and on the multichannel formula [2] for calculations of non-adiabatic transition probabilities. It has been shown [2] that the data obtained by the model approach and by full quantum calculations are in good agreement for processes with large cross sections, i.e. the processes of the main interest for astrophysical applications.

2 Brief theory

A transition probability for a single passing of a non-adiabatic region created by molecular states k and $k+1$ is calculated within the Landau–Zener model [3]

$$p_k = \exp\left(-\frac{\xi_k^{LZ}}{v}\right), \quad \xi_k^{LZ} = \frac{\pi}{2\hbar}\sqrt{\frac{Z_k^3}{Z_k''}}\Bigg|_{R=R_c}, \tag{1}$$

with Z_k being a local minimum of an adiabatic splitting (see [3] for details). The total probability for a transition from an initial state i to a final state f is obtained by the multichannel formula [2]

[1] Dept. Theoretical Physics and Astronomy, Herzen University, St. Petersburg, Russia

V. Grinin et al. (eds) Radiation mechanisms of astrophysical objects. Yerevan: Edit Print, 2017, pp. 269–270.

$$P_{if}^{tot} = 2p_f(1-p_f)(1-p_i)\prod_{k=f+1}^{i-1} p_k \left\{1 + \sum_{m=1}^{2(f-1)} \prod_{k=1}^{m} \left(-p_{f-\left[\frac{k+1}{2}\right]}\right)\right\} \times \left\{1 - \frac{\prod_{k=i}^{F} p_k^2 \left(1 + \sum_{m=1}^{2(i-1)} \prod_{k=1}^{m} \left\{-p_{i-\left[\frac{k+1}{2}\right]}\right\}\right)}{\sum_{m=1}^{2F} \prod_{k=1}^{m} \left(-p_{F+1-\left[\frac{k+1}{2}\right]}\right)}\right\}, \quad (2)$$

where F is a total number of open channels. The cross sections and rate coefficients are calculated as usual.

3 Results

Cross sections and rate coefficients of inelastic low-energy beryllium-hydrogen collisions for 12 covalent states and one ionic are calculated. The labels are shown in Fig. 1, where the channel $j = 13$ corresponds to the ionic one, $Be^+(2s\ ^2S)+H^-$. Rate coefficients are presented in Fig. 1 in form of heatmap. It is seen that the largest rate coefficients correspond to non-adiabatic transitions between the ionic state, the $Be(2s3p\ ^{1,3}P)$, $Be(2s3d\ ^3D)$ and $Be(2s3s\ ^1S)$ states.

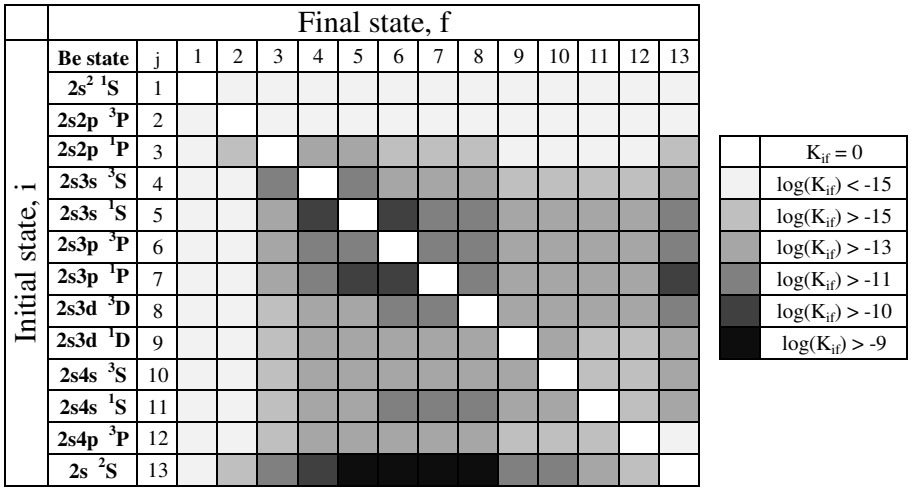

Figure 1: Calculated rate coefficients for Be+H, Be^++H^- collisions for $T = 6000$ K.

Acknowledgments. A support from the Ministry for Education and Science (Russia) is acknowledged.

References

1. *A.K. Belyaev*, Phys. Rev. A, **88**, 052704, 2013.
2. *A.K. Belyaev, S.A. Yakovleva, P.S. Barklem*, Astron. Astrophys., **572**, A103, 2014.
3. *A.K. Belyaev, O.V. Lebedev*, Phys. Rev. A, **84**, 014701, 2011.

Section IV
High-Energy Astrophysics
and Cosmology

Polarimetric Method for Measuring Black Hole Masses in Active Galactic Nuclei Based on Theory of V.V. Sobolev and S. Chandrasekhar

Yu.N. Gnedin[1], M.Yu. Piotrovich[1]

E-mail: *gnedin@gao.spb.ru*

The V.V. Sobolev and S. Chandrasekhar theory of polarized radiation presents the main basis for modern science of the polarized emission of cosmic objects including X-rays and gamma-rays. The accreting supermassive black holes (SMBH) in active galactic nuclei (AGN) are found in the center of modern astrophysics. The main problem is connected with determining the masses of these objects. The virial theorem accepted to a flattened configuration of a broad line region (BLR) in AGNs allows us to get a direct connection between the mass of SMBH and the inclination angle of the accretion flow. The inclination angle itself can be derived from the spectropolarimetric data of broad emission lines using the theory for generation of polarized radiation developed by Sobolev and Chandrasekhar. As a result, the new estimates of SMBH masses in AGN with measured polarization of BLR emission are presented. It is essential that the polarimetric data allow also to determine the value of the virial coefficient that is important for determining SMBH masses and to estimate the recoiling velocity of SMBH.

1 Introduction

AGNs are powered by accretion to a SMBHs, and the broad emission lines seen in Type I AGN are produced in the special region that is named as the broad line region (BLR). Unfortunately, the structure and kinematics of BLR remain unclear. Really, broad emission lines are emitted in the vicinity of SMBH in AGN, but this region is not resolved in interferometric observations. Nevertheless, the properties of the broad emission lines are used to estimate the mass of the central SMBH.

The commonly accepted method for estimating the SMBH mass is to use the virial theorem. It allows to get the following relation [1, 2]:

$$M_{BH} = f\frac{R_{BLR}V_{BLR}^2}{G}, \tag{1}$$

[1] Central Astronomical Observatory at Pulkovo, St. Petersburg, Russia

V. Grinin et al. (eds) Radiation mechanisms of astrophysical objects. Yerevan: Edit Print, 2017, pp. 273–283.

where M_{BH} is the mass of a black hole, f is a virial parameter that defines the geometry, velocity field and orientation of BLR, R_{BLR} is the radius of BLR and V_{BLR} is the velocity dispersion that is usually measured as the full width of the emission line at a half of height in the radiation spectrum, i.e. FWHM. The BLR radius R_{BLR} is usually determined by the reverberation method, i.e. with time delay between continuum and emission line variations.

Determination of the f value is strongly depending on accepted BLR model. Labita et al. [3] found that the model of an isotope BLR fails to reproduce the observed line widths and shapes. They claimed that a disk model is preferred. A disk-like geometry of the BLR has been proposed by several authors [4]. Collin et al. [5] suggested that the disk may have a finite half thickness H, or a profile with H increasing more than linearly with the disk radius. Other models propose the existence of warped disks [6].

The authors of [7] and [8] found that the hydrogen lines are emitted in a more flattened BLR configuration in comparison to the highly ionized lines. They estimated the ratios of H/R in BLR for a number of AGNs and obtained the interval of $H/R \sim 0.07$–0.5. Also Pancoast et al. [9] found that the geometry of the BLR is generally a thick disk viewed close to face on. Eracleous and Halpern [10] have found that the inclination angle of BLR is 24–30°. Eracleous et al. [11] estimated the inclination angle of the BLR as $i = 19$–$42°$. It is interesting to note that the polarimetric observations do not contradict these estimates [12, 13, 14].

The virial coefficient f depends strongly on the BLR geometry, velocity field and orientation. Usually the authors used the value $f \approx 1$. Peterson and Wandel [15] used $f = 3/4$. Onken et al. [16] suggested to use the mean value of the virial coefficient $f = 1.4$. McLure and Dunlop [17] have shown that for a disk inclined at an inclination angle i the virial coefficient value is

$$f = \frac{1}{4\sin^2 i}. \tag{2}$$

Collin et al. [5] have considered the situation when the opening angle of the BLR disk should be large, i.e. $\Omega/4\pi \geq 0.1$. It means that the half thickness H of the disk should be large enough and the ratio of H to the radius R should be larger than $H/R = 0.1$. As a result, the virial coefficient has a form:

$$f = \frac{1}{4\big[(H/R)^2 + \sin^2 i\big]}. \tag{3}$$

This way, the relation (2) is a particular case of Eq. (3).

We adopted the disk-like model for the BLR of a number of Seyfert galaxies and, therefore, will use the expression for the virial coefficient f given by Eq. (2). The required value of the inclination angle can be determined from polarimetric observations using the standard Chandrasekhar–Sobolev theory [18, 19] of multiple scattering of the radiation on free electrons and Rayleigh scattering on gas molecules and small dist particles. According to these classical works, the polarization degree of scattered radiation depends strongly on the inclination

angle. The scattered radiation has the maximum linear polarization $P_l = 11.7\%$ when the line of sight is perpendicular to the normal to the semi-infinite atmosphere (Milne problem). Chandrasekhar [18] and Sobolev [19] presented the solution of this Milne problem. They have considered the multiple scattering of light in optically thick flattened atmospheres. The Milne problem corresponds to the propagation and scattering of light in optically thick disk-like region, i.e. this solution can be directly applied to BLR problem.

2 Polarimetric determining of the virial coefficient

We use the theory of multiple scattering of polarized radiation [18, 19, 20] and the disk-like model for the BLR.

We take into account the process of absorption of radiation. In this case the degree of polarization depends on the parameter $q = \sigma_a/(\sigma_a + \sigma_{SC})$, where σ_a is the cross-section of intrinsic absorption and σ_{SC} is the scattering cross-section. For the standard accretion disk model $\sigma_{SC} = \sigma_{Th}$, where $\sigma_{Th} = 6.65 \times 10^{-25}$ cm^2 is the cross-section for scattering of radiation on electrons, which in the non-relativistic case is the classical Thomson scattering cross-section. For some cases it is convenient to use the analytical formula for the polarization degree $P_l(\mu)$ obtained by Silant'ev et al. [21]. Using Eq. (2), we can obtain the values of the polarization degree and their dependence of the virial coefficient f. The results of these calculations are presented in Table 1.

For the model of a disk shaped BLR, the sine of the inclination angle is determined by [22]

$$\sin i = \frac{1}{2}\left(\frac{R_{BLR}}{R_g}\right)^{1/2}\frac{FWHM}{c}, \tag{4}$$

where i is the inclination angle, R_{BLR} is the radius of the BLR, $FWHM$ is the full width half maximum of a given line, which can be measured directly, c is the speed of light, $R_g = GM_{BH}/c^2$ is the gravitational radius. The value of $R_{BLR}V_{BLR}^2/G$ is called the "virial product" (VP). This quantity is based on two observable quantities: BLR radius and emission line width and has units of mass. The VP corresponds to the quantity of the virial coefficient $f = 1$ and with accordance to Eq. (2) corresponds to the inclination angle $i = 30^\circ$. According to [18] and [19], it means that the observed BLR emission polarization is $P_l(\mu) = 0.43\%$.

Equation (2) has been used for determining the virial coefficient. The polarimetric data that are necessary for determining the value of the inclination angle and the virial coefficient are presented in the spectropolarimetric atlas of Smith et al. [12]. They obtained the values of polarization degree and position angle for 36 Type 1 Seyfert galaxies during a number of different runs at the Anglo-Australian and William Herschel telescopes. From 36 objects presented in [12] 13 AGNS have the equal polarization degree values for H_α line and continuum. Also these objects have equal values of the position angle with the error limits. For most of the observed objects, there is a difference between

Table 1: Polarization degree P_l [%] dependence on q and μ, f is virial coefficient

μ	f	$q = 0.0$	$q = 0.01$	$q = 0.05$	$q = 0.1$	$q = 0.2$	$q = 0.3$
0.000	0.2500	11.713	12.592	16.074	20.349	28.636	36.642
0.025	0.2502	10.041	10.937	14.488	18.852	27.324	35.516
0.050	0.2506	8.986	9.889	13.473	17.879	26.440	34.723
0.075	0.2514	8.150	9.057	12.656	17.085	25.691	34.019
0.100	0.2525	7.449	8.357	11.961	16.395	25.015	33.354
0.125	0.2540	6.844	7.751	11.349	15.776	24.382	32.704
0.150	0.2558	6.312	7.215	10.799	15.209	23.776	32.056
0.175	0.2579	5.838	6.735	10.297	14.679	23.187	31.403
0.200	0.2604	5.410	6.301	9.834	14.178	22.607	30.737
0.225	0.2633	5.022	5.904	9.401	13.699	22.031	30.056
0.250	0.2667	4.667	5.539	8.994	13.237	21.455	29.356
0.275	0.2705	4.342	5.201	8.608	12.789	20.876	28.636
0.300	0.2747	4.041	4.887	8.240	12.352	20.291	27.895
0.325	0.2795	3.762	4.594	7.887	11.922	19.700	27.132
0.350	0.2849	3.502	4.318	7.547	11.498	19.100	26.346
0.375	0.2909	3.260	4.059	7.217	11.078	18.491	25.538
0.400	0.2976	3.033	3.813	6.897	10.660	17.872	24.707
0.425	0.3051	2.820	3.581	6.584	10.244	17.242	23.854
0.450	0.3135	2.620	3.359	6.278	9.829	16.602	22.979
0.475	0.3228	2.431	3.148	5.977	9.414	15.950	22.083
0.500	0.3333	2.252	2.947	5.681	8.997	15.287	21.166
0.525	0.3451	2.083	2.753	5.389	8.580	14.612	20.230
0.550	0.3584	1.923	2.568	5.100	8.160	13.926	19.275
0.575	0.3735	1.771	2.389	4.813	7.737	13.230	18.302
0.600	0.3906	1.627	2.217	4.529	7.312	12.522	17.312
0.625	0.4103	1.489	2.050	4.246	6.883	11.803	16.306
0.650	0.4329	1.358	1.889	3.965	6.452	11.074	15.285
0.675	0.4592	1.233	1.732	3.684	6.016	10.335	14.250
0.700	0.4902	1.113	1.580	3.404	5.577	9.586	13.202
0.725	0.5270	0.998	1.433	3.124	5.135	8.828	12.143
0.750	0.5714	0.888	1.289	2.844	4.688	8.061	11.072
0.775	0.6260	0.783	1.148	2.563	4.237	7.285	9.992
0.800	0.6944	0.682	1.011	2.282	3.782	6.502	8.903
0.825	0.7828	0.585	0.876	2.001	3.323	5.710	7.807
0.850	0.9009	0.492	0.744	1.719	2.861	4.912	6.704
0.875	1.0667	0.402	0.615	1.435	2.394	4.107	5.595
0.900	1.3158	0.316	0.488	1.151	1.923	3.296	4.482
0.925	1.7316	0.233	0.363	0.865	1.448	2.479	3.365
0.950	2.5641	0.152	0.240	0.578	0.969	1.658	2.245
0.975	5.0633	0.075	0.119	0.290	0.486	0.831	1.123
1.000	–	0.000	0.000	0.000	0.000	0.000	0.000

the values of polarization degree and the position angle. This phenomenon can testify to the difference in the inclination between the disk shaped BLR and the accretion disk that can be described by Shakura–Sunyaev model [23]. Continuum polarization degree of AGN from Palomar–Green catalog has been measured on 6 m telescope of Special Astrophysical Observatory [14].

Some results for the virial coefficient f are presented in Table 1 of our paper [24]. In the second column of this table the values for the BLR inclination angles are presented. These data are obtained from polarimetric data derived by Smith et al. [12]. The values of inclination angles have been obtained with use of the standard Chandrasekhar–Sobolev theory of multiple scattering of polarize radiation in the disk-like electron atmosphere and with use of Eq. (4). The virial factor for most of data in Table 1 from [24] corresponds to $f \sim 1$ within error limits, in accordance with [25]. For some objects, including Mrk 841, Mrk 896, Mrk 976, NGC 3516, NGC 3783 and NGC 5548, the virial coefficient is close to the mean value of $f = 1.4$ [16].

For a number of objects, including Fairall 51, Mrk 6, MC 1849.2-78.32, NGC 6814, UGC 3478 and WAS 45, their inclination angle exceeds considerably the value of $i = 30°$. It means that their virial factor $f < 1.0$. This situation corresponds better to the BLR model of random orbits.

3 Determining SMBH masses

Equation (1) allows to derive the SMBH mass if the virial coefficient is known. The observed full width of emission lines is presented in [1, 26, 27, 28]. The radius R_{BLR} is estimated usually by the reverberation mapping that is related to the continuum monochromatic luminosity λL_λ. An increasing body of measurements is now available for H_β time lags [29, 30, 4, 31]. For example, from Bentz et al [31] one can obtain the following estimate for R_{BLR}:

$$\log\left(R_{BLR}/1\,\mathrm{ltd}\right) = K + \alpha \log \frac{\lambda L(5100\,\text{Å})}{10^{44}\,\mathrm{erg/s}}, \tag{5}$$

where $K = 1.527^{+0.031}_{-0.03}$, $\alpha = 0.533^{+0.035}_{-0.039}$ and R_{BLR} is measured in light days (ltd).

Equation (5) allows to present the BLR radius in the form

$$R_{BLR} = 10^{16.94} \left(\frac{\lambda L_\lambda(5100\,\text{Å})}{10^{44}\,\mathrm{erg/s}}\right)^{0.533}. \tag{6}$$

Then, using Eqs. (2) and (4), one can get the values of the SMBH masses. The value of $\sin i$ can be derived from the data on the degree of polarization that is strongly dependent on the inclination angle.

The results of our calculations of the SMBH masses are presented in Table 2 [24]. In the last column of this table the published values for SMBH masses are presented. There is a difference for a number of objects. For example, for Fairall 9 our estimate of the SMBH mass looks lower, but our upper

Table 2: The masses of SMBH in AGNs determined via measured polarization of broad H_α emission

Object	$M_{BH}/M_\odot$ (observations)	$M_{BH}/M_\odot$ (literature)
Akn 120	$(3.23^{+0.44}_{-0.32}) \times 10^8$	$(4.49 \pm 0.93) \times 10^8$
Akn 564	$(1.2^{+0.94}_{-0.49}) \times 10^6$	$\sim 1.1 \times 10^6$
Fairall 9	$(1.34^{+0.76}_{-0.36}) \times 10^8$	$(2.55 \pm 0.56) \times 10^8$
I Zw 1	$10^{7.6 \pm 0.17}$	$10^{7.441^{+0.093}_{-0.119}}$
Mrk 6	$(1.09^{+0.37}_{-0.25}) \times 10^8$	$(1.36 \pm 0.12) \times 10^8$
Mrk 279	$(8.13^{+1.24}_{-1.26}) \times 10^7$	$(15.2^{+3.25}_{-3.18}) \times 10^7$
Mrk 290	$(3.94 \pm 0.19) \times 10^7$	$(2.43 \pm 0.37) \times 10^7$
Mrk 304	$10^{8.4^{+0.09}_{-0.02}}$	$10^{8.511^{+0.093}_{-0.113}}$
Mrk 335	$(1.56^{+0.19}_{-0.15}) \times 10^7$	$(1.42 \pm 0.37) \times 10^7$
Mrk 509	$(1.35 \pm 0.12) \times 10^8$	$(1.39 \pm 0.12) \times 10^8$
Mrk 705	$10^{7.07^{+0.11}_{-0.09}}$	$10^{6.79 \pm 0.5}$
Mrk 841	$10^{8.55 \pm 0.1}$	$10^{8.523^{+0.079}_{-0.052}}$
Mrk 871	$10^{7.04^{+0.09}_{-0.06}}$	$10^{7.08 \pm 0.5}$
Mrk 876	$10^{8.57^{+0.19}_{-0.52}}$	$10^{9.139^{+0.096}_{-0.122}}$
Mrk 896	$10^{7.07 \pm 0.06}$	$10^{7.01}$
Mrk 926	$10^{8.8^{+0.19}_{-0.11}}$	$10^{8.36 \pm 0.02}$
Mrk 985	3.18×10^7	5.71×10^7
NGC 3516	$10^{8.06 \pm 0.27}$	$10^{7.88^{+0.04}_{-0.03}}$
NGC 3783	$10^{7.7 \pm 0.11}$	$10^{7.47^{+0.07}_{-0.09}}$
NGC 4051	$(1.64^{+0.67}_{-0.55}) \times 10^6$	$(1.58^{+0.50}_{-0.65}) \times 10^6$
NGC 4593	$(8.25^{+3.46}_{-3.06}) \times 10^6$	$(9.8 \pm 2.1) \times 10^6$
NGC 5548	$(7.84^{+0.53}_{-0.46}) \times 10^7$	$(7.827 \pm 0.017) \times 10^7$
NGC 6104	$10^{7.16^{+0.09}_{-0.08}}$	$10^{7.39}$
NGC 6814	$10^{6.94^{+0.077}_{-0.09}}$	$10^{7.02 \pm 0.5}$
NGC 7213	$10^{6.83^{+0.84}_{-0.33}}$	$10^{6.88 \pm 0.5}$
NGC 7469	$10^{7.54^{+0.17}_{-0.22}}$	$10^{7.19 \pm 0.13}$
PG 1211+143	$10^{8.34^{+0.29}_{-0.20}}$	$10^{7.961^{+0.082}_{-0.101}}$

limit value coincides with the low order limit value of BH mass obtained by Reynolds [32]. For Ark 120 the situation looks the same: there is a coincidence between our estimated value and the low order value of BH mass obtained by Vestergaard and Peterson [1]. The similar situation occurs also for NGC 3516, NGC 3783, NGC 5548, and Mrk 279. The extreme case is Mrk 290. Our low order estimate appears 1.34 times higher than the upper limit of BH mass presented by Feng et al. [28].

This difference between our and other estimates of mass values for some black holes can be associated with the real determination of the virial coefficient f from the Eq. (1). Value of virial coefficient from the papers [17, 25] allows us

to determine this parameter directly from Eq. (2) but only in the situation when the inclination angle of the BLR is certain. Polarimetric observations have preference because the value of polarization degree is directly associated with the inclination angle value, especially for standard Chandrasekhar–Sobolev theory of the generation of polarization in the plane-parallel atmosphere. Other methods for determination of inclinations of BLRs and accretion disks are considerably uncertain. Unfortunately, the size of the BLR cannot be directly measured from single epoch spectra, which are used for estimation of BH masses. Most popular estimates of BLR size rely on the R_{BLR} scales with a certain power of continuum luminosity of the AGN.

4 Determining recoiling velocities of black holes ejected by gravitational radiation in galaxy mergers

We demonstrate that polarimetric observations allow to derive the recoiling velocity of black hole ejected by gravitational radiation produced in the process of black holes merging. Really merging of spinning black holes can produce recoil velocities ("kicks") of the final merged black holes via anisotropic gravitational radiation up to several thousands km/s [33, 34, 35]. The basic feature of the gravitational wave (GW) recoil effect is the situation when the SMBH spends a significant fraction of time off nucleus at scales beyond that of the molecular obscuring torus. For example, according to [36], isophotal analysis of M87, using data from Advanced Camera for Surveys, reveals a projected displacement of 68 ± 0.8 pc ($\sim 0.''1$) between the nuclear point source and the photo-center of the galaxy itself.

It is very important that a recoiling SMBH in an AGN retains the inner part of its accretion disk. Bonning et al. [37] have shown that the accretion disk will remain bound to the recoiling BH inside the radius $R_{out} = 1.3 \times 10^{18} M_8 / V_3^2$ cm ($M_8 = M_{BH}/10^8 M_\odot$, $V_3 = V/10^3$ km/s), where the orbital velocity V is equal to the recoil velocity V_K. In this case the retained disk mass appears less than the BH mass because of stability requirement [33].

If we suggest that $R_{BLR} \approx R_K$, we obtain the following relation instead of Eq. (4):

$$\sin i = 0.492 \left(\frac{FWHM}{V_K} \right). \tag{7}$$

In this case, when $FWHM = 1500$ km/s and $V_K = 10^3$ km/s, we obtain $P_l(H_\beta) = 1.24\%$. For $V_K = 3 \times 10^3$ km/s, we obtain $P_l(H_\beta) = 0.1\%$. According to [38], for merging black hole with spin value $a = 1.0$, the kick velocity has magnitude of $V_K = 4925.94$ km/s. For $FWHM = 5 \times 10^3$ km/s the polarization degree is $P_l(H_\beta) = 0.624\%$. For H_α emission line, the values of polarization degree are practically the same because of the practical equality of FWHMs [39].

According to [33], the accretion disk remains bound to the ejected BH within the region where the accreting matter orbital velocity is larger than the ejection

speed. For example, the ejected disk of $10^7 M_\odot$ BH has a characteristic size of tens of thousands of Schwarzschild radii and an accretion lifetime of $\sim 10^7$ years. But in this case the ejected BH could traverse a considerable distance and appears as an off-center galaxy region. Loeb [33] claimed that only small fraction of all quasars could be associated with an escaping SMBH.

Equation (7) allows us to find the candidates for escaping BHs. According to [40] and [5], the virial coefficient can be presented in the form

$$f = \frac{1}{4\left[\left(\frac{V_K}{V_{orb}}\right)^2 + \sin^2 i\right]}. \tag{8}$$

In this case Eq. (4) is transforming in the expression

$$\sqrt{\left(\frac{V_K}{V_{orb}}\right)^2 + \sin^2 i} = \frac{FWHM}{2c}\left(\frac{R_{BLR}}{R_g}\right)^{1/2}. \tag{9}$$

The value of $\sin i$ can be obtained from polarimetric observations, naturally if we use the theory of multiple scattering of polarized radiation developed by Chandrasekhar and Sobolev. If we consider the situation $R_K \approx R_{BLR}$ and $V_K < V_{orb}$, we obtain instead of Eq. (7) the following relation:

$$\sqrt{\left(\frac{V_K}{V_{orb}}\right)^2 + \sin^2 i} = 0.492\left(\frac{FWHM}{V_K}\right). \tag{10}$$

For example, for $V_K = 0.5\,V_{orb}$, $\sin i = 0.847$, that corresponds to $P_l(\mu) = 2.05\%$. We estimated the values of kick velocity from a number of AGN using the polarimetric data from [12] and estimates of R_{BLR} obtained in [41]. For estimates of M_{BH}, we used the relation (6) from [1].

As a result we obtained the following estimates of the recoiling velocities: $V_K = 0.22\,V_{orb}$ for Ark 120 and Mrk 279, $V_K = 0.42\,V_{orb}$ for NGC 3516, $V_K = 0.288\,V_{orb}$ for NGC 3783, $V_K = 0.31\,V_{orb}$ for NGC 4593. It is interesting that for NGC 4051 the situation occurs when $V_K \approx V_{orb}$.

Of course, our results have a preliminary character, because another situation can be considered when the coefficient $A = H/R$, where H is the geometrical thickness of the BLR [5]. It means that the BLR is the geometrically thick accretion disk compared with the geometrically thin accretion disk that provides the continuum polarization.

5 Conclusions

We demonstrated that V.V. Sobolev and S. Chandrasekhar theory of the multiple scattering of polarized radiation is an efficient instrument for an analysis and interpretation of the polarimetric data of AGNs. The virial theorem accepted to a disk-like configuration of BLR in AGN allows us to determine the real mass of AGN if the inclination angle of the accretion flow is known. Namely,

the polarimetric observations allow us to derive the inclination angle itself using the theory for the generation of polarized radiation developed by Sobolev and Chandrasekhar. As a result we have demonstrated the possibility of polarimetric determining of the virial coefficient and, as the final result, determining the mass of SMBH in AGN. In principle, polarimetric observations allow us to derive the recoil velocity of a black hole ejected by gravitational radiation as a result of a galaxy merger.

Acknowledgments. This research was supported by the Basic Research Program P-7 of Presidium of RAS and the program of the Department of Physical Sciences of RAS No. 2.

References

1. *M. Vestergaard, B.M. Peterson*, Astrophys. J., **641**, 689, 2006.
2. *S. Fine, S.M. Croom, P.F. Hopkins et al.*, Mon. Not. Roy. Astron. Soc., **390**, 1413, 2008.
3. *M. Labita, A. Treves, R. Falomo, M. Uslenghi*, Mon. Not. Roy. Astron. Soc., **373**, 551, 2006.
4. *R. Decarli, M. Labita, A. Treves, R. Falomo*, Mon. Not. Roy. Astron. Soc., **387**, 1237, 2008.
5. *S. Collin, T. Kawaguchi, B.M. Peterson, M. Vestergaard*, Astron. Astrophys., **456**, 75, 2006.
6. *S. Tremaine, S.W. Davis*, Mon. Not. Roy. Astron. Soc., **441**, 1408, 2014.
7. *W. Kollatschny, M. Zetzl, M. Dietrich*, Astron. Astrophys., **454**, 459, 2006.
8. *W. Kollatschny, M. Zetzl*, Astron. Astrophys., **558**, A26, 2013.
9. *A. Pancoast, B.J. Brewer, T. Treu, LAMP2008 Collaboration, LAMP2011 Collaboration*, Amer. Astron. Soc. Meet. Abstr., **221**, 309.08, 2013.
10. *M. Eracleous, J.P. Halpern*, Astrophys. J. Suppl., **90**, 1, 1994.
11. *M. Eracleous, J.P. Halpern, M. Livio*, Astrophys. J., **459**, 89, 1996.
12. *J.E. Smith, S. Young, A. Robinson et al.*, Mon. Not. Roy. Astron. Soc., **335**, 773, 2002.
13. *J.E. Smith, A. Robinson, D.M. Alexander et al.*, Mon. Not. Roy. Astron. Soc., **350**, 140, 2004.
14. *V.L. Afanasiev, N.V. Borisov, Y.N. Gnedin et al.*, Astron. Lett., **37**, 302, 2011.
15. *B.M. Peterson, A. Wandel*, Astrophys. J. Lett., **521**, L95, 1999.
16. *C.A. Onken, L. Ferrarese, D. Merritt et al.*, Astrophys. J., **615**, 645, 2004.
17. *R.J. McLure, J.S. Dunlop*, Mon. Not. Roy. Astron. Soc., **327**, 199, 2001.
18. *S. Chandrasekhar*, Radiative Transfer. Oxford: Clarendon Press, 1950.

19. *V.V. Sobolev*, A Treatise on Radiative Transfer. Princeton: Van Nostrand, 1963.

20. *N.A. Silant'ev*, Astron. Astrophys., **383**, 326, 2002.

21. *N.A. Silant'ev, M.Y. Piotrovich, Y.N. Gnedin, T.M. Natsvlishvili*, Astron. Rep., **54**, 974, 2010.

22. *B. Agís-González, G. Miniutti, E. Kara et al.*, Mon. Not. Roy. Astron. Soc., **443**, 2862, 2014.

23. *N.I. Shakura, R.A. Sunyaev*, Astron. Astrophys., **24**, 337, 1973.

24. *M.Y. Piotrovich, Y.N. Gnedin, N.A. Silant'ev et al.*, Mon. Not. Roy. Astron. Soc., **454**, 1157, 2015.

25. *R.J. McLure, M.J. Jarvis*, Mon. Not. Roy. Astron. Soc., **337**, 109, 2002.

26. *L.C. Ho, J. Darling, J.E. Greene*, Astrophys. J. Suppl., **177**, 103, 2008.

27. *J.-G. Wang, X.-B. Dong, T.-G. Wang et al.*, Astrophys. J., **707**, 1334, 2009.

28. *H. Feng, Y. Shen, H. Li*, Astrophys. J., **794**, 77, 2014.

29. *S. Kaspi, P.S. Smith, H. Netzer et al.*, Astrophys. J., **533**, 631, 2000.

30. *M.C. Bentz, B.M. Peterson, H. Netzer et al.*, Astrophys. J., **697**, 160, 2009.

31. *M.C. Bentz, K.D. Denney, C.J. Grier et al.*, Astrophys. J., **767**, 149, 2013.

32. *C.S. Reynolds*, Space Sci. Rev., **183**, 277, 2014.

33. *A. Loeb*, Phys. Rev. Lett., **99**, 041103, 2007.

34. *G.A. Shields, E.W. Bonning*, Astrophys. J., **682**, 758, 2008.

35. *S. Komossa, D. Merritt*, Astrophys. J. Lett., **689**, L89, 2008.

36. *D. Batcheldor, A. Robinson, D.J. Axon et al.*, Astrophys. J. Lett., **717**, L6, 2010.

37. *E.W. Bonning, G.A. Shields, S. Salviander*, Astrophys. J. Lett., **666**, L13, 2007.

38. *C.O. Lousto, Y. Zlochower*, Phys. Rev. Lett., **107**, 231102, 2011.

39. *J.E. Greene, L.C. Ho*, Astrophys. J., **630**, 122, 2005.

40. *X.-B. Wu, J.L. Han*, Astrophys. J. Lett., **561**, L59, 2001.

41. *J.E. Greene, C.E. Hood, A.J. Barth et al.*, Astrophys. J., **723**, 409, 2010.

Black Holes in Binary Systems and Nuclei of Galaxies

A.M. Cherepashchuk[1]

E-mail: *Cherepashchuk@gmail.com*

During last 45 years, a big progress has been achieved in observational investigations of stellar mass black holes in X-ray binary systems and supermassive black holes in galactic nuclei. Masses of several dozens of stellar mass black holes ($M_{BH} = 4 \div 20 M_\odot$) as well as many hundreds of supermassive black holes ($M_{BH} = 10^6 \div 10^{10} M_\odot$) were measured. Recent discovery of gravitational waves from a binary black hole merger opens new era in investigations of black holes.

1 Introduction

In the last 45 years, following pioneering papers by Ya.B. Zeldovich [1] and E.E. Salpeter [2] in which powerful energy release from non-spherical accretion of matter onto black holes (BH) was predicted, many observational investigations of BHs in the Universe have been carried out. To date, the masses of several dozens stellar-mass BH ($M_{BH} = 4 \div 20 M_\odot$) in X-ray binary systems and many hundreds supermassive BH ($M_{BH} = 10^6 \div 10^{10} M_\odot$) in galactic nuclei have been measured. The estimated radii of these massive and compact objects do not exceed several gravitational radii.

Observations suggest (taking into account observational selection effects) that the number of stellar-mass BHs ($M = 8 \div 10 M_\odot$) in our Galaxy amounts to at least 10^7 or 0.1% of the baryonic matter. A great discovery was made recently by American gravitational wave antennas LIGO1 and LIGO2: gravitational waves were detected from a binary black hole merger GW150914 [3].

Black holes are derived from the collapse of massive objects. According to modern concepts taking into account general relativity effects, if the mass of the stellar core where thermonuclear burning occurs exceeds $3M_\odot$ the gravitational core collapse results in the formation of a BH. If the mass of the stellar core is less than $3M_\odot$, the stellar evolution ends up with the formation of neutron star or a white dwarf.

A black hole is an object (more precisely, a space-time region) with such a strong gravitational field that no signal, including light, can escape from it to the space infinity. Characteristic dimension of BH is given by the gravitational (Schwarzschild) radius: $r_g = 2GM/c^2$, where M is the mass of the object, G is the Newtonian constant of gravitation, and c is the speed of light in vacuum.

[1] Lomonosov Moscow State University, Sternberg Astronomical Institute, Russia

V. Grinin et al. (eds) Radiation mechanisms of astrophysical objects. Yerevan: Edit Print, 2017, pp. 283–295.

In this review, we describe the present-day observational status of BHs and discuss further prospects for studies of these extreme objects.

2 Stellar-mass black holes in X-ray binary systems

Black holes can be found in X-ray binary systems ($M_{BH} = 4 \div 20 M_\odot$), and in galactic nuclei ($M_{BH} = 10^6 \div 10^{10} M_\odot$).

After the great discovery of gravitational waves [3], it is clear that black holes can be found also in BH+BH and BH+NS binary systems (here BH is black hole, NS is neutron star).

An X-ray binary consists of a normal optical star (the donor of matter) and relativistic object, a neutron star or black hole, which accretes matter from its companion. To date, specialized X-ray satellites (Uhuru, Einstein, Rosat, Mir-Kvant, Granat, Ginga, Chandra, XMM-Newton, Integral, etc.) have discovered more than one thousand X-ray binaries, which serve as a powerful tool in the detection and studies of stellar-mass BHs. The theory of disk accretion was developed in 1972–1973 in papers by Shakura and Sunyaev [4], Pringle and Rees [5], Novikov and Thorne [6].

X-ray and optical observations of X-ray binary systems perfectly complement each other. X-ray observations from space vehicles allow one to foresee the presence of a compact object in a binary system, while measurements of rapid X-ray time variability on timescales Δt as short as 10^{-3} s provide an estimate the characteristic size of a compact star: $r \leq c\Delta t$. These estimates imply that the sizes of compact X-ray sources never exceed several gravitational radii. At the same time, spectral and photometric observations by ground-based optical telescopes enable us to study the motion of the normal star in an X-ray binary system and to deduce using the star as a "test body", the mass of BH or neutron star from Newton's law of gravitation. A great contribution to the theory of absorption and emission lines formation in the stellar atmospheres was done by Sobolev [7]. If the measured mass of an X-ray source exceeds $3M_\odot$, it can be considered as a BH candidate. Just this determines the strategy of searching for stellar-mass BHs in binary systems.

The first optical identifications of X-ray binary systems and studies of their optical manifestations (ellipticity and reflection effects) were carried out in 1972–1973 and reported in papers [8]–[11]. Based on these studies, reliable methods of estimating the BH masses in X-ray binaries were developed.

Methods of interpreting light curves, line profiles and radial velocity curves of X-ray binaries were developed by assuming that the optical star has an ellipsoidal or pear-like shape in the framework of Roche model with a complex surface temperature distribution due to gravitational darkening and X-ray heating effects [12]. To date, some scientific groups (from USA, the UK, Germany, Netherlands, France, Russia and some other countries) have measured the masses of 26 stellar-mass BHs ($M_{BH} = 4 \div 20 M_\odot$), as well as the masses of $\sim$70 neutron stars ($M_{NS} \approx 1 \div 2 M_\odot$) in binary systems (see Fig. 1).

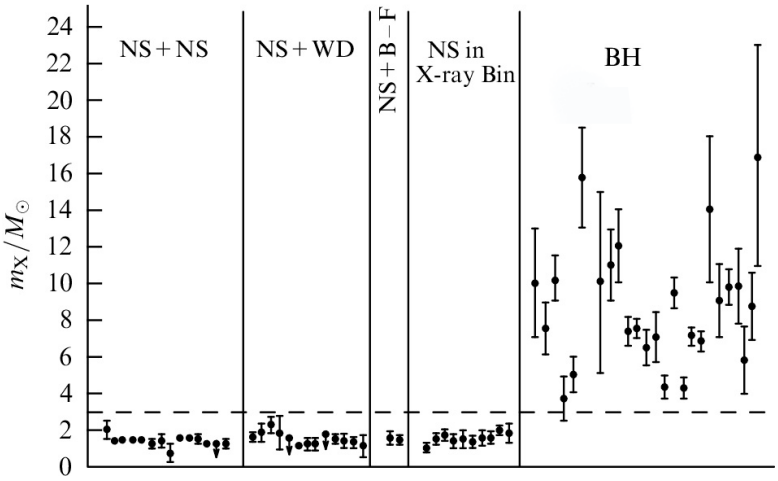

Figure 1: Measured masses of neutron stars and black holes in binary stellar systems: NS+NS – binary radio pulsars with neutron stars, NS+WD – binary radio pulsars with white dwarfs, NS+B–F – binary radio pulsars with an optical non-degenerate stars of the B–F spectral class, NS in X-ray Bin – binary X-ray pulsars. The dashed horizontal line shuts off the value of $3M_\odot$ being the absolute upper limit of neutron star mass predicted by GR.

The measured masses of neutron stars lie within the range of $1 \div 2M_\odot$, with the mean mass being $\sim 1.4M_\odot$. Fine differences in various types of neutron stars have already been found. For example, the masses of rapidly rotating old neutron stars (spin period of about several ms) which have been recycled by accretion in close binary systems [13], are on average $\sim 0.15M_\odot$ higher than the masses of slowly rotating neutron stars (spin periods about several s) [14]. This inference is consistent with theoretical predictions [15].

All neutron stars with measured masses demonstrate clear signatures of their observable surfaces – they are either radio pulsars, X-ray pulsars or type I X-ray bursters.

Thus, in all ~ 70 cases where a compact object demonstrates clear signatures of an observable surface, its measured mass ranges $1 \div 2M_\odot$ and does not exceed $3M_\odot$, in full agreement with the GR prediction of the existence of an upper mass limit $3M_\odot$ for neutron stars.

The measured masses of 26 BH candidates fall within the range ($M_{BH} = 4 \div 20M_\odot$) with the mean mass being of order $9M_\odot$. As BHs have no observable surface, they should not show up as a radio pulsar, X-ray pulsar, or type I X-ray burster. This is indeed the case for 26 BH candidates: none (!) of these massive ($M > 3M_\odot$), compact (radii do not exceed a few r_g) X-ray sources has shown evidence of radio pulsar, X-ray pulsar, or type I X-ray burster.

All of them demonstrate only irregular or quasi-periodic (but not strictly periodic) X-ray emission variability down to timescales as short as $\sim 10^{-3}$ s. In the model which takes into account oscillation of the inner parts the accretion

disk or the orbital motion of hot spots in the inner parts of the disk, it is possible to show (e.g., [16]) that such a rapid X-ray variability of BH candidates is due to their very small sizes not exceeding several gravitational radii.

Thus, a remarkable result gradually emerges with the increasing bulk of information on the masses of relativistic objects: neutron stars and BH candidates differ not only in masses, but also in other observational manifestations, in full agreement with GR.

New results have recently been obtained in studies of the rotation of stellar-mass BHs. The possibility of determining the angular momentum of a BH stems from the fact that if BH co-rotates with the accretion disk, the inner edge of the disk comes much closer to the BH than in the case of a non-rotating BH, since the radius of the event horizon of a rotating BH is smaller than that of a non-rotating BH.

The measured values of dimensionless angular momentum of stellar mass BH lie within the range

$$a_* = 0.98\,(\text{system GRS1915+105}) \div 0.12\,(\text{system A0620}-00). \qquad (1)$$

A remarkable result was recently obtained by Narayan and McClintock [17]. They found a correlation between the observed radio fluxes from collimated jets from accreting BHs, P_{jet}, and the value of dimensionless angular momentum a_* of the BHs: $P_{jet} \sim a_*^2$. This is the first observational evidence that the relativistic jets from accreting stellar-mass BHs can be generated from the conversion of the rotational energy of BH into the kinetic energy of regular bulk motion of matter in collimated relativistic jets with outflow velocities close to the speed of light. Here, the well-known Blandford–Znajek mechanism seems to be operative [18].

Relativistic collimated jets are observed in many X-ray binary systems (most spectacular example is the SS433 binary system, e.g., [19, 20]). Studies of X-ray binaries with relativistic collimated jets, called microquasars, are of special interest, since the physical processes in microquasars are microscopic versions of processes occurring in quasars – very active galactic nuclei, as well as in the nuclei of other galaxies.

3 Supermassive black holes in galactic nuclei

The first estimates of the masses of supermassive BHs (SMBHs) in quasars were made as early as 1964 in the pioneering paper by Zeldovich and Novikov [21] under reasonable assumption that the quasar luminosity is close to the critical Eddington luminosity.

Presently, the masses of SMBHs in galactic nuclei estimated by assuming that the motion of "test bodies" (gas disks, gas clouds, individual stars) near the SMBH is governed by the gravitational field of the central SMBH. In this case the mass of SMBH can be estimated by the formula

$$M_{BH} = \eta V^2 r/G, \qquad (2)$$

where V is the velocity of the test body, r is its distance from the center of SMBH, G is the Newtonian constant of gravitation, $\eta \cong 1 \div 3$ is the factor that takes into account the character of test body motions around the central SMBH.

The two most reliable methods of SMBH mass determination in galaxy centers are the resolved kinematics method and reverberation mapping method.

The method of resolved kinematics is based on direct observations of the motion of test bodies (e.g., [22]). It can be applied to nearby galaxies, for which the telescope angular resolution allows "watching" the test bodies residing in the galactic nucleus and direct measurement of their velocities and distances from the central SMBH. For example, there is a SMBH with mass $(4.31 \pm 0.36) \times 10^6 M_\odot$ in the center of our Galaxy. The mass of this SMBH is determined with an accuracy of better than 10% from the motion of 28 stars orbiting it in elliptic orbit [23]. Using very long baseline radio interferometers, by resolved kinematics method the mass of the SMBH in the center of galaxy NGC4257 was reliably determined to be $M_{BH} = 3.9 \times 10^7 M_\odot$ [24]. For more detailed results of SMBH mass estimations by resolved kinematics methods using basically Hubble Space Telescope, see review by Kormendy and Ho [22].

Unfortunately, the angular resolution of telescopes for the most of remote galaxies is insufficient to directly see individual test bodies; in these cases, one has to apply the reverberation mapping method when estimating the mass of SMBHs. In this method, the velocities and distances of test bodies are estimated indirectly. In the case of active galactic nuclei the velocity V is estimated from Doppler width of emission lines formed in gas clouds, rotating around the central SMBH.

The characteristic distance r of the gas clouds from the central SMBH is determined from the time delay of the emission lines variability relative to that of the continuum spectrum, which is formed in the central parts of the galaxy nucleus.

The time delay between the variability in emission lines relative to the continuum in active galactic nuclei was discovered in 1970–1972 by Cherepashchuk and Lyutyi [25]. It turned out that although due to non-stationary processes in galactic nuclei both the lines and continuum change chaotically, a correlation is revealed between their changes: the line intensity variations repeat those of the continuum intensity with a time delay Δt, which in different galaxies varies from a week to several months. It was noted [25] that a comparatively high gas density in the clouds corresponding to broad components of emission lines implies a short gas recombination time, so the time delay Δt is basically the time of flight of hard emission photons, which are created near the central accreting source to the gas clouds – test bodies emitting spectral lines. Then, the characteristic distance from the test bodies to the central SMBH can be estimated using formula $r \cong c\Delta t$. The SMBH mass can ultimately be estimated from the known characteristic distance r and velocity V using formula (1). The reverberation mapping method for SMBH mass estimates has been widely applied to evaluate SMBH masses in active galactic nuclei.

There are also indirect, less reliable methods of SMBH mass estimates. These include, for instance, the use of widths and absolute intensities of emission lines in active galactic nucleus spectra (e.g., [26]), the empirical relation between SMBH mass and velocity dispersion of stars in the galactic central regions and kink frequency in the power spectra of X-ray irregular variability of galactic nuclei. Such methods enable a quick mass estimation of a large number of SMBHs, which is essential for statistical studies. As a rule, the results obtained with these indirect methods are calibrated by SMBH masses which were reliably measured using resolved kinematics and reverberation mapping methods.

To date, the masses of several hundreds SMBHs have been measured applying resolved kinematics and reverberation mapping methods. They all lie within the range of $10^6 \div 10^{10} M_\odot$. The most reliable mass estimates of SMBH in 44 elliptical and 41 spirals (see the recent review by Kormendy and Ho [22]) span the interval from $(0.94 \div 1.34)\, 10^6 M_\odot$ to $(0.49 \div 3.55)\, 10^{10} M_\odot$. Here, the values in parenthesis stand for the mass determination errors. Reliable values of mass of SMBHs and central star clusters were summarized recently by Zasov and Cherepashchuk [27] for 82 galaxies with known rotational velocities (i.e. with known total galactic masses, including the dark matter halo mass).

Indirect mass evaluations were made for many thousand SMBHs in active galactic nuclei. For example, the targeted spectrophotometric Sloan digital sky survey (SDSS) allowed about 60 000 SMBH mass in centers of quasars to be estimated by indirect method, and statistical dependence of SMBH masses on redshift to be constructed in the redshift range $z = 0.1 \div 4.5$ [28]. It turned out that on average the SMBH mass increases with redshift (i.e. with a decrease in the proper age of a quasar). This effect, if free of a strong observational selection, can hardly be explained in the framework of the model of an SMBH mass increase due to the accretion of circumnuclear matter in quasars.

But the most difficult question to explain relates to the discovery of more than a dozen quasars with very high redshifts $z = 6 \div 8$ (proper age of less than one billion years [29]). How could such massive ($M_{BH} = 10^8 \div 10^{10} M_\odot$) SMBHs be formed in a time of less than 10^9 years? This important observational fact poses a serious theoretical problem.

In recent years (e.g., [30]), the analysis of iron K_α line profiles in X-ray spectra of galactic nuclei has allowed the dimensionless angular momentum $a_* = cj/(GM_{BH}^2)$ to be estimated for some SMBHs. These parameters found to be less than the critical value of $a_* = 0.998$, in agreement with theoretical predictions [31]. The parameter a_* can be estimated also from the kinetic energy flux in relativistic jets from SMBH [32]. These estimates require the magnetic field value in the last stable orbit in the accretion disk or the SMBH event horizon to be known. Spectropolarimetric observations of the nuclei of active galaxies made by Gnedin group [33] allowed the values of parameter a_* to be estimated for a dozen SMBHs. The values found range from $a_* = 0.920 \div 998$ to $a_* = 0.550 \div 0.650$ and do not exceed the theoretical upper limit $a_* = 0.998$.

Limits on the radii of SMBHs are set by observations of fast variability of the optical, infrared and X-ray emission from some galactic nuclei on timescales smaller than tens of minutes. Strong but model-dependent constraints on the SMBH radii can be obtained by analyzing the broad X-ray profiles of the iron K_α emission line at 6.4 keV. The line width of this asymmetric profile corresponds to velocities as high as $\sim 10^5$ km/s. The analysis of this component in the galaxy MCG6–30–15 [34] implies that the inner edge of the accretion disk in this case is located at a distance smaller than $3r_g$ from central SMBH, possibly due to its rapid rotation.

In the last few years, direct measurements of the radii of SMBHs in the center of our Galaxy ($M_{BH} \cong 4.3 \times 10^6 M_\odot$) and galaxy M87 ($M_{BH} = 6 \times 10^6 M_\odot$) have been carried out using VLBI-interferometry at short wavelengths ($\lambda \cong 1.3$ mm) with an angular resolution close to 10^{-5} seconds [35, 36]. It is shown that the dimension of the SMBHs "shadow" at the center of the accretion flow is several gravitational radii ($r_g = 9.1 \times 10^{-6}$ arcseconds for SMBH in our Galaxy and $r_g = 7.8 \times 10^{-6}$ arcseconds for the SMBH in the galaxy M87). A great contribution to the problem of measuring the dimensions of SMBHs will be done by the space radiointerferometers RADIOASTRON and MILLIMETRON.

Accordingly to S.S. Doelman, international effort has been done recently to create an Event Horizon Telescope (EHT) through a millimeter wavelength VLBI network. The EHT is the global effort to carry out the investigations of BH "shadow" and strong gravity effects in the vicinity of the event horizon of SMBH. The Black Hole Cam team, along with groups from Taiwan, Japan, Chile, USA and Germany are all working within the EHT.

New results of measurement on EHT of linear polarization and intensity of radioemission on the scale about 6 gravitational radius for the supermassive black hole in the galaxy M87 have been published recently [37].

Thus, supermassive ($M_{BH} = 10^6 \div 10^{10} M_\odot$) and very compact objects (with sizes not exceeding several gravitational radii) have been discovered to date in the nuclei of many galaxies. All their features most likely suggest that they comprise black holes.

4 Demography of stellar-mass and supermassive black holes

Black hole demography studies the formation and growth of black holes and their evolutionary connection to other astrophysical objects – stars, galaxies, etc.

In the last few years, a close similarity has been established between the observational manifestations of BHs in X-ray binary systems and in galactic nuclei [38]. In particular, the statistical dependence, called the fundamental plane, was discovered for supermassive and stellar-mass BHs [39]

$$\lg L_r = (0.60^{+0.11}_{-0.11}) \lg L_x + (0.78^{+0.11}_{-0.09}) \lg M_{BH} + 7.33^{+4.05}_{-4.07}, \qquad (3)$$

where L_r is the observed radio luminosity (mainly due to relativistic jet radio emission), L_x is the X-ray luminosity (from the accretion disk and the jet base), and M_{BH} is the black hole mass (for both stellar-mass BHs and SMBHs).

The variability of active galactic nuclei containing accreting supermassive BHs was related to be similar to that of accreting stellar-mass BHs in X-ray binary systems if the variability time is normalized depending on the BH mass [38].

In X-ray binaries with BHs, in addition to irregular variability there are two types of quasi-periodic (i.e., not strictly periodic) oscillations (QPO) of an X-ray flux: low frequency QPOs (LFQPOs) with the characteristic frequencies $0.1 \div 30$ Hz, and high-frequency QPOs (HFQPOs) with frequencies falling in the range of $40 \div 450$ Hz.

Quasi-periodic X-ray oscillations were recently discovered from accreting SMBHs in the nuclei of some galaxies. For example, QPOs with the characteristic period of about one hour were observed in the active nucleus of the galaxy REJ1034+396 [40]. With a central SMBH mass of about $10^7 M_\odot$, this quasiperiod corresponds to an orbit radius of about $3r_g$, which yields an upper limit on the size of this very massive and compact object, giving support to its BH nature.

Interesting results were obtained in studies of the mass distribution of stellar-mass BHs. It turned out that in binary systems there is no dependence of masses of relativistic objects on their companion masses. The neutron star and black hole mass distribution turned out to be unusual as well [41, 42], – see Fig. 2. The number of studied stellar-mass BHs does not increase with decreasing of their masses. This looks strange, since the stellar mass distribution in the Galaxy (the most massive stellar objects are progenitors of the relativistic compact objects) is such that the number of stars very strongly (as M^{-5}) increases with decreasing stellar mass.

In addition, a mass distribution dip between $2M_\odot$ and $4M_\odot$ seems to exist for neutron star and BH masses. In this mass range, no neutron stars or BHs have been observed. The mass dip within the range $(2-4)M_\odot$ for neutron stars and BH mass distributions, if confirmed in further observations (especially from observations of X-ray binaries in other galaxies), will require a serious theoretical elucidation.

Let us briefly discuss the problem of SMBH demography (see the recent review by Kormendy and Ho [22]). As noted above, the formation time of SMBHs in galactic nuclei is relatively short, namely less than 10^9 years. Such a rapid formation of very massive BH is difficult to explain in the model assuming their mass growth due to gas accretion onto a low-mass seed BH that has been formed via the core collapse of a massive ($M = 100 \div 1000 M_\odot$) population III star, even if the mass accretion rate is as high as the Eddington luminosity.

Recently, in addition to SMBHs, the important role of massive stellar clusters located in galaxy center has been revealed [43, 44].

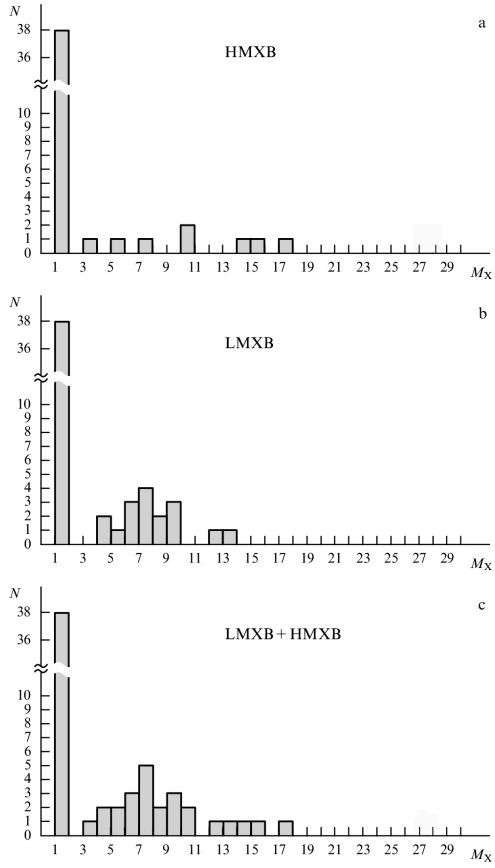

Figure 2: Neutron star and black hole mass distributions in binary systems: (a) black hole masses in high-mass X-ray binaries (HMXB) with massive optical stars of O–B and WR spectral classes; (b) black hole masses in low-mass X-ray binaries (LMXB), and (c) the total black hole and neutron star mass distributions (in low-mass and high-mass X-ray binaries). The high peaks in the left part of the panels (a)–(c) correspond to neutron star masses.

An important correlation is also revealed between SMBH masses, the masses of central star clusters, and parameters of spheroidal galactic components:

$$M \sim \sigma^{\beta},$$

where M is the mass of the SMBH or a stellar cluster, and σ is the star velocity dispersion in the spheroidal component. The index of a power is $\beta = 4 \div 5$ for SMBHs (e.g., [45]), and β falls within the range from 1.57 ± 0.24 [45] to 2.73 ± 0.29.

Although the dispersion of the exponent β for central star clusters is large ($\beta = 1.57 \div 2.73$), the dependence of mass M on the velocity dispersion σ for central star cluster may be considered as weaker compared to SBMHs. This allows us to assume that the formation and evolution of central SMBHs and massive star clusters in galactic nuclei are related to different mechanisms.

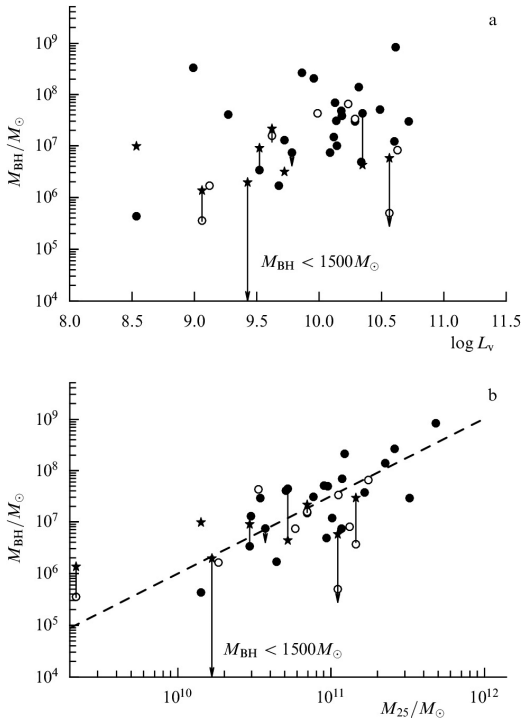

Figure 3: SMBH mass as function: (a) total optical luminosity L_V of the host galaxy characterizing the baryonic mass, and (b) the indicative mass of the galaxy $M_{25} = V_{far}^2 R_{25}/G$, which includes both baryonic and dark-matter masses. The filled "star" symbols correspond to central stellar clusters. Linear segments join circles (BHs) and filled "stars" (clusters). Arrows show the upper limits (taken from paper by Zasov et al. [43]).

Of special interest is the possible association of central SMBHs and massive star clusters with dark matter in galaxies. Our observations of the galactic rotation in galaxies with known heavy central black hole masses are aimed at solving this problem [43, 46, 27]. As shown in studies performed by A.V. Gurevich's group [47], the gravitational instability in proto-galaxy dark matter clumps form sharp and deep minima of gravitational potential (cusps), into which baryonic matter "falls" to produce a stellar population of the forming galaxy.

This process can also stimulate the formation of an SMBH in galaxy nucleus. Therefore, the association of the central SMBH mass with the mass of the galactic halo dominated by dark matter is rather expectable Indeed, due to coalescence of galaxies at early stages of their formation, as well as star formation in galactic centers, this association can be rather indirect. Nevertheless, the search for a correlation between the central SMBH mass and the dark matter-dominated galactic halo mass is a very important observational task.

In Fig. 3 important correlations obtained in our paper [43] are presented. They demonstrate the important role of dark matter in the central SMBH formation in the galactic nucleus. The figure depicts two dependencies: $M_{BH}(L_V)$ and

$M_{BH}(M_{25})$, where L_V is the total optical luminosity of the galaxy, which is a single-valued function of the total baryonic mass of the galaxy, and M_{25} is the so-called indicative mass of the galaxy: $M_{25} = V_{far}^2 R_{25}/G$, where V_{far} is the observed maximum rotational velocity of the galaxy (which tends to a plateau at large distances from the nucleus), and R_{25} is the radius of the galactic region limited by the surface brightness isophot reaching the 25th stellar magnitude per square arcsecond, which determines the boundary of the visible part of the galaxy. Apparently, there is virtually no correlation between the SMBH mass and the total baryonic mass of the whole galaxy. At the same time, if we consider the indicative galactic mass M_{25} for the same galaxies as comprising both baryonic and substantial fraction of dark matter, a good $M_{BH}(M_{25})$ correlation is revealed. This result immediately indicates that the influence of dark matter on central SMBH formation, although indirect, remains quite significant.

The linkage of central SMBH and stellar clusters with the kinematics and color of host galaxies was studied in more detail in the paper by Zasov and Cherepashchuk [27].

5 Conclusions

After 45 years of observational studies of BHs, there are almost no doubts that these extreme objects really exist in the Universe. This is due to the fact that all observations of these massive and very compact objects are in beautiful agreement with GR prediction for black holes.

Recent discovery of gravitational waves from a binary black hole merger GW150914 [3] opens a new era in investigations of black holes.

References

1. *Ya.B. Zeldovich*, Sov. Phys. Dokl., **9**, 195, 1964.
2. *E.E. Salpeter*, Astrophys. J., **140**, 796, 1964.
3. *B.P. Abbott, R. Abbott, T.D. Abbott et al.*, Phys. Rev. Lett.,**116**, 061102, 2016.
4. *N.I. Shakura, R.A. Sunyaev*, Astron. Astrophys., **24**, 337, 1973.
5. *J.E. Pringle, M.J. Rees*, Astron. Astrophys., **21**, 1, 1972.
6. *I.D. Novikov, K.S. Thorne*, in Black Holes. Eds. C. De Witt, B.S. De Witt. New York: Gordon and Breach, 1973, p. 343.
7. *V.V. Sobolev*, A Treatise on Radiative Transfer. Princeton: Van Nostrand and Co. Inc., 1963.
8. *A.M. Cherepashchuk, Yu.N. Efremov, N.E. Kurochkin et al.*, Inf. Bull. Var. Stars, No. 720, 1, 1972.
9. *J.N. Bahcall, N.A. Bahcall*, Astrophys. J. Lett., **178**, L1, 1972.
10. *V.M. Lyutyi, R.A. Sunyaev, A.M. Cherepashchuk*, Sov. Astron., **17**, 1, 1973.

11. *V.M. Lyutyi, R.A. Sunyaev, A.M. Cherepashchuk*, Sov. Astron., **18**, 684, 1974.

12. *E.A. Antokhina, A.M. Cherepashchuk, V.V. Shimansky*, Astron. Zh., **82**, 131, 2005.

13. *G.S. Bisnovatyi-Kogan, B.V. Komberg*, Sov. Astron., **18**, 217, 1974.

14. *B. Kiziltan, A. Kottlas, S.E. Thorsett*, Astrophys. J., **778**, 2013.

15. *M.A. Alpar, A.F. Cheng, M.A. Ruderman, J. Shaham*, Nature, **300**, 728, 1982.

16. *J.E. McClintock, R.A. Remillard*, in Compact Stellar X-ray Sources. Eds. W. Lewin, M. Van der Klis. Cambridge Astrophys. Ser., vol. 39. Cambridge: Cambridge Univ. Press, 2006, p. 157.

17. *R. Narayan, J.E. McClintock*, Mon. Not. Roy. Astron. Soc., **419**, L69, 2012.

18. *R.D. Blandford, R.I. Znajek*, Mon. Not. Roy. Astron. Soc., **179**, 433, 1977.

19. *A.M. Cherepashchuk*, Mon. Not. Roy. Astron. Soc., **194**, 761, 1981.

20. *B. Margon*, Ann. Rev. Astron. Astrophys., **22**, 507, 1984.

21. *Ya.B. Zeldovich, I.D. Novikov*, Sov. Phys. Dokl., **9**, 834, 1964.

22. *J. Kormendy, L.C. Ho*, Ann. Rev. Astron. Astrophys., **51**, 511, 2013.

23. *S. Gillessen, F. Eisenhauer, S. Trippe et al.*, Astrophys J., **692**, 1075, 2009.

24. *J.M. Moran, L.J. Greenhill, J.R. Herrnstein*, J. Astrophys. Astron., **20**, 165, 1999.

25. *A.M. Cherepashchuk, W.M. Lyutyi*, Astrophys. Lett., **13**, 165, 1973.

26. *E.A. Dibai*, Sov. Astron., **28**, 123, 1984.

27. *A.V. Zasov, A.M. Cherepashchuk*, Astron. Rep., **57**, 797, 2013.

28. *Y. Shen, J.E. Greene, M.A. Strauss et al.*, Astrophys. J., **680**, 169, 2008.

29. *M. Volonteri, M.J. Rees*, Astrophys. J., **650**, 669, 2006.

30. *L.W. Brenneman, C.S. Reynolds, M.A. Nowak et al.*, Astrophys. J., **736**, 103, 2011.

31. *K.S. Thorne*, Astrophys. J., **191**, 507, 1974.

32. *R.A. Daly*, Mon. Not. Roy. Astron. Soc., **414**, 1253, 2011.

33. *Yu.N. Gnedin*, Phys. Usp., **56**, 709, 2013.

34. *J. Wilms, C.S. Reynolds, M.C. Begelman et al.*, Mon. Not. Roy. Astron. Soc., **328**, L27, 2001.

35. *S.S. Doelman, J. Weintroub, A.E.E. Rogers et al.*, Nature, **455**, 78, 2008.

36. *S.S. Doelman, V.L. Fish, D.E. Schenck et al.*, Science, **338**, 355, 2012.

37. *M.D. Johnson, V.L. Fish, S.S. Doelman et al.*, Science, **350**, 1242, 2015.

38. *I.M. McHardy, E. Koerding, C. Knigge et al.*, Nature, **444**, 730, 2006.

39. *A. Merloni, S. Heinz, T. Di Matteo*, Mon. Not. Roy. Astron. Soc., **345**, 1057, 2003.

40. *M. Gierliński, M. Middleton, M. Ward, C. Done et al.*, Nature, **455**, 369, 2008.

41. *A.M. Cherepashchuk*, Astron. Rep., **45**, 120, 2001.

42. *A.M. Cherepashchuk*, Phys. Usp., **45**, 896, 2002.

43. *A.V. Zasov, A.M. Cherepashchuk, I.Yu. Katkov*, Astron. Rep., **55**, 595, 2011.

44. *L. Ferrarese, P. Côté, J.-C. Cuillandre et al.*, Astrophys. J. Lett., **644**, L21, 2006.

45. *A.W. Graham*, Mon. Not. Roy. Astron. Soc., **422**, 1586, 2012.

46. *A.M. Cherepashchuk, V.L. Afanas'ev, A.V. Zasov, I.Yu. Katkov*, Astron. Rep., **54**, 578, 2010.

47. *A.S. Ilyin, K.P. Zybin, A.V. Gurevich*, J. Exp. Theor. Phys., **98**, 1, 2004.

Continuum Variations with Luminosity in Accreting X-Ray Pulsars

M.I. Gornostaev[1,2], K.A. Postnov[1,2], D. Klochkov[3], N.I. Shakura[2]

E-mail: *mgornost@gmail.com*

Two-dimensional structure of accretion columns in the radiation-diffusion limit is calculated for two possible geometries (filled and hollow cylinder) for mass accretion rates $\dot{M}$ ranging from 10^{17} to 1.2×10^{18} g s^{-1}. The observed spectral hardening in the transient X-ray pulsars with increasing $\dot{M}$ can be reproduced by a Compton-saturated sidewall emission from optically thick magnetized accretion columns with taking into account the emission reflected from the neutron star atmosphere. At $\dot{M}$ above some critical value $\dot{M}_{cr} \sim (6–8)\times10^{17}$ g s^{-1}, the height of the column becomes such that the contribution of the reflected component to the total emission starts decreasing, which leads to the saturation and even slight decrease of the spectral hardness. Hollow-cylinder columns have a smaller height than the filled-cylinder ones, and the contribution of the reflected component in the total emission does not virtually change with $\dot{M}$ (and hence the hardness of the continuum monotonically increases) up to higher mass accretion rates than $\dot{M}_{cr}$ for the filled columns.

1 Observations

After the discovery of X-ray pulsars in 1971 [1] it was realized that in bright pulsars the radiation plays a crucial role in braking of the accreting matter onto the surface of a neutron star with strong magnetic field. It is now well recognized that once the radiation density above the polar cap starts playing the role in the accreting matter dynamics, an optically thick accretion column above the polar cap is formed [2] (see [3] for the latest investigation). The characteristic height of the column increases with accretion rate, most of the emission escapes through sidewalls, and it can be expected that above some X-ray luminosity the dependence of the observed properties of the continuum emission on the X-ray luminosity can become different from that in the low-luminosity regime.

Indeed, a similar bimodality is observed in the dependence of the X-ray continuum hardness on luminosity. This dependence can be studied using, for example, data from all-sky monitors such as RXTE/ASM and MAXI,

[1] Faculty of Physics, M.V. Lomonosov Moscow State University, Russia
[2] Sternberg Astronomical Institute, Moscow M.V. Lomonosov State University, Russia
[3] Institute of Astronomy and Astrophysics, Karl-Eberhard University, Germany

V. Grinin et al. (eds) Radiation mechanisms of astrophysical objects. Yerevan: Edit Print, 2017, pp. 297–304.

i.e. without dedicated spectroscopic observations which are necessary to measure CRSFs. Following this approach, we measured the hardness ratio as a function of luminosity in the accreting pulsars GX 304–1, 4U 0115+63, V 0332+53, EXO 2030+375, A 0535+26 and MXB 0656–072 using the data from different energy bands of RXTE/ASM. The result is shown in Fig. 1. To convert the ASM count rates into X-ray luminosities, we used published distances to the sources (GX 304–1: ∼2 kpc [4]; 4U 0115+63: ∼7 kpc [5], V 0332+53: ∼7 kpc [6]; EXO 2030+375: ∼7 kpc [7]; A 0535+26: ∼2 kpc [8]; MXB 0656-072: ∼3.9 kpc [9]) and their broadband X-ray spectra from the archival pointed observations with INTEGRAL and RXTE available to us. One can see that at lower fluxes the hardness ratio increases with flux. At a certain flux, however, a flattening of the hardness ratio is observed in 4U 0115+63, V 0332+53, EXO 2030+375, A 0535+26 and MXB 0656–072. This "turnover" occurs at the flux roughly corresponding to luminosities (3–7) × 10^{37} erg s^{-1}. In GX 304–1, which does not show such a turnover, this "critical" luminosity has simply not been reached during the outbursts registered by RXTE/ASM.

A similar dependence of spectral properties on the X-ray flux at luminosities below ∼10^{37} erg s^{-1} was also reported from spectroscopic observations of the transient Be-X-ray pulsar GRO J1008-57 [10].

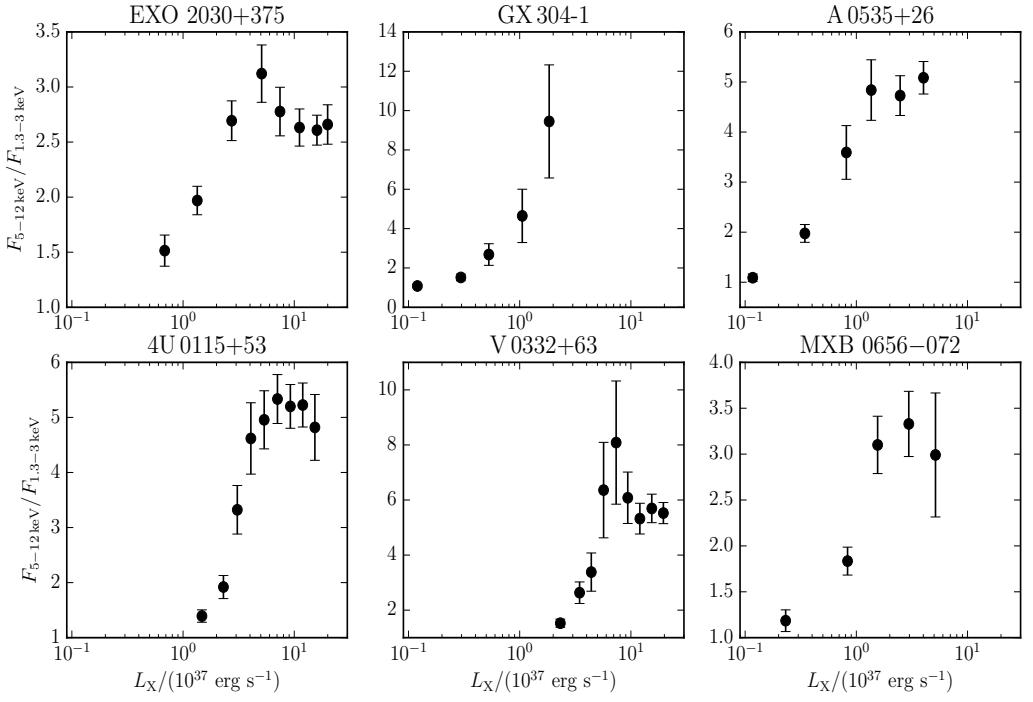

Figure 1: The ratio of the fluxes in 5–12 keV and 1.33–3 keV ranges (referred to as "hardness ratio" in text) measured with RXTE/ASM for six transient accreting pulsars as a function of the total ASM flux in the 1.33–12 keV range.

2 Numerical simulations of accretion column in radiation-diffusion approximation

2.1 Boundary conditions

We introduce cylindrical coordinates r, φ, z centered at the columns axis and $z = 0$ at the neutron star surface. The initial velocity of the falling matter at high altitude above the surface of the neutron star is $v_0 = 10^{10}$ cm s^{-1}. At the cylinder base ($z = 0$), the velocity is $v = 0$. As a boundary condition at the column side surface we used the relation between the radial energy flux and the energy density U in the form $F_r(r_0, z) = 2cU(r_0, z)/3$, which roughly corresponds to the conditions expected in the scattering atmospheres in the Eddington approximation.

2.2 Basic equations

The cylindrical symmetry of the problem makes it essentially two-dimensional. The steady-state momentum equation (ignoring gravity, which is very good approximation as discussed, e.g., in [2]) for accretion braking by the radiation with energy density U reads $(\boldsymbol{S} \cdot \nabla)\, \boldsymbol{v} = -\frac{1}{3}\nabla U$. The mass continuity equation is $\boldsymbol{S} = \rho \boldsymbol{v} = \text{const}$. The integration of momentum equation yields

$$U = 3S(v_0 - v). \tag{1}$$

Following [11], the energy equation can be written as

$$\nabla \cdot \boldsymbol{F} = -\boldsymbol{S} \cdot \nabla \left(\frac{v^2}{2} \right), \tag{2}$$

where we has neglected the flow of internal energy of the falling matter.

The radiative transfer equation for the components of the radiation energy flux in cylindrical coordinates yields

$$F_r = \frac{-\frac{c}{3\varkappa_\perp \rho} \frac{\partial U}{\partial r}}{1 + \frac{1}{3\varkappa_\perp \rho} \frac{1}{U} \left| \frac{\partial U}{\partial r} \right|}, \quad F_z = \frac{-\frac{c}{3\varkappa_\parallel \rho} \frac{\partial U}{\partial z} - \frac{4}{3} U v}{1 + \frac{1}{3\varkappa_\parallel \rho} \frac{1}{U} \left| \frac{\partial U}{\partial z} \right|}, \tag{3}$$

where the denominators are introduced to use the modified diffusion approximation [12].

The system of equations (1)–(3) was solved numerically for accretion rates onto one pole in the range 10^{17}–1.2×10^{18} g s^{-1}for the geometry of filled cylinder with radius r_0 and the hollow cylinder with wall thickness $0.1r_0$ (see [13] for details). The column structure at different accretion rates is shown in Fig. 2.

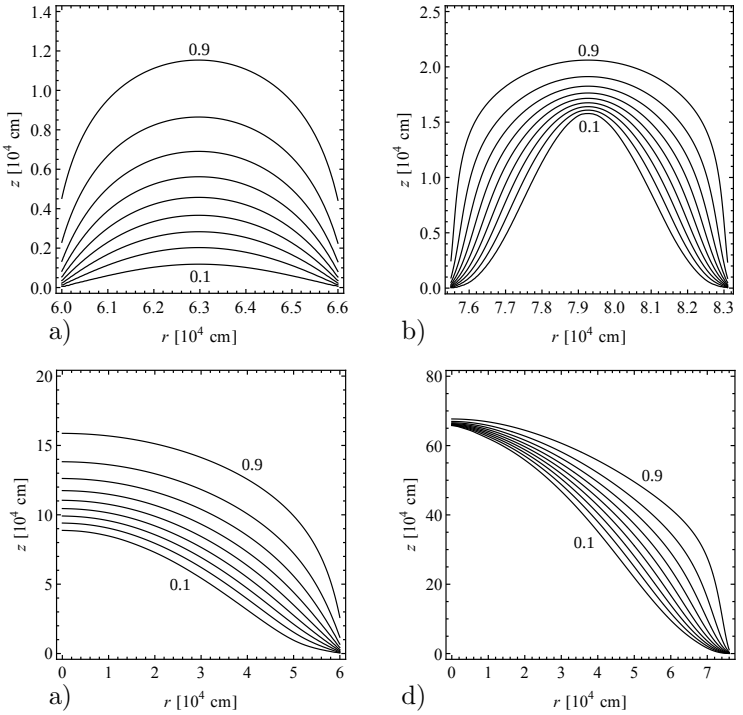

Figure 2: Contours of constant Q (0.9 to 0.1, from top to bottom). The hollow cylinder geometry calculated for $\dot{M}_{17} = 1$ (a) and $\dot{M}_{17} = 5$ (b). The filled cylinder geometry for $\dot{M}_{17} = 1$ (c) and $\dot{M}_{17} = 5$ (d).

3 Hardness ratio variations

3.1 Saturated Compton spectrum of sidewall emission

The LTE treatment of the spectrum of the sidewall emission from accretion columns is clearly a strong oversimplification. To take into account the scattering on electrons in the optically thin boundary of the column, we can use the model calculations of the radiation transfer problem in a semi-infinite plane-parallel atmosphere with strong magnetic field. In this case the emerging spectrum will be formed in the saturated Compton regime, with the mode 1 photons (extraordinary, i.e. polarized perpendicular to the $\boldsymbol{k}-\boldsymbol{B}$-plane, where $\boldsymbol{k}$ is the photon wavevector and $\boldsymbol{B}$ is the magnetic field vector) predominantly escaping through sidewalls [14]. The intensity of mode 2 (ordinary, i.e. polarized in the $\boldsymbol{k}-\boldsymbol{B}$ plane) photons is comparable to that of mode 1 photons only at large angles to the normal, $\mu' \sim 0$, and thus insignificantly contributes to the total flux from the unit surface area due to the geometrical factor.

In this regime, the specific intensity of extraordinary photons at energies far below the cyclotron resonance can be written as $I'_\nu = (1+2\mu')\frac{2\sqrt{3}}{5}\frac{h\nu\nu_g^2}{c^2\tau_0}e^{-\frac{h\nu}{kT}}$ [14], where $\mu' = \cos\theta'$ is the angle between the normal to the atmosphere and the

escaping radiation direction in the plasma reference frame, τ_0 is the characteristic optical depth of the problem, $\nu_g = \frac{eB}{2\pi m_e c}$ is the electron gyrofrequency in the magnetic field. By expressing the characteristic optical depth τ_0 through the emergent radiation flux Φ using (34)–(37) from [14], we find

$$I_\nu = \frac{I'_\nu}{1+2\mu'} = \frac{3}{10\pi}\left(\frac{h\nu}{kT}\right)^2 \frac{\Phi}{\nu} e^{-\frac{h\nu}{kT}}. \tag{4}$$

Therefore, we are in the position to calculate the emerging spectrum from the column in this approximation using the solutions for the column structure obtained above. To do this, it is sufficient to substitute the total radial energy flux at each height of the column $\Phi \to F_r(z)/2$ ($F_r(z)$ in Eq. (3) is known from our numerical calculations), and temperature $T \to T(z)$ estimated deep inside the column (at the optical depth $\sim$1), so that $T(z) = (U(z)/a_r)^{1/4}$.

3.2 Account for the reflected component

Now we should take into account the fact that the electrons in the optically thin part of the column are moving with high velocity $v_0 \sim 1/3c$, and thus the emission beam of the column (4) should be Doppler-boosted towards the neutron star surface and reflected from the neutron star atmosphere, as discussed in [15] and [16]. The reflection coefficient in the case of single Compton electron scattering in strong magnetic field is determined by the ratio $\lambda(\nu) = \kappa_{sc}/(\kappa_{sc} + \kappa_{abs})$, where κ_{sc} and κ_{abs} are the scattering and absorption coefficients for photons in the strong magnetic field, respectively. Since the calculated X-ray albedo turns out to be very similar for both extraordinary and ordinary photons and is virtually insensitive to the photon incident angle to the magnetic field, below we shall use its mode-averaged value for the angle $\pi/4$.

Let α be the angle between the photon wavevector and the plasma bulk velocity vector. The critical value α^* within which the radiation from the height z will be intercepted by the neutron star (in the Schwarzschild metric and with taking into account the difference between the polar axis and the column cylinder side) is

$$\alpha^*(z) = \arcsin\left(\frac{R_{NS}}{\sqrt{(R_{NS}+z)^2+r_0^2}}\sqrt{\frac{1-r_S/\sqrt{(R_{NS}+z)^2+r_0^2}}{1-r_S/R_{NS}}}\right) - \arctan\frac{r_0}{R_{NS}+z},$$

where $r_S = 2GM/c^2$ is the Schwarzschild radius (cf. [16]).

Let Σ be the surface of the column, $\Sigma'(\varphi, z)$ be a point on the surface and $d\Sigma = r_0 d\varphi dz$ be the elementary area. The flux from the surface element at frequency ν (in conventional notations) reads $f_\nu(\Sigma') = dE(\Sigma')/(dtd\nu d\Sigma)$ and can be separated into three parts in accordance to the angle relative to the observer. Photons escaping with angles $\alpha > \alpha^*$ to the column are directly seen as the proper column radiation f_ν^{col}. The second part includes the radiation f_ν^{ref} intercepted by the neutron star and reflected from the neutron star surface with

X-ray albedo $\lambda(\nu)$. The third part f_ν^{abs} is the radiation absorbed and re-radiated by the neutron star atmosphere. Then we can write

$$\begin{aligned} f_\nu(\Sigma') &= \int\limits_{-1}^{1} \frac{df_\nu(\Sigma')}{d\cos\alpha} d\cos\alpha \\ &= \int\limits_{-1}^{\cos\alpha^*} \frac{df_\nu(\Sigma')}{d\cos\alpha} d\cos\alpha + \lambda(\nu) \int\limits_{\cos\alpha^*}^{1} \frac{df_\nu(\Sigma')}{d\cos\alpha} d\cos\alpha + (1-\lambda(\nu)) \int\limits_{\cos\alpha^*}^{1} \frac{df_\nu(\Sigma')}{d\cos\alpha} d\cos\alpha \\ &= f_\nu^{col}(\Sigma') + f_\nu^{ref}(\Sigma') + f_\nu^{abs}(\Sigma'). \end{aligned} \tag{5}$$

The integrands [16] in the cylindrical coordinates with account for the axial symmetry ($I_\nu(\Sigma') = I_\nu(z)$, giving by (4)) have the form

$$\frac{df_\nu(\Sigma')}{d\cos\alpha} = I_\nu(z) \frac{2D^3}{\gamma} \sin\alpha \left(1 + \frac{\pi D}{2} \sin\alpha\right),$$

where the Doppler factor is $D = 1/(\gamma(1 - \beta\cos\alpha))$, $\gamma = 1/\sqrt{1-\beta^2}$ is the plasma Lorentz factor and $\beta = v/c$. Then for the total radiation from the column at frequency ν we obtain

$$\begin{aligned} L_\nu &= \iint\limits_{\Sigma} f_\nu(\Sigma') d\Sigma = 2\pi r_0 \int\limits_0^{z_{max}} \left(f_\nu^{col}(z) + f_\nu^{ref}(z) + f_\nu^{abs}(z)\right) dz \\ &= L_\nu^{col} + L_\nu^{ref} + L_\nu^{abs}, \end{aligned} \tag{6}$$

where z_{max} is the upper limit of the computational area. The observed X-ray flux from one column is $F_\nu = (L_\nu^{col} + L_\nu^{ref})/(4\pi d^2)$, where d is the distance to the source. For the illustrative purposes, we assume $d = 5$ kpc. Taking into account the radiation absorbed by the neutron star atmosphere L_ν^{abs} will add more soft photons to the total spectrum.

Since we are observing both the direct and reflected radiation from the column, the total change in the hardness of the spectrum depends on the fraction of the reflected radiation in the total flux. This, in turn, depends on the height of the column. We have calculated the total flux as the sum of the direct and reflected component as a function of $\dot{M}$ with taking into account the photon ray propagation in the Schwarzschild metric of the neutron star with a fiducial mass $M = 1.5M_\odot$ and radius $R = 10$ and 13 km. The magnetic field of the neutron star is set to 3×10^{12} G, so that the CRSF energy is about 35 keV. The result is presented in Fig. 3. It is seen that the hardness ratio

$$\mathrm{HR} = \int\limits_{5\ \mathrm{keV}}^{12\ \mathrm{keV}} F_\nu d\nu \Bigg/ \int\limits_{1.3\ \mathrm{keV}}^{3\ \mathrm{keV}} F_\nu d\nu$$

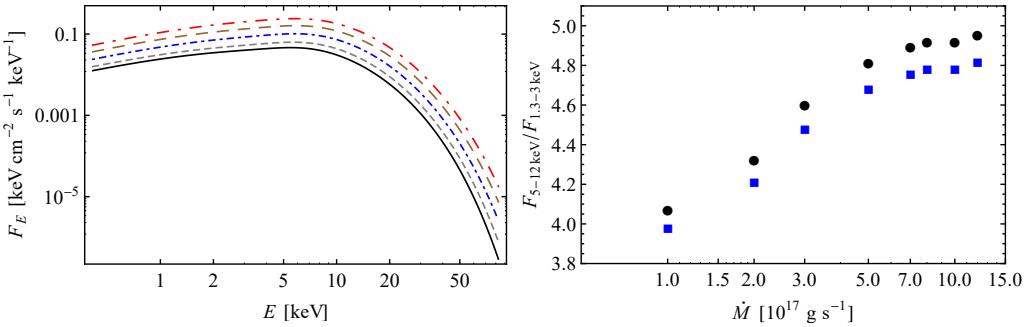

Figure 3: *Left:* the total spectrum of direct sidewall and reflected from the neutron star atmosphere from the optically thick filled accretion column for mass accretion rates $\dot{M}_{17} = 2$, 3, 5, 8 and 12 (from bottom to up, respectively). *Right:* the hardness ratio HR of the total spectrum. Shown are calculations for the neutron star radius $R_{NS} = 10$ km (squares) and $R_{NS} = 13$ km (circles).

first increases with the mass accretion rate (X-ray luminosity), but starting from $\dot{M}_{cr} \sim (6-8)\times 10^{17}$ g s^{-1}, it gets saturated. This is in agreement with observations shown in Fig. 1.

For the hollow cylinder accretion columns which have smaller height (see Fig. 2), the fraction of the reflected component in the total emission does not virtually change with mass accretion rate within the calculated range, therefore the hardness ratio of the total spectrum monotonically increases with $\dot{M}$ in this range. Note also that in this case the spectrum is harder than in the case of the filled column because the reflected (harder) emission dominates in the total spectrum.

4 Summary and conclusions

Therefore, our model calculations lead to the following conclusions:

1. The spectral hardening in X-ray pulsars with positive CRSF energy dependence on X-ray flux can be explained by increasing of the Comptonization parameter y in the slab atmosphere of the accretion mound. It is in this regime that positive correlation of the cyclotron line is observed, for example, in Her X-1 [17].
2. At high accretion rates, the radiation-supported optically thick accretion column grows above the polar cap, the sidewall emission from the column is formed by extraordinary photons in the saturated Compton regime. The spectrum of this emission gets harder with increasing mass accretion rate.
3. With further increasing mass accretion rate the height of the column increases, such that the fraction of radiation reflected from the neutron star atmosphere starts decreasing. As the reflected radiation is harder than the incident one,

the spectrum of the total emission (direct plus reflected) stops hardening (and even becomes slightly softer).

4. In the frame of this model, the saturation of the spectral hardness in the case of a hollow cylinder geometry of the accretion column can be achieved at much higher accretion rates (roughly, scaled with the relative thickness of the column wall, b), because the characteristic height of the column in this case is correspondingly smaller than that of the filled column.

References

1. *R. Giacconi, H. Gursky, E. Kellogg et al.*, Astrophys. J. Lett., **167**, L67, 1971.
2. *M.M. Basko, R.A. Sunyaev*, Mon. Not. Roy. Astron. Soc., **175**, 395, 1976.
3. *A.A. Mushtukov, V.F. Suleimanov, S.S. Tsygankov, J. Poutanen*, Mon. Not. Roy. Astron. Soc., **447**, 1847, 2015.
4. *G.E. Parkes, P.G. Murdin, K.O. Mason*, Mon. Not. Roy. Astron. Soc., **190**, 537, 1980.
5. *I. Negueruela, A.T. Okazaki*, Astron. Astrophys., **369**, 108, 2001.
6. *I. Negueruela, P. Roche, J. Fabregat, M.J. Coe*, Mon. Not. Roy. Astron. Soc., **307**, 695, 1999.
7. *C.A. Wilson, M.H. Finger, M.J. Coe et al.*, Astrophys. J., **570**, 287, 2002.
8. *I.A. Steele, I. Negueruela, M.J. Coe, P. Roche*, Mon. Not. Roy. Astron. Soc., **297**, L5, 1998.
9. *V.A. McBride, J. Wilms, M.J. Coe et al.*, Astron. Astrophys., **451**, 267, 2006.
10. *M. Kühnel, S. Müller, I. Kreykenbohm et al.*, Phys. J. Web Conf., **64**, 6003, 2014.
11. *K. Davidson*, Science, **246**, 1, 1973.
12. *Y.-M. Wang, J. Frank*, Astron. Astrophys., **93**, 255, 1981.
13. *K.A. Postnov, M.I. Gornostaev, D. Klochkov et al.*, Mon. Not. Roy. Astron. Soc., **452**, 1601, 2015.
14. *Y.E. Lyubarskii*, Astrophys., **25**, 577, 1986.
15. *Y.E. Lyubarskii, R.A. Syunyaev*, Astron. Lett., **14**, 390, 1988.
16. *J. Poutanen, A.A. Mushtukov, V.F. Suleimanov et al.*, Astrophys. J., **777**, 115, 2013.
17. *R. Staubert, N.I. Shakura, K. Postnov et al.*, Astron. Astrophys., **465**, L25, 2007.

* The color figures are available online in the Proceedings at *http://www.astro.spbu.ru/sobolev100/*.

A 2D Model of Non-Stationary Accretion onto a Magnetized Neutron Star

V.V. Grigoryev[1], A.M. Krassilchtchikov[2]

E-mail: *vitaliygrigoryev@yandex.ru, kra@astro.ioffe.ru*

A 2D non-stationary model of column accretion over the surface of a magnetized neutron star is presented. It is found that collisionless shocks appear and evolve in the column on the time scales of about 10^{-7} s, and their surface is not flat. A significant non-uniformity of flow parameters across the column is observed. In general, the modeling results agree with those of the previously developed 1D model.

1 Introduction

Accretion onto compact stellar objects was recognized as an efficient source of hard X-ray emission already 50 years ago [1, 2]. Ya.B. Zeldovich [3, 4] showed that the spectrum emitted from the vicinity of a neutron star surface critically depends on the accretion regime, namely, on whether the infalling matter comes as separate particles (free-fall) or as a hydrodynamic flow.

The accretion models developed in 1970–80 postulated the existence of a collisionless shock in the column, and its height over the surface of the star was a model parameter. However, for the substantially super-Eddington case J. Arons and R. Klein [5] and their collaborators [6] showed that non-stationary radiation-dominated shocks appear and evolve in the accretion column.

Apart from gas dynamics in an accretion column, some studies were devoted to the problem of radiation transfer in the column. Thus, R. Araya, A. Harding considered the influence of Compton processes on the transfer of cyclotron line emission and computed line profiles for a set of column parameters [7].

In 2004 A.M. Bykov and A.M. Krassilchtchikov [8] developed a 1D model of non-stationary accretion in a column of a magnetized neutron star. They did not postulate the existence of a shock in the column, rather, such a shock appeared as a natural result of evolution of an accreting flow. In this model a collisionless shock formed on the scales of 10^{-5} s. Thus, the aim of the present work was to extend the model of [8] to the 2D case and compare the resulting flow profiles.

[1] St. Petersburg State University, Russia
[2] Ioffe Institute, St. Petersburg, Russia

V. Grinin et al. (eds) Radiation mechanisms of astrophysical objects. Yerevan: Edit Print, 2017, pp. 305–310.

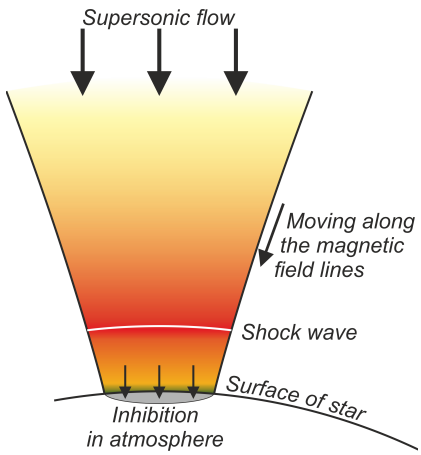

Figure 1: A sketch of the modeled accretion column.

2 The accretion column model

We consider a numerical model of sub-Eddington non-stationary accretion in a 2D column over a magnetic pole of a neutron star. We do not postulate the existence of a shock in the column as an initial condition. The model takes into account various interactions of two sorts of particles (electrons and ions) within the infalling hydrodynamical flow, as well as interaction of the plasma and radiation field. We consistently describe the dynamics of the plasma flow in the strong magnetic field of the star which is considered stationary. A sketch of the modeled system is presented in Fig. 1.

One of the main features of the presented model is a Godunov-type hydrodynamical approach which allowed us to treat discontinuous flows and describe shocks dynamics. Another feature of the model is the use of 2D dipole geometry, which is a natural choice to describe the flow of gas along the force lines of the dipole magnetic field.

The main global parameters of the employed model are as follows: the accretion rate $\dot{M}$ (typically $\dot{M} \sim 10^{15}$ g/s), the induction of the dipole magnetic field of a neutron star B ($\sim 10^{12}$ G), the radius of the star ($\sim$10 km), the mass of the star ($\sim$1.4 Solar mass), the area of the accretion spot on the star surface ($\sim$1 km^2).

3 Input physics and the numerical approach

The accreting plasma flow is treated in the 1-flow hydrodynamical approximation, due to the very short time scale of 2-flow instabilities. Hence, we model a flow of two fluids (electrons and ions) moving at the same velocity, but having different temperatures. The magnetic field of the neutron star is kept constant on the considered times scales.

The flow evolution is described by the following set of equations:

$$\begin{cases} \frac{\partial \rho}{\partial t} + \mathrm{div}(\rho \vec{u}) = 0, \\ \frac{\partial (\rho \vec{u})}{\partial t} + \nabla P + \nabla \cdot (\vec{u} \oplus (\rho \vec{u})) = \vec{\mathcal{F}}, \\ \frac{\partial}{\partial t}\left[\rho_s \left(E_s + \frac{u^2}{2}\right)\right] + \mathrm{div}\left[\rho_s \vec{u}\left(E_s + \frac{u^2}{2}\right) + p_s \vec{u}\right] = \mathcal{Q}_s, \end{cases} \tag{1}$$

where $\rho = \rho_e + \rho_i$, $p = p_e + p_i$, $\mathcal{F}$ and $\mathcal{Q}_s$ denote the sources of momentum and energy, respectively, and s is the sort of particles (i for ions, and e for electrons).

The set has to be completed with equations of state for each sort of particles. The ideal gas approximation $E_s(\gamma_s - 1) = p_s/\rho_s$ is valid for the considered ranges of temperatures and densities, but to account for the mild relativism achieved at the highest temperatures of the flow, we treat the adiabatic indexes as temperature-dependent values.

For mildly relativistic particles ($k_B T_s \ll m_s c^2$) the adiabatic index can be approximated as $\gamma_s \approx \gamma_{0s}\left(1 - \frac{k_B T_i}{m_i c^2}\right)$ [9], where $\gamma_{0i} = 5/3$ is the usual non-relativistic value for particle distributions with 3 degrees of freedom, and $\gamma_{0e} = 3$ as the electrons appear quasi-one-dimensional in the considered strong magnetic fields.

As we consider both the (resonant) cyclotron line emission, which provides substantial radiative pressure on the flow, and the (non-resonant) continuum emission, the transfer equation is solved by numerical iterations via a custom 2-step procedure with different emission and absorption coefficients at each step.

The force term $\vec{\mathcal{F}}$ is the sum of several forces: the gravitational force, the non-resonant and resonant radiative forces, and the viscous resistive force in the atmosphere of the neutron star (which is, in fact, an extended boundary condition at the bottom of the correction column). The force of resonant radiation acting on the electrons accounts for the scattering phase function (according to [10]), while the non-resonant force is due to Thomson scattering.

The ions change their energy due to the following processes: small-angle scattering with the electrons, collisional excitation of electrons to Landau levels, collisional relaxation in the atmosphere, and the work of the effective ambipolar force.

The electrons change their energy due to the following processes: small-angle scattering with the ions, Bremsstrahlung cooling in collisions with electrons and ions, excitation to Landau levels in collisions with electrons and ions, Compton processes, and the work of the effective ambipolar force.

The complete set of equations is rewritten in dipole geometry and numerically integrated. As the multi-component accreting flow may contain discontinuities, in particular, shocks, a modified Godunov-type approach [11, 12] has been employed. The radiation transfer equation is integrated within a first order finite-difference scheme.

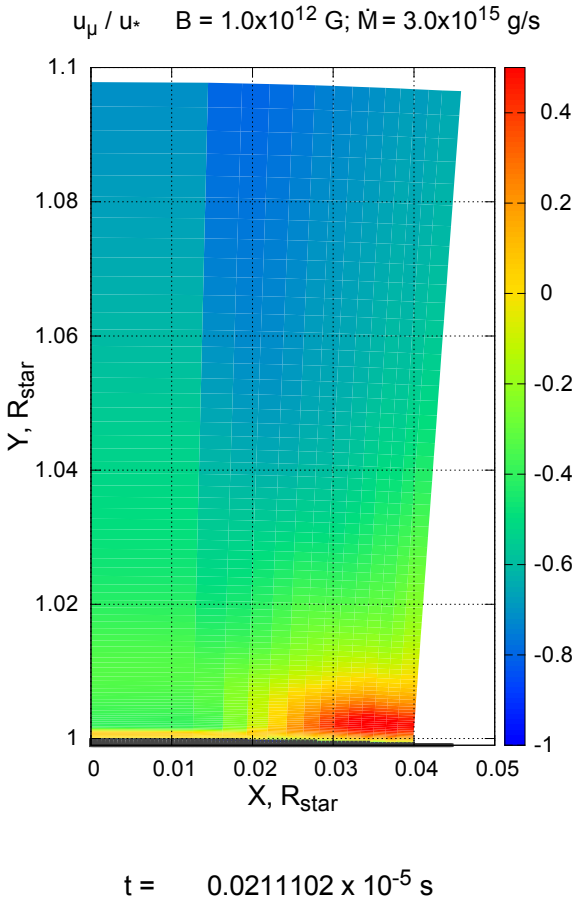

Figure 2: Distribution of velocity projection along the field lines (color) in the cross section of the accretion column.

4 Results

The performed modeling showed collisionless shocks to appear and evolve on the time scales of about 10^{-7} s. The 2D modeling also allows to see that the surface of the evolving shock is not flat, but rather resembles an "upside down hat": at the borders of the column the shock position is higher than over the pole.

A cross section of a modeled column (projection of 2D velocity onto the field lines) is shown in Figs. 2 and 3 to illustrate the form of the shock.

The 2D model allowed us to account for the flow motion and radiation transfer across the force lines. We also implemented an improved approach to the treatment of radiation transfer accounting for the scattering phase function both for non-resonant and resonant emission.

The presented results of 2D modeling are consistent with those of the 1D model [8]. Namely, the column profiles of accreting plasma parameters of the 2D model near the pole force line are in a qualitative agreement with the profiles

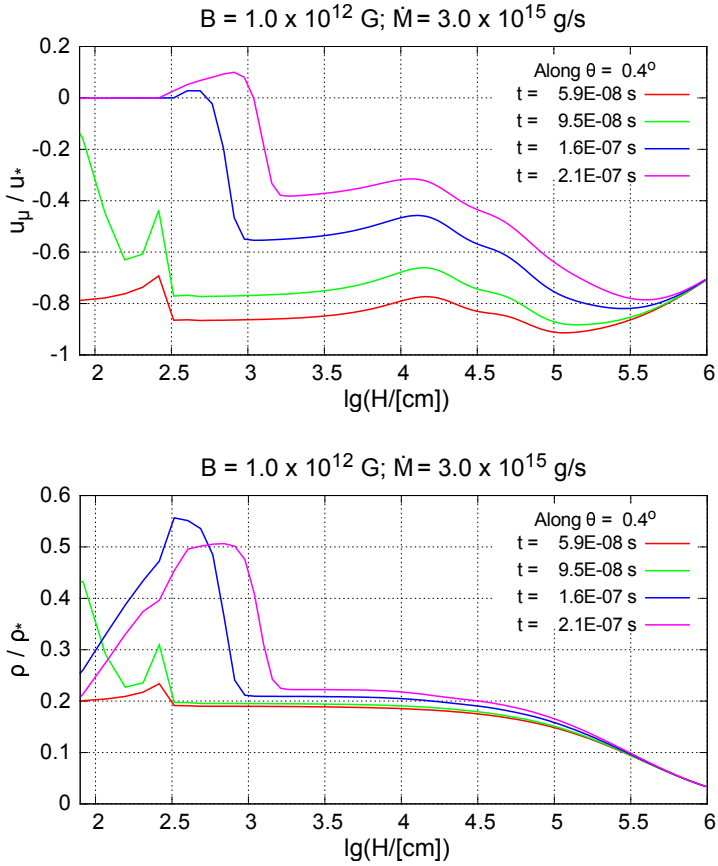

Figure 3: Velocity projection (up) and density (down) along the force line started at the magnetic pole, normalized by $u_* = 1.9 \times 10^{10}$ cm/s and $\rho_* = 10^{20}$ g/cm^3, respectively.

obtained with the 1D model. However, with the new model we also obtain a new effect which could not have been studied before – the inhomogeneity of the flow across the field lines.

References

1. *Ya.B. Zel'dovich*, Dokl. Acad. Nauk SSSR, **155**, 67, 1964.
2. *E.E. Salpeter*, Astrophys. J., **140**, 796, 1964.
3. *Ya.B. Zel'dovich*, Trans. XIII IAU Meet., Prague, 1967.
4. *Ya.B. Zel'dovich, N.I. Shakura*, Astron. Zh., **46**, 255, 1969.
5. *R.I. Klein, J. Arons*, Proc. 23rd ESLAB Symp. on Two-Topics in X-Rays Astronomy. Noordwijk, 1989, p. 89.
6. *R.I. Klein, J. Arons, G. Jernigan, J.J.-L. Hsu*, Astrophys. J. Lett., **457**, L85, 1996.
7. *R.A. Araya, A.K. Harding*, Astrophys. J., **517**, 334, 1999.

8. *A.M. Bykov, A.M. Krasil'shchikov*, Astron. Lett., **30**, 351, 2004.

9. *S. De Groot, W. van Leeuwen, Ch. van Weert*, Relativistic Kinetic Theory. Amsterdam: North-Holland, 1980.

10. *A.K. Harding, D. Lai*, Rep. Prog. Phys., **69**, 2631, 2006.

11. *S.K. Godunov, A.V. Zabrodin, M.Ya. Ivanov et al.*, Numerical Integration of Multidimensional Gas-Dynamic Problems. Moscow: Nauka, 1976 (in Russian).

12. *R.J. LeVeque*, J. Comput. Phys., **131**, 327, 1997.

* The color figures are available online in the Proceedings at *http://www.astro.spbu.ru/sobolev100/*.

Generation of Hot Plasma and X-Rays in Comets

S. Ibadov[1,2]

E-mail: *ibadovsu@yandex.ru*

Generation of hot plasma and X-rays in comets due to high-velocity collisions between cometary and interplanetary dust particles is analytically considered. The results are presented as a brief summary of our researches carried out in the field during the last three decades. It is found that in the inner heliosphere, i.e., at relative velocities of colliding dust particles more than 50–70 km/s (for retrograde and quasi-retrograde comets), initial temperatures of short-living dense plasma clumps produced by these collisions will be more than 10^5 K. Observable indicators of the phenomenon are multicharge ions as well as X-ray radiation of the hot clumps. The study of comets like Halley 1986 III and Hyakutake 1996 B2, having dust to gas production rates ratio more than 0.1, perihelion distances less than 1 AU and almost retrograde orbital motion, providing the dominant role of high-velocity (d-d) collisions in the gas-dust comet comas, is especially important to reveal peculiarities of the new radiation process/mechanisms in the Solar System objects using soft X-ray observatories like ROSAT and XMM. Such researches can expand the role of comets as natural space probes.

1 Introduction

The passage of bright dusty comets through circumsolar region is accompanied by intense collisions between cometary and interplanetary dust particles. Indeed, comet nuclei approaching the Sun become intense sources of gas-dust matter. According to the data of in situ measurements by VEGA 1/2 and GIOTTO missions, carried out at the comet heliocentric distance $R = 0.8$–0.9 AU, the gas and dust production rates of the nucleus of comet Halley 1986 III are $Q_g = 4 \times 10^7$ and $Q_d = 10^7$ g/s, respectively. These data lead to the dust to gas production rate ratio around 0.25 [1, 2].

Calculations show that for the Halley type dusty comets the dominant interaction mechanism of the gas-dust coma of the comet with interplanetary dust particles, IPD, will be no meteor-like phenomenon (i.e., intense gradual thermal evaporation of IPD due to irradiation by the cometary coma gas molecules), but collisions between comet dust and IPD, (d-d) process, that can lead to high-temperature phenomena: impulse generation of hot plasma, multicharge ions and soft, 0.1–1 keV, X-rays [3, 4, 5].

[1] Moscow State University, Sternberg Astronomical Institute, Russia
[2] Institute of Astrophysics, Tajik Academy of Sciences, Dushanbe, Tajikistan

V. Grinin et al. (eds) Radiation mechanisms of astrophysical objects. Yerevan: Edit Print, 2017, pp. 311–314.

Meantime, discovery of soft cometary X-rays was made on 27 March 1996 by orbital telescope ROSAT during observations of bright and dusty comet Hyakutake 1996 B2 having quasi-retrograde orbit [6]. To carry out these observations results of a theoretical consideration [7] was used, as a motivation (Dennerl, Lisse, Truemper, 1998, 1999, private communications).

We present here a brief review of basic results of theoretical investigations on the generation of hot plasma and X-rays in comets due to high-velocity collisions between dust particles as well as some prospects for further X-ray observations of dusty comets.

2 Generation of hot plasma and X-rays in comets by (d-d) process

Collisions between dusty coma of comets and interplanetary/zodiacal dust cloud, (d-d) process, in the inner heliosphere have high-velocity character for comets with retrograde and quasi-retrograde orbits. This phenomenon will lead to production of hot quickly expanding/short-living dense plasma clumps. The initial temperature of the plasma and the mean charge of ions can be analytically presented as $T = T_*(V/V_*)^2$ and $z = z_*(V/V_*)^{(2/s_i)}$ ($s_i = 1.3$ is the parameter of the curve of ionization potentials, $I(z)$, of dust particle atoms), so that at $R_* = 1$ AU we have $V = V_* = 7 \times 10^6$ cm/s and $T_* = 3 \times 10^5$ K, $z_* = 4$ for the Halley 1986 III type comets.

Calculations show that radiation mechanism of hot dense/quickly expanding plasma clumps with the initial radii around and more than 10^{-5} cm will be like the black-body one, due to suffice large "optical/photon thickness" of the plasma clots consisting of multicharge ions of heavy/multielectron atoms of elements like Fe, Si, O, etc. Such plasma blobs during their expansion become optically thin and hence can give line emission too.

The efficiency of conversion of the kinetic energy of colliding dust particles into the energy of X-ray photons, k_x, was calculated for the both cases taking into account both bremsstrahlung and recombination radiation mechanisms. It is found that the maximum value of the efficiency will be around $k_x = 0.1$. The most probable energy of photons from the cometary coma hot plasma clumps will raise at decreasing the comet heliocentric distance and change in the range 0.1–1 keV at the range of $R = 1$–0.1 AU, respectively [7, 8, 9].

X-ray luminosity of dusty comets like comet Hyakutake 1996 B2 due to (d-d) process will be more than 10^{15} erg/s at $R < 1$ AU [10]. This value is close to the measured soft X-ray luminosity of comet Hyakutake 1996 B2 by ROSAT as $L_x(0.09{-}2\,\mathrm{keV}, R = 1\,\mathrm{AU}) = 4{\times}10^{15}$ erg/s, with strong temporal variations [6].

It should be noted that an essential contribution to the X-ray luminosity of comets can also give line emission due to recombination of multicharge ions of the solar wind plasma via charge exchange process with cometary coma atoms and molecules that occurs effectively near the cometopause [11].

The maximum brightness of the X-ray emission of the cometary gas-dust coma, produced by these radiation mechanisms, should be located/shifted in the direction to the Sun because gas-dust matter from the comet nucleus always is being ejected, basically, towards the Sun. It is compatible with observations of such bright comet as Mrkos 1957d/1957 V showed emissions of Na-atoms with anomalous distribution at high angular resolution, as well as with data of the Vega 1/2 and Giotto in situ television observations of comet Halley 1986 III (cf. [1, 2, 12, 13, 14]).

3 Conclusions

It is analytically shown that high-velocity collisions between cometary and interplanetary dust particles in the comas of dusty comets with retrograde and quasi-retrograde orbital motion, (d-d) process, will lead to generation of hot short-living dense plasma clumps in the inner heliosphere. Such component of the cometary atmospheres plasma is able to emit 0.1–1 keV photons, i.e., soft X-rays.

Modern soft X-ray space telescopes like ROSAT and XMM have carried out X-ray observations of comets only at heliocentric distances close and more than 1 AU. For revealing and identification of X-ray generation mechanisms of comets as well as using comets as natural space probes it is important appropriate observations of bright dusty comets in the inner heliosphere and determining the dependence of X-ray luminosity and spectra of comets on the heliocentric distance.

Acknowledgments. The author is grateful to the Organizing Committee of the International Conference "Sobolev100: Radiation Mechanisms of Astrophysical Objects: Classics Today" (St. Petersburg, Russia, September 21–25, 2015) for hospitality and financial support, Dr. G.M. Rudnitskij, SAI MSU for useful discussions.

References

1. *R.Z. Sagdeev, J. Blamont, A.A. Galeev et al.*, Nature, **321**, 259, 1986.
2. *R. Reinhard*, Nature, **321**, 313, 1986.
3. *S. Ibadov*, Proc. Int. Conf. on Cometary Exploration. Budapest: Hungar. Acad. Sci., 1983, p. 227.
4. *S. Ibadov*, Europ. Space Agen. Sp. Publ., **SP-250**, 377, 1986.
5. *S. Ibadov*, Europ. Space Agen. Sp. Publ., **SP-278**, 655, 1987.
6. *C.M. Lisse, K. Dennerl, J. Englhauser et al.*, Science, **274**, 205, 1996.
7. *S. Ibadov*, Icarus, **86**, 283, 1990.
8. *S. Ibadov*, Adv. Space Res., **17**, 93, 1996.
9. *S. Ibadov*, Physical Processes in Comets and Related Objects. Moscow: Cosmos-inform, 1996.

10. *S. Ibadov*, Proc. IAU Symp. No. 274. Advances in Plasma Astrophysics. Cambridge: Cambridge Univ. Press, 2011, p. 76.

11. *T.E. Cravens*, J. Geophys. Res. Lett., **24**, 105, 1997.

12. *G.L. Greenstein, C. Arpigny*, Astrophys. J., **135**, 892, 1962.

13. *S. Ibadov*, Comets Meteors, No. 37, 8, 1985.

14. *S. Ibadov*, 10th Europ. Reg. Astron. Meet. Prague: Czech. Acad. Sci., 1987, p. 51.

The Evolution of a Supermassive Retrograde Binary in an Accretion Disk

P.B. Ivanov[1,2], J.C.B. Papaloizou[2], S.-J. Paardekooper[3], A.G. Polnarev[3]

E-mail: *pbi20@cam.ac.uk*

In this contribution we discuss the main results of a study of a massive binary with unequal mass ratio, q, embedded in an accretion disk, with its orbital rotation being opposed to that of the disk. When the mass ratio is sufficiently large, a gap opens in the disk, but the mechanism of gap formation is very different from the prograde case. Inward migration occurs on a timescale of $t_{ev} \sim M_p/\dot{M}$, where M_p is the mass of the less massive component (the perturber), and $\dot{M}$ is the accretion rate. When $q \ll 1$, the accretion takes place mostly onto the more massive component, with the accretion rate onto the perturber being smaller than, or of order of, $q^{1/3}M$. However, this rate increases when supermassive binary black holes are considered and gravitational wave emission is important. We estimate a typical duration of time for which the accretion onto the perturber and gravitational waves could be detected.

1 Statement of the problem

Supermassive black hole binaries (SBBH) may form as a consequence of galaxy mergers (see, e.g., [6, 1]). Since the directions of the angular momenta associated with the motion of the binary and the gas in the accretion disk are potentially uncorrelated, the binary may be on either a prograde or retrograde orbit with respect to the orbital motion in the disk when it becomes gravitationally bound and starts to interact with it. The prograde case has been considered in many works beginning with [3] and [2]. The retrograde case has received much less attention, with relatively few numerical simulations available to date (see, e.g., [7]). However, the retrograde case may be as generic as the prograde case when the interaction of SBBH with an accretion disk is considered. Note that although the disk is likely to be inclined with respect to the binary orbital plane initially, alignment on a length scale corresponding to the so-called alignment radius is attained relatively rapidly, the direction of rotation of the disk gas being either retrograde or prograde with respect to orbital motion, depending on the initial inclination (see, e.g., [3]). Here we briefly review recent results on the evolution of retrograde SBBH published in detail in [4].

[1] Astro Space Centre, P.N. Lebedev Physical Institute, Moscow, Russia
[2] DAMTP, University of Cambridge, UK
[3] Astronomy Unit, Queen Mary University of London, UK

V. Grinin et al. (eds) Radiation mechanisms of astrophysical objects. Yerevan: Edit Print, 2017, pp. 315–318.

2 Numerical simulations of massive retrograde perturbers embedded in an accretion disk

In this section we consider numerical simulations for which the perturber is massive enough to significantly perturb the accretion disk and open a surface density depression called hereafter "a gap" in the vicinity of its orbit. For that we require mass ratio, q, of the perturber with mass M_p to the dominant mass M, to be larger than $\sim 1.57(H/r_p)^2$, where r_p is the radius of perturber's orbit and H is the disk semi-thickness. We consider values of $q = 0.01$ and 0.02 below. Note that the alternative case of a low mass perturber which is insufficiently massive to open a gap has been considered by [4]. The perturber was initiated on a retrograde circular orbit of radius r_0 which is taken to be the simulation unit of length. For simulation unit of time, we take the orbital period of a circular orbit with this radius, the disk aspect ratio was constant and equal to 0.05, for other details see [4]. The structure of the disk gaps for $q = 0.02$ is illustrated in the surface density contour plots presented in Fig. 1 at various times. Note that an animation of the process of gap formation can be found on the website *http://astro.qmul.ac.uk/people/sijme-jan-paardekooper/publications*. The semi-major axis is shown as a function of time for $q = 0.02$ and $q = 0.01$ with a gravitational softening length of $b = 0.1H$ and for $q = 0.01$ with $b = 0.6H$ in Fig. 2. The behavior depends only very weakly on whether the perturber is allowed to accrete from the disk or not.

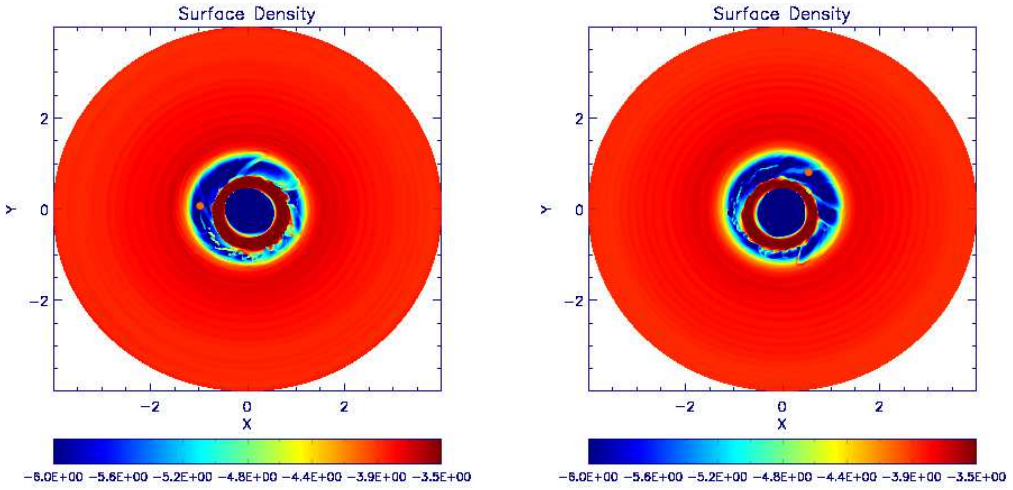

Figure 1: $\log \Sigma$ contours for $q = 0.02$ with softening length $0.1H$ after 50 orbits (left panel) and after 100 orbits (right panel). In these simulations the companion, its position in each case being at the center of the small red circle located within the gap region, was allowed to accrete. The width of the gaps slowly increases while the accretion rates, on average, slowly decrease with time. Short wavelength density waves in the outer disks are just visible. Note that values of $\log \Sigma$ below the minimum indicated on the color bar are plotted as that minimum value.

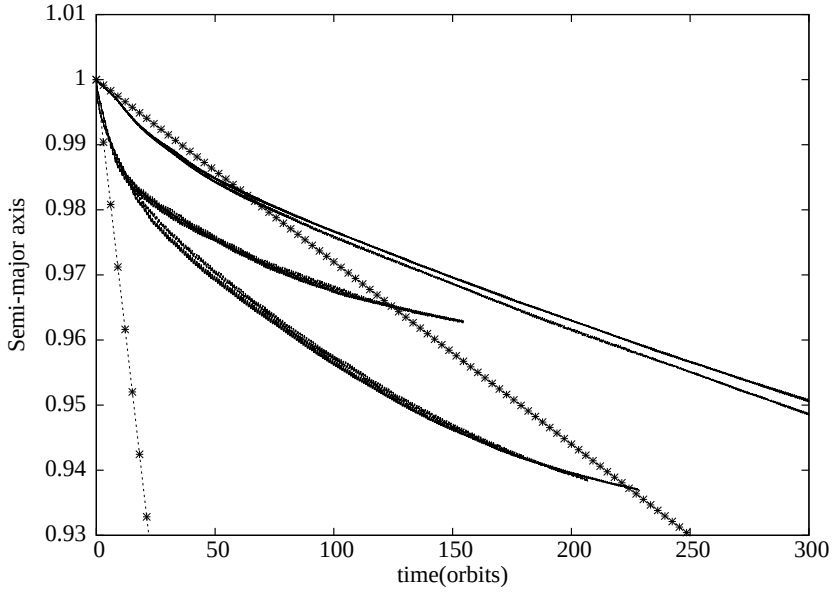

Figure 2: Semi-major axis, in units of the initial orbital radius, as a function of time for $q = 0.02$ and 0.01 with gravitational softening length $b = 0.1H$ and for $q = 0.01$ with $b = 0.6H$. Two curves without imposed crosses, which are very close together, are shown for each of these three cases. The uppermost pair of curves corresponds to $q = 0.01$ with $b = 0.6H$ and the lowermost pair to $q = 0.01$ with $b = 0.1H$. The central pair does to $q = 0.02$ with $b = 0.1H$. The lower of the pair of curves for the cases of $b = 0.1H$ corresponds to runs with accretion from the disk included. For the case of $b = 0.6H$, this situation is reversed. The straight lines which have imposed crosses are obtained adopting the initial Type I migration rate. The line with more widely separated crosses corresponds to $q = 0.01$ with $b = 0.1H$ while the other line corresponds to $q = 0.01$ with $b = 0.6H$.

3 Results

Our numerical results are confirmed by an analytic approach developed in [4]. In this paper the following general results have been obtained:

1) When the mass ratio q is small, but larger than $\sim 1.6(H/r_p)^2$ a gap in the vicinity of the perturber opens due to an increase of radial velocity of the gas in this region. Its size is smaller than the orbital distance r_p in this limit.
2) For such systems for which the perturber's mass is larger than a typical disk mass within a distance $\sim r_p$, the disk structure outside the gap is approximately quasi-stationary. The inner disk has nearly zero angular momentum flux, while the outer disk has an angular momentum flux equal to the product of the mass flux and the binary specific angular momentum. The orbital evolution timescale $t_{ev} = M_p/(2\dot{M})$ is then determined by conservation of angular momentum. Note that this picture differs from the prograde case with similar parameters, where there is a pronounced cavity instead of an inner disk and the orbital evolution is somewhat faster.

3) When the orbital evolution is determined by interaction with the disk, the mass flux onto the more massive component $\sim\dot{M}$, while the average mass flux onto the perturber is smaller $\sim q^{1/3}\dot{M}$. However, the latter exhibits strong variability on timescales on the order of the orbital period. The mass flux onto the perturber can increase significantly during the late stages of the inspiral of SBBH when the emission of gravitational waves controls the orbital evolution.
4) When the binary is sufficiently eccentric and the disk is sufficiently thin, the opening of a "conventional" cavity within the disk is also possible due to the presence of Lindblad resonances.

Additionally, we estimated a time duration for which the emitted gravitational waves would have sufficient amplitude for detection by a space-borne interferometric gravitational wave antenna with realistic parameters, as well as the appropriate range of frequencies as a function of the primary BH mass in [5].

Note that all these results have been obtained under the assumption that the binary orbit and the disk are coplanar. This may break down at late times. An estimate for the time required for their mutual inclination angle measured at large distances to change is given in [4] for an initially retrograde binary. The typical timescale is on the order of, or possibly even smaller than, t_{ev} depending on the mass ratio and disk parameters. Thus, this effect should be taken into account in future studies of these systems.

References

1. *M.C. Begelman, R.D. Blandford, M.J. Rees*, Nature, **287**, 307, 1980.
2. *A. Gould, H.-W. Rix*, Astrophys. J. Lett., **532**, L29, 2000.
3. *P.B. Ivanov, J.C.B. Papaloizou, A.G. Polnarev*, Mon. Not. Roy. Astron. Soc., **307**, 79, 1999.
4. *P.B. Ivanov, J.C.B. Papaloizou, S.-J. Paardekooper, A.G. Polnarev*, Astron. Astrophys., **576**, A29, 2015.
5. *P.B. Ivanov, J.C.B. Papaloizou, S.-J. Paardekooper, A.G. Polnarev*, Balt. Astron., **24**, 166, 2015.
6. *B.V. Komberg*, Sov. Astron., **11**, 727, 1968.
7. *C.J. Nixon, A.R. King, J.E. Pringle*, Mon. Not. Roy. Astron. Soc., **417**, L66, 2011.

* The color figure is available online in the Proceedings at *http://www.astro.spbu.ru/sobolev100/*.

Search for the Giant Pulses – an Extreme Phenomenon in Radio Pulsar Emission

A.N. Kazantsev[1,2], V.A. Potapov[1]

E-mail: *kaz.prao@bk.ru*

Here we present results of our search for Giant Pulses (GPs) from pulsars of Northern Hemisphere. Our survey was carried out at a frequency of 111 MHz using the Large Phased Array (LPA) radio telescope. Up to now we have detected regular generation of strong pulses satisfying the criteria of GPs from 2 pulsars: B1133+16, B1237+25.

1 Introduction

Slow pulse-to-pulse variation of intensity is very typical for overwhelming majority of known pulsars. However, a handful of pulsars have mysterious mechanism which can break such a stability.

Phenomenon of generation GPs was first detected for Crab pulsar (B0531+21) [1] and the millisecond pulsar B1937+21 [2]. In following studies a set of typical characteristics of GPs was determined. These are: very narrow components in pulse's microstructure (up to several nanoseconds), high peak flux density (up to several MJy), and power-law distribution of the peak flux density of GPs. It is important to emphasize that B0531+21 and B1937+21 have very strong magnetic field on the light cylinder ($B_{LC} \approx 10^6$ G) and are considered as "classical" pulsars with GPs. In course of time, GPs were detected from 5 pulsars with very strong magnetic field on the light cylinder ($B_{LC} \approx 10^5$–10^6 G): B0218+42 [3], B0540–69 [4], B1821–24 [5], J1823–3021 [6] and B1957+20 [3].

However, later a similar phenomenon was detected (mostly at low radio frequencies between 40 and 111 MHz) for a set of pulsars with B_{LC} in the range from several to several hundreds Gauss: J0034–0721 [7], J0529–6652 [8], J0659+1414 [9], J0953+0755 [10, 11], J1115+5030 [12] and J1752+2359 [13].

In present work we describe the results of our observations that were held to search for new pulsars generating GPs or anomalous strong pulses at low radio frequencies.

[1] P.N. Lebedev Phys. Inst. of the RAS, Pushchino Radio Astronomy Observatory, Russia
[2] Pushchino State Institute of Natural Sciences, Russia

V. Grinin et al. (eds) Radiation mechanisms of astrophysical objects. Yerevan: Edit Print, 2017, pp. 319–322.

2 Observations and processing

The observations were made during 2012 and 2014 at the Pushchino Radio Astronomy Observatory with the Large Phased Array radio telescope. This is the transit telescope with the effective area of about 20000 ± 4000 m^2 in the zenith direction. The main frequency of the observations was 111 MHz with a bandwidth of 2.3 MHz (460×5 kHz channels digital receiver with post-detector DM (Dispersion Measure) removal). The sampling interval was 1.2288 ms and the duration of each observation session was about 3.5 min (153 periods of PSR B1237+25).

We have processed the results of 66 observational sessions containing 11 091 pulses of B1133+16 and 89 observational sessions containing 13 617 pulses of B1237+25.

Average pulse of pulsar was obtained by summing and averaging of all individual pulses during one session of pulsar's observation. We have analyzed every pulse with a peak flux density $> 4\sigma_{noise}$ and located at the phase of the average pulse. Pulses with peak flux density more than 30 peak flux density of the average (per session) pulse were marked as GPs candidates.

For PSR B1133+16 we calculated peak flux density distribution separately for two main components of the average pulse of pulsar.

3 Results and conclusion

B1133+16 and B1237+25 are active second period (normal) radio pulsars with multicomponent average pulses having two and five main components, respectively. B1133+16 has a rotational period $P = 1.1879$ s and $B_{LC} = 11.9$ G, for B1237+25 $P = 1.3824$ s and $B_{LC} = 4.14$ G. We have regularly observed strong pulses from each pulsar during entire period of our observation [14, 15].

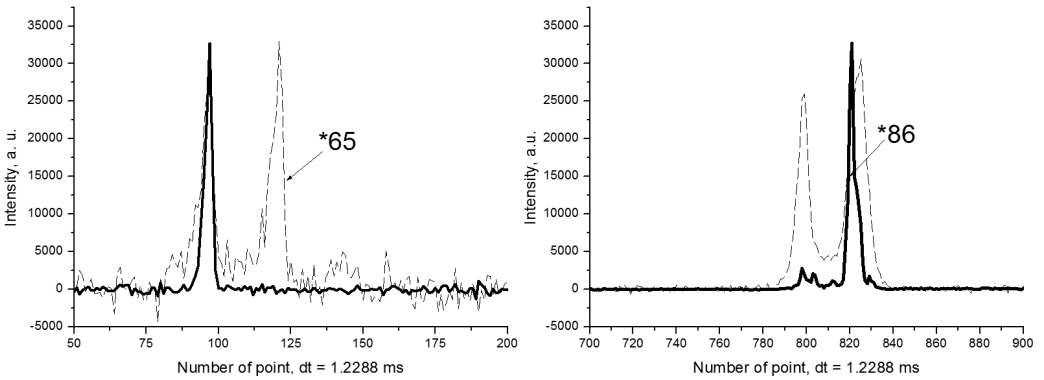

Figure 1: Strong pulses of PSR B1237+25 observed on May 14, 2012 (left panel), and of PSR B1133+16 observed on March 14, 2014 (right panel). The average pulse (dashed line) is shown multiplied by 65 and 86, respectively.

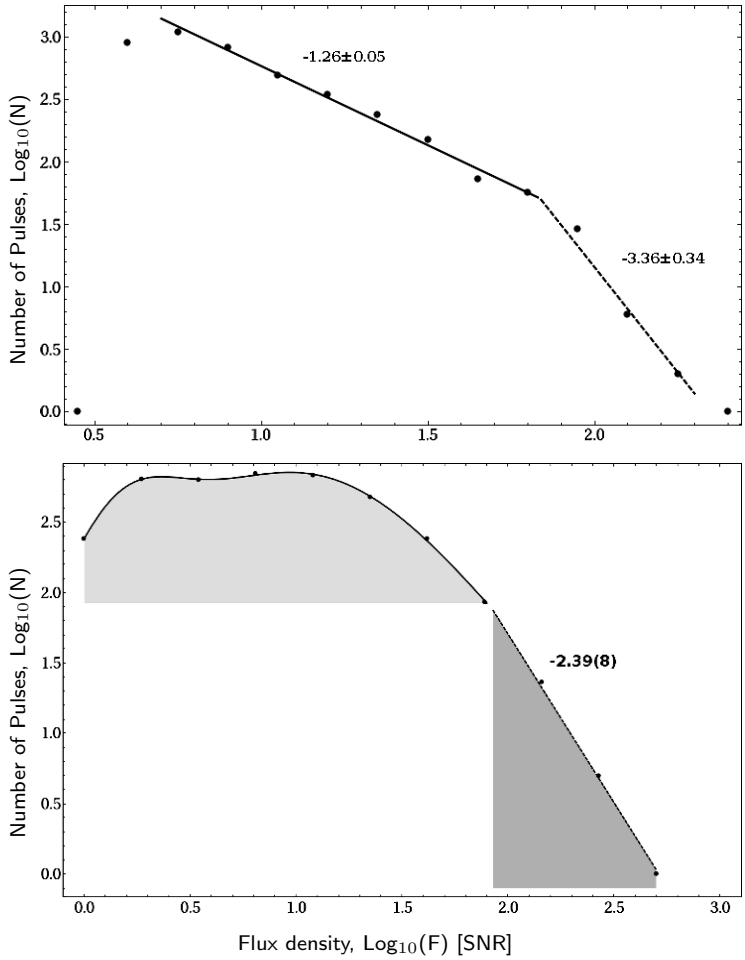

Figure 2: Histograms of distributions of the peak flux density of individual pulses for B1237+25 (top panel), and for the second (right-hand) component of B1133+16 (bottom panel) shown in the Log-Log scale. Data was fitted by the combination of two power-law distributions, and two log-normal plus power-law distribution, respectively.

An example of GPs from B1237+25 and B1133+16 are shown in Fig. 1. The most powerful GP of B1237+25 was detected on August 12, 2012, and has a flux density of 900 ± 130 Jy. There are around 12 GP events per 10000 pulses for B1237+25, and around 16 GP events per 10000 pulses for B1133+16.

The distribution of the peak flux density (in signal to noise ratio units) in the Log-Log scale is shown in Fig. 2. For B1237+25 distribution of the strong pulses has a bimodal power-law shape with exponents -1.26 ± 0.05 and -3.36 ± 0.34, which is quite typical of GPs and obviously differs from log-normal individual pulses distribution of regular pulses. The distribution for B1133+16 has a complex character and may be fitted as a combination of two log-normal distributions for the first component of pulse and two log-normal and one power-law components with an exponent -2.39 ± 0.08 for the second.

We can conclude that strong individual pulses of PSR B1133+16 and PSR B1237+25 observed at 111 MHz satisfy the main criteria of GPs. It is worth noting that B1133+16 and PSR B1237+25 are pulsars with low magnetic field on light cylinder. This is the further confirmation of our earlier assumptions that such pulsars (including J0034–0721, J0529–6652, J0659+1414, J0953+0755, J1115+5030 and J1752+2359) may be referred as a sub-class of pulsars with GP, having low magnetic field on light cylinder and generating GPs mostly at low radio frequencies.

Acknowledgments. This work was supported by the Program of the Presidium of the Russian Academy of Sciences 41P "Transitional and explosive processes in astrophysics", and by Scientific Educational Complex Program of P.N. Lebedev Institute of the RAS.

References

1. *D.N. Staelin, E.C. Reifenstein*, IAU Astron. Telegram Circ., No. 2110, 1968.
2. *A. Wolszczan, J. Cordes, D. Stinebring*, NRAO Workshop, 1984, p. 63.
3. *B.C. Joshi, M. Kramer, A.G. Lyne et al.*, Proc. IAU Symp. No. 218, 2004, p. 319.
4. *S. Johnston, R.W. Romani*, Astrophys. J. Lett., **590**, L95, 2003.
5. *S. Johnston, R.W. Romani*, Astrophys. J. Lett., **557**, L93, 2001.
6. *H.S. Knight, M. Bailes, R.N. Manchester, S.M. Ord*, Astrophys. J., **625**, 951, 2005.
7. *A.D. Kuzmin, A.A. Ershov, B.Ya. Losovsky*, Astron. Lett., **30**, 247, 2004.
8. *F. Crawford, D. Altemose, H. Li, D.R. Lorimer*, Astrophys. J., **762**, 97, 2013.
9. *A.D. Kuzmin, A.A. Ershov*, Astron. Lett., **32**, 583, 2006.
10. *A.K. Singal*, Astrophys. Space Sci., **278**, 61, 2001.
11. *T.V. Smirnova*, Astron. Rep., **54**, 430, 2012.
12. *A.A. Ershov, A.D. Kuzmin*, Astron. Lett., **29**, 91, 2003.
13. *A.A. Ershov, A.D. Kuzmin*, Chin. J. Astron. Astrophys., **6**, 30, 2006.
14. *A.N. Kazantsev, V.A. Potapov*, Astron. Tsirk., **1620**, 1, 2015.
15. *A.N. Kazantsev, V.A. Potapov*, Astron. Tsirk., **1628**, 1, 2015.

Testing the Variation of Fundamental Constants by Astrophysical Methods: Overview and Prospects

S.A. Levshakov[1,2]

E-mail: *lev@astro.ioffe.rssi.ru*

By measuring the fundamental constants in astrophysical objects one can test basic physical principles as space-time invariance of physical laws along with probing the applicability limits of the standard model of particle physics. The latest constraints on the fine structure constant α and the electron-to-proton mass ratio μ obtained from observations at high redshifts and in the Milky Way disk are reviewed. In optical range, the most accurate measurements have already reached the sensitivity limit of available instruments, and further improvements will be possible only with next generation of telescopes and receivers. New methods of the wavelength calibration should be realized to control systematic errors at the sub-pixel level. In radio sector, the main tasks are the search for galactic and extragalactic objects suitable for precise molecular spectroscopy as well as high resolution laboratory measurements of molecular lines to provide accurate frequency standards. The expected progress in the optical and radio astrophysical observations is quantified.

1 Introduction

The idea that the fundamental physical constants may vary on the cosmological time scale has been discussing since 1937, when Milne and Dirac argued about possible variations of the Newton constant G during the lifetime of the universe [1, 2]. Currently, the subject of the cosmological variation of fundamental constants is closely related to emergence considerations of different cosmological models inspired by the discovery of late time acceleration of the expansion of the universe [3, 4]. The possibility that dimensionless coupling constants such as electron-to-proton mass ratio $\mu = m_{\rm e}/m_{\rm p}$ and the fine structure constant $\alpha = e^2/\hbar c$ may roll with cosmic time has recently been reviewed in [5, 6, 7, 8].

The variation of fundamental constants would imply a violation of the Einstein equivalence principle (EEP), that is, local position invariance (LPI) and local Lorentz invariance (LLI). In particular, a changing α accompanied by variation in other coupling constants can be associated with a violation of LLI [9], and LPI postulates that the fundamental physical laws are space-time invariant.

[1] A.F. Ioffe Physical-Technical Institute, St. Petersburg, Russia
[2] St. Petersburg Electrotechnical University "LETI", Russia

V. Grinin et al. (eds) Radiation mechanisms of astrophysical objects. Yerevan: Edit Print, 2017, pp. 323–330.

The standard model of particle physics (SM) is based on the EEP; thus, we can probe the applicability limits of the SM and new types of interactions by experimental validation of the EEP.

In spite of some claims that changes in α or μ were marginally detected at high redshifts, to date no confirmed variation of dimensionless coupling constants has been found on astronomical space-time scales. Below we review current observational constraints on α and μ variations which provide limits on the allowed deviations from the SM and ΛCDM cosmology.

2 Basics of the astronomical measurements

Two dimensionless coupling constants μ and α are of particular interest for astronomical studies since their fractional changes $\Delta\mu/\mu = (\mu_{\rm obs} - \mu_{\rm lab})/\mu_{\rm lab}$, and $\Delta\alpha/\alpha = (\alpha_{\rm obs} - \alpha_{\rm lab})/\alpha_{\rm lab}$ can be accurately measured from spectral line profiles of Galactic and extragalactic sources.

Differential measurements of $\Delta\mu/\mu$ and $\Delta\alpha/\alpha$ are based on the comparison of the line centers in the absorption/emission spectra of cosmic objects and the corresponding laboratory values. It was shown that electro-vibro-rotational lines of H_2 [10] and CO [11] have their own sensitivities to μ-variation. Similarly, each atomic transition is characterized by its individual sensitivity to α-variation [12]. The dependence of an atomic frequency ω on α in the comoving reference frame of a distant object located at redshift z is given by $\omega_z = \omega + qx + O(x^2)$, where $x \equiv (\alpha_z/\alpha)^2 - 1$. Here ω and ω_z are the frequencies corresponding to the present-day value of α and that at a redshift z. The so-called q factor is an individual parameter for each atomic transition [12]. If $\alpha_z \neq \alpha$, then $x \neq 0$ and the corresponding frequency shift $\Delta\omega = \omega_z - \omega$ is $\Delta\omega/\omega = Q\Delta\alpha/\alpha$, where $Q = 2q/\omega$ is the dimensionless sensitivity coefficient.

For two lines of the same element with the sensitivity coefficients Q_1 and Q_2, the fractional changes $\Delta\mu/\mu$ and $\Delta\alpha/\alpha$ are equal to $\Delta v/(c\Delta Q)$, where $\Delta v = v_1 - v_2$ is the difference of the measured radial velocities of these lines, and $\Delta Q = Q_2 - Q_1$ is the corresponding difference between their sensitivity coefficients [13, 14].

The Q values of atomic transitions observed in quasar spectra are very small, $|Q| \ll 1$ [12]. Similar low sensitivity coefficients were calculated for electro-vibro-rotational transitions in H_2 and CO (for references, see [14]). Small values of Q and ΔQ put tough constraints on optical methods to probe $\Delta\alpha/\alpha$ and $\Delta\mu/\mu$. For instance, at $\Delta\alpha/\alpha \sim 10^{-5}$, the required line position accuracy must be $\sigma_v \lesssim 0.25$ km s^{-1} in accord with the inequality [14]: $\sigma_v/c < (\Delta Q/\sqrt{2})(\Delta\alpha/\alpha)$. A typical error of the line center measurements of an unsaturated absorption line in quasar spectra is about $1/10th$ of the pixel size [15]. For high redshift objects, the UV-Visual Echelle Spectrograph (UVES) at the ESO Very Large Telescope (VLT) provides a pixel size $\Delta\lambda_{\rm pix} \sim 0.06$ Å at $\lambda \sim 5000$ Å, that is $\sigma_v \sim 0.5$ km s^{-1}, which is comparable to the velocity offset due to a fractional change in α at the level of 10^{-5}. This shows that special care and additional calibrations are

required to probe $\Delta\alpha/\alpha$ and $\Delta\mu/\mu$ at a level of 10^{-6} by optical methods. Such measurements have been carried out at the VLT/UVES as described in the next section.

3 VLT/UVES Large Program for testing fundamental physics

The ESO Large Programme 185.A–0745 (2010–2013) was especially aimed at testing the hypothetical variability of physical constants [16, 17, 18, 19]. Its prime goal was to study systematic errors in wavelength scales of quasar spectra. For this purpose, quasars were observed almost simultaneously with bright asteroids, whose reflected sunlight spectra contain many narrow features with positions as accurate as a few m s^{-1} [20]. Additionally, bright stars were observed through an iodine gas absorption cell, providing a precise transfer function for part of the wavelength range.

As a result, there were revealed distortions of the wavelength scale with a jigsaw pattern and peak-to-peak amplitude of several hundreds m s^{-1} along the echelle orders. The presence of long range wavelength dependent velocity drifts ranging between $\sim$0.5 and 1.0 km s^{-1} and showing opposite sign as compared with the Keck/HIRES spectra of quasars was found as well [21].

A stringent bound for $\Delta\alpha/\alpha$ was obtained for the absorber at $z_{\rm abs} = 1.69$ towards the quasar HE2217–2818 [16]. The fractional change of α in this system is $\Delta\alpha/\alpha = (1.3 \pm 2.4_{\rm stat} \pm 1.0_{\rm sys}) \times 10^{-6}$ if AlII λ1670 Å and three FeII transitions are used, and $\Delta\alpha/\alpha = (1.1 \pm 2.6_{\rm stat}) \times 10^{-6}$ in a slightly different analysis with only FeII transitions used. Together with another system observed with the UVES/VLT at $z_{\rm abs} = 1.58$ towards HE0001–2340 where $\Delta\alpha/\alpha = (-1.5 \pm 2.6_{\rm stat}) \times 10^{-6}$ [22], and eight HIRES/Keck quasar absorbers with the mean $\Delta\alpha/\alpha = (-0.1 \pm 2.6) \times 10^{-6}$ [23], these values are the tightest bounds to date on α-variation at high redshifts. As seen, they do not show any evidence for changes in α at the precision level of $\sim 3 \times 10^{-6}$ (1σ confidence level, C.L.).

For the electron-to-proton mass ratio, the analysis of the H_2 absorption lines of the $z_{\rm abs} = 2.40$ damped Ly-α system towards HE0027–1836 yields $\Delta\mu/\mu = (2.5 \pm 8.1_{\rm stat} \pm 6.2_{\rm sys}) \times 10^{-6}$ [17]. When corrections to the wavelength dependent velocity drift are applied then $\Delta\mu/\mu = (7.6 \pm 8.1_{\rm stat} \pm 6.3_{\rm sys}) \times 10^{-6}$. At higher redshift $z_{\rm abs} = 4.22$ the analysis of H_2 absorption lines in the spectrum of J1443+2724 gives $\Delta\mu/\mu = (9.5 \pm 5.4_{\rm stat} \pm 5.3_{\rm sys}) \times 10^{-6}$ [24]. These results are consistent with a null μ-variation at the $\sim 2 \times 10^{-5}$ (1σ C.L.) precision level over a lookback time of $\approx$ 12.4 Gyr (10% of the age of the Universe today).

4 Microwave and submillimeter molecular transitions

Radio astronomical observations allow us to probe variation of the fundamental constants on the cosmological time scale at a level deeper than 10^{-5}. In the microwave range there are a good deal of molecular transitions arising

in galactic and extragalactic sources. Electronic, vibrational, and rotational energies in molecular spectra are scaled as $E_{\rm el} : E_{\rm vib} : E_{\rm rot} = 1 : \mu^{1/2} : \mu$. This means that the sensitivity coefficients for pure vibrational and rotational transitions are equal to $Q_{\rm vib} = 0.5$ and $Q_{\rm rot} = 1$. Molecules have also fine and hyperfine structures, Λ-doubling, hindered rotation, accidental degeneracy between narrow close-lying levels of different types and all of them have a specific dependence on the physical constants. Some of these molecular transitions are $\sim$100 times more sensitive to variations of μ and α than atomic, and electro-vibro-rotational transitions of H_2 and CO which are detected in six quasar absorbers between $z = 1.6$ and 2.7 [25]. In addition, positions of narrow molecular lines arising from cold dark clouds in the Milky Way disk can be measured with uncertainties of $\sigma_v \lesssim 0.01$ km s^{-1} [26], that is, the resulting sensitivity in radio bands is about three orders of magnitude higher as compared with optical spectra.

The molecular transitions with enhanced sensitivity coefficients which are the prime targets for testing the constancy of the fundamental constants by radio astronomical methods were recently reviewed in [14]. For instance, inversion transitions of ammonia NH_3 – one of the most abundant molecules in the interstellar medium – have sensitivity coefficients $Q_\mu = 4.5$ [27]. This enhancement occurs due to the tunneling effect depending on the action S which is proportional to μ^{-1}: the ground state tunneling frequency $\omega \propto e^{-S}$. Observations of the NH_3(1,1) inversion line and five HC_3N rotational lines at $z_{\rm abs} = 0.89$ towards PKS1830–211 [28], as well as the inversion (NH_3) and rotational (CS, H_2CO) lines at $z_{\rm abs} = 0.69$ towards B0218+357 [29] led to constraints (1σ C.L.): $|\Delta\mu/\mu| < 5 \times 10^{-7}$ and $|\Delta\mu/\mu| < 1 \times 10^{-7}$, respectively.

The second molecule which is extremely sensitive to μ-variation and which is observed in galactic and extragalactic molecular clouds is methanol CH_3OH. The sensitivity coefficients Q_μ for different transitions in CH_3OH range from -53 to 42 [30, 31]. A distinctive feature of methanol is strong interaction between the internal (hindered) and overall rotations. Transitions, in which both the internal and overall rotation states are changed, have strongly enhanced Q_μ-factors. However, the magnetic hyperfine structure of methanol transitions which was partly resolved in laboratory measurements [32] puts natural restriction on the methanol method at the level of $\sim 10^{-8}$ in $\Delta\mu/\mu$ tests. The hyperfine coupling in methanol is due to the well known magnetic spin-rotation and spin-spin couplings leading to small line splittings of $\sim$10 kHz. The large amplitude internal rotation may also lead to a less known magnetic coupling – the so-called spin-torsion coupling – which has not yet been conclusively evidenced.

So far, methanol absorption lines were detected at $z_{\rm abs} = 0.89$ in the gravitationally lensed system PKS1830–211 [33]. This system provides the most stringent limit on changes in μ over a lookback time of ≈ 7.5 Gyr: $|\Delta\mu/\mu| < 2 \times 10^{-7}$ (1σ C.L.) [34].

Cold ($T_{\rm kin} \sim 10$ K) and dense ($n_{\rm H_2} \sim 10^4$ cm^{-3}) molecular cores in the Milky Way disk are another perspective targets to probe μ. The molecular cores are the ammonia emitters exhibiting some of the narrowest ($\Delta v \lesssim 0.2$ km s^{-1} (FWHM))

lines ever observed [35, 36]. The NH_3 line widths Δv of some of them correspond to a pure thermal broadening at a minimum gas temperature of $T_{\rm kin} \approx 8$ K coming mainly from the heating by cosmic rays [37]. A lifetime of molecular cores is $\sim 10^{6-7}$ yr [38], and they are located at regions with different gravitational potentials.

A sample of the molecular cores were studied with the Medicina 32-m, Nobeyama 45-m, and Effelsberg 100-m telescopes in [26, 39, 40]. The main result of these measurements is the most stringent limit on μ-variation for the period of $\sim 10^{6-7}$ yr obtained by astronomical methods [26]: $|\Delta\mu/\mu| < 7 \times 10^{-9}$ (1σ C.L.). This upper limit is comparable with the current constraint stemming from laboratory experiments, $\dot{\mu}/\mu < 6 \times 10^{-16}$ yr^{-1} [41].

An independent test that α and μ may differ between the high- and low-density environments of the Earth and the interstellar medium was performed with CH and OH in [42]. In the Milky Way, the strongest limit to date on α-variation is $|\Delta\alpha/\alpha| < 1.4 \times 10^{-7}$ (1σ C.L.).

Thus, the Einstein heuristic principle of LPI is validated all over the universe, that is, neither α at the level of $\sim few \times 10^{-6}$, no μ at the level of $\sim few \times 10^{-7}$ deviates from its terrestrial value for the passed 10^{10} yr. Locally, no statistically significant deviations of $\Delta\mu/\mu$ from zero were found at even more deeper level of $\sim few \times 10^{-9}$. For the fine structure constant, such limit is $\sim 10^{-7}$.

5 Future prospects

In previous sections we demonstrated that the radio observations of NH_3 and CH_3OH lines are an order of magnitude more sensitive to fractional changes in μ than the optical constraints derived from H_2. However, at cosmological distances there are only five radio molecular absorbers known and all of them are located at $z < 1$, whereas H_2 lines are detected at redshifts $2 \lesssim z \lesssim 4$.

As was emphasized in [14], the improvements in measurements of $\Delta\alpha/\alpha$ and $\Delta\mu/\mu$ at the level of, respectively, 10^{-8} and 10^{-9}, can be achieved if two main requirements will be fulfilled: (*i*) increasing precision of the laboratory measurements of the rest frame frequencies of the most sensitive molecular transitions, and (*ii*) increasing sensitivity and spectral resolution of astronomical observations.

The second requirement is expected to be realized in a couple of years when the Next Generation Very Large Array (ngVLA) will start regular operations [43]. The ngVLA will provide ten times the effective collecting area of the JVLA and ALMA, operating from 1 GHz to 115 GHz, with ten times longer baselines (300 km). The increased sensitivity of the ngVLT by an order of magnitude over the VLA would allow discovery of new molecular absorbers at $z > 1$ and, thus, would extend the sample of targets suitable to test the EEP at early cosmological epochs.

In optical sector, the forthcoming generation of new optical telescopes such as the Thirty Meter Telescope (TMT) and the European Extremely Large

Telescope (E-ELT) equipped by high-resolution ultra-stable spectrographs will significantly improve the constancy limits of fundamental couplings. The future high precision optical measurements should achieve sensitivities of $\sim 10^{-7}$ for individual absorbers. Thanks to a large sample of absorption-line systems, a few times deeper limit is expected for the ensemble average.

In spite of a far higher sensitivity of radio methods as compared to that of next-generation optical facilities, the unresolved (or partly resolved) magnetic hyperfine structure of molecular transitions prevents the radio measurements to achieve the accuracy better than $\sim 10^{-9}$.

For example, the hyperfine structure of several transitions in methanol CH_3OH was recently recorded in the microwave domain using the Fourier transform microwave (FT-MW) spectrometer in Hannover and the molecular beam FT-MW spectrometer in Lille [32]. With the line splitting of $\sim$10 kHz revealed in these laboratory studies, and the difference between the sensitivity coefficients $\Delta Q_\mu \sim 10$ for the 48.372, 48.377, and 60.531 GHz methanol lines observed at $z_{\rm abs} = 0.89$ towards PKS1830–211 [34], one finds the uncertainty of $\Delta\mu/\mu$ of about 3×10^{-8}, which is entirely caused by the unresolved hyperfine structure of methanol lines.

It should be obvious that further progress in radio sector is in need of accurate laboratory measurements of the rest frame molecular frequencies. The required uncertainty of laboratory frequencies is $\lesssim 1$ m s^{-1}. There is currently a shortage of such data. Among molecules with high sensitivity coefficients to changes in μ and α only NH_3 [44] and CH [42, 45] transitions fulfill this requirement.

6 Conclusions

In this short review we highlighted the most important observational results which mark the frontier of most precise spectroscopic measurements of line positions in optical and radio sectors aimed at different tests of the variation of fundamental physical constants by astrophysical methods.

Current null results from the VLT and Keck optical telescopes as well as from different radio telescopes validate the Einstein equivalence principle at a rather deep level of $\sim 10^{-7} - 10^{-6}$ for extragalactic sources and at $\sim 10^{-8}$ within the Milky Way disk. This is a tremendous step forward in experimental justification of basic principles of the general relativity and the standard model of particle physics as compared with the first astrophysical constraint on $|\Delta\alpha/\alpha| < 3 \times 10^{-3}$ towards radio galaxy Cygnus A ($z = 0.057$) obtained 60 years ago by Savedoff [46].

It should be emphasized that both optical and radio methods complement each other and in future will provide independent tests of $\Delta\alpha/\alpha$ and $\Delta\mu/\mu$ variability using the next-generation radio and optical telescopes.

References

1. *E.A. Milne*, Proc. Roy. Soc. A., **158**, 324, 1937.
2. *P.A.M. Dirac*, Nature, **139**, 323, 1937.

3. *A.G. Riess, A.V. Filippenko, P. Challis et al.*, Astron. J., **116**, 1009, 1998.
4. *S. Perlmutter, G. Aldering, G. Goldhaber et al.*, Astrophys. J., **517**, 565, 1999.
5. *J.-P. Uzan*, Living Rev. Rel., **14**, 2, 2011.
6. *S. Liberati*, Class. Quant. Grav., **30**, 133001, 2013.
7. *C.J.A.P. Martin*, Gen. Rel. Grav., **47**, 1843, 2014.
8. *M. Martinelli, E. Calabrese, C.J.A.P. Martin*, J. Cosmol. Astropart. Phys., **11**, 030, 2015.
9. *V.A. Kostelecký, R. Lehnert, M.J. Perry*, Phys. Rev. D, **68**, 123511, 2003.
10. *D.A. Varshalovich, S.A. Levshakov*, J. Exp. Theor. Phys., **58**, 231, 1993.
11. *E.J. Salumbides, M.L. Niu, J. Bagdonaite et al.*, Phys. Rev. A, **86**, 022510, 2012.
12. *V.A. Dzuba, V.V. Flambaum, J.K. Webb*, Phys. Rev. Lett., **82**, 888, 1999.
13. *S.A. Levshakov, M. Dessauges-Zavadsky, S. D'Odorico, P. Molaro et al.*, Mon. Not. Roy. Astron. Soc., **333**, 373, 2002.
14. *M.G. Kozlov, S.A. Levshakov*, Ann. Phys., **525**, 452, 2013.
15. *S.A. Levshakov, M. Centurión, P. Molaro, S. D'Odorico*, Astron. Astrophys., **434**, 827, 2005.
16. *P. Molaro, M. Centurión, J.B. Whitmore et al.*, Astron. Astrophys., **555**, 68, 2013.
17. *H. Rahmani, R. Srianand, N. Gupta et al.*, Mon. Not. Roy. Astron. Soc., **425**, 556, 2013.
18. *P. Bonifacio, H. Rahmani, J.B. Whitmore et al.*, Astron. Nachr., **335**, 83, 2014.
19. *T.M. Evans, M.T. Murphy, J.B. Whitmore et al.*, Mon. Not. Roy. Astron. Soc., **445**, 128, 2014.
20. *P. Molaro, S.A. Levshakov, S. Monai et al.*, Astron. Astrophys., **481**, 559, 2008.
21. *J.B. Whitmore, M.T. Murphy*, Mon. Not. Roy. Astron. Soc., **447**, 446, 2015.
22. *I.I. Agafonova, P. Molaro, S.A. Levshakov, J.L. Hou*, Astron. Astrophys., **529**, A28, 2011.
23. *A. Songaila, L.L. Cowie*, Astrophys. J., **793**, 103, 2014.
24. *J. Bagdonaite, W. Ubachs, M.T. Murphy, J.B. Whitmore*, Phys. Rev. Lett., **114**, 071301, 2015.
25. *P. Noterdaeme, P. Petitjean, R. Srianand et al.*, Astron. Astrophys., **526**, L7, 2011.
26. *S.A. Levshakov, D. Reimers, C. Henkel et al.*, Astron. Astrophys., **559**, A91, 2013.
27. *V.V. Flambaum, M.G. Kozlov*, Phys. Rev. Lett., **98**, 240801, 2007.
28. *C. Henkel, K.M. Menten, M.T. Murphy et al.*, Astron. Astrophys., **500**, 725, 2009.
29. *N. Kanekar*, Astrophys. J. Lett., **728**, L12, 2011.
30. *P. Jansen, L.-H. Xu, I. Kleiner et al.*, Phys. Rev. Lett., **106**, 100801, 2011.

31. *S.A. Levshakov, M.G. Kozlov, D. Reimers*, Astrophys. J., **738**, 26, 2011.

32. *L.H. Coudert, C. Gutlé, T.R. Huet et al.*, J. Chem. Phys., **143**, 044304, 2015.

33. *S. Muller, A. Beelen, M. Guélin et al.*, Astron. Astrophys., **535**, A103, 2011.

34. *N. Kanekar, W. Ubachs, K.M. Menten et al.*, Mon. Not. Roy. Astron. Soc., **448**, L104, 2015.

35. *J. Jijina, P.C. Hyers, F.C. Adams*, Astrophys. J. Suppl., **125**, 161, 1999.

36. *S.A. Levshakov, D. Reimers, C. Henkel*, Astron. Astrophys., **586**, A126, 2016.

37. *P.F. Goldsmith, W.D. Langer*, Astrophys. J., **222**, 881, 1978.

38. *C.W. Lee, P.C. Myers*, Astrophys. J. Suppl., **123**, 233, 1999.

39. *S.A. Levshakov, P. Molaro, A.V. Lapinov et al.*, Astron. Astrophys., **512**, A44, 2010.

40. *S.A. Levshakov, A.V. Lapinov, C. Henkel et al.*, Astron. Astrophys., **524**, A32, 2010.

41. *M.C. Ferreira, M.D. Julião, C.J.A.P. Martins et al.*, Phys. Rev. D, **86**, 125025, 2012.

42. *S. Truppe, R.J. Hendricks, S.K. Tokunaga et al.*, Nature Commun., **4**, 2600, 2013.

43. *G.C. Bower, P. Demorest, J. Braatz et al.*, arXiv: astro-ph.HE/1510.06432, 2015.

44. *S.G. Kukolich*, Phys. Rev., **156**, 83, 1967.

45. *S. Truppe, R.J. Hendricks, S.K. Tokunaga et al.*, J. Molec. Spectrosc., **300**, 70, 2014.

46. *M.P. Savedoff*, Nature, **178**, 688, 1956.

A Viscous-Convective Instability in Laminar Keplerian Thin Discs

K.L. Malanchev[1,2], K.A. Postnov[1,2], N.I. Shakura[1]

E-mail: *malanchev@physics.msu.ru*

Using the anelastic approximation of linearized hydrodynamic equations, we investigate the development of axially symmetric small perturbations in thin Keplerian discs. Dispersion relation is found as a solution of general Sturm–Liouville eigenvalue problem for different values of relevant physical parameters (viscosity, heat conductivity, disc semi-thickness). The analysis reveals the appearance of overstable mode for Prandtl parameter higher than some critical value. These modes have a viscous-convective nature and can serve as a seed for turbulence in astrophysical discs even in the absence of magnetic fields.

1 Introduction

The problem of linear stability of sheared astrophysical flows has been actively studied. The recent papers [1] and [2] used the Boussinesq and anelastic approximations, respectively, with taking into account microscopic viscosity and thermal conductivity of the gas. These analyses have revealed the presence of overstable viscous modes whose physical origin is likely to be connected to development of convective motions in vertically stratified accretion flows. However, in those papers averaging over vertical disc structure was performed, which restricted applications of the obtained results. In the present paper, we take into account more realistic polytropic structure of a Keplerian accretion disc and solve linearized general Sturm–Liuville eigenvalue problem. Our analysis confirms the appearance of the overstable modes in the wide range of microscopic parameters of the gas described by the Prandtl number.

2 Basic equations

The system of hydrodynamic equations for axially symmetric accretion flow can be written as follows:

[1] M.V. Lomonosov Moscow State University, Sternberg Astronomical Institute, Russia
[2] M.V. Lomonosov Moscow State University, Faculty of Physics, Russia

V. Grinin et al. (eds) Radiation mechanisms of astrophysical objects. Yerevan: Edit Print, 2017, pp. 331–338.

1. Continuity equation

$$\frac{\partial \rho}{\partial t} + \frac{1}{r}\frac{\partial (\rho r u_r)}{\partial r} + \frac{\partial (\rho u_z)}{\partial z} = 0\,. \tag{1}$$

The anelastic approximation for gas velocity is $\boldsymbol{u}$ is $\nabla \cdot \rho_0 \boldsymbol{u} = 0$.

2. The radial, azimuthal and vertical components of the Navier–Stokes momentum equation are, respectively,

$$\frac{\partial u_r}{\partial t} + u_r\frac{\partial u_r}{\partial r} + u_z\frac{\partial u_r}{\partial z} - \frac{u_\phi^2}{r} = -\frac{\partial \phi_g}{\partial r} - \frac{1}{\rho}\frac{\partial p}{\partial r} + \mathcal{N}_r\,, \tag{2}$$

$$\frac{\partial u_\phi}{\partial t} + u_r\frac{\partial u_\phi}{\partial r} + u_z\frac{\partial u_\phi}{\partial z} + \frac{u_r u_\phi}{r} = \mathcal{N}_\phi\,, \tag{3}$$

$$\frac{\partial u_z}{\partial t} + u_r\frac{\partial u_z}{\partial r} + u_z\frac{\partial u_z}{\partial z} = -\frac{\partial \phi_g}{\partial z} - \frac{1}{\rho}\frac{\partial p}{\partial z} + \mathcal{N}_z\,, \tag{4}$$

where $\mathcal{N}_r$, $\mathcal{N}_\phi$ and $\mathcal{N}_z$ are viscous forces. For their specific form see for instance [3].

In this work we will drop the second derivatives of velocities u with respect to the vertical coordinate z in the Navier–Stokes equations following [2]. This assumption makes the problem simpler and the more general problem will be solved in [4].

3. Energy equation

$$\frac{\rho \mathcal{R} T}{\mu}\left[\frac{\partial s}{\partial t} + (\boldsymbol{u}\nabla)\cdot s\right] = Q_{\text{visc}} - \nabla \cdot \boldsymbol{F}\,, \tag{5}$$

where s is specific entropy per particle, Q_{visc} is the viscous dissipation rate per unit volume, R is the universal gas constant, μ is the molecular weight, T is the temperature and terms on the right stand for the viscous energy production and the heat conductivity energy flux F, respectively. The energy flux due to the heat conductivity is

$$\nabla \cdot \boldsymbol{F} = \nabla(-\kappa \nabla T) = -\kappa \Delta T - \nabla\kappa \cdot \nabla T\,. \tag{6}$$

In the Boussinesq approximation, in the energy equation the Eulerian perturbations should be zero: $p_1 = 0$. Following [1], we will also drop the term $\nabla\kappa \cdot \nabla T$ but keep $\kappa \Delta T$.

3 Linearized equations in the anelastic approximation

The perturbed hydrodynamic variables can be written in the form $x = x_0 + x_1$, where x_0 stands for the unperturbed background quantities and $x_1 = (\rho_1, p_1, u_{r\,1}, u_{z\,1}, u_{\phi\,1})$ are small perturbations. We take all these small perturbations in the form $x_1 = f(z)\ \exp(\mathrm{i}\omega t - \mathrm{i}k_r r)$. We will consider thin discs with semi-thickness $z_0/r \ll 1$ and relatively large radial wavenumbers of perturbations $k_r r \gg 1$. Small thickness of the disc and large wavenumbers allow us to set the radial derivatives to zero, $\partial x_0/\partial r = 0$. Under these assumptions, linearizing of the system of equations (1—5) yields the following system of equations [1, 2]:

1. Continuity equation

$$\frac{\partial u_z}{\partial z} - \mathrm{i}k_r u_r + \frac{1}{\rho_0}\frac{\partial \rho_0}{\partial z} u_z = 0. \tag{7}$$

2. Momentum equations

$$(\mathrm{i}\omega + \nu k_r^2) u_r - 2\Omega u_\phi = \mathrm{i}k_r \frac{p_1}{\rho_0}\,, \tag{8}$$

$$(\mathrm{i}\omega + \nu k_r^2) u_\phi + \frac{\varkappa^2}{2\Omega} u_r = 0\,, \tag{9}$$

$$(\mathrm{i}\omega + \nu k_r^2) u_z = -\frac{1}{\rho_0}\frac{\partial p_1}{\partial z} + \frac{\rho_1}{\rho_0}\frac{1}{\rho_0}\frac{\partial p_0}{\partial z}. \tag{10}$$

3. Energy equation

$$\frac{\rho_1}{\rho_0}\left[\mathrm{i}\omega + \frac{\nu k_r^2}{\mathrm{Pr}} - \alpha_{\mathrm{visc}}\frac{\nu}{\mathrm{Pr}}\frac{1}{T_0}\frac{\partial^2 T_0}{\partial z^2} - \alpha_{\mathrm{visc}}\nu\left(r\frac{d\Omega}{dr}\right)^2 \frac{\mu}{\mathcal{R}T_0}\right] = \frac{2\mathrm{i}k_r \nu r (d\Omega/dr)}{c_p \mathcal{R}T_0/\mu} u_\phi + \frac{1}{c_p}\frac{\partial s_0}{\partial z} u_z, \tag{11}$$

where Pr is the Prandtl number, $\mathcal{R}$ is the universal gas constant, $\varkappa$ is the epicyclic frequency, $\nu \sim T_0^{\alpha_{\mathrm{visc}}}/\rho_0$ is the kinematic viscosity coefficient. The kinematic viscosity in the disc equatorial plane is $\nu|_{z=0} = (v_s/v_\phi)\,(l/r)\Omega r^2$, where v_s is the sound velocity and l is the mean free path of particles. We assume the gas to be fully ionized so that $\alpha_{\mathrm{visc}} = 5/2$.

It is necessary to set the background solution of hydrodynamic equations to find solution for perturbations. As the background state, we will use adiabatic polytropic discs [5]

$$T_0(z) = T_{\mathrm{c}}\left(1 - \left(\tfrac{z}{z_0}\right)^2\right), \quad \rho_0(z) = \rho_{\mathrm{c}}\left(1 - \left(\frac{z}{z_0}\right)^2\right)^{3/2},$$

$$p_0(z) = p_{\mathrm{c}}\left(1 - \left(\tfrac{z}{z_0}\right)^2\right)^{5/2}, \quad s_0(z) = c_p \log\left(\frac{p_0^{3/5}}{\rho_0}\right) = const.$$

This system of algebraic and differential equations can be transformed to one second-order differential equation for pressure perturbations p_1

$$\frac{\partial^2 p_1}{\partial z} - \alpha(\omega)\frac{z}{z_0^2}\frac{\partial p_1}{\partial z} - (\alpha(\omega)+\beta(\omega))\,\frac{1}{z_0^2}p_1 = 0\,, \tag{12}$$

where $z_0 = \sqrt{3}\,(v_s/v_\phi)\,r$ is the disc semi-thickness [5], and the dimensionless coefficients α and β reads

$$\alpha(\omega) = \left(\frac{v_s}{v_\phi}\right)\left(\frac{l}{r}\right)\frac{\varkappa^2}{(\mathrm{i}\omega+\nu k_r^2)^2} \times \frac{(-d\ln\Omega/d\ln r)}{c_p\left[\mathrm{i}\omega + \dfrac{\nu k_r^2}{\mathrm{Pr}} + 2\dfrac{\alpha_{\mathrm{visc}}}{z_0^2}\dfrac{\nu}{T_0} - \alpha_{\mathrm{visc}}\nu\left(r\dfrac{d\Omega}{dr}\right)^2\dfrac{\mu}{\mathcal{R}T_0}\right]}\,\frac{(k_r r)^2}{1+\dfrac{\varkappa^2}{(\mathrm{i}\omega+\nu k_r^2)^2}}\,, \tag{13}$$

$$\beta(\omega) = \frac{(k_r r)^2}{1+\dfrac{\varkappa^2}{(\mathrm{i}\omega+\nu k_r^2)^2}}\,, \tag{14}$$

The pressure perturbation p_1 must vanish at the disc boundary ($z = z_0$), and the function $p_1(z)$ should be even or odd because of the plane symmetry of the problem. Bellow we will consider the case of even $p_1(z)$ with the boundary conditions

$$\left.\frac{\partial p_1}{\partial z}\right|_{z=0} = 0\,, \tag{15}$$

$$p_1|_{z=z_0} = 0\,. \tag{16}$$

We are searching for the least oscillating solutions, which means that $p_1(z)$ should not have zeros between $z = 0$ and $z = z_0$. This condition comes from our previous assumption about the smallness of the secondary derivatives of velocities in the Navier–Stokes equations (2–4).

Using a new variable $x \equiv z/z_0$, equation (12) transforms to

$$\frac{\partial^2 p_1}{\partial x^2} - \alpha(\omega)\,\frac{\partial p_1}{\partial x} - (\alpha(\omega)+\beta(\omega))p_1 = 0. \tag{17}$$

Let us introduce a new function $Y(x)$

$$Y \equiv p_1\,\exp\left(\frac{1}{2}\int_0^x -\alpha(\omega)x'dx'\right) = p_1\,\exp\left(-\frac{\alpha(\omega)\,x^2}{4}\right). \tag{18}$$

Then (17) transforms to

$$\frac{\partial^2 Y}{\partial x^2} + \left(-\beta(\omega) - \frac{\alpha(\omega)}{2} - \frac{\alpha^2(\omega)\,x^2}{4}\right)Y = 0. \tag{19}$$

After introducing the new variable $\zeta \equiv \sqrt{\alpha(\omega)}\, x$, the eigenvalue problem (12), (15), (16) takes the form

$$\frac{\partial^2 Y}{\partial \zeta^2} - \left(\frac{\zeta^2}{4} + \left[\frac{\beta(\omega)}{\alpha(\omega)} + \frac{1}{2} \right] \right) Y = 0, \tag{20}$$

$$\left. \frac{\partial Y}{\partial \zeta} \right|_{\zeta=0} = 0, \tag{21}$$

$$Y|_{\zeta=\sqrt{\alpha(\omega)}} = 0. \tag{22}$$

Our boundary condition (21) and the plane symmetry of the problem enable us to use an even solution of equation (20) [6]

$$\begin{aligned} Y_\eta(\zeta) &= e^{-\zeta^2/4}\, M(-\frac{\eta}{2}, \frac{1}{2}, \frac{\zeta^2}{2}) \\ &= e^{-\zeta^2/4} \left\{ 1 + (-\eta)\frac{\zeta^2}{2!} + (-\eta)(-\eta+2)\frac{\zeta^4}{4!} + ... \right\}, \end{aligned} \tag{23}$$

where M is the confluent hypergeometric function, $\eta(\omega) \equiv -1 - \beta(\omega)/\alpha(\omega)$.

An eigenfunction of the problem (with the boundary condition (22)) must satisfy the following relation:

$$Y_{\eta(\omega)}(\sqrt{\alpha(\omega)}) = 0. \tag{24}$$

The last relation can be regarded as an equation for the unknown variable ω, then the solutions to this equations are eigenvalues of our problem, and the corresponding $Y_\eta(\zeta)$ will be its eigenfunctions.

4 Dispersion relation

Solution of the eigenvalue problem depends of the sign of the linearized term $\kappa\Delta T$, which appears in the energy equation (11) in the form

$$\alpha_{\rm visc} \frac{\nu}{\rm Pr} \frac{1}{T_0} \frac{\partial^2 T_0}{\partial z^2} + \alpha_{\rm visc} \nu \left(r \frac{d\Omega}{dr} \right)^2 \frac{\mu}{\mathcal{R} T_0}\,. \tag{25}$$

If the Prandtl number $\rm Pr \leq 8/45$ and this relation is negative, there is only one mode of the dispersion equation which corresponds to a decaying mode (see Fig. 1). Otherwise, if $\rm Pr > 8/45$, an additional overstable mode appears (see Fig. 2).

Fig. 3 shows the dependence of $\mathrm{Im}(\omega)$ of the overstable mode on the viscosity parameters l/r and v_s/v_ϕ. Fig. 4 shows $p_1(x)$ corresponding to the eigenfunction of the overstable mode for $\rm Pr = 0.2$, $k_r r = 40$, $l/r = 0.01$ and $v_s/v_\phi = 0.01$.

5 Conclusions

Using the anelastic approximation of linearized hydrodynamic equations, we studied the development of axially symmetric small perturbations in thin Keplerian discs. Dispersion relation is derived as a solution of general Sturm–Liouville eigenvalue problem for pressure perturbations. An overstable mode is discovered for different values of the disc thickness and microscopic viscosity and thermal conductivity of the gas. The overstability appears when the Prandtl parameter exceeds a critical value 8/45. The unstable mode has viscous-convective nature and can serve as a seed for turbulence in astrophysical discs even in the absence of magnetic fields.

Acknowledgments. We thank R.A. Sunyaev for useful discussions. The work is supported by the Russian Foundation for Basic Research grant 14-02-91345.

References

1. *N. Shakura, K. Postnov*, Mon. Not. Roy. Astron. Soc., **448**, 3707, 2015.
2. *N. Shakura, K. Postnov*, Mon. Not. Roy. Astron. Soc., **451**, 3995, 2015.
3. *S. Kato, J. Fukue, S. Mineshige*, Black-Hole Accretion Disks: Towards a New Paradigm. Kyoto: Kyoto University Press, 2008.
4. *K. Malanchev, N. Shakura, K. Postnov*, in preparation.
5. *N. A. Ketsaris, N. I. Shakura*, Astron. Astroph. Trans., **15**, 193, 1998.
6. *M. Abramowitz, I. A. Stegun*, Handbook of Mathematical Functions: with Formulas, Graphs, and Mathematical Tables. Washington: Nat. Bur. Stand., 1972.

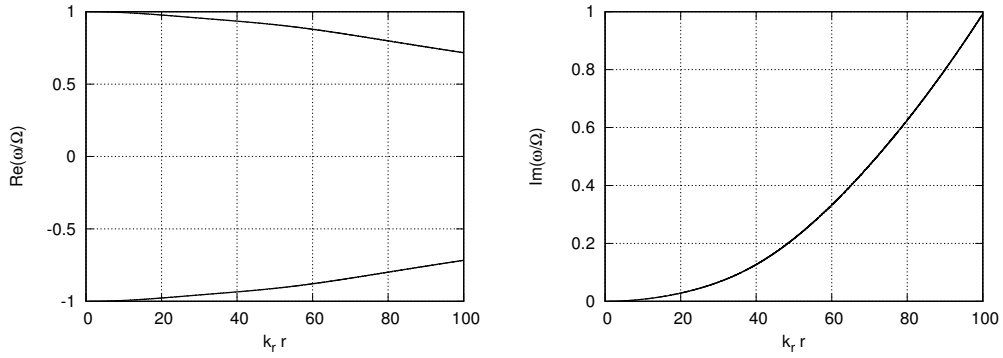

Figure 1: The dispersion equation for the critical Prandtl number $\mathrm{Pr} = 8/45$, the mean-free path length of particles $l/r = 0.01$ and disc semi-thickness parameter $v_s/v_\phi = 0.01$. The left panel shows the real part of two decaying modes in terms of dimensionless frequency ω/Ω and the dimensionless wavenumber $k_r r$. The right panel shows the imaginary part of the dispersion relation which is the same for both decaying modes.

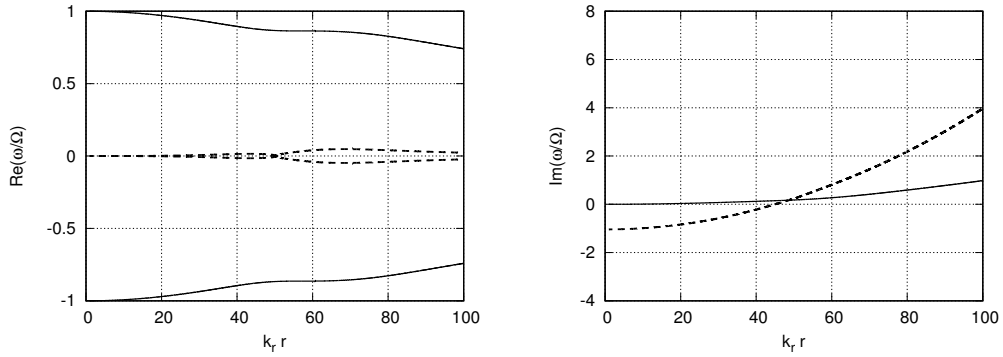

Figure 2: Dispersion relation for $\mathrm{Pr} = 0.2$, $l/r = 0.01$ and $v_s/v_\phi = 0.01$. Left panel shows the real part of two decaying (the solid line) and to the overstable modes (the dashed line) in terms of the dimensionless frequency ω/Ω and the dimensionless wavenumber $k_r r$. Right panels shows the imaginary part of these modes.

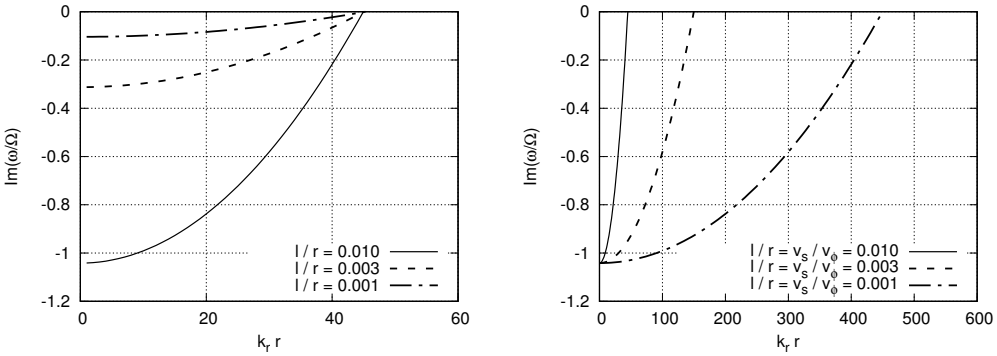

Figure 3: The imaginary part of the dispersion relations for $\mathrm{Pr} = 0.2$ and different values of l/r and v_s/v_ϕ. In the left panel, the value of $v_s/v_\phi = 0.01$ is constant for all curves. The viscosity changes in proportion to l/r and $\mathrm{Im}(\omega)$ changes in the same way. On the right panel both v_s/v_ϕ and l/r changes in the same way so that the term (25) keeps constant. Here the range of wavenumbers $k_r r$ of the overstable mode decreases inversely proportional to the disc thickness.

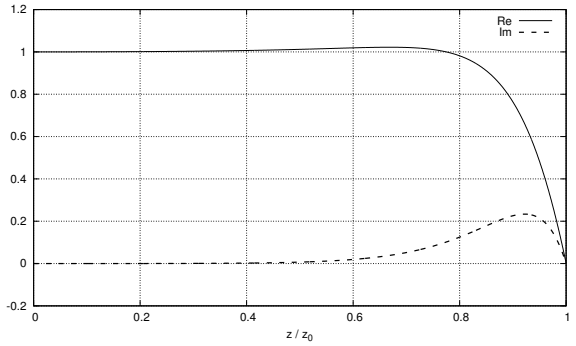

Figure 4: The overstable solution of the problem (12, 15, 16) for variable $x = z/z_0$ with the following parameters: $k_r r = 40$, $\mathrm{Pr} = 0.2$, $l/r = 0.01$ and $v_s/v_\phi = 0.01$. Figure shows the normalized eigenfunction $p_1(x)$. The solid line shows the real part of $p_1(x)$, the dashed line shows the imaginary part of the pressure perturbation $p_1(x)$.

X-Ray Pulsars in a Wide Luminosity Range

A. Mushtukov[1,2,3], V. Suleimanov[4,5], S. Tsygankov[3], D. Nagirner[6], A. Lutovinov[7,8], J. Poutanen[3,9]

E-mail: *al.mushtukov@gmail.com*

A picture of X-ray pulsars (XRPs) behavior in a wide luminosity range is presented. The characteristic accretion luminosity values are discussed as well as connection between XRPs and ultraluminous X-ray sources (ULXs).

1 X-ray pulsars

XRPs stand out from the other classes of accreting NSs due to their strong magnetic field ($\gtrsim 10^{12}$ G), which affects both the geometry of the accretion flow in the vicinity of NS and elementary processes of interaction between radiation and matter.

Magnetic field interrupts the accretion disc (or stellar wind) at the magnetospheric radius, where the magnetic and plasma stresses balance. The magnetospheric radius is given by

$$R_{\rm m} = k \left(\frac{\mu^4}{GM\dot{M}^2} \right)^{1/7},$$

where M and μ are the NS mass and magnetic moment, respectively, $\dot{M}$ is the mass accretion rate and $k \leq 1$ is a constant which depends on the accretion flow geometry ($k = 1$ for the case of spherical accretion and $k < 1$ for the case of accretion from the disc, see [1]). Inside the magnetospheric radius, the magnetic field channels the gas towards the magnetic poles, where the captured matter releases its gravitational energy as X-ray radiation. Some questions concerns the interaction of the accretion flow (stellar wind or accretion disc) and NS magnetosphere [2]. They are important for a self-consistent picture, but beyond the scope of this text.

[1] Anton Pannekoek Institute, University of Amsterdam, The Netherlands
[2] Pulkovo Observatory of the Russian Academy of Sciences, St. Petersburg, Russia
[3] Tuorla Observatory, Department of Physics and Astronomy, Univ. of Turku, Finland
[4] Institut für Astronomie und Astrophysik, Universität Tübingen, Germany
[5] Kazan (Volga region) Federal University, Russia
[6] Sobolev Astronomical Institute, St. Petersburg State University, Russia
[7] Space Research Institute of the Russian Academy of Sciences, Moscow, Russia
[8] Moscow Institute of Physics and Technology, Russia
[9] Nordita, KTH Royal Institute of Technology and Stockholm University, Sweden

V. Grinin et al. (eds) Radiation mechanisms of astrophysical objects. Yerevan: Edit Print, 2017, pp. 339–344.

High magnetic field modifies the elementary processes of interaction between radiation and matter including Compton scattering [3], which defines the radiation pressure and affects spectrum of emergent radiation. In the case of strong magnetic fields, the scattering has a number of special features. Its cross-section can be much smaller than the Thompson scattering cross-section $\sigma_{\rm T}$ depending on magnetic field strength, photon momentum and polarization state. At the same time electron transition between Landau levels causes the resonant scattering at some photon energies, where the cross-section can exceed $\sigma_{\rm T}$ by several orders of magnitude [4, 5]. The resonant scattering leads to appearance of absorption features in the spectra of XRPs – cyclotron lines – and affects the radiation pressure.

2 Below and above the critical luminosity

The accretion luminosity of XRPs is observed to be close or even higher than the Eddington limit $L_{\rm Edd}$ [6], which is commonly used as a restriction of possible isotropic luminosity of the object with a given mass M

$$L_{\rm Edd} = \frac{4\pi G M m_{\rm H} c}{\sigma_{\rm T}(1+X)} \approx 1.4\times10^{38}\frac{M}{M_\odot}\,{\rm erg\,s^{-1}}, \qquad (1)$$

where $m_{\rm H}$ is the hydrogen mass and X is its mass fraction.

The theory of accretion onto magnetized NS is based on two important effects: the accretion flow is channeled by strong magnetic field, which makes the problem essentially non-spherically symmetrical, and the effective cross-section $\sigma_{\rm eff}$ of the interaction between radiation and matter can be much different from the cross-section in the non-magnetic case.

At low mass accretion rates ($< 10^{16}\,{\rm g\,s^{-1}}$) radiation pressure has only a minor effect on the infalling material. The accretion flow heats up the NS surface and the observed spectrum is shaped by plasma deceleration in the NS atmosphere and by interaction of already emitted radiation with the accretion flow.

The higher the mass accretion rate, the higher the radiation pressure. If the radiation pressure is high enough, it affects the accretion flow velocity. The changes of the accretion flow velocity can be detected from variations of cyclotron line position in the spectrum: the line forms due to the resonant scattering in the accretion flow and, as a result, it is affected by Doppler shifting in the accretion channel [7].

At sufficiently high mass accretion rate the matter is fully stopped by the radiation pressure above stellar surface and an accretion column begins to grow. The corresponding luminosity, which is called critical luminosity, can be estimated as follows [8, 9]:

$$L^* = 4\times10^{36}\,\frac{M/M_\odot}{R/10^6{\rm cm}}\left(\frac{l_0}{2\times10^5{\rm cm}}\right)\frac{\sigma_{\rm T}}{\sigma_{\rm eff}}\ {\rm erg\,s^{-1}}, \qquad (2)$$

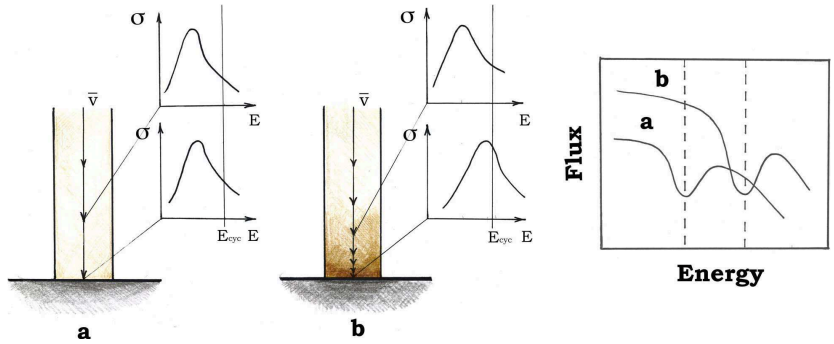

Figure 1: The schematic presentation of the dependence of the cyclotron line energy on the velocity profile in the line-forming region for the case of sub-critical XRPs (see [7] for details).

where R is the NS radius, l_0 is the length of the accretion channel cross-section on the NS surface and $\sigma_{\rm eff}$ is the effective scattering cross-section in strong magnetic field. The value of L^* depends on the surface magnetic field strength due to the strong dependence of the scattering cross-section on the field strength. The critical luminosity is not a monotonic function of B and has its minimum value of $\sim(3 \div 5) \times 10^{36}\,\mathrm{erg\,s^{-1}}$ at B-field strength of $\sim 10^{12}\,\mathrm{G}$, when the peak in the source spectrum is close to $E_{\rm cycl}$ and the effective radiation pressure reaches its maximum value [9]. For higher magnetic field strength, the critical luminosity value increases due to decrease of the effective scattering cross-section (see Fig. 1).

At the accretion luminosity $L > L^*$ for a given magnetic field strength the accretion flow stops at the radiation dominated shock above the NS surface and slowly settles in inside a sinking region. The luminosity of highly magnetized NS featuring an accretion column above its surface can be much higher than the Eddington luminosity value, because the radiation pressure is balanced by the strong magnetic pressure (instead of gravity), which supports the column. The luminosity of the NS with an accretion column of height H above its surface can be roughly estimated as follows [10]:

$$L^{**}(H) \approx 38 \left(\frac{l_0/d_0}{50}\right) \frac{\sigma_{\rm T}}{\sigma_\perp} f\left(\frac{H}{R}\right) L_{\rm Edd}, \qquad f(x) = \log(1+x) - \frac{x}{1+x}, \tag{3}$$

where d_0 is the thickness of the accretion channel, $\sigma_\perp$ is the effective Compton scattering cross-section across the magnetic field direction. For a column as high as the NS radius, the accretion luminosity becomes $L^{**}(H = R) \approx (2 \div 3) \times 10^{39} \left(\frac{l_0/d_0}{50}\right) \frac{\sigma_{\rm T}}{\sigma_\perp}\,\mathrm{erg\,s^{-1}}$.

From the comparison of XRPs spectra variability with the theoretical models, we can conclude that the height of the accretion column increases with the mass accretion rate and, indeed, can be comparable to the NS radius [12].

The height of the accretion column is obviously limited by the magnetosphere's radius ($H < R_{\rm m}$). However, many additional conditions have to be taken

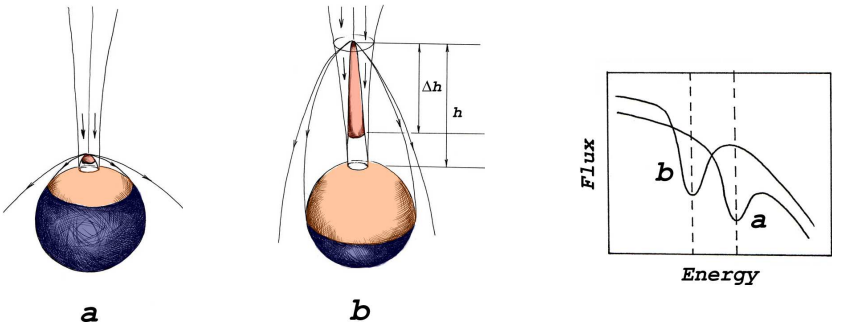

Figure 2: The schematic presentation of the dependence of the cyclotron line energy on the velocity profile in the line-forming region for the case of super-critical XRPs (see [12] for details).

into account. The gas and radiation pressure inside the column should not be higher than the magnetic pressure. This is important for fields of strength below $\sim 2 \times 10^{13}$ G. If the magnetic field strength is higher than $\sim 2 \times 10^{13}$ G, the internal column temperature can reach the value of $\sim 10^{10}$ K, when the electron-positron pair creation with further annihilation into neutrino and anti-neutrino becomes important: $e^+ + e^- \longrightarrow \nu_e + \overline{\nu}_e$. In this case part of accretion luminosity can be released by neutrino rather than by photons. However, it was shown that the accretion columns above NS with surface B-field strength $\gtrsim 5 \times 10^{13}$ G cannot be significantly higher than NS radius and their internal temperature does not reach values of $\sim 10^{10}$ K [10].

The accretion column structure determines the beam pattern of XRPs [14]. The height of the accretion column, where the matter is stopped by the radiation dominated shock, is different inside the accretion channel. It is caused by the fact that the radiation energy density drops towards the accretion channel edges. As a result, the height reaches its maximum value in the center of the channel and it decreases towards the edges. Therefore, the radiation from the already stopped matter has to penetrate through the layer of fast moving plasma. It leads to the radiation beaming towards the NS surface, where the radiation is intercepted and reprocessed. Changes of the accretion column height and corresponding variability of the illuminated region on the NS surface explain naturally variations of the cyclotron line centroid energy [11] with the accretion luminosity: the higher the mass accretion rate, the higher the column, the lower the magnetic field strength averaged over the illuminated part of the NS, the lower the observed cyclotron line centroid energy [12, 13].

3 XRPs and ULXs

ULXs are point-like extragalactic X-ray sources with an observed X-ray luminosity in excess of $L \sim 10^{39}\,\mathrm{erg\,s^{-1}}$, assuming that they radiate isotropically. The bolometric luminosity of ULXs exceeds the Eddington limit for accretion on

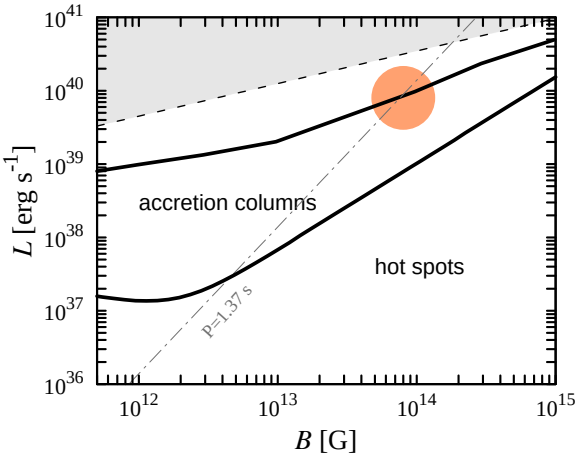

Figure 3: The critical L^* and maximum accretion luminosity values as functions of the B-field strength are given by thick solid lines. The grey region corresponds to the conditions when the accretion disc becomes super-critical. The lower limit on the X-ray luminosity for the case of NS spin period $P = 1.37$ s is shown by dashed-dotted line. It is related to the inhibition of accretion by the propeller effect. The position of the ULX X-2 in galaxy M82 is given by the orange circle.

a $10M_\odot$ black hole (BH). This is, indeed, intriguing since ULXs may be a possible manifestation of sub-critical accretion onto intermediate-mass (masses in the range $\sim 10^2 \div 10^5 M_\odot$) BHs.

At the present time their true nature is not well understood and in fact there may be several types of objects in this category. Most of the models are focused on accretion onto intermediate or stellar mass BHs.

However, it was found by the *NuSTAR* observatory that the ULX X-2 in galaxy M82 shows coherent pulsations with an average period of 1.37 s, which means that the compact object in this particular case is not a BH but a NS [15]. This discovery implies that accreting NS can reach luminosities of about 10^{40} erg s^{-1} (see Fig. 3), which is two orders of magnitude higher than the Eddington limit. Such high mass accretion luminosity can be explained by extremely high NS magnetic field $\sim 10^{14}$ G, which reduces the scattering cross-section and confines the accretion flow to accretion column [10].

It is already confirmed that in this particular case we see accretion onto NS with magnetar-like magnetic field $\sim 10^{14}$ G [16]. According to simple estimations, an accreting NS at such high mass accretion rate reaches the spin equilibrium (when the corotation and magnetosphere radii are equal) within a few hundreds years. As a result, small changes in the mass accretion rate lead to dramatic changes of the accretion luminosity due to the so-called "propeller"-effect, which has been observed in a few XRPs [17]. The mass accretion rate, at which the "propeller"-effect appears, depends on the B-field strength, and the latter can be estimated from the known mass accretion rate. The "propeller"-effect has been observed in ULX M82 X-2 and magnetic field $\sim 10^{14}$ G has been confirmed [16].

The discovery of NSs as compact objects in ULXs puts an additional important question: what fraction of ULXs are accreting NSs? It is interesting that no other pulsating ULX has been observed yet. According to our recent results, the accretion luminosity of a few$\times 10^{40}\,\mathrm{erg\,s^{-1}}$ is a good estimation for maximum NS accretion luminosity [10]. This luminosity coincides with the cut-off observed in the HMXBs luminosity function (ULXs are taken into account there as HMXB) which otherwise does not show any features at lower luminosities [18]. Therefore one can conclude that a substantial fraction of ULXs are accreting NSs.

References

1. *J. Frank, A. King, D. Raine*, Accretion Power in Astrophysics. Cambridge: Cambridge Univ. Press, 2002.
2. *D. Lai*, Phys. J. Web Conf., **64**, 1001, 2014.
3. *A.K. Harding, D. Lai*, Rep. Prog. Phys., **69**, 2631, 2006.
4. *A.A. Mushtukov, D.I. Nagirner, J. Poutanen*, Phys. Rev. D, **85**, 103002, 2012.
5. *A.A. Mushtukov, D.I. Nagirner, J. Poutanen*, Phys. Rev. D, **93**, 105003, 2016.
6. *R. Walter, A.A. Lutovinov, E. Bozzo, S.S. Tsygankov*, Astron. Astrophys. Rev., **23**, 2, 2015.
7. *A.A. Mushtukov, S.S. Tsygankov, A.V. Serber et al.*, Mon. Not. Roy. Astron. Soc., **454**, 2714, 2015.
8. *M.M. Basko, R.A. Sunyaev*, Mon. Not. Roy. Astron. Soc., **175**, 395, 1976.
9. *A.A. Mushtukov, V.F. Suleimanov, Sergey S. Tsygankov, J. Poutanen*, Mon. Not. Roy. Astron. Soc., **447**, 1847, 2015.
10. *A.A. Mushtukov, V.F. Suleimanov, S.S. Tsygankov, J. Poutanen*, Mon. Not. Roy. Astron. Soc., **454**, 2539, 2015.
11. *S.S. Tsygankov, A.A. Lutovinov, E.M. Churazov, R.A. Sunyaev*, Mon. Not. Roy. Astron. Soc., **371**, 19, 2006.
12. *J. Poutanen, A.A. Mushtukov, V.F. Suleimanov et al.*, Astrophys. J., **777**, 115, 2013.
13. *A.A. Mushtukov, J. Poutanen, V.F. Suleimanov et al.*, Phys. J. Web Conf., **64**, 2005, 2014.
14. *A.A. Lutovinov, S.S. Tsygankov, V.F. Suleimanov et al.*, Mon. Not. Roy. Astron. Soc., **448**, 2175, 2015.
15. *M. Bachetti, F.A. Harrison, D.J. Walton et al.*, Nature, **514**, 202, 2014.
16. *S.S. Tsygankov, A.A. Mushtukov, V.F. Suleimanov, J. Poutanen*, Mon. Not. Roy. Astron. Soc., **457**, 1101, 2016.
17. *S.S. Tsygankov, A.A. Lutovinov, V. Doroshenko et al.*, Astron. Astrophys., **593**, A16, 2016.
18. *S. Mineo, M. Gilfanov, R. Sunyaev*, Mon. Not. Roy. Astron. Soc., **419**, 2095, 2012.

* The color figures are available online in the Proceedings at *http://www.astro.spbu.ru/sobolev100/*.

Strongly Magnetized Atmospheres and Radiating Surfaces of Neutron Stars

A.Y. Potekhin[1,2,3]

E-mail: *palex@astro.ioffe.ru*

The theory of thermal emission from the surface layers of magnetized neutron stars is reviewed, including radiative transfer in partially ionized atmospheres with magnetic fields $B \sim 10^{10}$–10^{15} G and radiation from condensed surfaces at $B \gtrsim 10^{12}$ G. Applications of the theory to observations of thermally emitting isolated neutron stars with strong magnetic fields are summarized.

1 Introduction

A detailed study of the thermal spectra of neutron stars can yield precious information about properties of plasmas at extreme conditions in their atmospheres and interiors, about the neutron star masses M, radii R, temperatures T, and magnetic fields $\boldsymbol{B}$, and eventually help to constrain the equation of state (EOS) of the ultradense matter in the neutron star cores. In recent years, the number and quality of measured thermal spectra of neutron stars increased dramatically thanks to the data collected by the X-ray observatories *Chandra* and *XMM-Newton*. Some of the spectra can be understood with models of non-magnetic atmospheres (e.g., [1] and references therein). However, thermal spectra of many isolated neutron stars (INSs) are significantly affected by strong magnetic fields. The theory of these effects is reviewed in the present paper. Section 2 describes the theory of partially ionized neutron star atmospheres with strong magnetic fields, Sect. 3 considers the model of a condensed radiating surface and hybrid models of a condensed surface covered by a thin atmosphere, Sect. 4 describes synthetic energy and polarization spectra, and Sect. 5 presents examples of applications of the theory to observations.

2 Theory of strongly magnetized atmospheres

We call an atmosphere *strongly magnetized*, if a magnetic field strongly (non-perturbatively) affects opacities and radiative transfer of thermal photons. This occurs if the electron cyclotron energy $\hbar\omega_{\rm c} \equiv \hbar eB/m_{\rm e}c \approx 11.577\,(B/10^{12}\ {\rm G})$ keV is greater than either the photon energies $\hbar\omega$ or the atomic binding energies, or both. Here, ω is the photon angular frequency, $m_{\rm e}$ and $-e$ are the electron

[1] Ioffe Institute, St. Petersburg, Russia
[2] Central Astronomical Observatory at Pulkovo, St. Petersburg, Russia

V. Grinin et al. (eds) Radiation mechanisms of astrophysical objects. Yerevan: Edit Print, 2017, pp. 345–352.

mass and charge, and c is the speed of light. These conditions imply (see [2] for discussion) $B \gtrsim 10^{10}\,T_6$ G, where $T_6 \equiv T/10^6$ K, and $B \gtrsim B_0$, where $B_0 = m_{\rm e}^2\,c\,e^3/\hbar^3 \approx 2.35 \times 10^9$ G is the atomic unit of magnetic field. It is also convenient to define the relativistic magnetic-field parameter $b \equiv \hbar\omega_{\rm c}/m_{\rm e}c^2 = B/4.414 \times 10^{13}$ G. We call magnetic field *superstrong* if $b \gtrsim 1$. The superstrong fields are believed to exist at the surfaces of magnetars and high-B pulsars [3, 4].

At typical conditions in neutron star photospheres one can describe radiative transfer in terms of specific intensities of two normal polarization modes [5, 6], called extraordinary (X-mode) and ordinary (O-mode), which have different polarization vectors $\boldsymbol{e}_j$, depending on ω and on the angle θ_{kB} between the wave vector $\boldsymbol{k}$ and the magnetic field $\boldsymbol{B}$. The system of radiative transfer equations (RTE) for the two normal modes is presented in [7].

The polarization vectors of normal modes $\boldsymbol{e}_{\omega,j}$ are determined by the complex polarizability tensor $\boldsymbol{\chi}(\omega)$ and magnetic permeability tensor [5]. The anti-Hermitian part of $\boldsymbol{\chi}(\omega)$ is determined by the absorption opacities, and the Hermitian part can be obtained from it using the Kramers–Kronig relation [8, 9].

In strong magnetic fields, the effects called polarization and magnetization of vacuum can be important (see, e.g., [10]). At $B \lesssim 10^{16}$ G, they linearly add to $\boldsymbol{\chi}$ and can be parametrized by three numbers, called vacuum polarizability and magnetization coefficients, which were fitted by analytic functions of b in [9]. Convenient expressions of $\boldsymbol{e}_j$ through $\boldsymbol{\chi}(\omega)$ with account of the vacuum polarization were presented in [11].

Opacities for the X-mode are strongly reduced, if $\omega_{\rm c} \gg \omega$. The opacities also depend on θ_{kB}. Nevertheless, at large optical depth radiation is almost isotropic: the magnitude of the diffusive radiative flux is much smaller than the mean intensity. In this case an approximate solution to the RTE is provided by the diffusion approximation [7], which serves as a starting point to an iterative method [12], allowing one to solve the RTE system accurately. To this end, one must know the dependencies of the temperature and densities of particles on the depth. These dependencies can be found from the equations of thermal, hydrostatic, and ionization equilibrium supplemented with the EOS. The plasma composition, EOS, and opacities are affected by the field, as reviewed in [2].

As first noticed in [13], atoms and ions with bound states should be much more abundant at $B \gg B_0$ than at $B \lesssim B_0$ in a neutron star atmosphere at the same temperature. This difference is caused by the increase of atomic binding energies and decrease of atomic sizes at $B \gg B_0$. Therefore, bound-bound and bound-free transitions are important in strong magnetic fields even for light-element atmospheres, which would be almost fully ionized at $B = 0$.

Many authors studied atoms with an infinitely heavy (fixed in space) nucleus in strong magnetic fields (see, e.g., [14], for review). This model, however, is only a crude approximation. If the ratio B/B_0 is not negligibly small compared to the nucleus-to-electron mass ratio, one should take into account quantum oscillations of an atomic nucleus, which depend on the quantum state. Moreover, the astrophysical simulations assume finite temperatures, hence thermal motion

of particles. The theory of motion of a system of point charges q_i at points $\boldsymbol{r}_i$ in a constant magnetic field was reviewed in [15]. Instead of the canonical momentum $\boldsymbol{P}$, a relevant conserved quantity is pseudomomentum $\boldsymbol{K} = \boldsymbol{P} + (1/2c)\,\boldsymbol{B} \times \sum_i q_i \boldsymbol{r_i}$. The specific effects related to collective motion of a system of charged particles are especially important in neutron star atmospheres at $B \gg B_0$. In particular, so called *decentered states* may become populated, where an electron is localized mostly in a "magnetic well" aside from the Coulomb center. Binding energies and wave functions of the hydrogen atom moving across a strong magnetic field were calculated in [16, 17]. Bound-bound, bound-free, and free-free radiative transitions were studied in [17–21]. The absorption cross-sections have peaks at the multiples of both the electron and ion cyclotron frequencies for all polarizations α, but unlike the electron cyclotron harmonics, the ion harmonics, except the fundamental, are weak and can be neglected. The dependencies of energies and oscillator strengths on the transverse pseudomomentum $\boldsymbol{K}_\perp = \boldsymbol{K} - (\boldsymbol{B} \cdot \boldsymbol{K})\boldsymbol{B}/B^2$ cause a "magnetic broadening" of the spectral lines and ionization thresholds, which can be much larger than the usual Doppler and plasma broadenings.

The He^+ ion moving across a strong magnetic field was studied in [22, 23]. The basic differences from the case of a neutral atom are that the Cartesian components of the operator $\boldsymbol{K}_\perp$ do not commute and the values of K^2 are quantized [15]. Currently there is no detailed calculation of binding energies, oscillator strengths, and photoionization cross-sections for atoms and ions other than H and He^+, arbitrarily moving in a strong magnetic field. A practical method of calculation of the quantum-mechanical characteristics of multielectron atoms and ions, based on a combination of several perturbation theories with respect to different physical parameters, has been developed in [24].

Since the quantum-mechanical characteristics of an atom in a strong magnetic field depend on $K_\perp$, the atomic distribution over $K_\perp$ cannot be written in a closed form, and only the distribution over longitudinal momenta K_z remains Maxwellian. The first EOS calculations with account of these effects have been performed in [25] for hydrogen and in [26] for helium plasmas. To date, self-consistent calculations of the EOS and opacities, including both centered and decentered bound states (i.e., small and large $K_\perp$), have been realized only for neutron-star atmospheres composed of hydrogen [20, 27, 28]. For atoms and ions with several bound electrons (C, O, Ne), calculations have been performed in terms of a perturbation theory [29, 30].

3 Condensed surfaces and thin atmospheres

Ruderman [31] suggested that a strong magnetic field may cause a condensation of matter. Properties of the resulting condensed magnetic surfaces were studied in a number of papers (see [32] and references therein). Thermal radiation of the surface is determined by its emissivities in two normal modes, which are related to the reflectivities through the Kirchhoff law. They were calculated and fitted in [33] (see references therein for older approaches). Moreover, Motch et al. [34]

suggested that some neutron stars can possess a hydrogen atmosphere of a finite thickness above the solid iron surface. If the optical depth of such atmosphere is small for some wavelengths and large for others, the thermal spectrum differs from that of thick atmospheres. Such spectra were calculated in [35–37] using simplified boundary conditions for the radiative transfer equation at the bottom of the atmosphere. More accurate boundary conditions [33] take into account that any polarized wave, falling from the atmosphere on the surface, gives rise to reflected waves of both normal polarizations, whose intensities add to the respective intensities of the waves emitted by the condensed surface.

Local spectra of radiation emitted by thin hydrogen atmospheres over a condensed surface may reveal a narrow absorption line corresponding to the proton cyclotron resonance in the atmosphere, features related to atomic transitions broadened by the motion effects, and a kink corresponding to the ion cyclotron energy of the substrate ions. Some of these features may be absent, depending on the atmosphere thickness and magnetic field strength. At high energies, the spectrum is determined by the condensed-surface emission, which is softer than the spectrum of the thick hydrogen atmosphere.

One may also envisage an atmosphere having a helium layer beneath the hydrogen layer. The spectrum of such "sandwich atmosphere" can have two or three absorption lines in the range $E \sim (0.2\text{–}1)\,\mathrm{keV}$ at $B \sim 10^{14}$ G [36].

4 Synthetic energy and polarization spectra

The strong gravity of a neutron star induces a significant redshift of the local photon frequency ω to $\omega_\infty = \omega/(1+z_g)$ in the remote observer's reference frame, where $z_g = (1-2GM/c^2R)^{-1/2} - 1$ is the gravitational redshift, and G the gravitational constant. Accordingly, a thermal spectrum with effective temperature $T_{\rm eff}$ transforms for the remote observer into a spectrum with a lower "observed" temperature $T_{\rm eff}^\infty = T_{\rm eff}/(1+z_g)$. Along with the radius R that is determined by the equatorial length $2\pi R$ in the local reference frame, one often considers an *apparent radius* for a remote observer, $R_\infty = R\,(1+z_g)$, so that the apparent photon luminosity $L_{\rm ph}^\infty$ is determined by the Stefan–Boltzmann law $L_{\rm ph}^\infty = L_{\rm ph}/(1+z_g)^2 = 4\pi\sigma_{\rm SB}\,R_\infty^2\,(T_{\rm eff}^\infty)^4$, where $\sigma_{\rm SB}$ is the Stefan–Boltzmann constant, and $L_{\rm ph} = 4\pi\sigma_{\rm SB}\,R^2T_{\rm eff}^4$ is the luminosity in the local reference frame.

The spectral flux that comes to an observer is distorted by the light bending in strong gravity. It can be calculated using equations presented in [38] provided that the emitted specific intensity distribution is known for the entire visible surface of the neutron star. The problem is complicated by nontrivial surface distributions of the magnetic field and effective temperature. A fiducial model for the magnetic field distribution is the relativistic dipole [39], but recent numerical simulations of the magnetothermal evolution produce more complicated distributions (see [40, 41] and references therein). The temperature distribution, consistent with the magnetic-field distribution, is found from calculations of heat transport in neutron star envelopes (see [42] for review).

Synthetic spectra of partially ionized hydrogen atmospheres were calculated in [43], including averaging over the stellar surface with realistic temperature and magnetic field distributions. The spectra depend on the magnetic axis orientation relative to the line of sight. As the star rotates, the latter dependence leads to a rotational phase dependence of the spectra. Model spectra of partially ionized, strongly magnetized neutron star atmospheres composed of hydrogen, carbon, oxygen, and neon with magnetic fields $B \sim 10^{10}$–10^{13} G are included in the open database *XSPEC* [44] under the names NSMAX [30, 43] and NSMAXG [30, 45, 46], with the latter allowing for varying surface gravity.

Thermal radiation emergent from neutron stars with strong magnetic fields is expected to be strongly polarized. Since the opacity is smaller for the X-mode, this mode escapes from deeper and hotter layers in the atmosphere, therefore the X-mode polarization prevails in the thermal radiation [47]. Polarization of the observed radiation depends on the distribution of magnetic field and temperature over the visible neutron star surface. As the star rotates, the polarization pattern shows periodic variations, so that measuring the polarization pulse profile allows one to constrain the orientation of the rotation axis and the field strength and geometry [48, 49]. Therefore, future X-ray polarization measurements are expected to resolve degeneracies that currently hamper the determination of magnetar physical parameters using thermal models [50, 51].

After a photon has left the surface of a neutron star with a strong magnetic field, it travels through the magnetosphere and experiences the influence of vacuum polarization, which induces a change in the wave electric field as photon propagates. If the magnetic field is sufficiently strong, then in the vicinity of the star a photon propagates adiabatically, so that its polarization instantaneously adapts to the variation of the magnetic field direction [52, 53]. Farther from the star the field decreases, and eventually photons leave the adiabatic region and maintain their polarization. The rays that leave the adiabatic region pass through only a small solid angle; consequently, polarizations of the rays originating in different regions will tend to align together. This effect can enhance the net observed polarization [54]. A comparison of polarizations assuming either gaseous atmospheres or condensed surfaces was analyzed in [55].

5 Theory versus observations

As argued above, models of strongly magnetized ($B \gg 10^9$ G) neutron-star atmospheres must take the bound species and their radiative transitions into account. Currently there are the following examples of application of models of *strongly magnetized and partially ionized* atmospheres to studies of thermal radiation of neutron stars with strong magnetic fields:

– RX J1856.5–3754, which is the closest and brightest of the class of X-ray INSs (XINSs, also known as the Magnificent Seven), whose X-ray spectra are apparently of purely thermal nature. Its measured spectrum was fitted in the entire range from X-rays to optical within observational error bars

with the use of the model of a thin magnetized hydrogen atmosphere on top of a condensed iron surface [35] (see also a discussion in [46]).

- phase-resolved spectrum and light curve of XINS RX J1308.6+2127 (RBS1223) have been described in [56] by the model with a magnetized iron surface covered by a partially ionized hydrogen atmosphere;
- the X-ray spectrum of thermally emitting INS 1E 1207.4–5209 appears to have been explained by cyclotron absorption harmonics, corresponding to $B \approx 7 \times 10^{10}$ G [28, 57];
- the *XMM-Newton* spectrum of thermally emitting INS 2XMM J104608.7–594306 has been analyzed in [58] with the blackbody model and hydrogen atmosphere model NSMAXG;
- the spectrum of INS 1WGA J1952.2+2925 is equally well fitted either by the blackbody model with a temperature of $T \approx 2.5 \times 10^6$ K and an emitting area radius of ≈ 0.6 km or by the magnetized atmosphere model NSMAX with $T_{\rm eff} \sim 10^6$ K and emission from the entire neutron-star surface [59];
- rotation powered pulsars PSR J1119–6127, B0943+10, J0357+3205, and J0633+0632, whose thermal parts of spectra were analyzed in [60–63] using magnetized atmosphere model NSMAX.

A more detailed discussion of the interpretations of observations of the above-listed objects is given in [46].

References

1. *V.F. Suleimanov, J. Poutanen, D. Klochkov, K. Werner*, Eur. Phys. J. A, **52**, 20, 2016.
2. *A.Y. Potekhin*, Phys. Usp., **57**, 735, 2014.
3. *S. Mereghetti, J.A. Pons, A. Melatos*, Space Sci. Rev., **191**, 315, 2015.
4. *R. Turolla, S. Zane, A.L. Watts*, Rep. Prog. Phys., **78**, 116901, 2015.
5. *V.L. Ginzburg*, The Propagation of Electromagnetic Waves in Plasmas (2nd ed.). London: Pergamon, 1970.
6. *Yu.N. Gnedin, G.G. Pavlov*, Sov. Phys. JETP, **38**, 903, 1974.
7. *A.D. Kaminker, G.G. Pavlov, Yu.A. Shibanov*, Astrophys. Space Sci., **86**, 249, 1982.
8. *T. Bulik, G.G. Pavlov*, Astrophys. J., **469**, 373, 1996.
9. *A.Y. Potekhin, D. Lai, G. Chabrier, W.C.G. Ho*, Astrophys. J., **612**, 1034, 2004.
10. *G.G. Pavlov, Yu.N. Gnedin*, Sov. Sci. Rev. E: Astrophys. Space Phys., **3**, 197, 1984.
11. *W.C.G. Ho, D. Lai*, Mon. Not. Roy. Astron. Soc., **338**, 233, 2003.
12. *Yu.A. Shibanov, V.E. Zavlin*, Astron. Lett., **21**, 3, 1995.
13. *R. Cohen, J. Lodenquai, M. Ruderman*, Phys. Rev. Lett., **25**, 467, 1970.
14. *H. Ruder, G. Wunner, H. Herold, F. Geyer*, Atoms in Strong Magnetic Fields. Berlin: Springer, 1994.

15. *B.R. Johnson, J.O. Hirschfelder, K.H. Yang*, Rev. Mod. Phys., **55**, 109, 1983.
16. *M. Vincke, M. Le Dourneuf, D. Baye*, J. Phys. B: Atom. Mol. Phys., **25**, 2787, 1992.
17. *A.Y. Potekhin*, J. Phys. B: Atom. Mol. Opt. Phys., **27**, 1073, 1994.
18. *G.G. Pavlov, A.Y. Potekhin*, Astrophys. J., **450**, 883, 1995.
19. *A.Y. Potekhin, G.G. Pavlov*, Astrophys. J., **483**, 414, 1997.
20. *A.Y. Potekhin, G. Chabrier*, Astrophys. J., **585**, 955, 2003.
21. *A.Y. Potekhin*, Astron. Astrophys., **518**, A24, 2010.
22. *V.G. Bezchastnov, G.G. Pavlov, J. Ventura*, Phys. Rev. A, **58**, 180, 1998.
23. *G.G. Pavlov, V.G. Bezchastnov*, Astrophys. J. Lett., **635**, L61, 2005.
24. *K. Mori, C.J. Hailey*, Astrophys. J., **564**, 914, 2002.
25. *A.Y. Potekhin, G. Chabrier, Yu.A. Shibanov*, Phys. Rev. E, **60**, 2193, 1999.
26. *K. Mori, J. Heyl*, Mon. Not. Roy. Astron. Soc., **376**, 895, 2007.
27. *A.Y. Potekhin, G. Chabrier*, Astrophys. J., **600**, 317, 2004.
28. *A.Y. Potekhin, G. Chabrier, W.C.G. Ho*, Astron. Astrophys., **572**, A69, 2014.
29. *K. Mori, C.J. Hailey*, Astrophys. J., **648**, 1139, 2006.
30. *K. Mori, W.C.G. Ho*, Mon. Not. Roy. Astron. Soc., **377**, 905, 2007.
31. *M.A. Ruderman*, Phys. Rev. Lett., **27**, 1306, 1971.
32. *Z. Medin, D. Lai*, Mon. Not. Roy. Astron. Soc., **382**, 1833, 2007.
33. *A.Y. Potekhin, V.F. Suleimanov, M. van Adelsberg et al.*, Astron. Astrophys., **546**, A121, 2012.
34. *C. Motch, V.E. Zavlin, F. Haberl*, Astron. Astrophys., **408**, 323, 2003.
35. *W.C.G. Ho, D.L. Kaplan, P. Chang et al.*, Mon. Not. Roy. Astron. Soc., **375**, 821, 2007.
36. *V. Suleimanov, A. Potekhin, K. Werner*, Astron. Astrophys., **500**, 891, 2009.
37. *V. Suleimanov, V. Hambaryan, A.Y. Potekhin et al.*, Astron. Astrophys., **522**, A111, 2010.
38. *J. Poutanen, A.M. Beloborodov*, Mon. Not. Roy. Astron. Soc., **373**, 836, 2006.
39. *V.L. Ginzburg, L.M. Ozernoi*, Sov. Phys. JETP, **20**, 689, 1965.
40. *D. Viganò, N. Rea, J.A. Pons et al.*, Mon. Not. Roy. Astron. Soc., **434**, 123, 2013.
41. *J.G. Elfritz, J.A. Pons, K. Glampedakis, D. Viganò*, Mon. Not. Roy. Astron. Soc., **456**, 4461, 2016.
42. *A.Y. Potekhin, J.A. Pons, D. Page*, Space Sci. Rev., **191**, 239, 2015.
43. *W.C.G. Ho, A.Y. Potekhin, G. Chabrier*, Astrophys. J. Suppl., **178**, 102, 2008.
44. *K.A. Arnaud*, in Astronomical Data Analysis Software and Systems V. Eds. G. Jacoby, J. Barnes. Astron. Soc. Pacif. Conf. Ser., **101**, 17, 1996.
45. *W.C.G. Ho*, in Magnetic Fields Throughout Stellar Evolution Proc. IAU Symp.

No. 302. Eds. M. Jardine, P. Petit, H.C. Spruit. Cambridge: Cambridge University Press, 2014, p. 435.

46. *A. Y. Potekhin, W.C.G. Ho, G. Chabrier*, in The Modern Physics of Compact Stars 2015. Ed. A. Sedrakian. Proc. Sci., PoS(MPCS2015)016, 2016.
47. *G.G. Pavlov, Yu.A. Shibanov*, Sov. Astron., **22**, 43, 1978.
48. *G.G. Pavlov, V.E. Zavlin*, Astrophys. J., **529**, 1011, 2000.
49. *D. Lai, W.C.G. Ho*, Phys. Rev. Lett., **91**, 071101, 2003.
50. *M. van Adelsberg, R. Perna*, Mon. Not. Roy. Astron. Soc., **399**, 1523, 2009.
51. *R. Taverna, F. Muleri, R. Turolla et al.*, Mon. Not. Roy. Astron. Soc., **438**, 1686, 2014.
52. *J.S. Heyl, N. Shaviv*, Mon. Not. Roy. Astron. Soc., **311**, 555, 2000.
53. *J.S. Heyl, N. Shaviv*, Phys. Rev. D, **66**, 023002, 2002.
54. *J.S. Heyl, N. Shaviv, D. Lloyd*, Mon. Not. Roy. Astron. Soc., **342**, 134, 2003.
55. *R. Taverna, R. Turolla, D.G. Caniulef et al.*, Mon. Not. Roy. Astron. Soc., **454**, 3254, 2015.
56. *V. Hambaryan, V. Suleimanov, A.D. Schwope et al.*, Astron. Astrophys., **534**, A74, 2011.
57. *V.F. Suleimanov, G.G. Pavlov, K. Werner*, Astrophys. J., **751**, 15, 2012.
58. *A.M. Pires, C. Motch, R. Turolla et al.*, Astron. Astrophys., **583**, A117, 2015.
59. *A. Karpova, D. Zyuzin, A. Danilenko, Yu. Shibanov*, Mon. Not. Roy. Astron. Soc., **453**, 2241, 2015.
60. *C.-Y. Ng, V.M. Kaspi, W.C.G. Ho et al.*, Astrophys. J., **761**, 65, 2012.
61. *N.I. Storch, W.C.G. Ho, D. Lai et al.*, Astrophys. J. Lett., **789**, L27, 2014.
62. *A. Kirichenko, A. Danilenko, Yu. Shibanov et al.*, Astron. Astrophys., **564**, A81, 2014.
63. *A. Danilenko, P. Shternin, A. Karpova, D. Zyuzin*, Publ. Astron. Soc. Austral., **32**, e038, 2015.

Behavior of Perturbations in an Accretion Flow on to a Black Hole

A.V. Semyannikov[1]

E-mail: *avsemyannikov@gmail.com*

We investigate the behavior of small acoustic perturbations in the spherical adiabatic relativistic accretion flow on to a non-rotating black hole. The Das model of the accretion [1, 2] is a general relativistic generalization of the classical spherical Bondi accretion. We consider a general relativistic linear wave equation for small acoustic perturbations and fulfill the mode analysis of solutions. We find numerically that perturbations remain finite in amplitude on the event horizon due to the effects of the general relativity in contrast to predictions of the non-relativistic model based on the Bondi accretion approximation [3]. This circumstance downranges the possibilities for detection of black holes.

1 Motivation

It is known that converging flows are often subject to hydrodynamic instabilities. For example, small acoustic perturbations have to increase without limit in the spherical adiabatic accretion flow on to a non-rotating black hole [3]. The predictions of the referenced article are based on the non-relativistic Bondi model of the adiabatic spherical accretion on to a point gravitating mass. However, the more realistic model of accretion taking into account the relativistic nature of flow near the event horizon should take proper account of the finiteness of the accretor's radius (the Schwarzschild radius r_g) and the velocity limit (the light speed c). The aim of the present work is to find the influence of relativistic effects on the efficiency of amplification of small acoustic perturbations in the spherical accretion flow.

2 Model

We examine the spatial stability of spherical adiabatic flow of a non-self-gravitating non-viscous homogeneous matter on to a black hole from infinity. The model of accretion is described by the general relativistic hydrodynamic equations: equation of fluid motion

$$u^\nu \nabla_{;\nu} u^\mu = -\frac{1}{n}\left(g^{\mu\nu} + \frac{u^\mu u^\nu}{c^2}\right)\nabla_{;\nu} p, \tag{1}$$

[1] Volgograd State University, Russian Federation

V. Grinin et al. (eds) Radiation mechanisms of astrophysical objects. Yerevan: Edit Print, 2017, pp. 353–356.

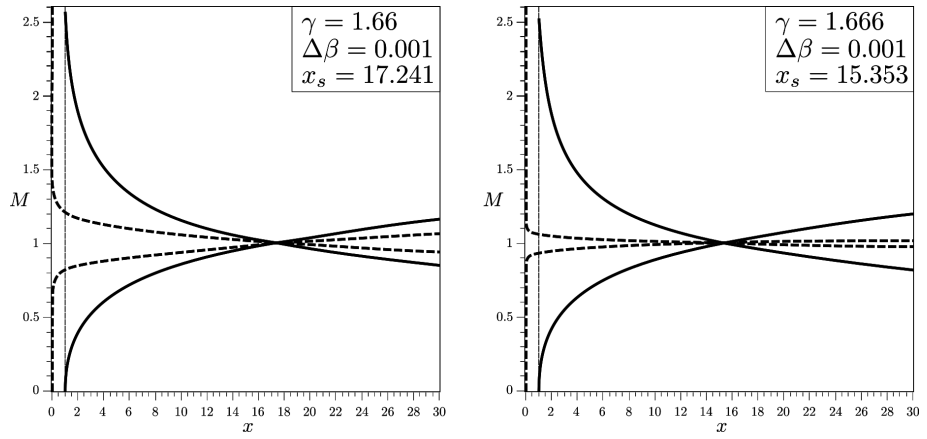

Figure 1: The Mach number M as the function of the dimensionless radial coordinate x (red lines). The subsonic (lower curve) and the supersonic (upper curve) separatrices of a relativistic solution (solid line) and a classic solution (dashed line).

and continuity equation

$$\nabla_{;\mu}(nu^{\mu}) = 0. \tag{2}$$

Here c is a speed of light, $g^{\mu\nu}$ a contravector of metric tensor, u^{μ} a geometrical contravector 4-velocity

$$u^{\mu} = \frac{dx^{\mu}}{d\tau}, \tag{3}$$

n is a specific relativistic density, and the pressure

$$p = Kn^{\gamma}. \tag{4}$$

A specific enthalpy is

$$h = mc^2 + \frac{\gamma}{\gamma - 1} Kn^{\gamma - 1}. \tag{5}$$

The equation of state (4) allows us to formulate an equation for the speed of sound c_s

$$c_s^2 = c^2 \frac{K\gamma n^{\gamma-1}}{mc^2 + K\frac{\gamma}{\gamma-1} n^{\gamma-1}}. \tag{6}$$

Here K is the gaseous constant, m the rest mass of matter, γ the adiabatic constant. In the case of the steady state spherically symmetric flow the system (1)–(2), (6) is reduced to the algebraic system of two integrals of motion, the mass flux conservation [1, 2]

$$yzx^2 \sqrt{\frac{1 - \frac{1}{x}}{1 - y^2}} = \lambda, \tag{7}$$

and the Bernoulli integral

$$(1 + z^{\gamma-1}) \sqrt{\frac{1 - \frac{1}{x}}{1 - y^2}} = \beta, \tag{8}$$

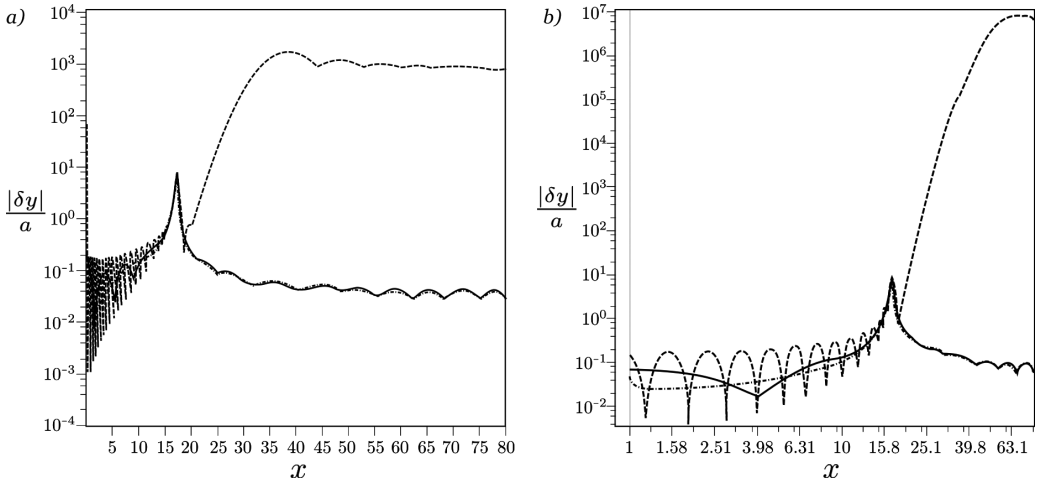

Figure 2: The ratio of the acoustic perturbations of radial velocity $|\delta y|$ for different azimuthal numbers l of spherical harmonics in the non-relativistic (a) and relativistic (b) cases. Dashed line with points is for $l = 0$, solid line for $l = 1$, and dashed line for $l = 10$. The frequency for all calculations $\omega = 0.01$, the adiabatic constant $\gamma = 1.66$, the energy $\Delta\beta = 0.001$.

and the equation for the non-dimensionalized sound speed a

$$a^2 = \frac{(\gamma - 1)z^{\gamma-1}}{1 + z^{\gamma-1}}. \tag{9}$$

Here λ and β are the mass flux and the Bernoulli constant, respectively. The non-dimensionalized flow variables are defined as follows:

$$x = \frac{r}{r_g}, \quad y = \frac{V_r}{c}, \quad z = \left(\frac{K\gamma}{mc^2(\gamma - 1)}\right)^{-\frac{1}{\gamma-1}} n, \quad a = \frac{c_s}{c}. \tag{10}$$

3 Solution

The perturbations are sought in the form

$$n = \delta n + n, \quad u^\mu = \delta u^\mu + u^\mu. \tag{11}$$

Potential of a 4-velocity is

$$u^\mu h = \nabla^{;\mu}\phi. \tag{12}$$

We find a solution in the form

$$\delta\phi = \delta\tilde{\phi}(x)Y_{lm}(\theta, \varphi)e^{-i\omega t}. \tag{13}$$

Cauchy-Lagrange integral is

$$\delta n = -\frac{u_{\sigma,0}}{K\gamma c^2 n_0^{\gamma-2}}\nabla^{;\sigma}\delta\phi. \tag{14}$$

Wave equation

$$\nabla_{;\mu}(d^{\mu\nu}\nabla_{,\nu}\delta\phi) = 0, \tag{15}$$

where d^{μ}_{ν} is a strange tensor

$$d^{\mu}_{\nu} = \frac{1}{K\gamma n_0^{\gamma-2}}\left(\frac{c_s^2}{c^2}g^{\mu}_{\nu} - \left(1 - \frac{c_s^2}{c^2}\right)\frac{u_0^{\mu}u_{\nu,0}}{c^2}\right). \tag{16}$$

A general relativistic wave equation

$$\delta\tilde{\phi}''d^{rr} + \delta\tilde{\phi}'\left(\frac{1}{\sqrt{-g}}\frac{\partial}{\partial x}\left(\sqrt{-g}d^{rr}\right) - 2i\omega d^{rt}\right) + \\ - \delta\tilde{\phi}\left(-\frac{\omega^2}{c^2}d^{tt} - i\frac{\omega}{c}\frac{1}{\sqrt{-g}}\frac{\partial}{\partial x}\left(\sqrt{-g}d^{tr}\right) - d^{\theta\theta}l(l+1)\right) = 0. \tag{17}$$

A classical limit of reduced wave equation

$$\delta\tilde{\phi}''\left(a^2 - y^2\right) + \delta\tilde{\phi}'\left(2\mathrm{i}\omega y - \left(y^2 + a^2\right)\frac{y'}{y} + 2y^2\frac{a'}{a}\right) + \\ + \delta\tilde{\phi}\left(\omega^2 - 2\mathrm{i}\omega y\frac{a'}{a} - a^2\frac{l(l+1)}{x^2}\right) = 0. \tag{18}$$

4 Results

We find that the acoustic perturbations are amplified significantly (many order of magnitudes) inside the sonic sphere in a spherical accretion flow, though remain finite compared to the case of the non-relativistic Bondi model.

References

1. *T.K. Das*, Astrophys. J., **577**, 880, 2002.
2. *T.K. Das*, Class. Quant. Grav., **21**, 5253, 2004.
3. *I.G. Kovalenko, M.A. Eremin*, Mon. Not. Roy. Astron. Soc., **298**, 861, 1998.

RM Synthesis: Problems and Perspectives

D.D. Sokoloff[1,2]

E-mail: *sokoloff.dd@gmail.com*

Main bulk of our knowledge concerning magnetic fields of spiral galaxies comes from observations of radio emission of the galaxies and in particular from Faraday rotation measures. We consider here traditional methods of this procedure in context of the new method known as RM Synthesis. RM Synthesis looks as an important tool for investigation of magnetic fields of spiral galaxies. Long wavelength observations allows a limited application of the method while expected facilities of SKA should allow such application in the full extent. Of course, it is desirable to combine RM Synthesis with options based on solution of inverse problem for multiwavelength observations.

1 Introduction

Magnetic field of the Milky Way is known for more than 60 years, and magnetic field of external spiral galaxies has been investigated since the 1980s. The main bulk of contemporary knowledge in this field comes from observations of polarized synchrotron emission in radio range. Polarization gives a hint that spiral galaxies contain magnetic fields of the scale comparable with galactic radius, while Faraday rotation of polarization plane confirms presence of this field and gives an estimate for it strength. The large-scale magnetic field component is almost parallel to the central galactic plane, and its direction is close to the azimuthal direction. The magnetic field strength is about several μG, i.e. magnetic field energy is close to equipartition with turbulent flows in the interstellar medium (see for a review, e.g., [1]).

Observations supporting the above understanding of galactic magnetism were obtained mainly at Effelsberg and VLA at 4 wavelengths (about 3, 6, 18, and 22 cm. A new generation of radio telescopes, which includes LOFAR and forthcoming SKA, opens a new perspective to obtain instructive information concerning galactic magnetic fields. The main novelty here is that it becomes possible to observe polarized radio emission at many (hundreds and possibly thousands) wavelengths instead of few ones only. Importance of this novelty is obvious for experts (see below), the question is, however, how to use this new ability. The aim of this paper is to discuss available suggestions in this respect.

[1] Department of Physics, Moscow State University, Russia
[2] IZMIRAN, Troitsk, Russia

V. Grinin et al. (eds) Radiation mechanisms of astrophysical objects. Yerevan: Edit Print, 2017, pp. 357–362.

2 Rotation measures and polarization angles

Starting points to use polarization data to get information concerning large-scale galactic magnetic fields are as follows. Synchrotron emission is polarized and its polarization angle is determined by magnetic field direction. If magnetic field is a small-scale random field, the emission becomes to be depolarized because of cancellation of many incomes with various polarization angles which contribute in one beam. In fact, the observed degree of polarization p (about 10–20%) is much lower than the initial one p_0 (about 70%) that gives a hint that a small-scale magnetic field b is superimposed on the large-scale one B, which leads to substantial depolarization. A simple estimate [2]

$$p = p_0/(1 + b^2/B^2) \tag{1}$$

tells that b is about two times larger than B. This estimate is supported by other available information (see for details [1]), however the point is that from one hand depolarization by small-scale magnetic field is far to be the only source of depolarization (see [2, 3]), and from the other hand anisotropic small-scale magnetic field can give polarization without large-scale one (so-called Laing effect – see, e.g., [3]).

Faraday rotation of polarization plane gives more direct information concerning large-scale magnetic field than just polarization. If polarized emission propagates through a slab with the line of sight magnetic field component $\mathbf{B}_{||}$, electron density n_e and thickness L, then its polarization angle ψ scales with λ as

$$\psi = \psi_0 + 0.81\ [\mathrm{rad\,m^{-2}cm^3}\mu\mathrm{G^{-1}pc^{-1}}]\ B_{||} n_e L \lambda^2, \tag{2}$$

where the coefficient at λ^2 is known as rotation measure (RM).

An important point is that from the observational point of view ψ varies in the range $-\pi/2 \le \psi \le \pi/2$, while Eq. (2) does not take into account this constraint. This is known as $\pm k\pi$ problem. A natural resolution of the problem is to use such range of wavelengths, where $\mathrm{RM}\lambda^2 \le \pi$ (Faraday thin source [4]) and include λ short enough to makes $\mathrm{RM}\lambda^2$ comparable with observational uncertainties. The range 3–22 cm fits more or less the requirements.

Basing on RM obtained observationally and known electron density, one obtains the line of sight magnetic field component only. Reconstruction of magnetic configuration in galactic disc as a whole requires fitting of a magnetic configuration model based on theoretical expectation from galactic dynamo to RM [5] or position angles [6] distribution in projection of galactic disc on the sky plane. This fitting is a highly non trivial task because the theoretical expectations are far to be very firm. Correspondingly, quite a lot of time and efforts are required to obtain a self-consistent model of galactic magnetic field from polarized observations.

3 Multiwavelength observations

The traditional procedure of magnetic configuration reconstruction from observational data has several substantial constraints. First of all, it does not take into account in an explicit form degree of polarization p and polarized intensity. A possible way to include such data in consideration is to fit a model to observed Stokes parameters $Q(\lambda^2)$ and $U(\lambda^2)$ [7].

A much more substantial point is that Eq. (2) implies that emission and Faraday rotation occur in separate regions at the line of sight so the case of so-called Faraday screen is considered. It happens, e.g., for Faraday rotation of radiation of extragalactic radio sources propagating through a nearby galaxy, say M 31, what can be used for reconstruction of magnetic field in such a galaxy [8]. A much more usual situation is, however, the case of radiation emitted and rotated in the same region in the galaxy in investigation. If such source is Faraday thick, polarization angle may deviate from the simple scaling Eq. (2) [3]. An important additional point is that LOFAR is constructed to observe at wavelengths of about 1 m and longer, so almost all spiral galaxies are expected to be Faraday thick in this spectral range.

If available observations cover a more or less homogeneous spectral range from several cm and up to 1 m and longer, there is an attractive option to fit a particular model of depolarization to available observations to obtain (provided a realistic distributions of electron density and relativistic electrons are somehow known) spatial distribution of magnetic field along the line of sight. Such possibility mentioned already in [9] remains, however, an attractive perspective only. In particular, one needs 25 times longer observational time to get data of comparable quality at 100 wavelengths than at 4 wavelengths. Multiwavelength observations of spiral galaxies are available at the instant for a quite narrow spectral range located at long wavelengths [10]. Expectation that future development of the observational basis will open a possibility to formulate and solve an adequate inverse problem for magnetic field distribution along the line of sight is supported by a positive experience in technique of inverse Doppler imaging in investigations of stellar activity [11] and helioseismology (e.g., [12]), but mathematical problems to be resolved remain very substantial.

4 Concept of RM Synthesis

A fruitful compromise, which allows to use multi-wavelength observations and avoid an extended usage of high-brow mathematical technique of inverse problem theory, was suggested as RM Synthesis in [13].

It was Burn [2] who noted that complex polarized intensity $P = Q + iU$ obtained from a radio source is related to the Faraday dispersion $F(\phi)$ (which

is determined by emissivity and intrinsic position angle, see below) as

$$P(\lambda^2) = \int_{-\infty}^{\infty} F(\phi) e^{2i\phi\lambda^2} d\phi. \tag{3}$$

Here the Faraday depth ϕ is defined by

$$\phi(z) = -0.81 \int B_{||} n_e dz'. \tag{4}$$

Following Eq. (3), P is the inverse Fourier transform of F. Correspondingly, the Faraday dispersion function F is the Fourier transform $\hat{P}$ of complex polarized intensity

$$F(\phi) = \frac{1}{\pi} \hat{P}(k), \tag{5}$$

where $k = 2\phi$.

The idea of RM Synthesis is to use multi-wavelength data in order to find Faraday dispersion F as a function of Faraday depth ϕ. Of course, Faraday depth is far to be the desired magnetic field (or at least its line of sight component $B_{||}$) as a function of position at the line of sight however the quantities are reasonably related one to the other to make finding of F an attractive destination (e.g., [14]). Comparison of various realizations of RM Synthesis in application to unresolved radio sources is presented in [15].

5 Wavelet based RM Synthesis

Realization of the attractive idea described above faces at least two obvious problems. From one hand, a straightforward understanding of Eq. (5) requires integration over the parameter λ^2 from $-\infty$ to $+\infty$ while according to its physical meaning $\lambda^2 > 0$. This problem can be resolved using the fact that the galactic magnetic field is symmetric in the respect to the galactic central plane. This symmetry gives a link between complex P for $\lambda^2 > 0$ and that one formally calculated for $\lambda^2 < 0$ [16]. Fortunately, exactly the same symmetry follows from the assumption that the source contains just one spectral detail in Faraday dispersion function [17]. The last assumption usually is exploited for RM Synthesis of unresolved radio sources.

From the other hand, performing a Fourier transform (even using symmetry argument), one needs to know the function for all values of λ^2 while in fact observations provide P for a limited spectral range $\lambda_{\min} < \lambda < \lambda_{\max}$. This problem can be in principle resolved by wavelet technique which allows to calculate contributions to the Fourier transform from each spectral range separately [16, 17]. Of course, a limited spectral range allows to isolate some spectral details in Faraday dispersion function only. Analysis performed in [18] shows that one can expect to isolate such details for which $\phi\lambda^2_{\min} \leq \pi$, i.e. galaxy is Faraday thin at least at the shortest wavelength. It means that using

LOFAR data RM Synthesis can give information concerning turbulent components of galactic magnetic field only. Direct investigation of large-scale galactic magnetic field requires forthcoming facilities of SKA. This result looks for the first sight slightly disappointing, however each telescope allows to observe only some feature of celestial body of an interest and nobody expects that an optical telescope allows to see something, say, inside the Sun. Nevertheless, analysis of [18] stresses the important role of short wavelength observations.

There are indications [19] that RM Synthesis can be used for observational identification of helicity, i.e. crucial driver of galactic dynamo.

6 Conclusions

Summarizing results from the above cited papers, we conclude that RM Synthesis looks as an important tool for investigation of magnetic fields of spiral galaxies. Long wavelength observations allow a limited application of the method, while the expected facilities of SKA should allow such application in the full extent. Of course, it is desirable to combine RM Synthesis with options based on solution of inverse problem for multi-wavelength observations. Of course, fitting of any models to observational data needs to adopt the model to the contemporary understanding of magnetic field symmetries in a celestial body of interest. For spiral galaxies that is magnetic field symmetry in respect to the central plane of the galaxy, however for, say, magnetic field of a jet such symmetry has to be isolated in a particular research.

Acknowledgments. Fruitful discussions with S.A. Mao, R. Beck, P. Frick, L. Rudnick, R. Stepanov are acknowledged. The paper is supported by RFBR under grant 15-02-01407.

References

1. *R. Beck, A. Brandenburg, D. Moss et al.*, Ann. Rev. Astron. Astrophys., **34**, 155, 1996.
2. *B.J. Burn*, Mon. Not. Roy. Astron. Soc., **133**, 67, 1966.
3. *D.D. Sokoloff, A.A. Bykov, A. Shukurov et al.*, Mon. Not. Roy. Astron. Soc., **299**, 189, 1998.
4. *A.G. Pacholczyk*, Radio Galaxies. Oxford: Pergamon Press, 1977.
5. *A. Ruzmaikin, D. Sokoloff, A. Shukurov, R. Beck*, Astron. Astrophys., **230**, 284, 1990.
6. *E.M. Berkhuijsen, C. Horellou, M. Krause et al.*, Astron. Astrophys., **318**, 700, 1997.
7. *S.A. Mao, E. Zweibel, A. Fletcher et al.*, Astrophys. J., **800**, 92, 2015.
8. *D. Moss, A. Shukurov, D.D. Sokoloff et al.*, Astron. Astrophys., **335**, 500, 1998.
9. *A.A. Ruzmaikin, D.D. Sokoloff*, Astron. Astrophys., **78**, 1, 1979.
10. *G. Heald, R. Brawn, R. Edmonds*, Astron. Astrophys., **503**, 409, 2009.

11. *A.V. Goncharskij, V.V. Stepanov, V.L. Khokhlova, A.G. Yagola*, Sov. Astron., **26**, 690, 1982.

12. *A.G. Kosovichev, K.V. Parchevskii*, Sov. Astron. Lett., **14**, 201, 1988.

13. *M.A. Brentjens, A.G. de Bruyn*, Astron. Astrophys., **441**, 1217, 2005.

14. *A.G. de Bruyn, M.A. Brentjens*, Astron. Astrophys., **441**, 931, 2005.

15. *X.H. Sun, L. Rudnick, T. Akahori et al.*, Astrophys. J., **149**, 60, 2015.

16. *P. Frick, D. Sokoloff, R. Stepanov, R. Beck*, Mon. Not. Roy. Astron. Soc., **401**, L24, 2010.

17. *P. Frick, D. Sokoloff, R. Stepanov, R. Beck*, Mon. Not. Roy. Astron. Soc., **414**, 2540, 2011.

18. *R. Beck, P. Frick, D. Sokoloff, R. Stepanov*, Astron. Astrophys., **543**, A113, 2012.

19. *A. Brandenburg, R. Stepanov*, Astrophys. J., **786**, 91, 2014.

Low Multipoles Anomalies of CMB Maps

O.V. Verkhodanov[1]

E-mail: *vo@sao.ru*

We consider anomalies of cosmic microwave background observed at low multipoles of the WMAP and Planck cosmic missions. The possible origin of these features is discussed. We study difference of both missions data which is apparently connected with the local sources emission and/or systematics.

1 Introduction

The last decade of the cosmic microwave background (CMB) study was marked by several marvelous discoveries which changed the observational cosmology. The main cosmological parameters were measured with two satellites – WMAP and Planck.

The observations of the CMB radiation by the Wilkinson Microwave Anisotropy Probe (WMAP, *http://lambda.gsfc.nasa.gov*) [1, 2] were revolutionary in modern cosmology. The data were recorded in five bands: 23, 33, 41, 61, and 94 GHz with the measurements of intensity and polarization. The mission results include the CMB maps of anisotropy and polarization, the maps of foreground components (synchrotron and free-free emission, dust radiation), their power spectrum. The resolution of the CMB map restored with implementing the Internal Linear Combination (ILC) method [1] is $40'$. The angular power spectrum of CMB produced by the WMAP experiment allowed one to measure all the main cosmological parameters at the most precise level of observational cosmology (with accuracy less than 10%) [3].

The second set of maps and corresponding data were obtained in the European Space Agency experiment Planck (*http://www.rssd.esa.int/Planck/*) [4] and produced new possibilities in investigation of foreground components and radio sources in millimeter and submillimeter wavelengths. Planck observations were carried out at low frequency instrument (LFI bandwidths: 30, 44, 70 GHz) and high frequency instrument (HFI bandwidths: 100, 143, 217, 353, 545, 857 GHz). The resolution of the Planck CMB maps is $\sim 5'$. The Planck mission allowed one to obtain new and independent observational data.

Results of both experiments also contain some anomalies violated our expectation from the CMB Gaussian distribution. The most discussed ones [5] are Axis of Evil [6], Cold Spot [7], violation of parity in the power spectrum [8], asymmetry "North – South" in galactic coordinate system [9]. The Planck data

[1] Special astrophysical observatory RAS, Nizhnij Arkhyz, Russia

V. Grinin et al. (eds) Radiation mechanisms of astrophysical objects. Yerevan: Edit Print, 2017, pp. 363–370.

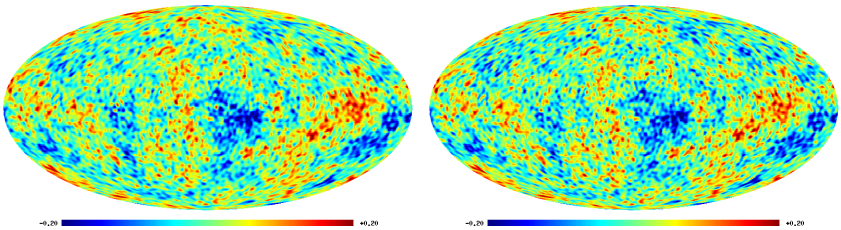

Figure 1: CMB maps restored from the WMAP (left, ILC map) and Planck (right, SMICA map) observational data and smoothed upto $\ell_{\max} = 100$.

added a new unexpected phenomena – too low amplitude of low harmonics [10]. All these anomalies occur at the largest angular scales ($\theta > 1^\circ$) and demonstrate observation statistical anisotropy being a sign of non-Gaussianity at low multipoles.

There are two basic approaches in understanding the origin of anomalies. The first one is based on suggestion of complex processes during early stages of the Universe. The second one follows the idea of connection of the anomalies with foregrounds and/or data analysis procedures.

Two basic properties of CMB allow one to separate its signal from foregrounds: (1) black body emission, so it has the same temperature at all wavelengths, and (2) correlation of CMB and foregrounds should be close to zero, because CMB is a random Gaussian process. In the simple case, the sought ILC temperature can be written as a linear combination of signal from the maps for different frequencies. The different versions of the ILC method and its variations exist both in pixel space and in harmonic space [11]. The maps restored in WMAP and Planck experiments are shown in Fig. 1.

For the restored CMB signal, the angular power spectrum is calcluated using the so called $a_{\ell m}$-coefficients $C(\ell) = \frac{1}{2\ell+1} \sum_{m=-\ell}^{\ell} |a_{\ell m}|^2$. The $a_{\ell m}$-coefficients are obtained in the standard decomposition of the measured temperature variations on the sky, $\Delta T(\theta, \phi)$, in spherical harmonics (multipoles):

$$\Delta T(\theta, \phi) = \sum_{\ell=2}^{\infty} \sum_{m=-\ell}^{m=\ell} a_{\ell m} Y_{\ell m}(\theta, \phi). \qquad (1)$$

2 The main WMAP and Planck CMB data anomalies

Axis of Evil. The Axis of Evil (Fig. 2) is the most famous among non-Gaussian features of the WMAP CMB data. The Axis unifies some problems which require special explanations. They are the planarity and alignment of the two harmonics, quadrupole and octupole, and, partly, the problem of extremely low amplitude of the quadrupole. Different estimations of the significance of existence of this axis, and several hypotheses on its origin were made. Various studies (e.g., [12, 13]) investigated the contribution of background components and their influence on the alignment of multipoles ($\ell = 2$ and $\ell = 3$), and indicated a small probability

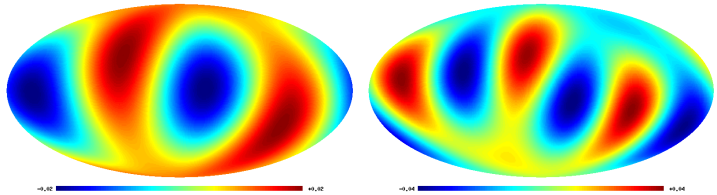

Figure 2: Axis of Evil: planarity and alignment of the quadrupole (left) and the octupole (right) on the WMAP CMB map.

of the background effect on the orientation of the low multipoles. Randomness of such an effect is estimated by the authors as unlikely at the significance level exceeding 98% and excludes the effect of residual contribution of background components.

Some cosmological models were developed to explain the prominence of the axis in the orientation of multipoles. They include the anisotropic expansion of the Universe, rotation and magnetic field [14, 15].

There are some hints demonstrating that the problem of existence of Axis of Evil can be connected with the instability of CMB reconstruction at low multipoles ($2 \leq \ell \leq 10$) in ILC method [16, 17]. Another possible solution of the problem is to construct the separation methods on the homogeneous samples of pixels where possible to tune selection of subsample in such a way that the quadrupole amplitude of the restored map grows and phase changes, so, no axis of evil exists [18].

Using new data, the Planck team [10] detected the angle between planes of quadrupole and octupole is equal $\sim 13^\circ$ (against $\sim 3^\circ$ or $\sim 9^\circ$ for WMAP data at different observational years) and declared that significance of the quadrupole-octupole alignment is substantially smaller than for the WMAP data, falling to almost 98% confidence level. Later, Copi et al. [19] demonstrated that the WMAP and Planck data confirm the alignments of the largest observable CMB modes in the Universe. Using different statistical methods to control the mutual alignment between the quadrupole and octupole, and the alignment of the plane defined by the two harmonics with the dipole direction, the authors obtained that both phenomena are at the greater than 3σ level for Planck CMB maps studied.

Cold Spot. The next exited feature discussed is the Cold Spot (CS) (Fig. 3). This is a cold region exhibiting a complex structure identified in the CMB using spherical Mexican hat wavelets [7]. The non-Gaussianity of the signal in the Southern hemisphere was explained precisely by the existence of this region. The galactic coordinates of center of the spot are $b = -57^\circ, l = 209^\circ$. The probability of the signal in CS, being consistent with the Gaussian model if spherical wavelets are used, is about 0.2% [7]. After obtaining indication of the signal non-Gaussianity at the CS as well as messages on the reduced density of source [20] in smoothed maps of radio survey NVSS at 1.4 GHz, several hypotheses concerning the origin of the Cols Spot were discussed which were related to the integrated Sachs–Wolfe effect, the topological defect, anisotropic expansion, the artifact of data analysis,

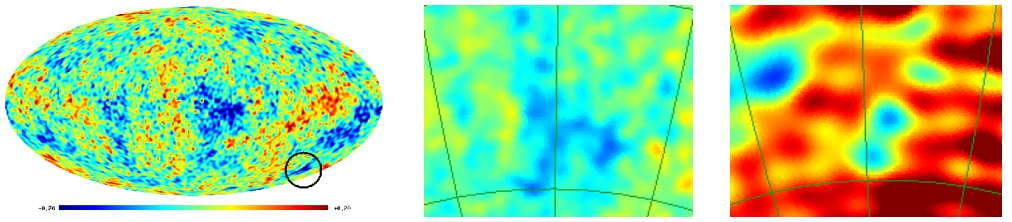

Figure 3: Cold Spot: position of the Cold Spot on the WMAP CMB map (left) and its shape (center) and 408 MHz map (right) with synchrotron emission.

and simply a random deviation (see the review [21]). As was noted in [22], the possible galactic foreground residuals in the CMB maps can produce such a type of the spot as a part of non-Gaussianity at low multipoles. We should add that the CS is also manifested in the data of 1982 in maps of a low-frequency survey where synchrotron radiation contributes significantly to the background (Fig. 3, right). In favor of the hypothesis of the CS being the Galactic phenomena, the following fact testifies. There exists the high correlation of positions of peaks of CMB fluctuation and galactic magnetic field distribution [23].

Violation of the power spectrum parity. A remarkable manifestation of non-Gaussian properties of low multipoles consists in parity asymmetry first noticed in [8] and confirmed in Planck data [10]. For a Gaussian random field of primary perturbations $\Phi(\mathbf{k})$ with a flat power spectrum, the presence of a plateau in the CMB angular power spectrum is expected at low multipoles, which is due to the Sachs–Wolfe effect, namely, to the fact that $\ell(\ell+1)C_\ell \approx const$. Spherical harmonics change as $Y_{\ell m}(\widehat{\mathbf{n}}) = (-1)^\ell Y_{\ell m}(-\widehat{\mathbf{n}})$, when the coordinates are reversed. Therefore, an asymmetry in the angular power spectrum for even and odd harmonics can be regarded as the asymmetry of the power of even and odd components of map. The authors [8] found the power of odd multipoles to systematically exceed the power of even multipoles of low ℓ and termed this phenomenon "parity asymmetry". To describe such an asymmetry quantitatively, the following quantities are proposed for consideration: $P^+ = \sum_{\text{even } \ell<\ell_{max}} \ell(\ell+1)C_l/2\pi$, $P^- = \sum_{\text{odd } \ell<\ell_{max}} \ell(\ell+1)C_l/2\pi$. Using the data of WMAP power spectrum and the results of Monte Carlo simulations, the authors [8] calculated the ratio P^+/P^- for the multipole ranges $2 \le \ell \le \ell_{\max}$, where $\ell_{\max}$ lies between 3 and 23. Comparing P^+/P^- for the WMAP data with the simulated maps ratio allows estimating the quantity p equal to the fraction of simulated spectra in which P^+/P^- is less than or equal to the same quantity for the WMAP map. The value of p was found to reach its lower boundary at $\ell_{\max} = 18$, where p equals 0.004 and 0.001 for the data obtained by the WMAP mission during five and three years of observations, respectively. This fact means that there is a preference for odd multipoles $2 \le \ell \le 18$ in the WMAP data at a confidence level of 99.6% with a screening mask imposed on the data, and of 99.76% without any mask. The authors believe the low amplitude of the WMAP CMB quadrupole may be part of the same anomaly as the parity asymmetry.

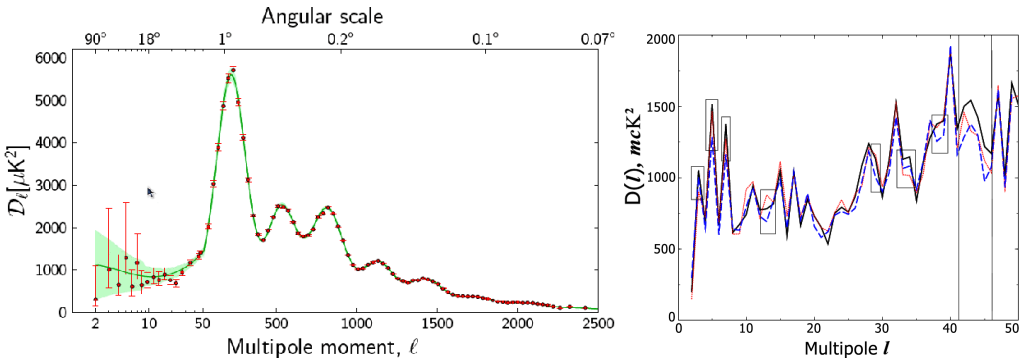

Figure 4: Right: CMB angular power spectrum of the 1st Planck data release. Left: the angular power spectrum $D(\ell) = \ell(\ell+1)C_\ell/2\pi$ for $2 \le \ell < 50$. The solid line shows the 7th year WMAP ILC data release. The dotted line marks WMAP9 ILC data. The Planck data are marked by the dashed line. The rectangulars show the most different amplitudes. The vertical lines mark limits of $\ell \in [41, 46]$.

Hemispherical Asymmetry. The asymmetry of hemispheres power (see, e.g., Fig. 1) was detected just after publishing the first year all sky maps of the WMAP [9]. Then, in [24], the some calculations based on the angular power spectrum were presented and shown that this spectrum, when estimated locally at different positions on the sphere, appears not to be isotropic. Park [25] also presented evidence for the existence of such hemispherical asymmetry, in which a particular statistical measure is considered to change discontinuously between two hemispheres on the sky, applying Minkowski functionals to the WMAP data. Since the preferred direction according to Eriksen et al. [9] lays close to the ecliptic plane, it was also demonstrated that the large-angular scale N-point correlation functions were different in behavior when computed on ecliptic hemispheres.

The observed properties of the Planck data are consistent with a remarkable lack of power in a direction towards the north ecliptic pole, consistent with the simpler one-point statistics [10].

3 Difference of WMAP and Planck power spectra

One of the main anomalies first detected in the Planck data was the lack of power at low multipoles detected for angular power spectrum $C(\ell)$. Using the WMAP and Planck officially published spectra, we can compare them via the calculation of the difference of maps including only the harmonics with maximum $C(\ell)$ difference (Fig. 4, right).

Following [26], let us consider the differences of maps corresponding to the harmonics having the maximum difference of power. These ranges are marked by rectangulars on Fig. 4. The vertical lines demonstrate limits of the multipole range in $\ell \in [41, 46]$. On Figs. 5, 6, there are shown maps of harmonic differences at $\ell = 5$ and $\ell = 7$, respectively. Some features of these differences show the

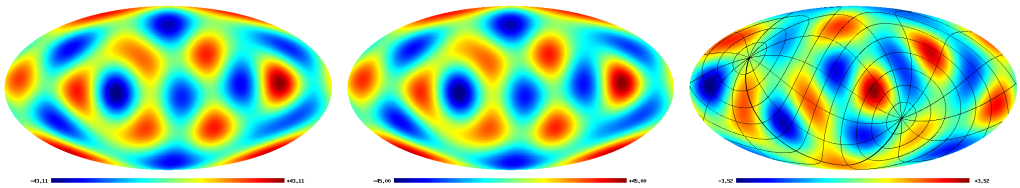

Figure 5: Left to right: the map of $\ell = 5$ of the Planck CMB map SMICA, the $\ell = 5$ of the ILC WMAP9 map, and the map of these signals difference. The equatorial coordinate grid is overlaid on the map of difference.

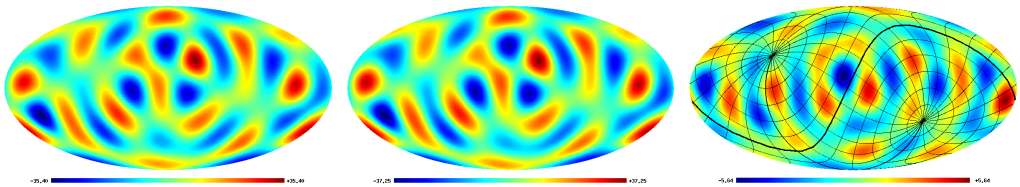

Figure 6: Left to right: the map of $\ell = 7$ of the Planck CMB map SMICA, the $\ell = 7$ of the ILC WMAP9 map, and the map of these signals difference. The ecliptic coordinate grid is overlaid on the map of difference.

position of spots along the Galactic plane, sensitivity of difference map at $\ell = 5$ to the equatorial coordinate system (equatorial poles are placed in singular points – saddles), and the axis of the multipole $\ell = 7$ lays on the Galactic plane and simultaneously, the saddle points of $\ell = 7$ are placed in ecliptic poles. The map of multipole difference at $\ell = 13$ (angular size of $\sim$6.5°) contains a feature similar to the harmonic $\ell = 7$ where the ecliptic poles are placed in singular points – local map minima and maxima. The multipole difference at the scales $\ell = 29$ ($\sim$3°) and $\ell = 37$ ($\sim$2.5°) contains a similar structure of spots placement. One line drawn by the very contrast spots formed with m-modes combinations of the $\ell = 29$ and $\ell = 37$ coincides with the ecliptic plane. Curiously, that a structure of the bright spots placement for $\ell = 29$ and $\ell = 37$ in the right hemisphere corresponds the anisotropic model Bianchi$_{\mathrm{VIIh}}$ discussed in [10]. There is the range of multipoles ($\ell \in [41; 46]$) where the spectrum strongly differ for the WMAP and Planck data (Figs. 4, 7). The map difference for these multipole range shows the extended structure near the Galactic center.

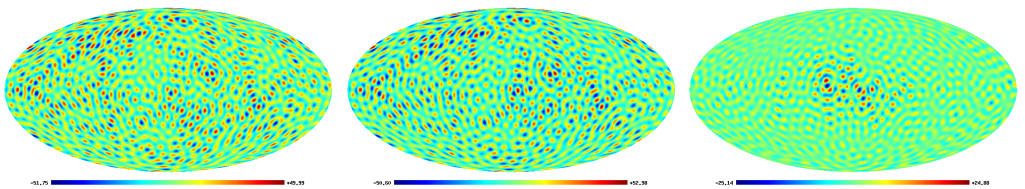

Figure 7: Left to right: the summarized signal of multipole $\ell \in [41, 46]$ for the Planck CMB map SMICA, harmonics $\ell = 41$–46 of WMAP9 ILC, and difference of these signals.

Note, that there are two important moments observed in multipole differences. First, all the maps of multipole difference with high amplitude contain features tied with galactic, ecliptic or/and equatorial (terrestrial) coordinate systems. Second, there is the $\Delta\ell = 8$ period for multipoles numbers having a big difference in amplitude. Peculiar harmonics have numbers $\ell = 5, 13, 29, 37, 45$.

4 Summary

As we can see from the details of the CMB anomalies mentioned above, most of them manifest the properties sensitive to local environment. Three main environments of the cosmic observatory are displayed in the CMB signal distribution. They are our Galaxy, the Solar (ecliptic) system and some features from the equatorial system. The Galaxy is a source of the non-Gaussian residuals visible in CMB spots positions (see [21]). The Cold Spot is a feature visible on a synchrotron map and on a map of the Faraday rotation depth. It could be due to any ionized cloud from Galaxy or its vicinity.

The Solar system objects are an additional residual source on the CMB map which is difficult to account using standard component separation methods. Possible sources of a residual signal are the antenna far sidelobes sensitive to the Sun and bright planets, a solar wind focusing by the Earth magnetosphere and passing through the Lagrange point L2, the objects at boundary of Solar system like the Kuiper belt.

The equatorial system features detected in some CMB correlation maps or in the single harmonic maps can be due by the influence of the Earth microwave emission via the antenna back lobes or possible Solar wind emission modulated by the Earth magnetosphere where the magnetic axis is close the Earth rotation axis.

It is necessary to note that there are some anomalies in the Planck data detected at high ($\ell > 600$) harmonics. There is a disagreement between cosmological parameters determination using the CMB angular power spectrum (including or not other experiments) and using only the Sunyaev–Zeldovich clusters [27]. Such a discordance, as discussed also in this paper, can be explained by the biased estimates of cluster parameters with the X-ray data.

And we can note that

1) WMAP and Planck data have practically the same low multipole anomalies, all the visible anomalies probably can be understood in the frame of the local (galactic and ecliptic) sources of microwave emission,
2) the difference of WMAP and Planck power spectra looks like one due to systematic effects of maps preparation (e.g. due to beam residuals).

Acknowledgments. Author is thankful to Conference Organizing Committee for hospitality. Author is also grateful to NASA for possibility to use NASA Legacy Archive where WMAP maps stored and ESA for open access to observational results in the Planck Legacy Archive. The GLESP (*http://www.glesp.nbi.dk*) package [28] was used to process the CMB maps on a sphere.

References

1. *C.L. Bennett, M. Halpern, G. Hinshaw et al.*, Astrophys. J. Suppl., **148**, 1, 2003.
2. *N. Jarosik, C.L. Bennett, J. Dunkley et al.*, Astrophys. J. Suppl., **192**, 14, 2011.
3. *C.L. Bennett, D. Larson, J.L. Weiland et al.*, Astrophys. J. Suppl., **208**, 20, 2013.
4. *Planck Collaboration*, Astron. Astrophys. **571**, A1, 2014.
5. *C.L. Bennett, R.S. Hill, G. Hinshaw et al.*, Astrophys. J. Suppl., **192**, 17, 2011.
6. *K. Land, J. Magueijo*, Phys. Rev. Lett., **95**, 071301, 2004.
7. *M. Cruz, E. Martinez-Gonzalez, P. Vielva, L. Cayon*, Mon. Not. Roy. Astron. Soc., **356**, 29, 2005.
8. *J. Kim, P. Naselsky*, Astrophys. J. Lett., **714**, L265, 2010.
9. *H.K. Eriksen, F.K. Hansen, A.J. Banday et al.*, Astrophys. J., **605** 14, 2014.
10. *Planck Collaboration*, Astron. Astrophys., **571**, A23, 2014.
11. *S.M. Leach, J.-F. Cardoso, C. Baccigalupi et al.*, Astron. Astrophys., **491**, 597, 2008.
12. *C.J. Copi, D. Huterer, D.J. Schwarz, G.D. Starkman*, Mon. Not. Roy. Astron. Soc., **367**, 79 (2006).
13. *A. Gruppuso, C. Burigana*, J. Cosmol. Astropart. Phys., **08**, 004, 2009.
14. *M. Demianski, A.G. Doroshkevich*, Phys. Rev. D, **75l**, 3517, 2007.
15. *T. Koivisto, D.F. Mota*, J. Cosmol. Astropart. Phys., **06**, 018, 2008.
16. *P.D. Naselsky, O.V. Verkhodanov*, Astrophys. Bull., **62**, 203, 2007.
17. *P.D. Naselsky, O.V. Verkhodanov, M.T.B. Nielsen*, Astrophys. Bull., **63**, 216, 2008.
18. *A.G. Doroshkevich, O.V. Verkhodanov*, Phys. Rev. D, **83**, 3002, 2011.
19. *C.J. Copi, D. Huterer, D.J. Schwarz, G.D. Starkman*, Mon. Not. Roy. Astron. Soc., **449**, 3458, 2015.
20. *L. Rudnick, S. Brown, L.R. Williams*, Astrophys. J., **671**, 40, 2007.
21. *O.V. Verkhodanov*, Phys. Usp., **55**, 1098, 2012.
22. *P.D. Naselsky, P.R. Christensen, P. Coles et al.*, Astrophys. Bull., **65**, 101, 2010.
23. *M. Hansen, W. Zhao, A.M. Frejsel et al.*, Mon. Not. Roy. Astron. Soc., **426**, 57, 2012.
24. *F.K. Hansen, A.J. Banday, K.M. Górski*, Mon. Not. Roy. Astron. Soc., **354**, 641, 2004.
25. *C.-G. Park*, Mon. Not. Roy. Astron. Soc., **349**, 313, 2004.
26. *O.V. Verkhodanov*, Astrophys. Bull., **69**, 330, 2014.
27. *Planck Collaboration*, Astron. Astrophys., **571**, A20, 2014.
28. *A.G. Doroshkevich, O.V. Verkhodanov, P.D. Naselsky et al.*, Int. J. Mod. Phys. D, **20**, 1053, 2011.

* The color figures are available online in the Proceedings at *http://www.astro.spbu.ru/sobolev100/*.

Structure of Galaxy Groups and Clusters and Measurement of Their Masses

A.I. Kopylov[1], F.G. Kopylova[1]

E-mail: *flera@sao.ru*

We report the results of measurement and comparison of masses for a sample of 29 groups and clusters of galaxies ($z < 0.1$). We use the SDSS archive data to determine dynamical masses from the one-dimensional dispersion of radial velocities for virialized regions of radii R_{200} and $R_{\rm e}$. Our method for determination of effective radius of galaxy systems from the cumulative distribution of the number of galaxies depending on squared cluster-centric distance allowed us to estimate masses $M_{1/2}$ (within $R_{\rm e}$), which are related to the masses enclosed within R_{200}: $M_{200} \sim 1.65\,M_{1/2}$. A comparison of the inferred dynamic masses and the hydrostatic masses determined from the radiation of hot gas in galaxy groups and clusters (based on published data) led us to conclude that the inferred masses for the main sample of 21 groups and clusters agree to within 12%.

Galaxy clusters are the largest gravitationally bound structures in the Universe. About 80–90% of their mass is in the form of dark matter, and the remaining mass is represented by baryons, most of which (10–20%) are in the form of hot diffuse plasma with $T > 10^7$ K (it is the main component of the inner medium of galaxy clusters), which emits mostly in the X-ray domain. Galaxies contribute only several percent of the cluster mass. The mass function of galaxy clusters is sensitive to cosmological parameters, turning the measurement of their accurate masses a challenging task [1].

The aim of this study is to measure the dynamical masses of 29 groups and clusters of galaxies using various methods, intercompare the resulting mass estimates, and compare them with the masses inferred from the X-ray emission of gas. We have determined dynamical masses M_{200} of the clusters from the dispersion of radial velocities of galaxies assuming that the systems are in virial equilibrium. The empirical radius R_{200} and the group or cluster mass can be estimated by the equations: $R_{200} = \sqrt{3}\sigma/(10H(z))$ Mpc [2] and $M_{200} = 3G^{-1}R_{200}\sigma^2$, where $H(z)$ is the Hubble constant at redshift z, and G is the gravitational constant. The masses $M_{1/2}$ of spheroidal galaxies and clusters of galaxies with measured dispersions of radial velocities can be determined for the characteristic radius, which is approximately equal to the 3D radius of the galaxy containing half of its luminosity. Thus, the virial mass of the cluster is measured, which is independent of the anisotropy of galaxy velocities,

[1] Special Astrophysical Observatory RAS, Nizhnij Arkhyz, Russia

V. Grinin et al. (eds) Radiation mechanisms of astrophysical objects. Yerevan: Edit Print, 2017, pp. 371–372.

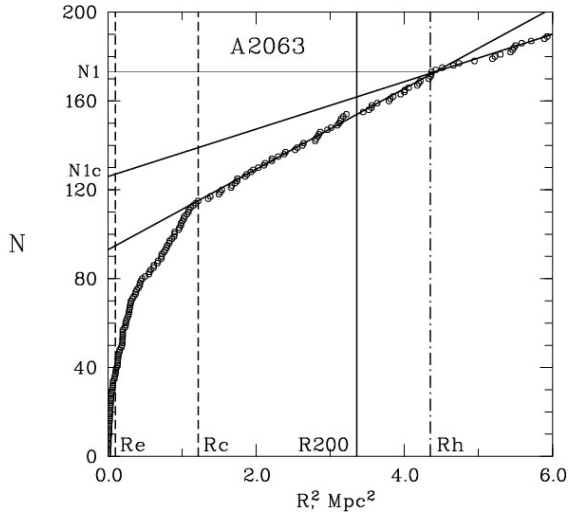

Figure 1: Cumulative distribution of the number of galaxies as a function of squared clustercentric distance for the A 2063. The solid vertical line indicates the R_{200}. The dashed-and-dotted line indicates the $R_{\rm h}$ radius bounding the cluster: core (c) and halo (h); the dashed lines indicate the $R_{\rm c}$ and $R_{\rm e}$ radii. The two solid lines show the distribution of galaxies located inside the halos of groups and clusters and the distribution of galaxies that do not belong to the cluster.

$M_{1/2} = 3G^{-1}\,\sigma^2_{1/2}\,r_{1/2}$ [3], where $r_{1/2} = 4/3R_e$ (R_e is the effective radius containing half of the luminosity emitted by the cluster or group).

We use a graphical method to determine the size and the number of galaxies of the system (R_h, N_h) and its effective radius containing half of the near-infrared luminosity (Fig. 1).

Our main results are as follows (see also [4]):

1. We developed an empirical method for identifying galaxy groups or clusters from the observed cumulative distribution of the number of galaxies depending on squared cluster-centric distance.
2. We show that the dynamic masses of galaxy groups and clusters for regions of radii R_{200} and $R_{\rm e}$ are related as $M_{200} \sim 1.65\,M_{1/2}$.
3. The inferred dynamic (M_{200} and $1.65\,M_{1/2}$) and hydrostatic ($M_{X,200}$) masses for 21 groups and clusters of galaxies agree with each other to within 12%.

References

1. *A.A. Vikhlinin, A.V. Kravtsov, M.L. Markevich et al.*, Uspekhi Fiz. Nauk, **184**, 349, 2014.
2. *R.G. Carlberg, H.K.C. Yee, E. Ellingson et al.*, Astrophys. J. Lett., **485**, L13, 1997.
3. *J. Wolf, G.D. Martinez, J.S. Bullock et al.*, Mon. Not. Roy. Astron. Soc., **406**, 1220, 2010.
4. *A.I. Kopylov, F.G. Kopylova*, Astron. Bull., **70**, 243 2015.

The Fundamental Plane and Other Scaling Relations of Groups and Clusters of Galaxies

F.G. Kopylova[1], A.I. Kopylov[1]

E-mail: *flera@sao.ru*

We present the scaling relations of galaxy groups and clusters derived by using archival data from SDSS and 2MASX catalogs. We applied a new method for determining the size of the galaxy clusters [1] and their effective radius as the radius enclosing half of the galaxies (not half of the luminosity), since the luminosity of the brightest galaxies in groups can exceed 50% of the total luminosity of the group. The characteristics $\log L_K$, $\log R_e$ and $\log \sigma_{200}$ obtained for 94 systems of galaxies ($0.012 < z < 0.09$ and Virgo) define the Fundamental Plane (FP) relation with the scatter of 0.15 that is similar in slope to the FP of clusters of galaxies measured in [2, 3] by other methods and in other bands. We find that the FP of the stellar population of the systems of galaxies in the near-infrared has the slope $L_K \propto R_e^{0.70\pm0.13}\sigma^{1.34\pm0.13}$ and the FP of the hot gas does $L_X \propto R_e^{1.15\pm0.39}\sigma^{2.56\pm0.40}$ or $L_K \propto R_e^{0.81\pm0.21} \log L_X^{0.30\pm0.05}$.

Dynamical and photometric parameters of the early-type galaxies (central stellar velocity dispersion σ, effective radius R_e, mean surface brightness $\langle I_e \rangle$) form the so-called Fundamental Plane [4, 5]. The FP of the galaxies has a significantly lower scatter compared with the earlier obtained Faber–Jackson relation between luminosity and velocity dispersion and the Kormendy relation between surface brightness and radius. Originally, the FP of clusters of galaxies was constructed using observational characteristics of a sample of 16 rich clusters of galaxies ($z < 0.2$) [2]. As a result of fitting, with residuals being minimized in L, they obtained the FP in the form: $L \propto R_e^{0.89\pm0.15}\sigma^{1.28\pm0.11}$.

To construct the scaling relations of our systems of galaxies (see the resume above), we used the one-dimensional dispersion of radial velocities of galaxies σ_{200} found within the radius R_{200}, near-infrared luminosity L_K, and effective radius R_e, enclosing half of galaxies, derived from the observed cumulative galaxy distribution considered as a function of the squared cluster-centric distance. The X-ray luminosity is based on the published data, e.g. [6, 7, 8]. We have found that the form of the FP of groups and clusters is consistent with the FP of the early-type galaxies (Fig. 1) defined in the same way. But they have different zero-points occurring, as we established, due to the difference in the mass-to-light ratio of galaxies and systems of galaxies. The fourth variable, the mass-to-light ratio, included by us in our FP reduces the scatter by about 16% [9], but the slope of the FP does not change.

[1] Special Astrophysical Observatory RAS, Nizhnij Arkhyz, Russia

V. Grinin et al. (eds) Radiation mechanisms of astrophysical objects. Yerevan: Edit Print, 2017, pp. 373–374.

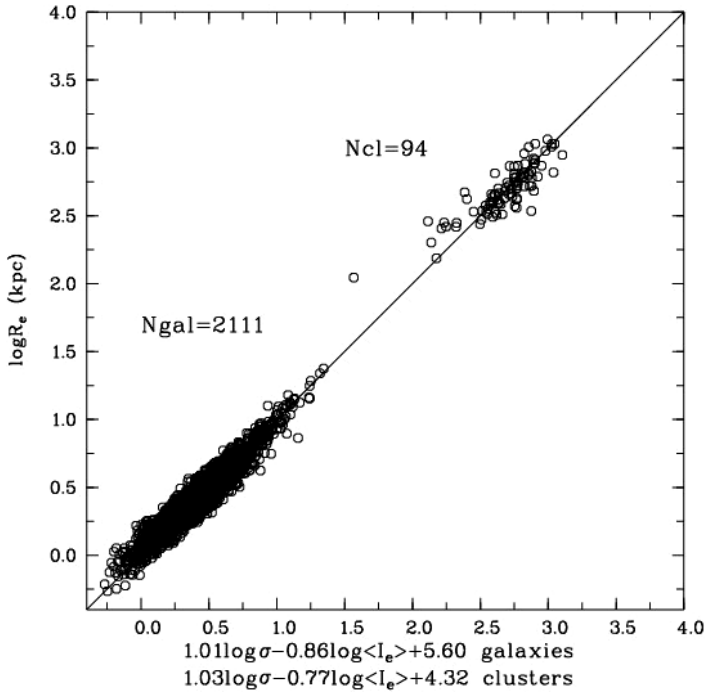

Figure 1: The Fundamental Plane of the galaxies, groups and clusters of galaxies. The effective radius R_e is the radius enclosing half of the galaxies.

References

1. *A.I. Kopylov, F.G. Kopylova*, Astroph. Bull., **70**, 243, 2015.
2. *R. Schaeffer, S. Maurogordato, A. Cappi, F. Bernardeau*, Mon. Not. Roy. Astron. Soc., **263**, L21, 1993.
3. *M. D'Onofrio, D. Bettoni, D. Bindoni et al.*, Astron. Nachr., **334**, 373, 2013.
4. *S. Djorgovski, M. Davis*, Astrophys. J., **313**, 59, 1987.
5. *A. Dressler, D. Lynden-Bell, D. Burstein et al.*, Astrophys. J., **313**, 42, 1987.
6. *H. Ebeling, A.C. Edge, H. Böhringer et al.*, Mon. Not. Roy. Astron. Soc., **301**, 881, 1998.
7. *H. Böhringer, W. Voges, J.P. Huchra et al.*, Astrophys. J. Suppl., **129**, 435, 2000.
8. *A. Mahdavi, M.J. Geller*, Astrophys. J., **607**, 202, 2004.
9. *F.G. Kopylova, A.I. Kopylov*, Astroph. Bull., **71**, 2016.

Simulation of CH_3OH Masers

A.V. Nesterenok[1]

E-mail: *alex-n10@yandex.ru*

A model of CH_3OH maser is presented. Two techniques are used for the calculation of molecule level populations: the accelerated lambda iteration (ALI) method and large velocity gradient (LVG), or Sobolev, approximation. The methods are found to give similar results, provided the gas velocity change across the cloud due to the velocity gradient is much larger than the Doppler line width.

1 Introduction

Intense maser transitions of the CH_3OH molecule are observed towards high-mass star-forming regions. The high brightness temperature of the maser emission permits us to observe them with the very long baseline interferometry (VLBI) technique, achieving both very high angular and velocity resolutions. Modeling of the maser pumping can provide estimates of the physical conditions in the maser regions [1]. The current study is aimed at modeling of the pumping mechanism of methanol masers. The zone of validity of the LVG approximation is discussed.

2 Results

We consider the one-dimensional model of a flat gas-dust cloud. The cloud consists of a mixture of H_2 and CH_3OH molecules, He atoms, and dust particles. The physical parameters of the cloud are the following: number density of H_2 molecules $N_{H2} = 5 \times 10^6$ cm^{-3}, number density of CH_3OH (A- and E-species) $N_m = 100$ cm^{-3}, gas temperature $T_g = 150$ K, dust temperature $T_d = 150$ K, micro-turbulent speed $v_{turb} = 0.5$ km s^{-1}, velocity gradient $dv/dz = 0.05$ km s^{-1} AU^{-1}. Let us define the resonance region length $\Delta z_D = v_D\, dv/dz$, where v_D is the velocity width of the spectral line profile. The LVG approximation with the full treatment of continuum effects [2] and the ALI method [3] were used in the calculations of methanol level populations and line intensities. The detailed description of the model is given in our paper [4].

Fig. 1 shows the dependence of the gain of the maser line at 6.7 GHz at the line center on the cloud depth calculated by means of the ALI method and the LVG approximation. There is a significant discrepancy in the results of two methods at the cloud height $H = 30$ AU. The gain has negative values at almost all cloud depths according to accurate calculations, while the LVG approximation provides

[1] Ioffe Institute, Saint Petersburg, Russia

V. Grinin et al. (eds) Radiation mechanisms of astrophysical objects. Yerevan: Edit Print, 2017, pp. 375–376.

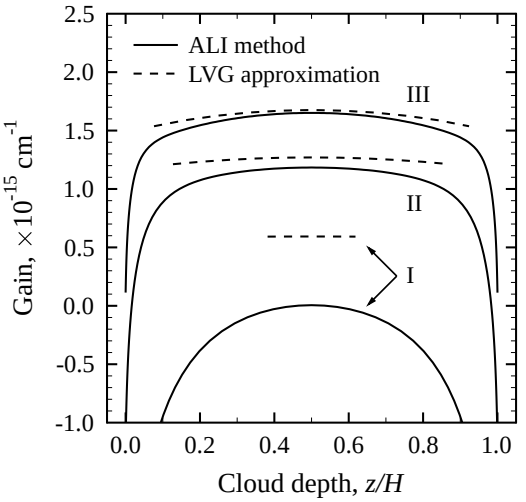

Figure 1: The gain of the 6.7 GHz $5_1 \rightarrow 6_0$ A^+ maser line as a function of the cloud depth. The results are presented for three values of the cloud height: (I) 30 AU; (II) 90 AU; (III) 150 AU. At the parameters in question, $\Delta z_D = 11.5$ AU.

high positive values of the maser gain. There is an agreement between the results of two techniques at large cloud height – the difference between the gain values at the cloud centre is about 10 per cent at $H = 90$ AU and about 2 per cent at $H = 150$ AU. The LVG approximation reproduces the results of accurate radiative transfer calculations at large cloud heights and high velocity gradients: the cloud height has to be of the order of or greater than 5–10 lengths of the resonance region.

References

1. *A.M. Sobolev, M.D. Gray*, Proc. IAU Symp. No. 287, 2012, p. 12.
2. *D.G. Hummer, G.B. Rybicki*, Astrophys. J., **293**, 258, 1985.
3. *G.B. Rybicki, D.G. Hummer*, Astron. Astrophys., **245**, 171, 1991.
4. *A.V. Nesterenok*, Mon. Not. Roy. Astron. Soc., **455**, 3978, 2016.

Correlation of Radial Fluctuations in Deep Galaxy Surveys

S.I. Shirokov[1], Yu.V. Baryshev[1]

E-mail: *lakronous@mail.ru*

Fluctuations of the number of galaxies in different catalogs are compared using the method of estimation of sizes and amplitudes of the radial fluctuations for different redshift bins. The Pearson correlation coefficient of fluctuations derived for these samples has the value $\rho = 0.7 \pm 0.12$ for the redshift interval $0.1 < z < 1.7$. This correlation of independent surveys of different research groups confirms the existence of super-large galaxy structures with sizes up to 1000 Mpc/h.

1 Statement of the problem

Determination of the maximum size of large-scale inhomogeneities in the distribution of galaxies is one of the most important problems in the modern observational cosmology.

For example, the Sloan Digital Sky Survey shows that at small redshifts there are inhomogeneity structures with a size of 400 Mpc/h. This work shows that there are similar and larger structures on large redshifts in the beam surveys. These structures should be correlated in the same fields in independent surveys of different research groups.

2 The method

Estimation of the fluctuation amplitude and size within galaxy distributions method (Fig. 1) was first proposed in [1] and modified in [2]. The left panel of the figure illustrates the wide-angle (CfA, 2df, SDSS) and beam (zCOSMOS, UVISTA, ALHAMBRA) surveys. The right panel shows the visible and model (uniform) galaxy distributions for the beam survey. The gray areas indicate the fields of deficiency or excess of the galaxy number. The fluctuation amplitude is a ratio of the visible galaxy number to the model galaxy number. The fluctuation size is a distance between the zero intersections of fluctuations with different signs.

The compared catalogs are as follows: ALHAMBRA [3], UltraVISTA [4], 10k-zCOSMOS [5], XMM-COSMOS [6], and HDF-N [7].

Table 1 shows the Pirson correlation coefficient ρ, its error σ_ρ, and its authenticity R from Student's table that were used to indicate the catalogs correlation.

[1] Saint Petersburg State University, Russia

V. Grinin et al. (eds) Radiation mechanisms of astrophysical objects. Yerevan: Edit Print, 2017, pp. 377–378.

Table 1: Correlation coefficients

The catalogs pair	ρ	σ_ρ	R
ALH-F4 & XMM-COSMOS	0.82	0.29	0.975
ALH-F4 & UVISTA	0.59	0.36	0.9
ALH-F4 & zCOSMOS	0.58	0.2	0.995
ALH-F5 & HDF-N	0.61	0.21	0.99

3 Results

In the deep COSMOS field there are fluctuations of the number of galaxies on the redshift $z \sim 2$ with the amplitude of 20% and the linear dimensions varying from 500 to 1500 Mpc.

The independent beam surveys of the COSMOS field are consistent in both the amplitudes and the linear dimensions of inhomogeneities with the correlation coefficient equal to 0.7 ± 0.12.

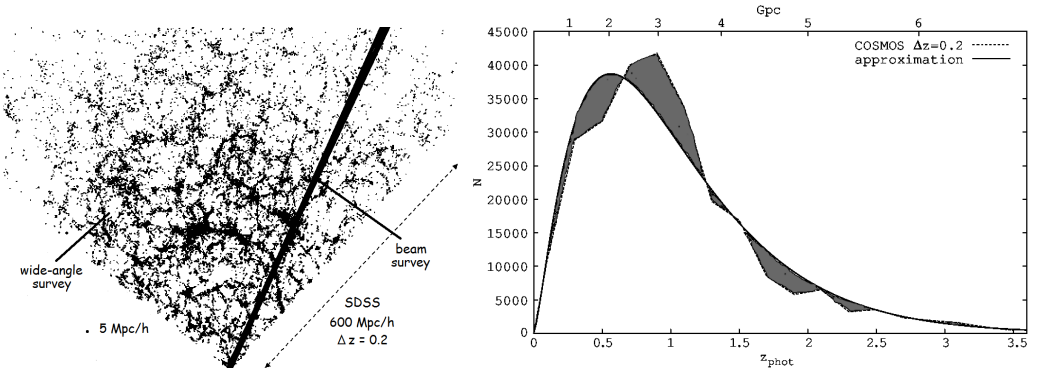

Figure 1: The method illustration.

Acknowledgments. S.S. and Yu.B. thank for the partial financial support the St. Petersburg State University research project No. 6.38.18.2014.

References

1. *N.V. Nabokov, Yu.V. Baryshev*, Astrophys., **53**, 91, 2010.
2. *S.I. Shirokov, D.I. Tekhanovich, Yu.V. Baryshev*, Vestn. Leningr. Univ., 1, **59**, 659, 2014.
3. *A. Molino, N. Benitez, M. Moles et al.*, Mon. Not. Roy. Astron. Soc., **441**, 2891, 2014.
4. *A. Muzzin, D. Marchesini, M. Stefanon et al.*, Astrophys. J. Suppl., **206**, 8, 2013.
5. *K. Kovac, S.J. Lilly, O. Cucciati et al.*, Astrophys. J., **708**, 505, 2010.
6. *M. Brusa, F. Civano, A. Comastri et al.*, Astrophys. J., **716**, 348, 2010.
7. *http://www.stsci.edu/ftp/science/hdf/hdf.html*

The influence of Small Scale Magnetic Field on the Polar Cap X-Ray Luminosity of Old Radio Pulsars

A.I. Tsygan[1], D.P. Barsukov[1,2], K.Y. Kraav[2]

E-mail: *bars.astro@mail.ioffe.ru*

The influence of small-scale magnetic field on the polar cap heating by reverse positrons is considered. We use the polar cap model with steady space charge limited electron flow. To calculate the electron-positron pairs production rate we take into account only the curvature radiation of primary electrons and its absorption in magnetic field. The reverse positron current is calculated in the framework of two models: rapid and gradually screening. It is shown that some pulsars are better described by the rapid screening model and some other pulsars have better agreement with calculation by the gradually screening model.

The polar caps of old radio pulsars are heated by reverse positrons. Such positrons emerge nearby the upper plate of the inner gap, are accelerated within it and hit to the neutron star surface causing the polar cap heating. The reverse positron current is calculated in the framework of two models: rapid [1] and gradual [2, 3] screening. In the first model electron-positron plasma rapidly screens the electric field above the inner gap that leads to a small reverse positron current and hence not so large polar cap heating. In the second model small electric field exists above the inner gap. It causes a substantial increasing of the reverse positron current and hence leads to a strong polar cap luminosity L_{pc}.

The result of calculation of L_{pc} for various ratios of small scale surface magnetic strength B_{sc} to strength B_{dip} of dipolar field is shown in Fig. 1. The polar cap luminosity L_{pc} calculated in the framework of the rapid screening model is shown by slant hatched region and calculated in the framework of the gradually screening model is shown by vertically hatched region.

The discrepancy between the calculated and observed values may be due to presence of some viscous force acting on positrons. The force may be related to the radiation closed inside the gap [11] or radiation coming from deep layers of a neutron star [12].

Acknowledgments. The work of D.P.B. was partly supported by the RFBR (project 13-02-00112).

[1] Ioffe Institute, Saint Petersburg, Russia
[2] SPbPU, Saint Petersburg, Russia

V. Grinin et al. (eds) Radiation mechanisms of astrophysical objects. Yerevan: Edit Print, 2017, pp. 379–380.

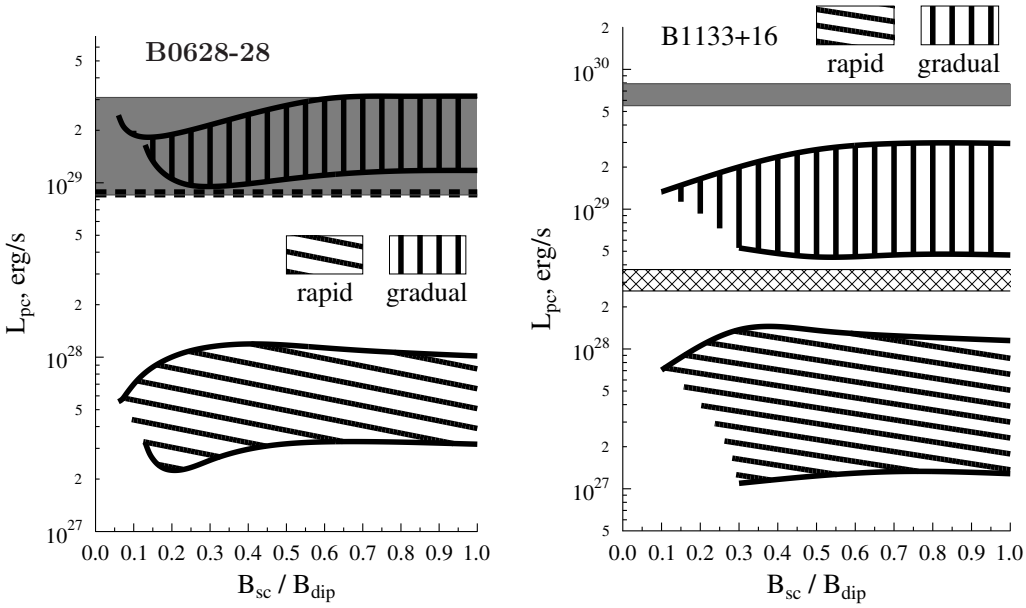

Figure 1: Left: the polar cap luminosity L_{pc} for B0628–28, $B_{dip} = 6.0 \times 10^{12} G$, $P = 1.24s$, $\tau = 2.8 \times 10^6$ years [4], inclination angle $\chi = 30°$ is taken from [5]. The observed L_{pc} range taken from [6] is shown by gray area, L_{pc} from [7] is shown by dashed line. Distance $D = 332^{+52}_{-40}$ pc is taken from [8]. Right: the polar cap luminosity L_{pc} for B1133+16, $B_{dip} = 4.26 \times 10^{12} G$, $P = 1.19s$, $\tau = 5.04 \times 10^6$ years [4], $\chi = 55°$ [9]. The observed L_{pc} value taken from [10] is shown by cross hatched area, L_{pc} range from [6] is shown by gray area.

References

1. *J. Arons, W.M. Fawley, E.T. Scharlemann*, Astrophys. J., **231**, 854, 1979.
2. *A.K. Harding, A.G. Muslimov*, Astrophys. J., **556**, 987, 2001.
3. *Yu.E. Lyubarskii*, Astron. Astrophys., **261**, 544, 1992.
4. *R.N. Manchester, G.B. Hobbs, A. Teoh, M. Hobbs*, Astron. J., **129**, 1993, 2005.
5. *I.F. Malov, E.B. Nikitina*, Astron. Rep., **56**, 693, 2012.
6. *J. Gil, F. Haberl, G. Melikidze et al.*, Astrophys. J., **686**, 497, 2008.
7. *A. Szary*, arXiv: astro-ph/1304.4203, 2013.
8. *A.T. Deller, S.J. Tingay, M. Bailes, J.E. Reynolds*, Astrophys. J., **701**, 1243, 2009.
9. *I.F. Malov, E.B. Nikitina*, Astron. Rep., **55**, 19, 2011.
10. *O. Kargaltsev, G.G. Pavlov, G.P. Garmire*, Astrophys. J., **636**, 406, 2006.
11. *V.M. Kontorovich, A.B. Flanchik*, J. Exp. Theor. Phys. Lett., **85**, 267, 2007.
12. *D.M. Sedrakian, A.S. Harutunyan, M.V. Hayrapetyan*, Astrophys., **57**, 530, 2014.

Faint Radio Galaxies on the Planck Mission Maps

O.V. Verkhodanov[1], E.K. Majorova[1], O.P. Zhelenkova[1], D.I. Solovyov[2], M.L. Khabibullina[1], O.S. Ulakhovich[3]

E-mail: *vo@sao.ru*

We investigate the distribution of emission on the multifrequency Planck maps toward radio sources of several samples separated by spectral index, redshift, morphology.

The "Cold" surveys were conducted at the RATAN-600 radio telescope in the centimeter and decimeter wavelength ranges. The RC (RATAN-Cold) catalog [1] contains multifrequency flux density measurements. The limiting sensitivity of the RCR (RC Refined) catalog is 10 mJy at 1.4 GHz. We investigated the regions with a radius of 1.5 beam widths at the Planck high frequencies for occurrence of a positive signal at the level of the signal-to-noise ratio $1 < S/N < 3$. We prepared the catalog of 117 radio sources with the measurement data and corresponding continuous spectra from the radio to submm range [2, 3]. Independent flux density estimations of the investigated radio sources, which are presented in the Planck catalog (there are 16 such objects in our list), give evidence of the satisfactory accuracy of flux estimation in the introduced method. Energy distribution in radio source spectra is marked by a rise in the submillimeter range and shows evidence of a dust component which present in AGN. The presence of such sources, difficult to clear out from the CMB maps, complicates the statistical analysis of the Planck CMB maps at scales $<7'$. Statistics of CMB peaks in the region of the investigated RCR radio sources show distinction for objects of different types: 1) on average, the flat-spectrum sources (i.e., from the spectral range $-0.5 < \alpha \leq 0.5$) fall into the positive peaks region 1.2 times more often than the steep-spectrum objects if the 1σ detection level is set; 2) the average number of cold spots in the range of $S/N > 2.0$ in the $7'$ vicinity of the RCR sources is very small in comparison both with the data on hot spots and with the models. This fact can prove that the selection of the sources in the microwave range is not random.

The stacked images of the Planck CMB maps for different object populations are shown on Fig. 1. Some topological features, e.g. minima and maxima, are visible in the objects areas. We can conclude that the CMB maps contain signal from radio galaxies and/or their parent galaxy, probably, due to a dust

[1] Special Astrophysical Observatory RAS, Nizhnij Arkhyz, Russia
[2] St. Petersburg Brunch of Special Astrophysical Observatory RAS, Pulkovo, Russia
[3] Physical Faculty of Kazan Federal University, Russia

V. Grinin et al. (eds) Radiation mechanisms of astrophysical objects. Yerevan: Edit Print, 2017, pp. 381–384.

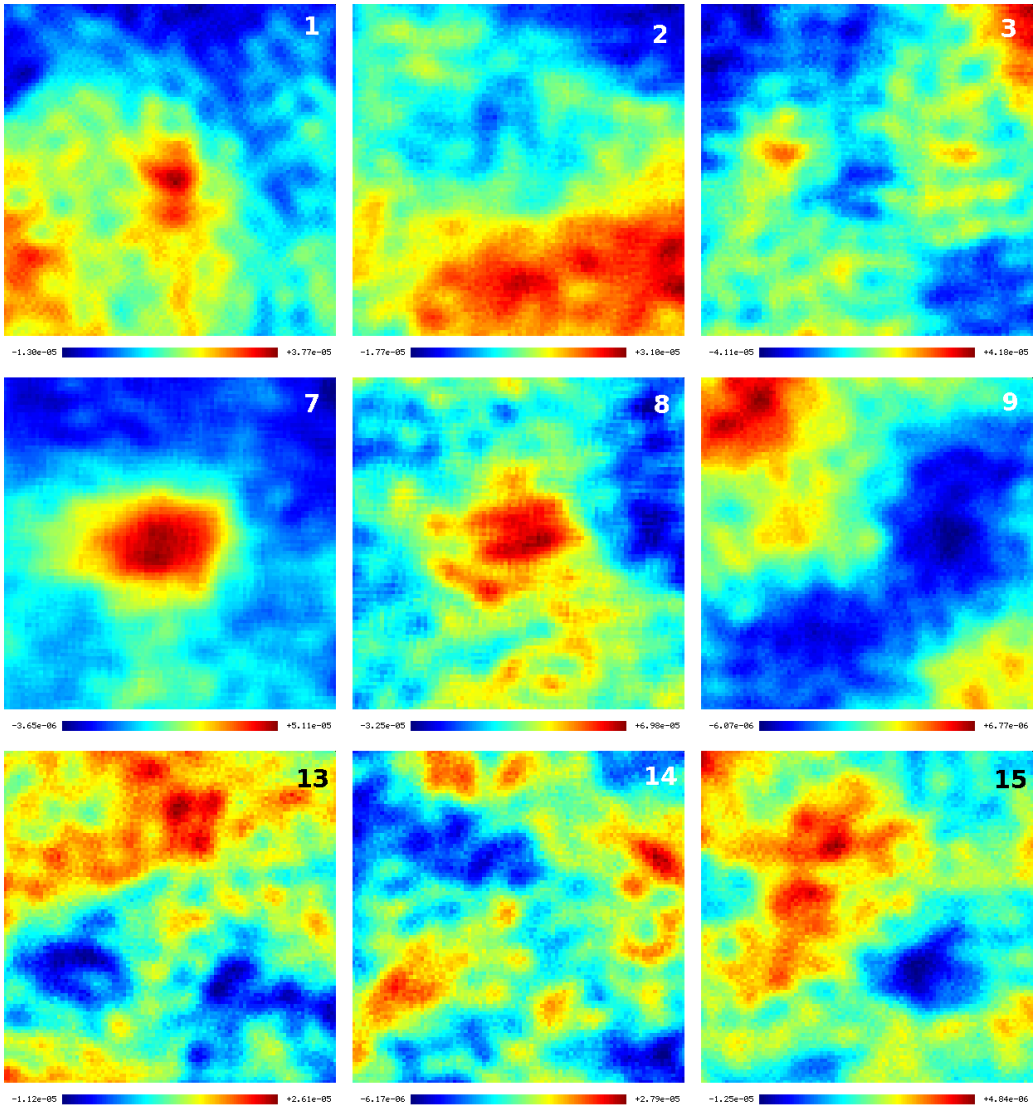

Figure 1: A response from stacking areas from the Planck 2.02 CMB maps around: **(1)** RCR-objects (117 stacked objects); **(2)** giant radio galaxies larger $\theta > 4'$ and 1 Mpc (89 obj.); **(3)** gE and CD galaxies (25 obj.); **(4)** WENSS radio sources (RS) with the radio spectral index $\alpha < -1.1$ (224 obj.); **(5)** WENSS RS, $-1.1 \leq \alpha < -0.75$ (661 obj.); **(6)** WENSS RS, $-0.75 \leq \alpha < -0.5$ (497 obj.); **(7)** WENSS RS, $-0.5 \leq \alpha < 0$ (238 obj.); **(8)** WENSS RS, $\alpha \geq 0$ (19 obj.); **(9)** distant RG, $0.3 \leq z < 0.7$ (1797 obj); **(10)** HZRG, $0.7 \leq z < 1.0$ (205 obj.); **(11)** HZRG, $1.0 \leq z < 1.5$ (149 obj.); **(12)** HZRG, $1.5 \leq z < 2.0$ (103 obj.); **(13)** HZRG, $2.0 \leq z < 2.5$ (77 obj.); **(14)** HZRG, $z \geq 2.5$ (81 obj.); **(15)** BATSE events with t <2s (495 obj.); **(16)** BATSE, t >2s (1540 obj.); **(17)** BeppoSAX, t <2s (87 obj.); **(18)** BeppoSAX, t >2s (694 obj.).

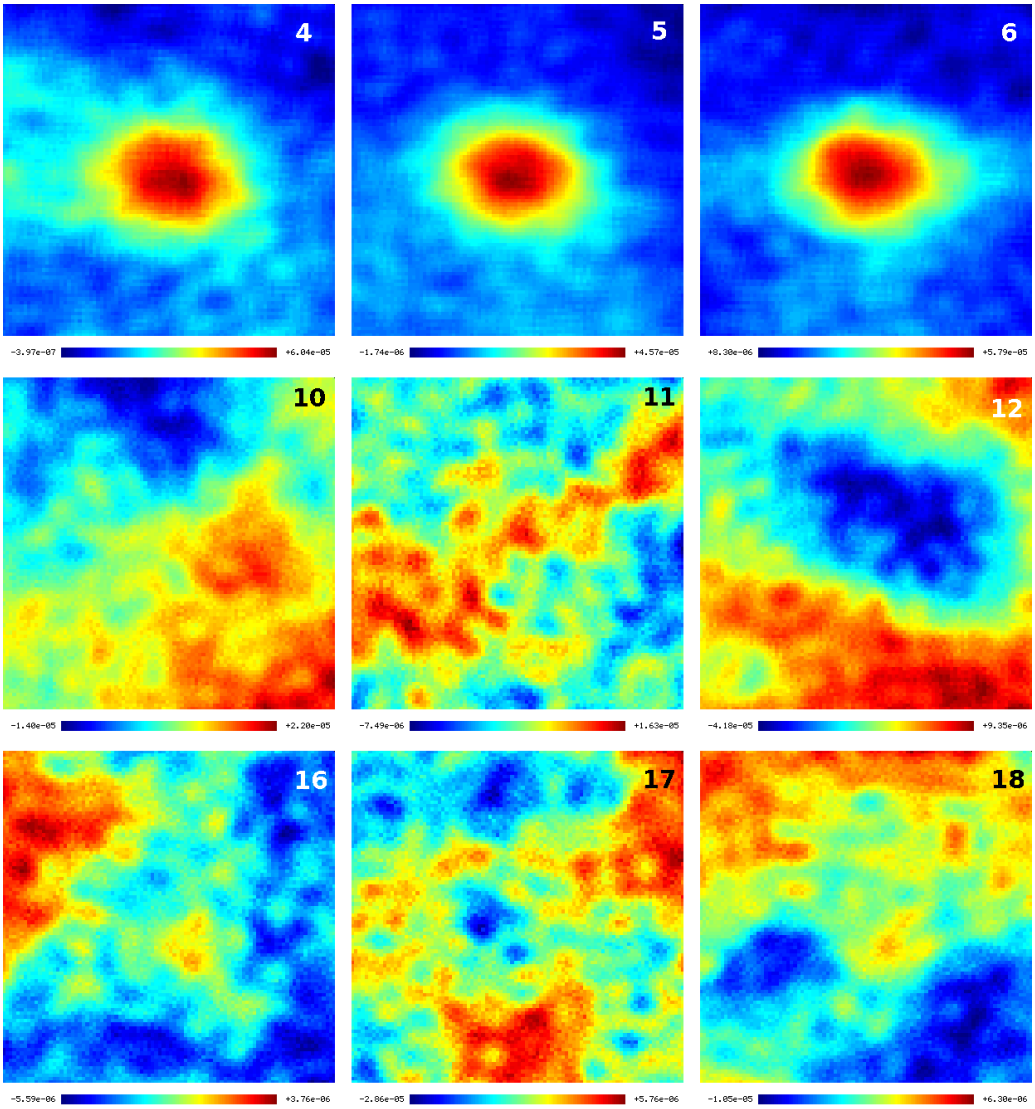
4
-3.97e-07
+6.04e-05
5
-1.74e-06
+4.57e-05
6
+8.30e-06
+5.79e-05
10
-1.40e-05
+2.20e-05
11
-7.49e-06
+1.63e-05
12
-4.18e-05
+9.35e-06
16
-5.59e-06
+3.76e-06
17
-2.86e-05
+5.76e-06
18
-1.05e-05
+6.30e-06

component. This signal contaminates the resulting CMB maps [4]. Objects of different population in the stacked area on CMB maps demonstrate different map topology. Some average zones are connected with response similar to Zeldovich–Sunyaev effect observing like minima on the CMB map. Other ones are gE-galaxies often being a center of clusters, distant RGs with $1.5 \leq z < 2$ in the epoch of active cluster formation. Short BATSE events, probably, connected with neutron stars merging in elliptical galaxies, and giant radio galaxies demonstrate inverse Compton scattering of CMB photons with the RG radio lobes electrons.

References

1. *Yu.N. Parijskij, N.N. Bursov, N.M. Lipovka et al.*, Astron. Astrophys. Suppl., **87**, 1, 1991.
2. *O.V. Verkhodanov, E.K. Majorova, O.P. Zhelenkova et al.*, Astron. Lett., **41**, 457, 2015.
3. *O.V. Verkhodanov, E.K. Majorova, O.P. Zhelenkova et al.*, Astrophys. Bull., **70**, 156, 2015.
4. *O.V. Verkhodanov, D.I. Solovyov, O.S. Ulakhovich, M.L. Khabibullina*, Astrophys. Bull., **71**, 139, 2016.

* The color figures are available online in the Proceedings at *http://www.astro.spbu.ru/sobolev100/*.

Appendices

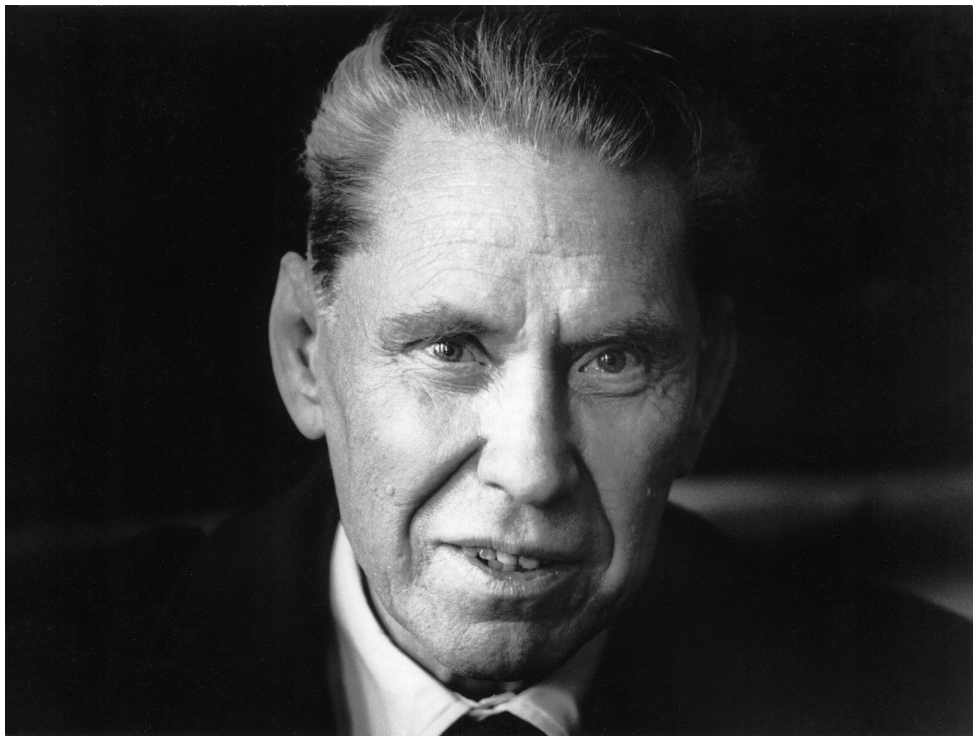

Памяти В.В. Соболева

В.В. Иванов[1]

E-mail: *viva1934@yahoo.com*

I. Жизненный путь

В.В. Соболев прожил долгую спокойную жизнь. По российским меркам XX века, драматических событий в ней не было. Канва этой жизни проста.

Родился в Петрограде 2 сентября 1915 г. Среднее образование получил в одной из лучших школ города – наследнице знаменитой перед революцией Петершуле. Окончив школу, Виктор Соболев поступил на математико-механический факультет Ленинградского университета. В то время его привлекала в первую очередь чистая математика (уже в зрелые годы он говорил, что если бы все же стал математиком, то занимался бы, вероятно, теорией чисел). Однако под влиянием В.А. Амбарцумяна, в то время молодого профессора ЛГУ, интересы студента Соболева сместились – он занялся теоретической астрофизикой. Ей он оставался верен всю жизнь.

[1] Санкт-Петербургский государственный университет

V. Grinin et al. (eds) Radiation mechanisms of astrophysical objects. Yerevan: Edit Print, 2017, pp. 387–421.

Аспирант В.В. Соболев (справа) со своим научным руководителем профессором В.А. Амбарцумяном (фото 1940-х годов)

Окончив университет в 1938 г., В.В. Соболев поступает в аспирантуру к В.А. Амбарцумяну. Весной 1941 г. он защитил кандидатскую диссертацию, поистине замечательную (см. раздел II), и был оставлен в университете. С этого момента до конца жизни В.В. Соболев непрерывно работал в Ленинградском – Петербургском университете, и только в нем – никаких совместительств нигде и никогда, на всем пути от скромного ассистента до всемирно признанного мэтра – академика.

Вскоре после начала войны, в июле 1941 г., В.В. Соболев, освобожденный от призыва в армию по состоянию здоровья, с группой сотрудников ЛГУ эвакуируется в Елабугу, небольшой городок на Каме. Работа в Елабуге оставила глубокий след в душе В.В. Соболева. Трудясь изо дня в день буквально бок о бок – в одной отапливавшейся буржуйкой комнате – с такими гигантами как В.А. Фок, В.И. Смирнов, В.А. Амбарцумян и др., В.В. Соболев за короткое время получает ряд первоклассных научных результатов и одновременно выполняет важные работы оборонного характера.

Вернувшись осенью 1944 г. в Ленинград, В.В. Соболев приступает к преподаванию на кафедре астрофизики в должности ассистента, а вскоре становится доцентом. В 1946 г. – защита докторской диссертации, в 1947 г. – опуб-

ликование по ее материалам первой монографии – «Движущиеся оболочки звезд» (Издательство ЛГУ, 113 стр.). Этой книге суждено было стать классикой теоретической астрофизики. И сегодня, полвека спустя, астрофизики всего мира продолжают широко ее цитировать. В 1948 г., став профессором, В.В. Соболев принимает заведование кафедрой астрофизики от ее основателя, своего учителя В.А. Амбарцумяна, переехавшего к этому времени из Ленинграда в Армению. В этой должности В.В. Соболев проработал более 40 лет, до 1989 г., профессором же астрономического отделения университета он оставался до конца жизни.

В 1956 г. выходит вторая монография В.В. Соболева «Перенос лучистой энергии в атмосферах звезд и планет» (Гостехиздат, М., 391 стр., далее кратко ПЛЭ). По широте охвата рассматривающихся в ней проблем теории многократного рассеяния света она и по сей день остается непревзойденной. В 1958 г. В.В. Соболева избирают членом-корреспондентом АН СССР. К этому времени им было опубликовано около 40 статей.

Человек по натуре властный, ярко выраженный лидер, В.В. Соболев тем не менее старался избегать высоких официальных административных постов. Лишь короткое время, в 1961–62 гг., продолжая оставаться заведующим кафедрой, он был одновременно директором Астрономической обсерватории университета на общественных началах. Убедившись на опыте, что формальное администрирование сильно ограничивает возможность распоряжаться собой и мешает активному личному научному творчеству и преподаванию, ВВ в дальнейшем сумел найти для себя другие, во многом более эффективные способы научно-организационной деятельности. Подробнее об этом мы скажем в разделе IV.

Свое 50-летие В.В. Соболев отмечает окончанием работы над рукописью «Курса теоретической астрофизики» (далее – КТА), вскоре увидевшего свет (Физматгиз, М., 1967, 528 стр.). Второе издание этого учебника вышло из печати в 1975 г. – в год 60-летнего юбилея ВВ, третье – в 1985 г., когда автору книги исполнилось 70 лет. Зная характер ВВ, трудно отделаться от впечатления, что это – не простая случайность, а как бы своеобразные подарки, которые он дарил себе – и одновременно своим читателям, хотя он об этом, конечно, никогда не говорил.

В 1972 г. в выпускавшейся в те годы издательством «Физматгиз» серии монографий «Проблемы теоретической астрофизики», созданной, кстати говоря, по инициативе ВВ, выходит в свет еще одна его книга – «Рассеяние света в атмосферах планет» (325 стр.; далее – РСАП). Ядро этой монографии составляют новые глубокие результаты, полученные В.В. Соболевым в теории многократного рассеяния света в конце 60-х – начале 70-х годов.

В 1981 г. никогда не работавший в системе Академии Наук СССР беспартийный профессор Ленинградского университета В.В. Соболев избирается действительным членом АН СССР – случай по тем временам редчайший, если не уникальный. В 1985 г. В.В. Соболеву присваивается звание Героя Социалистического Труда.

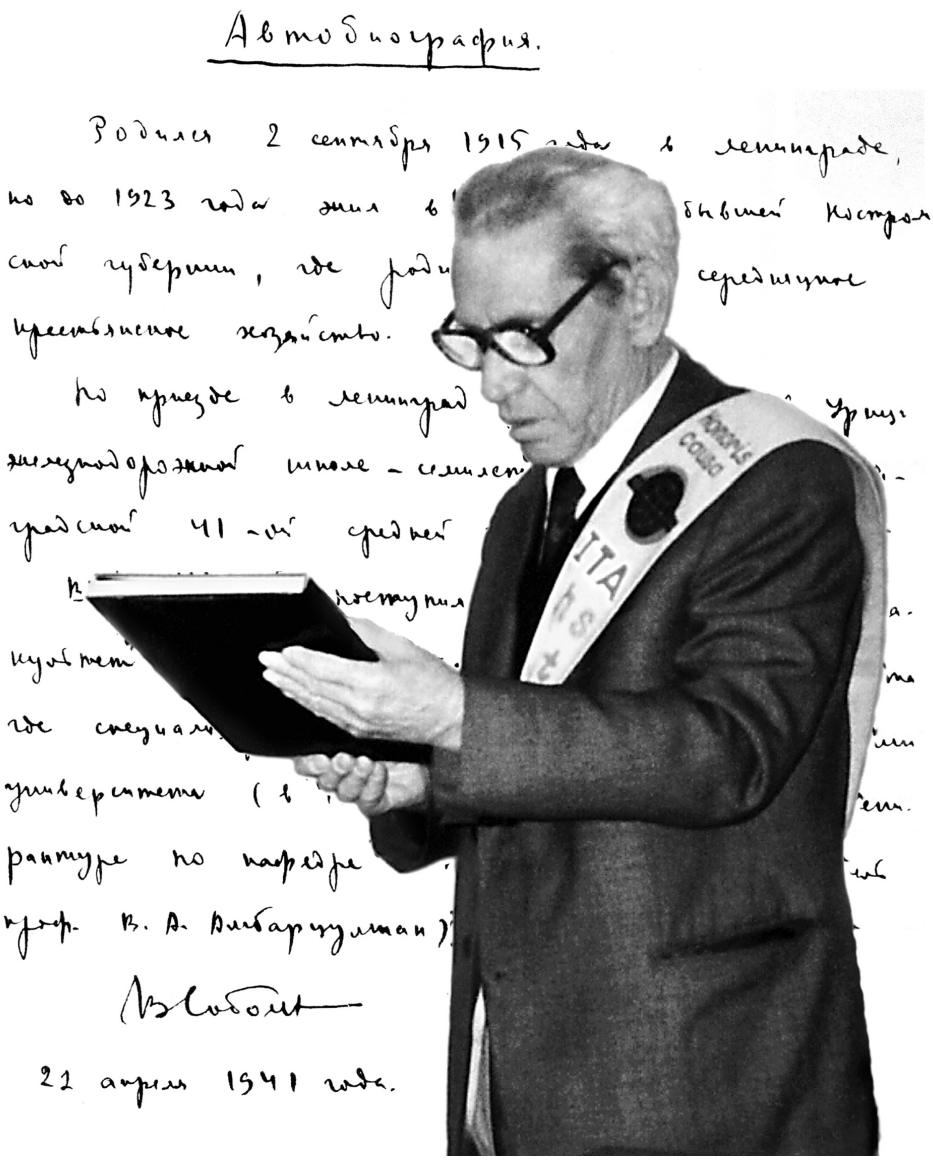

На юбилейном заседании, посвященном 80-летию В.В. Соболева (сентябрь 1995 г.), на фоне рукописной автобиографии, написанной 21 апреля 1941 г.

Достигший высот почета и признания, окруженный многочисленными учениками, на склоне лет, как и всю жизнь, Виктор Викторович продолжает активно работать и много публиковать. Ведь, по Соболеву, «ученый – не тот, кто занимается наукой, а тот, кто не может ею не заниматься». За несколько дней до смерти он завершает вторую корректуру фундаментальной коллективной монографии «История астрономии в России и СССР» объемом 40 печатных листов, написанной под его патронажем и, разумеется, при его участии в качестве автора.

В.В. Соболев в ранние годы

II. Ученый

Содержанием жизни Виктора Викторовича Соболева была наука – та, которую он творил, и та, которую он преподавал. В этом разделе мы опишем то главное из сделанного В.В. Соболевым, что прочно вошло в астрофизику. Область, в которой его вклад был особенно значителен – это аналитическая теория переноса излучения. В сегодняшней астрофизике она стоит несколько особняком, примерно на том же месте, что и теория чисел в математике. Ею занимаются немногие. Любое продвижение вперед трудно. Понять, что здесь делают, и особенно как здесь делают, нелегко – но все согласны в том, что это Наука.

Мы постараемся описать важнейшие результаты В.В. Соболева так, чтобы они стали понятны, хотя бы в общих чертах, по возможности более широкому кругу астрофизиков. Расположение материала – в первом приближении хронологическое, упорядоченное по времени первого обращения ВВ к той или иной проблеме.

Энергетический баланс в газовых туманностях. Сегодня мало кому известно, что обычный ныне метод расчета температур в разреженных астрофизических газовых средах – приравнивание темпа притока энергии к газу

темпу потерь на излучение – был предложен аспирантом В.В. Соболевым в его кандидатской диссертации и опубликован в 1941 г. в «Трудах Астрономической обсерватории ЛГУ», т. 12. К сожалению, почти весь тираж этого издания погиб во время блокады Ленинграда. Шестью годами позже, в 1947 г., этот метод (с небольшими уточнениями) был изложен ВВ в «Движущихся оболочках звезд»; впоследствии он вошел также в КТА. Термостатирующее влияние возбуждаемых столкновениями запрещенных линий в газовых туманностях, о котором узнает сегодня каждый астроном-третьекурсник, было впервые осознано и аккуратно учтено В.В. Соболевым.

Д. Мензел с сотрудниками в одной из статей своего известного цикла работ «Физические процессы в газовых туманностях», датированной 1938 г., также рассматривал энергетический баланс электронного газа, но считал туманность чисто водородной и потому не способной излучать в запрещенных линиях – и в итоге предсказал сильную зависимость температур туманностей T_e от температур T_* возбуждающих их звезд, чего на самом деле нет. В статье того же цикла, вышедшей в 1941 г., уже говорится о термостатирующей роли излучения в запрещенных линиях и приводятся соответствующие оценки, но уравнения энергетического баланса, аккуратно это учитывающего, все еще нет. И только в 1953 г. Л. Аллер получает почти то же уравнение, связывающее T_e и T_*, что и В.В. Соболев в 1941 г. Впрочем, если быть по-соболевски точным, то надо отметить, что у Аллера нет члена, учитывающего энергетические потери на столкновительное возбуждение нейтрального водорода, так что и его результат «не дотягивает» до соболевского.

Приближение полного перераспределения по частотам (ППЧ) в теории образования спектральных линий. Это – один из краеугольных камней всей современной теории звездных спектров. Оно появляется (правда, мельком, без детального обсуждения), еще в 1941 г. в кандидатской диссертации В.В. Соболева (и впоследствии неоднократно переоткрывается: 1942 г. – Дж. Хаутгаст, 1944 г. – Л. Спитцер, 1947 г. – Л.М. Биберман, тот же 1947 г. – Т. Холстейн). В докторской диссертации ВВ (1946 г.) обсуждение приближения ППЧ и вывод соответствующего интегрального уравнения переноса излучения в частотах линии, часто теперь называемого уравнением Бибермана–Холстейна, хотя, как видим, его правильнее было бы называть уравнением Соболева, занимает уже видное место. Здесь же им было введено и широко использовавшееся впоследствии приближенное решение этого уравнения, известное на Западе как on-the-spot-approximation, а у нас – как метод вынесения.

В чем суть приближения ППЧ и почему оно так важно? При рассеянии атомом фотона спектральной линии (т.е. при фотовозбуждении атома с последующим возвращением его на исходный уровень) частота фотона в силу нескольких причин слегка меняется. Так, из-за эффекта Доплера, обусловленного тепловым движением атомов, характерное относительное смещение по частоте $\Delta\nu/\nu \sim u/c$, где u – тепловая скорость. При $T \sim 10^4$ К оказывается

Эта фотография, сделанная в 1950-е годы на астрономической наблюдательной площадке на крыше математико-механического факультета университета, очень нравилась ВВ. Он называл ее в шутку «бандиты на крыше». Слева направо: К.Ф. Огородников, В.В. Домбровский, В.А. Амбарцумян, В.В. Соболев, В.Г. Горбацкий, В.В. Шаронов, О.А. Мельников

$\Delta\nu/\nu \sim 10^{-5}$. Малость этой величины несколько десятилетий буквально завораживала астрофизиков. Казалось, что столь малым эффектом вполне можно пренебречь и считать, что фотоны спектральных линий при рассеяниях строго сохраняют свою частоту (так называемое когерентное, или монохроматическое рассеяние). При этом упускалось из виду, что коэффициент поглощения в линии зависит от частоты очень сильно. Поэтому даже очень малое изменение частоты фотона спектральной линии может сильно менять длину его свободного пробега – параметр, определяющий весь процесс переноса излучения. Эффект оказывается колоссальным. Так, при смещении частоты фотона на 3 доплеровские ширины от центра линии длина его свободного пробега меняется в $\exp(3^2) \sim 10^3$ раз.

Приближение ППЧ, или, как его первоначально называли, приближение полностью некогерентного рассеяния, в определенном смысле противоположно предположению о строгом сохранении частоты при рассеянии. Оно состоит в том, что при каждом рассеянии фотон полностью «забывает» свою первоначальную частоту и может быть переизлучен на любой частоте в пределах линии с вероятностью, пропорциональной значению коэффициента поглощения в линии на этой частоте. В действительности, конечно, между частотами фотона до и после рассеяния есть корреляция, т.е. происходит не пол-

ное, а так называемое частичное перераспределение по частотам. Однако всего после нескольких рассеяний информация о первоначальной частоте фотона во многих случаях полностью замывается – и в этом суть того, почему в сильно рассеивающих средах приближение ППЧ обычно хорошо работает.

Возможность больших изменений длин пробегов фотонов при рассеяниях *качественно* меняет весь процесс переноса излучения. Он оказывается совершенно не похож на обычную диффузию. Удаленные объемы газа получают возможность эффективно взаимодействовать напрямую, обмениваясь фотонами в крыльях линий, и поэтому процесс переноса становится существенно нелокальным. Аппаратом для описания таких явлений служат интегральные, но никак не дифференциальные уравнения. Уравнение диффузии здесь не годится даже в качестве первого приближения. Поэтому введение приближения ППЧ фактически открыло новую главу в физике явлений переноса. Сегодня приближение ППЧ широко используется не только в астрофизике, но и в оптике газового разряда, в физике плазмы, при изучении люминесценции и даже в теории экситонов.

В 40-е – 50-е годы В.В. Соболев несколько раз возвращался к проблемам образования линий в рассеивающих атмосферах с учетом перераспределения по частотам. Им впервые были получены точные решения задачи об образовании линий в звездных спектрах в приближении ППЧ для модели Милна–Эддингтона (1949 г.). Важные дополнения, связанные с интерпретацией центральных остаточных интенсивностей сильных резонансных фраунгоферовых линий, были сделаны в работе 1954 г. Не ограничиваясь приближением ППЧ, в 1955 г. В.В. Соболев (одновременно с В. Унно) получил выражения для усредненных по углам функций перераспределения, известных теперь как R_I и R_{II}. Сравнив численные решения уравнения переноса излучения в приближении ППЧ и при частичном перераспределении по частотам при чисто доплеровском уширении (т.е. с R_I), В.В. Соболев впервые количественно оценил точность приближения ППЧ. Было доказано, что в этом конкретном случае она очень высока. И это было сделано еще в докомпьютерную эпоху!

Многократное рассеяние поляризованного излучения. В 1943 г., находясь в эвакуации в Елабуге, не достигший и 30 лет В.В. Соболев выполняет еще одну важную работу. Он получает уравнение переноса излучения с учетом поляризации (для случая рэлеевского рассеяния) и исследует его решения. К сожалению, публикация полученных результатов из-за трудностей военного и послевоенного времени задержалась. Впервые доложенные на юбилейной научной сессии ЛГУ в 1944 г., о чем есть краткое сообщение в Трудах этой сессии, в полном виде эти важные результаты увидели свет лишь пятью годами позже, в 1949 г., в первом послевоенном выпуске «Трудов АО ЛГУ» (том 13). [Впоследствии без изменений и дополнений они вошли в ПЛЭ, гл. V]. Между тем в начале 1946 г. С. Чандрасекар также получил векторное уравнение переноса излучения для рэлеевского рассеяния и приступил к деталь-

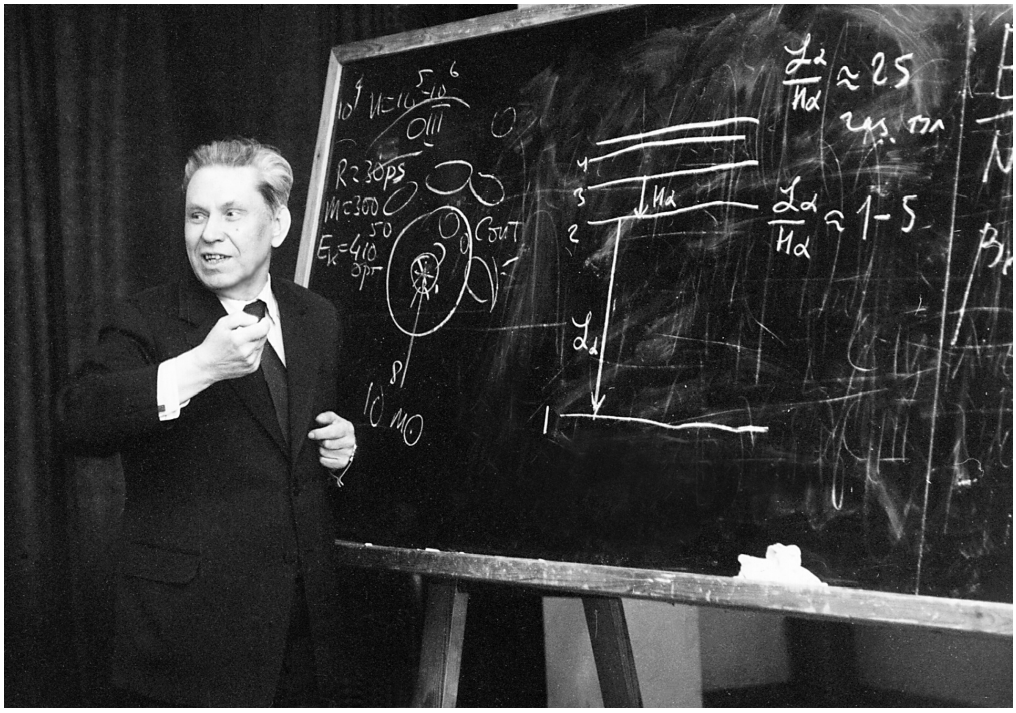

В.В. Соболев на семинаре (1970-е годы)

ному исследованию его решений. В том же 1946 г. первые его результаты были опубликованы в Astrophysical Journal. Поэтому на Западе принято считать, что многократное рассеяние поляризованного излучения впервые было исследовано С. Чандрасекаром. В действительности же В.В. Соболев, пользуясь иным (более простым) математическим аппаратом, получил решения тех же задач примерно тремя годами раньше.

Любопытный исторический факт: ни Чандрасекар, ни Соболев в действительности не были первыми, кто правильно написал уравнение переноса поляризованного излучения. Задолго до них, еще в 1924 г., это было сделано Р. Гансом, однако его работа была полностью забыта (и лишь в 70-х годах ее «раскопал» соболевский ученик Х.Домке). Однако, судя по всему, В.В. Соболев был в самом деле первым, кто получил *решения* векторного уравнения переноса.

То, что побудило ВВ начать исследование переноса поляризованного излучения, к астрономии отношения не имело. В Елабуге по заданию военных организаций В.В. Шаронов занимался проблемами видимости предметов и огней в атмосфере. В.В. Соболев вспоминает: «Однажды В.В. Шаронов сказал мне, что рассеянный свет является поляризованным, и если надеть очки, которые пропускают только одну компоненту света, то видимость можно улучшить. В связи с этим я приступил к разработке теории рассеяния поляризованного света».

В работе ВВ, выполненной в Елабуге в 1943 г., были решены три задачи. Во-первых, был рассчитан ход поляризации по диску звезды с рассеивающей чисто электронной атмосферой и установлено, что вблизи края она должна достигать почти 12%. Другим методом тот же результат в 1946 г. был найден Чандрасекаром. Во-вторых, была рассчитана поляризация (и интенсивность) излучения, диффузно отражаемого от чисто молекулярной планетной атмосферы, освещаемой солнечными лучами, падающими строго по вертикали. В-третьих, В.В. Соболевым впервые был поставлен (и разрешен) вопрос о нахождении поля поляризованного излучения в глубоких слоях освещаемой извне атмосферы, в которой происходит неконсервативное рэлеевское рассеяние. Этот вопрос С. Чандрасекар не рассматривал вовсе.

Метод, использовавшийся В.В. Соболевым для расчета интенсивности и поляризации излучения, выходящего из плоско-параллельной атмосферы, состоял по существу в применении к уравнению переноса преобразования Лапласа по пространственной переменной. Это позволяет, после ряда преобразований, получить линейные интегральные уравнения для непосредственно наблюдаемых величин – интенсивностей (точнее, векторов Стокса) выходящего из атмосферы излучения. Этот метод, развитый В.В. Соболевым в Елабуге, первоначально был применен им к задачам изотропного и анизотропного рассеяния без поляризации (соответствующие результаты были опубликованы в трех статьях 1949 г.; они составляют содержание гл. IV монографии ПЛЭ), а затем тут же – и к проблемам рэлеевского рассеяния с поляризацией.

После первой своей пионерской работы по поляризации В.В. Соболев надолго теряет интерес к этой тематике. Лишь тридцать лет спустя, в 1979 г., он снова обращается к многократному рэлеевскому рассеянию. Был найден простой способ получения асимптотик векторов Стокса излучения, диффузно отраженного и диффузно пропущенного оптически толстой атмосферой. Совместно с В.М. Лоскутовым были также выполнены обширные расчеты поляризации излучения, выходящего из плоского слоя с различного вида распределенными внутренними источниками и даны применения полученных результатов к истолкованию поляризации излучения рентгеновских двойных и квазаров.

Асимптотики полей излучения. ВВ любил красивые простые формулы. Цитируя Эпикура, он говорил своим ученикам, что в этом мире все важное просто, а все сложное – не важно. В.В. Соболев получил в теории переноса много простых красивых важных формул. Почти все они описывают те или иные предельные режимы полей излучения, которые чаще всего и реализуются в природе.

Первые формулы такого рода были найдены ВВ еще в Елабуге (частично совместно с В.А. Амбарцумяном). Это были асимптотические выражения для интенсивностей излучения, диффузно отраженного и диффузно пропущенного оптически толстой изотропно рассеивающей атмосферой. Они были

В.В. Соболев и В.В. Иванов беседуют с С. Чандрасекаром
(Бюракан, Армения, 1981 г.)

выражены через величины, описывающие поле излучения в атмосфере бесконечно большой оптической толщины. Эти результаты были опубликованы далеко не сразу – лишь в 1956 г., в ПЛЭ, гл. III. Ряд других близких к этим по своей природе результатов, получивших впоследствии не совсем точное название глубинных асимптотик, был найден ВВ в начале 50-х годов и также впервые опубликован в ПЛЭ. В предшествовавшей этой книге В.В. Соболева знаменитой монографии С. Чандрасекара "Radiative Transfer" (Oxford, 1950) результатов такого типа фактически нет.

Большинство асимптотик, относящихся к анизотропному рассеянию, было получено несколько позже. Они неоднократно переоткрывались многими авторами (в том числе и В.В. Соболевым). Изложение этих результатов занимает заметное место в РСАП.

Другой тип асимптотик, существование которых было обнаружено В.В. Соболевым (и независимо Х. ван де Хюлстом), появляется в случае почти чисто рассеивающих сред. Асимптотическая теория позволяет по известному полю излучения при чистом рассеянии находить поправки, вызываемые тем, что в среде происходит гибель фотонов из-за (малого) истинного поглощения.

Привив своим ученикам вкус к изучению асимптотических режимов, ВВ полностью оставил на их долю исследование нетривиальных асимптотик полей излучения в частотах линий, а также асимптотических режимов в нестационарных задачах теории переноса.

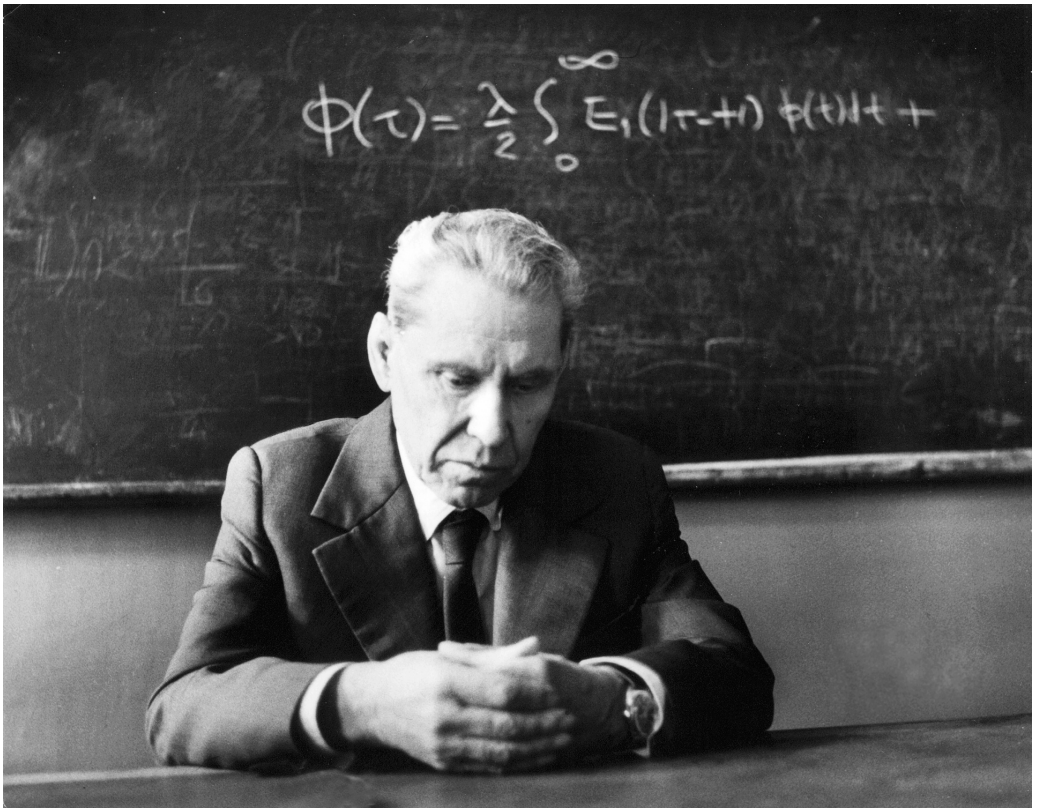

В.В. Соболев размышляет (фото 1980-х годов)

Теория образования линий в движущихся средах, или то, что на Западе известно как the Sobolev theory. Это, несомненно, самое известное – и самое замечательное – из всего, сделанного В.В. Соболевым. Основная мысль очень проста, но извлеченные из нее В.В. Соболевым следствия поистине удивительны.

Если в движущейся среде есть градиент скорости (точнее, градиент проекции скорости на направление распространения излучения), то из-за сильной зависимости коэффициента поглощения в линии от частоты доплеровские смещения должны сильно изменять длины свободных пробегов фотонов. Пролетев достаточно большое расстояние, фотон практически теряет способность возбуждать атомы, так как смещается по частоте за пределы линии. В итоге, если градиент скорости велик, то удаленные объемы почти перестают взаимодействовать за счет обмена фотонами в линиях. Это ведет к колоссальным упрощениям. Нелинейная система уравнений стационарности, «сцепленных» с интегро-дифференциальными уравнениями переноса излучения в линиях, радикально упрощается – она алгебраизуется, хотя и остается нелинейной. Теория Соболева впервые (еще до появления компьютеров) позволила рассчитать населенности уровней атомов в газе в условиях, когда вклад ради-

ативных возбуждений собственным излучением среды является определяющим, но условия очень далеки от локального термодинамического равновесия. Вопреки тому, что принято было думать, наличие макроскопических движений, происходящих со сверхзвуковыми скоростями, ведет не к усложнению, а к радикальному упрощению проблемы.

Построенную им теорию В.В. Соболев применил к интерпретации интенсивностей и профилей линий в спектрах звезд Вольфа-Райе, Ве и близких к ним по кинематике объектов. Позже теория Соболева нашла широкое применение при количественной интерпретации особенностей спектров также многих других объектов – квазаров, активных ядер галактик, космических мазеров и др. Эта теория лежит в основе современных детальных количественных теорий звездного ветра. Ее популярность среди теоретиков-астроспектроскопистов очень велика.

В учебнике Д. Михаласа «Звездные атмосферы» (Freeman and Co., San Francisco, 1978) есть раздел "Sobolev theory", а в книге Дж. Кассинелли и Х. Ламерса "Introduction to Stellar Winds", печатающейся сейчас в издательстве Кембриджского университета, вводятся следующие понятия: the Sobolev limit, the Sobolev region, the Sobolev optical depth, the Sobolev length, the Sobolev approximation и the Sobolev point.

Несколько исторических замечаний о не совсем обычной судьбе этой теории. В 1944–1947 гг. появились три статьи В.В. Соболева в Астрономическом журнале, в которых содержались основные идеи этой теории. И тут же, в 1947 г., увидела свет та ее окончательная форма, которая широко известна по «Движущимся оболочкам звезд». Лишь один раз, в ставшей впоследствии хорошо известной статье 1957 г., также опубликованной в Астрономическом журнале, В.В. Соболев вернулся к этой теории и заметно ее дополнил. Отказавшись от делавшегося ранее предположения о том, что градиент скорости велик, он распространил свою теорию на случай произвольного градиента скорости и произвольного профиля поглощения. За это пришлось заплатить дорогую цену – ограничиться рассмотрением модели атома с двумя уровнями, причем вместо алгебраических уравнений появились интегральные.

Среди отечественных астрофизиков теория Соболева быстро завоевала популярность, однако на Западе на нее долгое время не обращали внимания, даже и после появления в 1960 г. в издательстве Гарвардского университета английского перевода «Движущихся оболочек звезд». Как-то в конце 60-х годов, узнав, что на эту его книгу в Америке по-прежнему ссылаются мало, ВВ спокойно заметил: «Значит, время еще не пришло. Придется подождать» (а к тому моменту со времени создания теории прошло уже более 20 лет). И все же он оказался прав. Начиная со второй половины 70-х годов the Sobolev approximation стало в теории образования линий едва ли не столь же стандартным, как и общеизвестное приближение Эддингтона – в проблемах монохроматического рассеяния.

Судьба соболевской теории расчета возбуждения атомов и формирования линейчатых спектров в движущихся средах уникальна и еще в одном отношении. Не будь эта теория построена Соболевым в раннее докомпьютерное время, ее, возможно, так никогда и не развили бы. Теперь, когда мощные компьютеры позволяют решать нелинейные задачи методом грубой силы, «в лоб», точные численные решения были бы, конечно, получены и без соболевского приближения. Но физическое истолкование результатов таких расчетов и сегодня фактически основывается на том понимании сути дела, которое дала теория Соболева.

Любопытно, что толчком к развитию обрисованной только что в общих чертах теории (как и к введению приближения ППЧ) послужила для ВВ весьма частная задача о расчете светового давления в линии L_α в планетарных туманностях.

За полвека, прошедшие с момента создания соболевской теории, появилось немало работ, в которых она обобщается, уточняется, дополняется за счет учета тех или иных ранее не принимавшихся во внимание факторов, таких как поглощение в континууме, поляризация и т.п. Это естественно. Однако теория в целом блестяще выдержала испытание временем. Все дополнения выглядят как небольшие переделки и малые пристройки к зданию, которое изначально было построено добротно и стоять которому суждено еще долго.

Резольвентный метод Соболева. Как и во всякой области физики, в теории многократного рассеяния света есть набор стандартных задач, решаемых до конца, которые составляют основную базу теории. В данном случае ими служат задачи о нахождении полей излучения в плоских оптически однородных атмосферах.

При изотропном монохроматическом рассеянии, а также при рассеянии в линии с ППЧ дело сводится к решению некоторого линейного интегрального уравнения с симметричным разностным ядром. Это основное интегральное уравнение теории переноса излучения. Его решение – так называемая функция источников.

Для полного решения проблемы при произвольном распределении в среде внутренних первичных источников надо найти резольвенту $\Gamma(\tau, \tau')$ этого интегрального уравнения. В середине 50-х годов В.В. Соболев установил, что $\Gamma(\tau, \tau')$, представляющая собой функцию двух переменных (и параметра τ_0 – оптической толщины среды) может быть выражена через функцию одной переменной $\Phi(\tau)$ (и параметра τ_0). Функция $\Phi(\tau)$ является частным значением резольвенты: $\Phi(\tau) = \Gamma(0, \tau)$. Ее называют резольвентной функцией Соболева. При $\tau_0 = \infty$ (полубесконечная атмосфера) функцию $\Phi(\tau)$ удается найти в явном виде.

ВВ указал два способа получения этих важных результатов. Один из них (он приводится в ПЛЭ, гл. VI) был по своему духу эвристическим, родственным принципам инвариантности. Он основывался на вероятностной интерпретации задач о многократном рассеянии света, введенной ВВ за несколько лет

Учитель и ученик снова вместе в Ленинградском университете:
В.А. Амбарцумян (слева) и В.В. Соболев в дни празднования 100-летия
Астрономической обсерватории ЛГУ (май 1980 г.)

до этого (в 1951 г.). Другой способ (1958 г.) был чисто формальным и основывался на анализе интегрального уравнения для функции источников. Ключевую роль в этом втором подходе играет тот факт, что ядерная функция основного интегрального уравнения представляет собой суперпозицию экспонент. Этот подход позволил продвинуться несколько дальше, чем это было сделано первоначально (в ПЛЭ) из эвристических соображений. Эти результаты были включены ВВ в английское издание ПЛЭ ("A Treatise on Radiative Transfer", Princeton, 1963) в виде отдельного приложения и стали известны на Западе как резольвентный метод Соболева.

ВВ установил, что при $\tau_0 = \infty$ резольвентная функция $\Phi(\tau)$ удовлетворяет некоторому уравнению Вольтерра. Решив его, т.е. найдя $\Phi(\tau)$, мы получаем $\Gamma(\tau, \tau')$ и тем самым – решение исходного интегрального уравнения для функции источников (типа Винера–Хопфа) при произвольном свободном члене. Сходное (несколько более сложное) уравнение было получено для $\Phi(\tau, \tau_0)$ и при конечных τ_0.

Резольвентный метод Соболева нашел широкое применение. Он стал мощным средством получения точных и асимптотических решений широкого круга проблем многократного рассеяния. По используемому в нем матема-

тическому аппарату он значительно проще не только классического метода Винера–Хопфа, опирающегося на довольно тонкие идеи теории функций комплексной переменной, но и появившегося почти одновременно с ним метода Кейза, состоящего в разложении решения по сингулярным собственным функциям оператора переноса.

Тем, для кого слова про интегральные уравнения, резольвенты, сингулярные собственные функции и т.п., звучат пугающе, попробуем пояснить суть сделанного В.В. Соболевым в чисто физических терминах. Пусть требуется научиться находить поле излучения в рассеивающих плоских атмосферах с распределенными в них источниками излучения. Считается, что мощность источников зависит только от одной координаты – глубины, причем источники испускают излучение во все стороны одинаково (изотропно). Излучаемые ими фотоны испытывают многократные рассеяния в среде, причем после каждого рассеяния фотоны переизлучаются во все стороны с равной вероятностью. Имеется также некоторая вероятность того, что фотон при рассеянии гибнет. Кроме того, фотоны могут выбывать из процесса многократных рассеяний, вылетая из среды через ее границы. Подчеркнем, что зависимость мощности источников от глубины в атмосфере произвольная. Так вот, В.В. Соболев сумел показать, что для решения *всех* таких задач, различающихся распределением первичных источников, достаточно решить всего *одну* задачу – именно, найти поле излучения в атмосфере, на границе которой имеется тонкий светящийся слой. Согласитесь, это кажется весьма неожиданным.

Общая теория анизотропного рассеяния света. В конце 40-х годов С. Чандрасекар на нескольких частных примерах показал, что в задачах об анизотропном многократном рассеянии света наряду с обычным уравнением переноса можно построить некоторое другое, гораздо более простое уравнение, решение которого также позволяет получить полное поле излучения. Суть упрощения состояла в том, что С. Чандрасекару удалось решение *системы* интегральных уравнений, возникающих в задачах анизотропного рассеяния, заменить решением *одного* уравнения. Общей теории С. Чандрасекар не развил, ограничившись исследованием двух простейших частных случаев – линейно-анизотропного рассеяния и рассеяния с рэлеевской индикатрисой. Он писал, что «полное исследование... прольет некоторый свет на основную структуру теории переноса».

Штурм проблемы продолжался 20 лет. Хотя за это время и были сделаны существенные шаги вперед, в частности, И. Кущером и И. Басбридж, до полного решения было, как потом оказалось, еще далеко. Полное решение проблемы было дано В.В. Соболевым в серии работ конца 60-х годов. Это – ядро его монографии РСАП. Удалось установить, что при *любой* разлагающейся по полиномам Лежандра индикатрисе рассеяния расчет каждой из азимутальных гармоник поля излучения сводится к решению всего *одного* интегрального уравнения. Показать это очень непросто. Физической интер-

В рабочем кабинете в Петергофе (начало 1980-х годов)

претации вводимых в ходе преобразований величин и окончательных уравнений нет. Замечательно, что получающиеся уравнения имеют симметричные разностные ядра и их можно решить описанным выше в общих чертах резольвентным методом.

Как и предполагал Чандрасекар, полное решение проблемы действительно пролило свет на основную структуру теории переноса, причем этот свет оказался очень ярким.

В.В. Соболев не ограничился развитием теории анизотропного рассеяния в направлении, намеченном С. Чандрасекаром. Он получил также линейные интегральные уравнения для непосредственно наблюдаемых величин – интенсивностей выходящего из атмосферы излучения (при ее освещении извне). Этот подход позволил полностью обойти нахождение поля излучения внутри среды, и в этом одно из его преимуществ. Другое его достоинство – нет нужды в разложении индикатрисы по сферическим функциям.

Другие исследования. Результаты, описанные выше, стали в свое время заметными вехами в развитии нескольких разделов астрофизики. Они вошли в учебники и справочные руководства и продолжают активно использоваться по сей день.

У ВВ было много и других работ высокого класса, но они все же, пожалуй, «не дотягивают» до тех, о которых говорилось выше. Впрочем, подобные оценки всегда субъективны, и давать их надо с большой осторожностью.

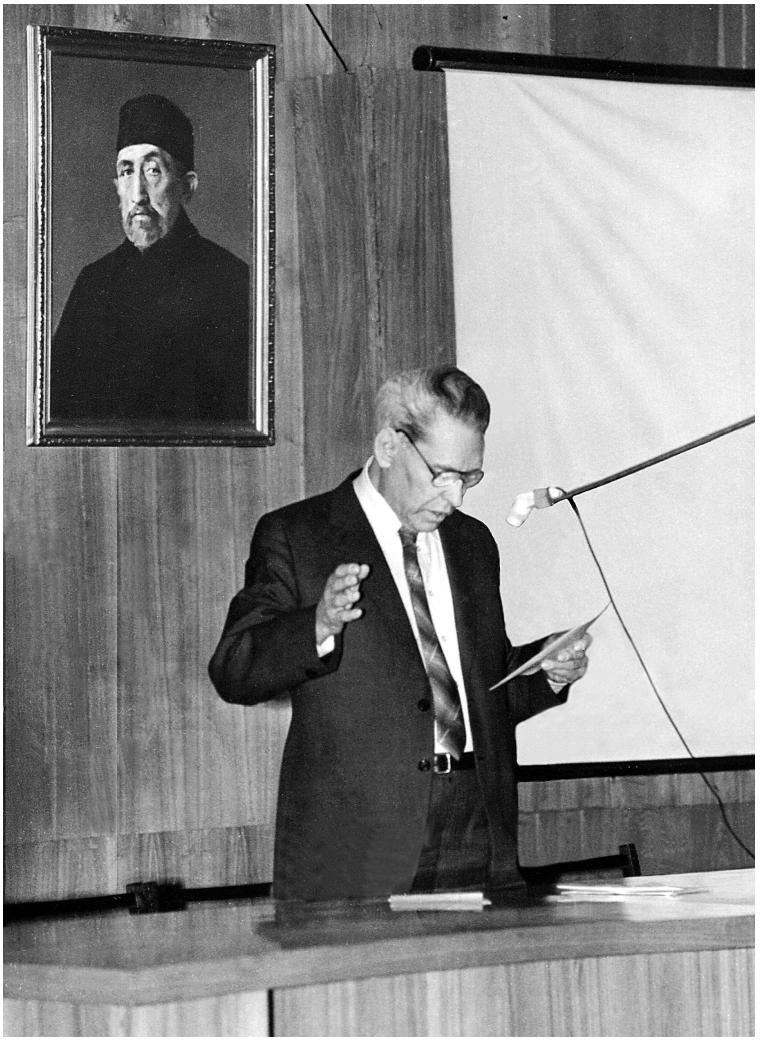

Выступление на хвольсоновском симпозиуме (октябрь 1990 г.)

Несколько интересных работ было посвящено исследованию полей излучения в планетных атмосферах. В 1944 г. ВВ опубликовал используемый и сегодня приближенный способ расчета полей излучения в планетных атмосферах. Суть приближения состоит в том, что рассеяние первого порядка учитывается точно, рассеяния же старших порядков – приближенно, путем удержания в разложении по полиномам Лежандра индикатрисы рассеяния и интенсивности излучения лишь двух членов. В нескольких работах (1944, 1964, 1968 гг.) исследовались свойства частиц облачного слоя Венеры. По данным об изменении блеска и поляризации с фазой были оценены альбедо частиц (оказавшееся очень близким к единице) и степень вытянутости их индикатрисы рассеяния. В 1972 г. ВВ построил теорию формирования слабых линий поглощения в рассеивающих планетных атмосферах большой оптической толщины.

Ряд работ ВВ 40-х и 50-х годов был посвящен применению теории движущихся оболочек звезд к конкретным объектам – звездам WR, Be и др. Эти ранние работы сейчас представляют, пожалуй, лишь исторический интерес. Им исследовалось также влияние электронного рассеяния в атмосферах звезд ранних типов и у сверхновых на особенности их спектров.

В рамках простой кинематической модели, без детального рассмотрения гидродинамики разлета оболочек, были интерпретированы кривые блеска новых (1954 г.) и сверхновых (1979 г.) звезд. Несмотря на то, что впоследствии появились многочисленные рафинированные гидродинамические численные расчеты, простые решения Соболева сохраняют свое значение и используются в теории сверхновых до сих пор.

Исследования вспыхивающих звезд, выполненные ВВ совместно с В.П. Грининым (1977 г.), показали, что вспышки, по-видимому, происходят глубже, чем считалось до этого.

Этот обзор «прикладных» работ ВВ, сделанный скороговоркой, далеко не полон. Были еще работы и о белых карликах, и о красных гигантах, и о солнечных протуберанцах, и о пылевых туманностях, и даже по звездной статистике – всего не перечесть.

Подведем общий итог. Исследования В.В. Соболева – это в первую очередь разработка новых методов анализа сложных процессов взаимодействия излучения и вещества в космосе – от планетных атмосфер до квазаров, и лишь в гораздо меньшей степени – изучение конкретных астрономических объектов. Образно говоря, В.В. Соболев был оружейником – он создавал то оружие, которым другие ведут штурм астрономических крепостей природы.

III. Педагог

В.В. Соболев был не только глубоким исследователем, но и замечательным педагогом – настоящим Учителем.

Все астрофизики бывшего СССР, и не только они, прекрасно знают его «Курс теоретической астрофизики» (КТА). Они или учились по нему сами, или учили своих студентов. Этот курс, выдержавший у нас три издания и переведенный в Америке и во Франции, вырос из лекций, которые ВВ многие годы читал в Ленинградском университете. Появление этого учебника фактически установило стандарт, которому старались следовать едва ли не во всех университетах СССР, где готовили астрономов. Появлению КТА предшествовало опубликование двух других учебников астрофизики на русском языке: В.А. Амбарцумян, Э.Р. Мустель, А.Б. Северный, В.В. Соболев – Теоретическая астрофизика (ГИТТЛ, М., 1952) и Курс астрофизики и звездной астрономии, под ред. А.А. Михайлова (т. I – ГИТТЛ., М., 1951; т. II – Физматгиз, М., 1962). В обоих этих учебниках В.В. Соболеву принадлежало по нескольку глав. Их материал в дополненном и переработанном виде впоследствии вошел в КТА.

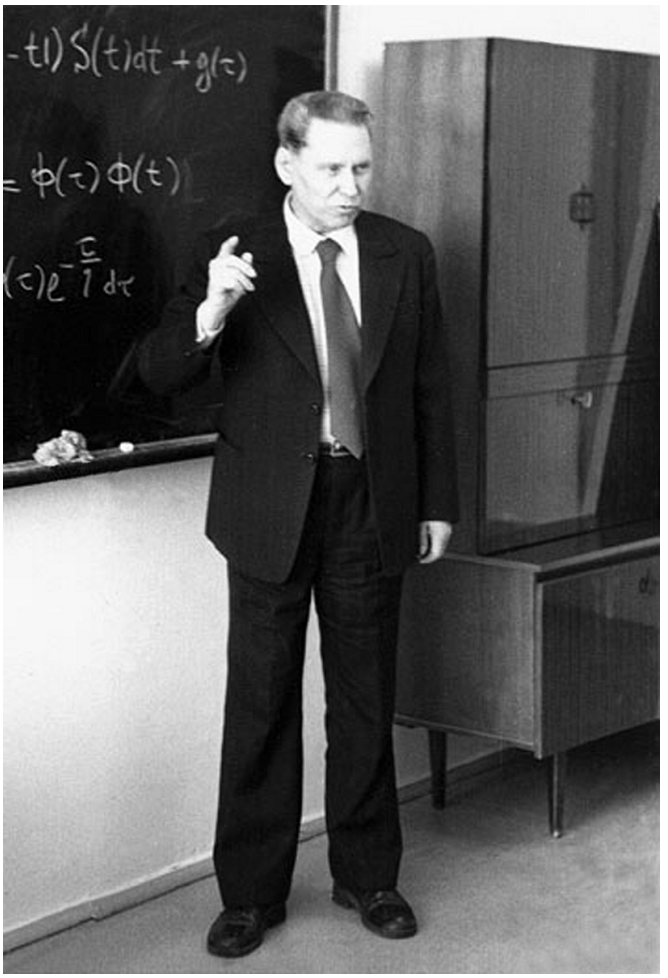

На лекции в начале 1980-х годов

Те, кому посчастливилось в 50-е – 70-е годы слушать лекции ВВ, неторопливые, спокойные, без внешних эффектов – но удивительно ясные, глубокие, лаконичные – будут помнить их всегда как высший образец того, какими должны быть лекции университетского профессора.

Сделать доклад на соболевском астрофизическом семинаре считалось честью. Нелегко было и получить у В.В. Соболева согласие на защиту диссертации в руководимом им Ученом совете. Чтобы работа была принята к защите, ВВ должен был лично убедиться, что ее уровень соответствует соболевским стандартам – а они были явно выше ВАКовских. Те, кто получил степень в ученом совете «у Соболева», потом всегда гордились этим.

После всего сказанного едва ли приходится удивляться тому, что Виктор Викторович создал пользующуюся широким признанием научную школу. С. Чандрасекар писал об “important contributions to the theory of radiative

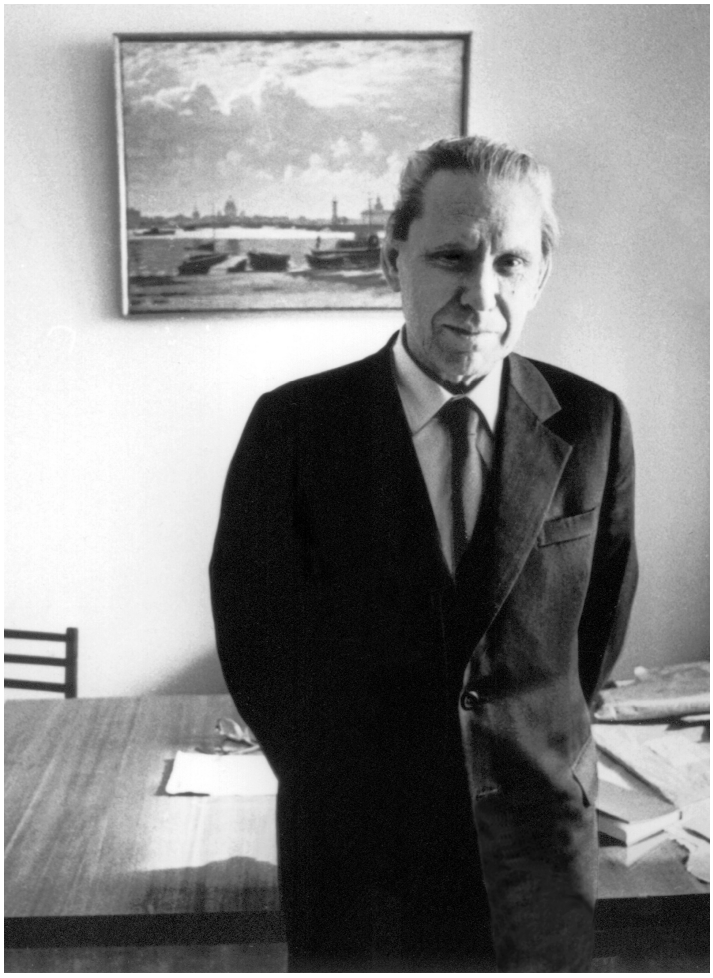

В университете в Петергофе (1990-е годы)

transfer by the Leningrad School and most especially by Professor V.V. Sobolev", Д. Хаммер и Дж. Райбики (США) говорят об "important work of the Leningrad School", Э. Фриш (Франция) пишет о методах, "developed by the Sobolev's School in Leningrad" и т.д.

По суммарному вкладу, внесенному в аналитическую теорию переноса излучения, В.В. Соболев и его школа – вне конкуренции в мировой астрофизике. Действительно, в этой теории можно выделить – разумеется, несколько условно – семь основных разделов: 1) идеи, понятия, математические методы; 2) теория монохроматического анизотропного рассеяния; 3) исследование нестационарных полей излучения; 4) поля излучения в неоднородных средах; 5) перенос поляризованного излучения; 6) многократное рассеяние излучения в частотах спектральных линий; 7) перенос излучения в движущихся средах. Школа Соболева – это единственный научный коллектив, который внес суще-

На летней школе по оптике рассеивающих сред (оз. Свитязь, Белоруссия, 1969 г.). Слева направо: *сидят* – И.Н. Минин, В.В. Соболев, В.В. Иванов; *стоят* – В.П. Гринин, А.К. Колесов, О.И. Смоктий, Э.Г. Яновицкий, Д.И. Нагирнер

ственный вклад во все эти разделы. Только среди членов этой школы одновременное свободное владение теорией анизотропного монохроматического рассеяния и теорией переноса линейчатого излучения – это норма. И лишь один человек за всю историю астрофизики не только внес фундаментальный вклад в каждый из этих семи основных разделов теории переноса излучения, но и стоял у истоков пяти из них. Этот человек – Виктор Викторович Соболев.

Школа Соболева – это несколько десятков астрофизиков, выпестованных им. ВВ гордился тем, что почти каждый второй из тех, у кого он был научным руководителем по кандидатской диссертации, стал впоследствии доктором наук.

Попасть в ученики к ВВ было нелегко. Каждый подвергался тому или иному испытанию, обычно неформальному. Мне, помнится, было предложено прочесть одну из глав незадолго до того появившейся книги по звездной динамике (sic!) и попытаться найти имеющиеся в ней серьезные ошибки. У всех проверялось также знание русской поэзии XIX века, особенно Пушкина, и отечественной истории. Мог быть задан, скажем, вопрос об отчестве Петра Великого или даже князя Андрея Курбского. Впрочем, провал «по литературе» и «по истории» прощался. Однако провалившийся обычно начинал перечитывать Пушкина и открывал для себя Ключевского... Впрочем, подоб-

ному «тестированию» подвергались не только молодые люди, но и практически все, с кем ВВ впервые знакомился лично. В 1981 г. я был свидетелем того, как подобный экзамен ВВ учинил... Чандрасекару во время его визита в Ленинград. Чандрасекар сдал экзамен блестяще, поразив Соболева прекрасным знанием произведений Толстого и Достоевского.

Молодых людей ВВ учил прежде всего личным примером. Все мы были свидетелями того, сколь тщательно им обдумывалось и подбиралось буквально каждое слово в любом тексте, даже в мелкой бюрократической бумажке, не говоря уже о статьях. Все рукописи статей своих учеников он внимательно прочитывал, в большинстве случаев возвращая после этого их на доработку, порой по много раз (известный мне рекорд – 14 раз!). Особенно внимательно, почти придирчиво, относился он к ссылкам и к тому, как в обзорной части статьи излагались и оценивались работы предшественников. Многие годы неукоснительно соблюдалось правило: прежде чем статья любого сотрудника ВВ будет отправлена в печать, она должна быть обсуждена на руководимом Соболевым семинаре. Неудивительно, что соболевский стиль чувствуется в публикациях всех его учеников.

«В молодости нужен быстрый успех, пусть хоть небольшой, чтобы человек поверил в себя» – любил повторять ВВ. И он старался помочь каждому своему ученику обрести этот первый успех как можно раньше. Зато потом наступал трудный период – нужно было хоть немного проплыть самому. Если это получалось плохо, ВВ в конце концов «включался» снова, быстро доводил человека до защиты диссертации, но в дальнейшем уже редко когда тратил на него свои силы и время.

Каждому из тех учеников, кого он считал толковым, на несколько лет давалось «на откуп» то или иное узкое направление, или, точнее сказать, четко очерченная научная тема. ВВ очень внимательно, порой жестко, следил за тем, чтобы между членами его школы не возникло нежелательных «интерференционных эффектов». Вот как был им нарезан научный пирог. В.Г. Горбацкий получил в свое ведение звезды с яркими линиями, И.Н. Минину было определено заниматься планетарными туманностями, а немного позже – нестационарными задачами теории переноса, В.В. Иванов был «брошен» на проблемы переноса излучения в частотах линий. Вскоре его как «не потянувшего» получить точные решения усилили Д.И. Нагирнером. Э.Г. Яновицкому назначено было изучать перенос излучения в неоднородных планетных атмосферах. В.М. Лоскутов получил в свое ведение поляризацию, А.К. Колесов – анизотропное рассеяние излучения в средах сферической геометрии, Х. Домке, в соответствии с указанием АН ГДР, предписывавшим, чтобы в его исследованиях было магнитное поле, – образование линий в атмосферах с магнитными полями, С.И. Грачев – движущиеся атмосферы, В.П. Гринин – вспыхивающие звезды и возникающие в связи с их исследованием задачи теории переноса и т.д. и т.п.

После защиты докторской диссертации, или около того, ограничения ослаблялись. Образно говоря, с этого момента давалось право на свободное

плавание по просторам современной астрофизики, и такое плавание поощрялось. Тем, кто преподавал в университете, доверялось выбрать для чтения собственный спецкурс. ВВ считал также, что только с этого момента он может поручить (или разрешить) своему ученику написать книгу. Впрочем, был случай, когда он отступил от этого последнего правила; именно тогда оно и стало нам известно.

Привыкшие к жестким рамкам ограничений, налагавшихся на них ВВ в пору их научной молодости, не все стремились воспользоваться предоставлявшейся им с некоторого момента «научной свободой». И все же: В.Г. Горбацкий ушел в космическую газодинамику, а позже увлекся внегалактическими проблемами; И.Н. Минин перекочевал в геофизику; В.В. Иванов чтением спецкурса и парой публикаций удовлетворил свое студенческое увлечение теорией строения и эволюции звезд (после чего вернулся «в родные края» – к проблемам формирования линий, но теперь уже с учетом поляризации); Д.И. Нагирнер постепенно откочевал в астрофизику высоких энергий (комптоновское рассеяние); В.П. Гринин стал интересоваться главным образом физической картиной явлений в оболочках Ae/Be звезд Хербига, планировать и проводить соответствующие наблюдения и почти перестал писать громоздкие формулы (сохранив, однако, интерес к численным расчетам спектров, формирующихся в движущихся средах); В.В. Витязев стал астрометристом; Х. Домке, к большому сожалению ВВ, вовсе оставил науку, уйдя в политику, где, впрочем, он вскоре достиг больших высот...

Когда несколько лет назад пришла пора бороться за гранты «на научные школы», ВВ стал, посмеиваясь, повторять присказку пресловутого Вл. Львова – «есть школы, школки, школенки». У Соболева же была и осталась – Школа.

IV. Организатор

В.В. Соболев много и охотно занимался организацией науки и преподавания, как в масштабе своего университета, так и страны в целом. Такого рода делами он стал активно интересоваться с конца 50-х годов, после избрания его членом-корреспондентом Академии Наук.

Став на академической лестнице на ступеньку выше своих университетских коллег-астрономов и возглавив астрономическую методическую комиссию, а вскоре – и все астрономическое отделение Ленинградского университета, он получил возможность проводить реформы преподавания, не встречая серьезного противодействия и не тратя на это слишком много сил. Он не преминул этим воспользоваться.

ВВ вник во все подробности учебного плана подготовки астрономов в ЛГУ и стал постепенно его улучшать. Это заняло лет десять-пятнадцать. Было прекращено преподавание геодезии, введен курс радиоастрономии, существенно улучшено преподавание математики для астрономов, сильно расширен –

На совещании, посвященном 40-летию введения принципов инвариантности (Бюракан, Армения, октябрь 1981 г.).
Слева направо: Э.Г. Яновицкий, Х. Домке, В.В. Иванов, В.В. Соболев, И.Н. Минин, В.П. Гринин, Д.И. Нагирнер, В.М. Лоскутов, О.В. Пикичян, С.И. Грачев

фактически заново поставлен – курс теоретической физики и т.д. Учитывая реалии Ленинградского университета, все предложения решительных изменений, таких как полный перевод всей астрономии или хотя бы астрофизики на физический факультет с математико-механического, или введение в ЛГУ двух разных учебных планов – для классических астрономов (небесные механики и астрометристы) и для астрофизиков – он решительно отвергал. Лишь незадолго до смерти, уже отойдя от подобных дел, в разговорах со мной ВВ несколько раз возвращался к тому, что все же было бы правильнее, если бы астрофизиков в Петербургском университете, как и во всем мире, готовили на физическом факультете. К сожалению, теперь этого едва ли удастся добиться скоро.

Предметом постоянных забот ВВ было также создание энергично работающего коллектива астрономов-исследователей в ЛГУ. Пока Астрономическая обсерватория (АО) ЛГУ оставалась государственным учреждением III категории, о привлечении сюда активной молодежи всерьез говорить не приходилось. ВВ нашел неожиданный выход: в 1960 г. он создал группу теоретической астрофизики в другом университетском подразделении – Научно-

исследовательском институте математики и механики, имевшем статус учреждения I категории. Когда несколькими годами позже при активном участии ВВ для АО ЛГУ удалось также добиться статуса I категории, эта группа была тут же переведена в АО. Так возникла лаборатория теоретической астрофизики АО ЛГУ, так сказать, штаб-квартира соболевской научной школы.

Как уже упоминалось, с 60-х годов ВВ был заведующим астрономическим отделением ЛГУ. Но не столько этот официальный пост, сколько высочайший личный авторитет, которым он пользовался, позволял В.В. Соболеву фактически держать в своих руках все основные рычаги управления астрономией в ЛГУ. Пользовался он этим очень умело. Не вникая в мелочи, ВВ оставлял решение всех стратегических вопросов за собой. Принимая порой неожиданные решения, он с годами сумел создать у себя в университете активно работающий дружный астрономический коллектив. Дрязги, склоки и подсиживания при ВВ были немыслимы.

Не одно десятилетие ВВ прилагал усилия к тому, чтобы преобразовать АО ЛГУ в Астрономический институт. В 1992 г. тогдашнему директору АО М.К. Бабаджанянцу удалось, опираясь и на поддержку ВВ, поставить последнюю точку в этом затянувшемся деле – столь желанное ВВ преобразование свершилось.

С 1958 по 1972 г. В.В. Соболев возглавлял Комиссию по физике звезд и туманностей Астрономического Совета АН СССР. В первые годы ее существования число астрономов у нас в стране быстро росло. Приходило новое поколение. Многочисленные совещания и конференции, проводившиеся возглавлявшейся ВВ Комиссией, сыграли важную роль в установлении тесных личных контактов между астрофизиками этого поколения, как теоретиками, так и наблюдателями, в первую очередь – оптиками. Совещания проходили, как правило, в крупных обсерваториях или в университетских центрах и привлекали большое число участников. Пожалуй, главный итог всей деятельности ВВ в этом направлении – возникновение в тогдашнем СССР еще одной спаянной общими научными интересами, личными симпатиями и антипатиями астрономической корпорации – астрофизической, подобной сложившимся существенно раньше корпорациям астрометристов и солнечников.

В 1973 г. В.В. Соболев стал председателем Совета по подготовке астрономических кадров (СПАК). На протяжении почти двух десятилетий ВВ уделял СПАКу очень много внимания. Совещания СПАКа проводились, как правило, на базе тех провинциальных педвузов, где преподавание астрономии было поставлено хорошо. Главным в работе СПАКа было отстаивание «суверенитета астрономии» в учебных планах университетов, педагогических институтов и средних школ. Твердая позиция В.В. Соболева, поддержанная его высоким академическим званием, позволяла успешно отбивать атаки тех, кто предлагал резко сократить либо вовсе упразднить преподавание астрономии или же влить астрономию в физику. То, что этого не произошло лет 20 назад – во многом заслуга В.В. Соболева. Увы, многое из достигнутого тогда сегодня пошло прахом...

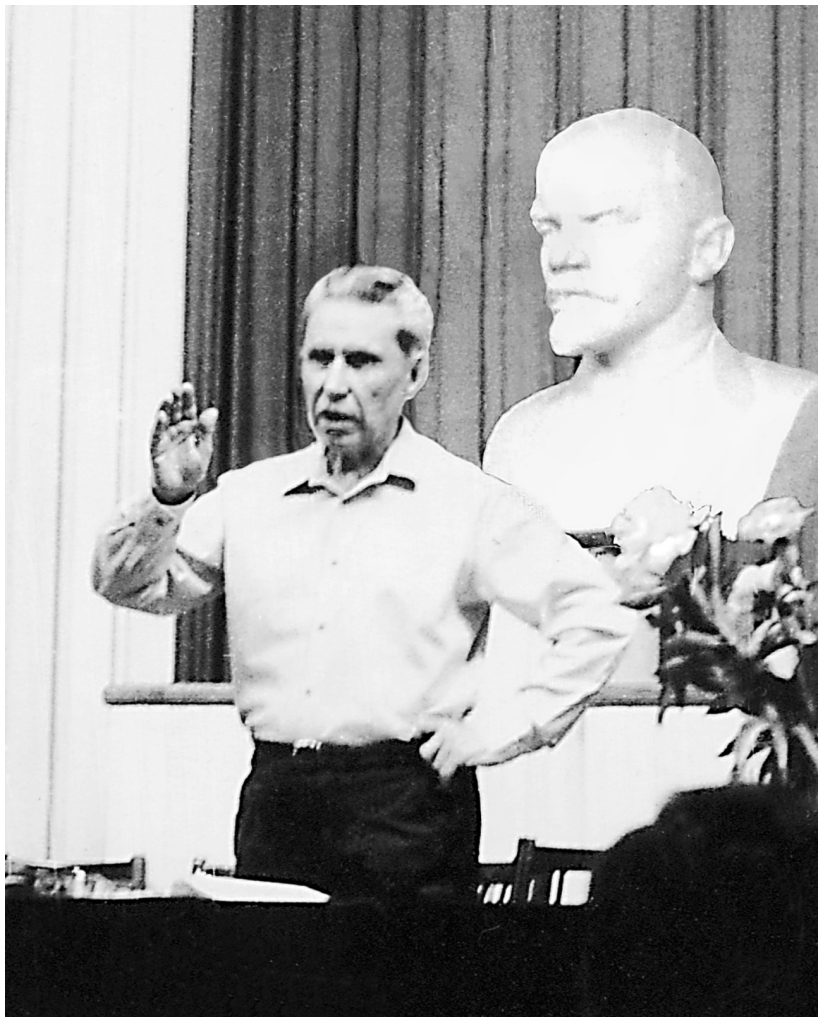

Выступление на одном из заседаний Совета по подготовке астрономических кадров (Полтава, 1983 г.)

В середине 70-х годов вошел в строй шестиметровый телескоп – первый общегосударственный телескоп бывшего СССР. Остро встал вопрос о распределении наблюдательного времени на нем. Была создана Комиссия по Тематике Шестиметрового Телескопа (КТШТ). Возглавить ее предложили В.В. Соболеву. Он согласился. Что из этого получилось, нынешние члены КТШТ оценивают так: «Как теоретик, он стоял над схваткой, не лоббировал интересы тех или иных групп наблюдателей, что в конечном итоге и предопределило устойчивую работу Комитета. Принципы работы Комитета, заложенные им, работают и по сей день уже более 20 лет».

Последняя крупная академическая организационная структура, которую возглавлял В.В. Соболев – Объединенный Научный Совет по Астрономии (ОНСА). На посту его главы он находился до конца жизни.

В.В. Соболев и Э.С. Парсамян на съезде Международного астрономического союза (Москва, Кремль, 1958 г.)

V. Человек

Теперь – самое трудное: постараться дать представление о том, каким В.В. Соболев был в жизни. Это трудно потому, что ВВ был личностью весьма необычной и многогранной. На людях он никогда не выставлял себя напоказ, скорее наоборот – стремился, если возможно, остаться за кадром. Поэтому для многих, даже часто видевших ВВ и время от времени общавшихся с ним, он оставался окружен ореолом таинственности. Было широко известно, что он человек сдержанный, очень умный, наблюдательный и проницательный, да к тому же обладает замечательной памятью – и потому его побаивались. Реальных оснований к этому, однако, не было.

С годами люди сильно меняются – это естественно. Когда уходит из жизни очень пожилой человек, обычно остается не так уж много людей, которые хорошо знали его в пору расцвета. Их свидетельства могут быть интересны не только тем, кто лично не встречался с ушедшим из жизни человеком, но и тем, кто застал его лишь на склоне лет.

В жизни ВВ можно выделить два периода – ленинградский и петергофский. «Ленинградский Соболев» заметно отличался от более позднего «петергофского Соболева», т.е. Соболева петергофского периода, начавшегося с конца 70-х годов, когда университетская астрономия вместе с несколькими естественными факультетами переехала с Васильевского острова в Петергоф, примерно за 40 км от города.

По пути домой из университета (фото 1970-х годов)

«Петергофский Соболев» бывал в университете сравнительно редко. Он приезжал для прочтения лекции или проведения семинара, подписывал бумаги, проводил короткие деловые встречи и сразу же уезжал домой – его ждала академическая машина, и задерживать ее он не мог. Общение с ВВ в этот период затрудняло также то, что он стал плохо слышать, и слух ослабевал все больше и больше. Основным способом его связи с внешним миром в этот период стал телефон. Естественно, что образ В.В. Соболева, который складывался у людей, не знавших его в ленинградский период, был искаженным. Далее мы даем отдельные штрихи к портрету В.В. Соболева ленинградской поры.

«Ленинградский Соболев» почти каждый день приходил из дома в университет пешком. Он жил сравнительно недалеко – на Мойке, прямо напротив Новой Голландии, на которую и смотрели окна его квартиры. В университете он проводил со своими сотрудниками и аспирантами часов по пять в день. Нельзя сказать, чтобы это были часы напряженной работы, скорее наоборот. Собрав около себя человек пять–шесть, ВВ вел с ними неторопливые беседы на самые разные темы – скажем, о реформах Витте или о Чехове и Толстом. Предметом детального обсуждения могли быть и планы экскурсий и поездок, которые хорошо бы организовать во время очередного совещания, готовившегося в это время ВВ. Писались также разные деловые бумаги (но не статьи!), причем все присутствовавшие при сем призывались активно помогать ВВ в этом деле. Мы выслушивали от ВВ массу любопытных, часто смешных историй, героями которых чаще всего были его коллеги-астрономы, и т.д.

и т.п. «Околонаучная» тематика в этих беседах занимала заметно больше времени, чем чисто научная. Пожалуй, час или полтора в день все же приходились и на серьезные научные обсуждения.

Для ВВ такое времяпрепровождение было чем-то вроде тех семейных бесед, которые обычно ведутся по вечерам, когда собирается вся семья. Если не считать чтения лекций (обычно по четыре часа в неделю) и проведения семинаров, то в университете ВВ главным образом отдыхал или не торопясь делал второстепенные дела. Всерьез же работал он дома по ночам, когда никто и ничто его не отвлекало.

ВВ любил ездить по своей стране и знакомиться с новыми местами, особенно связанными с русской историей и литературой. Организовывались такие поездки весьма своеобразным способом. В брежневские времена существовал термин «научный туризм». Так назывались поездки по приглашению на заграничные научные конференции. Так вот, Соболев создал свою, совершенно особую разновидность «научного туризма». Во-первых, он был внутрисоюзным, а не заграничным. Во-вторых, место и время проведения совещания выбирал сам ВВ. Наконец, в-третьих, тематика совещания подбиралась так, что ВВ имел возможность пригласить на него тех, кого он хотел повидать. Так им были созваны совещания в Полтаве и Вологде, Кинешме, Рязани, Ульяновске и никому из нас дотоле неведомой совершенно очаровательной Коломые (Западная Украина). Как это делалось? Местным властям заранее посылалась умело составленная деловая бумага. Провинциальное советское и партийное начальство не могло не откликнуться на предложение из Ленинграда провести у них в городе в пединституте нечто Всесоюзное, к тому же организуемое – ни мало ни много – самой Академией Наук СССР! Никакого обмана ни в чем никогда, конечно, не было.

А за границу ВВ не ездил ни разу. «Идти в райком, унижаться – нет, никогда». Он был человеком с обостренным чувством собственного достоинства.

В поездках любил комфорт. На шум и грязь вокруг себя реагировал болезненно. Поэтому в поездах не ездил никуда, кроме Москвы, во все другие места летал. А вообще-то был человеком очень скромным. К роскоши был абсолютно безразличен. Очень долго жил в коммунальной квартире, и только когда уже стал членкором, переехал в предоставленную ему университетом отдельную квартиру.

ВВ обладал удивительной памятью. Мельчайшие детали событий он помнил десятилетиями. Записной книжкой не пользовался – все телефоны запоминал с первого раза. В 50-е годы он даже жаловался, что такая память ему мешает. Помнить слишком много мелочей, видимо, было обременительно. Но зато черновиков рукописей у него не было. Сначала он тщательно обдумывал работу в целом и мысленно составлял ее план. Затем, сидя на диване или прохаживаясь по комнате, он «писал» в уме целый абзац. Только окончательно отредактировав его, тоже в уме, ВВ садился за стол и записывал окончательный текст. Разумеется, всему этому предшествовала основная часть работы – вывод формул, расчеты и т.п., и тут без бумаги не обходилось.

В.В. Соболев и группа его друзей, называвшие себя Гончими Псами, в 1950–60-е годы часто играли в пинг-понг. На снимке: α Гончих Псов (фото 1950-х годов)

Хорошо знавших ВВ людей его память не переставала поражать, тех же, кто сталкивался с нею впервые, пугала. ВВ знал это и пользовался этим как одним из средств, чтобы «устанавливать дистанцию». Эта дистанция всегда оказывалась – по вертикали.

Как уже говорилось, все сотрудники ВВ знали, что главной своей работой – наукой – он занимался по ночам. Поэтому звонить ему домой до полудня не полагалось. Помню, как-то раз, придя в университет по обыкновению около часа дня, ВВ со смехом поведал о том, что в этот день телефонный звонок поднял его с постели около восьми утра. Только что прилетевший в Ленинград молодой человек, собиравшийся в этот день доложить на семинаре у ВВ свою кандидатскую диссертацию, боялся опоздать к началу семинара и позвонил ВВ из аэропорта, чтобы узнать, как ему быстрее добраться до университета... Смеялся же ВВ потому, что, оказывается, есть еще на свете люди, которые не боятся вести себя с ним столь непринужденно, да еще и перед защитой диссертации. Доклад молодого человека Соболеву понравился, и вскоре он благополучно защитил диссертацию в совете у ВВ.

ВВ был человеком консервативным и менять свои привычки не любил. Лет двадцать ушло на то, чтобы убедить его начать пользоваться авторучкой. Дело в том, что в начале 50-х годов он попробовал было решиться на это,

но на несчастье как-то в самолете авторучка у него в пиджаке протекла и испортила ему рубашку. В итоге все свои книги, кроме, быть может, последней (РСАП), он написал, макая ручку с пером в чернильницу! В последние годы он стал изредка пользоваться пишущей машинкой, но компьютер так и остался неосвоенным.

Для пишущего эти строки любая организационная деятельность, требующая контактов с бюрократическими структурами, – это почти проклятие. Поэтому то, как В.В. Соболев относился к подобным вещам, долгое время было выше моего понимания. Порой казалось, что бюрократическое бумаготворчество доставляет ему удовольствие. Постепенно я понял, что ВВ воспринимал свое неизбежное взаимодействие с бюрократией как некую игру, или лучше сказать, спортивное состязание, которое надо стараться выиграть. Если он ввязывался в такую игру всерьез, то обычно выигрывал.

Вся обширная научно-организационная деятельность ВВ осуществлялась им путем писания бумаг и раздачи поручений хорошо лично ему знакомым людям. Сам ВВ по инстанциям не то что не бегал – никогда не ходил. В Москве в Министерстве он не был ни разу. На приеме у ректора университета за полвека работы в нем он побывал, кажется, всего дважды. «Толково составленная деловая бумага, требующая ответа в письменном виде, на порядок действеннее, чем визиты и устные согласования» – это был его принцип. И еще: «В делах, требующих соблюдения четко установленных правил, таких, например, как защита диссертации, надо скрупулезно соблюдать все формальности. Тогда сбоев не будет». Можно сказать – ВВ был идеально законопослушным. Он внимательнейшим образом изучал разные правила, инструкции и прочие бюрократические установления и требовал того же от своих сотрудников (чем порой сильно им досаждал). При этом он неизменно находил в подобных документах слабые места и умело ими пользовался, чтобы, ничего не нарушая, все же добиться желаемого результата. Он бил бюрократов их же собственным оружием, которым владел в совершенстве.

Когда жизнь ставила ВВ в затруднительное положение, он умел находить нестандартные решения. Вот пример. Приближалось 75-летие ВВ. Этот свой юбилей отмечать традиционным образом он не хотел. Тогда ВВ предложил отпраздновать 100-летие интегрального уравнения переноса излучения, приходившееся на тот же год! Конференция получилась замечательная, съехались многочисленные ученики ВВ. Но обычных славословий, вручения адресов и подарков не было, а именно этого ВВ и хотел избежать.

Мы привыкли к тому, что все вокруг вечно торопятся, спешат, куда-то бегут, опаздывают, жалуются на нехватку времени. ВВ был неторопliв, даже медлителен, никогда не спешил – но удивительным образом все делал вовремя, никуда никогда не опаздывал. Если что-то обещал, то обязательно выполнял. В общем-то, он был педантом.

Помню, как-то раз, вернувшись из Москвы, он с улыбкой рассказывал о том, как Э.Р. Мустель, в ту пору председатель Астросовета, целых полчаса кряду плакался ВВ, как невероятно он занят и сколько у него сегодня неот-

За шахматной доской на волжском теплоходе (фото 1950-х годов)

ложных дел, которые он никак не успевает сделать – «вместо того, чтобы взять да и потратить это время на эти самые дела».

Убедить ВВ взяться за какое-нибудь дело, в отличие от Мустеля, было очень и очень непросто. Зато уж если он соглашался, успех был почти обеспечен. Наоборот, если ВВ решил кого-то попросить что-нибудь сделать, отказаться или как-то увильнуть было почти невозможно – он умел давить и добиваться желаемого.

Неторопливость ВВ плохо вяжется в уме с тем, сколько он сумел сделать за свою жизнь. На самом деле за этим стоит жесткая самодисциплина и огромное трудолюбие, скрытое от людских глаз почти ночным образом жизни. Он умел быстро сосредотачиваться и концентрировать внимание только на том, что может оказаться существенным. При общении с ВВ сразу чувствовалось, когда он «включился».

Философствуя, ВВ говорил, что счастье – это некий баланс желаний и возможностей к их удовлетворению. Он полагал, что люди слишком часто зря тратят огромные силы на то, чтобы увеличить возможности удовлетворения своих желаний, тогда как счастья гораздо легче можно достичь, научившись умерять свои желания. Видимо, для него это были не просто красивые слова, а скорее принцип, которому он старался следовать и в науке, и в жизни вообще.

На отдыхе с В.Г. Горбацким (Алма-Ата, 1985 г.)

Знакомый каждому вечный конфликт разума и эмоций, казалось, был неведом ВВ. Разум диктаторски правил его чувствами. И все же была область, где эмоции полностью побеждали. Это был футбол. Соболев был страстным болельщиком. Впрочем, он считал себя не просто болельщиком, а профессионалом в этом деле. Решиться прийти на работу, не зная счета во вчерашнем победном матче его любимого «Зенита» – значило пасть в глазах ВВ очень низко. Если мне не изменяет память, как-то раз дата совещания в Бюракане специально подбиралась В.В. Соболевым и Э.Е. Хачикяном так, чтобы они смогли вместе сходить в Ереване на матч «Зенит» – «Арарат». Имя зенитовского футболиста Завидонова годами звучало из уст ВВ едва ли не чаще, чем имя любого из астрофизиков мира. В отличие от большинства футбольных болельщиков, зимой переключающихся на хоккей, к нему ВВ был безразличен.

Другим его увлечением были шахматы. В молодости он был шахматным композитором, его задачи печатались. Играл ВВ много и, говорят, хорошо (я не шахматист, и потому сам судить не берусь). В 50-е – 60-е годы раз или два в неделю ВВ можно было застать вечерами в его кабинете за шахматной доской. Сходив около шести вечера домой пообедать, он возвращался затем специально для заранее с кем-нибудь назначенного на вечер шахматного поединка. Порой игра затягивалась часов до девяти, а то и до десяти. Да и днем, если выяснялось, что его именитый визитер играет в шахматы, на столе тут же появлялись доска и часы. Через такой неожиданный для них

шахматный экзамен прошли Х. ван де Хюлст, М. Ситон, Лео Голдберг и многие другие.

А еще в жизни Соболева были стихи. Они были с ним всегда и везде, он возил их с собой – в своей памяти. Больше всего он любил Пушкина, которого знал великолепно. Начав что-нибудь читать наизусть, иногда вдруг останавливался, запнувшись, и делал вид, что дальше забыл. Просил подсказать следующую строку, а если никто сделать этого не мог, как бы вдруг вспоминал сам, и продолжал читать дальше. Хорошо знал не только Пушкина, но и вообще русскую поэзию XIX века – и Лермонтова, и Тютчева, и даже Никитина и поэтов его круга. Часто нараспев читал Есенина. Говорят, в последнее время от него можно было услышать Бродского, но мне не доводилось. Гостей своей дачи в Комарово ВВ неизменно водил на комаровское кладбище, где обязательно подводил их к могиле Ахматовой, но стихов ее почему-то почти никогда не читал. Теперь он сам покоится на этом кладбище.

ВВ был убежденным холостяком. Всю жизнь он вместе с матерью (до ее смерти) прожил в семье своей сестры и ее дочери. Он был полностью избавлен от бытовых забот и всегда окружен теплом и вниманием. В последние годы жизни, когда ВВ стал серьезно болеть, близкие трогательно заботились о нем.

Как-то раз, поздравляя Виктора Викторовича 2 сентября с днем рождения, я спросил: «Как Вы отдохнули? Погода нынче летом была прекрасная...» А он в ответ: «Ужасная была погода! Когда идет дождь, можно спокойно сидеть и работать. Когда же все время светит солнце, родные мне велят идти гулять – и невозможно нормально работать...»

Санкт-Петербург
7 января – 16 февраля 1999 г.